Quantum Transport in Non-Collinear Magnetic Nanostructures

Dissertation

zur Erlangung des akademischen Grades des Doktors der Naturwissenschaften (Dr. rer. nat.) an der Universität Konstanz, Fachbereich Physik

vorgelegt von

Christian Wickles

Tag der mündlichen Prüfung: 01. Juli 2011
Referenten: Prof. Dr. Wolfgang Belzig
Prof. Dr. Ulrich Nowak

Contents

0. Deutsche Zusammenfassung **V**

1. Introduction **1**

2. Electron Transport in Ferromagnetic Conductors with Inhomogeneous and Time-dependent Magnetic Order Parameter **5**
2.1. Introduction . . . 5
2.2. Quantum Transport Equation for Ferromagnetic Conductors . . . 7
2.2.1. Model and Hamiltonian . . . 7
2.2.2. Keldysh Technique . . . 9
2.2.3. Impurity Scattering . . . 12
2.2.4. Kinetic Equation in Linear Response . . . 15
2.2.5. Self-consistency Condition – from *s-d* Model to Stoner Model . . . 20
2.3. Diffusive Transport in Quasi-1-Dimensional Systems – Domain-wall Resistance 23
2.3.1. Model of the Contact . . . 24
2.3.2. Kinetic Equation - Boundary Condition versus Source Terms . . . 26
2.3.3. A Hierarchy of Equations . . . 27
2.3.4. Solving the Hierarchy of Equations . . . 29
2.3.5. Results and Discussion of the Domain-wall Resistance . . . 33
2.4. Electron Transport in Presence of Inhomogeneous and Time-dependent Magnetization . . . 38
2.4.1. Magnetization Gradient Corrections in Equilibrium . . . 38
2.4.2. Spin-Charge Continuity and Diffusion Equation . . . 39
2.4.3. Transverse Spin-dynamics in a System with Rapid Precession . . . 44
2.4.4. Change in the Conductivity due to Magnetization Gradients . . . 45
2.4.5. Domain-wall Resistance in Diffusive Wires for CPW and CIW Geometry 46
2.4.6. Transverse Conductivity . . . 53
2.4.7. Spin-current in Presence of Inhomogeneous Magnetization . . . 56
2.5. Magnetization Dynamics . . . 59
2.5.1. From Non-equilibrium Spin-excitations to Spin Torque . . . 60
2.5.2. Spin Torque and Landau-Lifshitz-Gilbert Equation . . . 63
2.5.3. Force on the Magnetization in the *s-d* Model . . . 65
2.5.4. Charge Current Induced by a Moving Domain-wall . . . 66
2.6. Conclusions and Outlook . . . 68

3. Effective Quantum Theories for Transport in Inhomogeneous Systems with Non-trivial Band Structure **71**
3.1. Effective Quantum Theories and Berry Curvatures . . . 71
3.1.1. The Wigner Representation and the Systematic Diagonalization Scheme 73

3.1.2. Gauge Invariance . . . 79
3.1.3. Canonical versus Kinetic Variables and Gauge Invariant Description . 80
3.1.4. Electronic Spectrum and Magnetic Dipole Energy . . . 90
3.1.5. Equations of Motion . . . 92
3.1.6. Some Notes on Requantization . . . 100
3.2. Hierarchy of Effective Theories and Inclusion of the Electromagnetic Field . . 102
3.2.1. General Hierarchy . . . 102
3.2.2. Inclusion of the Electromagnetic Field . . . 103
3.3. The Dirac Equation . . . 107
3.4. Topological Insulators Exchange Coupled to a Ferromagnet with General Magnetization Texture . . . 112
3.4.1. General Two Band Model . . . 112
3.4.2. Topological Properties . . . 114
3.4.3. Towards, and In The Metallic Regime . . . 116
3.4.4. Magnetization Dynamics and Transport Properties . . . 119
3.5. Conclusions and Outlook . . . 123

4. Transport and Bound States on Topological Insulators with Induced Ferromagnetism 127
4.1. Introduction to Topological Insulators . . . 127
4.1.1. 3D Strong Topological Insulators (STI) . . . 128
4.1.2. Strong Topological Insulator with Induced Ferromagnetism . . . 129
4.2. General Properties of Dirac Fermions with Induced Ferromagnetism . . . 130
4.2.1. Densities and Quantum Equations of Motion . . . 130
4.2.2. Gauge Transformation . . . 133
4.2.3. Wave Equation in the Schrödinger Form . . . 134
4.2.4. External Magnetic Field . . . 135
4.2.5. Semiclassical Orbits . . . 136
4.3. Interface States and Zero Energy Bound States . . . 138
4.3.1. F-F Interface on Top of a Topological Insulator . . . 138
4.3.2. Zero Energy Bound States . . . 141
4.3.3. Zero Energy Bound States in a Perpendicular Magnetic Field – Zeroth Landau Level . . . 143
4.3.4. Zero Energy Bound State in 2-Dimensional Structures . . . 144
4.4. Finite Width Domain Wall - The x-y Configuration . . . 146
4.4.1. Bulk Properties . . . 148
4.4.2. Symmetries . . . 150
4.4.3. The Exact Solution of the Problem . . . 151
4.4.4. Bound States at the Domain Wall . . . 152
4.4.5. Scattering States and Ballistic Transport . . . 156
4.4.6. Negative Energies . . . 162
4.5. Finite Width Domain Wall - The z-y Configuration . . . 162
4.5.1. The Exact Solution . . . 163
4.5.2. Scattering States and Ballistic Transport . . . 165
4.6. Conclusion and Outlook . . . 169

5. Conclusions and Outlook 171

A. The Wigner function **173**

B. Beyond linear response **175**

C. Details on deriving the hierarchy of equations **180**

D. Details on solving the kinetic equation in the general time-dependent case **186**

E. The Hypergeometric function ${}_2F_1$ and the Gamma function Γ **189**

0. Deutsche Zusammenfassung

In dieser Arbeit geht es hauptsächlich um die Transporteigenschaften von leitenden Materialien, welche zusätzlich zu den metallischen Eigenschaften auch ferromagnetisch sind und einen räumlich und zeitlich variierenden ferromagnetischen Ordnungsparameter aufweisen.

Im ersten Teil dieser Arbeit wird zunächst eine semi-klassische Transport Gleichung aus einem mikroskopischen Model im Rahmen der Quantentheorie hergeleitet. Diese Gleichung besitzt Gültigkeit im Grenzfall mesoskopischer Systeme, in denen die typischen Längenskalen in der Größenordnung von mehr als 10 nm betragen. Im Gegensatz zu herkömmlichen Theorien für Niedrig-Energie Transport ist die hier vorgestellte Theorie für beliebige Größe des ferromagnetischen Ordnungsparameters gültig und beschreibt somit experimentell oft verwendete leitendete ferromagnetische Materialien wie Permalloy. Dies muss sich durch die Unterscheidung von sogenannten hoch- und niedrig-Energie Beiträgen erkauft werden, was in dieser Arbeit in konsistenter Weise erfolgt. Mit Hilfe dieser Transportgleichung wird zunächst der Einfluss einer ferromagnetischen Domänenwand auf den Widerstand des Metalls untersucht. Es folgt eine ausführliche Diskussion die Unterschiede zu anderen veröffentlichten Theorien und deren Probleme ausführlich erläutert. Es wird auf verschiedene Mechanismen eingegangen die zum Domänenwand-Widerstand führen, und warum eine Domänenwand den Widerstand unter Umständen auch verringern kann, was zunächst der Intuition widerspricht. Es wird auch auf die Unterschiede eingegangen die von zwei unterschiedlichen Modellen des Ferromagnetismus herrühren. Im ersten Fall sitzen die für den Ferromagnetismus verantwortlichen Elektronen auf festen Plätzen im Kristallgitter, und wechselwirken durch die Austauschwechselwirkung mit den Leitungselektronen. In einem zweiten Modell wird der Ferromagnetismus von den für den Ladungstransport verantwortlichen Elektronen selbst getragen. Schließlich wird auch die Abhängigkeit des Domänenwand-Widerstands von magnetischen Verunreinigungen untersucht, die sich experimentell z.B. durch verschiedene Dotierung des Metalls untersuchen lässt.

Im weiteren Verlauf wird vor Allem auf die Folgen zeitabhängiger Magnetisierung eingegangen, die z.B. zu Ladungsströmen im Metall führen kann, oder die Magnetisierungsdynamik selbst beeinflusst. Viele in der Literatur bereits veröffentlichen Resultate werden bestätigt und teilweise durch fehlende Teile ergänzt. Das schöne der hier vorgestellten Beschreibung ist, dass sie sämtliche Effekte des Magnetotransports in einer einheitlichen und konsistenten Beschreibung zusammenfasst und andere, zum Teil phänomenologische Theorien, auf eine solide Basis stellt.

In dem zweiten Teil dieser Arbeit wird die im ersten Teil erfolgreich angewandte semiklassische Beschreibung auf allgemeine Quantensysteme verallgemeinert. Gerade im Hinblick auf die vor wenigen Jahren entdeckten topologischen Materialien ist diese Beschreibung nützlich. Diese zeichnen unter anderem auch dadurch aus, dass beim Transport oder bei dynamischen Phänomenen Berry Phasen eine zentrale Rolle spielen. Diese werden in der

semi-klassischen Beschreibung in konsistenter Weise implementiert, so dass Transport im mesoskopischen Grenzfall beschreiben lässt, ohne auf die ursprüngliche umfassendere Theorie zurückgreifen zu müssen. Nicht zuletzt ist die semi-klassische Beschreibung auch deshalb interessant, da sich aus ihr oft anschauliche Erklärungen ergeben. In diesem Zusammenhang wird auch ganz allgemein die Struktur, die eine effektive Quantentheorie aufweisen muss um in sich konsistent zu sein, analysiert. Es wird argumentiert, dass in bestimmten Fällen Zur Illustration verschiedener Aspekte wird dieser Formalismus auf die relativistische Dirac-Gleichung und ein allgemeines zwei-Bänder Modell angewandt, und dessen Verhalten ausführlich untersucht.

Der dritte und letzte Teil ist schließlich vollständig den topologischen Isolatoren gewidmet, die sich durch die Existenz metallischer Oberflächenzustände auszeichnen, während das Material im inneren im Idealfall nicht zum Transport beiträgt. Im Gegensatz zu Oberflächenzuständen die auch in gewöhnlichen Isolatoren auftreten können, besitzen die hier untersuchten Zustände eine ungewöhnliche Spin-Struktur, welche letztlich zu den interessanten topologischen Eigenschaften dieser besonderen Isolatoren führt. Aus fundamentaler Sicht interessant ist es, dass sich Anregungen auf dieser Oberfläche so verhalten wie relativistische Teilchen, sogenannte Dirac-Fermionen. Um diese Materialien hat sich innerhalb weniger Jahre ein sehr aktives Forschungsfeld entwickelt, nicht zuletzt da sie eine Reihe von exotischen Anregungen verspricht, die man bereits im Rahmen der Teilchenphysik theoretisch untersucht hat, nur aber die Möglichkeit sieht diese in Festkörpersystem unter kontrollierten Bedingungen zu studieren. Ganz speziell für Anwendungen interessant ist die Kombination dieser Isolatoren mit anderen Materialien, die ihrerseits wieder spezielle Eigenschaften verfügen. Bringt man z.B. einen isolierenden Ferromagneten in die Nähe dieser Oberfläche, so wird dort ein sogenanntes ferromagnetisches Austauschfeld induziert, das mit dem auf der Oberfläche befindlichen Dirac-Fermionen wechselwirkt, was wiederum zu ganz neuem Verhalten und Eigenschaften führt. Zunächst werden generelle Eigenschaften und Folgen dieses Zusammenspiels aus Dirac-Fermionen und Ferromagnetismus untersucht, vor Allem das Auftreten von gebundenen Zuständen an inhomogenen Magnetisierungsstrukturen wie Domänenwänden oder sogenannter Wirbel.

Schließlich wird noch ausführlich untersucht, welche Auswirkungen Domänenwände endlicher Breite und verschiedener Konfigurationen auf die Oberflächenzustände haben, und wie sie den Transport auf der Oberfläche beeinflusst. Für die quantentheoretische Beschreibung dieses Systems wird dazu die häufig verwendete effektive Beschreibung der Oberflächenzustände verwendet, zusammen mit einem analytischen Modell von Domänenwänden, welches schon im ersten Teil dieser Arbeit Anwendung fand. Der Hamiltonoperator wurde analytisch exakt diagonalisiert, was einem letztlich eine genaue Analyse sämtlicher Eigenschaften dieses Modells erlaubt. Daraus lässt sich ableiten, dass an einer Domänenwand endlicher Breite mehrere gebundene Zustände entstehen können, im Gegensatz zu einer abrupten Domänenwand, wo man nur einen solchen Zustand findet. Es wird die Dispersion diese Zustände bestimmt, wobei zwei besondere Typen von Domänenwänden unterschieden werden: Im ersten Fall bleibt die Magnetisierungsrichtung ausschließlich in der Ebene der Oberfläche des topologischen Isolators. Im zweiten Fall steht die Magnetisierungsrichtung senkrecht zur Oberfläche und öffnet damit eine Bandlücke, wodurch die Dirac-Fermionen eine Masse erhalten. Diese fiktiven Massen haben unterschiedliches Vorzeichen auf beiden Seiten der Wand. Deren unterschiedliches Verhalten zeigt sich auch besonders deutlich in den Transporteigenschaften, zum Beispiel die hier Untersuchte ballistische Leitfähigkeit. Im Falle der zu einer Bandlücke führenden Domänenwand

zeigt sich das interessante Verhalten, dass bei bestimmten Wandbreiten die Reflektion an der Wand komplett unterdrückt wird, die Wand aus Sicht der Dirac Fermionen also vollständig transparent wird. Das ist zwar auch beim anderen Typ Domänenwand der Fall, allerdings nur für bestimmte Dirac Fermionen, und ist damit in der Leitfähigkeitsänderung kaum bemerkbar. Vermutlich handelt es sich hierbei um einen Interferenzeffekt, der von den besonderen topologischen Eigenschaften des Isolators herrührt.

Acknowledgements

I would like to thank two people primarily, since without their help this work would not exist in this form. First, I wish to express my gratitude to my supervisor Wolfgang Belzig for his support, discussions and the friendly relation. And second, to my beloved Cholidah Febrilyasari for her support in many ways that ultimately allowed me to finish this work in the present form.
I would also like to thank the members of the Quantum Transport Group of Wolfgang Belzig for providing a comfortable environment. In particular, I am grateful to my longtime officemate Jan Hammer and the part-time officemates Sebastian Gattenlöhner and Simon Reinbold for entertaining, but also more serious scientific discussions.

1. Introduction

Since the very early ages of computer technology, ferromagnetic materials have been very successfully utilized as magnetic data storage. Its biggest drawback are the large magnetic fields required to manipulate the magnetization along with the mechanical components part of this design, making these devices slower and more prone to malfunction, in mobile devices in particular. Recently, the idea was put forward to combine the advantages of magnetic data storage and an all-electric read/write scheme, the racetrack memory [1]. The key idea is to use ferromagnetic metals in a nano-wire geometry where the data is stored by creating domains of different magnetization which are separated by a domain-wall (DW), a finite region over which the magnetization rotates its direction to connect the two domains of opposite magnetization direction. It has been realized that a spin-polarized current flowing through such a wall interacts with it causing it to move under certain conditions and it is referred to as domain wall motion. On the other side, a dynamic magnetization like the moving domain induces a charge- and spin-current that can be used to detect the presence of a domain-wall, an effect useful for data retrieval in an all-electrical magnetic data-storage. Furthermore, the generation of spin-currents is of fundamental interest in the field of spintronics and the experimentally widespread method is to use spin-pumping due to a dynamic magnetization, especially in non-magnetic materials like semiconductors. This mutual interaction between an inhomogeneous and time-varying magnetization and the freely movable conduction electrons, together with the many interesting effects it exhibits, is the central theme of this work.

Ferromagnetic conductors

Microscopically, this interaction between the spin of the conduction electrons and a spatially or time-varying magnetization is due to the exchange interaction between conduction electron spin and local magnetization and consequently, it is a genuine quantum mechanical effect. But not only is the magnetization affected by the current flow or a non-equilibrium spin-accumulation in the conduction electron system, the reciprocal effect should also exist. This is for example the domain-wall resistance (DWR) which quantifies the change in resistance due to the presence of a magnetization structure. In the presence of non-coplanar magnetization textures, this resistance can even acquire off-diagonal elements giving rise to a transverse Hall current similar to a metal in an external magnetic field.

In addition to the purely quantum-mechanical exchange interaction, the whole scenario is significantly influenced by magnetic and non-magnetic impurities. To this end, we will perform a theoretical study using a microscopic quantum theory that describes the exchange interaction along with magnetic and non-magnetic impurities and a simple band structure applicable for metals. Within this microscopic model and a consistent mathematical framework utilizing a Boltzmann transport equation, we will derive various results that include the domain-wall resistance, pumped charge- and spin-currents and the spin torque. All the results emerge

from the same model under the same assumptions and approximations and thus, they are directly comparable and consistent with each other. Treating two distinct models of ferromagnetism, we will thoroughly discuss the behavior of the domain-wall resistance and in the limiting cases of strongly and weakly ferromagnetically polarized metal, and we will discuss its underlying mechanisms in order to understand the appearance of positive and negative domain-wall resistance, since both signs have been also found experimentally. We will also discuss the major role played by impurity scattering, thus requiring a consistent treatment of impurities on the Hamiltonian level. Essentially, in the first part of this work, we calculate the full non-equilibrium behavior in response to an external magnetic field and a dynamic magnetization within one coherent framework, and we will discuss other theories and differences to our treatment.

Effective quantum theories

Having discussed the system of conduction electrons exchange coupled to inhomogeneous and time-dependent magnetization textures, and we will often distinguish intrisic effects like the Hall current or charge pumping from extrinsic ones. In literature, there is a trend to formulate these intrinsic effects in terms of real-space Berry phases and curvatures. On the other side, there is quite some research activity around the anomalous Hall effect (AHE) which is due to the interplay of spin-orbit interaction and ferromagnetism. These and related effects can be formulated in terms of momentum space Berry curvatures. Another development that underlined the importance of Berry phases was the discovery of Graphene in 2005 and the Berry phase of π associated with the special electronic band structure which coupled the momentum linearly to the pseudo-spin [2].

Generally, one has to take into account the spin-orbit interaction which is of particular importance for semiconductors like GaAs. This spin-orbit coupling mechanism gives rise to a variety of additional effects which are studied extensively in the field named spintronics, and are sought to be exploited for novel spin-electrical devices [3]. This interaction is described theoretically in an effective band theory applicable for low-energy excitations in the system. This is the main driving force that leads us to develop a general formalism suited for systems that intricately couple the spin-degree of freedom to the momentum $\boldsymbol{p}$ via a spin-orbit interaction, and to the position operator $\boldsymbol{r}$ via an inhomogeneous magnetization, the latter possibly also time-varying. In general, this gives rise to a complicated dynamics, and other common methods like gauge-transformations that attempt to locally diagonalize spin-space fail to work due to non-commutativity of $\boldsymbol{r}$ and $\boldsymbol{p}$.

In that respect, we will investigate what an effective quantum theory should look like in the most general case and how it emerges from a more comprehensive theory. We will see how Berry curvatures and related quantities arise in the course of this reduction procedure. We argue that for a complete effective quantum theory, knowing only the Hamiltonian is generally not enough and one needs to distinguish between canonical and kinetic operators, and only then can dynamical observables like the current be defined in a gauge-invariant manner. This is relevant for the non-relativistic Pauli Hamiltonian, but also for the study of spin-orbit coupled semiconductors.

To this end, we will develop a general consistent and gauge-invariant framework that incorpo-

rates intrinsic effects in terms of Berry curvatures. Subsequently, we consider the two specific examples of the relativistic Dirac equation and a general two-band model that describes for example the surface of a topological insulator with proximity induced ferromagnetism. And finally, the investigation thereof gives some interesting insight into the structure of quantum mechanics itself and the role that canonical and kinetic operators play in effective quantum theories.

Topological insulators with proximity induced ferromagnetism

The discovery of topological insulators has recently attracted many researchers and has lead to a drastic increase of activity in this field. These new materials show good prospects in regard to both fundamental research and technological applications. For example, due to the topologically protected surface states and the resulting spin-momentum locking, it shows great potential for magneto-electronic applications at room temperature. Of course, these topological materials show their true potential only in combination with additional systems, like conventional ferromagnetism to which we will devote our work. We study the interplay of these surface Dirac Fermions with a proximity induced inhomogeneous ferromagnetic order parameter.

As a direct application of the framework of effective theories derived within this work, we calculate the topological and non-topological response of this system in the diffusive limit. We calculate the domain-wall resistance but also the dynamical response of the system that gives us for example the anisotropic Gilbert damping contribution mediated by the surface Dirac Fermions.

Furthermore, we will exactly solve the Dirac equation in presence of a finite size domain wall in two different wall configurations. Finally, we calculate the transport through domain walls and calculate the change in the ballistic conductance evoked by the presence of the wall. We find an interesting interference behavior that leads to characteristic oscillations in the conductance change, and it is related to the topological nature of the surface state.

In summary, the central theme of this work is the study of inhomogeneous and time-dependent magnetization structures and its interplay with two very different materials: ordinary metals and topological metals.

2. Electron Transport in Ferromagnetic Conductors with Inhomogeneous and Time-dependent Magnetic Order Parameter

2.1. Introduction

Conducting magnetic materials are an active research topic at present due to promising applications like magnetic memory storage devices which make use of magnetization reversal in pillar multilayer nanostructures [4, 5, 6, 7, 8] or domain wall motion [9, 10, 11, 12, 13] as proposed for the racetrack memory [1] or the nanowire shift register [14]. On one hand, domain wall motion is realized by sending spin-polarized current through the domain wall, so that the mutual interaction of the electron spin with the ferromagnetic order parameter leads to a motion of the wall. This is due to the so called spin-torque [15, 16, 17, 4, 18], the transfer of spin-angular momentum. A number of theoretical works exist that deal with the problem of magnetization dynamics and spin-transfer torque, or the impact of an inhomogeneous magnetization on the itinerant electrons [19, 20, 21, 22, 23, 24, 25, 26, 27, 28, 29]. Many other interesting phenomena are predicted for these systems and have been already confirmed experimentally, like the charge current induced by a moving domain wall [30] which could be utilized to read the state of a magnetic memory device [31].

On the other hand, the electronic current flow is also affected by the presence of an inhomogeneous magnetization. Most prominently, there is a change in the resistance when the current runs through a domain wall in comparison to the resistance in the absence of the domain wall. The resistance change can have different origins that can be separated into the *extrinsic* and *intrinsic* domain-wall resistance (DWR). The former includes anisotropic magneto-resistance. The latter contains the direct influence the domain wall has on the electronic conduction channels: if the magnetization direction is not homogeneous in space, the spin majority and minority channels are no longer eigenstates, which in turn changes the conduction properties and also can have influence on the impurity scattering rates. There is also spin accumulation in the vicinity of the domain wall which leads to an additional potential drop. In any case, the *extrinsic* mechanisms have to be carefully identified in order to obtain the intrinsic domain-wall resistance from experiment. The DWR has been studied in a number of works in the past, both theoretically [32, 33, 34, 35, 36, 37, 38, 39, 40] and experimentally [41, 42, 43, 44]. Reviews about DWR in nanowires made from ferromagnetic transition metals, experimental measurements and details on the treatment of extrinsic magneto resistance can be found in [45, 46].

We mentioned a large number of theoretical works that deal with the phenomena like DWR,

charge/spin-pumping or spin-torque. They all differ in the microscopic models used and the regime of validity or other approximations made like employing phenomenological scattering times. However, we use a model that treats the electrons on a quantum mechanical basis while impurity scattering is treated on a microscopic level. We will use this theoretical framework to investigate equilibrium properties and the non-equilibrium response of the system. This allows us to obtain all results within one theoretical framework and consistent approximations. We reproduce many known results but also identify new terms. Primary focus is also put on the domain wall resistance for walls in the mesoscopic regime, which has been consistently treated in this work as opposed to other works. This includes the influence of magnetization corrections to the spectrum, scattering parameters, chemical potential, and the effective exchange field. We identify different contributions for different wall geometries and identify some of their origins and the dominant contributions in certain limiting cases. We also study the influence of the amount of magnetic impurities on the domain wall resistance.

The assumption that the Fermi and exchange energy are much larger than other energies in the system will play a major role in the calculations performed in this chapter, and it applies to common ferromagnetic metals like permalloy. However, no assumption on the relative size between exchange energy and Fermi level is made and they can even be of the same order allowing us to treat the regime of strong polarization where transport and physical properties are dominated by the majority spin channel. Essentially, we restrict ourselves to the limiting case of adiabatically varying magnetization, which means that magnetization structure is smooth on the scale of the Fermi-wavelength λ_{F}. Furthermore, the length and time-scales associated with precession are assumed to be much smaller than other scales of external perturbations, relaxation processes or the magnetization texture. This allows us to derive a kinetic equation in linear response including a consistent treatment of impurities within the Boltzmann transport framework by employing a collision integral with gradient corrections included. In fact, the domain-wall resistance crucially depends on scattering and in particular, on the asymmetry of the two scattering channels which are intricately modified in presence of magnetization gradients. This gives rise to important contributions to the domain-wall resistance that have been neglected so far in other theoretical works.

We will study two models of ferromagnetism, the Stoner model of itinerant ferromagnetism where the magnetization and transport is carried by the same s-electrons. The other scenario is the s-d limit where the electrons responsible for the ferromagnetism sit in localized d-orbitals and are coupled via the exchange interaction with the itinerant s-electrons. Treating the Stoner model allows us to additionally study the effect of a local reduction in the exchange field which also strongly affects the domain-wall resistance. In particular, we will find that the Stoner limit has a stronger tendency to exhibit negative DWR. This and other influences like magnetic impurity scattering on the DWR will be studied in detail, and mechanisms for the DWR can be identified in limiting cases of weak and strong polarization of the ferromagnet. In the general case, it is difficult to isolate various sources since the DWR has contributions from s, p and d-wave components which are mixed in a complicated manner due to impurity scattering described by the collision integral. The importance of the d-wave component has been also overlooked in studies utilizing the Boltzmann transport equation. Furthermore, we will illuminate the role played by spin-flip scattering, which also has significance for the DWR since the non-equilibrium spin-accumulation that exists in the vicinity of the domain-wall requires spin-flip scattering to relax towards the equilibrium value. Spin-flip scattering has not been discussed in connection with the DWR before.

In addition to the DWR, more complex two- or three-dimensional magnetization structures can exhibit a transverse current similar to the Hall effect. This behavior is studied explicitly in the case of a vortex domain wall in thin nanowires.

Within our theoretical description, it is also possible to treat time-dependent magnetization and we discuss the charge and spin-pumping effects due to time-dependent magnetization. The spin-currents will exert a spin-torque on the magnetization which is studied in 2.5. There, we will identify all contributions to the spin-torque that appear up to order $\partial_t \boldsymbol{\partial}_r^2 \vec{m}$ and $\boldsymbol{E}\boldsymbol{\partial}_r \vec{m}$ ($\boldsymbol{E}$ is the external electric field) and obtain known expressions for the Gilbert damping constant α and the non-adiabatic coefficient β. Furthermore, we obtain non-local damping terms and various non-local corrections to the other adiabatic and non-adiabatic terms. These terms will be relevant for short walls where magnetization gradients give important corrections. We will compare our results to other theories available and discuss the differences.

2.2. Quantum Transport Equation for Ferromagnetic Conductors

In this section, we will derive a quantum transport equation from a model Hamiltonian that describes the kinetics of conduction electrons in ferromagnetic materials with inhomogeneous magnetization profile. We use a non-equilibrium approach in order to treat the influence of an external electric field, and the description includes time-dependent phenomena as well. The resulting quantum kinetic equation will serve as a basis for all subsequent sections.

2.2.1. Model and Hamiltonian

The single particle Hamiltonian for the system of non-interacting electronic quasi-particle excitations, coupled to the ferromagnetic order parameter, reads

$$\begin{aligned} \hat{\mathcal{H}} &= \hat{H} - e\varphi(\boldsymbol{r})\hat{1} + \hat{\mathcal{V}}_{\text{imp}} \\ &= \left(\epsilon_{\boldsymbol{k}} - \delta\mu(\boldsymbol{r},t) - e\varphi(\boldsymbol{r})\right)\hat{1} - \frac{\Delta - \delta\Delta(\boldsymbol{r},t)}{2}\vec{m}(\boldsymbol{r},t)\hat{\vec{\sigma}} + \hat{\mathcal{V}}_{\text{imp}} \ . \end{aligned} \tag{2.1}$$

The convention in this chapter is that vectors in spin space are denoted by an arrow while vector quantities in real-space are printed boldface. The first term is the spin-independent part of the Hamiltonian and $\epsilon_{\boldsymbol{k}}$ is the usual parabolic approximation for the energy of the quasi-particles with the dispersion relation $\epsilon_{\boldsymbol{k}} \equiv \frac{\hbar^2 \boldsymbol{k}^2}{2m_{\text{e}}}$, effective mass m_{e} and $\boldsymbol{k} = -i\boldsymbol{\nabla}_{\boldsymbol{r}}$. Further contributions in our model are the external electric potential $\varphi(\boldsymbol{r})$ felt by the quasi-particles of charge $-e$, while $\delta\mu$ constitutes the additional screening potential in the presence of a magnetization gradient $\boldsymbol{\partial}_r \vec{m}$, which later turns out to be of order $\delta\mu = O(\boldsymbol{\partial}_r \vec{m})^2$ and is determined in section 2.2.5 by enforcing local charge neutrality.

In a mean-field approximation, the second term describes the coupling of the electron spin to the exchange field, the latter consisting of constant magnitude Δ, and the time and space dependent local magnetization direction denoted by the unit vector $\vec{m}(\boldsymbol{r},t)$. It turns out that in the presence of a magnetization gradient, the magnitude is reduced by $\delta\Delta = O(\boldsymbol{\partial}_r \vec{m})^2$ due to the hybridization between non-collinear spin-states [47]. The 2×2 matrix spin structure is denoted by $\hat{}$ and $\hat{\vec{\sigma}} = (\hat{\sigma}_1, \hat{\sigma}_2, \hat{\sigma}_3)$ is the vector of Pauli matrices, such that the electron spin operator is given by $\hat{\boldsymbol{S}} = \frac{\hbar}{2}\hat{\vec{\sigma}}$. The unit matrix in that space is denoted as $\hat{1}$.

In accordance with the mean-field approach, the variations in time and space are taken to be much larger than the relevant atomic scales. More specifically, the conditions for the smoothness of the exchange field $\vec{m}$ read

$$\begin{aligned} |\boldsymbol{\partial}_r \vec{m}| &\ll k_\mathrm{F} \ , \\ \hbar|\partial_t \vec{m}| &\ll E_\mathrm{F} \ , \end{aligned} \tag{2.2}$$

where k_F is the Fermi wave-vector and E_F denotes the Fermi-energy in the system. The exchange field is created by electrons that align their spin preferably in the same direction due to the (here ferromagnetic) exchange interaction. In conducting ferromagnets, the electrons contributing to the local magnetization can either be localized and, thus, do not participate in transport (d-electron character) or delocalized and, hence, are subject to electronic transport phenomena (dominant s-electron character). These extreme cases constitute two distinct models with the major difference being the way in which the self-consistency condition for the exchange-field is employed and which is explained in section 2.2.5. These two limiting cases are known as s-d model and *itinerant* Stoner model, the latter one describing a system in which transport and magnetism arise in fact both from the same delocalized electrons. However, in real physical systems, one always deals with something in between, but usually one orbital character dominates, so it is interesting to look at these two limiting cases. Furthermore, fluctuations in the order parameter (e.g. due to temperature), are neglected.

Finally, the impurity scattering potential has two contributions,

$$\hat{\mathcal{V}}_\mathrm{imp} = V_\mathrm{i}\hat{1} + \hat{V}_\mathrm{mag} \ . \tag{2.3}$$

V_i describes scattering from randomly distributed impurities which, for point-like scatterers, has the property

$$\langle V_\mathrm{i}(\boldsymbol{r}) V_\mathrm{i}(\boldsymbol{r'})\rangle_\mathrm{imp} = \chi^{(i)}\delta(\boldsymbol{r}-\boldsymbol{r'}) \ , \tag{2.4}$$

equivalent to the treatment of V_i as a delta-correlated fluctuating Gaussian field. $\chi^{(i)}$ is the strength of the impurity scattering potential and $\langle\rangle_\mathrm{imp}$ denotes the averaging over all impurity configurations.

In a similar way, scattering at impurities that have internal spin-degrees of freedom makes the scattering vertex spin-dependent, such that

$$\langle \hat{V}_\mathrm{mag}(\boldsymbol{r})\hat{X}\hat{V}_\mathrm{mag}(\boldsymbol{r'})\rangle_\mathrm{imp} = \sum_{i,j=1}^{3} \chi_{ij}^{(m)} \hat{\sigma}_i \hat{X} \hat{\sigma}_j \delta(\boldsymbol{r}-\boldsymbol{r'}) \ , \tag{2.5}$$

where $\hat{X}$ is an arbitrary disorder independent spin-matrix. Therefore, magnetic impurity scattering in the point-like limit can be treated as delta-correlated fluctuating Gaussian magnetic field which couples to the electron spin by the usual Zeeman term. The size of these spatial fluctuations can generally be spin-anisotropic, which manifests itself in the tensor structure of $\chi_{ij}^{(m)}$.

Usually, in the ferromagnetic conductors under investigation, there is also the presence spin-orbit coupling which leads to effects like the anisotropic magneto-resistance (AMR) or the anomalous Hall effect (AHE) [48, 49]. The AMR leads to a resistance depending on the angle between magnetization and current direction and the AHE leads to a finite transverse Hall

conductivity in ferromagnetic materials, but in absence of an external magnetic field. Instead, it is due to the interplay of the ferromagnetic exchange field and the spin-orbit interaction.

Spin-orbit effects like AMR or AHE are effects of zeroth order in magnetization gradients, but here, we are primarily interested in the effects like change in conductivity imposed by the presence of magnetization textures. To leading order in magnetization gradients, they are simply additive, while in higher order, the effects of a magnetization gradient and the spin-orbit mechanism underlying the AMR interfere and a more general description is necessary. Note that in addition, the anomalous Hall effect (AHE) comes into play in higher order. In following, we focus on the effects which are due to time-dependence and spatial inhomogeneity in the magnetization $\vec{m}(\boldsymbol{r}, t)$, and note that we can either neglect AMR and AHE effects, or they can be simply added to the contributions of the present study or distinguished experimentally.

2.2.2. Keldysh Technique

The standard way to proceed in non-equilibrium many-particle physics is to set up the kinetic equation for the Keldysh Greens function. For the remaining part of this chapter, we set $\hbar = 1$ and only restore it in the final results.

The further treatment is done in the Wigner representation which is obtained from usual spatio-temporal representation via the transformation

$$\check{G}(\boldsymbol{k}, \epsilon, \boldsymbol{r}, t) = \int \mathrm{d}^3 z \int \mathrm{d}\tau \; e^{-i\boldsymbol{k}\boldsymbol{z} + i\epsilon\tau} \check{G}(\boldsymbol{r} + \frac{\boldsymbol{z}}{2}, t + \frac{\tau}{2}; \boldsymbol{r} - \frac{\boldsymbol{z}}{2}, t - \frac{\tau}{2}) \; , \tag{2.6}$$

where now, operator multiplication has to be carried out by applying the Moyal product $*$. Explicitly, this product is defined as

$$C(\boldsymbol{k}, \epsilon, \boldsymbol{r}, t) = A(\boldsymbol{k}, \epsilon, \boldsymbol{r}, t) * B(\boldsymbol{k}, \epsilon, \boldsymbol{r}, t) \equiv A(\boldsymbol{k}, \epsilon, \boldsymbol{r}, t) \; e^{\frac{i}{2}(\overleftarrow{\partial_{\boldsymbol{r}}}\overrightarrow{\partial_{\boldsymbol{k}}} - \overleftarrow{\partial_t}\overrightarrow{\partial_\epsilon} - \overleftarrow{\partial_{\boldsymbol{k}}}\overrightarrow{\partial_{\boldsymbol{r}}} + \overleftarrow{\partial_\epsilon}\overrightarrow{\partial_t})} \; B(\boldsymbol{k}, \epsilon, \boldsymbol{r}, t) \; , \tag{2.7}$$

where $\overleftarrow{\partial}$ and $\overrightarrow{\partial}$ denote derivatives acting only to the left and right, respectively. The transformation (2.6) introduces center of mass coordinates $\boldsymbol{r}$, t and Fourier transformed relative coordinates that are, respectively, $\boldsymbol{k}$ and ϵ. For a short summary of useful properties of the Wigner transformation, see Appendix A.

The Greens function $\check{G}$ is defined as expectation value of the field operators, time ordered along the Keldysh contour [50]. The ordering along back and forward time Keldysh contour gives rise to an additional 2×2 matrix structure (denoted by $\check{}$) which in an appropriate basis takes the convenient form [51]

$$\check{G} = \begin{pmatrix} \hat{G}^{\mathrm{R}} & \hat{G}^{<} \\ 0 & \hat{G}^{\mathrm{A}} \end{pmatrix} \; . \tag{2.8}$$

$\hat{G}^{\mathrm{R}}$ and $\hat{G}^{\mathrm{A}}$ are the retarded and advanced Greens functions, well known from equilibrium theory and carry information about the spectrum of the system, in particular, one obtains the spectral density simply from

$$\hat{A} = i(\hat{G}^{\mathrm{R}} - \hat{G}^{\mathrm{A}}) = -2\mathrm{Im}\, \hat{G}^{\mathrm{R}} \; , \tag{2.9}$$

which generally obeys the normalization condition

$$\int_{-\infty}^{\infty} \frac{\mathrm{d}\epsilon}{2\pi}\ \hat{A}(\boldsymbol{k},\epsilon,\boldsymbol{r},t) = \hat{1}\ .$$

The lesser component $\hat{G}^{<}(\boldsymbol{k},\epsilon,\boldsymbol{r},t)$ describes the occupation of states of the many particle system and is given in terms of electron field operators by

$$\hat{G}^{<}_{\alpha,\beta}(\boldsymbol{r},\boldsymbol{r}',\boldsymbol{t},\boldsymbol{t}') = i\left\langle \psi^{\dagger}_{\beta}(\boldsymbol{r}',\boldsymbol{t}')\psi_{\alpha}(\boldsymbol{r},\boldsymbol{t})\right\rangle\ , \tag{2.10}$$

where the grand canonical average is taken and the indices α,β are one of $\uparrow,\downarrow$. In equilibrium, it takes the form

$$\hat{G}^{<}(\boldsymbol{k},\epsilon,\boldsymbol{r}) = i\hat{A}(\boldsymbol{k},\epsilon,\boldsymbol{r})f_{\mathrm{D}}(\epsilon) \tag{2.11}$$

with the Fermi-Dirac distribution function

$$f_{\mathrm{D}}(\epsilon) = \frac{1}{e^{\beta(\epsilon-E_{\mathrm{F}})}+1}\ ,$$

where $\beta = 1/k_{\mathrm{B}}T$ denotes the inverse temperature.

With the knowledge of $\hat{G}^{<}$ at hand, one can easily obtain various physical quantities of interest such as the quasi-particle spin-charge density

$$\hat{N}(\boldsymbol{r},t) = \int \frac{\mathrm{d}^3k}{(2\pi)^3}\int_{-\infty}^{\infty}\frac{\mathrm{d}\epsilon}{2\pi i}\ \hat{G}^{<}(\boldsymbol{k},\epsilon,\boldsymbol{r},t)\ , \tag{2.12}$$

and spin-charge current density

$$\hat{\boldsymbol{J}}(\boldsymbol{r},t) = \int \frac{\mathrm{d}^3k}{(2\pi)^3}\int_{-\infty}^{\infty}\frac{\mathrm{d}\epsilon}{2\pi i}\ \boldsymbol{v}_k\hat{G}^{<}(\boldsymbol{k},\epsilon,\boldsymbol{r},t)\ , \tag{2.13}$$

with the quasi-particle group velocity given by $\boldsymbol{v}_k = \boldsymbol{\partial}_k\epsilon_{\boldsymbol{k}} = \boldsymbol{k}/m$.

The spin-charge density $\hat{N}$ is a 2×2 matrix in spin space and its trace yields the charge-density $N_c = -e\mathrm{Tr}\hat{N}$, while the spin-density is given by $\boldsymbol{S} = \frac{\hbar}{2}\mathrm{Tr}(\hat{\vec{\sigma}}\hat{N})$. In a similar manner, we obtain the charge current $\boldsymbol{j}_c = -e\mathrm{Tr}\,\hat{\boldsymbol{J}}$ and the spin-k current $\boldsymbol{j}_k = \frac{\hbar}{2}\mathrm{Tr}(\hat{\sigma}_k\hat{\boldsymbol{J}})$.

In order to find $\check{G}$ for our specific physical system, we need an equation of motion, called the Dyson equation

$$\begin{aligned}\left[((\epsilon+e\varphi(\boldsymbol{r}))\hat{1}-\hat{H})\ \check{1}-\check{\Sigma}\right]*\check{G} &= \check{1}\ ,\\ \check{G}*\left[((\epsilon+e\varphi(\boldsymbol{r}))\hat{1}-\hat{H})\ \check{1}-\check{\Sigma}\right] &= \check{1}\ ,\end{aligned} \tag{2.14}$$

where $\check{1}$ is the unit matrix in spin and Keldysh space.

Impurity scattering due to $\hat{\mathcal{V}}_{\mathrm{imp}}$ is described in terms of the self-energy $\hat{\Sigma}$, and is to be discussed in a moment. In Keldysh space, $\hat{\Sigma}$ possesses the same structure as the Greens function $\check{G}$,

$$\check{\Sigma} = \begin{pmatrix}\hat{\Sigma}^{\mathrm{R}} & \hat{\Sigma}^{<}\\ 0 & \hat{\Sigma}^{\mathrm{A}}\end{pmatrix}\ . \tag{2.15}$$

We assume throughout the rest of this article that scattering is weak such that

$$\Sigma \ll E_{\mathrm{F}} \ , \tag{2.16}$$

where E_{F} is the Fermi-level for the conduction electrons, and which will allow us later to take advantage of the quasi-particle approximation.

Spectral Density

First, we have a look at equilibrium properties of the system by calculating the retarded Greens function, from which we readily obtain the spectral density $\hat{A}$ using Eq. (2.9). Essentially, we do this by first solving for the retarded Greens function and taking the imaginary part thereafter. The starting point is the Dyson equation for the Greens function and taking the retarded component of (2.14), we explicitly obtain

$$\left([\epsilon - \epsilon_{\boldsymbol{k}} + \delta\mu(\boldsymbol{r},t)]\,\hat{1} + \frac{\Delta - \delta\Delta}{2}\vec{m}(\boldsymbol{r},t)\hat{\vec{\sigma}} \right) * \hat{G}^{\mathrm{R/A}} = \hat{1} \ . \tag{2.17}$$

$\hat{G}^{\mathrm{R/A}}$ only differs by the boundary condition which can be simply incorporated by substituting $\epsilon \to \epsilon \pm i0^+$ in Eq. (2.17). Furthermore, since $\Sigma \ll E_{\mathrm{F}}$, we will not include self-energy corrections to the spectrum, i.e. we neglect the line broadening and assume a delta-peaked spectrum, commonly referred to as quasi-particle approximation. Also, the external electric field affects the spectrum only in second order of the field [51].

To proceed, we expand the Moyal product

$$* \approx 1 + \frac{i}{2}(\overleftarrow{\partial_{\boldsymbol{r}}}\overrightarrow{\partial_{\boldsymbol{k}}} - \overleftarrow{\partial_t}\overrightarrow{\partial_\epsilon} - \overleftarrow{\partial_{\boldsymbol{k}}}\overrightarrow{\partial_{\boldsymbol{r}}} + \overleftarrow{\partial_\epsilon}\overrightarrow{\partial_t}) + \dots \ , \tag{2.18}$$

commonly referred to as gradient expansion, and iteratively determine $\hat{G}^{\mathrm{R/A}}$ in orders of gradients, whereas, for our purpose, we need only up to order $\boldsymbol{\partial}_r^2$. The zeroth order term of the spectral density $\hat{A} = \hat{A}_0 + \hat{A}_1 + \dots$ is readily found to be

$$\hat{A}_0 = 2\pi \left[\hat{P}_\uparrow \delta(\epsilon - \epsilon_{\boldsymbol{k}}^\uparrow) + \hat{P}_\downarrow \delta(\epsilon - \epsilon_{\boldsymbol{k}}^\downarrow) \right] \ , \tag{2.19}$$

and for higher order terms we refer to Eq. (D.3) in the Appendix. Here, we defined the projectors in spin-space $\hat{\mathcal{P}}_{\uparrow,\downarrow} = \frac{1}{2}(\hat{1} \pm \vec{m}\hat{\vec{\sigma}})$ that project on the local spin up/down direction, and $\epsilon_{\boldsymbol{k}}^{\uparrow,\downarrow} \equiv \epsilon_{\boldsymbol{k}} \mp \frac{\Delta}{2}$ is the dispersion relation for majority and minority spin bands (see Fig. 2.1).

The $\boldsymbol{k}$-integration of the spectral function yields the density of states, here defined as number of states per unit energy and volume,

$$\int \frac{\mathrm{d}^3k}{(2\pi)^3}\ \hat{A}(\boldsymbol{k},\epsilon,\boldsymbol{r},t) = 2\pi\hat{\nu}(\epsilon,\boldsymbol{r},t) \ . \tag{2.20}$$

The matrix density of states in zeroth order correction or without magnetization gradient present is due to $\hat{A}_0$,

$$\hat{\nu}_0 = \hat{\mathcal{P}}_\uparrow \nu_\uparrow + \hat{\mathcal{P}}_\downarrow \nu_\downarrow = \nu_0(\hat{1} + P\ \vec{m}(\boldsymbol{r},t)\hat{\vec{\sigma}}) \ , \tag{2.21}$$

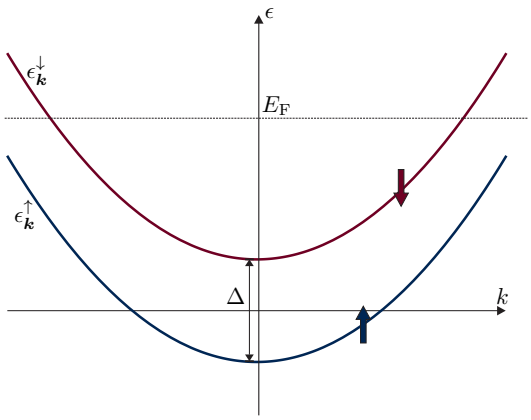

Figure 2.1.: The parabolic band structure for the spin-up and down bands is split by the ferromagnetic exchange field Δ. The Fermi level E_{F} is measured with respect to the mid-point of the two band-edges.

where we have introduced the polarization of the Fermi surface

$$P = \frac{\nu_\uparrow - \nu_\downarrow}{\nu_\uparrow + \nu_\downarrow} \,, \tag{2.22}$$

and $\nu_0 = \frac{1}{2}(\nu_\uparrow + \nu_\downarrow)$ denotes the average density of states. The density of states for majority and minority spin bands are

$$\nu_{\uparrow,\downarrow}(\epsilon) = \int \frac{\mathrm{d}^3 k}{(2\pi)^3} \, \delta(\epsilon - \epsilon_{\boldsymbol{k}}^{\uparrow,\downarrow}) \,. \tag{2.23}$$

$\nu_{\uparrow,\downarrow}$ without energy argument denotes the density of states at the Fermi-level E_{F}. For smooth $\vec{m}(\boldsymbol{r}, t)$, the density of states adiabatically follows the variations of the magnetization, and higher order terms $\hat{A}_1$, $\hat{A}_2$, ... constitute corrections due to non-adiabaticities.

The polarization parameter at the Fermi level explicitly reads

$$P(\Delta, E_{\mathrm{F}}) = \frac{\Delta}{2E_{\mathrm{F}} + \sqrt{4E_{\mathrm{F}}^2 - \Delta^2}} \,, \tag{2.24}$$

and, in place of Δ will be used as a fundamental parameter in the subsequent investigations. For $\Delta \to 0$, the polarization vanishes, and in the opposite limiting case when $\Delta \to 2E_{\mathrm{F}}$, the Fermi-level reaches the band edge of the spin-down band and the system is fully polarized, i.e. the half-metallic regime with $P = 1$. E_{F} is measured with respect to the mid-point between the two band-edges (zero on the energy axis). The situation is depicted in Figure 2.1.

2.2.3. Impurity Scattering

The self-energy $\hat{\Sigma}$ incorporates scattering by magnetic and non-magnetic impurities, commonly calculated in the self-consistent Born approximation which truncates the series of irreducible diagrams due to multiple scattering after the first one:

$$\check{\Sigma} = \quad = \langle \hat{\mathcal{V}} \check{G} \hat{\mathcal{V}} \rangle_{\rm imp} \ .$$

In physical terms, this means that all kinds of interference effects like weak localization are dropped from the theory. In this approximation, the self-energy for spin-independent impurity scattering takes the form

$$\check{\Sigma}_{\rm i} \ = \ \chi^{(i)} \int \frac{{\rm d}^3 k}{(2\pi)^3} \ \check{G} \ , \tag{2.25}$$

and likewise for magnetic impurity scattering,

$$\check{\Sigma}_{\rm mag} \ = \ \sum_{i,j=1}^{3} \chi^{(m)}_{ij} \int \frac{{\rm d}^3 k}{(2\pi)^3} \ \hat{\sigma}_i \check{G} \hat{\sigma}_j \ . \tag{2.26}$$

The tensorial structure of $\underline{\chi}^{(m)}$ accounts for situations in which scattering is non-isotropic in spin space. We note that the impurity concentration has been incorporated into $\chi^{(i)}$ and $\underline{\chi}^{(m)}$, which then simply scales linearly with the density of impurities. We can rewrite the magnetic self-energy using simple algebra and the properties of the Pauli matrices

$$\begin{aligned} \sum_{i,j=1}^{3} \chi^{(m)}_{ij} \hat{\sigma}_i \hat{G} \hat{\sigma}_j \ &= \ \sum_{ij} \chi^{(m)}_{ij} \hat{\sigma}_i (g_0 \hat{1} + \vec{g} \hat{\vec{\sigma}}) \hat{\sigma}_j \\ &= \ \hat{G} \ {\rm tr} \underline{\chi}^{(m)} - 2{\rm Tr}\{\hat{\vec{\sigma}} \hat{G}\} \left(\underline{\underline{1}} {\rm tr} \underline{\chi}^{(m)} - \underline{\chi}^{(m)} \right) \hat{\vec{\sigma}} \ , \end{aligned}$$

where Tr takes the trace over the spin degrees of freedom, while ${\rm tr}\underline{\chi}^{(m)} = \sum_{i=1}^{3} \chi^{(m)}_{ii}$.

The explicit structure of $\underline{\chi}^{(m)}$ to be used throughout this chapter is motivated in the following. If there exists a ferromagnetic exchange coupling between the internal impurity spin and the ferromagnetic order parameter, the spin is preferably aligned along this direction. Consequently, the impurity will scatter the electron with a different magnitude depending on its spin. In the case of uniaxial symmetry (the symmetry axis is denoted by $\vec{n}$),

$$\chi^{(m)}_{ij} = \chi^{(m)}_{\perp} (\delta_{ij} - n_i n_j) + \chi^{(m)}_{\parallel} n_i n_j \ .$$

For the above example of ferromagnetic interaction between impurity spins and order parameter, the unit vector $\vec{n}$ actually corresponds to the local magnetization direction, $\vec{m} = \vec{n}$. In the Born approximation and restricting ourselves to this special case of uniaxial symmetry, the self-energy for both spin-isotropic and magnetic impurity scattering is written in the compact notation

$$\check{\Sigma} = \check{\Sigma}_{\rm i} + \check{\Sigma}_{\rm mag} = \int \frac{{\rm d}^3 k}{(2\pi)^3} \ \hat{\underline{\chi}} \check{G} \ , \tag{2.27}$$

where the operation $\hat{\underline{\chi}}$ on a general spin-matrix $\hat{X}$ is defined as

$$\hat{\underline{\chi}} \hat{X} = (\chi^{(i)} + {\rm tr} \underline{\chi}^{(m)}) \left(\hat{X} - \frac{\tau}{T_2} \vec{x}_{\perp} \hat{\vec{\sigma}} - \frac{\tau}{T_1} x_{\parallel} \vec{m} \hat{\vec{\sigma}} \right) = \frac{1}{2\pi\nu_0} \left(\frac{\hat{X}}{\tau} - \frac{\vec{x}_{\perp} \hat{\vec{\sigma}}}{T_2} - \frac{x_{\parallel} \vec{m} \hat{\vec{\sigma}}}{T_1} \right) \ , \tag{2.28}$$

where we write for the longitudinal component $\vec{x}_{\parallel} = \frac{1}{2} {\rm Tr}\{\vec{m} \hat{\vec{\sigma}} \hat{X}\} \vec{m}$, the transverse spin part $\vec{x}_{\perp} = \frac{1}{2} {\rm Tr}\{\hat{\vec{\sigma}} \hat{X}\} - x_{\parallel} \vec{m}$ and the charge component $x_{\rm c} = {\rm Tr} \hat{X}$. Furthermore, we define the spin-$\uparrow$ and $\downarrow$ channels as $x_{\uparrow,\downarrow} = \frac{1}{2} x_c \pm x_{\parallel}$.

Our model of impurities introduces various types of relaxation which are summarized in the table below along with the explicit expressions in terms of the parameters of our model.

Momentum relaxation in Spin-↑,↓ channel	$1/\tau_{\uparrow,\downarrow}$	$= 2\pi\chi^{(i)}\nu_{\pm} + 2\pi(\chi_{\parallel}^{(m)}\nu_{\pm} + 2\chi_{\perp}^{(m)}\nu_{\mp})$
Transverse momentum relaxation	$1/\tau$	$= 2\pi\nu_0(\chi^{(i)} + \mathrm{tr}\underline{\underline{\chi}}^{(m)})$
Longitudinal, spin-flip	$1/T_1$	$= 4\pi\nu_0\ 2\chi_{\perp}^{(m)}$
Transverse, spin-dephasing	$1/T_2$	$= 4\pi\nu_0\,(\chi_{\parallel}^{(m)} + \chi_{\perp}^{(m)})$

Transverse spin excitations are also subject to momentum relaxation, albeit with the elastic mean-free time τ which is different from the elastic mean-free time $\tau_{\uparrow,\downarrow}$ in the spin-↑,↓ conduction channels. The longitudinal, or spin-flip relaxation time T_1 describes the time it takes for a non-equilibrium magnetization in the direction of $\vec{m}$ to relax to its equilibrium value. The transverse, or spin-dephasing time T_2 describes the decay of transverse spin-excitations. Mathematically, this behavior is already evident from the specific form of the self energy which is essentially given by (2.28). We will see this more explicitly later, when we derive the extended Bloch equation (2.121) along with the scattering term (2.129).

Our specific model of impurity scattering has three independent parameters $\chi^{(i)}$, $\chi_{\perp}^{(m)}$ and $\chi_{\parallel}^{(m)}$, therefore, we take τ, T_1 and T_2 as independent parameters of our system. Then the momentum relaxation time, or the elastic mean-free time for the spin-up and down conduction channels can be expressed as

$$\frac{1}{\tau_{\uparrow,\downarrow}} = \frac{1 \pm P\gamma}{\tau} \ , \tag{2.29}$$

where we defined the scattering asymmetry $\gamma \equiv (1 - \frac{\tau}{T_1})$ and we see that $\frac{2}{\tau} = \frac{1}{\tau_\uparrow} + \frac{1}{\tau_\downarrow}$, even though γ is not an independent parameter in our model.

Before continuing, let us inspect the range of possible values for our parameters. First, τ is dominated by $\chi^{(i)}$ when magnetic scattering is weak, and essentially can be chosen arbitrarily. T_1 and T_2 are of course not affected by non-magnetic impurities, and from their explicit expression, we see that the spin-flip time T_1 is only affected by the transverse fluctuating field $\chi_{\parallel}^{(m)}$, while for the spin-dephasing time T_2, both components $\chi_{\parallel}^{(m)}$ and $\chi_{\perp}^{(m)}$ contribute equally. For the spin-isotropic situation $\chi_{\parallel}^{(m)} = \chi_{\perp}^{(m)}$, both times are equal $T_1 = T_2$, and for a vanishing perpendicular component, we have of course $T_1 = \infty$. On the other side, a vanishing longitudinal fluctuating field $\chi_{\parallel}^{(m)} = 0$ leads to $T_1 = T_2/2$, so that in general, one has the condition

$$2T_1 \geq T_2 \ , \tag{2.30}$$

which is a well known inequality in the field of nuclear spin dynamics [52]. In addition, non-magnetic impurities always contribute to momentum relaxation, so one is not free in the choice of τ with respect to T_2 und usually, non-magnetic scatterers are dominant, so that $\tau < T_2$. Even in the best case scenario $\chi^{(i)} = 0$, the momentum relaxation time τ ranges from T_2 to $2T_2$, so in order to cover all situations, we keep $\tau \leq T_2, T_1$.

2.2.4. Kinetic Equation in Linear Response

In the following, we derive a transport equation for the low energy dynamics including gradient corrections to the collision integral and to first order in external perturbations, i.e. in linear response. This kinetic equation will be the foundation of our subsequent investigations, and we will use it to study different aspects involving various magnetization structures. We need to use the full non-equilibrium apparatus, since we have in mind to also study time-dependent phenomena.

Full quantum kinetic equation

To obtain a kinetic equation for the non-equilibrium distribution function [50], we subtract the left- and right-conjugated Dyson equations (2.14),

$$\Big[((\epsilon + e\varphi(\boldsymbol{r}))\hat{1} - \hat{H})\ \check{1} - \check{\Sigma}\ \overset{*}{,}\ \check{G}\Big] = 0 \tag{2.31}$$

and write down the equation for the lesser component $\hat{G}^{<}(\boldsymbol{k}, \omega, \boldsymbol{r}, t)$

$$\begin{aligned} -i\left[(\epsilon - \epsilon_{\boldsymbol{k}} + \delta\mu + e\varphi)\hat{1} + \frac{\Delta - \delta\Delta}{2}\vec{m}\hat{\vec{\sigma}}\ \overset{*}{,}\ \hat{G}^{<}\right] \\ = \frac{1}{2}\left\{\hat{A}\ \overset{*}{,}\ \hat{\Sigma}^{<}\right\} - \frac{1}{2}\left\{\hat{\Gamma}\ \overset{*}{,}\ \hat{G}^{<}\right\} - i\left[\mathrm{Re}\,\hat{\Sigma}^{\mathrm{R}}\ \overset{*}{,}\ \hat{G}^{<}\right] + i\left[\mathrm{Re}\,\hat{G}^{\mathrm{R}}\ \overset{*}{,}\ \hat{\Sigma}^{<}\right] . \end{aligned} \tag{2.32}$$

The (anti-)commutators are defined by $\{\hat{A}\ \overset{*}{,}\ \hat{B}\} = \hat{A} * \hat{B} + \hat{B} * \hat{A}$ and $[\hat{A}\ \overset{*}{,}\ \hat{B}] = \hat{A} * \hat{B} - \hat{B} * \hat{A}$.

Taking a suitable combination of the retarded and advanced components of (2.31), a similar equation can be found for the spectral density $\hat{A}(\boldsymbol{k}, \omega, \boldsymbol{r}, t)$,

$$-i\left[(\epsilon - \epsilon_{\boldsymbol{k}} + \delta\mu + e\varphi)\hat{1} + \frac{\Delta - \delta\Delta}{2}\vec{m}\hat{\vec{\sigma}} - \mathrm{Re}\,\hat{\Sigma}\ \overset{*}{,}\ \hat{A}\right] - i\left[\hat{\Gamma}\ \overset{*}{,}\ \mathrm{Re}\,\hat{G}\right] = 0\ . \tag{2.33}$$

Between the spectral density $\hat{A}$ and $\mathrm{Re}\,\hat{G}^{\mathrm{R}}$, there exists a Kramers-Kronig relation,

$$\mathrm{Re}\,\hat{G}^{\mathrm{R}}(\epsilon) = \frac{1}{2}(\hat{G}^{\mathrm{R}} + \hat{G}^{\mathrm{A}}) = \frac{1}{2\pi}\mathcal{P}\int_{-\infty}^{\infty} \mathrm{d}\epsilon'\ \frac{\hat{A}(\epsilon')}{\epsilon - \epsilon'}\ , \tag{2.34}$$

where $\mathcal{P}$ denotes the principal value of the integral. The imaginary part of the self-energy

$$\hat{\Gamma} = -2\mathrm{Im}\,\hat{\Sigma}^{\mathrm{R}} = i(\hat{\Sigma}^{\mathrm{R}} - \hat{\Sigma}^{\mathrm{A}}) \tag{2.35}$$

describes relaxation due to impurity scattering, while the real part is responsible for changes in the dispersion relation for the quasi-particle excitations. Likewise, there exists a Kramers-Kronig relation between real and imaginary parts of the self-energy

$$\mathrm{Re}\,\hat{\Sigma}^{\mathrm{R}}(\epsilon) = \frac{1}{2}(\hat{\Sigma}^{\mathrm{R}} + \hat{\Sigma}^{\mathrm{A}}) = \frac{1}{2\pi}\mathcal{P}\int_{-\infty}^{\infty} \mathrm{d}\epsilon'\ \frac{\hat{\Gamma}(\epsilon')}{\epsilon - \epsilon'}\ . \tag{2.36}$$

However, as can be seen from the integral representation in this formula, the real part depends on the complete electronic spectrum of the system, since the scattering rate is directly related

to the density of states, $\hat{\Gamma}(\epsilon) = 2\pi\underline{\hat{\chi}}\hat{\nu}(\epsilon)$ according to (2.20) and (2.27). Considering that the dynamics accompanied by a rotation of the magnetization direction, be it in time or space, is affecting only an energy region of the order of Δ, these changes constitute only a tiny fraction of the whole energy range. Thus, corrections due to magnetization dynamics to the real part can be neglected when compared to the whole background contribution, which then is just a constant (however formally diverging due to the assumption of $\boldsymbol{k}$-independent impurity scattering) and merely renormalizes the electronic spectrum. In fact, the only reason to include impurity scattering is to add momentum and spin relaxation to the conduction electron system, as contained in the imaginary part of the self-energy, $\hat{\Gamma}$. The real part can however become significant if one goes beyond the self-consistent Born approximation. Important contributions from higher order diagrams are relevant for skew and side-jump scattering which give rise to the anomalous Hall effect [48, 49]. In our case, we assume that scattering is weak and thus, there is no necessity to go beyond the first order diagram for our study. Therefore, the two commutators involving real parts can be dropped from equation (2.32).

Kinetic equation for the low-energy dynamics

Generally, we can distinguish the contributions appearing in the kinetic equation as emerging from two regions in energy. The electronic states deep inside the Fermi sea are affected by an inhomogeneous exchange splitting $\Delta\vec{m}(\boldsymbol{r})$. The fraction of the Fermi sea that contributes is given by Δ/E_{F} and not necessarily small. However, due to the Pauli principle, these states are fully occupied for all reasonable temperatures and the change in the spectrum does not affect the dynamics of the mobile electrons close to the Fermi surface. These are responsible for the dynamics in the quantum kinetic equation, since the electrons in an energy window given by the temperature, voltage or other low-energy scales have the freedom to move. These differences can be used to eliminate the high-energy contribution from our quantum kinetic equation. Possible high-energy contribution can be simply added later, once the low-energy result has been obtained. Essentially, the high-energy contributions can be interpreted in terms of Berry phases, which is treated in depth in chapter 3. Furthermore, a change in the spectrum due to magnetization structures modifies the Berry curvature, which therefore can affect the intrinsic AHE contribution. The AHE however, is beyond the scope of this work as discussed previously. To conclude, it is therefore important to carefully check for contributions from the Fermi sea and it is in particular important for the investigations in sections 2.4 and 2.5, where we calculate non-diagonal resistivities for 2 or 3-dimensional magnetization structures, for example.

As a reference, let us summarize the present version of our kinetic equations we are going to work with. Dropping the terms involving real parts, the Eq. (2.32) for $\hat{G}^{<}(\boldsymbol{k},\omega,\boldsymbol{r},t)$ becomes

$$-i\left[(\epsilon-\epsilon_{\boldsymbol{k}}+\delta\mu+e\varphi)\hat{1}+\frac{\Delta-\delta\Delta}{2}\vec{m}\vec{\hat{\sigma}}\overset{*}{,}\hat{G}^{<}\right] \;=\; \hat{\mathcal{I}}_{\epsilon}[\hat{G}^{<}]\;. \tag{2.37}$$

The right-hand side of this equation is the collision integral $\hat{\mathcal{I}}_{\epsilon}$, and takes the explicit form

$$\hat{\mathcal{I}}_{\epsilon}[\hat{G}]=\int\frac{\mathrm{d}^3k'}{(2\pi)^3}\left[\frac{1}{2}\left\{\underline{\hat{\chi}}\hat{G}(\boldsymbol{k}',\epsilon,\boldsymbol{r},t)\overset{*}{,}\hat{A}(\boldsymbol{k},\epsilon,\boldsymbol{r},t)\right\}-\frac{1}{2}\left\{\underline{\hat{\chi}}\hat{A}(\boldsymbol{k}',\epsilon,\boldsymbol{r},t)\overset{*}{,}\hat{G}(\boldsymbol{k},\epsilon,\boldsymbol{r},t)\right\}\right]\;, \tag{2.38}$$

where the operation $\underline{\hat{\chi}}$ is defined by equation (2.28) and the index ϵ indicates that the collision integral still carries the full energy dependence, and is used to distinguish it later from the collision integral for low-energy excitations around E_{F}. $\mathcal{I}_\epsilon$ is a linear functional, $\mathcal{I}_\epsilon[\hat{B}+\hat{C}] = \mathcal{I}_\epsilon[\hat{B}]+\mathcal{I}_\epsilon[\hat{C}]$ and, as required by the form of $\hat{G}^<$ in equilibrium (see Eq. (2.11)), we also have the property $\mathcal{I}_\epsilon[\hat{A}(\boldsymbol{k},\epsilon,\boldsymbol{r},t)] = 0$. Therefore, the spectral density $\hat{A}(\boldsymbol{k},\omega,\boldsymbol{r},t)$ also satisfies the kinetic equation (2.37), since by substituting $\hat{A}$ for $\hat{G}^<$, we essentially obtain

$$-i\left[(\epsilon-\epsilon_{\boldsymbol{k}}+\delta\mu+e\varphi)\hat{1}+\frac{\Delta-\delta\Delta}{2}\vec{m}\hat{\vec{\sigma}}\,\tilde{*}\,\hat{A}\right]=0\ , \tag{2.39}$$

which is just (2.33) without the real part. Mathematically, this kinetic equation for the spectral density is not necessarily the best way to determine $\hat{A}$ due to the delta function type boundary condition. We will however use (2.39) during the following derivation.

The goal now is to separate the high-energy dynamics from the low-energy dynamics, where the latter describes processes taking place at the surface of the Fermi sea. Firstly, we eliminate the electric potential by the substitution $\omega = \epsilon + e\varphi$ which transforms the derivatives according to

$$\partial_\epsilon \to \partial_\omega\ , \qquad \boldsymbol{\partial}_r \to \boldsymbol{\partial}_r - e\boldsymbol{E}\partial_\omega\ ,$$

with the electric field $\boldsymbol{E} = -\boldsymbol{\partial}_r\varphi$. Accordingly, the Moyal product (2.7) has to take into account this transformation and we instead write

$$\tilde{*} \quad \equiv \quad \circ\, e^{\frac{i}{2}\left(\overleftarrow{\partial}_\omega\overrightarrow{\partial}_{\mathrm{neq}}-\overleftarrow{\partial}_{\mathrm{neq}}\overrightarrow{\partial}_\omega\right)}\ , \tag{2.40}$$

where $\circ$ denotes the Moyal product in $\boldsymbol{r},\boldsymbol{k}$ space. Furthermore, we define

$$\partial_{\mathrm{neq}} \equiv \partial_t - e\boldsymbol{E}\boldsymbol{\partial}_k\ , \tag{2.41}$$

which combines the two external driving forces that turn the system into a non-equilibrium state: electric field and time-dependent magnetization. Therefore, in our kinetic equation, non-equilibrium effects are essentially reduced to the differential operator ∂_{neq}. Thus, we will only include terms linear in ∂_{neq} in the following, which is equivalent to the linear response regime.

Generally, the transformation includes the difficulty that $\boldsymbol{\partial}_r$ also acts on $\boldsymbol{E}$, but here, we assumed that $\boldsymbol{E}$ is uniform, despite the situation of inhomogeneous magnetization which will modify the local electric field thus, making it spatially dependent. However, these corrections to the field are of order $(\boldsymbol{\partial}_r\vec{m})^2$, therefore of maximum order to be considered in this work. Any additional derivative as in $\boldsymbol{\partial}_r\boldsymbol{E}$, would yield terms beyond the regime of our investigation. Thus, we can treat the local electric field as being quasi-homogeneous, as long as the external electric field is constant, which we assume to be the case.

Secondly, we divide the lesser Greens function into equilibrium and non-equilibrium contributions by making the ansatz

$$\hat{G}^<(\boldsymbol{k},\omega,\boldsymbol{r},t) = i\hat{A}(\boldsymbol{k},\omega,\boldsymbol{r},t)\ f_{\mathrm{D}}(\omega) + \delta\hat{G}(\boldsymbol{k},\omega,\boldsymbol{r},t)\ . \tag{2.42}$$

We substitute this ansatz into the kinetic equation (2.37), and the first term essentially drops out by virtue of (2.39), except for terms proportional to $\frac{\partial f_{\mathrm{D}}}{\partial\omega}\partial_{\mathrm{neq}}(\dots)$ which become source terms in the kinetic equation. In particular, we obtain an expression that does no longer

contain any terms proportional to f_{D}, but only to $\frac{\partial f_{\mathrm{D}}}{\partial \omega}$ and higher order derivatives which are non-zero only in the vicinity of the Fermi-energy, provided the temperatures are sufficiently low. In fact, we use the zero-temperature approximation $\frac{\partial f_{\mathrm{D}}}{\partial \omega} = -\delta(\omega - E_{\mathrm{F}})$ throughout this work.

Concerning the second term in (2.42), the non-equilibrium part $\delta\hat{G}$ has two very practical properties. It is proportional to the electric field $\boldsymbol{E}$ or time-gradients of the magnetization $\partial_t \vec{m}$, which allows us to drop terms that are of quadratic order in either of the two sources of non-equilibrium excitations. More specifically, we keep terms of linear order in ∂_{neq}, since we are interested only in linear response to an external perturbation. Furthermore, $\delta\hat{G}$ is peaked around the Fermi-level, reflecting the fact that physical processes take place only in the vicinity of E_{F} for low-energy processes and low enough temperatures.
Consequently, we set $\omega = E_{\mathrm{F}}$ in all prefactors to $\delta\hat{G}$ in the collision integral on the right-hand side of equation (2.37), more specifically, the spectral densities in the collision integral become $\hat{A}(\boldsymbol{k}, E_{\mathrm{F}}, \boldsymbol{r}, t)$. In other words, we neglect the energy-dependence of the scattering rates when it comes to non-equilibrium excitations in the distribution function, since the energy range these excitations span is sharply peaked around E_{F} and is much smaller than typical scales of variation in the scattering rates. As shown in Appendix B, this is compatible with the linear response regime.

The third and final step consists of integrating the kinetic equation (2.37) over energy, i.e. we take $\int_{-\infty}^{\infty} \frac{\mathrm{d}\omega}{2\pi i}$ of this kinetic equation and arrive at a simpler equation for the quantity

$$\hat{g}(\boldsymbol{k}, \boldsymbol{r}, t) = \int \frac{\mathrm{d}\omega}{2\pi i}\, \delta\hat{G}(\boldsymbol{k}, \omega, \boldsymbol{r}, t) \ . \tag{2.43}$$

Performing all these steps, we eventually find the kinetic equation,

$$\boldsymbol{v}_k \boldsymbol{\partial}_r \hat{g} + \frac{1}{2i}\left[(\Delta - \delta\Delta)\vec{m}\hat{\vec{\sigma}} \circ \hat{g}\right] + (\boldsymbol{\partial}_r \delta\mu)\boldsymbol{\partial}_k \hat{g} = \hat{\mathcal{J}}_{\mathrm{t}} + \hat{\mathcal{J}}_{\mathrm{c}} + \hat{\mathcal{I}}[\hat{g}] \ , \tag{2.44}$$

where $\boldsymbol{v}_k = \boldsymbol{\partial}_k \epsilon_{\boldsymbol{k}} = \boldsymbol{k}/m$ is the quasi-particle velocity and the collision integral takes the form

$$\hat{\mathcal{I}}[\hat{g}] = \frac{1}{2}\int \frac{\mathrm{d}^3 k'}{(2\pi)^3}\left(\left\{\underline{\hat{\chi}}\hat{g}(\boldsymbol{k}', \boldsymbol{r}, t) \circ \hat{A}(\boldsymbol{k}, E_{\mathrm{F}}, \boldsymbol{r}, t)\right\} - \left\{\underline{\hat{\chi}}\hat{A}(\boldsymbol{k}', E_{\mathrm{F}}, \boldsymbol{r}, t) \circ \hat{g}(\boldsymbol{k}, \boldsymbol{r}, t)\right\}\right) \ , \tag{2.45}$$

and the spatial Moyal product $\circ$ acts on $\boldsymbol{r}$ and $\boldsymbol{k}$ only, but does *not* act on $\boldsymbol{k}'$. Additionally, external perturbations due to time-dependence or electric field gives rise to the following two source terms,

$$\hat{\mathcal{J}}_{\mathrm{t}} = \int \frac{\mathrm{d}\omega}{2\pi i} i\left[(\omega\hat{1} - \hat{H}) \stackrel{*}{,} i\hat{A}(\boldsymbol{k}, \omega) f_{\mathrm{D}}(\omega)\right] = \frac{1}{4\pi}\left\{\hat{A}(\boldsymbol{k}, E_{\mathrm{F}}, \boldsymbol{r}, t) \circ \partial_{\mathrm{neq}}\hat{H}\right\} \tag{2.46}$$

$$\hat{\mathcal{J}}_{\mathrm{c}} = \int \frac{\mathrm{d}\omega}{2\pi i}\, \mathcal{I}_\omega[i\hat{A} f_{\mathrm{D}}(\omega)] = \frac{1}{4\pi}\partial_{\mathrm{neq}} \int \frac{\mathrm{d}^3 k'}{(2\pi)^3}\, \frac{1}{2i}\left[\underline{\hat{\chi}}\hat{A}(\boldsymbol{k}', E_{\mathrm{F}}, \boldsymbol{r}, t) \circ \hat{A}(\boldsymbol{k}, E_{\mathrm{F}}, \boldsymbol{r}, t)\right] \ , \tag{2.47}$$

where $\hat{\mathcal{J}}_{\mathrm{t}}$ appears as a direct driving force in the kinetic equation, while $\hat{\mathcal{J}}_{\mathrm{c}}$ describes non-equilibrium corrections to the collision integral that appear as a result of the ansatz (2.42). $\hat{\mathcal{J}}_{\mathrm{t}}$ and $\hat{\mathcal{J}}_{\mathrm{c}}$ are additional contributions from the high-energy term that enter the equation for the low-energy dynamics. Eqs. (2.44)-(2.47) constitute a linear integro-differential equation for $\hat{g}$ and serve as the basis for our further analytical treatment. These equations provide a rather

general framework to investigate a large variety of transport problems and time-dependent phenomena like spin/charge pumping.

Provided we have found a solution for $\hat{g}(\boldsymbol{k},\boldsymbol{r},t)$, a task postponed to subsequent sections, we can finally determine the physical observables of interest by simply substituting the ansatz (2.42) into (2.12). In this way, we find for the quasi-particle spin-charge density

$$\hat{N}(\boldsymbol{r},t) = \hat{N}_{\mathrm{h}}(\boldsymbol{r},t) + \hat{n}(\boldsymbol{r},t) = \int \frac{\mathrm{d}\omega}{2\pi} f_{\mathrm{D}}(\omega) \int \frac{\mathrm{d}^3k}{(2\pi)^3} \hat{A}(\boldsymbol{k},\omega,\boldsymbol{r},t) + \hat{n}(\boldsymbol{r},t) \tag{2.48}$$

with the low-energy spin/charge density excitations $\hat{n}(\boldsymbol{r},t) = \int \frac{\mathrm{d}^3k}{(2\pi)^3} \hat{g}(\boldsymbol{k},\boldsymbol{r},t)$. The analogous expression for the current (2.13) is obtained in a straightforward manner.

On length scales much larger than the Thomas-Fermi screening length, which is of atomic order in metallic materials, local charge neutrality is fulfilled. We also assume that timescales of external perturbations are sufficiently small for screening to be instantaneous. This allows us to easily specify a condition for the chemical potential shift $\delta\mu(\boldsymbol{r},t)$, which has to be chosen such that the following relation holds,

$$-e\mathrm{Tr}\hat{N}(\boldsymbol{r},t) + Q_{\mathrm{Ion}} = 0 \ . \tag{2.49}$$

This implies that the total quasi-particle charge density (2.12) is constant throughout the ferromagnet and neutralizes the ionic background of charge density Q_{Ion}.

Feasibility of the gradient expansion for arbitrary Δ - separation of time-scales

One important remark about the validity of the derivation of the kinetic equation (2.44) is in order. Strictly speaking, we are allowed to make the gradient expansion only when the derivatives act on quantities which are smooth on the respective Fermi-scales. However, we put no restrictions on the value of the exchange field Δ and it can even be close to the Fermi level E_{F}, which implies that the precession length is of the order of the Fermi-wave length. This gives rise to fast oscillations, with gradients acting on these terms not necessarily small. A solution is to average out the rapid transverse precession, which leads to an effective equation for the averaged quantity $\langle\hat{g}\rangle$, which is formally identical to Eqs. (2.44)-(2.47). However, when solving our kinetic equations, it has to be kept in mind that derivatives do *not* act on fast precession terms, only on the slow envelope functions. This is also the reason why we could drop the term $\partial\hat{g}$ in Eq. (2.44) for the low-energy dynamics, because this term would be of second order in external perturbation and thus, beyond linear response.

To mathematically concretize this, we go back to the very beginning and consider the full kinetic equation for the Keldysh Greens function before introducing impurity self-energies,

$$\left[\epsilon\hat{1} - \hat{\mathcal{H}}\right] * \check{G} = \check{1} \ , \tag{2.50}$$

where the Hamiltonian $\hat{\mathcal{H}}$ is introduced in Eq. (2.1). This equation constitutes a differential equation for $\check{G}$, where the term $\frac{\Delta}{2}\vec{m}(\boldsymbol{r},t)\hat{\vec{\sigma}}$ gives rise to rapid precession in time and space. The main idea is to obtain an effective equation for the averaged propagator $\langle\check{G}\rangle$, eliminating the fast oscillations due to Δ. It turns out that we obtain an effective equation for $\langle\check{G}\rangle$, which

is formally identical to the original kinetic equation. However, care has to be taken concerning the term $\frac{\Delta}{2}\vec{m}(\boldsymbol{r},t)\hat{\vec{\sigma}}$ which would normally give rise to fast oscillations. The important aspect is that the derivatives in the effective equation act only on the slow dynamics and consequently, only the behavior of the envelope function $\langle \check{G} \rangle$ is well described.
From there on, all the derivations and definitions still apply, including the introduction of the self-energy $\hat{\Sigma}$, just with all quantities $\hat{G}, \hat{A}$, etc. replaced by averaged quantities. The benefit is clearly the feasibility of the gradient expansion in temporal and spatial coordinates which, in the case $\Delta \approx E_{\mathrm{F}}$, would not be possible to truncate before, since then gradients to all orders would be important.

Another way to explain what happens is the following. The truncation of the gradient series (2.18) leads to an incorrect description of the fast time-scale dynamics, however, the slow dynamics imposed by the external driving is still well described. Of course, the truncated equations still exhibit fast time-scale dynamics in an uncontrolled approximation, but this is not a big problem, since we are not interested in these rapid oscillations, only in the envelope function obtained after averaging. And the latter one is well described in the sense of the usual gradient expansion. In the end, this is possible due to a separation of time scales, since in our regime, the precession length/time is the smallest length/time-scale besides the respective Fermi-scales, so we implicitly keep in mind the averaging procedure outlined above.

In the limit $\Delta \ll E_{\mathrm{F}}$, our equations are valid without the need for some averaging procedure, so also the dynamics imposed by Δ is correctly described. Later in section 2.4.3, we will explicitly perform such an averaging procedure, and the steps leading to equation (2.137) illustrate the ideas discussed above.

2.2.5. Self-consistency Condition – from s-d Model to Stoner Model

Using functional Keldysh theory [24], one can derive an effective Hamiltonian

$$\hat{\mathcal{H}} = \mathcal{H}_0\hat{1} - \frac{\Delta_s}{2}\vec{m}_s\hat{\vec{\sigma}} - \frac{\Delta_d}{2}\vec{m}_d\hat{\vec{\sigma}} \ , \tag{2.51}$$

together with the self-consistency condition for the conduction electrons

$$\frac{U}{2}\left\langle \psi^\dagger(\boldsymbol{r},\boldsymbol{t})\hat{\vec{\sigma}}\psi(\boldsymbol{r},\boldsymbol{t})\right\rangle = \frac{U}{2}\mathrm{Tr}\hat{\vec{\sigma}}\hat{N}(\boldsymbol{r},\boldsymbol{t}) = \Delta_s\vec{m}_s \ , \tag{2.52}$$

where $\mathcal{H}_0$ describes the spin-independent part of the Hamiltonian (2.1) for our ferromagnetic conductor. Here, $\Delta_d\vec{m}_d$ describes the effective field due to the localized d-electrons and likewise for the itinerant s-electrons. U is the exchange coupling between the itinerant electrons and the self-consistency condition (2.52) remains the same in both cases, s-d and Stoner limit. The only difference is the Hamiltonian, to which we have to add an additional term $\hat{H}_{sd} = \frac{1}{2}\Delta_d\vec{m}_d\hat{\vec{\sigma}}$ in the s-d case. This latter term vanishes in the Stoner limit, as opposed to the s-d model, where Δ_d is the dominant term as compared to the mean-field contribution from the itinerant electrons described by the Δ_s term, i.e. $\Delta_d \gg \Delta_s$ in the s-d limit.

If we assume that time scales of external perturbations are much larger than the time scales of the spin dynamics of both s and d-electrons, we have $\vec{m}_s = \vec{m}_d$ incase of a ferromagnetic coupling between the two types of electrons. Then the two magnitudes Δ_s and Δ_d simply

add, and the situation intermediate between s-d and Stoner limit is no different to treat in our mathematical formalism than the two limiting cases. If the separation of timescales is not possible, the intermediate scenario is difficult due to the fact that $\vec{m}_s$ and $\vec{m}_d$ are not necessarily parallel and thus, adding up the contributions yields a strong variation of the magnitude of the total exchange field. Consequently, one has to relax the condition of constant Δ already to lowest order which then would yield terms due to gradients in the magnitude Δ not treated in the present work.

At any rate, in the present work we assume external perturbations to be much slower than any internal time-scales, so our calculations include also the intermediate situation. However, the two extreme cases of s-d and Stoner limit are interesting enough, and in the intermediate regime nothing qualitatively new is expected, so in the following we will mainly treat these two limiting cases.

Stoner limit

Let us first treat the Stoner limit, where we can write for the self-consistency condition for the magnetization of the conduction electrons

$$U\left(\vec{S}_0+\vec{S}_2\right)=\left(\Delta-\delta\Delta(\boldsymbol{r})\right)\vec{m}+\delta\vec{W}_\perp(\boldsymbol{r})\ , \tag{2.53}$$

where U is the effective exchange coupling energy between electrons and $-\delta\Delta(\boldsymbol{r})\vec{m}+\delta\vec{W}_\perp(\boldsymbol{r})$ are anticipated corrections to the self-consistent exchange field in presence of magnetization gradients. The density is obtained from Eq. (2.12) as $\hat{N}=\frac{N_\mathrm{c}}{2}\hat{1}+\vec{S}\hat{\vec{\sigma}}$, where N_c is the charge component and $\vec{S}=\vec{S}_0+\vec{S}_2$ the spin density as a series in gradients. To zeroth order, the spin density is $\vec{S}_0=\rho_s\vec{m}$ with $\rho_s=\frac{\nu_0\Delta}{2}(1+\frac{1}{3}P^2)$, and the correction second order in spatial gradients reads explicitly

$$\begin{aligned}\hat{S}_2=\nu_0\left[(-\frac{P}{2}\delta\Delta+\delta\mu)\hat{1}+(-\frac{1}{2}\delta\Delta+P\delta\mu)\vec{m}\hat{\vec{\sigma}}\right]+\frac{1}{2}\nu_0\left(1+\frac{P^2}{3}\right)\delta\vec{W}_\perp\hat{\vec{\sigma}}\\ +\nu_0\frac{(\boldsymbol{\partial}_r\vec{m})^2}{2m_\mathrm{e}}\left(\frac{P^2}{12}\hat{1}-\frac{P(10+P^2)}{60}\vec{m}\hat{\vec{\sigma}}\right)+\hat{S}_{2,\perp}\ ,\end{aligned} \tag{2.54}$$

where $\hat{S}_{2,\perp}$ is the transverse spin component not needed at present. In the Stoner limit of itinerant ferromagnetism, U is fixed by the equilibrium magnetization $U=\frac{\Delta}{\rho_s}=\frac{6}{\nu_0(3+P^2)}$ and is immediately obtained by solving Eq. (2.53) for the homogeneous case.

Solving (2.53) along with the local charge-neutrality condition (2.49), i.e. $\mathrm{Tr}\hat{S}_2=0$ yields

$$\delta\mu^{(\mathrm{St})}(\boldsymbol{r}) = \frac{15-P^2}{120}\frac{(\boldsymbol{\partial}_r\vec{m})^2}{2m_\mathrm{e}} \tag{2.55}$$

$$\delta\Delta(\boldsymbol{r}) = \frac{5+3P^2}{20P}\frac{(\boldsymbol{\partial}_r\vec{m})^2}{2m_\mathrm{e}}\ , \tag{2.56}$$

while $\delta\vec{W}_\perp$ exactly drops out from the equation, meaning that in principle it can be any value. However, adding a transverse part $\delta\vec{W}_\perp$ would yield modified equations, which however describe the same physics. In fact, we obtain the original equations by simply renormalizing

the magnetization $\Delta\vec{m} \to \Delta\vec{m} + \delta\vec{W}_\perp$ (to leading order, since corrections to the magnitude would be of oder $\delta\vec{W}_\perp^2$ which is of 4th order in gradients and thus beyond our treatment). Physically speaking, there should be no transverse corrections $\delta\vec{W}_\perp$, only the magnitude of the magnetization attains corrections $\delta\Delta(\boldsymbol{r})$. Thus, setting $\delta\vec{W}_\perp = 0$ and satisfying the transverse part of Eq. (2.53), amounts to $\hat{S}_{2,\perp} = 0$ which, as we will see in section 2.5.2, corresponds to $\vec{\mathcal{T}}_{\mathrm{el}} = 0$ and leads to the Landau-Lifshitz-Gilbert equation describing the magnetization dynamics. In fact, this corresponds to the zero-torque theorem [53] which in the Stoner limit emerges from the self-consistency condition for the transverse magnetization, and simply states that the itinerant electron system cannot exert a torque on itself.

Furthermore, in the limit $\Delta \to 0$ *viz.* $P \to 0$, the correction $\delta\Delta$ also drops out from the self-consistency equation (2.53) to leading order in P. This means that in the limit of weak itinerant ferromagnetism, a small correction $\delta\Delta$ to the self-consistent field induces a polarization in the electron gas, which in turn corresponds to a small additional effective field and exactly compensates the original perturbation $\delta\Delta$ in the field. Thus, longitudinal spin-perturbations in the itinerant electron gas cannot be screened efficiently in this limit and therefore, the screening field $\delta\Delta$ from Eq. (2.56) is inversely proportional to P, so that it is greatly enhanced in the limit $P \to 0$. Note that this is true also for additional small transverse fields, however for arbitrary strength of the itinerant field Δ, so transverse perturbations cannot be screened, and instead give rise to the magnetization dynamics mentioned above.

s-d limit

In the *s-d* limit, the effective exchange field $\Delta\vec{m}(\boldsymbol{r}, t)$ entering the equation for the itinerant electrons is simply given by the magnetization of the localized *d*-electrons, since we neglect the contribution from the itinerant electrons to the total magnetization, as it is assumed to be much smaller. Thus, we merely have to fulfill the charge neutrality condition for the conduction electrons, which yields

$$\delta\mu^{(\mathrm{sd})}(\boldsymbol{r}) = -\frac{P^2}{12}\frac{(\boldsymbol{\partial}_r\vec{m})^2}{2m_{\mathrm{e}}} \tag{2.57}$$

and of course $\delta\vec{W}_\perp = 0$ and $\delta\Delta = 0$.

To summarize, we have derived a fully microscopic equation for the spin transport in non-collinear magnetization textures. Our approach takes impurity scattering and spin-flip scattering into account on the Hamiltonian level. This paves the way to treat complex magnetic textures and derive microscopic expression for the domain-wall-induced resistance.

2.3. Diffusive Transport in Quasi-1-Dimensional Systems – Domain-wall Resistance

In this section, we will mainly focus on static magnetotransport and domain-wall resistance. We present a method of solving our kinetic equations using a truncated hierarchy of equations, and which will give us some insight into the structure of our equations. First, let us begin with a short review of work related to the domain-wall resistance (DWR) that has been published in literature.

On the theoretical side, two major research lines to magnetotransport have been followed in the last years. One line is a numerical approach using atomistic so-called first principle calculation to treat relatively small systems. The second line of research applicable to larger systems, in which structural details due to a microscopic disorder averages out, is based on analytical kinetic equation derived from field theoretical methods. We now briefly summarize a few main results obtained with both approaches.

Using numerical methods based on ab-initio approaches in combination with tight-binding transport calculations, detailed predictions for the linear conductance of multilayers have been made [54, 55, 56]. These include in particular all effects of the complex band structure and can also take into account the effect of disorder. The effects of a finite cross section were explored in Ref. [57] and an inhomogeneous magnetization has been accounted for in Ref. [58]. A method to overcome the linear response limit of these calculations have been recently proposed for non-magnetic materials [59]. These approaches are well suitable and very successful to describe multilayers and atomic size domain walls. The main disadvantage is that the computational effort limits the system size rather drastically and typical mesoscale domain walls with dimensions of the order of 10nm cannot be described. Furthermore, spin-flip scattering by magnetic impurities or disordered spin-orbit scattering are difficult to take into account by the microscopic tight-binding simulations. Since the latter mentioned systems will be the main focus of our work, we will therefore choose a different approach, based on analytical transport equations using non-equilibrium Green's function methods.

Using analytical methods, several limiting cases of the domain wall resistance have been investigated using a variety of theoretical approaches. The works [33, 34, 35] perform a diagrammatic evaluation of the Kubo-formula introducing scattering in the unperturbed Greens functions by two phenomenological parameters $\tau_{\uparrow,\downarrow}$, the momentum scattering times for spin up and down channels. In this calculation, spin-flip processes are not included. As we will discuss later, this leads to a spin accumulation that does not decay even arbitrarily far from the domain wall. Hence, this neglect of spin-flip is only possible, if the distance between the domain wall and leads is much smaller than the spin-diffusion length. In a complementary approach, Levy and Zhang [32] use a linearized Boltzmann equation. They do not consider changes in the electronic spectrum, i.e. they assume spin-independence of the wave vector $k_\uparrow = k_\downarrow$, restricting the validity to the regime of small exchange splitting. Their analytical calculation is done in a basis that diagonalizes the Hamiltonian, which is possible incase of a constant magnetization gradient, known as spin-spiral. Thus, they cannot take into account a finite contact geometry and finite domain wall length, but have to consider an infinitely extended spin-spiral for which they calculate the conductivity. Spin-flip processes are absent, so, again, the above statement concerning spin accumulation applies. Furthermore, they per-

form a multi-pole expansion of the distribution function but only include terms up to the p-wave component. However, as we will see during our calculation, this is not sufficient in general. Lastly, we believe the Boltzmann equation, they use, lacks terms that should appear as a result of the gauge transformation. Bergeret *et al.* use the Keldysh technique to derive a quasiclassical equation valid in the diffusive limit [38]. However, they consider a different regime of validity, in which the scattering mean free path l_s is the smallest length scale in the system (besides the Fermi-length), and not the precession length as will be the case in our treatment. Likewise, they do not consider spin-flip processes, even though during their calculation, they perform steps which implicitly require longitudinal spin excitations to relax. Finally, Simanek *et al.* [39, 40] used equations of motion for the quantum distribution function in Wigner space, which however contain a term that we cannot reproduce. Before, Bergeret *et al.* noted that this term violates particle conservation [38]. Nevertheless, this term does not affect the statement of Simanek *et al.* that there is quenching of the spin-accumulation due to rapid transverse precession. This also emerges from our theory and we will make use of it later (see the discussion around Eq. (2.89)).

In this section, we pursue a fully microscopical theoretical approach to the DWR in the limit of wide domain walls, so that quantum mechanical electron reflection at the domain wall can be neglected. This allows us to use a our semi-classical approximation and neglect spin-dependent scattering due to abrupt potential changes [60, 61, 62, 63]. We employ our model of quasi-free electrons with parabolic dispersion instead of a realistic band structure, since we are mainly interested in linear response properties, which limit the relevant energy scales to a small band around the Fermi level. Furthermore, we assume a width of the system larger than the mean free path, so that quantization effects due to a finite cross section do not interfere with the intrinsic DWR. Furthermore, we assume that the precession length should be much smaller than other typical lengths of the system. As opposed to other works, our approach includes spin-flip scattering, which is needed for a decay of the spin-accumulation away from the domain wall. Finally, scattering is included on a microscopic level and we include gradient corrections to the collision integral, which is required for a consistent description up to second order in spatial gradients of the magnetization.

We begin by introducing our transport setup and the model description of the domain wall, to which we apply the kinetic equation derived in the previous section. Then we solve these resulting equations analytically in the regime of small precession lengths, and finally discuss certain limiting cases and relate our results to existing theoretical works we are aware of dealing with the issue of DWR [32, 33, 34, 35, 36, 37, 38, 39, 40].

2.3.1. Model of the Contact

We treat a ferromagnet in a quasi one-dimensional geometry such that there are only gradients of the magnetization in the x direction, while in the y- and z-directions the system is homogeneous. Furthermore, we assume a coplanar magnetization which allows us to parameterize the magnetization direction by a single angle $\theta(x)$, defined as

$$\vec{m}(x) = \begin{pmatrix} 0 \\ \sin\theta(x) \\ \cos\theta(x) \end{pmatrix} \quad . \tag{2.58}$$

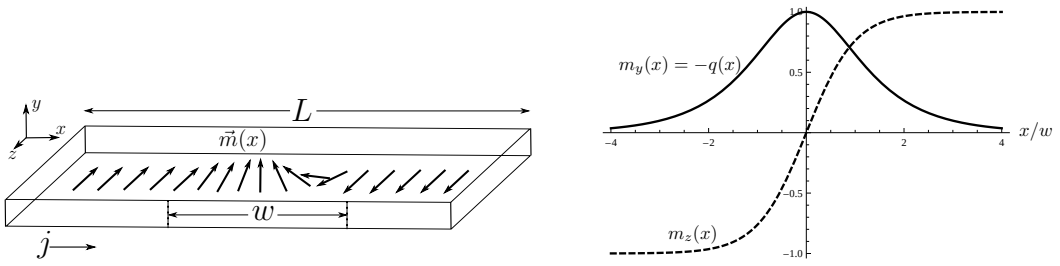

(a) (b)

Figure 2.2.: (a) Contact of length L with a Bloch domain wall of characteristic size w situated in between. The domain wall is described by the magnetization gradient $q(x) = \partial_x\theta(x)$. The plot in (b) shows $m_y(x) = -q(x)$ and $m_z(x)$ according to equation (2.61).

Current flow perpendicular to the domain wall implies that the direction of $\boldsymbol{j}$ is along the x-axis, so that the problem becomes effectively one-dimensional. Therefore, every quantity of interest only depends on x, so we can set $\partial_y = \partial_z = 0$. The contact of length L contains a domain wall of characteristic width w. The left- and rightmost parts have opposite magnetization directions and a so far arbitrary magnetization profile $\theta(x)$ connects the two magnetic domains. The situation is sketched in Fig. 2.2.

It is then convenient to perform a local SU(2) gauge transformation in order to rotate the coordinate system, used to represent the spin-orientation, such that its z-axis is always aligned to the local magnetization direction $\vec{m}$. The unitary operator ($\hat{\mathcal{U}}^\dagger = \hat{\mathcal{U}}^{-1}$)

$$\hat{\mathcal{U}} = e^{-\frac{i}{2}\theta\hat{\sigma}_x} \tag{2.59}$$

exactly performs this rotation in spin-space using the previously introduced angle θ, so that $\hat{\mathcal{U}}\ \vec{m}\vec{\hat{\sigma}}\ \hat{\mathcal{U}}^{-1} = \hat{\sigma}_z$. As θ is spatially dependent, the derivative obtains an additional term after the transformation,

$$\hat{\mathcal{U}}\ \partial_x\ \hat{\mathcal{U}}^{-1} = \hat{1}\partial_x + \frac{i}{2}q(x)\hat{\sigma}_x \equiv \hat{\partial}_x\ . \tag{2.60}$$

Henceforth, we have to deal with the gradient $q(x) = \partial_x\theta$ in our equations and which fully parameterizes the domain wall. Essentially, $q(x)$ can be interpreted as a Berry phase due to adiabatic transport in the domain wall profile $\vec{m}(x)$ and (2.60) is the covariant derivative. The gauge transformation (2.59) rotates the orthonormal basis system $(\boldsymbol{v}\times\vec{m}, \boldsymbol{v}, \vec{m})$ such that it becomes the canonical set of basis vectors, $(\boldsymbol{e}_x, \boldsymbol{e}_y, \boldsymbol{e}_z)$. The unit vector $\boldsymbol{v}$ points in the direction of change of the magnetization $\vec{m}$, i.e. $\partial_x\vec{m} = q\boldsymbol{v}$. Note that $\boldsymbol{v}$ is perpendicular to $\vec{m}$, since $\vec{m}$ is a unit vector.

An analytical form of the domain wall profile can be derived in the context of minimizing the free energy of the ferromagnetic material, commonly a compromise between exchange and anisotropy energy. Typically, one finds

$$\cos\theta(x) = \tanh(\tfrac{x}{w})\ , \tag{2.61}$$

so that

$$q^2(x) = \frac{1}{w^2\cosh^2(\frac{x}{w})} = \frac{1}{w}\frac{\partial}{\partial x}\tanh(\tfrac{x}{w})\ , \tag{2.62}$$

where w constitutes a typical length scale over which the domain wall extends.

Theoretically, as well as experimentally, contributions arising from spin-orbit coupling, such as the AMR which leads to a resistance depending on the angle between magnetization and current directions, can be separated from the true DWR and therefore are not included the following calculation. For the Bloch wall and the CPW-geometry (current perpendicular to wall) employed in our model (see FIG. 2.2), the AMR plays no role, since the magnetization direction is always perpendicular to the current direction. For other walls like Néel walls, the spin direction within the wall attains a component parallel to the current and the AMR has to be carefully distinguished from the DWR. As discussed above, the AMR contribution can simply be added to the DWR to leading order.

2.3.2. Kinetic Equation - Boundary Condition versus Source Terms

In the present investigation, we restrict ourselves to the *s-d* limiting case, so that $\delta\Delta = 0$. Furthermore, since we are dealing with a stationary problem (i.e. $\partial_t = 0$), we can reformulate the external electric driving in terms of appropriate boundary conditions to be specified below. Mathematically, this is equivalent to the formulation as source terms for our kinetic equation, as it is the case in Eq. (2.44).

We want to eliminate the source terms $\hat{\mathcal{J}}_\mathrm{t}$, $\hat{\mathcal{J}}_\mathrm{c}$ due to the electric potential $\varphi(\boldsymbol{r})$ in (2.44), which is achieved by a redefinition of $\hat{g}$ as,

$$\hat{g} \to \hat{g} + \frac{e}{2\pi}\varphi(\boldsymbol{r})\ \hat{A}(\boldsymbol{k}, E_\mathrm{F}, \boldsymbol{r})\ . \tag{2.63}$$

Therefore, we have to solve the kinetic equation

$$\boldsymbol{v}_k \boldsymbol{\partial}_r \hat{g} - i\frac{\Delta}{2}\left[\vec{m}\vec{\hat{\sigma}}\ ;\ \hat{g}\right] + (\boldsymbol{\partial}_r \delta\mu)\boldsymbol{\partial}_k \hat{g} = \hat{\mathcal{I}}[\hat{g}]\ , \tag{2.64}$$

together with the collision integral from Eq. (2.45) and the shift in the chemical potential given by Eq. (2.57). Now instead, the external electric potential enters as boundary condition for $\hat{g}$, which is seen by writing the density (2.48) for the redefined $\hat{g}$ and considering local charge neutrality (2.49). This brings us directly to the condition

$$-e\mathrm{Tr}\hat{n}(\boldsymbol{r}) = e^2\varphi(\boldsymbol{r})\frac{1}{2\pi}\int \frac{\mathrm{d}^3k}{(2\pi)^3}\mathrm{Tr}\hat{A}(\boldsymbol{k}, E_\mathrm{F}, \boldsymbol{r})\ , \tag{2.65}$$

since the charge component of the first term $\hat{N}_\mathrm{h}(\boldsymbol{r})$ of (2.48) corresponds to the equilibrium density which is constant by definition of the chemical potential shift $\delta\mu(\boldsymbol{r})$ and exactly neutralizes the material. Therefore, $\mathrm{Tr}\hat{n}(\boldsymbol{r})$ is directly related to the local electric potential, or screening potential, and thus, the local electric field $\boldsymbol{E}(\boldsymbol{r}) = -\boldsymbol{\partial}_r\varphi(\boldsymbol{r})$ in the system, which is a benefit of the above transformation. Essentially, the transformation (2.63) introduces unscreened quantities, whereas the original definition of $\hat{g}$ used in Eq. (2.44) incorporates charge screening effects.

Now, we consider a region far from any inhomogeneities in the magnetization for which we want to specify an appropriate boundary condition. In the absence of a magnetization gradient

and non-equilibrium spin-excitations in the conduction electron system, instead of (2.65) a less strict equality holds,

$$\hat{n}(\boldsymbol{r}) = -e\varphi(\boldsymbol{r})\frac{1}{2\pi}\int \frac{\mathrm{d}^3k}{(2\pi)^3}\hat{A}(\boldsymbol{k}, E_\mathrm{F}, \boldsymbol{r}) \ . \tag{2.66}$$

In a simple one-dimensional geometry and for the left and right terminals at $x_{\mathrm{L,R}}$, the boundary condition simply becomes

$$\hat{n}(x_{\mathrm{L,R}}) = -e\varphi(x_{\mathrm{L,R}})\nu_0\left(\hat{1} + P\vec{m}\hat{\vec{\sigma}}\right) \ . \tag{2.67}$$

For the present quasi-one dimensional situation of the DWR, it turns out that there are no additional high-energy contributions induced by the electric field, so we can fully concentrate on the low-energy part $\hat{g}$. Furthermore, the leading order contribution to the domain-wall resistance is of second order in gradients, so in the following treatment, we will include only terms up to order $\boldsymbol{\partial}_r^2$.

2.3.3. A Hierarchy of Equations

In light of the solution procedure that is to come, it is convenient to use a 4-component vector representation (which is denoted by an arrow to distinguish it from the 3-component real-space vectors set in boldface), in which the spin-charge density excitations and current density take the form, respectively,

$$\begin{aligned} \vec{n} &= (n_+, n_-, n_\uparrow, n_\downarrow) \ , \\ \vec{j} &= (j_+, j_-, j_\uparrow, j_\downarrow) \ . \end{aligned}$$

Starting from the 2×2-matrix representation after the gauge transformation, $\hat{n} = \frac{n_c}{2}\hat{1} + n_x\hat{\sigma}_x + n_y\hat{\sigma}_y + n_z\hat{\sigma}_z$, we define the spin-up/down densities $n_{\uparrow,\downarrow} = \frac{n_c}{2} \pm n_z$. Additionally, the transverse spin degrees of freedom are transformed according to $n_\pm = n_x \pm i n_y$ which correspond to circularly polarized transverse spin excitations. This basis is convenient because it diagonalizes the equations of motion for the transverse dynamics in absence of magnetization gradients, see Eq. (2.70) and following.

The full kinetic equation for $\hat{g}$ is still very involved, so we need to perform additional simplifying steps. Therefore, we multiply Eq. (2.64) with v_x^n ($n \geq 0$) and afterwards, we integrate over the whole $\boldsymbol{k}$-space. This involves evaluating terms of the form

$$\begin{aligned} \left\langle v_x^n \partial_{k_x}^m \hat{g}\right\rangle &= \int \frac{\mathrm{d}^3k}{(2\pi)^3} v_x^n \partial_{k_x}^m \hat{g} = (-1)^m \int \frac{\mathrm{d}^3k}{(2\pi)^3}\hat{g}\partial_{k_x}^m v_x^n \\ &= \begin{cases} \frac{(-1)^m}{m_\mathrm{e}^m}\frac{n!}{(n-m)!}\hat{g}^{(n-m)} & \text{if n} \geq \text{m} \\ 0 & \text{if n} < \text{m} \end{cases} \end{aligned} \tag{2.68}$$

and defining moments of the Greens function $\hat{g}$

$$\hat{g}^{(n)} = \int \frac{\mathrm{d}^3k}{(2\pi)^3} v_x^n \hat{g} \, . \tag{2.69}$$

The first two moments are $\hat{g}^{(0)} = \hat{n}$ and $\hat{g}^{(1)} = \hat{j}$, obviously. The kinetic equation (2.64) turns into an infinite hierarchy of equations relating these moments. It is nevertheless possible to find an analytical solution to these equations in form of a systematic series expansion in the function $q(x)$. As we will show below, it is then possible to truncate the hierarchy by setting $\hat{g}^{(5)} = 0$ in the calculation of the domain-wall resistance. The first two of these equations are reminiscent of spin-charge continuity and diffusion equations and take the explicit form

$$\hat{\underline{\underline{\Gamma}}}\vec{n} + \underline{\underline{\partial}}_x \vec{j} = O(q) \ , \tag{2.70}$$

$$\hat{\underline{\underline{\Pi}}}\left(\vec{j} + \underline{\underline{D}}\ \partial_x \vec{n}\right) = O(q) \ , \tag{2.71}$$

where we defined the covariant derivative $\underline{\underline{\partial}}_x$ in accordance to Eqn. (2.60),

$$\underline{\underline{\partial}}_x \equiv \underline{\underline{1}}\partial_x + q\underline{\underline{M}}_x \equiv \underline{\underline{1}}\partial_x + \frac{i}{2}q \begin{pmatrix} 0 & 0 & 1 & -1 \\ 0 & 0 & -1 & 1 \\ 1 & -1 & 0 & 0 \\ -1 & 1 & 0 & 0 \end{pmatrix} \ . \tag{2.72}$$

The right-hand sides of these equations include important contributions that are due to modification of various transport properties in presence of a magnetization gradient, like the change in the density of states which enters the collision integrals. Thus, the right-hand side vanishes as $q \to 0$. Their explicit form along with the equations for $\hat{g}^{(2)}$, etc. are rather lengthy and not needed for our following discussion. Further details can be found in the Appendix in equations (C.12)-(C.20).

The various scattering rates associated with momentum relaxation are combined in the tensor

$$\hat{\underline{\underline{\Pi}}} = \mathrm{diag}\left(\frac{1}{\tau} + i\Delta, \frac{1}{\tau} - i\Delta, \frac{1}{\tau_\uparrow}, \frac{1}{\tau_\downarrow}\right) \ , \tag{2.73}$$

while spin-flip and dephasing processes are due to the tensor

$$\hat{\underline{\underline{\Gamma}}} = \begin{pmatrix} \frac{1}{T_2} + i\Delta & 0 & 0 & 0 \\ 0 & \frac{1}{T_2} - i\Delta & 0 & 0 \\ 0 & 0 & \frac{1}{T_\uparrow} & -\frac{1}{T_\downarrow} \\ 0 & 0 & -\frac{1}{T_\uparrow} & \frac{1}{T_\downarrow} \end{pmatrix} \ . \tag{2.74}$$

We introduced the spin-flip relaxation times for spin-up/down electrons $T_{\uparrow,\downarrow} \equiv \frac{2\nu_0 T_1}{\nu_{\downarrow,\uparrow}}$, and the structure of $\hat{\underline{\underline{\Gamma}}}$ has the correct form such that it relaxes any non-equilibrium excitation towards the equilibrium magnetization value of the system. Note that spin precession is incorporated as well, and manifests itself as an imaginary part in the entries of the transverse subspace of $\hat{\underline{\underline{\Gamma}}}$ and $\hat{\underline{\underline{\Pi}}}$.

Furthermore, the matrix of diffusion constants is diagonal and reads

$$\underline{\underline{D}} = \mathrm{diag}\left(\frac{D_\perp}{1 + i\tau\Delta}, \frac{D_\perp}{1 - i\tau\Delta}, D_\uparrow, D_\downarrow\right) \ , \tag{2.75}$$

where we introduced the transverse diffusion constant $D_\perp = \frac{2E_\mathrm{F}}{3m_\mathrm{e}}\tau = \frac{1}{3}v_\mathrm{F}^2\tau$ and the diffusion constant for spin-up/-down channels $D_{\uparrow,\downarrow} = \frac{2E_\mathrm{F} \pm \Delta}{3m_\mathrm{e}}\tau_{\uparrow,\downarrow}$. Transverse spin excitations are also subject to precession as they diffuse, which results in the complex values of the effective transverse diffusion constants found in (2.75).

2.3.4. Solving the Hierarchy of Equations

We eliminate the higher order moments $\hat{g}^{(n\geq 1)}$ by iteratively substituting the equations into each other, carefully keeping terms that contribute up to order q^2. We find a differential equation for the vector of quasi-particle excitations $\vec{n}$ of the form

$$\left(\hat{\underline{\underline{\Gamma}}} - \underline{\underline{D}}\partial_x^2\right)\vec{n} \;=\; \underline{\underline{W}}(q)\vec{n}\;, \tag{2.76}$$

where the differential operator $\underline{\underline{W}}(q)$ vanishes for $q \to 0$ and contains all possible terms up to order q^2. In the homogeneous ($q = 0$) and collinear case, Eq. (2.76) corresponds to the transport equation used by Valet and Fert [64].

Generally, $\underline{\underline{W}}(q)$ contains terms of the form $\underline{\underline{Y}}_{ijk}\partial_x^i q\partial_x^j q\partial_x^k$, $\underline{\underline{Y}}_{ij}\partial_x^i q\partial_x^j$ and $\underline{\underline{Y}}_i\partial_x^i$, where the position of q and ∂_x is crucial, since ∂_x acts on everything to its right. The constant matrices $\underline{\underline{Y}}$ that depend on our set of parameters P, τ, T_1, T_2 can be obtained in a straightforward manner from equations (C.12)-(C.16) by collecting all terms associated with the corresponding factor $\partial_x^i q\partial_x^j q\partial_x^k$. Restricted to terms that contribute to DWR, its explicit form (see Eq. (C.18)) is given in Appendix C.

Since we have a perturbative treatment in q in mind, we determine the Greens function of Eq. (2.76),

$$\left(\hat{\underline{\underline{\Gamma}}} - \underline{\underline{D}}\partial_x^2\right)\underline{\underline{G}}(x) = \underline{\underline{1}}\delta(x)\;. \tag{2.77}$$

Separated into longitudinal (l) and transverse (t) subspace, the Greens function is

$$\begin{aligned}
\underline{\underline{G}}(x) &= \begin{pmatrix} \underline{G}_{\mathrm{tt}}(x) & 0 \\ 0 & \underline{G}_{\mathrm{ll}}(x) \end{pmatrix}\;, \\
\underline{G}_{\mathrm{ll}}(x) &= \underline{H}e^{-\frac{|x|}{\lambda}} + \underline{K}\frac{|x|}{\lambda}\;, && (2.78)\\
\underline{G}_{\mathrm{tt}}(x) &= \begin{pmatrix} f(x) & 0 \\ 0 & f^*(x) \end{pmatrix}\;, && (2.79)\\
f(x) &= \frac{1+i\tau\Delta}{D_\perp}\,\frac{i}{2k}e^{ik|x|}\;, \\
k^2 &= \left(\frac{2\pi}{l_{\mathrm{prec}}}\right)^2\left(1-\frac{i}{\tau\Delta}\right)\left(1-\frac{i}{T_2\Delta}\right)\;,
\end{aligned}$$

and the precession length is defined as $l_{\mathrm{prec}} \equiv 2\pi\frac{v_{\mathrm{F}}}{\sqrt{3}\Delta}$. Matrices in the 2×2 subspaces are denoted by a single underbar as compared to the double underbar which indicates a 4×4 matrix. The index l and t refers to longitudinal and transverse components, respectively, so that for example

$$\underline{\underline{W}} = \begin{pmatrix} \underline{W}_{\mathrm{tt}} & \underline{W}_{\mathrm{tl}} \\ \underline{W}_{\mathrm{lt}} & \underline{W}_{\mathrm{ll}} \end{pmatrix}\;.$$

The longitudinal component $\underline{G}_{\mathrm{ll}}$ consists of two contributions. The first term of $\underline{G}_{\mathrm{ll}}$ describes spatial damping of spin-up/down non-equilibrium excitations which manifests itself in the characteristic exponential decay on the spin-diffusion length,

$$\frac{1}{\lambda^2} \equiv \frac{1}{D_\uparrow T_\uparrow} + \frac{1}{D_\downarrow T_\downarrow}\;. \tag{2.80}$$

The second term of $\underline{G}_{\mathrm{ll}}$ describes the linear behavior of the chemical potential in a homogeneous system in the absence of a magnetization gradient. The two tensors

$$\underline{H} = \frac{\lambda^3}{2}\begin{pmatrix} \frac{1}{D_\uparrow^2 T_\uparrow} & -\frac{1}{D_\uparrow D_\downarrow T_\downarrow} \\ -\frac{1}{D_\downarrow D_\uparrow T_\uparrow} & \frac{1}{D_\downarrow^2 T_\downarrow} \end{pmatrix} \tag{2.81}$$

$$\underline{K} = -\frac{1}{2}\frac{\lambda^3}{D_\uparrow D_\downarrow}\begin{pmatrix} \frac{1}{T_\downarrow} & \frac{1}{T_\downarrow} \\ \frac{1}{T_\uparrow} & \frac{1}{T_\uparrow} \end{pmatrix} \tag{2.82}$$

obey the useful identities

$$\underline{\Gamma}_{\mathrm{ll}}\underline{K} = 0\,, \tag{2.83}$$

$$\left(\underline{\Gamma}_{\mathrm{ll}} - \frac{1}{\lambda^2}\underline{D}_{\mathrm{ll}}\right)\underline{H} = 0\,, \tag{2.84}$$

$$\frac{2}{\lambda}\underline{D}_{\mathrm{ll}}\left(\underline{H} - \underline{K}\right) = \underline{1}\,, \tag{2.85}$$

which can be invoked to easily verify that the longitudinal Greens function $\underline{G}_{\mathrm{ll}}(x)$ in fact fulfills equation (2.77). The real part of the complex wave-vector k describes the precession of transverse non-equilibrium spin excitations, while its imaginary part is the damping due to dephasing mechanisms. Therefore, the root of k has to be chosen such that is has a positive imaginary part in order to obtain physical damping.

In the following, we restrict ourselves to the regime $\tau\Delta \gg 1$, *viz.* a momentum relaxation rate much smaller than the exchange splitting. Again, since the leading order correction term turns out to be of order q^2, we drop any terms of higher order than that. Later, we will see that this restricts the validity of the result for the DWR to domain wall lengths larger than the spin-precession length l_{prec}.

In this regime, the transverse oscillations are very rapid on the scale of the magnetization gradient. Therefore, it is suitable to eliminate the transverse degrees of freedom by first splitting the equation of motion (2.76) for $\vec{n}$ into transverse and longitudinal parts,

$$\left(\hat{\underline{\Gamma}} - \underline{\underline{D}}\partial_x^2\right)_{\mathrm{tt}}\vec{n}_{\mathrm{t}} = \underline{W}_{\mathrm{tl}}\vec{n}_{\mathrm{l}} + \underline{W}_{\mathrm{tt}}\vec{n}_{\mathrm{t}} \tag{2.86}$$

$$\left(\hat{\underline{\Gamma}} - \underline{\underline{D}}\partial_x^2\right)_{\mathrm{ll}}\vec{n}_{\mathrm{l}} = \underline{W}_{\mathrm{ll}}\vec{n}_{\mathrm{l}} + \underline{W}_{\mathrm{lt}}\vec{n}_{\mathrm{t}}\,, \tag{2.87}$$

and writing down the formal solution for the transverse component

$$\vec{n}_{\mathrm{t}}(x) = \int_{-\infty}^{\infty}\mathrm{d}x'\underline{G}_{\mathrm{tt}}(x-x')\left[\underline{W}_{\mathrm{tl}}\vec{n}_{\mathrm{l}}(x') + \underline{W}_{\mathrm{tt}}\vec{n}_{\mathrm{t}}(x')\right]\,. \tag{2.88}$$

In the limit $\tau\Delta \gg 1$, $\underline{G}_{\mathrm{tt}}(x')$ varies on a scale determined by $\frac{2\pi}{k} = l_{\mathrm{prec}}$, and is much smaller than other length scales of interest, which are variation of $\vec{m}$ and the external electric field. In particular, for the length of the domain wall, $w \gg l_{\mathrm{prec}}$. Thus, to leading order in $1/\tau\Delta$, we can consider $\underline{G}_{\mathrm{tt}}$ as a representation of the Dirac δ-function and perform the integration. We obtain

$$\vec{n}_{\mathrm{t}}(x) = \underline{\mathcal{F}}\left[\underline{W}_{\mathrm{tl}}\vec{n}_{\mathrm{l}}(x) + \underline{W}_{\mathrm{tt}}\vec{n}_{\mathrm{t}}(x)\right]\,. \tag{2.89}$$

Here we introduced the spatially integrated transverse Greens function,

$$\underline{\mathcal{F}} = \int_{-\infty}^{\infty} dx\ \underline{G}_{\mathrm{tt}}(x) = \begin{pmatrix} F & 0 \\ 0 & F^* \end{pmatrix}\,, \tag{2.90}$$

where

$$F = \frac{1}{\frac{1}{T_2} + i\Delta} \approx -i\frac{1}{\Delta} \ . \tag{2.91}$$

Note that $\underline{\mathcal{F}}$ simply corresponds to the inverse of the transverse part of $\underline{\underline{\hat{\Gamma}}}$, a fact which becomes clear by noting that our approximation corresponds to the neglect of the transverse diffusion term.

Additionally, we only need to keep the first term of (2.89), since the backaction on the transverse dynamics, represented by the second term, appears only in higher orders in q and $1/\tau\Delta$. Explicitly, this is expressed by the fact that to leading order in q, $\underline{\underline{W}}_{\mathrm{tt}}$ vanishes, so that

$$\begin{aligned} \vec{n}_{\mathrm{t}}(x) &= \underline{\mathcal{F}}\ \underline{W}_{\mathrm{tl}}\vec{n}_{\mathrm{l}}(x) + \underline{\mathcal{F}}\ \underline{W}_{\mathrm{tt}}\underline{\mathcal{F}}\ \underline{W}_{\mathrm{tl}}\vec{n}_{\mathrm{l}}(x) + \dots \\ &= \underline{\mathcal{F}}\ \underline{W}_{\mathrm{tl}}\vec{n}_{\mathrm{l}}(x) + O\left(\tfrac{1}{\tau\Delta}\right)^3 \ . \end{aligned} \tag{2.92}$$

Putting this result back into the equation for the longitudinal dynamics yields the formal solution,

$$\vec{n}_{\mathrm{l}}(x) = \int_{-\infty}^{\infty} \mathrm{d}x'\ \underline{G}_{\mathrm{ll}}(x'-x)\ \left[\underline{W}_{\mathrm{ll}}\vec{n}_{\mathrm{l}}(x') + \underline{W}_{\mathrm{lt}}\underline{\mathcal{F}}\ \underline{W}_{\mathrm{tl}}\vec{n}_{\mathrm{l}}(x')\right] \ .$$

The boundary condition (2.67) for the left and right side of the contact reads

$$\vec{n}(\pm\tfrac{L}{2}) = -e\varphi\big(\pm\tfrac{L}{2}\big)\ \ (0,0,\nu_\uparrow,\nu_\downarrow) \ . \tag{2.93}$$

With externally applied bias voltage V, the zeroth order solution that satisfies this boundary condition is simply found to be

$$\vec{n}^{(0)}(x) = eEx\ \ (0,0,\nu_\uparrow,\nu_\downarrow) \ , \tag{2.94}$$

where $E = \frac{V}{L}$ is the constant external electric field in absence of the wall.

Substituting $\vec{n}^{(0)}(x)$ into the right-hand side of the solution (2.93) yields the second order correction in q, $\vec{n}^{(2)}(x)$. Due to charge-current conservation, the current flowing through the contact is still determined by $\vec{n}^{(0)}$ because $\partial_x\vec{n}^{(2)}(x)$ is taken to vanish at the boundaries by assuming that the contact is long enough for any finite size effects to become negligible, i.e. $L \gg \lambda$. In this regime, the exponential term in the longitudinal Greens function (2.78) can be neglected, which means that spin-accumulation has faded near the reservoirs. Then the current can be deduced directly from Eqs. (2.94), unaffected by the correction $\vec{n}^{(2)}$. Explicitly, this current reads

$$\vec{j}^{(0)} = -\underline{\underline{D}}\partial_x\vec{n}^{(0)} = -\frac{1}{e}\,(0,0,\sigma_\uparrow,\sigma_\downarrow)\,E \ , \tag{2.95}$$

where the spin-resolved Drude conductivity of majority and minority spin channels is given as usually by $\sigma_{\uparrow,\downarrow} = e^2\nu_{\uparrow,\downarrow}D_{\uparrow,\downarrow}$. Note that the additional factor $-1/e$ is due to our definition of $\vec{n}$ and $\vec{j}$ as particle densities, since they constitute a combined vector of spin- and charge degrees.

However, $\vec{n}^{(2)}(x)$ has an additional potential drop that is extracted from the asymptotic behavior and that stems from the second term in $\underline{G}_{\mathrm{ll}}(x)$,

$$-e\delta V\nu_0 = n_{\mathrm{c}}^{(2)}(x\to+\infty) - n_{\mathrm{c}}^{(2)}(x\to-\infty) = 2n_{\mathrm{c}}^{(2)}(x\to\infty) \ . \tag{2.96}$$

Here, we used that the charge component is $n_c = n_\uparrow + n_\downarrow$ and the second equality is due to symmetry of the contact. Keeping the current constant, the presence of the wall implies a change in the externally applied potential, which directly translates into a relative change in resistance. Hence, we define the DWR

$$\delta\rho_{\mathrm{DW}} \equiv \frac{\rho_{\mathrm{DW}} - \rho_0}{\rho_0} = \frac{\delta V}{V} = \frac{2\ n_{\mathrm{c}}^{(2)}(x \to \infty)}{n_{\mathrm{c}}^{(0)}(+L/2) - n_{\mathrm{c}}^{(0)}(-L/2)} \ . \tag{2.97}$$

Of course, due to the perturbative nature of our treatment, the correction $n^{(2)}$ has to be always smaller than $n^{(0)}$. Since it turns out that

$$\vec{n}^{(2)}(x \to \pm\infty) = \delta\rho_{\mathrm{DW}}\ \vec{n}^{(0)}(\pm\tfrac{L}{2}) \tag{2.98}$$

this condition is equivalent to $\delta\rho_{\mathrm{DW}} \ll 1$, which is always the case in the regime considered here.

Finally, let us stress that the reason for the inclusion of the moments up to $\hat{g}^{(4)}$ lies in the fact that in our regime of investigation, the precession length $l_{\mathrm{prec}} \equiv 2\pi\frac{v_{\mathrm{F}}}{\sqrt{3}\Delta}$ is, besides the Fermi-length, the smallest length scale in the system. As can be seen from the equation (2.79), l_{prec} describes the period of oscillation of transverse spin excitations. In the diffusive approximation, as for example used by Bergeret *et al.* [38], the scattering mean free path l_{s} is the smallest length scale in the system (besides the Fermi wave length) and not l_{prec}. Hence, it is possible to truncate the hierarchy of equations already by $\hat{g}^{(3)} = 0$, which results in only two equations that are just the spin-charge continuity and diffusion equation. In our treatment, the diffusion equation is obtained by plugging the equation for $\hat{g}^{(2)}$ into the equation for $\hat{g}^{(1)}$ (see also Appendix C for more details).

Screened versus unscreened spin-charge density excitations

We mentioned before that the transformation (2.63) introduces unscreened quantities. To illustrate this more explicitly, let $\vec{n}$ represent the unscreened spin-charge density excitations, while the true, screened quantity $\vec{n}^{(s)}$ is (see also Eq. (2.63))

$$-\,e n_{\uparrow,\downarrow}^{(s)}(x) = -e n_{\uparrow,\downarrow}(x) - \nu_{\uparrow,\downarrow}(x) e^2 \varphi(x) \ . \tag{2.99}$$

Here, only charge-excitations are assumed to be screened while spin-excitations remain unscreened since our model does not include a spin-dependent interaction. The former charge screening is implicitly incorporated by enforcing local charge neutrality, while physically, it is a result of the Coulomb interaction not explicitly included in our work. For reasons of simplicity, we only consider the homogeneous case $q = 0$. Charge neutrality then dictates that

$$n_\uparrow^{(\mathrm{s})}(x) + n_\downarrow^{(\mathrm{s})}(x) = 0 \ , \tag{2.100}$$

so that $n_s^{(\mathrm{s})}(x) = n_\uparrow^{(\mathrm{s})}(x) - n_\downarrow^{(\mathrm{s})}(x) = 2n_\uparrow^{(\mathrm{s})}(x) = -2n_\downarrow^{(\mathrm{s})}(x)$. The chemical potential is related to the screened density by

$$\tilde{\mu}_{\uparrow,\downarrow}(x) = \frac{-1}{e\nu_{\uparrow,\downarrow}} n_{\uparrow,\downarrow}^{(\mathrm{s})}(x) = -e\frac{D_{\uparrow,\downarrow}}{\sigma_{\uparrow,\downarrow}} n_{\uparrow,\downarrow}^{(\mathrm{s})}(x) \ , \tag{2.101}$$

where we made use of the Einstein relation $\sigma_{\uparrow,\downarrow} = e^2 \nu_{\uparrow,\downarrow} D_{\uparrow,\downarrow}$. Analogously, we introduce the electrochemical potential which is linked to the unscreened density via

$$\mu_{\uparrow,\downarrow}(x) = \frac{-1}{e\nu_{\uparrow,\downarrow}} n_{\uparrow,\downarrow}(x) = -e\frac{D_{\uparrow,\downarrow}}{\sigma_{\uparrow,\downarrow}} n_{\uparrow,\downarrow}(x) = \frac{-1}{e\nu_{\uparrow,\downarrow}} n^{(s)}_{\uparrow,\downarrow}(x) - e\varphi(x) = \tilde{\mu}_{\uparrow,\downarrow}(x) - e\varphi(x) \ . \quad (2.102)$$

Therefore, the diffusion equation becomes

$$j_{\uparrow,\downarrow} = \frac{\sigma_{\uparrow,\downarrow}}{e} \partial_x \mu_{\uparrow,\downarrow} \ , \quad (2.103)$$

and since

$$\frac{1}{T_\uparrow} n_\uparrow - \frac{1}{T_\downarrow} n_\downarrow = \frac{\nu_\downarrow}{2\nu_0 T_1} n^{(s)}_\uparrow - \frac{\nu_\uparrow}{2\nu_0 T_1} \underbrace{n^{(s)}_\downarrow}_{=-n^{(s)}_\uparrow} = \pm \left(\frac{\nu_\downarrow}{2\nu_0 T_1} + \frac{\nu_\uparrow}{2\nu_0 T_1} \right) n^{(s)}_{\uparrow,\downarrow} \ , \quad (2.104)$$

the continuity equation simply becomes

$$\partial_x j_{\uparrow,\downarrow} = -\frac{1}{T_1} n^{(s)}_{\uparrow,\downarrow} \ . \quad (2.105)$$

When using the electrochemical potential or the unscreened density, one has access to the local screening potential which is directly related to $n_{\uparrow,\downarrow}$ by virtue of relation (2.65). Then, knowing $n_{\uparrow,\downarrow}$ and $\varphi(x)$, one can readily obtain the screened density $n^{(s)}_{\uparrow,\downarrow}(x)$. However, the latter is the physically relevant quantity, while the local screening potential and the unscreened density are not directly seen in experiment.

Note that the spin-chemical potential is

$$\mu_s(x) = \mu_\uparrow(x) - \mu_\downarrow(x) = \tilde{\mu}_\uparrow(x) - \tilde{\mu}_\downarrow(x) = -\frac{1}{2e} \left(\frac{1}{\nu_\uparrow} + \frac{1}{\nu_\downarrow} \right) n^{(\mathrm{s})}_s(x) \ ,$$

and finally, the magnetic susceptibility χ relates μ_s and the induced magnetization $\delta M = \mu_\mathrm{B} n^{(\mathrm{s})}_s(x)$ via

$$(-e)\mu_s = \mu_\mathrm{B} \frac{\delta M}{\chi} \ ,$$

so that we obtain the Pauli susceptibility ($\mu_\mathrm{B} = \frac{e\hbar}{2m_\mathrm{e}}$)

$$\chi = \mu_\mathrm{B}^2 \frac{2\nu_\uparrow \nu_\downarrow}{\nu_\uparrow + \nu_\downarrow} \ . \quad (2.106)$$

2.3.5. Results and Discussion of the Domain-wall Resistance

Up to order $q^2 = (\partial_x \vec{m}(x))^2$ and neglecting terms of order $\frac{1}{(\tau\Delta)^2}$, the domain-wall resistance takes the form

$$\delta\rho_\mathrm{DW} \equiv \frac{\rho_\mathrm{DW} - \rho_0}{\rho_0} = E_\mathrm{w} \ \zeta \left(\frac{\Delta}{2E_\mathrm{F}}, \frac{\tau}{T_1}, \frac{\tau}{T_2} \right) \ , \quad (2.107)$$

where the function ζ will be discussed in a moment and analogously to Ref. [34], we introduce the domain wall energy

$$E_\mathrm{w} = \frac{\hbar^2}{2m_\mathrm{e}E_\mathrm{F}} \ \frac{1}{L} \int_{-L/2}^{+L/2} q^2(x)\mathrm{d}x = \frac{\hbar^2}{2m_\mathrm{e}E_\mathrm{F}} \ \frac{C}{wL} \ , \quad (2.108)$$

which here is dimensionless by defining it in units of the Fermi energy E_F. The constant C of order unity depends on the specific form of the wall and we find the geometric scaling to be $1/wL$. For the domain wall profile of Eq. (2.62), we obtain $C = 2$. The scaling with $1/wL$ can be easily understood by realizing that corrections to the resistance arising from a gradient q yield the behavior $\delta\rho_\mathrm{DW} \propto q^2 \propto \frac{1}{w^2}$. Due to physical reasons there cannot be a correction linear in q since the result should not depend on the sign of q, i.e. the sense of rotation of $\vec{m}$. Since the total length of the contact is L and the domain wall constitutes only a fraction w/L, the correction for the whole contact should indeed be $\delta g \propto 1/wL$.

A thorough investigation of the whole hierarchy of equations reveals that the result obtained for $\delta\rho_\mathrm{DW}$ is valid for wall lengths much larger than the spin-precession length, $w \gg l_\mathrm{prec}$. The mathematical reason for this condition is that, even though in the vicinity of the domain wall the detailed profile of the quasi-particle excitations $n^{(2)}(x)$ depends on the whole hierarchy of equations (unless $w \gg l_\mathrm{sd}$, with the transverse spin-diffusion length $l_\mathrm{sd}^2 \equiv T_2 D_\perp$), the asymptotic behavior of the correction $n^{(2)}(x)$, is not affected by higher order contributions of the multipole expansion. And in situations, in which finite size effects from the contact geometry are negligible, $\delta\rho_\mathrm{DW}$ is solely determined by these asymptotics. In short, to obtain the asymptotics, and thus the desired result valid up to order q^2, we need to take into account contributions only up to $\vec{g}^{(4)}$.

We note that our model of impurity scattering has 3 independent parameters, however, in the limit $\Delta\tau \gg 1$, we find that result (2.107) depends only on the two combinations $\frac{\tau}{T_1}$ and $\frac{\tau}{T_2}$, so effectively, one has to deal with only 2 parameters. The situations changes in higher orders of $\frac{1}{\tau\Delta}$, which however is not subject of the present work.

Before continuing with the discussion, let us reconsider the assumptions made during the derivation of result (2.107), $\tau\Delta \gg 1$ and $w \gg l_\mathrm{prec}$ along with (2.2). The former can be rewritten as $l_\mathrm{s} \gg l_\mathrm{prec}$ where l_s denotes the scattering mean free path. This in fact implies that l_prec is, besides the Fermi-length, the smallest length scale in the system. Note that no assumption was made on the relation between l_s and the length of the domain wall. However, we made the assumption of a diffusive contact which implies that $L \gg l_\mathrm{s}$.

Quasiclassical Regime $\Delta \ll E_\mathrm{F}$

Let us first investigate the limit $\Delta \ll E_\mathrm{F}$ *viz.* $P \ll 1$, commonly referred to as the quasi-classical regime. Note that for $\frac{\Delta}{2E_\mathrm{F}}, P \ll 1$, we have the simple relation $P = \frac{\Delta}{4E_\mathrm{F}} + O(\frac{\Delta}{E_\mathrm{F}})^3$. However, due to the restrictions imposed upon l_prec and discussed above, Δ cannot become arbitrarily small. In this regime, corrections to the electron density of states play no role and the density of states can be considered constant. Also, it turns out that gradient corrections to the self-energies play no role so that only the contribution from impurity scattering remains. We find in this limiting case

$$\zeta\left(P, \frac{\tau}{T_1}, \frac{\tau}{T_2}\right) \overset{P\ll 1}{\to} \frac{\tilde{\gamma}^2}{1-\tilde{\gamma}^2}\frac{1}{15P^2} \ , \tag{2.109}$$

with the scattering asymmetry parameter $\tilde{\gamma} = P(1 - \tau/T_1)$. We dropped a correction term of order τ/T_2 due to spin-dephasing, and here, we only refer to the complete result in the limit $P \to 0$ in equation (2.149) along with a discussion in section 2.4.5. At the moment, we

have in mind to compare our result with other existing theoretical works that generally do not treat spin-dependent scattering explicitly.

This result shows the strong enhancement by scattering asymmetry $\tilde{\gamma}$ as already noted in previous works [34]. It also displays the same Δ-dependence already found in various other works. Clearly, this result is due to different conductivities in the two spin channels which are mixed in regions of non-vanishing magnetization gradient q. A spin-up electron incident on a domain wall attains a spin-down component since electron spin direction does not instantaneously follow the local magnetization direction $\vec{m}$ (known as spin mistracking). Since the electronic spectrum plays no role in this limit, any asymmetry in the conductivity of the two channels is due to the scattering asymmetry $\tilde{\gamma}$, thus, there is no DWR as $\tilde{\gamma} \to 0$.

Note that the scattering asymmetry parameter in the works [33, 34, 35] is phenomenological, and thus does not vanish as $\Delta, P \to 0$. This is contrary to our study, where our scattering asymmetry is $\tilde{\gamma} = P\gamma$ instead, which exactly cancels the diverging $1/P^2$ in expression (2.109), and thus, our result remains finite in the limit $\Delta, P \to 0$. This remains a problem in the work of Brataas and coworkers [34], since there the impurity scattering times are introduced phenomenologically and thus, in their scenario no constriction is placed upon $\tilde{\gamma}$.

Comparing this result with the works [33, 34, 35], we find in this limit a different numerical prefactor and adopting to our notation, the authors mentioned found $\delta R_{\mathrm{DW}} = \frac{3}{5}\frac{\tilde{\gamma}^2}{1-\tilde{\gamma}^2}\frac{1}{4P^2}E_{\mathrm{w}}$. To fathom this discrepancy, we stress that the specific form of the longitudinal Greens function $\underline{G}_{\mathrm{ll}}(x)$ is a result of the presence of spin-flip processes. In absence on these processes (which is the case in aforementioned works), the spin-diffusion length diverges, so that properly performing this limit yields the longitudinal Greens function $\underline{G}_{\mathrm{ll}}(x) = \underline{\underline{H}}e^{-\frac{|x|}{\lambda}} + \underline{\underline{K}}\frac{|x|}{\lambda} \to (\underline{\underline{K}} - \underline{\underline{H}})\frac{|x|}{\lambda}$, which produces qualitatively different results. This additional contribution persists arbitrarily far away from the domain wall and leads to a different result for $\delta\rho_{\mathrm{DW}}$. Then calculating the DWR in the quasiclassical limit, we find that it is still smaller by a factor of 2 as compared to the result in [34]. Nevertheless, this shows that spin-flip processes are crucial and cannot be ignored, since the absence of the latter leads to spin accumulation that does not decay even infinitely far away from the domain wall and thus yields an additional contribution to the DWR.

Concerning the work of [32], the main critic has been mentioned in the introduction. Even restricting ourselves to the quasiclassical regime, the use of a system consisting of an infinite spin-spiral, the inclusion of only up to p-wave component and the lack of terms due to gauge transformation can be invoked to explain the discrepancy to our fully microscopic results.

Arbitrary exchange splitting $\Delta < 2E_{\mathrm{F}}$

Let us now have a closer look at the behavior in the whole range of valid values for Δ. In this regime, the gradient corrections in the collision integral become important, and so is the influence of the magnetization gradient on the electronic structure, *viz.*, the density of states.

In the half metallic limit, the spin-flip length becomes arbitrarily small, since $\lambda \to 0$ as $\Delta \to 2E_{\mathrm{F}}$, or equivalently, $P \to 1$. Writing $\Delta = 2E_{\mathrm{F}} - \epsilon$ and owing to the condition that no length should exceed the precession length $l_{\mathrm{prec}} \ll \lambda$, we obtain the requirement that

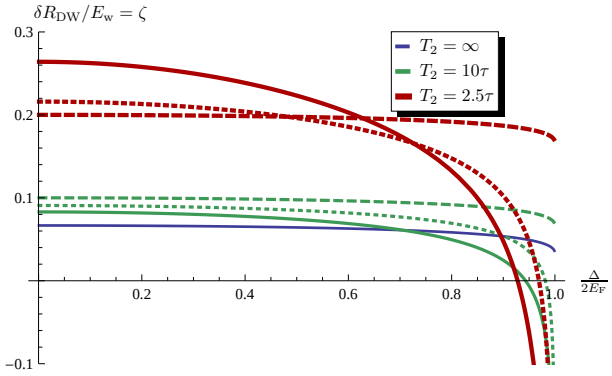

Figure 2.3.: Domain-wall resistance $\delta\rho_{\mathrm{DW}} = E_{\mathrm{w}}\,\zeta\left(\frac{\Delta}{2E_{\mathrm{F}}}, \frac{\tau}{T_1}, \frac{\tau}{T_2}\right)$ in the *s-d* limit as a function of exchange splitting Δ for the CPW geometry and for different values of spin-dephasing time T_2. The spin-flip time is linked to T_2 as follows: $T_1 = \infty$ (dashed), $T_1 = T_2$ (dotted), $T_1 = \frac{T_2}{2}$ (solid).

$\frac{\epsilon^2}{1-P\gamma} \gg \frac{1}{\tau T_1}$. However, this is not a big restriction considering our assumption that scattering is weak, so that $\tau, T_1, T_2 \gg 1/E_{\mathrm{F}}$.

For various values of T_1 and T_2, the DWR is shown in figure 2.3 as a function of exchange splitting. Note that this plot is identical to figure 2.5(a) with the only different that the diagram shown there is plotted as a function of P, the polarization of the density of states.

We can see that the DWR does not vary strongly with Δ when this parameter is small and decreases monotonously as Δ increases even to the point where the DWR can become negative as one approaches the half metallic regime. The latter happens only in the case of non-vanishing spin-flip scattering between the two bands.

This clearly is a band structure effect and we find that this also requires the inclusion of corrections to the collision integral. It turns out that the presence of a magnetization gradient modifies the density of states so that there are corrections of order q^2 to the scattering rates that decrease the momentum relaxation rate and thus, a reduction in resistivity. Furthermore, we find that the neglect of said corrections leads to a monotonic increase of the DWR with increasing Δ as opposed to the present result. As a side note, we remark that it is important to include corrections to the collision integral up to the same order as in the approximation of the transport part of the kinetic equation in order for the calculation to be consistent. However, predictions for a given material would require realistic band structure calculations, but the present calculation demonstrates the possibility to have a negative DWR.

Let us finally compare our approach to the one of Brataas *et al.* [34] by temporarily excluding spin-flip processes. In that case, we obtain for the domain wall resistance a strictly monotonic increase with Δ compatible to the findings of Brataas *et al.*, in particular, there is no negative DWR.

Summary and conclusions

All previous works dealing with DWR in the limit of wide walls obtain results that depend in a similar way on the microscopic parameters, that is, the DWR is essentially given by $C\alpha^2$, where C is a dimensionless prefactor and $\alpha = \frac{\hbar v_F}{\Delta w}$ is the spin mistracking angle. Hence, every theory predicts this sort of dependence, but with different proportionality factors, both in value and sign. This factor C however contains information about the scattering and DOS of the two spin channels and can depend in a complex manner on these properties. The most simple one is due to a model by Levy and Zhang [32], where C simply depends on the ratio of resistivities for spin up and down channels.

We did not take into account the possibility of magnetic moment softening, i.e. the reduction of the magnetic moment within the domain wall. This effect is most prominent in very sharp domain walls where canting of adjacent spin is large so that the non collinear spin states hybridize, which in turn leads to a reduction in the absolute value of the magnetic moment. As shown in [35], a reduction of the magnetic moment can lead to a negative DWR. In the next section, we will explicitly investigate this effect by also studying the Stoner model of itinerant ferromagnetism, in addition to the *s-d* model treated in this section. Furthermore, in the next section, we will pursue a slightly different approach to solve our kinetic equation and we will have the ability to study more complex magnetic textures, including the domain-wall resistance thereof, along with other interesting effects.

Finally, effects due to geometric confinement have not been considered, for example, surface scattering might become important. Also, the magnetization profile can be more complicated and might lead to eddy currents in the vicinity of the domain wall which might be relevant for interpretation of experimental results on the DWR in thin nanowires.

Having discussed our result in relation to other existing calculations of the DWR, we refer to section 2.4.5 for a more general and more detailed discussion of the DWR, including the current-in-wall (CIW) geometry and the treatment of the Stoner model.

2.4. Electron Transport in Presence of Inhomogeneous and Time-dependent Magnetization

Here, we present an alternative solution of the kinetic equations, which is mathematically compatible to the solution method and approximations of the previous section. However, the treatment in this section is extended to include time-dependent situations and also general magnetization textures which can vary in all directions of space. Nevertheless, the previous method enlightened some other aspects ignored in the following, like spin-diffusion. Thus, both treatments complement one another.

In order to deal with Eqs. (2.44)-(2.47), we introduce the moments of the Greens function $\hat{g}$,

$$\begin{aligned} \hat{n}(\boldsymbol{r},t) &= \int \frac{\mathrm{d}^3k}{(2\pi)^3}\hat{g}(\boldsymbol{k},\boldsymbol{r},t) \equiv \langle \hat{g} \rangle \\ \hat{\boldsymbol{j}}(\boldsymbol{r},t) &= \langle \boldsymbol{v}_{\boldsymbol{k}}\hat{g} \rangle \\ \underline{\underline{\hat{T}}}(\boldsymbol{r},t) &= \left\langle \left(\boldsymbol{v}_{\boldsymbol{k}} \circ \boldsymbol{v}_{\boldsymbol{k}} - \underline{\underline{1}}\frac{1}{3}v_{\boldsymbol{k}}^2 \right)\hat{g} \right\rangle \ , \end{aligned} \tag{2.110}$$

where the second moment $\underline{\underline{\hat{T}}}$ is defined such that the isotropic part is projected out. Note that the definitions represent quasi-particle densities, so in order to obtain the respective charge-densities, we simply have to multiply by the factor $(-e)$. We do not need more than the first three moments for the present study up to second order spatial magnetization gradients. More details are presented in Appendix D, and the resulting equations (D.4)-(D.6) can then be solved analytically by expanding into gradients of the magnetization and assuming rapid transverse precession as well as a sufficiently small spin-diffusion length, so that spin-accumulation plays no role on average. Note that for certain quantities averaged over the whole magnetization structure, like for the domain-wall resistance treated in section 2.3, it turns out that the condition of small spin-diffusion length can be relaxed by saying that any spin-accumulation due to the DW has decayed at the leads. This amounts to saying that the leads have to be much farer away from the domain-wall as compared to the spin-diffusion length. In the present study however, we neglect the spin-diffusion which would lead to a smearing of the spin-accumulation on the length scale of the spin-diffusion length.

2.4.1. Magnetization Gradient Corrections in Equilibrium

Let us first investigate the implications of an inhomogeneous magnetization in the absence of external perturbations so that the system is in equilibrium. For the gradient corrections $\delta\rho_s$ to the equilibrium magnetization density of the conduction electrons $\rho_{s,\boldsymbol{r}} \equiv \rho_s - \delta\rho_s$, we find

$$\begin{aligned} \delta\rho_s^{(\mathrm{sd})} &= \frac{\nu_0 P(5+3P^2)}{60 m_\mathrm{e}} \left(\boldsymbol{\partial}_r \vec{m}\right)^2 = \frac{2}{3}\nu_\mathrm{s} P\, \delta\Delta \ , \\ \delta\rho_s^{(\mathrm{St})} &= \frac{\nu_0 (3+P^2)(5+3P^2)}{240 m_\mathrm{e} P} \left(\boldsymbol{\partial}_r \vec{m}\right)^2 = \rho_s \frac{\delta\Delta}{\Delta} \ , \end{aligned} \tag{2.111}$$

i.e. $\rho_{s,\boldsymbol{r}}^{(\mathrm{St})} = (1 - \frac{\delta\Delta}{\Delta})\rho_s$ and the spin-density of states is $\nu_\mathrm{s} = P\nu_0$. Of course, the result for the itinerant Stoner model is not surprising, since according to section 2.2.5, $\Delta = U\rho_s$ and the proportionality remains when ρ_s becomes spatially dependent, i.e. $\Delta_{\boldsymbol{r}} = \Delta - \delta\Delta_{\boldsymbol{r}} = U\rho_{s,\boldsymbol{r}}^{(\mathrm{St})}$.

Furthermore, magnetization gradients induce a transverse equilibrium spin density which to leading order gradient correction reads

$$\hat{N}_{\rm xc} = \nu_0 \frac{(\boldsymbol{\partial}_r^2 \vec{m})_\perp \hat{\vec{\sigma}}}{2m_{\rm e}} \frac{P(5-P^2)}{30} = \frac{A}{\Delta} (\boldsymbol{\partial}_r^2 \vec{m})_\perp \hat{\vec{\sigma}} \tag{2.112}$$

and constitutes the exchange interaction contribution of the conduction electrons, as will become apparent in section 2.5.2. A corresponds to the exchange constant calculated within the Stoner model. The spin-charge current reads to leading order correction

$$\hat{\boldsymbol{J}}_{\rm xc} = -A(\vec{m} \times \boldsymbol{\nabla} \vec{m}) \hat{\vec{\sigma}} \ , \tag{2.113}$$

which is a pure spin current transverse to the local magnetization direction $\vec{m}$ and constitutes the spin-exchange current which transfers spin-angular momentum such that it tends to homogenize the magnetization texture. This interpretation is also supported by the common prefactor A, the exchange constant. From result (2.112), it is obvious that A vanishes as Δ^2 for $\Delta \to 0$.

In the third order correction, it is interesting to note that the equilibrium current not only constitutes a spin-current, but also a persistent charge current,

$$\boldsymbol{J}_{\rm eq,c} = {\rm Tr} \hat{\boldsymbol{J}}_{\rm eq}^{(3)} = \frac{\nu_0 P^3}{60 m_{\rm e}^2} \ \boldsymbol{\partial}_r \left[\vec{m} \cdot (\boldsymbol{\nabla} \vec{m} \times \boldsymbol{\partial}_r \vec{m}) \right] \ , \tag{2.114}$$

where the prefactor vanishes as Δ^3 for $\Delta \to 0$, a dependence which was also found by Tatara *et al.* in Refs [65, 66]. In this and the following expressions, our convention is that gradients $\boldsymbol{\partial}_r$ appear pairwise and should be contracted like in $\boldsymbol{\partial}_r \vec{m} \cdot \boldsymbol{\partial}_r \vec{m} = \partial_x \vec{m} \cdot \partial_x \vec{m} + \partial_y \vec{m} \cdot \partial_y \vec{m} + \partial_z \vec{m} \cdot \partial_z \vec{m}$, while the expression inherits its vector character from the single $\boldsymbol{\nabla}$. As it should be, this term does not violate charge conservation, since $\boldsymbol{\nabla} \cdot \boldsymbol{J}_{\rm eq,c} = 0$ and $\boldsymbol{J}_{\rm eq,c}$ is non-vanishing only in more complex magnetization structures like in vortices. This term can also be rewritten in terms of the fictitious magnetic field due to the Berry curvature, $\mathcal{B}_i = \frac{\epsilon_{ijk}}{2} \vec{m} \cdot (\partial_k \vec{m} \times \partial_j \vec{m})$ (c.f. Eq. (2.154)), so that

$$\boldsymbol{\nabla} \times \boldsymbol{\mathcal{B}} = \boldsymbol{\partial}_r \left[\vec{m} \cdot (\boldsymbol{\partial}_r \vec{m} \times \boldsymbol{\nabla} \vec{m}) \right] \ , \tag{2.115}$$

and thus, up to a prefactor, coinciding with the expression $\boldsymbol{J}_{\rm eq,c}$. This persistent charge current is such that the magnetic field it creates by virtue of $\mu_0 \mu \boldsymbol{J}_{\rm eq,c} = \boldsymbol{\nabla} \times \boldsymbol{B}_{\rm c}$ screens part of the fictitious magnetic field it originates from. Translated back into the picture of the original magnetization profile, this diamagnetic current attempts to homogenize the magnetization structure. On the other side, we can also argue that the fictitious magnetic field (2.154) or Berry curvature gives rise to a Lorentz force leading to curved orbits of the conduction electrons, which correspond to real diamagnetic currents. One can also motivate the persistent spin and charge currents by breaking of the time-reversal symmetry due to the non-commutativity of the SU(2) spin-algebra [67, 65]. The equilibrium currents derived in Ref. [68] are obtained in the limit $\Delta \to 0$ and are compatible with our expressions.

2.4.2. Spin-Charge Continuity and Diffusion Equation

In this part, we will investigate the kinetic equations in some more detail, since they are underlying the results to be presented in the remaining part of this chapter. We will explore

some implications of these equations, to which we will refer back in the discussions of the subsequent sections. Also, we will be able to compare our kinetic equation to other theories available in literature.

In this part of our work, high energy terms give important contributions to the results. In an attempt to include the high-energy part into our equations, let us write the equation (2.39) for the spectral density to leading order in time-gradients and electric field,

$$\partial_{\mathrm{neq}}\hat{A} + \boldsymbol{v}_k(\boldsymbol{\partial}_r - e\boldsymbol{E}\partial_w)\hat{A} + \frac{1}{2i}\left[\Delta_{\boldsymbol{r}}\vec{m}\hat{\vec{\sigma}} \circ \hat{A}\right] + (\boldsymbol{\partial}_r\delta\mu)\boldsymbol{\partial}_k\hat{A} + \frac{1}{2}\left\{\partial_t\hat{H} \circ \partial_w\hat{A}\right\} = 0 \ , \quad (2.116)$$

where $\Delta_{\boldsymbol{r}} \equiv \Delta - \delta\Delta$ denotes the magnitude of the exchange field with gradient-corrections included and $\hat{H}$ is the Hamilton Operator defined in Eq. (2.1). Using $\boldsymbol{v}_k = \boldsymbol{\partial}_k\epsilon_{\boldsymbol{k}} = \boldsymbol{\partial}_k\hat{H}$ and the definition $\partial_{\mathrm{neq}} \equiv \partial_t - e\boldsymbol{E}\boldsymbol{\partial}_k$, we can also write

$$\partial_{\mathrm{neq}}\hat{A} + \boldsymbol{v}_k\boldsymbol{\partial}_r\hat{A} + \frac{1}{2i}\left[\Delta_{\boldsymbol{r}}\vec{m}\hat{\vec{\sigma}} \circ \hat{A}\right] + (\boldsymbol{\partial}_r\delta\mu)\boldsymbol{\partial}_k\hat{A} + \frac{1}{2}\left\{\partial\hat{H} \circ \partial_w\hat{A}\right\} = 0 \ . \quad (2.117)$$

The high energy contribution is simply given by $\hat{g}_{\mathrm{h}} = \int \frac{\mathrm{d}\omega}{2\pi}\hat{A}f_{\mathrm{D}}(\omega)$, so that the total Greens function is $\hat{\mathcal{G}}(\boldsymbol{k},\boldsymbol{r},t) = \hat{g}_{\mathrm{h}}(\boldsymbol{k},\boldsymbol{r},t) + \hat{g}(\boldsymbol{k},\boldsymbol{r},t)$. Therefore, we multiply the equation for $\hat{A}$ by f_{D}, integrate over ω and partially integrate the derivate in the last term

$$\int \frac{\mathrm{d}\omega}{2\pi}f_{\mathrm{D}}(\omega)\frac{\partial\hat{A}}{\partial\omega} = \int \frac{\mathrm{d}\omega}{2\pi}\left(-\frac{\partial f_{\mathrm{D}}(\omega)}{\partial\omega}\right)\hat{A} = \frac{1}{2\pi}\hat{A}(\boldsymbol{k}, E_{\mathrm{F}}, \boldsymbol{r}, t)$$

invoking the zero-temperature approximation. We immediately see that the last term exactly corresponds to the source term $\hat{\mathcal{J}}_{\mathrm{t}}$ in Eq. (2.46), thus yielding

$$\partial_{\mathrm{neq}}\hat{g}_{\mathrm{h}} + \boldsymbol{v}_k\boldsymbol{\partial}_r\hat{g}_{\mathrm{h}} + \frac{1}{2i}\left[\Delta_{\boldsymbol{r}}\vec{m}\hat{\vec{\sigma}} \circ \hat{g}_{\mathrm{h}}\right] + (\boldsymbol{\partial}_r\delta\mu)\boldsymbol{\partial}_k\hat{g}_{\mathrm{h}} = -\hat{\mathcal{J}}_{\mathrm{t}} \ . \quad (2.118)$$

Adding the two equations for low- and high-energy dynamics (effectively restoring the $\partial_{\mathrm{neq}}\hat{g}$ term in Eq. (2.44)), the term $\hat{\mathcal{J}}_{\mathrm{t}}$ cancels, leaving only the contribution $\hat{\mathcal{J}}_{\mathrm{c}}$. We explicitly write the kinetic equation for the total quantity $\hat{\mathcal{G}}(\boldsymbol{k},\boldsymbol{r},t) = \hat{g}_{\mathrm{h}} + \hat{g}$,

$$\partial_{\mathrm{neq}}\hat{\mathcal{G}} + \boldsymbol{v}_k\boldsymbol{\partial}_r\hat{\mathcal{G}} + \frac{1}{2i}\left[\Delta_{\boldsymbol{r}}\vec{m}\hat{\vec{\sigma}} \circ \hat{\mathcal{G}}\right] + (\boldsymbol{\partial}_r\delta\mu)\boldsymbol{\partial}_k\hat{\mathcal{G}} = \hat{\mathcal{J}}_{\mathrm{c}} + \hat{\mathcal{I}}[\hat{g}] = \hat{\mathcal{I}}[\hat{\mathcal{G}}] + \hat{\mathcal{J}}_{\mathrm{eff}} \ , \quad (2.119)$$

where we used the linearity of the collision integral $\hat{\mathcal{I}}$ and we introduced

$$\hat{\mathcal{J}}_{\mathrm{eff}} \equiv \hat{\mathcal{J}}_{\mathrm{c}} - \hat{\mathcal{I}}[\hat{g}_{\mathrm{h}}] = \int \frac{\mathrm{d}\omega}{2\pi}\ \hat{\mathcal{I}}_\omega[\hat{A}(\omega)f_{\mathrm{D}}(\omega)] - \hat{\mathcal{I}}\left[\int \frac{\mathrm{d}\omega}{2\pi}\hat{A}f_{\mathrm{D}}(\omega)\right] \ . \quad (2.120)$$

Here, $\hat{\mathcal{I}}_\omega$ is the fully energy dependent collision integral from Eq. (2.38), while $\hat{\mathcal{I}}$ describes only low-energy collisions and is defined in (2.45). $\hat{\mathcal{J}}_{\mathrm{eff}}$ comprises important high-energy contributions to the collision integral and appears as a source term. Essentially, $\hat{\mathcal{J}}_{\mathrm{eff}}$ defines a quasi-equilibrium distribution which takes into account situations of external perturbations like time-dependence and external electric field described by ∂_{neq}. We will better understand what it represents, when deriving continuity and diffusion equations in a moment.

Formally, this equation corresponds to the previous equation for the low-energy dynamics, Eq. (2.44), except that the low-energy Greens function $\hat{g}$ is replaced by the total Greens function

$\hat{\mathcal{G}}$, while instead of the two sources $\hat{\mathcal{J}}_{\rm t}$ and $\hat{\mathcal{J}}_{\rm c}$, we have $\hat{\mathcal{J}}_{\rm eff}$. Note that now, we cannot neglect the term $\partial_{\rm neq}\hat{\mathcal{G}} \approx \partial_{\rm neq}\hat{g}_{\rm h}$. So in effect, we have to make the following adjustments to Eqs. (D.4)-(D.6) in order to obtain the new set of equations for the total quantities: replace the low energy densities by their total density counterparts, i.e. $\hat{n} \to \hat{N}$, $\hat{\boldsymbol{j}} \to \hat{\boldsymbol{J}}$, $\underline{\underline{\hat{T}}} \to \underline{\underline{\hat{T}}}_{\rm tot}$, replace the source terms $\hat{\mathcal{J}}_{\rm t} + \hat{\mathcal{J}}_{\rm c}$ by $\hat{\mathcal{J}}_{\rm eff}$ and add the term $\partial_{\rm neq}\hat{N}$, $\partial_{\rm neq}\hat{\boldsymbol{j}}$, etc.

Applying this procedure to the spin-charge continuity equation (D.4), we obtain

$$\partial_t \hat{N} + \underline{\underline{\hat{\Gamma}}}\hat{N} + \frac{\Delta_{\boldsymbol{r}}}{2i}\left[\vec{m}\hat{\vec{\sigma}}, \hat{N}\right] + \boldsymbol{\partial}_r \hat{\boldsymbol{J}} = \hat{N}_{\rm eff} = \hat{\mathcal{J}}_c^{(0)} + \underline{\underline{\hat{\Gamma}}}\hat{N}_{\rm h} \ , \tag{2.121}$$

where the source term explicitly reads

$$\begin{aligned}\hat{N}_{{\rm eff},\perp} = \big[&\beta A(\boldsymbol{\partial}_r^2\vec{m})_\perp + (\alpha\rho_s + \delta\alpha_{\boldsymbol{r}})\vec{m}\times\partial_t\vec{m} \\ &+\beta\alpha_1^{\rm nloc}\vec{m}\times\partial_t\boldsymbol{\partial}_r^2\vec{m} + \beta\alpha_2^{\rm nloc}(\boldsymbol{\partial}_r\vec{m}\cdot\partial_t\vec{m})\ \vec{m}\times\boldsymbol{\partial}_r\vec{m}\Big]\hat{\vec{\sigma}} \ ,\end{aligned} \tag{2.122}$$

which are the correct expressions up to order $O(\boldsymbol{\partial}_r\vec{m})^2$. The so-called non-adiabatic coefficient $\beta \equiv \frac{1}{T_2\Delta}$ will be recurring throughout the following sections. Furthermore, we will later find that $\alpha = \frac{\nu_0 P^2}{6\rho_s T_2}$ corresponds to the Gilbert damping constant and $\delta\alpha_{\boldsymbol{r}} = O(\boldsymbol{\partial}_r\vec{m})^2$ are gradient corrections thereof, which however will be not important in this work, since they turn out to be of higher order in $\frac{1}{\tau\Delta}$, while the dominant term comes from the current and is proportional to $\sigma_{\rm c}$ (see result (2.175)). $\alpha_{1,2}^{\rm nloc}$ constitute non-local diffusive type corrections to the Gilbert damping,

$$\alpha_2^{\rm nloc} = -\frac{\nu_0 P^3}{20 m_{\rm e}\Delta} \tag{2.123}$$

$$\alpha_1^{\rm nloc} = \alpha_2^{\rm nloc}\left(\frac{8}{3} - \frac{5}{3}\frac{T_2}{T_1}\right) \ , \tag{2.124}$$

The action of the scattering term $\underline{\underline{\hat{\Gamma}}}$ will be specified explicitly in a moment.

Similarly, for the spin-charge diffusion equation (D.5), we get

$$\partial_t\hat{\boldsymbol{J}} + \underline{\underline{\hat{\Pi}}}\hat{\boldsymbol{J}} + \frac{\Delta_{\boldsymbol{r}}}{2i}\left[\vec{m}\hat{\vec{\sigma}}, \hat{\boldsymbol{J}}\right] + \boldsymbol{\partial}_r\underline{\underline{\hat{T}}}_{\rm tot} + \hat{\boldsymbol{\mathcal{T}}}_{\hat{N}}^{(1)} = \frac{1}{2}\left\{\hat{\boldsymbol{a}}^{(1)}, \underline{\hat{\chi}}\hat{N}\right\} + \hat{\boldsymbol{\mathcal{C}}}_{\hat{N}}^{(1)} + \hat{\boldsymbol{J}}_{\rm eff} - \frac{e\boldsymbol{E}}{m_{\rm e}}\hat{N} \ , \tag{2.125}$$

where $\hat{\boldsymbol{J}}_{\rm eff} = \hat{\boldsymbol{\mathcal{J}}}_c^{(1)} + \underline{\underline{\hat{\Pi}}}\hat{\boldsymbol{J}}_{\rm h} - \frac{1}{2}\left\{\hat{\boldsymbol{a}}^{(1)}, \underline{\hat{\chi}}\hat{N}_{\rm h}\right\} - \hat{\boldsymbol{\mathcal{C}}}_{\hat{N}_{\rm h}}^{(1)}$ is the source term which incorporates a high-energy part of the complicated dynamics described by the collision integral. For a definition of the various quantities, see Appendix D.

Corrections to the scattering rates

Now, we want to discuss the relaxation described by $\underline{\underline{\hat{\Gamma}}}$ and $\underline{\underline{\hat{\Pi}}}$, and in particular, we are interested in gradient corrections to the various scattering times. For illustration, let us first have a look at transverse spin-dephasing which is explicitly given by

$$\underline{\underline{\hat{\Gamma}}}\hat{N}_\perp \equiv \frac{1}{2}\left\{\underline{\hat{\chi}}\hat{a}^{(0)}, \hat{N}_\perp\right\} - \frac{1}{2}\left\{\underline{\hat{\chi}}\hat{N}_\perp, \hat{a}^{(0)}\right\} = \frac{{\rm Tr}\hat{a}^{(0)}}{4\pi\nu_0 T_2}\hat{N}_\perp = \frac{1}{T_2(1+\delta T_2)}\hat{N}_\perp \equiv \frac{1}{T_{2,\boldsymbol{r}}}\hat{N}_\perp \ , \tag{2.126}$$

where we can see that only the charge component of $\hat{a}^{(0)}$ plays a role. T_2 is the spin-dephasing time of the homogeneous system, while $T_{2,\boldsymbol{r}} = T_2(1+\delta T_2)$ incorporates magnetization gradient corrections, which is indicated by the subindex $\boldsymbol{r}$.

The change in the local density of states is parametrized by the quantity

$$\eta_{\boldsymbol{r}} = E_{\boldsymbol{r}} \, \frac{(1+P^2)}{6(1-P^2)} \begin{cases} P^2 & s\text{-}d \text{ model} \\ \frac{11P^2-15}{20} & \textit{itinerant} \text{ Stoner model} \end{cases} \tag{2.127}$$

so that

$$\hat{a}^{(0)} = \sum_{\uparrow,\downarrow} \left\{ \nu_0(1 \pm P)\hat{\mathcal{P}}_{\uparrow,\downarrow} \pm \nu_0 \frac{(1 \mp P)^2}{2P} \eta_{\boldsymbol{r}} \hat{\mathcal{P}}_{\uparrow,\downarrow} \right\} - \frac{\nu_0 P^2}{6m_{\mathrm{e}}\Delta} (\boldsymbol{\partial}_r^2 \vec{m})_\perp \hat{\vec{\sigma}} \; , \tag{2.128}$$

where we introduced the dimensionless energy of magnetization gradients, $E_{\boldsymbol{r}} \equiv \frac{\hbar^2 (\boldsymbol{\partial}_r \vec{m})^2}{2m_{\mathrm{e}} E_{\mathrm{F}}}$ and $\eta_{\boldsymbol{r}} = \eta E_{\boldsymbol{r}}$.

The corrections to all the remaining scattering times are summarized in the following, and it turns out that all can be reduced to $\eta_{\boldsymbol{r}}$, which seems reasonable since in the end, the scattering rates are essentially given by the density of states. The action of the spin relaxation tensor $\hat{\underline{\underline{\Gamma}}}$ includes gradient corrections and is defined as ($\hat{N} = \frac{n_c}{2}\hat{1} + \hat{\vec{\sigma}}\vec{s}$)

$$\hat{\underline{\underline{\Gamma}}}\hat{N} \; = \; \frac{1-\eta_{\boldsymbol{r}}}{T_2} \vec{s}_\perp \hat{\vec{\sigma}} + \frac{1-\eta_{\boldsymbol{r}}}{T_1} s_\parallel \, \vec{m}\hat{\vec{\sigma}} - \frac{1}{T_1}\left(P + \frac{1+P^2}{2P}\eta_{\boldsymbol{r}} \right) \frac{n_c}{2} \, \vec{m}\hat{\vec{\sigma}} + \frac{P^2}{6m_{\mathrm{e}}T_2\Delta} \frac{n_c}{2} (\boldsymbol{\partial}_r^2 \vec{m})_\perp \hat{\vec{\sigma}} \tag{2.129}$$

and likewise, the momentum relaxation tensor $\hat{\underline{\underline{\Pi}}}$ performs the following action

$$\begin{aligned} \hat{\underline{\underline{\Pi}}}\hat{\boldsymbol{J}} = \frac{1-\eta_{\boldsymbol{r}}}{\tau} \boldsymbol{j}_\perp \hat{\vec{\sigma}} + \frac{1-\delta\tau_\uparrow}{\tau_\uparrow} \boldsymbol{j}_\uparrow \hat{\mathcal{P}}_\uparrow + \frac{1-\delta\tau_\downarrow}{\tau_\downarrow} \boldsymbol{j}_\downarrow \hat{\mathcal{P}}_\downarrow \\ - \left(\frac{1}{\tau} - \frac{1}{T_2} \right) \frac{P^2}{6m_{\mathrm{e}}\Delta} \left(\frac{\boldsymbol{j}_{\mathrm{c}}}{2} (\boldsymbol{\partial}_r^2 \vec{m})_\perp \hat{\vec{\sigma}} + (\boldsymbol{j}_\perp \cdot \boldsymbol{\partial}_r^2 \vec{m}) \hat{1} \right) \; , \end{aligned} \tag{2.130}$$

where the corrections to the scattering times for the spin-up/down channels read

$$\delta\tau_{\uparrow,\downarrow} \equiv \eta_{\boldsymbol{r}} \; \frac{1 \mp \gamma \frac{1+P^2}{2P}}{1 \pm P\gamma} \quad . \tag{2.131}$$

The definitions for the various spin components $s_\perp$, $s_\parallel$, $\boldsymbol{j}_{\uparrow,\downarrow}$ are found near Eq. (2.28).

Furthermore, we can see a channel mixing in the presence of magnetization gradients, for example, a transverse spin-current $\boldsymbol{j}_\perp$ has a finite contribution relaxing into the charge channel.

Current in the presence of non-equilibrium excitations

Let us now derive a diffusion equation in the regime where the elastic mean-free time is much shorter than the precession time, i.e. $\Delta\tau \ll 1$. In this limit, gradient corrections to the collision integral and the d-wave contribution $\boldsymbol{\partial}_r \hat{\underline{\underline{T}}}_{\mathrm{tot}}$ become irrelevant and, as it is the case usually in diffusive transport, we need to take into account only s- and p-wave components

for sufficiently weak perturbations so that the distribution function is nearly isotropic. This is contrary to the other sections, where we assumed that the precession time is shorter than τ which implies that precession due to Δ induces additional anisotropy in the spin-component of the distribution function, which requires us to also include the d-wave contribution.

Making use of all the simplifications allowed in the regime $\Delta\tau \ll 1$, in particular $\mathcal{J}_{\text{eff}} = 0$, the neglect of precession $\frac{\Delta}{2i}\left[\vec{m}\hat{\vec{\sigma}}, \hat{\boldsymbol{J}}\right]$ and additional terms due to high energy contributions $\boldsymbol{J}_{\text{h}}$, we can reduce Eq. (2.125) to

$$\partial_t \hat{\boldsymbol{j}} + \hat{\underline{\underline{\Pi}}}\hat{\boldsymbol{j}} + \frac{1}{2m_{\text{e}}}\left(\frac{2}{d}\boldsymbol{\nabla}\{\hat{E_{\text{F}}}, \hat{n}\} - \{\boldsymbol{\nabla}\hat{E_{\text{F}}}, \hat{n}\}\right) + \frac{e\boldsymbol{E}}{m_{\text{e}}}\hat{n} = 0 \ , \tag{2.132}$$

where the spin-resolved Fermi-energy is defined as $\hat{E_{\text{F}}} \equiv E_{\text{F}}\hat{1} + \frac{\Delta}{2}\vec{m}\hat{\vec{\sigma}}$ and $d = 3$ is the dimensionality of the system. Defining $\epsilon_d \equiv 1 - \frac{d}{2}$, we can rewrite this equation as ($\hat{n} = \frac{n_c}{2}\hat{1} + \hat{\vec{\sigma}}\vec{s}$)

$$\begin{aligned}\partial_t \hat{\boldsymbol{j}} + \hat{\underline{\underline{\Pi}}}\hat{\boldsymbol{j}} + \frac{1}{dm_{\text{e}}}\left[E_{\text{F}}\boldsymbol{\nabla}n_c + \Delta\vec{m}\boldsymbol{\nabla}\vec{s} + \epsilon_d\Delta\vec{s}\boldsymbol{\nabla}\vec{m}\right]\hat{1} \\ + \frac{1}{dm_{\text{e}}}\left[2E_{\text{F}}\boldsymbol{\nabla}\vec{s} + \frac{\Delta}{2}\vec{m}\boldsymbol{\nabla}n_c + \frac{\Delta}{2}\epsilon_d n_c\boldsymbol{\nabla}\vec{m}\right]\hat{\vec{\sigma}} + \frac{e\boldsymbol{E}}{m_{\text{e}}}\hat{N} = 0 \ .\end{aligned} \tag{2.133}$$

Note that for a two-dimensional electron gas $d = 2$, the gradient terms $\boldsymbol{\nabla}\vec{m}$ vanish, which is related to the fact that the density of states is a constant in that case.

We now assume a stationary situation, and by inverting $\hat{\underline{\underline{\Pi}}}$ and ignoring gradient corrections to the scattering, we can straightforwardly solve for the charge and spin-currents (note that now, there is an additional factor $(-e)$ included in $\hat{j}$ and $\hat{n}$),

$$\begin{aligned}\hat{\boldsymbol{j}} = \frac{1}{2}\left(\sigma_{\text{c}}\boldsymbol{E} - D_0\boldsymbol{\nabla}n_c - 2P_dD_0\vec{m}\boldsymbol{\nabla}\vec{s} - 2\mathcal{D}_c\vec{s}\boldsymbol{\nabla}\vec{m}\right)\hat{1} \\ + \frac{1}{2}\left[P_\sigma\sigma_{\text{c}}\boldsymbol{E} - 2D_0\boldsymbol{\nabla}\vec{s} - P_dD_0\boldsymbol{\nabla}n_c - 2\mathcal{D}_s\vec{s}\boldsymbol{\nabla}\vec{m}\right]\vec{m}\hat{\vec{\sigma}} - D_\perp(\boldsymbol{\nabla}\vec{s})_\perp\hat{\vec{\sigma}} - \mathcal{D}_\perp n_c\boldsymbol{\nabla}\vec{m}\hat{\vec{\sigma}} = 0 \ .\end{aligned} \tag{2.134}$$

Here, we defined the diffusion constants $D_{\uparrow,\downarrow} = \frac{2}{dm_{\text{e}}}(E_{\text{F}} \pm \frac{\Delta}{2})\tau_{\uparrow,\downarrow}$ for the spin-up and down channels, its average $D_0 \equiv \frac{1}{2}(D_\uparrow + D_\downarrow)$ and the polarization of the diffusion constants $P_d = \frac{D_\uparrow - D_\downarrow}{D_\uparrow + D_\downarrow}$. We also introduce the polarization of the conductivity, $P_\sigma \equiv \frac{\sigma_\uparrow - \sigma_\downarrow}{\sigma_\uparrow + \sigma_\downarrow}$. The transport properties of transverse spin-excitations are summarized in the transverse diffusion constant $D_\perp = \frac{2E_{\text{F}}}{dm_{\text{e}}}\tau$. We furthermore defined the off-diagonal diffusion constants $\mathcal{D}_{c/s} \equiv \frac{\epsilon_d\Delta}{2dm_{\text{e}}}(\tau_\uparrow \pm \tau_\downarrow)$ and $\mathcal{D}_\perp \equiv \frac{\epsilon_d\Delta}{2dm_{\text{e}}}\tau$ that appear as a result of gradient corrections to the spectrum and promote conversion between the spin-degree and the charge-degree of freedom. The latter coupling terms vanish as $\boldsymbol{\nabla}\vec{m} = 0$.

Finally, in the case of a homogeneous ferromagnet, Zhang *et al.* phenomenologically derived a set equations describing transport in ferromagnetic conductors in the diffusive limit $\Delta\tau \ll 1$ [69]. Thus, for the homogeneous ferromagnet ($\boldsymbol{\nabla}\vec{m} = 0$), we can compare our result for the current with the expression derived by Zhang *et al.*, and find agreement except for a different transverse diffusion constant $D_\perp$.

Finally, let us stress that in the opposite limit of rapid precession, $\Delta\tau \gg 1$, we still obtain an expression for the current like in (2.134), but with the d-wave term included along with some additional terms and renormalized transport parameters due to gradient corrections to the collision integral.

2.4.3. Transverse Spin-dynamics in a System with Rapid Precession

To illustrate the basic idea of how we solve the equations of motion in the following sections, let us consider a system that can attain a non-equilibrium spin-excitation like our system of conduction electrons. Let us assume that the dynamics of such a system is described by the simple Bloch equation for the spin $\vec{s}$

$$\partial_t \vec{s} + \Delta \vec{m}(t) \times \vec{s} + \beta\Delta \vec{s} = \vec{\mathcal{T}}(t) \ , \tag{2.135}$$

which also includes relaxation of spin-excitations given by the damping parameter $\beta\Delta = 1/T_2$ and a general torque $\vec{\mathcal{T}}(t)$ acting on the system. This essentially corresponds to our kinetic equation (2.121), with $T_1 = T_2$ and all other terms combined into the torque, $\vec{\mathcal{T}} = \vec{N}_{\rm eff} - \boldsymbol{\nabla}\underline{\underline{J}}_s$. It is assumed that the time-scales defined by $\vec{m}(t)$ and $\vec{\mathcal{T}}(t)$ are much slower than the period of oscillations due to the precession term Δ. We are now interested in the steady state dynamics for arbitrary $\vec{m}(t)$ and $\vec{\mathcal{T}}(t)$ with the rapid oscillations averaged out, in particular we do not need the transient behavior arising from arbitrary initial conditions.

Assuming $\vec{m}$ to be constant or smoothly varying as compared to Δ, we anticipate a solution of the form $\vec{s} = \vec{c}(t) + \vec{a}(t)\cos\Delta t + \vec{b}(t)\sin\Delta t$, where the coefficients $\vec{a}, \vec{b}, \vec{c}$ are smooth in time as compared to oscillations defined by Δ. Introducing the averaged solution $\langle\vec{s}\rangle = \vec{c}(t)$, the oscillatory terms drop out, but the differential equation for $\langle\vec{s}\rangle$ is formally identical. It is then possible to iteratively solve for the transverse part of the equation by simply rewriting (2.135) as

$$\langle\vec{s}_\perp\rangle \ = \ \frac{1}{\Delta}\frac{1}{1+\beta^2}\left(\beta - \vec{m}\times\right)\left[\vec{\mathcal{T}} - \partial_t\langle\vec{s}\rangle\right]_\perp \approx \frac{1}{\Delta}\left(\beta - \vec{m}\times\right)\left[\vec{\mathcal{T}} - \partial_t\langle\vec{s}\rangle\right]_\perp \ , \tag{2.136}$$

where we assume also that $\beta \ll 1$, which simply means that spin-dephasing is much slower than precession and we can drop terms of order β^2. We denote $(\dots)_\perp$ as taking the spin-component transverse to the direction of the exchange field $\vec{m}$. For completeness, we also specify the longitudinal component, which however is left unaffected by precession, $\vec{m}\cdot\vec{s} = T_2(\vec{m}\cdot\vec{\mathcal{T}}(t) - \vec{m}\cdot\partial_t\vec{s})$.

In the following, we are only interested in the transverse component and we iteratively solve (2.136) by starting from the zeroth order, or equilibrium solution $\vec{s}_0 = \rho_s\vec{m}$. Therefore, in the case of adiabatic variation of $\vec{m}$, we obtain to leading order in time-gradients and dropping terms of order β^2,

$$\begin{aligned}\langle\vec{s}_\perp\rangle = \frac{1}{\Delta}\left(\beta - \vec{m}\times\right)\vec{\mathcal{T}}_\perp - \rho_s\frac{1}{\Delta}\left(\beta - \vec{m}\times\right)\partial_t\vec{m} \\ + \frac{1}{\Delta^2}\left(\beta\partial_t\vec{m}\times\vec{\mathcal{T}} + 2\beta\vec{m}\times\partial_t\vec{\mathcal{T}} - \vec{m}\times\partial_t(\vec{m}\times\vec{\mathcal{T}})\right)_\perp \ .\end{aligned} \tag{2.137}$$

We thus can see that by mere increase of the spin-relaxation mechanism, we can increase the non-equilibrium spin-excitation in the electron gas proportional to β and this additional

component is aligned along $\vec{\mathcal{T}}_\perp$, while the much larger component attained by Δ is perpendicular to it. Note that the latter term gives rise to the Hall-conductivity while only the former component $\propto \beta$ gives a contribution to the domain-wall resistance, more specifically, it corresponds to the function g_a in Eqn. (2.142) which is for example relevant for the CPW DWR.

Finally, the torque acting on $\vec{m}$ is immediately obtained as

$$\begin{aligned}\Delta\vec{m}\times\langle\vec{s}_\perp\rangle &= \vec{\mathcal{T}}_\perp + \beta\vec{m}\times\vec{\mathcal{T}} + \frac{1}{\Delta}\vec{m}\times\partial_t\vec{\mathcal{T}} - 2\frac{\beta}{\Delta}\left[\partial_t\vec{\mathcal{T}}\right]_\perp - \rho_s\partial_t\vec{m} - \rho_s\beta\vec{m}\times\partial_t\vec{m} \\ &\hat{=} -\frac{1}{g\mu_\mathrm{B}}\vec{\mathcal{T}}_\mathrm{el}\ , \end{aligned} \tag{2.138}$$

and which enters the equation for the magnetization dynamics, $M_d\partial_t\vec{m}+\cdots=\vec{\mathcal{T}}_\mathrm{el}$. However, this is subject of section 2.5.

The derivation of the other quantities like the current goes along the same lines. Essentially, we apply this iterative procedure to the hierarchy of equations until we obtain the desired order which in this work is $O(\boldsymbol{\partial}_r^2\partial_t)$ and $O(\boldsymbol{E}\boldsymbol{\partial}_r^2)$.

2.4.4. Change in the Conductivity due to Magnetization Gradients

Before discussing the results, let us first introduce some quantities for the trivial homogeneous case. The charge current in spin-up/spin-down channels is simply $\boldsymbol{j}_{\uparrow,\downarrow}=\sigma_{\uparrow,\downarrow}\boldsymbol{E}$, where

$$\sigma_{\uparrow,\downarrow} = e^2\frac{\tau_{\uparrow,\downarrow}N_{\uparrow,\downarrow}}{m_\mathrm{e}} = e^2\frac{\tau_{\uparrow,\downarrow}}{m_\mathrm{e}}\,\frac{2E_\mathrm{F}\nu_0}{3}\,\frac{(1\pm P)^3}{1+P^2} \tag{2.139}$$

are simply the Drude conductivities and $N_{\uparrow,\downarrow}$ is the equilibrium particle density for spin-up/spin-down bands. The charge current is derived from $\boldsymbol{j}_c=\boldsymbol{j}_\uparrow+\boldsymbol{j}_\downarrow=\sigma_\mathrm{c}\boldsymbol{E}$, so that $\sigma_\mathrm{c}\equiv\sigma_\uparrow+\sigma_\downarrow$. Likewise, current of spin-angular momentum pointing along direction $\vec{m}$, the longitudinal spin-current, is $\boldsymbol{j}_s=-\frac{\hbar}{2e}(\boldsymbol{j}_\uparrow-\boldsymbol{j}_\downarrow)=\sigma_\mathrm{s}\boldsymbol{E}$, so that $\sigma_\mathrm{s}\equiv-\frac{\hbar}{2e}(\sigma_\uparrow-\sigma_\downarrow)$. Thus, in a homogeneous system, the spin-charge current simply takes the form $\hat{\boldsymbol{j}}=\left(\frac{\sigma_\mathrm{c}}{2}\hat{1}-\frac{e}{\hbar}\sigma_\mathrm{s}(\vec{m}\hat{\vec{\sigma}})\right)\boldsymbol{E}$. Let us now turn to the much more interesting situation of inhomogeneous and time-dependent magnetization.

We first discuss the scenario of a static magnetization profile $\vec{m}(\boldsymbol{r})$. For the gradient corrections to the conductivity $(\underline{\underline{\sigma}}_\mathrm{c})_{ij}=\sigma_\mathrm{c}\delta_{ij}+(\delta\underline{\underline{\sigma}}_\mathrm{c})_{ij}$, we obtain up to order $(\boldsymbol{\partial}_r\vec{m})^2$

$$(\delta\underline{\underline{\sigma}}_\mathrm{c})_{ij} = -\frac{\hbar^2\sigma_\mathrm{c}}{2m_\mathrm{e}E_\mathrm{F}}\left[\zeta_\mathrm{a}(\partial_i\vec{m}\cdot\partial_j\vec{m})+\zeta_\mathrm{i}\left(\boldsymbol{\partial}_r\vec{m}\right)^2\delta_{ij}\right] - \hbar\frac{\sigma_\uparrow\tau_\uparrow-\sigma_\downarrow\tau_\downarrow}{2m_\mathrm{e}}\vec{m}\cdot(\partial_i\vec{m}\times\partial_j\vec{m})\ , \tag{2.140}$$

so that one has to solve the equations $\boldsymbol{j}=\underline{\underline{\sigma}}_\mathrm{c}\boldsymbol{E}$ and $\boldsymbol{\nabla}\cdot\boldsymbol{j}=0$ in order to obtain the current distribution and electric field for a given magnetization structure $\vec{m}(\boldsymbol{r})$. The first two terms in Eq. (2.140) give rise to the domain-wall resistance, while the last term yields a transverse conductivity due to the Berry curvature. The anisotropic (a) term $\partial_i\vec{m}\cdot\partial_j\vec{m}$ is relevant only when there is a magnetization gradient in the direction of current flow like in the current perpendicular-to-wall geometry (CPW), while the isotropic (i) term $(\boldsymbol{\partial}_r\vec{m})^2$ is always present whenever there is a magnetization gradient. The constants ζ_a, ζ_i depend on the parameters of our microscopic model and are discussed below.

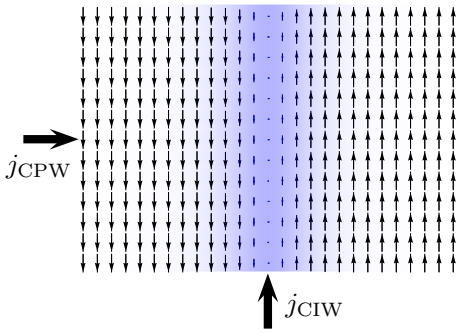

Figure 2.4.: Bloch wall of thickness w with current flowing perpendicular to the domain wall (CPW) and in the domain wall (CIW). The shading indicates the magnitude of the out-of-plane component of the magnetization.

In the general time-dependent situation, the charge current obtains two additional terms to first order in time-gradients,

$$\boldsymbol{j}_c = \underline{\underline{\sigma}}_{\mathrm{c}} \boldsymbol{E} - \sigma_{\mathrm{s}} \left[\vec{m} \cdot (\boldsymbol{\nabla} \vec{m} \times \partial_t \vec{m}) + \beta \boldsymbol{\nabla} \vec{m} \cdot \partial_t \vec{m} \right] \ , \tag{2.141}$$

while in our linear response treatment, the correction to the conductivity $\delta \underline{\underline{\sigma}}_{\mathrm{c}}(\boldsymbol{r}, t)$ simply inherits its time-dependence from $\vec{m}(\boldsymbol{r}, t)$, thus adiabatically following changes in time. In our case of a totally incompressible Fermi-liquid, i.e. perfect screening, Eq. (2.141) has to be solved together with charge current conservation $\boldsymbol{\nabla} \cdot \boldsymbol{j}_c = 0$. In the more general case, we have to solve Eq. (2.141) together with the continuity equation $\partial_t n_c + \boldsymbol{\nabla} \cdot \boldsymbol{j}_c = 0$ and the Poisson equation in order to obtain the charge-density, charge-current and electric field distributions. In the opposite limiting case of a totally compressible Fermi-liquid, one has the current directly given by (2.141), but then we would have unscreened charge excitations n_c required to satisfy the continuity equation.

The time-gradient terms in Eq. (2.141) describe charge pumping and are non-vanishing in presence of spatial variations, in addition to the time-dependence. Of course, in a homogeneous system but with time-dependent magnetization, no charge can be pumped. The first term is due to the electromotive force given by the time derivative of the Berry phase acquired by the electron spin in the magnetization structure and is discussed in Ref. [70]. The second term proportional to β has been first discussed by Duine [71, 72] and is only non-vanishing in presence of mechanisms that do not conserve the spin. $\beta \equiv \frac{1}{T_2 \Delta}$ denotes dephasing due to spin mistracking, and within our theory, it turns out to be equal to the non-adiabatic coefficient β which appears in the LLG equation (see section 2.5.2). However, in obtaining the expression for the average current, Duine does not solve the continuity equation. In a simple effective 1 dimensional geometry, incorporation of charge current conservation is trivial and the expressions coincide. For more complex geometries, the result of Duine corresponds to our expression for the current density (2.141) simply averaged over the system volume V.

2.4.5. Domain-wall Resistance in Diffusive Wires for CPW and CIW Geometry

Let us study the effect of a static magnetization profile on the resistivity by calculating the domain wall resistance from Eq. (2.140) for a Bloch wall of thickness w in a wire with sufficiently large diameter, so that the problem becomes effectively one-dimensional (Fig. 2.4).

The CPW geometry has been treated in section 2.3 with details on the approximations performed. Here, we will reproduce the result obtained there and extend it to the current-in-wall (CIW) geometry and also discuss the difference between Stoner and *s-d* model.

Compatible to (2.97), the domain-wall resistance is defined as

$$\delta R_{\mathrm{DW}} \equiv \frac{R_{\mathrm{DW}} - R_0}{R_0} \ ,$$

and we straightforwardly obtain $\delta R_{\mathrm{CIW}} = E_{\mathrm{w}}\zeta_{\mathrm{i}}$ for the CIW geometry and $\delta R_{\mathrm{CPW}} = E_{\mathrm{w}}(\zeta_{\mathrm{a}} + \zeta_{\mathrm{i}})$ CPW geometry, where

$$E_{\mathrm{w}} = \frac{\hbar^2}{2m_{\mathrm{e}}E_{\mathrm{F}}}\frac{1}{L}\int_{-L/2}^{+L/2} dx(\partial_x\vec{m})^2 = \frac{\hbar^2}{2m_{\mathrm{e}}E_{\mathrm{F}}}\frac{2}{wL}$$

constitutes an average over the magnetization profile and has been already introduced in (2.108).

In fact, we find that the results obtained in this section perfectly agree with result (2.107) for the DWR found the in the previous section. We have discussed the validity of the expression for the domain-wall in depth in section 2.3.5, and found that for a localized magnetization structure such as the domain wall, and the voltage probes much farer away from the wall than the spin-diffusion length, the result is valid for wall widths w much larger than the spin-precession length l_{prec}.

Let us first discuss the limiting case of a strong ferromagnet $\tau\Delta \gg 1$.

Results for $\tau\Delta \gg 1$

In order to shed some more light on the origin of the domain wall resistance, let us separate the pure spin-dephasing part by rewriting $\zeta_{\mathrm{a,i}}$ as

$$\zeta_{\mathrm{a}}\left(\frac{\tau}{T_2},\frac{\tau}{T_1}\right) = f_{\mathrm{a}}\left(\frac{\tau}{T_1}\right) + \frac{\tau}{T_2}\, g_{\mathrm{a}}\left(\frac{\tau}{T_1}\right) \ , \tag{2.142}$$

$$\zeta_{\mathrm{i}}^{(\mathrm{St/sd})}\left(\frac{\tau}{T_1}\right) = f_{\mathrm{i}}^{(\mathrm{St/sd})}\left(\frac{\tau}{T_1}\right) \ , \tag{2.143}$$

where the functions f, g depend only on $\frac{\tau}{T_1}$, the ratio of elastic mean-free time and spin-flip time T_1. ζ_{a} is the same in both *s-d* and Stoner limiting cases, in fact only ζ_{i} shows a dependence on the specific model of ferromagnetism, which is not surprising as the only source of difference are the corrections $\delta\mu$ and $\delta\Delta$, both proportional to $(\boldsymbol{\partial}_r\vec{m})^2$, and thus can contribute only to ζ_{i}. One can clearly see that ζ_{a}, and thus only δR_{CPW}, contains a term originating from spin-dephasing, and this term is strongly related to the non-adiabatic current-induced torque. Such contributions do not appear for the in-wall geometry where there is no magnetization gradient along the current-direction, only perpendicular to it. We explicitly find for $g_{\mathrm{a}} = \frac{2m_{\mathrm{e}}2E_{\mathrm{F}}}{\nu_0}\frac{1}{\Delta^2\tau}\frac{\sigma_{\mathrm{s}}^2}{\sigma_{\mathrm{c}}}$ and writing the full expression for this term, we get

$$\delta\sigma_{ij} = -\frac{2\beta}{\Delta\nu_0}\frac{\sigma_{\mathrm{s}}^2}{\sigma_{\mathrm{c}}}(\partial_i\vec{m}\cdot\partial_j\vec{m}) + f_{\mathrm{a}}\ldots \ , \tag{2.144}$$

which interestingly corresponds exactly to the lower bound for the domain-wall resistivity Tserkovnyak *et al.* obtain in a hypothetical regime, where the electron flow through the domain wall is ballistic, albeit with spin-dephasing present. They obtain this bound by enforcing the positivity of the dissipated power, for realistic scenarios however, this lower bound plays no role. The value of this lower bound is directly related to the non-adiabatic spin-transfer torque which corresponds to the term proportional to the β-term in equation (2.137), $\vec{s}_\perp = \frac{1}{\Delta}(\beta - \vec{m}\times)\,\vec{\mathcal{T}}_\perp + \ldots$. In fact, an external electric field gives rise to the longitudinal spin-current $\boldsymbol{j}_s = \sigma_\mathrm{s}\boldsymbol{E}$, and enters the spin-continuity equation through the torque $\vec{\mathcal{T}} = -\sigma_\mathrm{s}(\boldsymbol{E}\boldsymbol{\partial}_r)\vec{m}$. Therefore, this gives rise to the non-equilibrium spin-excitation

$$\vec{s} = \frac{1}{\Delta}(-\beta + \vec{m}\times)\,(\sigma_\mathrm{s}\boldsymbol{E}\boldsymbol{\partial}_r)\vec{m}\ ,$$

which acts back on the current via the spin-diffusion equation (2.125). It is exactly the term $\propto \beta$ that gives rise to the conductivity change $\frac{\tau}{T_2}\ g_\mathrm{a}(\frac{\tau}{T_1})$, (2.144) and thus, it arises due to spin-dephasing of the non-equilibrium spin induced by the spin-current $\boldsymbol{j}_s$. On a side note, the second term $\propto \vec{m}\times(\boldsymbol{E}\boldsymbol{\partial}_r)\vec{m}$, which as a consequence of precession is non-dissipative in nature, constitutes the transverse Hall conductivity found in the third term of (2.140). Thus an increase in spin-dephasing rate, for example by adding magnetic impurities, would also increase the non-equilibrium spin-excitation in regions of non-vanishing magnetization gradient, which in turn would reduce the charge current flow, resulting in an increase of the DWR[1]. However, adding magnetic impurities modifies the spin-flip T_1 time which affects also the other contributions to the DWR.

For the other contributions to the DWR, it is not straightforward to track different origins, since there are many different sources which includes for example changes to the spectrum, and thus modified transport parameters like scattering rates. Furthermore, to second spatial gradient of the magnetization considered here, the collision integral involves relaxation of s, p and d k-space moments in spin-space, giving rise to complicated dynamics. Although analytical expressions for f_i, f_a exist, they are quite lengthy and inconvenient, so we restrict ourselves to limiting cases, and only show plots of the full results.

The domain-wall resistance for both the CPW and CIW geometry, and thus also the functions $\zeta_\mathrm{a}, \zeta_\mathrm{i}$ are depicted in Fig. 2.5 as a function of the polarization P and for various scattering parameters. The values of the spin-flip time T_1 and the spin-dephasing time T_2 are measured in units of the momentum relaxation time τ. The plots for the Stoner limiting case covering the same parameter values are shown in Fig. 2.7. As an overall tendency, one can see that the in-plane domain wall resistance (CIW) is smaller than the resistance for the CPW geometry. Furthermore, one can see that the DWR can be both positive or negative, depending on the magnitude of the exchange-splitting Δ *viz.* polarization P, and this switching of the sign can be ultimately traced back to a band-structure effect which obviously appears in the limit of strong polarization $P \to 1$. Also, in the case of the *s-d* model, a negative DWR appears only in the presence of spin-flip relaxation. Concerning the overall tendency of the DWR, the situation for the *s-d* model and the Stoner model is quite opposite. For small P, the *s-d* model favors positive DWR, while for $P \to 1$, it tends to become negative. This is contrary to the Stoner limit, where for small P we have a stronger tendency for negative DWR, which however

[1] See result (2.134), even though d-wave terms and gradient corrections are missing, but it does not affect the statement concerning the spin-dephasing term

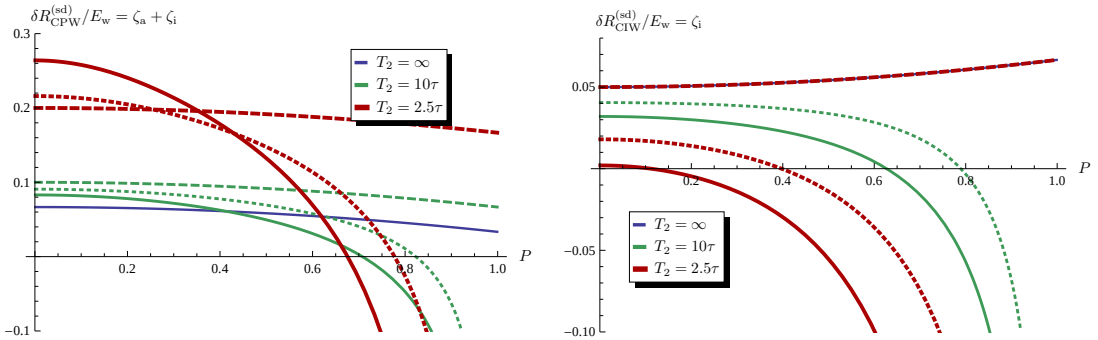

(a) Current perpendicular to wall, s-d model

(b) Current in wall geometry, s-d model

Figure 2.5.: (a) Domain-wall resistance δR_{DW} in the s-d limit as a function of the polarization of the Fermi surface $P = \frac{\nu_\uparrow - \nu_\downarrow}{\nu_\uparrow + \nu_\downarrow}$ for the CPW geometry and for various values of spin-dephasing time T_2. The spin-flip time is linked to T_2 as follows: $T_1 = \infty$ (dashed), $T_1 = T_2$ (dotted), $T_1 = \frac{T_2}{2}$ (solid). (b) DWR for the CIW geometry for the same parameter values as in (a).

becomes reversed as $P \to 1$. The behavior will be further illuminated in a moment, when we treat the two limiting cases of weak and strong polarization P analytically. In the limit of small exchange splitting Δ or polarization P, the DWR does not depend very strongly on P,Δ, whereas other calculations found a Δ^{-2} scaling [34, 35]. As discussed in section 2.3.5, this difference arises from the phenomenological origin of the scattering parameters $\tau_{\uparrow,\downarrow}$ in these works. The dependence on the domain-wall thickness is w^{-1} as opposed to other calculations that consider for example infinite spin-spirals [32].

In Fig. 2.6, we show the dependence of the DWR within the s-d model as one increases the magnetic impurity concentration, and with it the spin relaxation rates $1/T_1$, $1/T_2$. The analogue plots for the Stoner limiting case are shown in Fig. 2.8. We can see a general increase of the DWR with the impurity concentration, except for the CIW geometry in the s-d model, where we find a decrease or no change at all (see Fig. 2.6(b)). Especially curves with high polarization P tend to decrease.

Interestingly, in the case of vanishing spin-flip one obtains relatively simple expressions in terms of the polarization P,

$$\delta R^{(\mathrm{sd})}_{\mathrm{CPW}} \overset{T_1\to\infty}{=} E_{\mathrm{w}}(\zeta_{\mathrm{a}} + \zeta_{\mathrm{i}}) = \frac{E_{\mathrm{w}}}{15}\left(1 - \frac{1}{2}P^2 + 5\frac{\tau}{T_2}\right) , \tag{2.145}$$

$$\delta R^{(\mathrm{sd})}_{\mathrm{CIW}} \overset{T_1\to\infty}{=} E_{\mathrm{w}}\zeta_{\mathrm{i}} = \frac{E_{\mathrm{w}}}{20}\left(1 + \frac{1}{3}P^2\right) , \tag{2.146}$$

for the s-d limiting case in which the contributions of the conduction electrons to the magnetization is negligible. Likewise, we obtain for the Stoner limit

$$\delta R^{(\mathrm{St})}_{\mathrm{CPW}} \overset{T_1\to\infty}{=} E_{\mathrm{w}}(\zeta_{\mathrm{a}} + \zeta_{\mathrm{i}}) = \frac{E_{\mathrm{w}}}{120}\left(-7 - 13P^2 + 40\frac{\tau}{T_2}\right) , \tag{2.147}$$

$$\delta R^{(\mathrm{St})}_{\mathrm{CIW}} \overset{T_1\to\infty}{=} E_{\mathrm{w}}\zeta_{\mathrm{i}} = \frac{E_{\mathrm{w}}}{120}\left(-9 - 7P^2\right) . \tag{2.148}$$

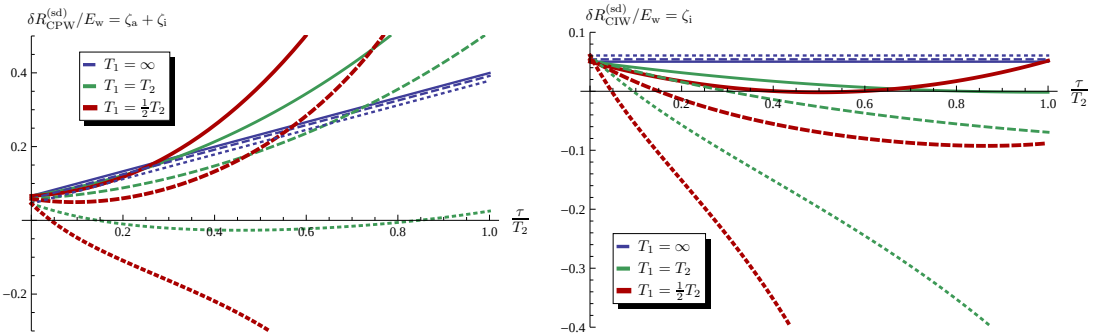

(a) Current perpendicular to wall, *s-d* model

(b) Current in wall geometry, *s-d* model

Figure 2.6.: (a) DWR in the *s-d* limit as a function of spin-dephasing rate $1/T_2$ in units of the momentum relaxation rate $1/\tau$ for the CPW geometry and for various values of polarization: $P = 0.1$ (solid lines), $P = 0.5$ (dashed lines) and $P = 0.8$ (dotted lines). For each curve, we keep the ratio of T_1/T_2 fixed, so that the spin-flip rate $1/T_1$ also increases linearly with $1/T_2$. This has the underlying assumption that an increase of a specific type of magnetic impurities in the sample changes the overall spin-relaxation, but not the ratio T_1/T_2. (b) DWR for the CIW geometry for the same parameter values as in (a). For $T_1 \to \infty$, we see straight lines with the slope given by g_a and the vertical shift by f_a, f_i.

Obviously, in the latter Stoner case, the DWR is negative, but $\delta R^{(St)}_{CPW}$ can turn positive for a sufficiently large ratio $\frac{\tau}{T_2}$. Negative domain-wall resistance in the Stoner limit has been also found by Gorkom *et al.* in Ref. [35].

Limit of weak polarization, $P \to 0$

Let us also investigate the limiting case $\Delta \to 0$ *viz.* $P \to 0$, or the quasiclassical limit, this time for general T_1. In the *s-d*-limit, we get

$$\delta R^{(sd)}_{CPW} \overset{P\to 0}{=} E_w(\zeta_a + \zeta_i) = \frac{E_w}{15}\left(1 - \frac{\tau}{T_1}\right)^2 + \frac{E_w}{12}\frac{\tau}{T_2}\left(2 + \frac{\tau}{T_1}\right)^2 , \tag{2.149}$$

$$\delta R^{(sd)}_{CIW} \overset{P\to 0}{=} E_w\zeta_i = \frac{E_w}{20}\left(1 - \frac{\tau}{T_1}\right)^2 = \frac{E_w}{20}\gamma^2 , \tag{2.150}$$

and in the Stoner limit

$$\delta R^{(St)}_{CPW} \overset{P\to 0}{=} E_w(\zeta_a + \zeta_i) = \frac{E_w}{120}\left(-7 - \frac{\tau}{T_1}\left(1 - 23\frac{\tau}{T_1}\right)\right) + \frac{E_w}{12}\frac{\tau}{T_2}\left(2 + \frac{\tau}{T_1}\right)^2 \tag{2.151}$$

$$\delta R^{(St)}_{CIW} \overset{P\to 0}{=} E_w\zeta_i = \frac{E_w}{40}\left(-3 + \frac{\tau}{T_1}\left(1 + 7\frac{\tau}{T_1}\right)\right) . \tag{2.152}$$

In the quasiclassical limit, there are no gradient corrections to the collision integral and no changes in the spectrum, so the result essentially depends on scattering asymmetry parameter $\gamma = 1 - \frac{\tau}{T_1}$ introduced in (2.29), which essentially depends on the ratio of elastic mean-free

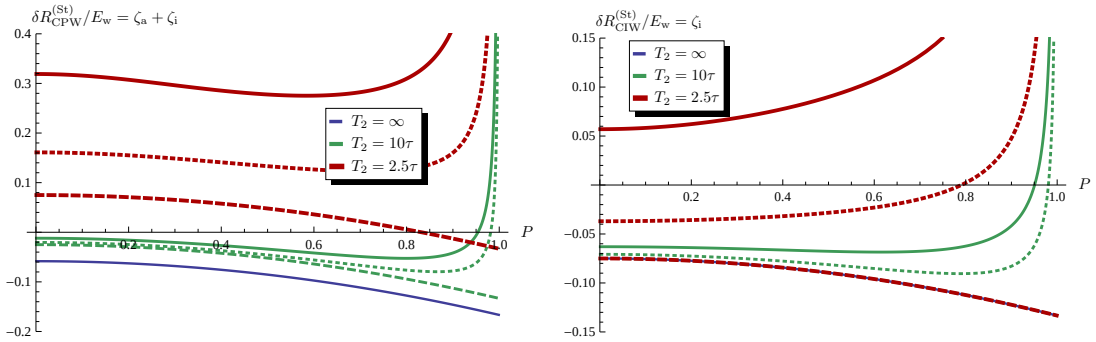

(a) Current perpendicular to wall, Stoner model

(b) Current in wall geometry, Stoner model

Figure 2.7.: (a) DWR in the Stoner limit as a function of the polarization P for the CPW geometry and for various values of spin-dephasing time T_2. The spin-flip time is linked to T_2 as follows $T_1 = \infty$ (dashed), $T_1 = T_2$ (dotted), $T_1 = \frac{T_2}{2}$ (solid). (b) DWR for the CIW geometry for the same parameter values as in (a). The parameters used in these figures are identical to Fig. (2.5).

time to spin-flip time T_1. In the case of the *s-d* model, the DWR vanishes as $\gamma \to 0$ leaving only the spin-dephasing contribution (see Eq. (2.149) and (2.150)). As discussed before, this suggests that the DWR arises from the different conductivities in the two spin-channels, which in the quasiclassical limit is solely due to $\tau_{\uparrow,\downarrow}$. Inside the domain wall, the spin is misaligned with respect to the local magnetization direction, thus slightly redistributing the current flow among the two channels, which ultimately gives rise to the DWR as discussed in section 2.3.5. On the other hand, the situation is different for the Stoner limiting case, where the DWR does not vanish when we remove the scattering asymmetry, i.e. $\gamma \to 0$. The reason can be found from (2.56), from which we find that the reduction of the exchange splitting becomes strongly enhanced in the quasiclassical limit, $\frac{\delta\Delta}{\Delta} = O(1/\Delta^2)$. In the end, this reduction of the magnetization from the itinerant electron due to hybridization leads to a decrease in the domain wall resistance. The reason can be seen from equation (2.29), $\tau_{\uparrow,\downarrow} = \frac{\tau}{1\pm P\gamma}$, which implies that a reduction of $\boldsymbol{\Delta}_{\boldsymbol{r}}$ (and thus also P) increases $\tau_\uparrow$ (and decreases $\tau_\downarrow$), and which in turn increases the local Drude conductivity (2.139) of the majority spin-channel $\sigma_\uparrow$ in areas of non-vanishing magnetization gradients. Therefore, we see a reduction in resistance. If we reduce the scattering asymmetry parameter to the point where it becomes zero $\gamma = 0$, the DWR still does not vanish, as opposed to the *s-d* limiting case. However, despite $\tau_\uparrow = \tau_\downarrow = \tau$, we find from Eqns. (2.131) and (2.127) that $\delta\tau = -\frac{1}{8}E_{\mathrm{w}}$ for $\gamma = 0$, so that the scattering times $\tau_{\uparrow,\boldsymbol{r}} = \tau_{\downarrow,\boldsymbol{r}} = \tau(1 + \delta\tau)$ increase locally in the domain wall, giving rise to the positive DWR $\delta R^{(\mathrm{St})}_{\mathrm{CPW}}(\gamma = 0) = \delta R^{(\mathrm{St})}_{\mathrm{CIW}}(\gamma = 0) = -\delta\tau = \frac{1}{8}E_{\mathrm{w}}$.

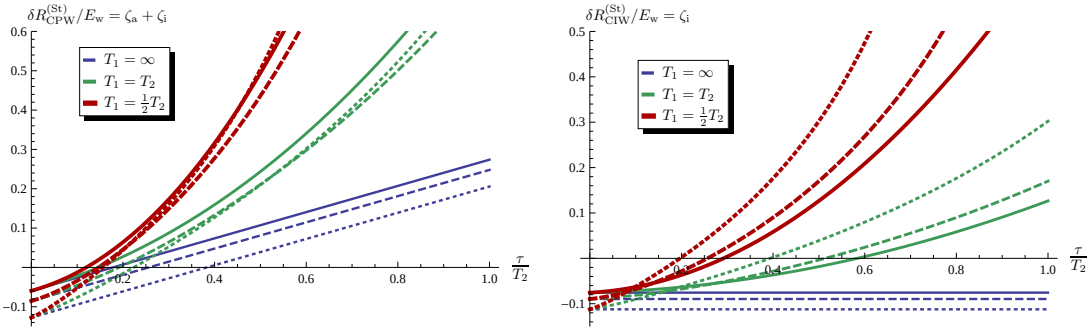

(a) Current perpendicular to wall, Stoner model

(b) Current in wall geometry, Stoner model

Figure 2.8.: (a) DWR in the Stoner limit as a function of spin-dephasing rate τ/T_2 in units of the momentum relaxation rate $1/\tau$ for the CPW geometry and for various values of polarization: $P = 0.1$ (solid lines), $P = 0.5$ (dashed lines) and $P = 0.8$ (dotted lines). For each curve, we keep the ratio of T_1/T_2 fixed. (b) DWR for the CIW geometry for the same parameter values as in (a). For $T_1 \to \infty$, we see straight lines with the slope given by g_{a} and the vertical shift by f_{a}, f_{i}. The parameters used in these figures are identical to Fig. (2.6).

Limit of strong polarization, $P \to 1$

In the limit $P \to 1$, we find that the DWR is dominated by the gradient corrections to elastic mean-free time for the scattering up channel,

$$\zeta_{\mathrm{i}} \overset{P\to 1}{\to} -\frac{\delta\tau_{\uparrow}}{E_{\boldsymbol{r}}} \overset{P\to 1}{\to} \frac{1}{30(1-P)} \frac{\tau}{2T_1 - \tau} \begin{cases} -5 & s\text{-}d \text{ model} \\ 1 & \textit{itinerant} \text{ Stoner model} \end{cases}, \tag{2.153}$$

where we used results (2.131) and (2.127), and which is diverging as $P \to 1$, while the anisotropic contribution to the DWR ζ_{a} yields a finite value in that limit. This change in the scattering times arises from a modification of the density-of-states in the presence of a magnetization gradient, so it ultimately is a band structure effect. This divergent behavior is inherited by the DWR in all possible configurations, since it arises from the isotropic contribution ζ_{i}. In particular, for the CIW and CPW geometries in the s-d limit shown in Figure 2.5, we can clearly recognize this singularity towards negative values of the DWR, as predicted by (2.153). In the Stoner limit however, we see from this expression that it goes towards positive values, albeit smaller by a factor 5 relative to the s-d model, so that this behavior becomes relevant only for larger values of P. This is exactly what we also find in the plots for the Stoner model in Fig. 2.7, where the singularity appears sharper towards positive values of the DWR, as $P \to 1$. Finally, for $T_1 \to \infty$, i.e. in the absence of spin-flip scattering, the leading order asymptotic term (2.153) vanishes and $\delta\tau_{\uparrow}$ attains a finite value in the limit $P \to 1$, so that also the divergence in Figures 2.5 and 2.7 disappears for this case.

This concludes the discussion of the regime $\Delta\tau \gg 1$, but before we leave the subject of the domain-wall resistance, we will have a quick look at what is expected to happen in the regime of intermediate impurity scattering strength.

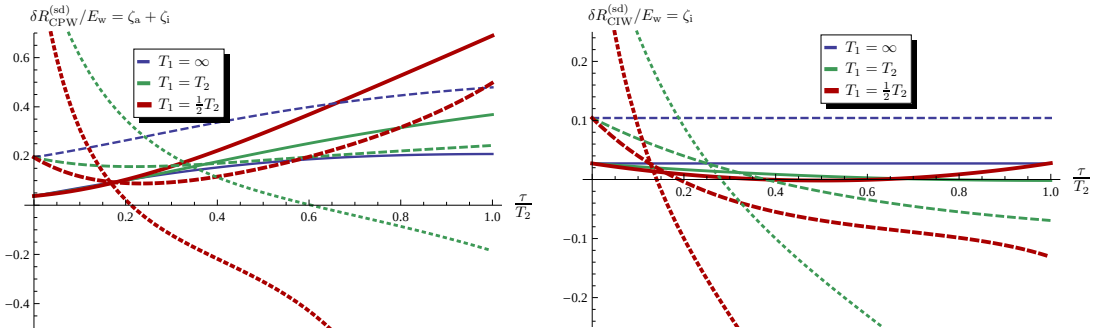

(a) Current perpendicular to wall, s-d model

(b) Current in wall geometry, s-d model

Figure 2.9.: DWR in the regime of intermediate impurity scattering, $\tau\Delta = 1$ in the s-d-limit and as a function of spin-dephasing rate τ/T_2. The parameters are the same as in Fig. 2.6, i.e. we vary the polarization: $P = 0.1$ (solid lines), $P = 0.5$ (dashed lines) and $P = 0.8$ (dotted lines). For each curve, we keep the ratio of T_1/T_2 fixed.

Results for intermediate impurity scattering $\tau\Delta = 1$

We can also treat the limiting case of intermediate impurity scattering, $\tau\Delta = 1$, in the sense of an extrapolation, since we neglect the broading of the spectrum and we also dropped the real parts from the kinetic equation, an approximation which can be doubted in the limit of intermediate or strong impurity scattering. Plots of the DWR as a function of the spin-dephasing time T_2 are shown in Fig. 2.9 for the s-d case and in Fig. 2.10 for the Stoner limit. The situation looks quite different as compared to the previous regime. In the Stoner limit in particular, we find minima of the DWR for a certain magnetic impurity concentration (see Fig. 2.10). For the s-d limit, curves with high polarization decrease strongly from positive to negative DWR as we increase the impurity concentration.

2.4.6. Transverse Conductivity

In more complex magnetization structures, in which the magnetization gradients in different directions are not collinear such that the vector product $\propto \vec{m}\cdot(\partial_i\vec{m} \times \partial_j\vec{m})$ in (2.140) does not vanish, there is a transverse current (or voltage drop depending on the experimental setup).

This transverse force on the electrons can be understood in terms of the Berry curvature or fictitious electromagnetic field which, in the limit of large exchange splitting, has the form [73]

$$\mathcal{B}_i = \frac{\epsilon_{ijk}}{2}\vec{m}\cdot(\partial_k\vec{m} \times \partial_j\vec{m}) \tag{2.154}$$

$$\boldsymbol{\mathcal{E}} = \vec{m}\cdot(\partial_t\vec{m} \times \boldsymbol{\nabla}\vec{m}) \ , \tag{2.155}$$

so that the spin-dependent force on an electron is $\boldsymbol{F}_{\uparrow,\downarrow} = \pm\frac{\hbar}{2}(\boldsymbol{\mathcal{E}} + \boldsymbol{v}_{\uparrow,\downarrow} \times \boldsymbol{\mathcal{B}})$ with the effective charge $\pm\frac{\hbar}{2}$ for spin-up/down channels. Therefore, the fictitious fields act with opposite sign on the spin-up and down channels. It is interesting to note that the fictitious fields obey the

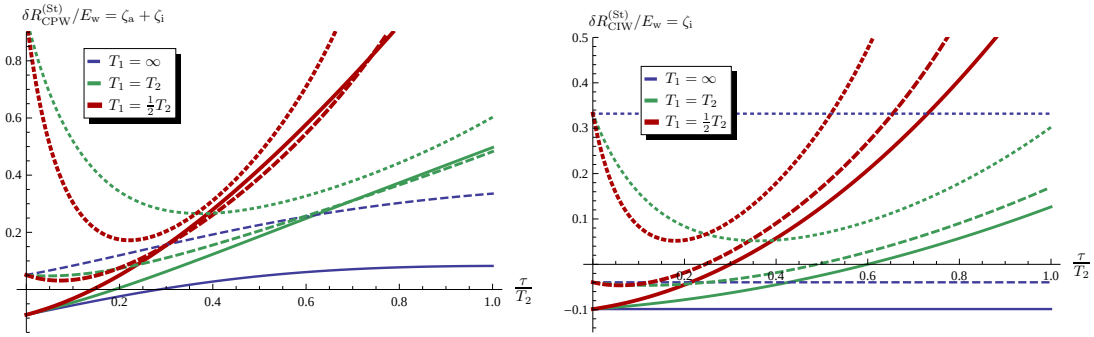

(a) Current in wall geometry, Stoner model

(b) Current in wall geometry, Stoner model

Figure 2.10.: DWR in the regime of intermediate impurity scattering, $\tau\Delta = 1$ in the Stoner limit and as a function of spin-dephasing rate τ/T_2. The parameters are the same as in Fig. 2.9, i.e. we vary the polarization: $P = 0.1$ (solid lines), $P = 0.5$ (dashed lines) and $P = 0.8$ (dotted lines). For each curve, we keep the ratio of T_1/T_2 fixed.

Maxwell relations

$$\begin{aligned} \boldsymbol{\nabla}\cdot\boldsymbol{\mathcal{B}} &= 0 \\ \boldsymbol{\nabla}\times\boldsymbol{\mathcal{E}} + \partial_t\boldsymbol{\mathcal{B}} &= 0\ , \end{aligned}$$

which is not surprising in the spirit of chapter 3 and result (3.64).

In the relaxation time approximation, we simply have $\boldsymbol{F}_{\uparrow,\downarrow} = m_{\mathrm{e}}\partial_t\boldsymbol{v}_{\uparrow,\downarrow} + \frac{m_{\mathrm{e}}}{\tau_{\uparrow,\downarrow}}\boldsymbol{v}_{\uparrow,\downarrow}$, where we can set $\partial_t\boldsymbol{v}_{\uparrow,\downarrow} = 0$ since it would be of higher order in external perturbations (the same reason why we omit $\partial_t\hat{g}$ in Eq. (2.44)). Since we are interested in the current, we multiply this equation with the particle density $n_{\uparrow,\downarrow}$ and average over the whole Fermi-sea of electrons:

$$\boldsymbol{j}_{\uparrow,\downarrow} = \pm\frac{\hbar}{2}\frac{\tau_{\uparrow,\downarrow}}{m_{\mathrm{e}}}\left(-en_{\uparrow,\downarrow}\boldsymbol{\mathcal{E}} + \boldsymbol{j}_{\uparrow,\downarrow}\times\boldsymbol{\mathcal{B}}\right) = \mp\frac{\hbar}{2e}\sigma_{\uparrow,\downarrow}\boldsymbol{\mathcal{E}} \pm \frac{\hbar}{2m_{\mathrm{e}}}\tau_{\uparrow,\downarrow}\boldsymbol{j}_{\uparrow,\downarrow}\times\boldsymbol{\mathcal{B}}\ , \tag{2.156}$$

and we immediately arrive at the charge current

$$\boldsymbol{j}_c = \boldsymbol{j}_\uparrow + \boldsymbol{j}_\downarrow = \sigma_{\mathrm{s}}\boldsymbol{\mathcal{E}} + \frac{\hbar}{2m_{\mathrm{e}}}\left(\sigma_\uparrow\tau_\uparrow - \sigma_\downarrow\tau_\downarrow\right)\boldsymbol{E}\times\boldsymbol{\mathcal{B}}\ . \tag{2.157}$$

Using the identity

$$(\boldsymbol{E}\times\boldsymbol{\mathcal{B}})_i = -E_j\ \vec{m}\cdot(\partial_i\vec{m}\times\partial_j\vec{m})\ , \tag{2.158}$$

we find equality to the Hall conductivity of the result (2.140) obtained within our model for $\Delta\tau \gg 1$. The first term of Eq. (2.157) corresponds to the time-gradient $\propto \sigma_{\mathrm{s}}$.

Tserkovnyak *et al.* [74] find compatible expressions for the transverse conductivity, which they treat in the half-metallic limit where only one spin-channel exists. In [65, 66], this so-called chirality-induced Hall effect can be also derived by considering two time-reversed paths of electrons which yield unequal contributions for a non-vanishing spin-chirality (non-coplanarity of the spin-structure), and corresponds to a Berry phase for the electron spin.

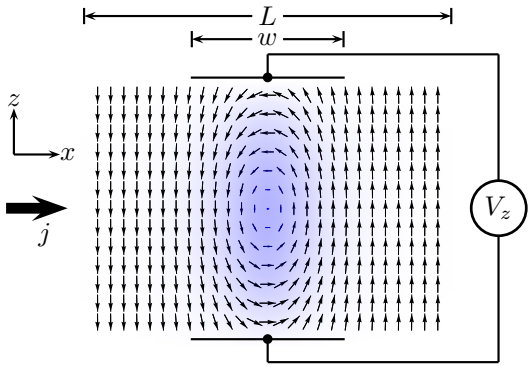

Figure 2.11.: Contact of length L containing a Bloch wall with Néel flux-closure caps (corresponds to a vortex wall). The characteristic width of the wall is w, and the transverse voltage drop is V_z. The shading indicates the magnitude of the out-of-plane component of the magnetization.

Transverse voltage across a domain wall

Let us investigate a transport experiment in which the transverse conductivity gives rise to a non-vanishing Hall voltage. As we mentioned, the term $\vec{m}\cdot(\partial_k\vec{m}\times\partial_j\vec{m})$ can only be finite when the magnetization rotates around different axis as one goes along different directions in space. This situation is for example realized in a Bloch wall with Néel flux-closure caps and is illustrated in Fig. 2.11. We apply a voltage V_x at a thin film, so that there is a current flow perpendicular to the domain wall (CPW geometry). Within the wall, the Hall conductivity is non-zero and one expects a transverse current which can be measured by detecting a voltage drop V_z at the ends of the domain-wall. Of course, this voltage drop appears only in the vicinity of the wall, and should be maximal at its center. A related effect has been found in frustrated ferromagnets [75] and also is known in literature as topological Hall effect [76], which is a result of the Berry phase picked up by the electrons as they adiabatically follow the magnetization. This Hall effect has been measured in a lattice of so-called Skyrmions which are topologically stable knots in the spin structure [77].

Let us now explicitly calculate this voltage drop for the geometry depicted in Fig. 2.11. According to (2.140), the current $\boldsymbol{j}=\underline{\underline{\sigma}}\boldsymbol{E}$ is given by

$$\begin{aligned} j_x &= \sigma_{\mathrm{c}}(E+\delta E_x) \\ j_z &= \sigma_{\mathrm{c}}\delta E_z - K\sigma_{\mathrm{c}}E\,\vec{m}\cdot(\partial_z\vec{m}\times\partial_x\vec{m}) \ , \end{aligned}$$

where $K\equiv\hbar\frac{\sigma_\uparrow\tau_\uparrow-\sigma_\downarrow\tau_\downarrow}{2m_{\mathrm{e}}\sigma_{\mathrm{c}}}$. We assume a general spin structure

$$\vec{m}=(\sin\theta\cos\phi,\sin\theta\sin\phi,\cos\theta)$$

varying only in two dimensions, $\theta(x,z)$ and $\phi(x,z)$, so that the expression corresponds to the determinant of the Jacobian $\vec{m}\cdot(\partial_z\vec{m}\times\partial_x\vec{m})=(\partial_x\cos\theta)(\partial_z\phi)-(\partial_z\cos\theta)(\partial_x\phi)=\frac{\partial(\cos\theta,\phi)}{\partial(x,z)}$. Of course, the spin-structure has to be non-coplanar in order for K to be non-zero, like the one depicted in Fig. 2.11. Employing the continuity equation $\boldsymbol{\nabla}\cdot\boldsymbol{j}=0$, we arrive at the equation

$$(\partial_x^2+\partial_z^2)\delta\varphi=-EK\partial_z\frac{\partial(\cos\theta,\phi)}{\partial(x,z)} \ ,$$

where we assume for simplicity that variation of the induced potential $\delta\varphi(x,z)$ in the x-direction is smaller than in the z-direction, so that we can neglect the derivative with respect to x, and taking into account boundary conditions leads to

$$\delta\varphi(x,z) = -EK \int^{z} \mathrm{d}z' \; \frac{\partial(\cos\theta,\phi)}{\partial(x,z')} \; .$$

The induced potential gives rise to the electric fields $\delta E_x = -\partial_x \delta\varphi$ and $\delta E_z = -\partial_z \delta\varphi$. We are interested in the voltage drop V_z across the width w of the domain wall, which we obtain from

$$\begin{aligned} V_z &= \frac{1}{w}\int_{-w/2}^{+w/2} [\varphi(x,+\infty) - \varphi(x,-\infty)]\,\mathrm{d}x = -EK\frac{1}{w}\int_{-w/2}^{+w/2}\mathrm{d}x \int_{-\infty}^{+\infty}\mathrm{d}z \; \frac{\partial(\cos\theta,\phi)}{\partial(x,z)} \\ &= -EK\frac{1}{w}\int \mathrm{d}\cos\theta \int \mathrm{d}\phi \; , \end{aligned}$$

and for the geometry depicted in Fig. 2.11, we have $\phi(z = w/2) - \phi(z = -w/2) = \pi$ (in the center of the wall) and $\cos\theta(x \to +\infty) - \cos\theta(x \to -\infty) = 2$, so that we finally obtain for the voltage drop in the limit $\tau\Delta \gg 1$

$$|V_z| = \frac{2\pi K}{wL} V_x = \frac{2\pi\hbar}{wL}\frac{\sigma_\uparrow\tau_\uparrow - \sigma_\downarrow\tau_\downarrow}{2m_\mathrm{e}\sigma_\mathrm{c}} V_x \; , \tag{2.159}$$

which for $T_1 \to \infty$ turns into

$$|V_z| \to \frac{\pi\hbar}{4m_\mathrm{e}wL}\tau^2\Delta \; V_x \; . \tag{2.160}$$

Finally, let us stress that the integration performed in (2.159) essentially corresponds to the Skyrmion number

$$N_\mathrm{Skyrmion} = \frac{1}{4\pi}\int \mathrm{d}x \int \mathrm{d}z \; \vec{m}\cdot(\partial_z\vec{m} \times \partial_x\vec{m}) \tag{2.161}$$

and is a topological number characterizing the spin structure [78].

2.4.7. Spin-current in Presence of Inhomogeneous Magnetization

The generation of spin-currents is of fundamental interest in the field of spintronics and the experimentally widespread method is to use spin-pumping due to a dynamic magnetization, especially in non-magnetic materials like semiconductors. Takeuchi *et al.* [68] calculated charge and spin-currents in presence of *s-d* exchange coupling and spin-orbit interaction due to an inhomogeneous scalar potential. However, they consider the dirty limit $\Delta\tau \ll 1$ and make a perturbation expansion in Δ and the spin-orbit interaction coupling. The spin-currents in the presence of magnetization dynamics have been investigated in Ref. [79], while they focus on the influence of spin-orbit interaction, which is not part of our study.

In contrast to the charge current, the spin-current can be directly obtained from a given magnetization profile without having to solve a differential equation. As discussed in the previous sections, the charge current has to be determined together with the electric field by solving the charge continuity equation and the Poisson equation. The reason for this difference is

the following: for the charge current, we have to satisfy the local charge neutrality condition in our case of an incompressible Fermi-liquid. This condition stems from the treatment of Coulomb interaction between electrons in the limiting case of small screening length. However, since we did not take into account any comparable interaction for the spin-degree of freedom, there is no analogue screening effect for the spin, and thus, what matters are the unscreened quantities. With respect to the spin-degree, the Fermi-liquid behaves as being totally compressible.

For the longitudinal spin-current, we obtain to leading order in $1/\tau\Delta$

$$\boldsymbol{j}_s = \underline{\underline{\sigma}}_{\rm s}\boldsymbol{E} - \frac{\hbar^2}{4e^2}\sigma_{\rm c}\,\left[\vec{m}\cdot(\boldsymbol{\nabla}\vec{m}\times\partial_t\vec{m}) + \beta\boldsymbol{\nabla}\vec{m}\cdot\partial_t\vec{m}\right] + \frac{A}{\Delta}\boldsymbol{\nabla}\vec{m}\cdot\partial_t\vec{m}\ , \tag{2.162}$$

where A is the exchange constant defined in formula (2.112), and for the correction to the spin-conductivity $(\underline{\underline{\sigma}}_{\rm s})_{ij} = \sigma_{\rm s}\delta_{ij} + (\delta\underline{\underline{\sigma}}_{\rm s})_{ij}$, we obtain up to order $(\boldsymbol{\partial}_r\vec{m})^2$

$$(\delta\underline{\underline{\sigma}}_{\rm s})_{ij} = \frac{\hbar^2\sigma_{\rm s}}{2m_{\rm e}E_{\rm F}}\left[\zeta_{\rm a}^{(\rm s)}(\partial_i\vec{m}\cdot\partial_j\vec{m}) + \zeta_{\rm i}^{(\rm s)}\,(\boldsymbol{\partial}_r\vec{m})^2\,\delta_{ij}\right] + \hbar^2\frac{\sigma_\uparrow\tau_\uparrow+\sigma_\downarrow\tau_\downarrow}{4em_{\rm e}}\,\vec{m}\cdot(\partial_i\vec{m}\times\partial_j\vec{m})\ , \tag{2.163}$$

with a structure analogue to $\delta\sigma_{\rm c}$ from Eq. (2.140). The prefactor $(-\frac{\hbar}{2e})^2$ of $\sigma_{\rm c}$ is due to the different units of charge- and spin-currents. Let us note that $\vec{m}\cdot(\boldsymbol{\nabla}\vec{m}\times\partial_t\vec{m})$ constitutes a dissipative term while $\boldsymbol{\nabla}\vec{m}\cdot\partial_t\vec{m}$ is reactive, in particular, the latter persists even in the absence of dissipative processes due to the intrinsic contribution $\frac{A}{\Delta}\boldsymbol{\nabla}\vec{m}\cdot\partial_t\vec{m}$. Interestingly, the prefactor of this intrinsic term is essentially the same as for the exchange current and spin-density, Eqs. (2.113) and (2.112).

Again, the spin-Hall term and the reactive time-gradient $\vec{m}\cdot(\boldsymbol{\nabla}\vec{m}\times\partial_t\vec{m})$ can be reproduced using the notion of the fictitious electric (2.155) and magnetic field (2.154),

$$\boldsymbol{j}_s = -\frac{\hbar}{2e}\,(\boldsymbol{j}_\uparrow - \boldsymbol{j}_\downarrow) = \left(\frac{\hbar}{2e}\right)^2\sigma_{\rm c}\boldsymbol{\mathcal{E}} - \frac{\hbar^2}{4m_{\rm e}e}\,(\sigma_\uparrow\tau_\uparrow+\sigma_\downarrow\tau_\downarrow)\,\boldsymbol{E}\times\boldsymbol{\mathcal{B}}\ , \tag{2.164}$$

which was done completely along the same lines as the derivation of (2.157) and in the regime $\tau\Delta \gg 1$.

We can introduce the spin-chemical potential induced by a time-dependent magnetization, $\vec{\mu}_p = \vec{m}\times\partial_t\vec{m}$ which gives rise to an effective spin-electric field acting on each spin component. In fact, we immediately recover the fictitious electric field $\boldsymbol{\mathcal{E}} = -\left[\boldsymbol{\nabla}\vec{\mu}_p\right]_\parallel \equiv -\vec{m}\cdot[\boldsymbol{\nabla}\vec{\mu}_p]$. Taking the gradient of $\vec{\mu}_p$ yields a tensor containing the various spin-electric fields as components and which describe effects like spin-pumping due to a time-dependent magnetization. The idea of the spin-chemical potential is analogue to the description of spin-accumulation due to pumping in magnetic multi-layers discussed in Ref. [18]. Then, we can simply write for the pumped charge and spin-currents (ignoring the β-term for the moment)

$$\begin{aligned}\boldsymbol{j}_c &= -\sigma_{\rm s}\left[\boldsymbol{\nabla}\mu_p\right]_\parallel \\ \boldsymbol{j}_s &= -\frac{\hbar^2}{4e^2}\sigma_{\rm c}\left[\boldsymbol{\nabla}\mu_p\right]_\parallel\ .\end{aligned}$$

The difference to the usual electric field is that the spin-electric field yields forces on spin-up/down channels of opposite sign. Therefore, in a non-magnetic medium where transport

quantities do not depend on the spin direction, i.e. $\sigma_\mathrm{s} = 0$, there is no charge current however, a spin-current $\propto \sigma_\mathrm{c}$ which is a direct consequence of the above relations.

It is also interesting to note that we can incorporate the β-term into the spin-chemical potential by defining instead $\vec{\mu}_p' = \vec{m} \times \partial_t \vec{m} - \beta \partial_t \vec{m}$, so that

$$\boldsymbol{\mathcal{E}}' = -\left[\boldsymbol{\nabla} \vec{\mu}_p'\right]_\parallel = \vec{m} \cdot (\partial_t \vec{m} \times \boldsymbol{\nabla} \vec{m}) - \beta \boldsymbol{\nabla} \vec{m} \cdot \partial_t \vec{m}$$

completely reproduces all the time-dependent terms in $\boldsymbol{j}_c$, however, in the longitudinal spin-current $\boldsymbol{j}_s$ we do not get the intrinsic contribution $\frac{A}{\Delta} \boldsymbol{\nabla} \vec{m} \cdot \partial_t \vec{m}$. In summary, the complete equations for the charge- and longitudinal spin-current can be compactly written as

$$\boldsymbol{j}_c = \underline{\underline{\sigma}} \boldsymbol{E} - \sigma_\mathrm{s} \left[\boldsymbol{\nabla} \mu_p'\right]_\parallel \tag{2.165}$$

$$\boldsymbol{j}_s = \underline{\underline{\sigma}}_\mathrm{s} \boldsymbol{E} - \frac{\hbar^2}{4e^2} \sigma_\mathrm{c} \left[\boldsymbol{\nabla} \mu_p'\right]_\parallel + \frac{A}{\Delta} \boldsymbol{\nabla} \vec{m} \cdot \partial_t \vec{m} \ . \tag{2.166}$$

Transverse spin currents

As we will find out later, the spin-current gives rise to a spin-torque and thus directly affects the magnetization dynamics. Therefore, it is also interesting to look at the transverse spin-current which is induced by a time-dependent magnetization, and in the limit $\tau\Delta \gg 1$ has the form

$$\hat{\boldsymbol{j}}_\perp = -\sigma_{d\perp} \left(\boldsymbol{\nabla} \vec{\mu}_p\right)_\perp \hat{\vec{\sigma}} + \sigma_{r\perp} \vec{m} \times \boldsymbol{\nabla} \vec{\mu}_p \hat{\vec{\sigma}} = -\sigma_{d\perp} \vec{m} \times (\partial_t \boldsymbol{\nabla} \vec{m})_\perp \hat{\vec{\sigma}} - \sigma_{r\perp} (\partial_t \boldsymbol{\nabla} \vec{m})_\perp \hat{\vec{\sigma}} \ , \tag{2.167}$$

Note that here we are omitting the additional transverse spin-current contribution induced by the electric field. Also, we did not explicitly write the exchange current (2.113), although it has to be added here in order to obtain the complete expression. We defined the transverse spin conductivity with the dissipative part $\sigma_{d\perp}$ and the reactive part $\sigma_{r\perp}$,

$$\sigma_{d\perp} = \frac{\nu_0}{12 m_\mathrm{e} P \Delta} \left(\frac{1 - P^4}{\tau} + \frac{1}{T_2} + \frac{P^2 (3 + P^2)}{T_1} \right) \ , \tag{2.168}$$

$$\sigma_{r\perp} = \frac{\nu_0 \left(5 + 5P^2 + 2P^4\right)}{60 m_\mathrm{e} P} \ . \tag{2.169}$$

The reactive part is due to precession in the exchange field Δ, while the dissipative part is due to momentum and spin-relaxation and vanishes in the absence of scattering mechanisms, $\tau, T_1, T_2 \to \infty$, so that in our case $\Delta\tau \gg 1$, we have $\sigma_{d\perp} \ll \sigma_{r\perp}$. In a fully polarized ferromagnet $P = 1$, we find that $\sigma_{d\perp}$ vanishes unless in the presence of spin-relaxation.

Tserkovnyak *et al.* derived expressions for the dissipative transverse conductivity by calculating the linear spin-density response to a transverse magnetic field [80]. Additionally evaluating the auto-correlator for the transverse spin-currents (the Kubo formula), they arrive at an expression which exactly corresponds to our result of $\sigma_{d\perp}$ in the absence of spin-relaxation $T_1, T_2 \to \infty$. They also noted that, formally, there is no difference between Stoner and *s-d* model, except for the different microscopic origin of the exchange field Δ, a result which we also find.

Finally, using the extended spin-chemical potential $\vec{\mu}'_p = \vec{m} \times \partial_t \vec{m} - \beta \partial_t \vec{m}$, we can also rewrite the transverse spin-current

$$\hat{\boldsymbol{j}}_\perp = -\sigma'_{d\perp} \left(\boldsymbol{\nabla} \vec{\mu}'_p \right)_\perp \hat{\vec{\sigma}} + \sigma'_{r\perp} \vec{m} \times \boldsymbol{\nabla} \vec{\mu}'_p \hat{\vec{\sigma}} \tag{2.170}$$

so that here, the transverse conductivities are related to the previous ones by $\sigma'_{d\perp} = \sigma_{d\perp} - \beta \sigma_{r\perp}$ and $\sigma'_{r\perp} = \sigma_{r\perp}$, dropping corrections of order β^2.

This concludes our investigations on the influence of an inhomogeneous and time-dependent magnetization structure $\vec{m}(\boldsymbol{r}, t)$ on the conduction electrons inside the ferromagnetic metal. In particular, we studied the implications on current-flow, also in the presence of an external electric field which gives rise to the domain-wall resistance, and in more complex 2-dimensional magnetization textures like a vortex, it leads to a transverse Hall conductivity.

2.5. Magnetization Dynamics

We will now switch sides and consider the system from the point of view of the magnetization dynamics and study the additional contributions from the conduction electrons which are intimately coupled to the magnetization through the exchange interaction, thus, giving rise to a spin-torque exerted on the magnetization $\vec{m}$. The concept of spin-torque is at the heart of magnetization dynamics described by the famous Landau-Lifshitz-Gilbert (LLG) equation. It is a widely used kinetic equation for the magnetization dynamics, and is used for example to the study domain-wall motion which is of fundamental interest for a new generation of magnetic data storage devices [1]. To this end, let us give a brief review of the existing studies and calculations of spin-torques and domain wall motion.

Theoretical spin-torque calculation have been performed by various groups [19, 22, 23, 26, 27, 28, 29] along with a gauge field formulation of adiabatic spin torques [25], using functional Keldysh theory [24], and the influence of momentum transfer has been investigated in Ref [20]. Xiao *et al.* argue that the non-adiabatic term cannot be due to spin-flip scattering since the non-equilibrium spin should be aligned along an effective field incorporating the magnetization gradient [21]. In fact, we find that the appearance of the non-adiabatic β-term requires a dissipative spin-dephasing mechanism, expressed by T_2 within our model. The spin-wave contributions to the damping are found to obey $\alpha_{sw} = \beta_{sw}$ [81] and many-body effects like electron-electron interaction on the Gilbert Damping constant have been considered in Refs [82, 83, 84, 85].

The theoretical study of domain-wall motion has been first carried out without the non-adiabatic coefficient β [86, 87], and later including the effect of the β-term which acts as an additional force on the magnetization structure [88, 89, 90, 91]. The influence of extrinsic pinning is considered in works [20, 92, 93]. Shibata *et al.* investigated the vortex wall motion driven by the current-induced spin-transfer torque [94] and the influence of eddy currents of a moving domain-wall has been studied in Ref [95]. A recent review of domain wall motion can be found in Ref [29]. A numerical investigation of domain-wall motion using a simple spin-conserving lattice Hamiltonian indicates a depinning below the critical current due to an emission of spin-waves in the case of short domain walls [96]. The non-adiabatic term is crucial for domain-wall motion in nanowires, or the current-in-plane geometry (CIP)

in magnetic multilayers. However, as described by Khvalkovskiy in Ref [97], much higher domain-wall velocities can be achieved in magnetic multilayers in the current perpendicular to plane geometry (CPP), in which case the larger (by a factor $1/\beta$) adiabatic spin-torque term drives the wall. The influence of finite temperature on the current-driven and field-driven domain wall motion has been investigated theoretically [98, 99], and the authors found a reduction of the depinning times due to the non-equilibrium fluctuations. An exact solution for the domain wall dynamics within the framework of the LLG equations is discussed in Ref [100].

In a slightly different line of research, Culcer *et al.* theoretically investigated the magnetization dynamics in ferromagnetic semiconductors and find to leading order an expression for the spin-torque which is not rotationally invariant [101]. The reason is that in semiconductors the intrinsic spin-orbit coupling is the dominant mechanism, while in ferromagnetic metals the intrinsic spin-orbit contribution is usually neglected and extrinsic contributions add only to spin-dephasing. This is compatible with Ref [102], who find an enhanced domain-wall mobility in (Ga,Mn)As materials along with a significant hole reflection at domain-walls which persists even in the adiabatic limit. All these effects are a result of the dominant spin-orbit mechanism while scattering mechanisms are secondary, which is in contrast to our study of metallic systems.

Experimentally, current-driven domain wall motion in metallic nanowires has been studied in Refs [10, 11, 12], thermally activated domain wall motion has been used to measure β [103] and $Ni_{80}Fe_{20}$ nanowires with low depinning fields have been utilized to obtain lower critical velocities [104].

Before we will investigate the spin-torque and its implications within our model, we first cover some basics by taking a look at the simple phenomenological Bloch equations.

2.5.1. From Non-equilibrium Spin-excitations to Spin Torque

The treatment will be similar as in section 2.4.3, though, we will be more specific here. In order to obtain the spin-torque, we need to find the transverse non-equilibrium spin-excitation in the system which we denote as $\vec{s}_\perp$. This quantity of interest is obtained by considering just the transverse part of the spin-continuity equation (2.121),

$$(\partial_t \vec{s})_\perp + \Delta_{\boldsymbol{r}}\, \vec{m}\times\vec{s}_\perp + (\boldsymbol{\nabla}\cdot\underline{\underline{J}}_s)_\perp = \vec{N}_{\text{eff},\perp} - \frac{1}{T_{2,\boldsymbol{r}}}\vec{s}_\perp \ , \tag{2.171}$$

along with $\vec{N}_{\text{eff},\perp}$ given in Eq. (2.122) and $(\dots)_\perp$ indicates that we take the vector component perpendicular to $\vec{m}$. The spin-dephasing time $T_{2,\boldsymbol{r}} = (1+\eta_{\boldsymbol{r}})T_2$ has gradient corrections included with $\eta_{\boldsymbol{r}}$ defined in (2.127). Furthermore, we introduce the spin-current tensor $(\underline{\underline{J}}_s)_{ij} \equiv \frac{\hbar}{2}\text{Tr}\frac{\hat{\sigma}_j}{2}\hat{j}_i$ which contains the spin-currents for the 3 spin-components and $(\boldsymbol{\nabla}\cdot\underline{\underline{J}}_s)_j \equiv \partial_{r_i}(\underline{\underline{J}}_s)_{ij}$ is the divergence thereof.[2] In the preceding sections, we already investigated the spin-currents in presence of time-dependent $\vec{m}$ and external electric field, so the spin-current tensor is explicitly given by Eqs. (2.162), (2.167) and (2.113).

[2]Here, the spin-current is defined with the usual factor $\frac{\hbar}{2}$ in order to obtain the current of angluar momentum.

We can solve this equation for the transverse dynamics iteratively by first solving for $\vec{s}_\perp$,

$$\vec{s}_\perp = \frac{1}{\Delta_{\boldsymbol{r}}}(\beta_{\boldsymbol{r}} - \vec{m}\times)\left(-(\partial_t\vec{s})_\perp - (\boldsymbol{\nabla}\cdot\underline{\underline{J}}_s)_\perp + \vec{N}_{\mathrm{eff},\perp}\right) , \tag{2.172}$$

where here, the non-adiabatic coefficient $\beta_{\boldsymbol{r}} \equiv \frac{1}{T_{2,\boldsymbol{r}}\Delta_{\boldsymbol{r}}}$ incorporates gradient-corrections and we drop terms of order β^2. We now start from the zeroth order solution which corresponds to the spin-density of the equilibrium system, $\vec{s}_0 = \rho_{s,\boldsymbol{r}}\vec{m} + \vec{N}_{\mathrm{xc}}$, and consists of the equilibrium spin-density $\rho_{s,\boldsymbol{r}} = \rho_s - \delta\rho_s$ including gradient corrections, Eq. (2.111), and the transverse spin-excitation due to the exchange current, respectively. Compatible to a linear response treatment, we then plug $\vec{s}_0$ into the right-hand side of expression (2.172). Finally, the corresponding spin-torque is given by $\vec{\mathcal{T}}_{\mathrm{el}} = -g\mu_{\mathrm{B}}\Delta_{\boldsymbol{r}}\vec{m}\times\vec{s}$, where $g \approx 2$ is the g-factor and $\mu_{\mathrm{B}} \equiv \frac{|e|\hbar}{2m_e}$ is the Bohr magneton [66]. Explicitly, we then obtain for the spin-torque

$$-\frac{1}{g\mu_{\mathrm{B}}}\vec{\mathcal{T}}_{\mathrm{el}} = \Delta_{\boldsymbol{r}}\vec{m}\times\vec{s}_\perp = (1+\beta_{\boldsymbol{r}}\vec{m}\times)\left(-\rho_{s,\boldsymbol{r}}\partial_t\vec{m} - (\partial_t\vec{N}_{\mathrm{xc}})_\perp - (\boldsymbol{\nabla}\cdot\underline{\underline{J}}_s)_\perp + \vec{N}_{\mathrm{eff},\perp}\right). \tag{2.173}$$

The time-derivative of the exchange term (2.113) becomes

$$(\partial_t\vec{N}_{\mathrm{xc}})_\perp = \frac{A}{\Delta}\left(\partial_t(\boldsymbol{\partial}_r^2\vec{m})_\perp\right)_\perp = \frac{A}{\Delta}\left[(\boldsymbol{\partial}_r\vec{m})^2\partial_t\vec{m} + (\partial_t\boldsymbol{\partial}_r^2\vec{m})_\perp\right] ,$$

but there are two more contributions related to exchange currents, the obvious one arising from $\underline{\underline{J}}_s$, and the other one a result of the distinction of high- and low-energy scattering, the former expressed in $\vec{N}_{\mathrm{eff},\perp}$. In fact, we find that it is exactly this term $\propto \beta A$ that is responsible for the cancelation of a "dissipative exchange torque" and that would otherwise appear due to the spin-mistracking originating from $\vec{N}_{\mathrm{xc}}$. Physically speaking, this is good news, as an intrinsic contribution like the exchange current (2.113) should not be subject to any dissipative mechanism like spin relaxation.

Explicitly writing all the exchange-related terms, we can rewrite the spin-torque in the form[3]

$$\begin{aligned}-\frac{1}{g\mu_{\mathrm{B}}}\vec{\mathcal{T}}_{\mathrm{el}} = &-(1+\beta\vec{m}\times)\left(\boldsymbol{\nabla}\cdot\underline{\underline{J}}_s\right)_\perp - \rho_{s,\boldsymbol{r}}\partial_t\vec{m} - \alpha\rho_s\,\vec{m}\times\partial_t\vec{m} \\ &+ \alpha_1^{\mathrm{nloc}}\vec{m}\times\partial_t\boldsymbol{\partial}_r^2\vec{m} + A\left[\left(1 - \frac{\beta}{\Delta}\partial_t + \frac{1}{\Delta}\vec{m}\times\partial_t\right)\vec{m}\times\boldsymbol{\partial}_r^2\vec{m}\right]_\perp ,\end{aligned} \tag{2.174}$$

where now, $\underline{\underline{J}}_s$ only contains true non-equilibrium contributions and thus, vanishes in absence of time-dependence and an external electric field.

We note that the Gilbert damping constant α emerges from $\vec{N}_{\mathrm{eff},\perp}$. Furthermore, in this and the following results, we can drop all gradient corrections which would only renormalize the Gilbert damping constant α, since the dominant term arises from $\boldsymbol{\nabla}\cdot\underline{\underline{J}}_s$ and is given by $\frac{\sigma_{\mathrm{c}}}{4e^2}$ (see result (2.175)), while all other corrections would be smaller by a factor $\frac{1}{\tau^2\Delta^2}$, and thus negligible in our regime of investigation. This is also the reason why we made the replacements $\beta_{\boldsymbol{r}} \to \beta$ and in the prefactor of α, $\rho_{s,\boldsymbol{r}} \to \rho_s$.

The last term on the right-hand side resembles the result of (2.138) with the exchange torque given by $\vec{\mathcal{T}} = A\vec{m}\times\boldsymbol{\partial}_r^2\vec{m}$, except for a factor of 2 whose origin lies in the term $\vec{N}_{\mathrm{eff},\perp}$ and was

[3] We make use of the vector identities $\partial_t\vec{m}\times\boldsymbol{\partial}_r^2\vec{m}|_\perp = \vec{m}\times\boldsymbol{\partial}_r^2 m + (\boldsymbol{\partial}_r\vec{m})^2\vec{m}\times\partial_t\vec{m}$ and $\vec{m}\times\partial_t(\vec{m}\times\boldsymbol{\partial}_r^2\vec{m}) = -(\partial_t\boldsymbol{\partial}_r^2\vec{m})_\perp - (\boldsymbol{\partial}_r\vec{m})^2\partial_t\vec{m}$

discussed above. The term $\frac{1}{\Delta}\vec{m}\times\partial_t\vec{\mathcal{T}}$ can be understood as the precession correction and the term $-\frac{\beta}{\Delta}(\partial_t\vec{\mathcal{T}})_\perp$ as the respective dissipative correction due to spin-dephasing.

Result (2.174) lets us identify the contributions to the non-local exchange (dynamic exchange) which do not directly originate from the non-equilibrium spin-currents $\underline{\underline{J}}_s$ induced by an external electric field or by the magnetization dynamics. However, in order to study all the terms explicitly appearing in the expression for the spin-torque, we substitute the spin currents using results (2.162), (2.167), and dropping terms of order β^2, we readily obtain[4]

$$
\begin{aligned}
-\frac{1}{g\mu_\mathrm{B}}\vec{\mathcal{T}}_\mathrm{el} = -(1+\beta\vec{m}\times)(\boldsymbol{j}_s\boldsymbol{\partial}_r)\vec{m} - \left(\rho_{s,\boldsymbol{r}} + \frac{A}{\Delta}\left(\boldsymbol{\partial}_r\vec{m}\right)^2\right)\partial_t\vec{m} - \alpha\rho_s\,\vec{m}\times\partial_t\vec{m} \\
+ A\vec{m}\times\boldsymbol{\partial}_r^2\vec{m} + \beta\frac{\hbar^2\sigma_\mathrm{c}}{4e^2}\left(\boldsymbol{\partial}_r\vec{m}\right)^2\partial_t\vec{m} - \frac{\hbar^2\sigma_\mathrm{c}}{4e^2}\left(\boldsymbol{\partial}_r(\partial_t\vec{m}\times\boldsymbol{\partial}_r\vec{m})\right)_\perp \\
+ \alpha_d^{(\mathrm{nl})}\vec{m}\times\partial_t\boldsymbol{\partial}_r^2\vec{m} + \alpha_r^{(\mathrm{nl})}\left[\boldsymbol{\partial}_r(\partial_t\boldsymbol{\partial}_r\vec{m})_\perp\right]_\perp \quad . \qquad (2.175)
\end{aligned}
$$

where the spin-current due to the external electric field is $\boldsymbol{j}_s = \sigma_\mathrm{s}\boldsymbol{E}$ (the current in units of spin-angular momentum) as introduced in section 2.4.4. The terms of first order in time-gradients and second order in spatial gradients include non-local contribution to various terms like Gilbert damping, and will be relevant for magnetization structures varying strongly in space, like short walls.

Taking into account spatial gradient corrections, the effective conduction electron magnetization density appearing in the LLG equation gets renormalized by the reduction of the spin-density $\delta\rho_s$ determined in (2.111), which is different for Stoner and s-d models. However, in addition to this straightforward term, we also have a renormalization due to the exchange current.

The non-local dissipative (Gilbert damping) and reactive ($\propto\beta\sigma_\mathrm{c}$) terms proportional to σ_c have also been found by Wong *et al.* in Ref [74]. Essentially, the reactive term renormalizes the effective electron spin-density by $\beta\frac{\hbar^2\sigma_\mathrm{c}}{4e^2}\left(\boldsymbol{\partial}_r\vec{m}\right)^2$, in addition to the corrections discussed above. Due to $\left(\boldsymbol{\partial}_r(\partial_t\vec{m}\times\boldsymbol{\partial}_r\vec{m})\right)_\perp = \left(\boldsymbol{\partial}_r\vec{m}\right)^2\vec{m}\times\partial_t\vec{m} - (\partial_t\vec{m}\cdot\boldsymbol{\partial}_r\vec{m})\vec{m}\times\boldsymbol{\partial}_r\vec{m}$, the dissipative term enhances the Gilbert damping constant α by an isotropic contribution $\frac{\hbar^2\sigma_\mathrm{c}}{4e^2}(\boldsymbol{\partial}_r\vec{m})^2$. The second term essentially modifies the non-adiabatic spin-torque due to the current $\boldsymbol{j}_s$, giving rise to a fictitious spin-current $\propto\frac{\hbar^2\sigma_\mathrm{c}}{4e^2}(\partial_t\cdot\boldsymbol{\partial}_r\vec{m})$.

The last two terms are identical for both Stoner and s-d model, namely the dissipative term $\alpha_d^{(\mathrm{nl})} = \sigma_{d\perp} + \beta\sigma_{r\perp} + \beta\alpha_1^{\mathrm{nloc}} - \beta\frac{A}{\Delta}$ and the reactive term $\alpha_r^{(\mathrm{nl})} = \sigma_{r\perp} - \frac{A}{\Delta}$. The dissipative term $\alpha_d^{(\mathrm{nl})}\vec{m}\times\partial_t\boldsymbol{\partial}_r^2\vec{m}$ has contributions from $\vec{N}_{\mathrm{eff},\perp}$ but also from the divergence of the spin-current, where the latter give rise to $\sigma_{d\perp} + \beta\sigma_{r\perp}$. This term describes additional dissipation mediated by the conduction electrons due to dynamical exchange and has been discussed in Ref. [80], however, there only the link to the transverse spin diffusion coefficient $\sigma_{d\perp}$ was established. In the end, this term can be interpreted as an anisotropic Gilbert damping contribution, which can be seen experimentally using microwave radiation to excite magnetization dynamics, and performing a wave-vector dependent measurement of the Gilbert damping constant $\alpha(\boldsymbol{q})$. The Gilbert damping is related to the broadening of the absorption line. Finally, $\alpha_r^{(\mathrm{nl})}$ is an

[4] We use the identities $\left(\boldsymbol{\partial}_r(\partial_t\vec{m}\times\boldsymbol{\partial}_r\vec{m})\right)_\perp = -\left[\vec{m}\cdot(\boldsymbol{\partial}_r\vec{m}\times\partial_t\vec{m}\right]\boldsymbol{\partial}_r\vec{m} = \left(\boldsymbol{\partial}_r\vec{m}\right)^2\vec{m}\times\partial_t\vec{m} - (\partial_t\vec{m}\cdot\boldsymbol{\partial}_r\vec{m})\vec{m}\times\boldsymbol{\partial}_r\vec{m}$ and $\left[\boldsymbol{\partial}_r(\partial_t\boldsymbol{\partial}_r\vec{m})_\perp\right]_\perp = (\partial_t\boldsymbol{\partial}_r^2\vec{m})_\perp + (\partial_t\vec{m}\cdot\boldsymbol{\partial}_r\vec{m})\,\boldsymbol{\partial}_r\vec{m}$

additional reactive term due to the transverse conductivity $\sigma_{r\perp}$ and the exchange interaction. In the experiment just mentioned, it would for example lead to a wave-vector dependent shift in the excitation frequency.

Note that we can identify dissipative terms in the torque by looking for terms which are odd under time-reversal, i.e. $\partial_t \to -\partial_t$, $\vec{m} \to -\vec{m}$ and $\boldsymbol{j}_s \to -\boldsymbol{j}_s$. The terms even under this transformation are denoted as reactive. It is clear that the dissipative terms vanish in absence of any time-reversal breaking mechanism, but is not true for all of the reactive terms, since they contain intrinsic contributions, like $\alpha_r^{(\mathrm{nl})}$. These contributions are reminiscent to the intrinsic contributions of the anomalous Hall effect originating from the spin-orbit interaction. However, we did not include any spin-orbit term in the usual sense in our model, but we have the Zeeman term coupling the electron spin to an inhomogeneous exchange field which actually does couple spin and orbital degrees of freedom, thus acting like a spin-orbit interaction. In fact, for the spatially homogenous case, only the usual Gilbert damping constant α remains, and this term vanishes as $T_2 \to \infty$.

The expression (2.175) is the main result of this section and constitutes the complete torque due to the conduction electrons acting on the magnetization $\vec{m}$. It emerges from a treatment that is consistent up to order $\partial_t(\boldsymbol{\partial}_r\vec{m})^2$ and $\boldsymbol{E}\boldsymbol{\partial}_r\vec{m}$ and is derived in the regime where precession dominates over other time-scales in the system, i.e. $\Delta\tau \gg 1$. In this case, β is much smaller than unity and we can neglect terms of order $O(\beta^2)$.

2.5.2. Spin Torque and Landau-Lifshitz-Gilbert Equation

In this section, we will study the implications of the spin-torque derived in the previous section on the magnetization dynamics for the two limiting cases of the *s-d* model and the Stoner model.

However, let us first remark on the exchange interaction term, usually treated on the level of the free energy $F[\vec{m}(\boldsymbol{r})]$ which is a functional of the magnetization $\vec{m}$. Here, it explicitly appears in the spin-torque (2.175), and constitutes the contribution mediated by the itinerant electrons, which in the Stoner model is already the total exchange interaction, while in the case of the *s-d* model, there are additional (larger) contributions from direct exchange between localized spins. The exchange term corresponds to an effective magnetic field $\vec{H}_{\mathrm{xc}} = A\boldsymbol{\partial}_r^2\vec{m}$ which in turn corresponds to a free energy term $F_{\mathrm{xc}}[\vec{m}(\boldsymbol{r})] = \frac{A}{2}\int \mathrm{d}^3r\ (\boldsymbol{\partial}_r\vec{m})^2$, so that $\vec{H}_{\mathrm{xc}}(\boldsymbol{r}) = -\frac{\delta F_{\mathrm{xc}}}{\delta\vec{m}[\boldsymbol{r}]}$.

Stoner model

In the Stoner limit of itinerant ferromagnetism, the self-consistency condition dictates $\vec{\mathcal{T}}_{\mathrm{el}} = 0$ (see Eq. (2.53)), and we readily obtain the LLG equation including the effective field term that incorporates the exchange interaction. Of course, other contributions to the effective field, like anisotropy or dipole-dipole interaction is not present in our microscopic Hamiltonian and thus do not emerge in (2.175), but they can be added by hand. In this limit, we can also directly specify the Gilbert damping (excluding other contributions to the damping like coupling to phonons) and which reads $\alpha = \frac{\nu_0}{2T_2\rho_s}$. The ratio $\beta/\alpha = \frac{2\rho_s}{\nu_0\Delta} = \left(1 + P^2/3\right)$ is not necessarily one, except for the case of small polarization $P \ll 1$. For non-negligible polarization, $\alpha < \beta$

which is in agreement with experimental findings [103, 10, 12, 105], but the measured ratio β/α is much higher, which indicates that additional mechanisms contribute to β. This result has been also found by Tatara and coworkers [22, 29, 66], however, they found a dependence on the anisotropy of magnetic impurity scattering ($\underline{\underline{\chi}}^{(m)}$ defined section 2.2.3) which our result does not exhibit. We believe the difference is due to different treatment of the anisotropy axis which in our case adiabatically follows $\vec{m}$, while Tatara *et al.* used the fixed z-axis and then considered small transverse fluctuations around this axis to obtain the torques. This is also the reason why in Ref. [22, 29] they find a correction $\propto \boldsymbol{j}_c$ in the current induced spin-torque which does not emerge in our result.

Finally, Burrowes *et al.* measured the non-adiabatic coefficient β in narrow domain walls ($1 - 10$ nm) and they find $\alpha \approx \beta$ and suggest magnetic dissipation to be the universal origin of both coefficients [106].

s-d model

In the case of the s-d model, the Landau-Lifshitz-Gilbert equation for the magnetization dynamics of the d-electrons reads

$$M_d(\partial_t \vec{m} + \alpha_d \vec{m} \times \partial_t \vec{m}) = -g\mu_{\mathrm{B}} M_d \vec{m} \times \vec{H}_{\mathrm{eff}} + \vec{\mathcal{T}}_{\mathrm{el}} \ , \tag{2.176}$$

where M_d is the magnetization of the d-electrons and we denote $M_s = -g\mu_{\mathrm{B}}\rho_s$ as the magnetization of the conduction electrons. According to Tatara and coworkers [66], one has $M_d = -g\mu_{\mathrm{B}}\frac{1}{a^3}S$, where S is the effective spin of a unit cell and a^3 is its volume.

α_d contains any other damping contributions to the d-electron magnetization dynamics which do not originate from the conduction electron system, like interaction with nuclear spins or with the lattice (relaxation due to phonons). $\vec{H}_{\mathrm{eff}}$ is an effective magnetic field that describes the exchange interaction, anisotropy and dipole-dipole interaction. One can readily identify the different contributions to the spin-torque (2.175). The term $M_s\partial_t\vec{m}$ simply renormalizes the magnetization magnitude in the LLG equation to be that of the total magnetization $M_{\mathrm{tot}} = M_d + M_s = -g\mu_{\mathrm{B}}\rho_{\mathrm{tot}}$, the term $\propto \vec{m}\times\partial_t\vec{m}$ yields the conduction electron contribution to the Gilbert damping constant $\alpha_{\mathrm{el}} = \frac{\nu_0}{2T_2\rho_{\mathrm{tot}}}$ which, when compared to α for the Stoner limit is essentially reduced by the fraction of conduction electron magnetization to total magnetization.

In our regime $\tau\Delta \gg 1$, the dominating contribution to the non-local Gilbert damping terms comes from the terms $\propto \sigma_{\mathrm{c}}$. But when Δ is small, and thus also P is small, the other terms can also become relevant since they are $\propto 1/P$. These damping terms of order $(\boldsymbol{\partial}_r\vec{m})^2$ correspond to the continuous version of the Gilbert damping enhancement which also exists as a discrete version in multilayers. A simple example is a magnetic layer, whose damping in one layer is influenced by the mere presence of another layer due to the exchange of spin-torque [18, 80]. Using simple vector-algebra, one can show that said terms proportional to σ_{c} also appear in the theory of Tserkovnyak *et al.* [74] except for the β^2-term which are beyond our regime. However, they do not get the other two intrinsic terms independent of impurity scattering (and thus arising purely from band-structure or Berry phase effects). This gives for example rise to the additional term $[\boldsymbol{\partial}_r(\partial_t\boldsymbol{\partial}_r\vec{m})_\perp]_\perp$ which cannot be absorbed into the already existing ones.

2.5.3. Force on the Magnetization in the s-d Model

In order to further understand the implications of a non-equilibrium spin excitation in the conduction electron system, we use the concept of a force in this section. In the s-d model, we can calculate the force that is exerted on the d-electron magnetization structure by the itinerant electrons, and it explicitly reads

$$\boldsymbol{F}_m = -\Delta(\boldsymbol{\nabla}\vec{m})\cdot\vec{s} \tag{2.177}$$

and with $\vec{s}$ obtained from result (2.175), we obtain

$$\begin{aligned}\boldsymbol{F}_m = -\rho_s\vec{m}\cdot(\partial_t\vec{m}\times\boldsymbol{\nabla}\vec{m}) + \alpha\rho_s(\boldsymbol{\nabla}\vec{m}\cdot\partial_t\vec{m}) \\ + \beta\sigma_\mathrm{s}(\boldsymbol{\nabla}\vec{m})\cdot(\boldsymbol{E}\boldsymbol{\partial}_r\vec{m}) + \sigma_\mathrm{s}\vec{m}\cdot(\boldsymbol{\nabla}\vec{m}\times\boldsymbol{E}\boldsymbol{\partial}_r\vec{m}) \ ,\end{aligned} \tag{2.178}$$

where we kept only the leading order terms in spatial gradients. Before investigating the dissipative terms, we note that we can once more derive the reactive force terms from the concept of the fictitious fields introduced in Eqs. (2.154) and (2.155). We find the averaged forces exerted by the magnetization structure on the spin-up/spin-down electrons

$$\langle\boldsymbol{F}_{\uparrow,\downarrow}\rangle = \frac{m_\mathrm{e}}{\tau_{\uparrow,\downarrow}}\frac{\boldsymbol{j}_{\uparrow,\downarrow}}{-e} = \pm\frac{\hbar}{2}\left(n_{\uparrow,\downarrow}\boldsymbol{\mathcal{E}} - \frac{1}{e}\boldsymbol{j}_{\uparrow,\downarrow}\times\boldsymbol{\mathcal{B}}\right) \ , \tag{2.179}$$

where we used expression (2.156) in the second step. Thus, we readily obtain for the force acting on the itinerant electrons

$$\boldsymbol{F}_e = \langle\boldsymbol{F}_\uparrow\rangle + \langle\boldsymbol{F}_\downarrow\rangle = \hbar\rho_s\boldsymbol{\mathcal{E}} + \sigma_\mathrm{s}\boldsymbol{E}\times\boldsymbol{\mathcal{B}} \ , \tag{2.180}$$

so that the force(-density) acting on the magnetization structure due to the conduction electron gas is simply given by $\boldsymbol{F}_m = -\boldsymbol{F}_e$. Comparing $-\boldsymbol{F}_e$ and Eq. (2.178), we can indeed find equality between the two reactive terms, the latter representing the Hall-force due to the fictitious magnetic field.

The dissipative terms can be illustrated by considering a simple quasi one-dimensional magnetization structure which only varies with a constant gradient along the z-direction, a so called spin spiral, so that $\partial_z\vec{m} = k\hat{e}_\varphi$. We first consider a rotation of the magnetization around the z-axis with constant angular frequency $\partial_t\vec{m} = \omega\hat{e}_\varphi$, so that effectively it looks as if the whole magnetization structure is moving to the left (see Fig. 2.12(a)). Calculating the respective force on the electrons due to the α-term, we obtain $F_e = -\rho_s\alpha(\partial_z\vec{m}\cdot\partial_t\vec{m}) = -\rho_s\alpha k\omega$, so that electrons are dragged along with the magnetization due to the dissipative Gilbert damping term. This electron drag gives rise to a charge current (flowing into the opposite direction, i.e. to the right in Fig. 2.12(a)) and should correspond to the one derived in (2.141), which for the given magnetization dynamics reads $\boldsymbol{j}_c = |\sigma_\mathrm{s}|\beta k\omega$. This shows that there is an intrinsic relation between α and β, even though the factor of proportionality depends on the specific band structure.

On the other side, applying an electric field leads to a spin current $j_s = \sigma_\mathrm{s}E$ (here opposite to the direction of E since $\sigma_\mathrm{s} < 0$), i.e. electrons are moving to the left (see Fig. 2.12(b)). The corresponding dissipative force on the magnetization due to this current is in our scenario $F_m = \beta(\partial_z\vec{m})\cdot(j_s\partial_z\vec{m}) = -|\sigma_\mathrm{s}|Ek^2$, so that the electrons drag the magnetization in the same direction due to the dissipative spin-torque.

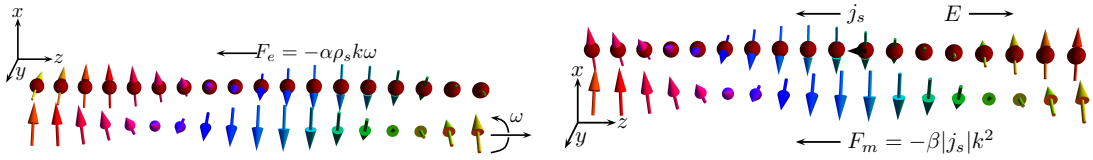

(a) Electron drag due to the α-term (b) Magnetization drag due to the β-term

Figure 2.12.: (a) Illustration of the electron drag due to the α-term in the force for a rotating magnetization with angular frequency ω around the z-axis. The upper row with the red spheres denotes the electrons and its spin, while the lower row depicts the magnetization $\vec{m}(\boldsymbol{r})$. Note the mistracking between electron spin and $\vec{m}(\boldsymbol{r})$ induced by the dynamics. (b) Dragging of the magnetization due to the β-term of the force F_m in the presence of moving electrons due to an applied electric field E.

Note that in the adiabatic limit, there is no simple correspondence between force and resistivity in the diffusive case. The equality derived by Tatara *et al.* [29, 66] relates the resistivity due to electron reflection at the domain wall to the force driven by the same reflection processes, but the probability of reflection vanishes exponentially in the adiabatic limit.

The force relates to the torque by $\boldsymbol{F} = \frac{1}{g\mu_\mathrm{B}}\boldsymbol{\nabla}\vec{m}\cdot(\vec{m}\times\vec{\mathcal{T}}_\mathrm{el})$, so that in the s-d model, we can rewrite the LLG equation (2.176) in term of the force,

$$\begin{aligned}\vec{m}\cdot(\boldsymbol{\nabla}\vec{m}\times\partial_t\vec{m}) + \alpha_d\boldsymbol{\nabla}\vec{m}\cdot\partial_t\vec{m} &= -g\mu_\mathrm{B}\boldsymbol{\nabla}\vec{m}\cdot\vec{H}_\mathrm{eff} - \frac{g\mu_\mathrm{B}}{M_d}\boldsymbol{F} \\ &= -g\mu_\mathrm{B}\boldsymbol{\nabla}\vec{m}\cdot\vec{H}_\mathrm{eff} + \frac{a^3}{S}\boldsymbol{F}\ . \end{aligned} \tag{2.181}$$

When $\alpha_d = \beta$, the left-hand side would formally correspond to the charge current induced by a dynamic magnetization (up to prefactors). Note that the first term on the left side represents the time-derivative of the Berry phase [70].

In the Stoner limit, the magnetization arises from the itinerant electrons itself and consequently, we cannot define a force this way. Therefore, we will continue with the study of a moving domain wall which according to the insight gained in this section is expected to drag electrons along with it and thus, it produces a charge current that we will calculate in the next section.

2.5.4. Charge Current Induced by a Moving Domain-wall

It is interesting to study the charge current induced by a field driven domain-wall due to the possible experimental determination of β [71, 72]. The electromotive force induced by a moving vortex wall has been measured by Yang and coworkers [30].

Let us first consider the case in which $\alpha = \beta$, although this is generally not the case [23, 22, 24]. In this scenario, we can recast the LLG-equation (2.176) into

$$(1+\beta\vec{m}\times)\left(\partial_t\vec{m} + \boldsymbol{v}_s\boldsymbol{\partial}_r\right)\vec{m} = -\vec{m}\times\vec{H}\ , \tag{2.182}$$

where $\boldsymbol{v}_s = \boldsymbol{j}_s/M$ and $\vec{H} = g\mu_{\rm B}\vec{H}_{\rm eff}$ is the effective field acting on the magnetization which in a straightforward case takes the form

$$\vec{H}[\vec{m}] = J\boldsymbol{\partial}_r^2\vec{m} - K_\perp(\vec{e}_x\vec{m})\vec{e}_x + K_z(\vec{e}_z\vec{m})\vec{e}_z + g\mu_{\rm B}\vec{B} = \vec{H}_0 + g\mu_{\rm B}\vec{B} \ . \tag{2.183}$$

Here, the various terms are exchange interaction, y-z easy-plane anisotropy with constant $K_\perp$, easy axis anisotropy along the z direction with K_z and externally applied magnetic field $\vec{B}$, respectively. Note that in equilibrium, a domain-wall solution is obtained by virtue of the condition $\vec{H}_0[\vec{m}]|_\perp = 0$, i.e. the absence of any torques which would otherwise induce time-dependent dynamics. We then cast the expression for the charge current (2.141) into the following form,

$$\begin{aligned} \boldsymbol{j}_c &= \underline{\underline{\sigma}}\boldsymbol{E} - \sigma_{\rm s}\vec{m}\cdot\boldsymbol{\nabla}\left[\vec{m}\times(1+\beta\vec{m}\times)\partial_t\vec{m}\right] \\ &= \underline{\underline{\sigma}}\boldsymbol{E} + \sigma_{\rm s}\vec{m}\cdot\boldsymbol{\nabla}\left[-\vec{H}|_\perp + \vec{m}\times(1+\beta\vec{m}\times)\boldsymbol{v}_s\boldsymbol{\partial}_r\vec{m}\right] \end{aligned} \tag{2.184}$$

where in the second step we used the LLG-equation for $\alpha = \beta$ to eliminate the time-gradients of $\vec{m}$. In the absence of external currents, $\boldsymbol{v}_s = 0$ and the equation simplifies to

$$\boldsymbol{j}_c = \underline{\underline{\sigma}}\boldsymbol{E} + \sigma_{\rm s}\vec{m}\cdot\boldsymbol{\nabla}(-\vec{H})_\perp = \underline{\underline{\sigma}}\boldsymbol{E} + \sigma_{\rm s}(\boldsymbol{\nabla}\vec{m})\cdot\vec{H} \ , \tag{2.185}$$

where now, there is no longer any explicit dependence on the dissipative term β. When we further assume a rigid domain wall structure, for example one that is characterized by the two collective coordinates domain-wall position $X(t)$ and chirality $\phi(t)$ [20], any additional dissipation due to emission of spin-waves is absent and the final result should not depend on $\alpha = \beta$ and thus yields a scenario equivalent to $\alpha = \beta = 0$ which has been considered by Barnes *et al.* in Ref. [70]. In fact, we can make use of the condition $\vec{H}_0[\vec{m}]|_\perp = 0$ valid for a rigid domain-wall structure[5], so that in the case of a field driven domain-wall with constant external magnetic field $\vec{B}$, we have

$$\boldsymbol{j}_c = \underline{\underline{\sigma}}\delta\boldsymbol{E} + \sigma_{\rm s}g\mu_{\rm B}\boldsymbol{\nabla}(\vec{m}\vec{B}) \ , \tag{2.186}$$

where $\delta\boldsymbol{E}$ is the induced electric field which is determined from the continuity equation $\boldsymbol{\nabla}\cdot\boldsymbol{j}_c = 0$. Introducing the potential $\delta\boldsymbol{E} = -\boldsymbol{\nabla}\delta\varphi$, we can write $\boldsymbol{j}_c = -\sigma_{\rm c}\boldsymbol{\nabla}\varphi$ with $\varphi(\boldsymbol{r}) = \delta\varphi(\boldsymbol{r}) - \frac{\sigma_{\rm s}}{\sigma_{\rm c}}g\mu_{\rm B}\vec{m}\vec{B}$, where $\delta\varphi$ has to be determined from the Poisson equation $\boldsymbol{\nabla}^2\varphi = 0$ together with appropriate boundary conditions. In the simple 1-dimensional scenario with a contact of length L containing a field driven magnetic domain wall, we easily find as solution for the Poisson equation $\varphi(x) = -Ex + \varphi_0$ which together with vanishing potential at the boundaries, $\delta\varphi(\pm\frac{L}{2}) = 0$ yields $E = \frac{\sigma_{\rm s}}{\sigma_{\rm c}}g\mu_{\rm B}\frac{2}{L}B$. The current thus obtained is $j_c = \sigma_{\rm s}\frac{2}{L}g\mu_{\rm B}B$ which is identical to what Duine finds in Ref. [71].

More generally with $\alpha \neq \beta$, we can also specify the pumped charge current due to a rigidly moving domain wall in one dimension, where we can parametrize the domain wall as $\vec{m} = (\sin\theta\cos\phi, \sin\theta\sin\phi, \cos\theta)$ with $\phi(t)$ being spatially constant and $\cos\theta = \tanh(\frac{x-X}{w})$ describing a rigidly moving Bloch domain wall at position $X(t)$ with width w. We then have

$$j_c = \sigma_{\rm c}\delta\boldsymbol{E} - \sigma_{\rm s}\left(\dot{\phi}\sin\theta\partial_x\theta + \beta\dot{\theta}\partial_x\theta\right) = \sigma_{\rm c}\delta\boldsymbol{E} + \sigma_{\rm s}q^2w\left(\dot{\phi} + \beta\frac{\dot{X}}{w}\right) \ , \tag{2.187}$$

[5]It is a bit more tricky if $\phi(t) \neq 0$, then there will be additional terms due to $\vec{H}_0$, however the overall contributions of these terms along the whole domain-wall structure vanishes if we consider the pumped charge current far away from the inhomogenity

where $q^2 = (\partial_x\theta)^2 = \frac{1}{w}\partial_x \cos\theta = -\frac{1}{w}\partial_x\theta \sin\theta$. Using $\partial_x j_c = 0$ and vanishing electric potentials at the end of the contacts, $\delta\varphi(\pm L/2) = 0$ where $\delta\boldsymbol{E} = -\boldsymbol{\nabla}\delta\varphi$, we eventually get

$$j_c(t) = \sigma_\mathrm{s}\left(\dot{\phi} + \beta\frac{\dot{X}}{w}\right)\frac{w}{L}\int_{-L/2}^{+L/2} q^2(x)\mathrm{d}x = \sigma_\mathrm{s}\left(\dot{\phi} + \beta\frac{\dot{X}}{w}\right)\frac{2}{L}\ . \tag{2.188}$$

We note that our results are compatible with the work of Duine [71]. From the same author, Ref. [72] also deals with the issue of spin-pumping due to a moving domain wall but uses a different approach than in Ref. [71]. However, the result of the pumped charge current in Ref. [72] shows the opposite sign of the β-term as compared to Ref. [71] and our result (2.188).

Let us briefly consider the kinetic equation for the force applied to this specific problem of a moving domain-wall. We straightforwardly obtain from Eq. (2.181), assuming a constant external magnetic field $\vec{B}_\mathrm{ext} = B_\mathrm{ext}\hat{e}_z$,

$$-wq^2(\dot{\phi} + \alpha\frac{\dot{X}}{w}) = -g\mu_\mathrm{B}B_\mathrm{ext}wq^2 + \frac{a^3}{S}q^2\beta j_s\ , \tag{2.189}$$

or

$$\dot{\phi} + \alpha\frac{\dot{X}}{w} = g\mu_\mathrm{B}B_\mathrm{ext} - \frac{a^3}{Sw}\beta j_s\ , \tag{2.190}$$

which is one of the well known equations for the two collective coordinates representing chirality ϕ and domain wall position X [29, 66]. We again recover the result $j_c = \sigma_\mathrm{s}\frac{2}{L}g\mu_\mathrm{B}B$ by comparing the last expression with the pumped charge current in Eq. (2.187) and assuming $\alpha = \beta$.

2.6. Conclusions and Outlook

We studied electronic transport in the presence of an inhomogeneous magnetization in ferromagnetic conductors by deriving a quantum kinetic equation for the low energy dynamics including gradient corrections to the collision integral and in linear response. Our method allows us to obtain various results for charge- and spin-transport and the magnetization dynamics within one microscopic model, mathematical framework and compatible approximations.

This equation has been first employed to calculate the domain-wall resistance for current perpendicular to wall (CPW) and current in-wall (CIW) geometries for a simple Bloch wall we found positive or negative values for the DWR. As opposed to previous studies of the DWR, dissipative spin-flip is taken into account and it gives rise to qualitatively different behavior, since in the absence of spin-flip processes, non-equilibrium spin-excitations do not relax, even infinitely far away from the domain wall which yields an additional potential drop at the domain-wall. Essentially, our treatment assumes that any spin-accumulation has decayed at the contact ends and thus, we neglect any finite size effects due to the contact geometry.

We have performed a detailed analysis of the domain-wall resistance in ferromagnetic conductors and identified important mechanisms. Our results differ in various aspects from other

theories and we extend the description by including magnetic impurity scattering which leads to dissipative spin-flip scattering and spin-dephasing. The difference to other theories has been discussed at length and originates mostly from an inconsistent treatment in these works like disregarding the d-wave component, the neglect of spin-flip processes and different approaches to include impurity scattering. While we use a fully microscopic approach for scattering, reflected in the full form of the collision integral (2.45) with gradient corrections and modification of the electronic structure properly taken into account, other works introduced momentum scattering rates phenomenologically.

We identified two distinct contributions to the DWR: the isotropic contribution that is always present in regions of non-vanishing magnetization gradient and an anisotropic term that contributes only when there is a magnetization gradient along the current flow. We found that transverse spin-dephasing contributes only to the anisotropic contribution, while the isotropic contribution does *not* depend on T_2. Also, the anisotropic component is identical for s-d and itinerant Stoner models. In the limit $\Delta\tau \gg 1$ mainly studied here, we found the general trend that the domain-wall resistance increases as we increase the magnetic impurity scattering strength.

In the limit of weak polarization, we find that the behavior of the DWR is dominated by the scattering asymmetry of $\tau_{\uparrow,\downarrow}$, i.e. the difference of the momentum relaxation rate in the spin-up and down channel. In the opposite limit of strong polarization, the behavior of the DWR is dominated by the gradient corrections to $\tau_\uparrow$. In the intermediate regime of P, it is difficult to isolate the various contributions to the DWR, especially since in our regime $\Delta\tau \gg 1$ we need to include the d-wave moment of the spin-charge distribution function, which gives rise to complicated scattering, and is consistently described in terms of the complete collision integral with gradient correction included to second order in spatial magnetization gradients. Other contributions arise from changes in the spectrum, the shift in the chemical potential, or local screening potential $\delta\mu$, and the reduction of the magnetic moment $\delta\Delta$.

Contrary to the s-d model, we found that the Stoner limit has an overall stronger tendency to exhibit negative domain-wall resistance in the regime of small to intermediate polarizations P, which has its origin in the local reduction of the exchange field in areas of non-vanishing magnetization gradient. The situation is opposite in the limit of strong polarization, where the behavior is dominated by the magnetization gradient corrections to the scattering time $\tau_\uparrow$, so that the DWR increases, eventually becoming positive again.

More complex domain-walls give rise to a transverse voltage due to the Berry curvature and we investigated this effect by calculating the transverse voltage drop induced by a charge current flowing through a vortex wall.

Employing our kinetic equation, we also have derived extended spin-charge continuity and diffusion equations which can be utilized to study magnetotransport and spin-transport in presence of an inhomogeneous magnetization in the mesoscopic limit. We calculated the full charge- and spin-current response due to the two sources of external perturbations: external electric field and a time-varying magnetization which least to charge- and spin-pumping. As application, we calculated the induced charge current by a moving domain wall. The results for the spin-current can then be directly used to obtain the spin-torque which affects the magnetization dynamics described in the framework of the Landau-Lifshitz-Gilbert equation, widely utilized to study for example domain-wall motion.

Finally, we have also illustrated the effects of the two dissipative terms, Gilbert damping and non-adiabatic spin-torque, which can be also understood in terms of friction between the electron system and the magnetization. On one hand, we saw that the Gilbert damping α leads to a electron drag and consequently, a charge current due to a dynamic magnetization. On the other hand, we directly calculated the pumped charge current (see Eq. (2.141)) with a contribution proportional to β. In the end, both pictures should yield the same current, so this suggests a deep connection between the Gilbert damping constant α and the non-adiabatic coefficient β.

In summary, the kinetic equation derived in the first part of this work allows for a unified treatment of the complete response of a ferromagnetic conductor with an inhomogeneous and time-dependent magnetization structure in the regime where the magnetization $\vec{m}$ is smooth on the scale of the Fermi-wavelength λ_{F} and the precession length l_{prec}. Aside from the thorough investigation of the domain wall resistance, we are able to confirm many findings published in literature using different methods and models, some of them of phenomenological nature, thus putting them on a solid ground. We also find new terms that have not been discussed before, in particular non-local corrections to various terms in the LLG equation that describe corrections relevant for strongly varying magnetization structures.

3. Effective Quantum Theories for Transport in Inhomogeneous Systems with Non-trivial Band Structure

3.1. Effective Quantum Theories and Berry Curvatures

In the previous chapter, we studied the electron dynamics in the presence of an arbitrary inhomogeneous and time-dependent exchange field using semiclassical transport equations and saw the emergence of many interesting phenomena. Now, one can make various generalizations like adding a spin-orbit coupling term, which would give rise to new effects as the anomalous Hall effect, and the latter would be additionally modified by the inhomogeneous magnetization. Furthermore, in the next chapter, we are going to study so-called topological insulators, in which the quasi-particle momentum is intimately coupled to the spin-degree of freedom and thus behaves similar to a Dirac Fermion. It is clear that the full quantum mechanical problem of the Dirac particles coupled to a general inhomogeneous and time-dependent magnetization texture will in general be very complex due to the locking of spin and momentum. This is different than the case of semiconductors, where the spin-orbit interaction can for example be treated as a small perturbation due to the presence of the dominant quadratic spin-independent dispersion. Contrary to the previous situation of quasi-free electrons without the spin-orbit term, we cannot perform a gauge transformation along the lines of the work from Tserkovnyak and Wong [73], since the spin $\boldsymbol{\sigma}$ couples strongly to both a spatially/time-dependent field $\boldsymbol{M}(\boldsymbol{r}, t)$ and momentum $\boldsymbol{p}$, which we consequently cannot easily diagonalize due to non-commutation of $\boldsymbol{r}$ and $\boldsymbol{p}$. If we construct the gauge transformation such that it diagonalizes just the spatial part $\boldsymbol{M}(\boldsymbol{r})\cdot\boldsymbol{\sigma}$, we get a term that is in general no less difficult to treat. It is clear that if one wants to diagonalize spin space, the unitary transformation has to involve the pair of canonical operators $\boldsymbol{r}$ and $\boldsymbol{p}$. Of course, if $\boldsymbol{r}$ and $\boldsymbol{p}$ are classical variables, such a unitary transformation is straightforward to find, and then one could resort to quantum corrections which are of the order $\hbar$. In this chapter however, we go one step further and study the dynamics of general Hamiltonians in the semiclassical limit. In fact, the initial idea is similar to the Foldy-Wouthuysen transformation in the case of the relativistic Dirac equation [107]. In principle, our approach here is a generalization to an arbitrary Hamiltonian and to transformations that require the use of $\boldsymbol{p}$ and $\boldsymbol{r}$ simultaneously, and is achieved by using the phase space or Wigner representation of quantum theory [108]. In our treatment, we will find that corrections due to non-adiabaticities will emerge very naturally in the shape of Berry phases.

The importance of Berry phases in condensed matter physics is beyond question [109, 110, 111]. For example, not long ago was it realized that the electric polarizability of a crystal can only be consistently formulated in terms of a Berry curvature [112]. Furthermore, magnetic

monopoles that appear in the definition of a momentum space effective magnetic field are found to give important modifications to universal conductance fluctuations [111]. Furthermore, the whole development in the field of the anomalous Hall effect (AHE) has shown that the intrinsic contribution is related to a Berry-curvature, which is a quantum mechanical property of a perfect crystal [113]. Finally, topological interference effects arise from spin Berry phases [114].

There are different ways to obtain semiclassical equations ([109, 110] and references therein), like wave-packet analysis [115], or, the rather formal diagonalization method of Gosselin and coworkers [116]. We are however presenting our own self-contained derivation of the semiclassical dynamics, which is rather naturally based on the Wigner representation or phase-space representation of quantum mechanics and is inspired by the work done in previous chapters, where such a representation showed its power for a semiclassical analysis. The big advantage is that one can obtain corrections systematically to arbitrary order in $\hbar$ and it is pretty straightforward to use. Also, a re-quantization of the effective theory is not necessary, which is a big drawback of the wave-packet analysis which derives the Lagrangian from the equations of motion for the wave-packet center of mass coordinates, and it is not always clear what the canonical conjugate variables are. The relation between canonical and kinetic pairs of conjugate variables, however, emerges naturally in our formalism. Furthermore, the techniques used by Gosselin are rather formal and, in fact, we reproduce some of their results by using the Wigner picture, but without any need to develop special mathematical tools. Our technique provides physical insight and it also extends some aspects to include hierarchies of effective theories and it addresses the important question of gauge invariance. The Löwdin partitioning, or quasi-degenerate perturbation theory, used in the book of Winkler [117] to derive effective models for certain bands in spin-orbit coupled semiconductors can also be related to our semiclassical treatment, however, there focus is only put on the Hamiltonian, not on the dynamical variables or other aspects of the system.

Our derivation also allows us to treat time-dependent phenomena using 4-vector notation, and thus incorporates time and energy on an equivalent basis with position and momentum parameters. Furthermore, in the course of our treatment, we will find how vector potentials or magnetic fields (real space or reciprocal space) appear in effective theories. In that respect, we will also investigate the difference between a physical magnetic field that already exists at the beginning as a gaugefield[1] and the coupling to an inhomogeneous exchange field, whose effects could also be expressed in terms of fictitious electric and magnetic fields, as discussed in the previous chapter. It is clear that both inhomogeneous exchange field and magnetic field cannot be treated on the same level, as the latter does not change the dynamical variables while the former does so by the well known Peierls substitution $\boldsymbol{p} \to \boldsymbol{p} - q\boldsymbol{A}$.

Despite the fact that we are performing formally an expansion in $\hbar$, it does not necessarily need to be restricted to the semiclassical regime. In fact, as pointed out later, our actual expansion parameter might be a different one, depending on the physical system and the regime under investigation. In certain systems, it will be formally equivalent to an expansion in inter-band couplings which would be more accurate for larger band separations (or weaker coupling). In the case of the Dirac theory, as we will discuss thoroughly later in this chapter,

[1] as we will see, it can be thought of as a Berry phase arising from the coupling to the electromagnetic field and which has been already eliminated by a suitable diagonalization scheme to obtain the effective theory we are starting from

the actual scale relevant for our expansion is the Compton wavelength $\lambda_c = \frac{\hbar}{mc}$ so, despite the fact we are formally expanding in $\hbar$, we are still completely in the quantum mechanical regime. To emphasize this fact, we will introduce the notation of $\not{\hbar}$ in this chapter to indicate that the expansion is not necessarily a semi-classical one.

We will now present the diagonalization scheme for a general Hamiltonian that consists of a N dimensional spinor structure (bands) and the goal is to obtain an effective theory for the description of the physics restricted to specific sub-bands.

The outline of this chapter is as follows: First, we will introduce the transformation that rotates the basis such that the Hamiltonian becomes band-diagonal and we will specify how observables change under this rotation. Since this transformation is not uniquely defined, we will discuss the implications of this additional gauge degree of freedom. This motivates a description in terms of kinetic variables which is manifestly gauge invariant. We will then thoroughly discuss what an effective description of the physical system restricted to a certain band looks like, i.e. we seek a projected theory without the necessity to refer back to the original Hamiltonian. To this end, we find equations of motion for the quasi-probability density, essentially a quantum Boltzmann equation applicable to a non-equilibrium description. For this description, we also find a conservation law corresponding to Liouville's theorem in classical mechanics. Furthermore, in order to calculate expectation values for physical observables, we need a suitable representation in the rotated frame. To that end, we obtain an expression that formally is analogous to the equations of motion for the center-of-mass motion of a wave-packet and in fact, the latter is just a special case of our formulation. Subsequently, we illustrate how to treat the external electromagnetic field. This can be done in the spirit of a hierarchy of effective theories, and we will find rules of how to simply incorporate the external fields into our formalism. After concluding the discussion of general systems, we apply the apparatus developed to the Dirac equation and readily find a relativistic version of the Pauli-Hamiltonian, thereby gaining some interesting insights into the structure of the Dirac equation. We briefly discuss the anomalous velocity of a relativistic electron and the notion of *Zitterbewegung*. Subsequently, we study the related model of the surface Dirac Fermions on a topological insulator with proximity induced ferromagnetic exchange field which can be both spatially and time-varying. We are able to relate a charging effect in the Fermi Sea due to magnetization gradients to a Berry curvature. Furthermore, we calculate the non-equilibrium current and spin-excitation, and reproduce known results in literature along with new terms and some generalizations.

3.1.1. The Wigner Representation and the Systematic Diagonalization Scheme

The Hamiltonian $\mathcal{H}$ will not be further specified at this point, except that it is written in its canonical representation using the operators $[r_i, p_j] = i\hbar$ and additionally carries the $N \times N$ dimensional matrix structure. The diagonal elements describe intra-band physics while the off-diagonal elements describe inter-band transitions. We now transform everything into the familiar Wigner representation so that our Hamiltonian and our observables are a function of the variables $\boldsymbol{r}, \boldsymbol{p}$ and time t. Multiplication of operators is now performed by the Moyal product [118],

$$* \equiv \exp \frac{i\hbar}{2}\Lambda \ , \tag{3.1}$$

where for the most general scenario of spatio-temporal dependency the differential operator Λ is given by

$$\Lambda = \overleftarrow{\partial_{\boldsymbol{r}}}\overrightarrow{\partial_{\boldsymbol{p}}} - \overleftarrow{\partial_t}\overrightarrow{\partial_\epsilon} - \overleftarrow{\partial_{\boldsymbol{p}}}\overrightarrow{\partial_{\boldsymbol{r}}} + \overleftarrow{\partial_\epsilon}\overrightarrow{\partial_t} = -\overleftarrow{\partial_{\boldsymbol{x}}}\overrightarrow{\partial_{\boldsymbol{\pi}}} + \overleftarrow{\partial_{\boldsymbol{\pi}}}\overrightarrow{\partial_{\boldsymbol{x}}} \tag{3.2}$$

where we introduced the compact 4-component vector notation $\boldsymbol{x} = (t, \boldsymbol{r})$ and $\boldsymbol{\pi} = (\epsilon, -\boldsymbol{p})$. Note that we always use $\boldsymbol{x}$, $\partial_{\boldsymbol{x}} = (\partial_t, \partial_{\boldsymbol{r}})$ and $\mathcal{A}_{\boldsymbol{x}} = (\mathcal{A}_t, \mathcal{A}_{\boldsymbol{r}})$ in contravariant notation whereas we implicitly assume covariant notation for the symbols $\boldsymbol{\pi}$, $\partial_{\boldsymbol{\pi}} = (\partial_\epsilon, -\partial_{\boldsymbol{p}})$ and $\mathcal{A}_{\boldsymbol{\pi}} = (\mathcal{A}_\epsilon, -\mathcal{A}_{\boldsymbol{p}})$. Since contraction will always be between pairs of $\boldsymbol{x}$ and $\boldsymbol{\pi}$, there is no need to indicate covariant vectors. In the operator representation of quantum mechanics, we can write the canonical commutation relation (quantities with hats indicate operators in this chapter),

$$[\hat{\boldsymbol{\pi}}_\mu, \hat{\boldsymbol{x}}^\nu] = i\hbar\delta_\mu^{\ \nu} \ . \tag{3.3}$$

The Wigner transformation explicitly reads in 4-component notation

$$\int \mathrm{d}^4 z \ e^{i\boldsymbol{z}\boldsymbol{\pi}/\hbar} A\left(\boldsymbol{x} + \frac{\boldsymbol{z}}{2}, \boldsymbol{x} - \frac{\boldsymbol{z}}{2}\right) = A(\boldsymbol{x}, \boldsymbol{\pi}) \ , \tag{3.4}$$

and the Moyal product obeys the axiom of associativity,

$$A * B * C = A * (B * C) = (A * B) * C \ , \tag{3.5}$$

and also

$$(A * B)^\dagger = B^\dagger * A^\dagger \ , \tag{3.6}$$

however, the Moyal product is non-commutative, i.e. $A{*}B \neq B{*}A$. In fact, the latter property encodes the non-commutativity of operators in quantum theory which one can explicitly see by considering the commutator of two general observables dependent on $\boldsymbol{x}$ and $\boldsymbol{\pi}$ and which are band-diagonal,

$$\begin{aligned}[A(\boldsymbol{x}, \boldsymbol{\pi}) \stackrel{*}{,} B(\boldsymbol{x}, \boldsymbol{\pi})] &= 2iA(\boldsymbol{x}, \boldsymbol{\pi}) \ \sinh(\hbar\Lambda/2) \ B(\boldsymbol{x}, \boldsymbol{\pi}) \\ &= i\hbar A(\boldsymbol{x}, \boldsymbol{\pi}) \ \Lambda \ B(\boldsymbol{x}, \boldsymbol{\pi}) + O(\hbar^3) = i\hbar \left\{A, B\right\}_{\mathrm{p}} + O(\hbar^3) \ .\end{aligned} \tag{3.7}$$

It becomes essentially an extended Poisson bracket in the semiclassical limit which reduces to the normal Poisson bracket when neither A nor B explicitly depend on ϵ which is usually the case.

At this point, an important remark is in order, and which is relevant for diagonalization matrixes $\mathcal{U}$ explicitly depending on time. Since then the energy parameter is affected as well by the transformation and thus, treating $\mathcal{H}$ alone is insufficient and one has to diagonalize the more fundamental object

$$\Xi \equiv \epsilon \mathbb{1}_N - \mathcal{H} \tag{3.8}$$

instead. The reason is that only Ξ represents the complete equation of motion, i.e. all kinetic equations involve this operator, and not $\mathcal{H}$ alone. For diagonalizations that do not require explicit dependency on the time parameter, treating $\mathcal{H}$ and Ξ is equivalent, and in

the following, we will use the term Hamiltonian equally for both objects. Essentially, Ξ is the inverse of the single-particle Greens function which for $\epsilon \to \epsilon + i0$ becomes the retarded one, and it can be explicitly calculated from $\Xi * \mathcal{G} = \mathbb{1}_N$ as has been done in section 2.2.4.

We are now looking for a unitary matrix $\mathcal{U}(\boldsymbol{x}, \boldsymbol{\pi})$ that transforms our initial Hamiltonian $\Xi(\boldsymbol{x}, \boldsymbol{\pi})$ into a band-diagonal Hamiltonian, denoted by $\bar{\Xi}(\boldsymbol{x}, \boldsymbol{\pi})$ in the following, i.e.

$$\mathcal{U} * \mathcal{U}^\dagger = \mathcal{U}^\dagger * \mathcal{U} = \mathbb{1} \tag{3.9}$$

$$\mathcal{U} * \Xi * \mathcal{U}^\dagger = \bar{\Xi} \ . \tag{3.10}$$

Note that Ξ does now explicitly depend on the energy operator (which is the variable ϵ in the Wigner picture), so that we write $\boldsymbol{\pi}$ as argument, but it also provides a symmetric and compact notation in the following treatment. In addition, the transformation (3.10) is generic, as Ξ can in turn be any other operator that might depend on ϵ explicitly (for example anything involving the Fermi distribution function). We also see that, upon transformation, $\mathcal{U} * \epsilon * \mathcal{U}^\dagger$ can acquire off-diagonal elements when $\mathcal{U}$ depends on time, thus requiring the diagonalization of the proper combination Ξ.

Of course, finding the exact matrix $\mathcal{U}(\boldsymbol{x}, \boldsymbol{\pi})$ is in general not always possible, but we can do it systematically order by order in $\hbar$ by doing a gradient expansion. To zeroth order in $\hbar$, one usually finds the matrix $\mathcal{U}_0$

$$\mathcal{U}_0 \, \Xi \mathcal{U}_0^\dagger = \bar{\Xi}_0 \qquad \Leftrightarrow \qquad \mathcal{U}_0 \mathcal{H} \mathcal{U}_0^\dagger = \bar{\mathcal{H}}_0 \tag{3.11}$$

by diagonalization of the $N \times N$ matrix $\mathcal{H}$, and subsequent construction of $\mathcal{U}_0$ from the eigenvalues. At any rate, we assume from now on that we know the diagonalization matrix $\mathcal{U}_0$ analytically. Note that all our matrixes parametrically depend on $\boldsymbol{x}$ and $\boldsymbol{\pi}$, so we essentially diagonalize locally at every point in $2 \times (3+1)$-dimensional parameter space, which is possible, as position $\boldsymbol{r}$, momentum $\boldsymbol{p}$, time t and energy ϵ become well-defined in the semiclassical limit. Furthermore, if the inter-band matrix elements only depend on either $\boldsymbol{x}$ or $\boldsymbol{\pi}$, then we already obtained the exact expression $\mathcal{U} = \mathcal{U}_0$. For example, in the previous chapter treating metallic ferromagnets, it just necessary to just diagonalize $\boldsymbol{m}(\boldsymbol{r})\boldsymbol{\sigma}$, since the energy dispersion was diagonal in spin-space. As we have seen, the effect of $\mathcal{U}$ is that $\boldsymbol{p}$ acquires an additional gauge potential: $\boldsymbol{p} \to \boldsymbol{p} - i\hbar \mathcal{U} \partial_{\boldsymbol{r}} \mathcal{U}^\dagger$. In the general situation treated in following, $\boldsymbol{x}$ and $\boldsymbol{p}$ will be transformed simultaneously and we will study its implications.

In order to proceed, we perform the gradient expansion on (for brevity we write $\mathcal{V} \equiv \mathcal{U}^\dagger$)

$$\mathcal{U} * \Xi * \mathcal{V} = \exp\left\{ \frac{i\hbar}{2} \left(\Lambda_{\mathcal{U}\Xi} + \Lambda_{\Xi\mathcal{V}} + \Lambda_{\mathcal{U}\mathcal{V}} \right) \right\} \mathcal{U}\Xi\mathcal{V} \ , \tag{3.12}$$

where we defined

$$\Lambda_{\mathcal{U}\mathcal{V}} = -\partial_{\boldsymbol{x}}^{(\mathcal{U})} \partial_{\boldsymbol{\pi}}^{(\mathcal{V})} + \partial_{\boldsymbol{\pi}}^{(\mathcal{U})} \partial_{\boldsymbol{x}}^{(\mathcal{V})}$$

to act only on one of $\mathcal{U}$, $\mathcal{V}$ or Ξ as denoted by the superscript on the derivatives. Now, all we have to do is to expand the exponential and collect terms of the same order in gradients (which in fact is the same as an expansion in $\hbar$). However, in the end, we want to express everything in the transformed basis, i.e. we want to write $\bar{\Xi}_0$ instead of Ξ, so we have to rewrite terms of the form

$$\left(\partial_{\{\alpha\}} \mathcal{U}\right) \left(\partial_{\{\beta\}} \Xi\right) \left(\partial_{\{\gamma\}} \mathcal{U}^\dagger\right) \ , \tag{3.13}$$

which, by inserting unities $\mathcal{U}_0^\dagger \mathcal{U}_0 = \mathbb{1}$ between each operator, turns into

$$\left(\partial_{\{\alpha\}}\mathcal{U}^\dagger\right)^\dagger \; \left[\partial_{\{\beta\}}, \Xi\right] \; \left(\partial_{\{\gamma\}}\mathcal{U}^\dagger\right) = \left(\bar{\partial}_{\{\alpha\}}\bar{\mathcal{U}}^\dagger\right)^\dagger \; \left[\bar{\partial}_{\{\beta\}}, \bar{\Xi}_0\right] \; \left(\bar{\partial}_{\{\gamma\}}\bar{\mathcal{U}}^\dagger\right) \; , \tag{3.14}$$

where we introduced the commutator notation $\left[\partial_{\{\beta\}}, \Xi\right]$ to formally restrict the action of the derivatives to Ξ alone, thus making the transformation straightforward. We introduced

$$\begin{aligned} \bar{\mathcal{U}} &= \mathcal{U}\mathcal{U}_0^\dagger = \mathbb{1} + \bar{\mathcal{U}}_1 + \bar{\mathcal{U}}_2 + \dots \\ \bar{\mathcal{U}}^\dagger &= \mathcal{U}_0\mathcal{U}^\dagger = \mathbb{1} + \bar{\mathcal{U}}_1^\dagger + \bar{\mathcal{U}}_2^\dagger + \dots \; , \end{aligned} \tag{3.15}$$

which describes the matrix that diagonizes our Hamiltonian Ξ to all order of $\hbar$. $\bar{\mathcal{U}}_1$ is $\propto \hbar$ and will be specified explicitly later.

Upon transformation, we obtain the covariant derivatives

$$\bar{\partial}_i = \mathcal{U}_0 \partial_i \mathcal{U}_0^\dagger = \partial_i - i\mathcal{A}_i \tag{3.16}$$

which acquire Berry phases

$$\mathcal{A}_i \equiv i\mathcal{U}_0 \partial_i \mathcal{U}_0^\dagger \; , \tag{3.17}$$

where i is a placeholder for any of the possible derivatives $\partial_t, \partial_\epsilon, \partial_{\boldsymbol{r}}$ and $\partial_{\boldsymbol{p}}$. Berry phases, or often called geometric phases, are omnipresent in modern physics, and describe phases picked up along a trajectory in curved geometries. Note that $\mathcal{A}_i$ is a $N \times N$ matrix which is Hermitian

$$\mathcal{A}_i^\dagger = -i(\mathcal{U}_0 \partial_i \mathcal{U}_0^\dagger)^\dagger = -i(\partial_i \mathcal{U}_0)\mathcal{U}_0^\dagger = i\mathcal{U}_0 \partial_i \mathcal{U}_0^\dagger = \mathcal{A}_i \; , \tag{3.18}$$

where the last step is due to $0 = \partial_i(\mathcal{U}_0\mathcal{U}_0^\dagger) = (\partial_i\mathcal{U}_0)\mathcal{U}_0^\dagger + \mathcal{U}_0(\partial_i\mathcal{U}_0^\dagger)$ and the diagonal elements of $\mathcal{A}_i$ describe the usual berry phases arising from transport within a certain band. The off-diagonal elements mix contributions from two bands and thus describe effects due to inter-band coupling during transport in a certain band. As we will see later, these inter-band transitions will give rise to important corrections for example the correction to the energy that appears to leading order in $\hbar$. Transforming higher order derivatives is straightforward, except for the additional freedom of exchanging partial derivatives, which leads to a general relation between Berry phase matrices $\mathcal{A}_i$. Starting from

$$\mathcal{U}_0 \partial_j \partial_i \mathcal{U}_0^\dagger = \bar{\partial}_j \bar{\partial}_i = (\partial_j - i\mathcal{A}_j)(\partial_i - i\mathcal{A}_i) \; , \tag{3.19}$$

and likewise,

$$\mathcal{U}_0 \partial_i \partial_j \mathcal{U}_0^\dagger = \bar{\partial}_i \bar{\partial}_j = (\partial_i - i\mathcal{A}_i)(\partial_j - i\mathcal{A}_j) \; , \tag{3.20}$$

and, if we assume symmetry of second derivatives $\partial_j\partial_i = \partial_i\partial_j$, the following relation should hold

$$\partial_i \mathcal{A}_j - \partial_j \mathcal{A}_i = i\left[\mathcal{A}_i, \mathcal{A}_j\right] \; . \tag{3.21}$$

In fact, this identity can be directly shown by using the definition of $\mathcal{A}$ (3.17) and the exchange of partial derivatives. For this to be true, we assume our unitary transformation $\mathcal{U}_0$ to be single valued.

Now we have everything at hand to systematically calculate $\bar{\Xi} = \bar{\Xi}_0 + \bar{\Xi}_1 + \bar{\Xi}_2 \dots$ to arbitrary order in $\hbar$ [2] and to first order, we explicitly obtain the following result for the transformed expression,

$$\bar{\Xi}_1 = \bar{\mathcal{U}}_1 \bar{\Xi}_0 + \bar{\Xi}_0 \bar{\mathcal{U}}_1^\dagger - \frac{\hbar}{2} \left\{ \mathcal{A}_{\boldsymbol{\pi}}, \partial_{\boldsymbol{x}} \bar{\Xi}_0 \right\} + \frac{\hbar}{2} \left\{ \mathcal{A}_{\boldsymbol{x}}, \partial_{\boldsymbol{\pi}} \bar{\Xi}_0 \right\} + \frac{i\hbar}{2} \left(\mathcal{A}_{\boldsymbol{\pi}} \bar{\Xi}_0 \mathcal{A}_{\boldsymbol{x}} - \mathcal{A}_{\boldsymbol{x}} \bar{\Xi}_0 \mathcal{A}_{\boldsymbol{\pi}} \right) \ . \quad (3.22)$$

We obtain an additional constraint for $\bar{\mathcal{U}}_n$ from the condition of unitarity (3.9), which to first order in $\hbar$ reads

$$\bar{\mathcal{U}}_1 + \bar{\mathcal{U}}_1^\dagger + \frac{i\hbar}{2} \left[\mathcal{A}_{\boldsymbol{\pi}}, \mathcal{A}_{\boldsymbol{x}} \right] \stackrel{!}{=} 0 \ , \quad (3.23)$$

and is obtained by simply substituting $\mathbb{1}$ for $\bar{\Xi}_0$ into the transformation relation Eq. (3.22). It fixes the diagonal part of $\bar{\mathcal{U}}_1$, or more specifically the real part thereof, but without loss of generality, we can set the imaginary part to zero. A non-zero imaginary diagonal part corresponds to the gauge freedom and can be thought of as the linear order expansion of the gauge phase factors $e^{i\chi(\boldsymbol{x},\boldsymbol{\pi})}$, and will be elaborated upon later. In fact, the same is true for any order in $\hbar$, so that these kinds of constraints completely fix the diagonal part of the matrices $\bar{\mathcal{U}}_n$. As we will see in a moment, the non-diagonal elements of these matrices are fixed by the condition that $\bar{\Xi}$ should be diagonal to all orders in $\hbar$. We call this part $\mathcal{Y}_n$, and equally distribute the diagonal part amongst $\bar{\mathcal{U}}_n$ and $\bar{\mathcal{U}}_n^\dagger$, so that we explicitly have

$$\begin{aligned} \bar{\mathcal{U}}_1 &= -\frac{i\hbar}{4} \left[\mathcal{A}_{\boldsymbol{\pi}}, \mathcal{A}_{\boldsymbol{x}} \right] + \mathcal{Y}_1 \\ \bar{\mathcal{U}}_1^\dagger &= -\frac{i\hbar}{4} \left[\mathcal{A}_{\boldsymbol{\pi}}, \mathcal{A}_{\boldsymbol{x}} \right] + \mathcal{Y}_1^\dagger \ , \end{aligned}$$

and it is obvious that $\mathcal{Y}_1 = -\mathcal{Y}_1^\dagger$ has to be anti-Hermitian. Plugging $\bar{\mathcal{U}}_1$ back into Eq. (3.22) yields $\bar{\Xi} = \bar{\Xi}_0 + \bar{\Xi}_1 + \dots$ with

$$\bar{\Xi}_1 = \left[\mathcal{Y}_1, \bar{\Xi}_0 \right] - \frac{\hbar}{2} \left\{ \mathcal{A}_{\boldsymbol{\pi}}, \left[\partial_{\boldsymbol{x}} - \tfrac{i}{2} \mathcal{A}_{\boldsymbol{x}}, \bar{\Xi}_0 \right] \right\} + \frac{\hbar}{2} \left\{ \mathcal{A}_{\boldsymbol{x}}, \left[\partial_{\boldsymbol{\pi}} - \tfrac{i}{2} \mathcal{A}_{\boldsymbol{\pi}}, \bar{\Xi}_0 \right] \right\} + O(\hbar^2) \ , \quad (3.24)$$

which displays anti-symmetry with respect to exchange of $\boldsymbol{x}$ and $\boldsymbol{\pi}$, a property inherited from the Moyal product (3.1).

Once $\mathcal{Y}_1$ has been determined, Eq. (3.24) constitutes the general expression for the transformation of any operator $\mathcal{O}$ with respect to our unitary matrix $\mathcal{U}$,

$$\bar{\mathcal{O}} = \bar{\mathcal{O}}_0 + \left[\mathcal{Y}_1, \bar{\mathcal{O}}_0 \right] - \frac{\hbar}{2} \left\{ \mathcal{A}_{\boldsymbol{\pi}}, \left[\partial_{\boldsymbol{x}} - \tfrac{i}{2} \mathcal{A}_{\boldsymbol{x}}, \bar{\mathcal{O}}_0 \right] \right\} + \frac{\hbar}{2} \left\{ \mathcal{A}_{\boldsymbol{x}}, \left[\partial_{\boldsymbol{\pi}} - \tfrac{i}{2} \mathcal{A}_{\boldsymbol{\pi}}, \bar{\mathcal{O}}_0 \right] \right\} + O(\hbar^2) \ , \quad (3.25)$$

and the back transformation is simply given by [3]

$$\begin{aligned} \mathcal{U}_0 \mathcal{O} \mathcal{U}_0^\dagger = \mathcal{U}_0 (\mathcal{U}^\dagger * \bar{\mathcal{O}} * \mathcal{U}) \mathcal{U}_0^\dagger = \bar{\mathcal{O}} - \hbar \left[\mathcal{Y}_1, \bar{\mathcal{O}} \right] + \frac{\hbar}{2} \left\{ \mathcal{A}_{\boldsymbol{\pi}}, \left[\partial_{\boldsymbol{x}} - \tfrac{i}{2} \mathcal{A}_{\boldsymbol{x}}, \bar{\mathcal{O}} \right] \right\} \\ - \frac{\hbar}{2} \left\{ \mathcal{A}_{\boldsymbol{x}}, \left[\partial_{\boldsymbol{\pi}} - \tfrac{i}{2} \mathcal{A}_{\boldsymbol{\pi}}, \bar{\mathcal{O}} \right] \right\} + O(\hbar^2) \ , \quad (3.26) \end{aligned}$$

[2] Basically, $\hbar$ emerges when terms like $\hbar\mathcal{A}$ appear during the expansion in $\hbar$.

[3] which can be easily obtained from equation (3.25) with the substitutions $\mathcal{A} \to -\mathcal{U}_0^\dagger \mathcal{A} \mathcal{U}_0$ and $\mathcal{Y}_1 \to \mathcal{U}_0^\dagger \mathcal{Y}_1^\dagger \mathcal{U}_0 = -\mathcal{U}_0^\dagger \mathcal{Y}_1 \mathcal{U}_0$ and $i \to -i$

which can be readily checked by plugging Eqn (3.25) into the back transformation (3.26) and dropping terms of order $\hbar^2$.

$\left[\mathcal{Y}_1, \bar{\Xi}_0\right]$ is completely off-diagonal and $\mathcal{Y}_1$ is chosen such that Ξ becomes diagonal (or block-diagonal). In order to do that, we define the matrix $\mathcal{P}_d$ that projects on the diagonal subspace which can also be block-diagonal to describe for example degenerate or nearly degenerate bands, while its counterpart $\mathcal{P}_o = \mathbb{1} - \mathcal{P}_d$ projects onto the remaining off-diagonal elements which describe the inter-band transitions. Thus, $\mathcal{P}_d$ defines the bands that, in the end, we want use for our effective theory. Of course, $\mathcal{P}_d$ has to be specified together with $\mathcal{U}_0$, since the unitary transformation has a freedom of how we distribute the bands amongst the entries of our matrix. A natural choice would be to sort the bands with respect to their energies.

We now write $\bar{\Xi}_1^{(o)}$ for the off-diagonal terms appearing to linear order in $\hbar$ on the right-hand side of equation (3.24), so that the condition for $\mathcal{Y}_1$ reads

$$\left[\mathcal{Y}_1, \bar{\mathcal{H}}_0\right] = \mathcal{P}_o \bar{\Xi}_1^{(o)} \mathcal{P}_o = \bar{\Xi}_1^{(o)} \ . \tag{3.27}$$

If we assume the most general case where $\bar{\mathcal{H}}_0$ can be also block-diagonal, we can write an explicit solution using a description analogous to the superoperator formulation of the von Neumann equation for the density matrix [119]. In fact, the commutator on the left side with the Hamiltonian $\bar{\mathcal{H}}_0$ is exactly what also appears in the von Neumann equation suggesting further that this term describes corrections due to inter-band dynamics. More specifically, introducing the "superoperator" $\mathcal{L} = \bar{\mathcal{H}}_0 \otimes \mathbb{1}_N - \mathbb{1}_N \otimes \bar{\mathcal{H}}_0$ (it corresponds actually to the Liouvillian to zeroth order in $\hbar$ and $\otimes$ denotes the Kronecker product) and rewriting $\mathcal{Y}_1$ and $\bar{\Xi}_1^{(o)}$ as a vector (indicated by boldface letters), we can write the general solution

$$\boldsymbol{\mathcal{Y}}_1 = \mathcal{P}_o \mathcal{L}^{-1} \mathcal{P}_o \bar{\boldsymbol{\Xi}}_1^{(o)} \mathcal{P}_o \ , \tag{3.28}$$

which reduces to

$$\Rightarrow (\mathcal{Y}_1)_{ij} = \frac{\left(\bar{\Xi}_1^{(o)}\right)_{ij}}{E_i - E_j} \tag{3.29}$$

for the case of a completely diagonalized $\bar{\mathcal{H}}_0$ and which is, as it should be, manifest anti-Hermitian. Note that $\mathcal{L}^{-1}$ is singular, so we have to take the pseudo-inverse, nevertheless, the inverse restricted to the off-diagonal subspace $\mathcal{P}_o \mathcal{L}^{-1} \mathcal{P}_o$ is mathematically well-defined. Here we also see that corrections due to $\mathcal{Y}$ are inversely proportional to the separation between bands, and thus, the expansion becomes better, the farer the bands are apart. In fact $\mathcal{Y}$-terms appear as corrections due to inter-band coupling.

At this point, we should point out that the difference between the diagonalization of Ξ and $\mathcal{H}$ is merely the modification of $\mathcal{Y}_1$ by that it acquires an additional contribution from the off-diagonal elements of the Berry phase $\mathcal{A}_t$. However, this term will become important, when we transform observables with non-trivial matrix structure into the rotated frame, since it incorporates the dynamical aspect of the transformation. As we will find out later, only then will the formalism yield consistent results.

Finally, introducing the projected Berry phases $\mathcal{A}_{\boldsymbol{\pi}}^{(d)} \equiv \mathcal{P}_d \mathcal{A}_{\boldsymbol{\pi}} \mathcal{P}_d$, we can write for the Hami-

tonian that is diagonalized up to first order in $\hbar$,

$$\bar{\mathcal{H}} = \bar{\mathcal{H}}_0 - \hbar\mathcal{A}_{\boldsymbol{\pi}}^{(d)}\partial_{\boldsymbol{x}}\bar{\mathcal{H}}_0 + \hbar\mathcal{A}_{\boldsymbol{x}}^{(d)}\partial_{\boldsymbol{\pi}}\bar{\mathcal{H}}_0 + \frac{i\hbar}{4}\mathcal{P}_d\left(\left\{\mathcal{A}_{\boldsymbol{\pi}}, \left[\mathcal{A}_{\boldsymbol{x}}, \bar{\mathcal{H}}_0\right]\right\} - \left\{\mathcal{A}_{\boldsymbol{x}}, \left[\mathcal{A}_{\boldsymbol{\pi}}, \bar{\mathcal{H}}_0\right]\right\}\right)\mathcal{P}_d \ . \tag{3.30}$$

As compared to expression (3.22), we can drop the two anti-commutators here, since after truncation, $\mathcal{A}^{(d)}$ and $\bar{\mathcal{H}}_0$ commute. As discussed more thoroughly below, this is even the case when either $\bar{\mathcal{H}}_0$ is block-diagonal and/or the projected Berry connections are non-Abelian.

Apart from the obvious term $\bar{\mathcal{H}}_0$ which can be understood as the classical energy, the first two terms appear to be Berry phase corrections to this energy. The meaning will become more apparent later, but before, we address the question of gauge invariance of the effective Hamiltonian (3.30). The last term of (3.30) can be thought of as correction to the energy due to inter-band transitions and gives for example rise to the magnetic Zeeman energy.

3.1.2. Gauge Invariance

We mentioned previously that there is an additional degree of freedom in the choice of unitary transformations $\mathcal{U}_0$ and $\mathcal{U}_0'$ which all yield the same diagonal Hamiltonian, $\bar{\Xi} = \mathcal{U}_0\Xi\mathcal{U}_0^\dagger = \mathcal{U}_0'\Xi\mathcal{U}_0'^\dagger$. These different unitary transformations are related by local phase factors in $2\times(3+1)$-dimensional parameter space, so that we can formally connect two unitary transformations $\mathcal{U}$ and $\mathcal{U}'$ by the (block-)diagonal $N \times N$ phase matrix

$$\Phi(\boldsymbol{x}, \boldsymbol{\pi}) = \begin{pmatrix} e^{i\chi_1(\boldsymbol{x},\boldsymbol{\pi})} & 0 & 0 & \\ 0 & e^{i\chi_2(\boldsymbol{x},\boldsymbol{\pi})} & 0 & \cdots \\ 0 & 0 & e^{i\chi_3(\boldsymbol{x},\boldsymbol{\pi})} & \\ & \vdots & & \ddots \end{pmatrix} , \tag{3.31}$$

where $\chi_n(\boldsymbol{x}, \boldsymbol{\pi})$ are arbitrary functions in our parameter space, which are appropriately termed gauge fields. In fact, $\mathcal{U}_0' = \Phi\mathcal{U}_0$ describes a gauge transformation and can be thought of as a local phase transformation in an extended phase space which includes time and energy. This gauge transformation changes the Berry connection matrices according to

$$\mathcal{A}_k' = i\mathcal{U}_0'\partial_k\mathcal{U}_0'^\dagger = \Phi\mathcal{A}_k\Phi^\dagger + i\Phi\partial_k\Phi^\dagger = \Phi\mathcal{A}_k\Phi^\dagger + \mathcal{X}_k \ , \tag{3.32}$$

where the field $\mathcal{X}_k = i\Phi\partial_k\Phi^\dagger = \partial_k\mathrm{diag}(\chi_1, \chi_2, \ldots, \chi_N)$ is a (block-)diagonal matrix containing the partial derivatives of the phases. $\Phi\mathcal{A}_k\Phi^\dagger$ modifies the off-diagonal elements by giving them additional phase-factors, while the change in diagonal elements is due to $\mathcal{X}_k$. In principle, we have to distinguish three different cases here, the first one being that $\bar{\Xi}_0$ is completely diagonalized with non-degenerate bands which corresponds to the situation just described. However, when we keep part of $\bar{\Xi}_0$ block-diagonal because bands are (nearly) degenerate and we can distinguish the bands, i.e. they have a physical meaning that we want to retain (for example we have spin-degenerate bands but want to describe spin-dependent physics) then we have only a U(1) gauge freedom within this sub-block. Third and last, if we have M degenerate bands, i.e. there is a M-dimensional sub block in $\bar{\Xi}_0$ that is proportional to the unit matrix, and furthermore, we cannot or do not want to distinguish between the degenerate bands, we have the additional degree of freedom to rotate within this degenerate

space giving us an additional SU(M) gauge invariance. Contrary to the first two cases, this last one describes a situation with the effective description of this M-dimensional subspace being a non-Abelian gauge theory with the symmetry group $\mathrm{U}(1) \times \mathrm{SU}(M)$ and consequently, $\mathcal{X}_k$ constitutes a non-Abelian field. We do not differentiate between these cases explicitly in the following because they are straightforwardly treated in our formulas, thus requiring us only to comment in situations where special care is required.

According to the preceding discussion, the projected Berry phase matrix is only modified due to $\mathcal{X}$,

$$\mathcal{A}'^{(d)}_{\boldsymbol{x}} = \mathcal{P}_d \mathcal{A}'_{\boldsymbol{x}} \mathcal{P}_d = \mathcal{A}^{(d)}_{\boldsymbol{x}} + \mathcal{X}_{\boldsymbol{x}} \ , \tag{3.33}$$

and the alternative transformation due to $\mathcal{U}'_0$ leads to the Hamiltonian

$$\begin{aligned} \bar{\Xi}' = \mathcal{U}' * \Xi * \mathcal{U}'^{\dagger} = \bar{\Xi}_0 - \frac{\hbar}{2} \left\{ \mathcal{A}'^{(d)}_{\boldsymbol{\pi}}, \partial_{\boldsymbol{x}} \bar{\Xi}_0 \right\} + \frac{\hbar}{2} \left\{ \mathcal{A}'^{(d)}_{\boldsymbol{x}}, \partial_{\boldsymbol{\pi}} \bar{\Xi}_0 \right\} \\ + \frac{i\hbar}{4} \mathcal{P}_d \left(\left\{ \mathcal{A}_{\boldsymbol{\pi}}, \left[\mathcal{A}_{\boldsymbol{x}}, \bar{\Xi}_0 \right] \right\} - \left\{ \mathcal{A}_{\boldsymbol{x}}, \left[\mathcal{A}_{\boldsymbol{\pi}}, \bar{\Xi}_0 \right] \right\} \right) \mathcal{P}_d + O(\hbar^2) \ . \end{aligned} \tag{3.34}$$

The last term, representing the inter-band transition corrections to the energy, does not change, since the additional terms due to $\mathcal{X}_{\boldsymbol{x}}$, $\mathcal{X}_{\boldsymbol{\pi}}$ are projected out by $\mathcal{P}_d$ and thus, as a consequence, are absorbed by $\mathcal{Y}'_1$ *viz.* $\bar{\mathcal{U}}'_1$ which of course does not need to coincide with $\bar{\mathcal{U}}_1$.

However, the other two terms linear in $\hbar$ do explicitly depend on the gauge, and therefore change the effective Hamiltonian. Clearly, this shows that the effective Hamiltonian alone is an incomplete description as it directly depends on this additional degree of freedom. Therefore, in order to make any sense out of this, we have to identify our physical observables, because in the end, the physical results from our effective theory should not depend on a specific gauge.

3.1.3. Canonical versus Kinetic Variables and Gauge Invariant Description

The previous section showed us that there is still an ingredient missing in our effective theories. In order to investigate this matter, let us study the dynamics of our system, and construct the effective theory such that the results obtained within this description are consistent with what one would obtain in the original frame.

The question is now, whether one can find a manifest gauge invariant formulation and clearly, the answer is yes, but first, let us review some basics. We can generally write quantum kinetic equations in the compact form

$$[\Xi, \ \mathcal{D}] = 0 \ , \tag{3.35}$$

where $\Xi \equiv \epsilon - \mathcal{H}$ and $\mathcal{D}$ represents any dynamical variable in the Schrödinger picture like the usual retarded or Keldysh Greens functions, density of states or the density matrix for which (3.35) reduces to the well-known von Neumann equation

$$i\hbar \partial_t \rho = [\mathcal{H}, \rho] \ , \tag{3.36}$$

where we used that $\epsilon = i\partial_t$. The properties of $\mathcal{D}$ (the type of Greens function, etc.) enter through appropriate boundary conditions in our parameter space. For the example just given,

we simply need to fix our density matrix at some initial time $\rho(t_0) = \rho_0$. In the case of Greens functions it is trickier, for example the retarded Greens function is required to have certain properties in the complex energy plane (all poles should have a positive imaginary part). At any rate, expression (3.35) might not be the best formulation to start from when actually doing explicit calculations. Nevertheless, it is well suited to make our point.

On the other hand, in the Heisenberg picture, we have for the Heisenberg operator $\mathcal{S}^{(H)}$ the equation of motion

$$\frac{\mathrm{d}\mathcal{S}^{(H)}}{\mathrm{d}t} = \frac{1}{i\hbar}\left[\Xi, \mathcal{S}^{(H)}\right] = \partial_t \mathcal{S}^{(H)} + \frac{1}{i\hbar}\left[\mathcal{S}^{(H)}, \mathcal{H}\right] \ . \tag{3.37}$$

Of course, in the end, both Schrödinger and Heisenberg description should yield the same result which we briefly verify by considering the time-evolution of the expectation value of the observable $\mathcal{S}$ in both pictures ($\rho^{(H)}$ does not depend on time in the Heisenberg picture)

$$\frac{\mathrm{d}}{\mathrm{d}t}\langle \mathcal{S} \rangle = \frac{\mathrm{d}}{\mathrm{d}t}\mathrm{Tr}\{\rho \mathcal{S}\} = \mathrm{Tr}\{\rho \partial_t \mathcal{S}\} + \frac{1}{i\hbar}\mathrm{Tr}\{\mathcal{S}\left[\mathcal{H}, \rho\right]\} \tag{3.38}$$

$$\frac{\mathrm{d}}{\mathrm{d}t}\langle \mathcal{S} \rangle = \frac{\mathrm{d}}{\mathrm{d}t}\mathrm{Tr}\left\{\rho^{(H)}\mathcal{S}^{(H)}\right\} = \mathrm{Tr}\left\{\rho^{(H)}\frac{\mathrm{d}\mathcal{S}^{(H)}}{\mathrm{d}t}\right\} = \mathrm{Tr}\left\{\rho^{(H)}\partial_t \mathcal{S}^{(H)}\right\} + \frac{1}{i\hbar}\mathrm{Tr}\left\{\rho^{(H)}\left[\mathcal{S}^{(H)}, \mathcal{H}\right]\right\} \tag{3.39}$$

where we made use of the cyclic property of the trace, and that we use once more to show $\mathrm{Tr}\{\mathcal{S}\left[\mathcal{H}, \rho\right]\} = \mathrm{Tr}\{\rho\left[\mathcal{S}, \mathcal{H}\right]\}$ and which establishes the final equality.

Parameter transformation to kinetic variables

Let us now perform the chain of transformations that brings us to our effective theory. First, the Wigner representation turns $\boldsymbol{x}$ and $\boldsymbol{\pi}$ into normal parameters on which our observables depend, i.e. $\Xi = \Xi(\boldsymbol{x}, \boldsymbol{\pi})$, but operator multiplication is now due to the Moyal product $*$. Let us consider the operator $\mathcal{S}$ that describes some physical observable of our system and, in performing the rotation that brings our Hamiltonian $\mathcal{H}$ into diagonal form, it transforms our observable $\mathcal{S}$ along with it. The observable in the rotated frame $\bar{\mathcal{S}}$ is then related to the original operator $\mathcal{S}$ by virtue of relation (3.25).

Lastly, we consider the projected system, i.e. we now have in mind to develop an effective, yet exhaustive description of the physics taking place within a certain band that is sufficiently well separated from all other bands in order to treat this band independently to a good approximation. For the moment, let us assume that our observable $\mathcal{S}$ is band-diagonal, i.e. it is simply a scalar function of $\boldsymbol{x}$ and $\boldsymbol{p}$, so that the last term in relation (3.25) vanishes and we simply have

$$\bar{\mathcal{S}} = \bar{\mathcal{S}}_0(\boldsymbol{x}, \boldsymbol{\pi}) - \frac{\hbar}{2}\left\{\mathcal{A}^{(d)}_{\boldsymbol{\pi}}, \partial_{\boldsymbol{x}}\bar{\mathcal{S}}_0\right\} + \frac{\hbar}{2}\left\{\mathcal{A}^{(d)}_{\boldsymbol{x}}, \partial_{\boldsymbol{\pi}}\bar{\mathcal{S}}_0\right\} + O(\hbar^2) \ , \tag{3.40}$$

where $\bar{\mathcal{S}}_0 = \mathcal{U}_0 \mathcal{S} \mathcal{U}_0^\dagger$. Later, we will lift this restriction and consider a matrix $\mathcal{O}$ with general structure in band space, so that we will also get this additional term, giving rise to important

contributions. However for the moment, (3.40) is nothing but a Taylor expansion of $\bar{\mathcal{S}}_0$ to first order in $\hbar$,

$$\bar{\mathcal{S}} = \bar{\mathcal{S}}_0(\boldsymbol{x} - \hbar\mathcal{A}^{(d)}_{\boldsymbol{\pi}}, \boldsymbol{\pi} + \hbar\mathcal{A}^{(d)}_{\boldsymbol{x}}) + O(\hbar^2) \ , \tag{3.41}$$

suggesting the parameter transformation to kinetic variables $\boldsymbol{X}$ and $\boldsymbol{\Pi}$

$$\boldsymbol{X} = \boldsymbol{x} - \hbar\mathcal{A}^{(d)}_{\boldsymbol{\pi}} \tag{3.42}$$

$$\boldsymbol{\Pi} = \boldsymbol{\pi} + \hbar\mathcal{A}^{(d)}_{\boldsymbol{x}} \ , \tag{3.43}$$

so that we can simply write

$$\bar{\mathcal{S}} = \bar{\mathcal{S}}_0(\boldsymbol{X}, \boldsymbol{\Pi}) + O(\hbar^2) \ . \tag{3.44}$$

The basis of all calculations within the Wigner representation of quantum theory is the Moyal bracket $\left[\bar{\mathcal{S}} \stackrel{*}{,} \bar{\mathcal{T}}\right]$ between two matrices $\bar{\mathcal{S}}$ and $\bar{\mathcal{T}}$ in the diagonal frame which we now want to rewrite in terms of kinetic variables only. Of course, the Moyal product has to be adjusted to account for the parameter transformation, which can be obtained by using the transformed derivatives

$$\partial_{\boldsymbol{x}} = \partial_{\boldsymbol{X}} + \partial\!\!\!/_{\boldsymbol{x}} = \partial_{\boldsymbol{X}} + \partial^{(\mathcal{A})}_{\boldsymbol{x}} - \hbar(\partial_{\boldsymbol{x}}\mathcal{A}^{(d)}_{\boldsymbol{\pi}_k})\partial_{\boldsymbol{X}_k} + \hbar(\partial_{\boldsymbol{x}}\mathcal{A}^{(d)}_{\boldsymbol{x}_k})\partial_{\boldsymbol{\Pi}_k} \tag{3.45}$$

$$\partial_{\boldsymbol{\pi}} = \partial_{\boldsymbol{\Pi}} + \partial\!\!\!/_{\boldsymbol{\pi}} = \partial_{\boldsymbol{\Pi}} + \partial^{(\mathcal{A})}_{\boldsymbol{\pi}} + \hbar(\partial_{\boldsymbol{\pi}}\mathcal{A}^{(d)}_{\boldsymbol{x}_k})\partial_{\boldsymbol{\Pi}_k} - \hbar(\partial_{\boldsymbol{\pi}}\mathcal{A}^{(d)}_{\boldsymbol{\pi}_k})\partial_{\boldsymbol{X}_k} \ , \tag{3.46}$$

where $\partial^{(\mathcal{A})}$ acts *only* on the Berry connections $\mathcal{A}^{(d)}$ that appear as a result of the transformation, i.e. $\partial^{(\mathcal{A})}$ explicitly acts only on the last two terms of (3.45) and (3.46). This is necessary since, generally, we are dealing with terms like $\partial^n_{\boldsymbol{x}}\bar{\mathcal{S}}$. The reason for writing the derivatives is that we can split the action of $\partial_{\boldsymbol{x}} = \partial_{\boldsymbol{X}} + \partial\!\!\!/_{\boldsymbol{x}}$ into two contributions. $\partial_{\boldsymbol{X}}$ now acts only on the operators like $\bar{\mathcal{S}}(\boldsymbol{X}, \boldsymbol{\Pi})$ as derivative with respect to kinetic variables, while the second partial $\partial\!\!\!/_{\boldsymbol{x}}$ only creates Berry connection terms that appear due to the transformation in the rotated frame, i.e. the terms that $\partial\!\!\!/$ generates are of order $\hbar$. Then using

$$\Lambda = (\overleftarrow{\partial}_{\boldsymbol{\Pi}} + \overleftarrow{\partial\!\!\!/}_{\boldsymbol{\pi}})(\overrightarrow{\partial}_{\boldsymbol{X}} + \overrightarrow{\partial\!\!\!/}_{\boldsymbol{x}}) - (\overleftarrow{\partial}_{\boldsymbol{X}} + \overleftarrow{\partial\!\!\!/}_{\boldsymbol{x}})(\overrightarrow{\partial}_{\boldsymbol{\Pi}} + \overrightarrow{\partial\!\!\!/}_{\boldsymbol{\pi}}) \ , \tag{3.47}$$

the Moyal product (3.1) becomes to leading order correction in $\hbar$

$$* = \star\left(1 + \frac{i\hbar}{2}\left(\overleftarrow{\partial}_{\boldsymbol{\Pi}}\overrightarrow{\partial\!\!\!/}_{\boldsymbol{x}} + \overleftarrow{\partial\!\!\!/}_{\boldsymbol{\pi}}\overrightarrow{\partial}_{\boldsymbol{X}} - \overleftarrow{\partial}_{\boldsymbol{X}}\overrightarrow{\partial\!\!\!/}_{\boldsymbol{\pi}} - \overleftarrow{\partial\!\!\!/}_{\boldsymbol{x}}\overrightarrow{\partial}_{\boldsymbol{\Pi}}\right) + O(\hbar^2)\right) \ , \tag{3.48}$$

where we defined the Moyal product $\star$ now with respect to kinetic variables $\boldsymbol{X}$ and $\boldsymbol{P}$.

In the case of block-diagonalization, we can have non-commutativity within such a sub-block, so we assume $\left[\bar{\mathcal{S}}, \bar{\mathcal{T}}\right] \neq 0$ to treat the most general scenario. Now using (3.48), taking some care of possibly non-Abelian Berry connections, we straightforwardly arrive at the transformed expressions for operator multiplication

$$\begin{aligned}\left[\bar{\mathcal{S}} \stackrel{*}{,} \bar{\mathcal{T}}\right] \to \left[\bar{\mathcal{S}} \stackrel{\star}{,} \bar{\mathcal{T}}\right] &+ i\hbar\Theta^{\boldsymbol{x}\boldsymbol{\pi}}_{ij}\left(\frac{1}{2}\left\{\frac{\partial\bar{\mathcal{S}}}{\partial\boldsymbol{X}_j} \stackrel{\star}{,} \frac{\partial\bar{\mathcal{T}}}{\partial\boldsymbol{\Pi}_i}\right\} - \frac{1}{2}\left\{\frac{\partial\bar{\mathcal{S}}}{\partial\boldsymbol{\Pi}_i} \stackrel{\star}{,} \frac{\partial\bar{\mathcal{T}}}{\partial\boldsymbol{X}_j}\right\}\right) \\ &+ i\hbar\Theta^{\boldsymbol{x}\boldsymbol{x}}_{ij}\frac{1}{2}\left\{\frac{\partial\bar{\mathcal{S}}}{\partial\boldsymbol{\Pi}_i} \stackrel{\star}{,} \frac{\partial\bar{\mathcal{T}}}{\partial\boldsymbol{\Pi}_j}\right\} + i\hbar\Theta^{\boldsymbol{\pi}\boldsymbol{\pi}}_{ij}\frac{1}{2}\left\{\frac{\partial\bar{\mathcal{S}}}{\partial\boldsymbol{X}_i} \stackrel{\star}{,} \frac{\partial\bar{\mathcal{T}}}{\partial\boldsymbol{X}_j}\right\} + O(\hbar^3) \ ,\end{aligned} \tag{3.49}$$

where we defined

$$\Theta_{ij}^{\boldsymbol{xx}} = \hbar \left(\frac{\partial \mathcal{A}_{\boldsymbol{x}_j}^{(d)}}{\partial \boldsymbol{x}_i} - \frac{\partial \mathcal{A}_{\boldsymbol{x}_i}^{(d)}}{\partial \boldsymbol{x}_j} - i \left[\mathcal{A}_{\boldsymbol{x}_i}^{(d)}, \mathcal{A}_{\boldsymbol{x}_j}^{(d)} \right] \right) \tag{3.50}$$

$$\Theta_{ij}^{\boldsymbol{\pi\pi}} = \hbar \left(\frac{\partial \mathcal{A}_{\boldsymbol{\pi}_j}^{(d)}}{\partial \boldsymbol{\pi}_i} - \frac{\partial \mathcal{A}_{\boldsymbol{\pi}_i}^{(d)}}{\partial \boldsymbol{\pi}_j} - i \left[\mathcal{A}_{\boldsymbol{\pi}_i}^{(d)}, \mathcal{A}_{\boldsymbol{\pi}_j}^{(d)} \right] \right) \tag{3.51}$$

$$\Theta_{ij}^{\boldsymbol{x\pi}} = \hbar \left(\frac{\partial \mathcal{A}_{\boldsymbol{\pi}_j}^{(d)}}{\partial \boldsymbol{x}_i} - \frac{\partial \mathcal{A}_{\boldsymbol{x}_i}^{(d)}}{\partial \boldsymbol{\pi}_j} - i \left[\mathcal{A}_{\boldsymbol{x}_i}^{(d)}, \mathcal{A}_{\boldsymbol{\pi}_j}^{(d)} \right] \right) \tag{3.52}$$

which are just Berry curvatures for non-Abelian Berry connections. A more compact way to write the Berry curvatures is to use the covariant derivative (3.16), for example

$$\Theta_{ij}^{\boldsymbol{xx}} = \hbar \left(\bar{\partial}_{\boldsymbol{x}_i} \mathcal{A}_{\boldsymbol{x}_j}^{(d)} - \bar{\partial}_{\boldsymbol{x}_j} \mathcal{A}_{\boldsymbol{x}_i}^{(d)} \right) \ . \tag{3.53}$$

It is easily shown that the Berry curvatures are invariant with respect to gauge transformations, and the commutator is essential as it provides the full SU(M) gauge invariance in the non-Abelian case. Note that incase we retain the full N-dimensional matrix structure of the Berry connections (that is, before the projection), the Berry curvatures identically vanish according to relation (3.21), and it is actually not surprising, since then our unitary $\mathcal{U}_0$ is connected by $SU(N)$ gauge invariance to the identity transformation which clearly has vanishing Berry curvature. Or in other words, when we are just thinking about the $N \times N$ Berry phase matrix structure and forgetting about the underlying Hamiltonian and variables of the actual system (or assuming their structure is trivial), $\mathcal{U}_0$ then constitutes nothing but a SU(N) gauge transformation and the Berry curvature is SU(N) gauge invariant.

We note that to leading order in $\hbar$, we can equally write $\mathcal{A}(\boldsymbol{x}, \boldsymbol{\pi}) = \mathcal{A}(\boldsymbol{X}, \boldsymbol{\Pi}) + O(\hbar)$, since Berry phase terms are already linear in $\hbar$. Similarly, we can substitute $(\boldsymbol{x}, \boldsymbol{\pi})$ with $(\boldsymbol{X}, \boldsymbol{\Pi})$ to leading order in $\hbar$ in the arguments of the Berry curvatures Θ, so our expression for the Moyal bracket (3.49) can now be easily given completely in terms of kinetic variables.

Up to now, we still use the full 4-component notation for our canonical or kinetic variables $\boldsymbol{X} = (T, \boldsymbol{R})$ and $\boldsymbol{\Pi} = (E, -\boldsymbol{P})$ and, after splitting spatial and temporal components again, we can for example write explicitly

$$\underline{\underline{\Theta}}_{ij}^{\boldsymbol{rp}} = \hbar \left(\frac{\partial \mathcal{A}_{\boldsymbol{p}_j}^{(d)}}{\partial \boldsymbol{r}_i} - \frac{\partial \mathcal{A}_{\boldsymbol{r}_i}^{(d)}}{\partial \boldsymbol{p}_j} - i \left[\mathcal{A}_{\boldsymbol{r}_i}^{(d)}, \mathcal{A}_{\boldsymbol{p}_j}^{(d)} \right] \right) \tag{3.54}$$

and we can write for the commutators of our kinetic pairs

$$\begin{aligned} [\boldsymbol{R}_i \stackrel{*}{,} \boldsymbol{P}_j] &= i\hbar \left(\delta_{ij} + \underline{\underline{\Theta}}_{ji}^{\boldsymbol{rp}} \right) \\ [\boldsymbol{R}_i \stackrel{*}{,} \boldsymbol{R}_j] &= i\hbar \epsilon_{ijk} \mathcal{B}_k^{(\boldsymbol{p})} \\ [\boldsymbol{P}_i \stackrel{*}{,} \boldsymbol{P}_j] &= i\hbar \epsilon_{ijk} \mathcal{B}_k^{(\boldsymbol{r})} \end{aligned} \tag{3.55}$$

which attains the additional Berry curvature terms as compared to the canonical commutator relations $[\boldsymbol{r}_i \stackrel{*}{,} \boldsymbol{p}_j] = i\hbar\delta_{ij}$ and $[\boldsymbol{r}_i \stackrel{*}{,} \boldsymbol{r}_j] = 0 = [\boldsymbol{p}_i \stackrel{*}{,} \boldsymbol{p}_j]$. Here, we introduced

$$\boldsymbol{\mathcal{B}}^{(\boldsymbol{r})} = \hbar \left(\partial_{\boldsymbol{r}} \times \mathcal{A}_{\boldsymbol{r}}^{(d)} \right) - i\hbar \left(\mathcal{A}_{\boldsymbol{r}}^{(d)} \times \mathcal{A}_{\boldsymbol{r}}^{(d)} \right) \tag{3.56}$$

$$\boldsymbol{\mathcal{B}}^{(\boldsymbol{p})} = \hbar \left(\partial_{\boldsymbol{p}} \times \mathcal{A}_{\boldsymbol{p}}^{(d)} \right) - i\hbar \left(\mathcal{A}_{\boldsymbol{p}}^{(d)} \times \mathcal{A}_{\boldsymbol{p}}^{(d)} \right) \ , \tag{3.57}$$

which can be considered a generalized magnetic field in real space and reciprocal (or momentum) space. Such a field did we already encounter earlier in the form of a fictitious magnetic (2.154) and electric field (2.155). These non-Abelian Berry curvatures are well known from Yang-Mills theories.

Let us have a closer look at our kinetic variables. $\boldsymbol{P} = \boldsymbol{p} - \hbar\mathcal{A}_{\boldsymbol{r}}$ is of course well known in the Hamilton formulation of particles in an electromagnetic field. In an analogous way, the position $\boldsymbol{R} = \boldsymbol{r} + \hbar\mathcal{A}_{\boldsymbol{p}}$ acquires an additional Berry phase with its corresponding Berry curvature, or momentum space magnetic field that gives rise to the so called anomalous velocity term. Furthermore, $E = \epsilon + \hbar\mathcal{A}_t$ attains a contribution which gives rise to an electromotive force and that we already encountered earlier in the form of an effective electric field (see section 2.4.4 and [70]). The same is true for the electromagnetic field, where the electric field can be also rewritten in terms of a time-dependent phase, effectively changing the gauge. Finally, for reasons of symmetry, one would also have $T = t - \hbar\mathcal{A}_\epsilon$ but, at least in non-interacting Hamiltonian systems, $\mathcal{A}_\epsilon$ is zero, since the energy-dependency in Ξ is trivial and there is no reason, why $\mathcal{U}_0$ should explicitly depend on ϵ.

In the case when the spinor structure of $\bar{\mathcal{S}}$ and $\bar{\mathcal{T}}$ is trivial such that they commute, we can simply write in usual 3-component notation of $\boldsymbol{R}$ and $\boldsymbol{P}$ (and the aforementioned absence of energy-dependence in the Berry curvatures),

$$\begin{aligned}\left[\bar{\mathcal{S}} \overset{*}{,} \bar{\mathcal{T}}\right] = i\hbar\left(\frac{\partial\bar{\mathcal{S}}}{\partial E}\frac{\partial\bar{\mathcal{T}}}{\partial T} - \frac{\partial\bar{\mathcal{S}}}{\partial T}\frac{\partial\bar{\mathcal{T}}}{\partial E}\right) + i\hbar\left(\frac{\partial\bar{\mathcal{T}}}{\partial\boldsymbol{P}}\underline{\underline{\mathcal{J}}}\frac{\partial\bar{\mathcal{S}}}{\partial\boldsymbol{R}} - \frac{\partial\bar{\mathcal{S}}}{\partial\boldsymbol{P}}\underline{\underline{\mathcal{J}}}\frac{\partial\bar{\mathcal{T}}}{\partial\boldsymbol{R}}\right)\\ + i\hbar\boldsymbol{\mathcal{E}}^{(\boldsymbol{r})}\cdot\left(\frac{\partial\bar{\mathcal{S}}}{\partial E}\frac{\partial\bar{\mathcal{T}}}{\partial\boldsymbol{P}} - \frac{\partial\bar{\mathcal{S}}}{\partial\boldsymbol{P}}\frac{\partial\bar{\mathcal{T}}}{\partial E}\right) - i\hbar\boldsymbol{\mathcal{E}}^{(\boldsymbol{p})}\cdot\left(\frac{\partial\bar{\mathcal{S}}}{\partial E}\frac{\partial\bar{\mathcal{T}}}{\partial\boldsymbol{R}} - \frac{\partial\bar{\mathcal{S}}}{\partial\boldsymbol{R}}\frac{\partial\bar{\mathcal{T}}}{\partial E}\right)\\ + i\hbar\boldsymbol{\mathcal{B}}^{(\boldsymbol{p})}\cdot\left(\frac{\partial\bar{\mathcal{S}}}{\partial\boldsymbol{R}}\times\frac{\partial\bar{\mathcal{T}}}{\partial\boldsymbol{R}}\right) + i\hbar\boldsymbol{\mathcal{B}}^{(\boldsymbol{r})}\cdot\left(\frac{\partial\bar{\mathcal{S}}}{\partial\boldsymbol{P}}\times\frac{\partial\bar{\mathcal{T}}}{\partial\boldsymbol{P}}\right) + O(\hbar^3)\ ,\end{aligned} \tag{3.58}$$

where, $\underline{\underline{\mathcal{J}}} \equiv \underline{\underline{1}} + \underline{\underline{\Theta}}^{\boldsymbol{rp}}$ and thus, the dimensionless tensor $\underline{\underline{\Theta}}^{\boldsymbol{rp}}$ describes the change in the metric of the phase-space due to the parameter transformation from canonical to kinetic variables (3.42). We can make this more apparent by relating it to the change in differentials

$$\mathrm{d}R_i = \left(\delta_{ij} + \hbar\partial_{r_j}\mathcal{A}_{p_i}\right)\mathrm{d}r_j \tag{3.59}$$

$$\mathrm{d}P_i = \left(\delta_{ij} - \hbar\partial_{p_j}\mathcal{A}_{r_i}\right)\mathrm{d}p_j\ , \tag{3.60}$$

so that

$$\begin{aligned}\mathrm{d}\boldsymbol{R}\cdot\mathrm{d}\boldsymbol{P} &= \mathrm{d}r_i\left(\delta_{ik} + \hbar\partial_{r_i}\mathcal{A}_{p_k}\right)\left(\delta_{kj} - \hbar\partial_{p_j}\mathcal{A}_{r_k}\right)\mathrm{d}p_j\\ &= \mathrm{d}r_i\left(\delta_{ij} + \hbar\partial_{r_i}\mathcal{A}_{p_j} - \hbar\partial_{p_j}\mathcal{A}_{r_i}\right)\mathrm{d}p_j + O(\hbar^2)\\ &= \mathrm{d}\boldsymbol{r}\left(\underline{\underline{1}} + \underline{\underline{\Theta}}^{\boldsymbol{rp}}\right)\mathrm{d}\boldsymbol{p} + O(\hbar^2) = \mathrm{d}\boldsymbol{r}\underline{\underline{\mathcal{J}}}\mathrm{d}\boldsymbol{p} + O(\hbar^2)\end{aligned} \tag{3.61}$$

and in the same way, $\mathrm{d}\boldsymbol{r}\cdot\mathrm{d}\boldsymbol{p} = \mathrm{d}\boldsymbol{R}\left(\underline{\underline{1}} - \underline{\underline{\Theta}}^{\boldsymbol{rp}}\right)\mathrm{d}\boldsymbol{P} = \mathrm{d}\boldsymbol{R}\underline{\underline{\mathcal{J}}}^{-1}\mathrm{d}\boldsymbol{P}$. For the non-Abelian case, we just need to use the covariant derivative $\bar{\partial}_k = \bar{\partial}_k - i\mathcal{A}_k$ and arrive at the same result.

In accordance with the effective magnetic fields (3.56) and (3.57), we introduced the effective electric fields

$$\boldsymbol{\mathcal{E}}^{(\boldsymbol{r})} = \hbar\left(\partial_{\boldsymbol{r}}\mathcal{A}_t^{(d)} - \partial_t\mathcal{A}_{\boldsymbol{r}}^{(d)} - i\left[\mathcal{A}_{\boldsymbol{r}}^{(d)}, \mathcal{A}_t^{(d)}\right]\right) \tag{3.62}$$

$$\boldsymbol{\mathcal{E}}^{(\boldsymbol{p})} = \hbar\left(\partial_{\boldsymbol{p}}\mathcal{A}_t^{(d)} - \partial_t\mathcal{A}_{\boldsymbol{p}}^{(d)} - i\left[\mathcal{A}_{\boldsymbol{p}}^{(d)}, \mathcal{A}_t^{(d)}\right]\right)\ , \tag{3.63}$$

which shows us indeed that $\mathcal{A}_t$ appears in the role of a generalized electric potential, however, it can also depend on momentum $\boldsymbol{P}$. In the Abelian case (for non-Abelian fields, it works if we take $\mathrm{Tr}_M \boldsymbol{\mathcal{E}}$ and $\mathrm{Tr}_M \boldsymbol{\mathcal{B}}$ or when we take the covariant derivatives (3.16) along with the full matrix structure of the Berry connections), these fictitious fields obey homogeneous Maxwell equations

$$\begin{aligned} \boldsymbol{\partial}_{\boldsymbol{r}/\boldsymbol{p}} \cdot \boldsymbol{\mathcal{B}}^{(r/p)} &= 0 \\ \boldsymbol{\partial}_{\boldsymbol{r}/\boldsymbol{p}} \times \boldsymbol{\mathcal{E}}^{(r/p)} + \partial_t \boldsymbol{\mathcal{B}}^{(r/p)} &= 0 \ , \end{aligned} \tag{3.64}$$

however, in order to determine these fields independently as in classical electrodynamics, we need two additional equations containing (effective) source terms as inhomogenities. Note that in the equations (3.64), we have to treat the momentum $\boldsymbol{P}$ as an additional parameter in $\boldsymbol{\mathcal{E}}^{(r)}$, $\boldsymbol{\mathcal{B}}^{(r)}$ and vice versa. As in (3.55), the effective magnetic fields can be also defined in terms of commutator relations

$$\begin{aligned} \boldsymbol{\mathcal{E}}^{(r)} &= \frac{1}{i\hbar} \left[E \overset{*}{,} \boldsymbol{P} \right] \\ \boldsymbol{\mathcal{E}}^{(p)} &= -\frac{1}{i\hbar} \left[E \overset{*}{,} \boldsymbol{R} \right] \ . \end{aligned} \tag{3.65}$$

There exists a sum rule for the fictitious fields

$$\begin{aligned} &\mathrm{Tr}_N \boldsymbol{\mathcal{B}}^{(p)} = 0 \ , \qquad \mathrm{Tr}_N \boldsymbol{\mathcal{B}}^{(r)} = 0 \ , \qquad \mathrm{Tr}_N \underline{\underline{\Theta}}^{rp} = 0 \ , \\ &\mathrm{Tr}_N \boldsymbol{\mathcal{E}}^{(p)} = 0 \ , \qquad \mathrm{Tr}_N \boldsymbol{\mathcal{E}}^{(r)} = 0 \ , \end{aligned} \tag{3.66}$$

which can be found by taking the trace over all bands (we denote this sum over bands as Tr_N here and throughout this chapter) and making use of the identity (3.21). This means that all the effective forces for each band balance each other in total, or in other words, an excitation that is equally spit amongst all bands (and thus, the density operator ρ is band diagonal) does not experience any net force.

Finally, we can interpret the appearance of the fictitious fields completely as a consequence of the metric of our $2 \times (3+1)$ dimensional parameter space, which becomes non-trivial after the parameter transformation, which itself is a consequence of the diagonalization.

Expectation values in the rotated frame

Let us now go back to the initial question of the dynamics of our system within the effective theory by studying the expectation values of physical observables, which can be obtained in the Wigner representation simply by the integration over the complete phase space,

$$\langle \mathcal{S} \rangle = \int \mathrm{d}^3 r \int \frac{\mathrm{d}^3 p}{(2\pi\hbar)^3} \ \mathrm{Tr}_N \left\{ \rho(\boldsymbol{x}, \boldsymbol{\pi}) * \mathcal{S}(\boldsymbol{x}, \boldsymbol{\pi}) \right\} \ , \tag{3.67}$$

and the trace is with respect to the matrix structure. Note that the factor $1/(2\pi\hbar)^3 = 1/h^3$ describes the proper quantization of the phase space volume and thus is directly obtained by transforming quantum averages into the Wigner representation.

If we assume the integration over the whole phase space to be unbounded and any surface contribution from the integrand at infinity to vanish, we can perform partial integrations to

show that all the partial derivatives in the Moyal product $*$ cancel each other, so that we can equally write

$$\langle \mathcal{S} \rangle = \int \mathrm{d}^3 r \int \frac{\mathrm{d}^3 p}{(2\pi\hbar)^3} \, \mathrm{Tr}_N \left\{ \rho(\boldsymbol{x}, \boldsymbol{\pi}) \mathcal{S}(\boldsymbol{x}, \boldsymbol{\pi}) \right\} \ . \tag{3.68}$$

The expression in the rotated frame is straightforwardly obtained by using

$$\begin{aligned} \langle \mathcal{O} \rangle &= \int \frac{\mathrm{d}^3 r \ \mathrm{d}^3 p}{(2\pi\hbar)^3} \, \mathrm{Tr}_N \left\{ \mathcal{O} * \mathcal{U}^\dagger * \mathcal{U} \right\} = \int \frac{\mathrm{d}^3 r \ \mathrm{d}^3 p}{(2\pi\hbar)^3} \, \mathrm{Tr}_N \left\{ \mathcal{U} (\mathcal{O} * \mathcal{U}^\dagger) \right\} \\ &= \int \frac{\mathrm{d}^3 r \ \mathrm{d}^3 p}{(2\pi\hbar)^3} \, \mathrm{Tr}_N \left\{ \mathcal{U} * \mathcal{O} * \mathcal{U}^\dagger \right\} = \langle \bar{\mathcal{O}} \rangle \ , \end{aligned} \tag{3.69}$$

where in the second step we used the property that one Moyal product can be made trivial by partial integration (however, we cannot remove both Moyal products in this manner) and then we used the cyclic property of the trace to move the factor $\mathcal{U}$ to the left, so that in the third step, we can reintroduce the Moyal product. Therefore, we can write

$$\langle \mathcal{S} \rangle = \langle \bar{\mathcal{S}} \rangle = \int \mathrm{d}^3 r \int \frac{\mathrm{d}^3 p}{(2\pi\hbar)^3} \, \mathrm{Tr}_N \left\{ \bar{\rho}(\boldsymbol{x}, \boldsymbol{\pi}) \bar{\mathcal{S}}(\boldsymbol{x}, \boldsymbol{\pi}) \right\} \ . \tag{3.70}$$

Henceforth, our formulation will be solely in the Heisenberg picture, so that in equilibrium, the density operator is simply obtained from

$$\rho(\boldsymbol{x}, \boldsymbol{\pi}) = f_{\mathrm{D}}(\epsilon) \, \delta(\bar{\Xi}) = f_{\mathrm{D}}(\epsilon) \ \delta(\epsilon - \bar{\mathcal{H}}(\boldsymbol{x}, \boldsymbol{\pi})) \ , \tag{3.71}$$

or, if we do not want our results to be energy resolved, we use directly

$$\rho(\boldsymbol{x}, \boldsymbol{p}) = \int \mathrm{d}\epsilon \ f_{\mathrm{D}}(\epsilon) \delta(\epsilon - \bar{\mathcal{H}}(\boldsymbol{x}, \boldsymbol{\pi})) \ , \tag{3.72}$$

which gives us simply the density in phase space and, as we will discuss later however, it is to be interpreted as a quasi-probability. Since we are using the Heisenberg picture, an explicitly time-dependent Hamiltonian $\bar{\mathcal{H}}(\boldsymbol{x}, \boldsymbol{\pi})$ has to be treated using (3.125) instead. If a band is completely filled, it becomes 1 at the diagonal element corresponding to that band. If energies are well separated, and we assume excitations localized in energy space, we can assume any off-diagonal elements in the density operator to vanish. In fact, those off-diagonal entries correspond to coherent excitations that are split amongst several bands, for example the transverse spin excitations discussed in 2.4.3 are rapidly oscillating due to their large energy splitting, so that on larger scales we only see the envelope which, in the present formulation, is described by Berry phase terms due to adiabatic transport. If all bands are completely filled, $\rho(\boldsymbol{x}, \boldsymbol{\pi}) = \mathbb{1}_N$, i.e. it is simply the unit matrix. Then the total number of electrons is

$$N_{\mathrm{el}} = \int \mathrm{d}^3 r \int \frac{\mathrm{d}^3 p}{(2\pi\hbar)^3} \, \mathrm{Tr}_N \bar{\rho}(\boldsymbol{x}, \boldsymbol{\pi}) = N \int \mathrm{d}^3 r \int \frac{\mathrm{d}^3 p}{(2\pi\hbar)^3} = N \frac{V}{V_{BZ}} \ , \tag{3.73}$$

where V is the volume of the system and V_{BZ} is the volume of the Brillouin zone and thus gives the correct number of particles. In the end, the projection operation defined by $\mathcal{P}_d$ is essentially enforced by the diagonal representation of the Hamiltonian $\bar{\Xi}$, and by the density

matrix ρ which gives us only those states that have coherences within bands (or nearly degenerate bands so that, again, the energy argument applies). In particular, this is certainly true for low energy transport, where physics takes place only in the vicinity of the Fermi level. Note that the "high energy" contributions we needed to take into account in previous chapters (c.f. section 2.2.4), are in the present description replaced by Berry phase contributions.

In order to proceed, let us transform the integration variables to kinetic ones, and in doing so, we also have to take into account how the volume element in phase space changes, which is given by the determinant of the Jacobian

$$D^{-1} \equiv \det \frac{\partial(\boldsymbol{R},\boldsymbol{P})}{\partial(\boldsymbol{r},\boldsymbol{p})} = \det\left(\underline{\underline{1}} + \hbar\frac{\partial(\mathcal{A}_{\boldsymbol{p}}^{(d)}, -\mathcal{A}_{\boldsymbol{r}}^{(d)})}{\partial(\boldsymbol{r},\boldsymbol{p})}\right)$$
$$= 1 + \hbar\mathrm{Tr}\frac{\partial(\mathcal{A}_{\boldsymbol{p}}^{(d)}, -\mathcal{A}_{\boldsymbol{r}}^{(d)})}{\partial(\boldsymbol{r},\boldsymbol{p})} + O(\hbar^2) = 1 + \mathrm{Tr}\underline{\underline{\Theta}}^{\boldsymbol{rp}} + O(\hbar^2)\ , \qquad (3.74)$$

or $D(\boldsymbol{X},\boldsymbol{\Pi}) = 1 - \mathrm{Tr}\underline{\underline{\Theta}}^{\boldsymbol{rp}} + O(\hbar^2)$ and therefore is also gauge invariant. In non-Abelian situations the non-trivial matrix structure of the Berry curvature will be inherited by D which will be accounted for by performing the integration before taking the trace, thus yielding

$$\langle\mathcal{S}\rangle = \mathrm{Tr}_N\left\{\int \frac{\mathrm{d}^3R\ \mathrm{d}^3P}{(2\pi\hbar)^3}\ D(\boldsymbol{X},\boldsymbol{\Pi})\ \bar{\rho}(\boldsymbol{X},\boldsymbol{\Pi})\bar{\mathcal{S}}(\boldsymbol{X},\boldsymbol{\Pi})\right\}\ . \qquad (3.75)$$

As we will see later, D describes for example charge accumulation in the case of a topological insulator with a exchange induced magnetization structure. This effect of the Berry curvature on the density of states has been already discovered by Xiao and coworkers [120]. The consequences of D will become clearer in the following sections, and we will give an example of this induced charge in section 3.4.

Let us look at this in another way, by transforming the observable $\bar{\mathcal{O}}$ back into the original frame (using result (3.26)),

$$\mathcal{U}_0\mathcal{O}\mathcal{U}_0^\dagger = \bar{\mathcal{O}} - \hbar\left[\mathcal{Y}_1,\bar{\mathcal{O}}\right] + \frac{\hbar}{2}\left\{\mathcal{A}_{\boldsymbol{\pi}},\partial_{\boldsymbol{x}}\bar{\mathcal{O}}\right\} - \frac{\hbar}{2}\left\{\mathcal{A}_{\boldsymbol{x}},\partial_{\boldsymbol{\pi}}\bar{\mathcal{O}}\right\}$$
$$- \frac{i\hbar}{4}\left(\left\{\mathcal{A}_{\boldsymbol{\pi}},\left[\mathcal{A}_{\boldsymbol{x}},\bar{\mathcal{O}}\right]\right\} - \left\{\mathcal{A}_{\boldsymbol{x}},\left[\mathcal{A}_{\boldsymbol{\pi}},\bar{\mathcal{O}}\right]\right\}\right) + O(\hbar^2) \qquad (3.76)$$

and let $\mathcal{S}$ be a general observable that can posses an arbitrary matrix structure, so that contrary to relation (3.40), the additional dipole term becomes relevant. In the end, we want to establish the connection with (3.75), so we are interested in expectation values or phase-space densities (which then are quasi-probability distributions),

$$s(\boldsymbol{x},\boldsymbol{\pi}) = \mathrm{Tr}_N\left(\frac{1}{2}\left\{\rho\overset{*}{,}\mathcal{S}\right\}\right) = \mathrm{Tr}_N\left(\mathcal{U}^\dagger * \frac{1}{2}\left\{\bar{\rho}\overset{*}{,}\bar{\mathcal{S}}\right\} * \mathcal{U}\right)\ , \qquad (3.77)$$

which links the density calculated in the original frame to the trace completely expressed in terms of quantities belonging to the rotated frame. We essentially have to substitute $\bar{\mathcal{O}} = \frac{1}{2}\left\{\bar{\rho}\overset{*}{,}\bar{\mathcal{S}}\right\}$, and then take the trace of (3.76),

$$s(\boldsymbol{x},\boldsymbol{\pi}) = \mathrm{Tr}_N\left\{\bar{\mathcal{O}} + \hbar\mathcal{A}_\pi\partial_{\boldsymbol{x}}\bar{\mathcal{O}} - \hbar\mathcal{A}_{\boldsymbol{x}}\partial_{\boldsymbol{\pi}}\bar{\mathcal{O}}\right\} + i\hbar\mathrm{Tr}\left\{\bar{\mathcal{O}}\left[\mathcal{A}_{\boldsymbol{x}},\mathcal{A}_{\boldsymbol{\pi}}\right]\right\} + O(\hbar^2)\ . \qquad (3.78)$$

According to the discussion above, it is reasonable to assume that our observable is given as a function of the kinetic variables, i.e. $\bar{\mathcal{O}}(\boldsymbol{X}, \boldsymbol{\Pi})$ and it is instructive to treat the inter-band and the intra-band contributions separately by splitting $\bar{\mathcal{O}} = \mathcal{P}_d \bar{\mathcal{O}} \mathcal{P}_d + \mathcal{P}_o \bar{\mathcal{O}} \mathcal{P}_o \equiv \bar{\mathcal{O}}^{(d)} + \bar{\mathcal{O}}^{(o)}$ and likewise for $\bar{\mathcal{S}} = \bar{\mathcal{S}}^{(d)} + \bar{\mathcal{S}}^{(o)}$, so that the contribution from the diagonal part becomes [4]

$$s^{(d)}(\boldsymbol{x}, \boldsymbol{\pi}) = \mathrm{Tr}_N \left\{ D(\boldsymbol{x}, \boldsymbol{\pi}) \; \bar{\mathcal{O}}^{(d)}(\boldsymbol{X} + \hbar \mathcal{A}^{(d)}_{\boldsymbol{\pi}}, \boldsymbol{\Pi} - \hbar \mathcal{A}^{(d)}_{\boldsymbol{x}}) \right\} + O(\hbar^2) \; , \tag{3.79}$$

which basically undoes the variable transformation so that we go back to the canonical pair of variables and can write simply

$$s^{(d)}(\boldsymbol{x}, \boldsymbol{\pi}) = \mathrm{Tr}_N \left\{ \bar{\rho}(\boldsymbol{x}, \boldsymbol{\pi}) \; D(\boldsymbol{x}, \boldsymbol{\pi}) \; \bar{\mathcal{S}}^{(d)}(\boldsymbol{x}, \boldsymbol{\pi}) \right\} + O(\hbar^2) \; . \tag{3.80}$$

In addition, we rewrote the last term with the help of identity (3.21), $i\,[\mathcal{A}_{\boldsymbol{x}}, \mathcal{A}_{\boldsymbol{\pi}}] = \partial_{\boldsymbol{x}} \mathcal{A}_{\boldsymbol{\pi}} - \partial_{\boldsymbol{\pi}} \mathcal{A}_{\boldsymbol{x}}$ and, according to our previous discussion, we have $\Theta^{\epsilon t} = 0$, as $\mathcal{U}_0$ was assumed to not explicitly depend on the energy parameter so we could replace this term with $\mathrm{Tr} \underline{\underline{\Theta}}^{\boldsymbol{rp}}$. This contribution gives rise to the correction factor $D(\boldsymbol{x}, \boldsymbol{\pi})$ that we already encountered before, and thus, the last result is consistent with relation (3.75). In particular, if we take $\bar{\mathcal{O}}$ to be simply the density matrix of completely filled bands (i.e. $\bar{\rho}_{ii} = 1$ for a set of i corresponding to the filled bands, and all other elements are zero), we obtain the same modification to the density due to factor $D(\boldsymbol{x}, \boldsymbol{\pi})$, as in (3.75).

The implications of the diagonal part of $\bar{\mathcal{S}}$ can be summarized as undoing the parameter transformation together with the appearance of the correction factor $D(\boldsymbol{x}, \boldsymbol{p})$ which locally changes the density. However, it is not always possible to ignore the off-diagonal part of the observable $\bar{\mathcal{S}}$, one prominent example will be the current which we are going to discuss later. With a series of straightforward manipulations involving the cyclic property of the trace along with identity (3.21), we eventually arrive at

$$s^{(o)}(\boldsymbol{x}, \boldsymbol{\pi}) = \partial_{\boldsymbol{x}} \mathrm{Tr}_N \bar{\rho} \frac{\hbar}{2} \Big\{ \mathcal{A}_{\boldsymbol{\pi}}, \bar{\mathcal{S}}^{(o)} \Big\} - \partial_{\boldsymbol{\pi}} \mathrm{Tr}_N \bar{\rho} \frac{\hbar}{2} \Big\{ \mathcal{A}_{\boldsymbol{x}}, \bar{\mathcal{S}}^{(o)} \Big\} + O(\hbar^2) \; , \tag{3.81}$$

so that both contributions to the expectation value, (3.80) and (3.81) together read

$$s = \mathrm{Tr}_N \bar{\rho} \, D \bar{\mathcal{S}}^{(d)} + \partial_{\boldsymbol{x}} \mathrm{Tr}_N \bar{\rho} \, \frac{\hbar}{2} \Big\{ \mathcal{A}_{\boldsymbol{\pi}}, \bar{\mathcal{S}}^{(o)} \Big\} - \partial_{\boldsymbol{\pi}} \mathrm{Tr}_N \bar{\rho} \, \frac{\hbar}{2} \Big\{ \mathcal{A}_{\boldsymbol{x}}, \bar{\mathcal{S}}^{(o)} \Big\} + O(\hbar^2) \; . \tag{3.82}$$

The importance of these last two terms will become clearer in the section discussing the kinetic equations of the effective theory.

Before continuing, let us briefly comment on observables with non-trivial band matrix structure $\mathcal{O}$, and its transformation into the rotated frame by virtue of relation (3.25), and considering the diagonal and off-diagonal part of $\bar{\mathcal{O}}_0 = \mathcal{U}_0 \mathcal{O} \mathcal{U}_0^\dagger$ separately,

$$\bar{\mathcal{O}}_0^{(d)}(\boldsymbol{X}, \boldsymbol{\Pi}) + \frac{i\hbar}{4} \mathcal{P}_d \left(\Big\{ \mathcal{A}_{\boldsymbol{\pi}}, \Big[\mathcal{A}_{\boldsymbol{x}}, \bar{\mathcal{O}}_0^{(d)} \Big] \Big\} - \frac{i\hbar}{4} \Big\{ \mathcal{A}_{\boldsymbol{x}}, \Big[\mathcal{A}_{\boldsymbol{\pi}}, \bar{\mathcal{O}}_0^{(d)} \Big] \Big\} \right) \mathcal{P}_d + O(\hbar^2) \; , \tag{3.83}$$

[4] Since $\mathcal{O}^{(d)}$ effectively projects the Berry-connection matrices $\mathcal{A}^{(d)}$, so that we have $[\bar{\mathcal{S}}^{(d)}, \mathcal{A}^{(d)}] = 0$, the Taylor expansion is mathematically well-defined. In the case of Abelian gauge fields, the situation is trivial, while in the non-Abelian case, we need to make the assumption not to probe the internal, degenerate structure and accordingly, $\bar{\mathcal{S}}_0$ should be diagonal in the corresponding sub-space in order to describe a meassurement of this kind.

and the contribution arising from the off-diagonal part of $\bar{\mathcal{O}}_0^{(o)}$,

$$\mathcal{P}_d \left(\left[\mathcal{Y}_1, \bar{\mathcal{O}}_0^{(o)} \right] - \frac{\hbar}{2} \left\{ \mathcal{A}_{\boldsymbol{\pi}}, \left[\partial_{\boldsymbol{x}} - \tfrac{i}{2} \mathcal{A}_{\boldsymbol{x}}, \bar{\mathcal{O}}_0^{(o)} \right] \right\} + \frac{\hbar}{2} \left\{ \mathcal{A}_{\boldsymbol{x}}, \left[\partial_{\boldsymbol{\pi}} - \tfrac{i}{2} \mathcal{A}_{\boldsymbol{\pi}}, \bar{\mathcal{O}}_0^{(o)} \right] \right\} \right) \mathcal{P}_d + O(\hbar^2) \ , \tag{3.84}$$

which are both independently gauge invariant. While the gauge invariance of the former is straightforward to show, the later requires more work and we have to take into account that $\mathcal{Y}_1$ is modified under a gauge transformation as

$$\mathcal{Y}_1 \to \mathcal{Y}_1 - \frac{i\hbar}{4} \left(\{ \chi_{\boldsymbol{x}}, \mathcal{A}_{\boldsymbol{\pi}} \} - \{ \chi_{\boldsymbol{\pi}}, \mathcal{A}_{\boldsymbol{x}} \} \right) \ , \tag{3.85}$$

along with $\partial_\alpha \bar{\mathcal{O}} \to \partial_\alpha \bar{\mathcal{O}} + i \left[\chi_\alpha, \bar{\mathcal{O}} \right]$ and $\mathcal{A}_\alpha \to \mathcal{A}_\alpha + \chi_\alpha$.

Is the diagonalization transformation canonical?

Before continuing, we would like to point out that without the truncation, $\boldsymbol{X}$ and $\boldsymbol{\Pi}$ still obey the canonical commutation relations, which can be easily seen by noting that the set of "complete" Berry curvatures (i.e. relations (3.50)-(3.52) with $\mathcal{A}^{(d)}$ replaced by the full Berry phase matrices $\mathcal{A}$) vanishes according to identity (3.21). That means, retaining all off-diagonal elements, our unitary transformation is a canonical one, however, since $\boldsymbol{X}$ and $\boldsymbol{\Pi}$ now posses a complicated matrix structure in the N-dimensional band space, they no longer commute with non-trivial matrices within this band space. For example, in a simple particle-hole symmetric two-band model

$$\mathcal{H} = \boldsymbol{E}(\boldsymbol{p}) \cdot \boldsymbol{\sigma} + V(\boldsymbol{r}) \mathbb{1}_2 \ , \tag{3.86}$$

our band-diagonalized Hamiltonian has the form

$$\bar{\mathcal{H}} = E(\boldsymbol{p}) \sigma_z + V(\boldsymbol{R}) \mathbb{1}_2 \ , \tag{3.87}$$

while $\boldsymbol{R} = \boldsymbol{r} + \hbar \mathcal{A}_{\boldsymbol{p}}$ acquires a 2×2 Berry connection matrix, so that $[\boldsymbol{R}_i, \boldsymbol{R}_j] = 0 = [\boldsymbol{P}_i, \boldsymbol{P}_j]$ and $[\boldsymbol{R}_i, \boldsymbol{P}_j] = i\hbar\delta_{ij}$, but $[\boldsymbol{R}, \sigma_z] = \hbar [\boldsymbol{\mathcal{A}}_{\boldsymbol{p}}, \sigma_z] \neq 0$. Instead, this commutator now encodes the complicated dynamics of inter-band scattering, making the problem as a whole not easier tractable so, in the general case, the only way out is the truncation scheme. And only due to the restriction of the Berry-phase matrices into a certain sub-space do the corresponding Berry curvatures yield a non-vanishing value.

To conclude this section, we see that when we use the kinetic terms $\boldsymbol{X}$ and $\boldsymbol{\Pi}$ as basic quantities for our observables, we end up with expressions that are manifest gauge invariant (c.f. Eqns (3.49) and (3.75)). In fact, these kinetic variables appear consistently in virtually all equations of physical relevance, and moreover, it is exactly these quantities that we obtain, if we transform the canonical variables into the rotated frame,

$$\begin{aligned} \boldsymbol{X} &= \mathcal{U} * \boldsymbol{x} * \mathcal{U}^\dagger = \boldsymbol{x} - i\hbar \mathcal{U} * \partial_{\boldsymbol{\pi}} \mathcal{U}^\dagger \\ \boldsymbol{\Pi} &= \mathcal{U} * \boldsymbol{\pi} * \mathcal{U}^\dagger = \boldsymbol{p} + i\hbar \mathcal{U} * \partial_{\boldsymbol{x}} \mathcal{U}^\dagger \ . \end{aligned}$$

3.1.4. Electronic Spectrum and Magnetic Dipole Energy

In course of the preceding discussion, we saw that rewriting the Hamiltonian in terms of kinetic variables would render it gauge invariant. However, in order to calculate the electronic spectrum, one essentially has to diagonalize it, and which has to be done in terms of canonical variables. But it turns out that this remaining gauge-dependence of the Hamiltonian in the canonical representation would only affect the wavefunctions or quantities that build upon them like the density operator or the corresponding retarded Greens function. These objects will acquire local phase-factors that depend on $\boldsymbol{x}$ and $\boldsymbol{p}$ and we will illustrate this point later by explicitly studying the situation in the case of the Dirac equation. At this point, we can conclude that the electronic spectrum of the system is also gauge-independent.

Let us briefly discuss the last term of the transformation equations like (3.30), and that we ignored by now,

$$\bar{\mathcal{H}}_{\mathcal{M}} = \frac{i\hbar}{4}\mathcal{P}_d \left(\left\{ \mathcal{A}_{\boldsymbol{r}}, \left[\mathcal{A}_{\boldsymbol{p}}, \bar{\mathcal{H}}_0 \right] \right\} - \left\{ \mathcal{A}_{\boldsymbol{p}}, \left[\mathcal{A}_{\boldsymbol{r}}, \bar{\mathcal{H}}_0 \right] \right\} \right) \mathcal{P}_d \ , \tag{3.88}$$

which gives rise to corrections due to virtual transitions to other bands. The term "magnetic" comes from the fact that $\bar{\mathcal{H}}_{\mathcal{M}}$ corresponds to the energy of a magnetic dipole in an external magnetic field, where the magnetic dipole is an intrinsic property of the band. For example, in the case of the Dirac equation, this term becomes essentially the magnetic Zeeman term, though in other scenarios, one obtains generalizations thereof, and even in the absence of external magnetic fields, $\bar{\mathcal{H}}_{\mathcal{M}}$ can be non-zero. Later, we will find an example thereof, where a non-trivial space dependency is imprinted onto the system. At any rate, this term is related to circular currents and is essentially is a magnetic dipole.

Since we will encounter terms like in $\bar{\mathcal{H}}_{\mathcal{M}}$ later, let us define the quantities (α, β are any combinations of $(t, \boldsymbol{r}, \boldsymbol{p})$)

$$\underline{\underline{\Omega}}_{\alpha,\beta} = \frac{i\hbar}{2}\mathcal{P}_d \left\{ \mathcal{A}_\alpha \left[\mathcal{A}_\beta, \bar{\mathcal{H}}_0 \right] \right\} \mathcal{P}_d \ , \tag{3.89}$$

which is an antisymmetric tensor in $\boldsymbol{x}, \boldsymbol{p}$-space[5], and in addition, it is a band-diagonal matrix, or block diagonal according to the structure defined by the projector $\mathcal{P}_d$. The explicit structure of $\underline{\underline{\Omega}}$ is

$$\underline{\underline{\Omega}} = \begin{pmatrix} 0 & -\boldsymbol{\Omega}^{\boldsymbol{tr}} & -\boldsymbol{\Omega}^{\boldsymbol{tp}} \\ \boldsymbol{\Omega}^{\boldsymbol{tr}} & \epsilon_{ijk}\Omega_k^{\boldsymbol{rr}} & \underline{\underline{\Omega}}^{\boldsymbol{rp}} \\ \boldsymbol{\Omega}^{\boldsymbol{tp}} & -\underline{\underline{\Omega}}^{\boldsymbol{rp}} & \epsilon_{ijk}\Omega_k^{\boldsymbol{pp}} \end{pmatrix} \ , \tag{3.90}$$

which has been defined in correspondence to the Berry curvatures

$$\underline{\underline{\Theta}}_{\alpha,\beta} = \hbar \left(\partial_\alpha \mathcal{A}_\beta^{(d)} - \partial_\beta \mathcal{A}_\alpha^{(d)} - i \left[\mathcal{A}_\alpha^{(d)}, \mathcal{A}_\beta^{(d)} \right] \right) \ , \tag{3.91}$$

or explicitly in terms of the fictitious fields

$$\underline{\underline{\Theta}} = \begin{pmatrix} 0 & -\boldsymbol{\mathcal{E}}^{(\boldsymbol{r})} & -\boldsymbol{\mathcal{E}}^{(\boldsymbol{p})} \\ \boldsymbol{\mathcal{E}}^{(\boldsymbol{r})} & \epsilon_{ijk}\mathcal{B}_k^{(\boldsymbol{r})} & \underline{\underline{\Theta}}^{\boldsymbol{rp}} \\ \boldsymbol{\mathcal{E}}^{(\boldsymbol{p})} & -\underline{\underline{\Theta}}^{\boldsymbol{rp}} & \epsilon_{ijk}\mathcal{B}_k^{(\boldsymbol{p})} \end{pmatrix} \ , \tag{3.92}$$

[5]This tensor should have certain properties with respect to rotations or Lorentz transformations.

which now makes the analogy of the structure between $\underline{\underline{\Omega}}$ and $\underline{\underline{\Theta}}$ obvious. The topleft part of $\underline{\underline{\Theta}}$ excluding the momentum dependent part is essentially the electromagnetic field tensor[6].

Now, we can express the energy term simply as

$$\bar{\mathcal{H}}_{\mathcal{M}} = \mathrm{Tr}\underline{\underline{\Omega}}^{\boldsymbol{rp}} \ , \tag{3.93}$$

where the trace is only with respect to coordinates, and not band indices, and we write explicitly

$$\underline{\underline{\Omega}}^{\boldsymbol{rp}}_{ij} = \frac{i\hbar}{2}\mathcal{P}_d \left\{ \mathcal{A}_{r_i} \left[\mathcal{A}_{p_j}, \bar{\mathcal{H}}_0 \right] \right\} \mathcal{P}_d \ . \tag{3.94}$$

As will become more apparent later, terms involving the $\underline{\underline{\Omega}}$ tensor are related to circular currents and give rise to important terms that should not be forgotten.

For the sake of completeness, and in order to establish the link to other treatments in literature (for example [109] and references therein), let us express our quantities $\underline{\underline{\Theta}}$ and $\underline{\underline{\Omega}}$ in terms of Bloch functions $(\mathcal{A}_{\boldsymbol{p}})_{ij} = \langle u_i | i\partial_{\boldsymbol{p}} | u_j \rangle$, with the Bloch band indices i and j. We continue by introducing the gauge-invariant transition elements

$$\Gamma^{(\alpha,\beta)}_{ij} \equiv -2\hbar \mathrm{Im} \left\{ (\mathcal{A}_\alpha)_{ij} (\mathcal{A}_\beta)_{ji} \right\} = -2\hbar \mathrm{Im} \left\{ \langle u_i | i\partial_\alpha | u_j \rangle \ \langle u_j | i\partial_\beta | u_i \rangle \right\} \ , \tag{3.95}$$

which are anti-Hermitian, $\Gamma^{(\alpha,\beta)}_{ij} = -\Gamma^{(\alpha,\beta)}_{ji}$ due to the Hermiticity of $\mathcal{A}$ and, as the name suggests, they describe corrections due to virtual transitions between band i and j.

Then the Berry curvatures projected onto band i can be expressed as

$$\underline{\underline{\Theta}}_{\alpha\beta} = \hbar(\partial_\alpha \mathcal{A}^{(d)}_\beta - \partial_\beta \mathcal{A}^{(d)}_\alpha)_{ii} = \sum_j \Gamma^{(\alpha,\beta)}_{ij} \ , \tag{3.96}$$

and one can interpret the Berry phases as being corrections to the kinetic variables $\boldsymbol{x}, \boldsymbol{\pi}$ due to virtual transitions into all other bands j. The sum rule (3.66) is then a direct consequence of the anti-Hermiticity of Γ. In the same spirit, the dipole terms projected on Bloch band i read

$$\underline{\underline{\Omega}}_{\alpha\beta} = \frac{1}{2} \sum_j (\epsilon_i - \epsilon_j) \, \Gamma^{(\alpha,\beta)}_{ij} \ , \tag{3.97}$$

where the energies are $\epsilon_i \equiv (\bar{\mathcal{H}}_0)_{ii}$.

As might be apparent from the above expressions, there exists a direct link between $\underline{\underline{\Theta}}$ and $\underline{\underline{\Omega}}$ in the case of a two-level system, and which we establish in the following. First, a general diagonal 2-level Hamiltonian $\bar{\mathcal{H}}_0$ can be divided into a symmetric part $\propto \mathbb{1}_2$ which consequently commutates out in expression (3.89), and an antisymmetric part $\propto \sigma_z$ responsible for a finite contribution. After some simple algebra, we find $\mathrm{Tr}_2 \sigma_z \underline{\underline{\Omega}} = 0$ which implies that $\underline{\underline{\Omega}}$ is band diagonal, and the two bands get the same contribution, in particular the magnetic dipole energy is the same for the two bands. The diagonal part is simply obtained by taking the trace and using its cyclic properties,

$$\begin{aligned} \mathrm{Tr}_2 \underline{\underline{\Omega}}_{\alpha,\beta} &= i\hbar \mathrm{Tr}_2 \bar{\mathcal{H}}_0 \left[\mathcal{A}_\alpha, \mathcal{A}_\beta \right] = \hbar \mathrm{Tr}_2 \bar{\mathcal{H}}_0 (\partial_\alpha \mathcal{A}^{(d)}_\beta - \partial_\beta \mathcal{A}^{(d)}_\alpha) \\ &= \mathrm{Tr}_2 \left(\bar{\mathcal{H}}_0 \underline{\underline{\Theta}}_{\alpha,\beta} \right) \ , \end{aligned} \tag{3.98}$$

[6] apart from a sign difference since we did not use Lorentz covariant notation

where in the last two steps, we used the identity (3.21) along with definition (3.96) to replace the commutator. We can finally cast the result into the form

$$\underline{\underline{\Omega}} = \frac{1}{2}\mathrm{Tr}_2\left(\bar{\mathcal{H}}_0\underline{\underline{\Theta}}\right)\ \mathbb{1}_2\ , \tag{3.99}$$

where in this expression, the diagonal contribution of $\bar{\mathcal{H}}_0$ drops out because of the sum rule $\mathrm{Tr}_2\Theta = 0$.

In particular, we can express the magnetic dipole energy as

$$\bar{\mathcal{H}}_{\mathcal{M}} = \frac{1}{2}\mathrm{Tr}_2\left(\bar{\mathcal{H}}_0\mathrm{Tr}\underline{\underline{\Theta}}^{\boldsymbol{rp}}\right)\ \mathbb{1}_2\ , \tag{3.100}$$

where $\mathrm{Tr}\underline{\underline{\Theta}}^{\boldsymbol{rp}} \equiv \sum_i \underline{\underline{\Theta}}^{\boldsymbol{rp}}_{ii}$, whereas Tr_2 denotes the trace with respect to the two level band space.

Having discussed some static properties, we are now interested in the dynamics of the systems, especially in a consistent effective descriptions of the physics within a certain band.

3.1.5. Equations of Motion

Heisenberg equations of motion

In this section, we want to derive the Heisenberg equations of motion for the kinetic variables $\boldsymbol{R}$ and $\boldsymbol{P}$, in order to study the dynamics of excitations in the system that are well defined in energy, for example a Gaussian wave-packet that is well beyond the limits of the Heisenberg uncertainty and is sharply centered around some point in phase-space. Let us derive the Heisenberg equation in the rotated frame by starting from the operator representation (3.39) and first, transform it into the Wigner picture and then go to the diagonalized frame (Tr_{Q} denotes the quantum average),

$$\begin{aligned}\frac{\mathrm{d}}{\mathrm{d}t}\langle\mathcal{S}\rangle &= \frac{1}{i\hbar}\mathrm{Tr}_{\mathrm{Q}}\left\{\mathrm{Tr}_N\left\{[\Xi,\mathcal{S}]\,\rho\right\}\right\} = \frac{1}{i\hbar}\int\frac{\mathrm{d}^3r\ \mathrm{d}^3p}{(2\pi\hbar)^3}\ \mathrm{Tr}_N\left\{[\Xi\overset{*}{,}\mathcal{S}]*\bar{\rho}\right\}\\ &= \int\frac{\mathrm{d}^3r\ \mathrm{d}^3p}{(2\pi\hbar)^3}\ \mathrm{Tr}_N\left\{\frac{1}{i\hbar}\left[\bar{\Xi}\overset{*}{,}\bar{\mathcal{S}}\right]\bar{\rho}\right\}\ ,\end{aligned} \tag{3.101}$$

where we used similar steps as in the derivation (3.69).[7] From this expression, we can readily identify the corresponding Heisenberg equations of motion in the diagonalized frame,

$$\frac{\mathrm{d}\bar{\mathcal{S}}}{\mathrm{d}t} = \frac{1}{i\hbar}\left[\bar{\Xi}\overset{*}{,}\bar{\mathcal{S}}\right]\ . \tag{3.102}$$

Using this result and (3.58), we can now immediately write down the equations of motion

$$\frac{\mathrm{d}\boldsymbol{R}}{\mathrm{d}t} = \frac{1}{i\hbar}\left[\bar{\Xi}\overset{*}{,}\boldsymbol{R}\right] = \frac{\partial\bar{\mathcal{H}}}{\partial\boldsymbol{P}}\underline{\underline{\mathcal{J}}} - \boldsymbol{\mathcal{E}}^{(\boldsymbol{p})} + \frac{\partial\bar{\mathcal{H}}}{\partial\boldsymbol{R}}\times\boldsymbol{\mathcal{B}}^{(\boldsymbol{p})} \tag{3.103}$$

$$\frac{\mathrm{d}\boldsymbol{P}}{\mathrm{d}t} = \frac{1}{i\hbar}\left[\bar{\Xi}\overset{*}{,}\boldsymbol{P}\right] = -\underline{\underline{\mathcal{J}}}\frac{\partial\bar{\mathcal{H}}}{\partial\boldsymbol{R}} + \boldsymbol{\mathcal{E}}^{(\boldsymbol{r})} + \frac{\partial\bar{\mathcal{H}}}{\partial\boldsymbol{P}}\times\boldsymbol{\mathcal{B}}^{(\boldsymbol{r})}\ , \tag{3.104}$$

[7] If $\bar{\mathcal{H}}$ explicitly depends on time, we need to solve the kinetic equation for ρ in the Schrödinger picture, as discussed around equation (3.125) below.

where $\underline{\underline{\mathcal{J}}} \equiv \underline{\underline{1}} + \underline{\underline{\Theta}}^{\boldsymbol{rp}}$ has been introduced in expression (3.58). Or, to leading order in $\hbar$,

$$\frac{\mathrm{d}\boldsymbol{R}}{\mathrm{d}t}(\underline{\underline{1}} - \underline{\underline{\Theta}}^{\boldsymbol{rp}}) = \frac{\partial \bar{\mathcal{H}}}{\partial \boldsymbol{P}} - \boldsymbol{\mathcal{E}}^{(\boldsymbol{p})} - \frac{\mathrm{d}\boldsymbol{P}}{\mathrm{d}t} \times \boldsymbol{\mathcal{B}}^{(\boldsymbol{p})} \tag{3.105}$$

$$(\underline{\underline{1}} - \underline{\underline{\Theta}}^{\boldsymbol{rp}}) \frac{\mathrm{d}\boldsymbol{P}}{\mathrm{d}t} = -\frac{\partial \bar{\mathcal{H}}}{\partial \boldsymbol{R}} + \boldsymbol{\mathcal{E}}^{(\boldsymbol{r})} + \frac{\mathrm{d}\boldsymbol{R}}{\mathrm{d}t} \times \boldsymbol{\mathcal{B}}^{(\boldsymbol{r})} \ , \tag{3.106}$$

where we see that the effect of $\underline{\underline{\Theta}}^{\boldsymbol{rp}}$ is related to a change of phase-space in the course of the diagonalization transformation. The beauty of this result is the symmetry in which effective magnetic and electric fields appear in these equations.

We are now performing a quantum average of the kinetic equations (3.105) and (3.106) with respect to a density matrix that is sharply peaked around a certain value $\boldsymbol{P}_c$ and $\boldsymbol{R}_c$, which in effect corresponds to an appropriate wave-packet. Then our equations of motion (3.105) and (3.106) essentially become classical ones with all kinetic variables simply replaced by P_c and R_c. These equations of motion for the center of mass coordinates of a wave packet have been directly obtained by Sundaram and coworkers [115]. The circular current terms in (3.114) and (3.115) vanish for the wave packet, which is to be expected physically, since this description reduces the electron to a point particle with coordinates $\boldsymbol{P}_c$ and $\boldsymbol{R}_c$, and which does not posses any internal motion described by the circular currents. Mathematically, after integration over the whole phase-space, one can rewrite them in terms of surface integrals which vanish for the well-localized wave-packet.

Quasi-probability distributions

Within the Wigner framework, the basic quantity is the quasi-probability distribution $\rho(\boldsymbol{r}, \boldsymbol{p})$, while the usual momentum and position probability distributions can be generally defined as marginals

$$\rho(\boldsymbol{r}) = \int \frac{\mathrm{d}^3 p}{(2\pi\hbar)^3} \ \rho(\boldsymbol{p}, \boldsymbol{r}) \ ,$$

$$\rho(\boldsymbol{p}) = \int \frac{\mathrm{d}^3 r}{(2\pi\hbar)^3} \ \rho(\boldsymbol{p}, \boldsymbol{r}) \ ,$$

and they are linked to the probability interpretation of quantum mechanics, i.e. $\rho(\boldsymbol{r}) = |\psi(\boldsymbol{r})|^2$ and $\rho(\boldsymbol{p}) = |\psi(\boldsymbol{p})|^2$. In the rotated frame however, one has to express them in terms of kinetic variables instead, in order to obtain gauge invariant results.

Now the goal which we want pursue in the following is to find proper quantities in the rotated frame that lead to a consistent physical description, when projected onto a certain band.

For compact notation, let us define the phase-space coordinates $\boldsymbol{\mathcal{X}} \equiv (\boldsymbol{X}, -\boldsymbol{\Pi}) = (t, \boldsymbol{R}, -E, \boldsymbol{P})$ and the phase-space derivative $\boldsymbol{\nabla}_{\boldsymbol{\mathcal{X}}} \equiv (\partial_{\boldsymbol{X}}, -\partial_{\boldsymbol{\Pi}})$, and we define the current density as

$$\frac{\mathrm{d}\boldsymbol{\mathcal{X}}}{\mathrm{d}t} = \frac{1}{i\hbar} \left[\bar{\Xi} \stackrel{\star}{,} \boldsymbol{\mathcal{X}} \right] \ , \tag{3.107}$$

and, inspired by result (3.82) for the expectation values in the rotated frame, we define the corresponding current density

$$\mathfrak{J}_{\boldsymbol{\mathcal{X}}} \equiv \mathrm{Tr}_N \left\{ D(\boldsymbol{\mathcal{X}}) \bar{\rho}(\boldsymbol{\mathcal{X}}) \ \frac{\mathrm{d}\boldsymbol{\mathcal{X}}}{\mathrm{d}t} \right\} + \boldsymbol{\nabla}_{\boldsymbol{\mathcal{X}}} \cdot \mathrm{Tr}_N \bar{\rho}(\boldsymbol{\mathcal{X}}) \ \underline{\underline{\Omega}}^D \ , \tag{3.108}$$

where $\underline{\underline{\Omega}}^D$ is the tensor dual to $\underline{\underline{\Omega}}$,

$$\underline{\underline{\Omega}}^D = \begin{pmatrix} \underline{\underline{\Omega}}^{\boldsymbol{\pi\pi}} & \underline{\underline{\Omega}}^{\boldsymbol{\pi x}} \\ \underline{\underline{\Omega}}^{\boldsymbol{x\pi}} & \underline{\underline{\Omega}}^{\boldsymbol{xx}} \end{pmatrix} \ . \tag{3.109}$$

The first four components of $\mathfrak{J}_{\boldsymbol{\mathcal{X}}}$ correspond to the usual definition of a 4-component current where the zeroth, or time component corresponds to the particle density and the spatial components equal the usual definition of the velocity operator, $\frac{1}{i\hbar}\left[\boldsymbol{R}\,^{*}_{,}\,\bar{\mathcal{H}}\right]$ in the diagonalized frame. The remaining 4 components are the energy current and momentum current, respectively.

Here, it is important to realize that the current matrices have an off-diagonal structure that one has to take into account in the light of expression (3.82) and which eventually leads to the second term in the current densities (3.108), and constitute divergence free, or circular currents. Explicitly for the 4-component current, this off-diagonal part takes the form

$$\mathcal{P}_o \frac{\mathrm{d}\boldsymbol{X}}{\mathrm{d}t} \mathcal{P}_o = -i\left[\bar{\mathcal{H}}_0, \mathcal{A}_{\boldsymbol{\pi}}\right] \tag{3.110}$$

and is completely expressed in terms of quantities of the rotated frame and arises due to the off-diagonal elements of the Berry connection matrix. As can be shown, the definition (3.108) of a current obeys a conservation law in extended phase space, or Liouville's theorem that states

$$\boldsymbol{\nabla}_{\boldsymbol{\mathcal{X}}} \cdot \mathfrak{J}_{\boldsymbol{\mathcal{X}}} = 0 \ , \tag{3.111}$$

and which can be shown by using the kinetic equation (3.123) for the density matrix $\bar{\rho}$ and a couple of identities between Berry curvatures (c.f. Eqns (3.116)). The last term of the current density (3.108) simply vanishes due to the anti-symmetry of $\underline{\underline{\Omega}}^D$.

Instead of keeping this compact notation for the following investigation, we will return to the more familiar description in terms of time, position and momentum, and furthermore, assume that the energy parameter E has been already integrated out, though it could be included straightforwardly. Liouville's theorem in the rotated frame then takes the usual form

$$\partial_t \mathfrak{n}(\boldsymbol{R}, \boldsymbol{P}, t) + \boldsymbol{\nabla}_{\boldsymbol{R}}\, \mathfrak{j}(\boldsymbol{R}, \boldsymbol{P}, t) + \boldsymbol{\nabla}_{\boldsymbol{P}}\, \mathfrak{q}(\boldsymbol{R}, \boldsymbol{P}, t) = 0 \ , \tag{3.112}$$

with the quasi-probability density $\mathfrak{n}$, current density $\mathfrak{j}$ and momentum current density $\mathfrak{q}$ given as follows

$$\mathfrak{n}(\boldsymbol{R}, \boldsymbol{P}, t) \equiv \mathrm{Tr}_N \left\{\bar{\rho}\ D\right\} \ , \tag{3.113}$$

$$\mathfrak{j}(\boldsymbol{R}, \boldsymbol{P}, t) \equiv \mathrm{Tr}_N \left\{\bar{\rho}\ D \frac{\mathrm{d}\boldsymbol{R}}{\mathrm{d}t}\right\} - \boldsymbol{\nabla}_{\boldsymbol{R}} \times \mathrm{Tr}_N \bar{\rho} \boldsymbol{\Omega}^{\boldsymbol{pp}} - \boldsymbol{\nabla}_{\boldsymbol{P}} \cdot \mathrm{Tr}_N \bar{\rho} \underline{\underline{\Omega}}^{\boldsymbol{rp}} \ , \tag{3.114}$$

$$\mathfrak{q}(\boldsymbol{R}, \boldsymbol{P}, t) \equiv \mathrm{Tr}_N \left\{\bar{\rho}\ D \frac{\mathrm{d}\boldsymbol{P}}{\mathrm{d}t}\right\} - \boldsymbol{\nabla}_{\boldsymbol{P}} \times \mathrm{Tr}_N \bar{\rho} \boldsymbol{\Omega}^{\boldsymbol{rr}} + \boldsymbol{\nabla}_{\boldsymbol{R}} \cdot \mathrm{Tr}_N \bar{\rho} (\underline{\underline{\Omega}}^{\boldsymbol{rp}})^T \ , \tag{3.115}$$

along with (3.103) and (3.104), and we used the relation $\underline{\underline{\Omega}}^{\boldsymbol{pr}} = -(\underline{\underline{\Omega}}^{\boldsymbol{rp}})^T$. We substitute these definitions into Liouville's theorem and establish the identity (3.112) after some algebra, using

the equality of second partial derivatives and dropping terms of order $O(\hbar^2)$. Furthermore, we need to use the following identities between Berry curvatures

$$\begin{aligned}\partial_t D - \boldsymbol{\nabla}_R \boldsymbol{\mathcal{E}}^{(\boldsymbol{p})} + \boldsymbol{\nabla}_P \boldsymbol{\mathcal{E}}^{(\boldsymbol{r})} &= 0 \ , \\ \partial_{R_i} D + \partial_{R_k} \underline{\underline{\Theta}}^{\boldsymbol{rp}}_{ik} - (\boldsymbol{\nabla}_P \times \boldsymbol{\mathcal{B}}^{(\boldsymbol{r})})_i &= 0 \ , \\ -\partial_{P_i} D - \partial_{P_k} \underline{\underline{\Theta}}^{\boldsymbol{rp}}_{ki} - (\boldsymbol{\nabla}_R \times \boldsymbol{\mathcal{B}}^{(\boldsymbol{p})})_i &= 0 \ ,\end{aligned} \tag{3.116}$$

which can be readily shown by plugging in the definitions (3.54),(3.56),(3.57)(3.62) and (3.63). This result strongly suggests the importance of including the correction factor $D(\boldsymbol{R}, \boldsymbol{P}, t)$ into the expectation values.

Just like the Wigner function is a quasi-probability and can be given physical sense only after taking expectation values, the same applies to $\mathfrak{n}$, $\mathfrak{j}$ and $\mathfrak{q}$. In particular, physical meaning can be given only to quantities like $n(\boldsymbol{R})$ or $\boldsymbol{j}(\boldsymbol{R})$. This is related to Heisenberg's uncertainty which states that momentum and position uncertainty have to be larger than Plank's constant $\hbar$, i.e. $\Delta P \Delta R \gtrsim \hbar$. The same is true for the conjugate variables time and energy.

Liouville's theorem constitutes a conservation law for the quasi-probability densities, and one can for example integrate (3.112) over all momenta in order to find a continuity equation for the probability densities of the particle and current densities,

$$\partial_t n(\boldsymbol{R}, t) + \boldsymbol{\nabla}_R \boldsymbol{j}(\boldsymbol{R}, t) = - \oint_{\partial V} \mathrm{d}^2 \boldsymbol{P} \ \mathfrak{q}(\boldsymbol{R}, \boldsymbol{P}, t) \ , \tag{3.117}$$

where the closed surface integral on the right-hand side has been obtained by virtue of Gauss's theorem, and it vanishes if we assume that there is no net momentum current flow through the surface at infinity. Explicitly, the particle density is

$$n(\boldsymbol{R}, t) = \int \frac{\mathrm{d}^3 P}{(2\pi\hbar)^3} \ \mathrm{Tr}_N \left(\bar{\rho} \ D \right) \ , \tag{3.118}$$

and likewise for the current density,

$$\boldsymbol{j}(\boldsymbol{R}, t) = \int \frac{\mathrm{d}^3 P}{(2\pi\hbar)^3} \ \mathrm{Tr}_N \left(\bar{\rho} \ D \frac{\mathrm{d}\boldsymbol{R}}{\mathrm{d}t} \right) - \boldsymbol{\nabla}_{\boldsymbol{R}} \times \int \frac{\mathrm{d}^3 P}{(2\pi\hbar)^3} \ \mathrm{Tr}_N \bar{\rho} \boldsymbol{\Omega}^{\boldsymbol{pp}} - \oint \frac{\mathrm{d}^2 \boldsymbol{P}}{(2\pi\hbar)^3} \mathrm{Tr}_N \bar{\rho} \underline{\underline{\Omega}}^{\boldsymbol{rp}} \ , \tag{3.119}$$

while the previous discussion has shown that these definitions are in fact meaningful physical quantities and constitute the central result of this section. We will see interesting implications of the additional dipole term in the current when studying various examples.

For the sake of completeness, we use result (3.82) to define densities corresponding to the physical quantity $\mathcal{S}$ in the diagonalized frame

$$S(\boldsymbol{R}, t) \equiv \int \frac{\mathrm{d}^3 P}{(2\pi\hbar)^3} \ \mathrm{Tr}_N \left(\bar{\rho} \ D \bar{\mathcal{S}} - \boldsymbol{\nabla}_{\boldsymbol{R}} \ \bar{\rho} \frac{\hbar}{2} \Big\{ \mathcal{A}_{\boldsymbol{P}}, \bar{\mathcal{S}}^{(o)} \Big\} \right) + \oint \frac{\mathrm{d}^2 \boldsymbol{P}}{(2\pi\hbar)^3} \mathrm{Tr}_N \bar{\rho} \frac{\hbar}{2} \Big\{ \mathcal{A}_{\boldsymbol{R}}, \bar{\mathcal{S}}^{(o)} \Big\} \ , \tag{3.120}$$

and likewise for $S(\boldsymbol{P})$.[8] These kinds of quantities can be used for an effective description of the physical processes only involving excitation restricted to a certain band that includes for

[8] This expression is consistent with the definition of a density operator $\delta(\boldsymbol{r} - \boldsymbol{r}_0) S(\boldsymbol{r}, \boldsymbol{p})$ which, when transformed into the rotated frame yields the given result. Furthermore, all the given expressions can still explicitly depend on energy via the gauge invariant parameter E, which however does not affect the discussion to follow.

example low-energy transport where physics is taking place only in the vicinity of the Fermi level. We will look into this problem in the following.

Non-equilibrium description

Now, it is just a matter of finding the density matrix $\bar{\rho}(\boldsymbol{R}, \boldsymbol{P}, t)$ in order to explicitly calculate anything within this framework, in particular, when one is interested in non-equilibrium phenomena. One way to proceed is within Keldysh formalism and to consider the kinetic equation for the lesser Greens function (like in (2.31)),

$$\left[\Xi \overset{*}{,} \mathcal{G}^{<}\right] = 0 \ , \tag{3.121}$$

which, after transformation into the rotated frame, can be evaluated to leading order correction in $\hbar$ by using (3.58) which by virtue of (3.103) and (3.104) can be recast into

$$\left[\partial_t + \frac{\mathrm{d}\boldsymbol{R}}{\mathrm{d}t}\boldsymbol{\nabla}_R + \frac{\mathrm{d}\boldsymbol{P}}{\mathrm{d}t}\boldsymbol{\nabla}_P + \left(\frac{\partial\bar{\mathcal{H}}}{\partial t} + \boldsymbol{\mathcal{E}}^{(\boldsymbol{r})}\frac{\partial\bar{\mathcal{H}}}{\partial\boldsymbol{P}} - \boldsymbol{\mathcal{E}}^{(\boldsymbol{p})}\frac{\partial\bar{\mathcal{H}}}{\partial\boldsymbol{R}}\right)\partial_E\right]\bar{\mathcal{G}}^{<} = 0 \ . \tag{3.122}$$

Using the definitions (3.107) from above, this equation can be written in a very compact manner as

$$\left(\frac{\mathrm{d}\boldsymbol{\mathcal{X}}}{\mathrm{d}t}\cdot\boldsymbol{\nabla}_{\boldsymbol{\mathcal{X}}}\right)\bar{\rho} = 0 \ . \tag{3.123}$$

When we integrate the lesser Greens function over energy, we simply obtain the density matrix

$$\bar{\rho}(\boldsymbol{R}, \boldsymbol{P}, t) = \int \frac{\mathrm{d}E}{2\pi}\ \bar{\mathcal{G}}^{<}(\boldsymbol{X}, \boldsymbol{\Pi}) \ , \tag{3.124}$$

and, since the terms proportional to $\partial_E\bar{\mathcal{G}}^{<}$ vanish after integrating (3.122) over all energies, we are left with the following differential equation for the density matrix,

$$\left(\partial_t + \frac{\mathrm{d}\boldsymbol{R}}{\mathrm{d}t}\boldsymbol{\nabla}_R + \frac{\mathrm{d}\boldsymbol{P}}{\mathrm{d}t}\boldsymbol{\nabla}_P\right)\bar{\rho}(\boldsymbol{R}, \boldsymbol{P}, t) = 0 \ , \tag{3.125}$$

which is nothing but a Boltzmann equation including quantum corrections in terms of Berry curvatures. In the end, it is quite analogous to the quantum Boltzmann equation along with the gradient expansion we used in section 2.2.4. Of course, the major difference is the absence of the collision integral in the present formulation, however it is possible to include it here as well, for example, the steps performed in section 2.2 can be straightforwardly transformed into the present formalism, which is however left for future investigations. Of course, $\bar{\rho}$ can additionally include discrete quantum degrees of freedom like the spin, which means that our rotated frame is block-diagonal and so is $\bar{\rho}$. This situation is straightforwardly treated by using result (3.49).

We now show how to obtain the distribution function, when it is known at some initial time, $\bar{\rho}(\boldsymbol{R}, \boldsymbol{P}, t = 0)$. In general, these problems can be formulated in terms of an inhomogeneous Boltzmann equation with a source term $S(\boldsymbol{R}, \boldsymbol{P}, t)$,

$$\left(\partial_t + \frac{\mathrm{d}\boldsymbol{R}}{\mathrm{d}t}\boldsymbol{\nabla}_R + \frac{\mathrm{d}\boldsymbol{P}}{\mathrm{d}t}\boldsymbol{\nabla}_P\right)\bar{\rho}(\boldsymbol{R}, \boldsymbol{P}, t) = S(\boldsymbol{R}, \boldsymbol{P}, t) \ . \tag{3.126}$$

To proceed in the usual way, we define the Greens function $\mathcal{G}_\mathrm{c}$,

$$\left(\partial_t + \frac{\mathrm{d}\boldsymbol{R}}{\mathrm{d}t}\boldsymbol{\nabla}_R + \frac{\mathrm{d}\boldsymbol{P}}{\mathrm{d}t}\boldsymbol{\nabla}_P\right)\mathcal{G}_\mathrm{c}(\boldsymbol{R},\boldsymbol{P},t,\boldsymbol{R}',\boldsymbol{P}',t') = \delta(t-t')\delta(\boldsymbol{R}-\boldsymbol{R}')\delta(\boldsymbol{P}-\boldsymbol{P}') \ , \tag{3.127}$$

for which we find the general solution

$$\mathcal{G}_\mathrm{c}(\boldsymbol{R},\boldsymbol{P},t,\boldsymbol{R}',\boldsymbol{P}',t') = \Theta(t-t') \ \delta(\boldsymbol{R}-\boldsymbol{R}_\mathrm{c}(t)) \ \delta(\boldsymbol{P}-\boldsymbol{P}_\mathrm{c}(t)) \ , \tag{3.128}$$

where Θ is the Heaviside step function, and $\boldsymbol{R}_\mathrm{c}(t)$ and $\boldsymbol{P}_\mathrm{c}(t)$ describe the classical orbits which obey the equations of motion

$$\begin{aligned} \dot{\boldsymbol{R}}_\mathrm{c} &= \frac{\mathrm{d}\boldsymbol{R}}{\mathrm{d}t} & \boldsymbol{R}_\mathrm{c}(t') &= \boldsymbol{R}' \ , \\ \dot{\boldsymbol{P}}_\mathrm{c} &= \frac{\mathrm{d}\boldsymbol{P}}{\mathrm{d}t} & \boldsymbol{P}_\mathrm{c}(t') &= \boldsymbol{P}' \ . \end{aligned}$$

This solution describes ballistic trajectories given by the kinetic equations (3.103) and (3.104) and which including the effects of the Berry curvatures, while the particle being initially at phase space coordinates $(\boldsymbol{R}',\boldsymbol{P}',t')$. For example, in the absence of any spatially dependent potential, one simply has straight lines described by the Greens function $\mathcal{G}_\mathrm{c} = \Theta(t-t_0) \ \delta(\boldsymbol{R}-\boldsymbol{V}(t-t_0)) \ \delta(\boldsymbol{P}-\boldsymbol{P}')$, where $\boldsymbol{V} = \frac{\partial\bar{\mathcal{H}}_0}{\partial\boldsymbol{P}}$ is the group velocity. This is analogous to other quasiclassical equations like the Eilenberger equation which can be also described in terms of classical trajectories [121, 50]. The result (3.128) constitutes the generalization to systems where the dispersion is non-trivial and one has Berry-curvature related phenomena like a spatial perturbation of the system in the form of a magnetization gradient that we will treat later in section 3.4.

Now, the solution is readily given by

$$\bar{\rho}(\boldsymbol{R},\boldsymbol{P},t) = \int_{-\infty}^{+\infty}\mathrm{d}t' \int \mathrm{d}^3R' \int \mathrm{d}^3P' \ \mathcal{G}_\mathrm{c}(\boldsymbol{R},\boldsymbol{P},t,\boldsymbol{R}',\boldsymbol{P}',t') \ S(\boldsymbol{R}',\boldsymbol{P}',t') \ , \tag{3.129}$$

where, due to the delta functions in $\mathcal{G}_\mathrm{c}$, we get contributions only from trajectories which end at $(\boldsymbol{R},\boldsymbol{P})$ at time t. Since the trajectory is well defined by the given pair $(\boldsymbol{R},\boldsymbol{P})$ already, we can find all corresponding points $(\boldsymbol{R}',\boldsymbol{P}')$ by going back in time so we can eventually rewrite the above integral as

$$\bar{\rho}(\boldsymbol{R},\boldsymbol{P},t) = \int_0^{+\infty}\mathrm{d}t' \ S(\boldsymbol{R}'_\mathrm{c}(-t'),\boldsymbol{P}'_\mathrm{c}(-t'),t-t') \ , \tag{3.130}$$

where now, the classical orbits are defined such that its position in phase space at time 0 is $\boldsymbol{R}'_\mathrm{c}(0) = \boldsymbol{R}$ and $\boldsymbol{P}'_\mathrm{c}(0) = \boldsymbol{P}$.

For the example of a simple parabolic dispersion $\frac{P^2}{2m}$ and a linear gradient $V(\boldsymbol{R}) = -\boldsymbol{E}\boldsymbol{R}$, one obtains

$$\bar{\rho}(\boldsymbol{R},\boldsymbol{P},t) = \int_0^{+\infty}\mathrm{d}t' \ S\left(\boldsymbol{R} - \frac{\boldsymbol{P}}{m}t' + \frac{\boldsymbol{E}}{2m}t'^2, \boldsymbol{P} - \boldsymbol{E}t', t-t'\right) \ , \tag{3.131}$$

which is straightforwardly checked to solve (3.126).

Let us now go back to the original initial value problem which we can easily solve by using the source term $\delta(t)\bar{\rho}(\boldsymbol{R},\boldsymbol{P},t=0)$, so that the general solution reads

$$\bar{\rho}(\boldsymbol{R},\boldsymbol{P},t)=\Theta(t)\ \bar{\rho}(\boldsymbol{R}'_{\rm c}(-t),\boldsymbol{P}'_{\rm c}(-t),t=0)\ , \tag{3.132}$$

which has the desired properties for $t\geq 0$. This indeed corresponds to a motion in phase space as an incompressible fluid, as stated by Liouville's theorem.

An alternative solution of the kinetic equation (3.125) is to resort to a treatment which is perturbative in the Berry curvatures. This is for example useful when external spatial perturbations are smooth on the scale of the Fermi wave-length, like in the treatment of the ferromagnetic exchange field $\boldsymbol{m}(\boldsymbol{R})$ in chapter 2. To illustrate this, we note that to zeroth order in Berry corrections, we have $\frac{{\rm d}\boldsymbol{R}}{{\rm d}t}=\frac{\partial\bar{\mathcal{H}}_0}{\partial\boldsymbol{P}}$ and $\frac{{\rm d}\boldsymbol{P}}{{\rm d}t}=-\frac{\partial\bar{\mathcal{H}}_0}{\partial\boldsymbol{R}}$, and subsequently use standard Greens function techniques to iteratively solve the quantum Boltzmann equation (3.125), or with the all the Berry curvature terms combined in the differential operator $\mathcal{W}$,

$$\left(\partial_t+\frac{\partial\bar{\mathcal{H}}_0}{\partial\boldsymbol{P}}\boldsymbol{\nabla}_R-\frac{\partial\bar{\mathcal{H}}_0}{\partial\boldsymbol{R}}\boldsymbol{\nabla}_P\right)\bar{\rho}=\bar{\mathcal{W}}(\boldsymbol{R},\boldsymbol{P},t)\bar{\rho}\ . \tag{3.133}$$

We note that also the external electromagnetic field is contained in the Berry curvatures, and it will be explicitly treated in section 3.2.2 so that at this point, we will just refer to equations (3.160)-(3.164).

Next, the zeroth order, or quasi-equilibrium solution for the density matrix is simply given by $\bar{\rho}_0=f_{\rm D}(E_{\rm F}-\bar{\mathcal{H}}_0)$, so that using result (3.130), one obtains for the first order correction in Berry curvatures,

$$\bar{\rho}_1(\boldsymbol{R},\boldsymbol{P},t)=\int_0^{+\infty}{\rm d}t'\ \left(\bar{\mathcal{W}}\bar{\rho}_0\right)(\boldsymbol{R}'_{\rm c}(-t'),\boldsymbol{P}'_{\rm c}(-t'),t-t')\ , \tag{3.134}$$

where now, $\boldsymbol{R}'_{\rm c}$ and $\boldsymbol{P}'_{\rm c}$ describe the trajectories defined by the classical energy of the Hamiltonian $\mathcal{H}_0$.

Even though we did not include scattering, we will get at least the ballistic conductivities, and one obtains the intrinsic contributions to various effects like the domain wall resistance of the anomalous Hall effect. In particular, the ballistic conductivity in linear response will be simply obtained from (see Eqns (3.104) and (3.125)

$$\bar{\mathcal{W}}\bar{\rho}_0=(\boldsymbol{\mathcal{E}}^{(\mathrm{r})}\boldsymbol{\nabla}_P)\ \bar{\rho}_0\ , \tag{3.135}$$

which, when plugged into (3.134), yields the ballistic conductance.

In order to illustrate this, we assume the system to be homogeneous, i.e. the Hamiltonian $\bar{\mathcal{H}}_0(\boldsymbol{P})$ depends on momentum only. Our system is confined along the x-direction between $-L_x/2$ and $+L_x/2$ and we apply the potential difference $V=EL_x$ in order to measure the conductance. Then,

$$\bar{\rho}_0(\boldsymbol{R},\boldsymbol{P})=\Theta\left(\frac{L_x}{2}-|\hat{\boldsymbol{e}}_{\boldsymbol{x}}\cdot\boldsymbol{R}|\right)\ f_{\rm D}(E_{\rm F}-\bar{\mathcal{H}}_0(\boldsymbol{P}))\ , \tag{3.136}$$

so that $\bar{\mathcal{W}}\bar{\rho}_0 = -\Theta\left(\frac{L_x}{2} - |x|\right)\ Ev_x f'_{\rm D}(E_{\rm F} - \bar{\mathcal{H}}_0)$ with the group velocity $v_x = \frac{\partial \bar{\mathcal{H}}_0}{\partial P_x}$ along x-direction. Plugging this into (3.134) readily yields

$$\begin{aligned}\bar{\rho}_1(\boldsymbol{R}, \boldsymbol{P}) &= -Ev_x f'_{\rm D}(E_{\rm F} - \bar{\mathcal{H}}_0) \int_0^{+\infty} {\rm d}t'\ \Theta\left(\frac{L_x}{2} - |x - v_x t'|\right) \\ &= -E\ \Theta(\tfrac{L_x}{2} - |x|)\ \left(x + \frac{L_x}{2}\,{\rm sgn}\, v_x\right) f'_{\rm D}(E_{\rm F} - \bar{\mathcal{H}}_0)\ , \end{aligned} \tag{3.137}$$

and in the present scenario, the total current along the x-direction is simply given by

$$j_x = \int \frac{{\rm d}^3P}{(2\pi\hbar)^3}\ v_x \bar{\rho}_1 = -\frac{EL_x}{2}\ \Theta(\tfrac{L_x}{2} - |x|) \int \frac{{\rm d}^3P}{(2\pi\hbar)^3}\ |v_x| f'_{\rm D}(E_{\rm F} - \bar{\mathcal{H}}_0)\ . \tag{3.138}$$

In the zero temperature approximation,

$$f'_{\rm D}(E_{\rm F} - \bar{\mathcal{H}}_0) = -\delta(\bar{\mathcal{H}}_0 - E_{\rm F}) = -\frac{1}{|v_x|}\left[\delta(P_x - (P_x)_{\rm F}) + \delta(P_x + (P_x)_{\rm F})\right]\ ,$$

so that for the conductance $G = e^2 \frac{L_y L_z}{E L_x} j_x$, we obtain the well known Landauer formula [122]

$$G = \frac{e^2}{2\pi\hbar}\ \sum_{k_\perp}^{k_{\rm F}} = \frac{e^2}{2\pi\hbar}\ N_\perp\ , \tag{3.139}$$

where $N_\perp$ the sum is over all transverse modes, and it is simply $N_\perp = \frac{k_{\rm F}^2}{4\pi} L_y L_z$ for a parabolic dispersion.

Note that the selection of the energy range taking part in transport is, like in the above expression, due to the gradient of $\bar{\rho}_0$ which yields the derivative of the Fermi-Dirac distribution function and thus, $\bar{\mathcal{W}}\bar{\rho}_0$ constitutes a function that is peaked around $E_{\rm F}$ with a characteristic width given by the temperature.

We remark that in the case of closed orbits, the integration in (3.134) is ill-defined, since one would go around the loop infinite times. This situation describes a bound state and integration over such a state would imply a resonance phenomenon which is not well described in the absence of dissipation. In fact, introduction of a relaxation mechanism by the aforementioned inclusion of impurity scattering would provide a natural cut-off of to the integral (3.134), rendering it convergent.

Polarization

Another way to interpret the kinetic variables is obtained by considering the electrical polarization which we pursue according to the pioneering work of Vanderbilt and coworkers [112]. They derive the polarization in terms of adiabatic transport, where some perturbation that leads to a polarization in the crystal, is adiabatically turned on. The current due to adiabatic transport is [123]

$$\boldsymbol{j} = \int \frac{{\rm d}^3r\ {\rm d}^3p}{(2\pi\hbar)^3}\ {\rm Tr}_N \frac{{\rm d}\boldsymbol{R}}{{\rm d}t} = -\int_{\rm BZ} \frac{{\rm d}^3p}{(2\pi\hbar)^3}\ {\rm Tr}_N \boldsymbol{\mathcal{E}}^{(\boldsymbol{p})}\ , \tag{3.140}$$

where integration is only within the Brillouin zone. The electric polarization is then simply obtained by integrating over time,

$$\mathfrak{P}(\boldsymbol{R}) = \int \mathrm{d}t \; \boldsymbol{j}(\boldsymbol{R}, t) \; . \tag{3.141}$$

The definition as an adiabatic transport process is necessary in order to obtain a truly gauge invariant result [112]. Within a simple, but physically rich model discussed in section 3.4, we will find an explicit example of a non-vanishing polarization and how to obtain it. In the periodic gauge however [109], it is nevertheless possible to construct

$$\mathfrak{P} = \int \frac{\mathrm{d}^3 p}{(2\pi\hbar)^3} \; \mathcal{A}_{\boldsymbol{p}} \; , \tag{3.142}$$

but in the general case, it is required to consider the full Berry phase structure (including in particular $\mathcal{A}_t$) in order to obtain the correct result for the polarization.

In the same spirit, one could define a polarization in momentum space which can be thought of as a Doppler effect in the rotated frame or also termed anomalous velocity.

In this sense, one could loosely interpret these Berry connections as shifts that the canonical variables acquire and which depend on full phase space, albeit these shifts are not directly physically observable, only when one does either an integration with respect to either the position or the momentum variable one obtains the observable electric polarization in real space or reciprocal space, respectively. This is analogous to the quasi-probability distribution $\rho(\boldsymbol{r}, \boldsymbol{p})$ in the Wigner picture, which can be given only physical interpretation as probability density when integrated either over whole momentum space or real space. However, if we try to transfer this idea, we still will have a shift that depends on the frame, i.e. it is still not gauge invariant. Only for a very specific gauge, one obtains the physical polarization.

In conclusion of this section, we found a consistent effective description of the physical system in the diagonalized frame, which is completely formulated in terms of kinetic variables and thus, it is manifest gauge invariant.

3.1.6. Some Notes on Requantization

In this section, we address the question of the quantum theoretical aspects of our semiclassical analysis. In particular, in literature there is the question of how to properly quantize the theory in the Lagrangian formalism, since one needs to identify the canonical pair of variables which is the starting point of the quantization. As mentioned previously, using wave packet analysis [109], one obtains the same set of equations of motion for the center of mass coordinates of the wave-packet as in (3.105) and (3.106). Then one can find the Lagrangian, but one does not know anything about canonical variables, and in the general case, it is not always easy or possible to find the pair of canonical variables [109].

However, in our framework, we did not encounter such problems, since firstly, we are working in the Hamilton formalism, where one knows the canonical variables and secondly, our theory is quantized at any time, albeit neglecting terms of order $O(\hbar^2)$. This quantization is encoded in the structure of the Moyal product, or more explicitly in the special structure of the

commutator in (3.49). Furthermore, without major effort, we can go back to the operator representation of quantum mechanics by simply undoing the Wigner transformation.

The Wigner representation has the very practical feature of automatically symmetrizing operators, when one transforms back into the operator formulation, for example using the back transformation of (3.4),

$$A(\boldsymbol{x}+\frac{\boldsymbol{z}}{2},\boldsymbol{x}-\frac{\boldsymbol{z}}{2})=\int\frac{\mathrm{d}^4\pi}{(2\pi\hbar)^4}\;e^{-i\boldsymbol{z}\boldsymbol{\pi}/\hbar}A(\boldsymbol{x},\boldsymbol{\pi})\;, \tag{3.143}$$

one obtains

$$xp\to\frac{1}{2}\left(\hat{x}\hat{p}+\hat{p}\hat{x}\right)\;, \tag{3.144}$$

so what is usually required to be put in by hand in usual quantum mechanics in order to obtain Hermitian observables, comes out automatically. Another, more direct way to see this is by using identities of the form

$$\frac{1}{2}\left(x*p+p*x\right)=xp\;. \tag{3.145}$$

Since many of our expressions (for example (3.24), (3.25), (3.42), etc.) are straightforwardly transformed back into the operator formulation of quantum mechanics, we formally obtain the same expression, except mixtures of $\boldsymbol{r}$ and $\boldsymbol{p}$ appear properly symmetrized in the so-called Wigner-Weyl ordering. In fact, we retain the full quantum theory which gives correct results at least to order $\hbar$. One just has pay attention that the Wigner transformation is *only* with respect to the canonical pair of variables so kinetic variables have to be replaced accordingly.

Furthermore, one should be careful that terms like $(\boldsymbol{p}-q\boldsymbol{A}(\boldsymbol{r}))^n$ are not directly translated into the Wigner representation, which can be seen when transforming this term into the Wigner picture by using the Moyal product to iteratively multiply factors. First, we note that a quadratic dispersion yields the straightforward result

$$(\boldsymbol{p}-q\boldsymbol{A}(\boldsymbol{r}))^2\to(\boldsymbol{p}-q\boldsymbol{A}(\boldsymbol{r}))*(\boldsymbol{p}-q\boldsymbol{A}(\boldsymbol{r})=(\boldsymbol{p}-q\boldsymbol{A}(\boldsymbol{r}))^2\;,$$

whereas

$$\begin{aligned}(\boldsymbol{p}-q\boldsymbol{A}(\boldsymbol{r}))^4\to&(\boldsymbol{p}-q\boldsymbol{A}(\boldsymbol{r}))^2*(\boldsymbol{p}-q\boldsymbol{A}(\boldsymbol{r})^2=\\&(\boldsymbol{p}-q\boldsymbol{A}(\boldsymbol{r}))^4+\hbar^2q(\boldsymbol{p}-q\boldsymbol{A}(\boldsymbol{r}))\partial_{\boldsymbol{r}}^2\boldsymbol{A}(\boldsymbol{r})-q^2\hbar^2\left(\boldsymbol{\nabla}\boldsymbol{A}(\boldsymbol{r})\right)^2\;.\end{aligned}$$

One should pay attention to these details, when one wants to treat a problem beyond semi-classical accuracy. For example, consider the following Hamiltonian $\mathcal{T}(\boldsymbol{p})+\mathcal{V}(\boldsymbol{r})$ where $\mathcal{T}(\boldsymbol{p})$ possesses no internal structure, i.e. it is diagonal in band space, while we want to diagonalize the non-trivial potential $\mathcal{V}(\boldsymbol{r})$ (this is actually the scenario of 2.4.5). Then there is a good chance that the diagonalization matrix $\mathcal{U}(\boldsymbol{r})$ is known exactly, and we get the gauge invariant kinetic momentum $\boldsymbol{P}=\boldsymbol{p}-\hbar\mathcal{A}_{\boldsymbol{r}}(\boldsymbol{r})$. The band energy term then is

$$\mathcal{U}(\boldsymbol{r})*\mathcal{T}(\boldsymbol{p})*\mathcal{U}^\dagger(\boldsymbol{r})=\mathcal{T}(\mathcal{U}(\boldsymbol{r})*\boldsymbol{p}*\mathcal{U}^\dagger(\boldsymbol{r})*)\;, \tag{3.146}$$

where we used $\mathcal{T}(\boldsymbol{p}) = \mathcal{T}(\boldsymbol{p}*) = \mathcal{T}(\boldsymbol{p} - i\hbar\partial_{\boldsymbol{r}})$, so that we can properly insert unities $\mathcal{U}^\dagger * \mathcal{U} = \mathbb{1}$ in order to obtain the last equality. Using the kinetic momentum, we can simply write for the band diagonalized Hamiltonian $\mathcal{T}(\boldsymbol{P}*) + \mathcal{V}(\boldsymbol{r})$ which is now straightforwardly transformed back to the operator representation of quantum mechanics,

$$\mathcal{T}(\boldsymbol{p} - \hbar\mathcal{A}_{\boldsymbol{r}}(\boldsymbol{r})) + \mathcal{V}(\boldsymbol{r}) \ . \tag{3.147}$$

As discussed at the end of section 3.1.5, $\boldsymbol{P}$ and $\boldsymbol{r}$ are still canonical variables, so there is no problem with commutation within $\mathcal{T}(\boldsymbol{P})$, despite the non-trivial matrix structure of $\boldsymbol{P}$ inherited from $\mathcal{A}_{\boldsymbol{r}}$. However, this is only true as long as no projection occurred yet.

3.2. Hierarchy of Effective Theories and Inclusion of the Electromagnetic Field

Sometimes, one already starts from an effective theory, because either, it is much more simple to handle, or one does not know the more complete theory. In this case, one already deals with gauge invariant momentum and/or position operators. It is now interesting to ask, whether new phenomena emerge in effective theories at lower level in the hierarchy.

3.2.1. General Hierarchy

In order to give an answer to this question, let us perform two diagonalization steps, the first one $\mathcal{U}(\boldsymbol{x}, \boldsymbol{\pi})$ yields the block-diagonal Hamiltonian $\bar{\Xi}(\boldsymbol{X}, \boldsymbol{\Pi})$ and gives us the pair of kinetic variables

$$\begin{aligned}\boldsymbol{X} &= \mathcal{U} * \boldsymbol{x} * \mathcal{U}^\dagger = \boldsymbol{x} - i\hbar\mathcal{U} * \partial_{\boldsymbol{\pi}}\mathcal{U}^\dagger = \boldsymbol{x} - \hbar\mathcal{A}_{\boldsymbol{\pi}}(\boldsymbol{x}, \boldsymbol{\pi}) \\ \boldsymbol{\Pi} &= \mathcal{U} * \boldsymbol{\pi} * \mathcal{U}^\dagger = \boldsymbol{p} + i\hbar\mathcal{U} * \partial_{\boldsymbol{x}}\mathcal{U}^\dagger = \boldsymbol{\pi} + \hbar\mathcal{A}_{\boldsymbol{x}}(\boldsymbol{x}, \boldsymbol{\pi}) \ .\end{aligned}$$

To make the situation not too complicated and focus and the essential aspects, we assume non-Abelian Berry connections throughout this section. Note that the above definition of the Berry phases $\mathcal{A}_{\boldsymbol{\pi}}(\boldsymbol{x}, \boldsymbol{\pi}) \equiv i\mathcal{U} * \partial_{\boldsymbol{\pi}}\mathcal{U}^\dagger$ is an exact one, if we assume to know the unitary matrix $\mathcal{U}$ that completely diagonalizes Ξ to all orders of $\hbar$. Completely in analogy to (3.21), one can show the identity (α,β is a placeholder for any combination of $\boldsymbol{x}$, $\boldsymbol{\pi}$)

$$\partial_\alpha\mathcal{A}_\beta - \partial_\beta\mathcal{A}_\alpha = i\left[\mathcal{A}_\alpha \overset{*}{,} \mathcal{A}_\beta\right] \ , \tag{3.148}$$

which can be directly used to show that the diagonalization due to $\mathcal{U}$ is a canonical transformation, i.e. it preserves (μ,ν is the 4-component index)

$$\begin{aligned}[\boldsymbol{\Pi}_\mu \overset{*}{,} \boldsymbol{X}^\nu] &= i\hbar\delta_\mu^\nu \\ [\boldsymbol{X}_\mu \overset{*}{,} \boldsymbol{X}^\nu] &= 0 = [\boldsymbol{\Pi}_\mu \overset{*}{,} \boldsymbol{\Pi}^\nu] \ .\end{aligned}$$

We find the second transformation matrix $\mathcal{U}'(\boldsymbol{X}, \boldsymbol{\Pi})$ in terms of kinetic variables which yields a new, further or completely diagonalized Hamiltonian $\bar{\mathcal{H}}'(\boldsymbol{X}', \boldsymbol{\Pi}')$ along with the transformation of the kinetic variables

$$\boldsymbol{X}' = \mathcal{U}' * \boldsymbol{X} * \mathcal{U}'^\dagger = \mathcal{U}' * \boldsymbol{x} * \mathcal{U}'^\dagger - \hbar\mathcal{A}_{\boldsymbol{\pi}}(\mathcal{U}' * \boldsymbol{x} * \mathcal{U}'^\dagger *, \ \mathcal{U}' * \boldsymbol{\pi} * \mathcal{U}'^\dagger *) \ ,$$

where $\mathcal{A}_{\boldsymbol{\pi}}(\mathcal{U}' * \boldsymbol{x} * \mathcal{U}'^{\dagger} *,\ \mathcal{U}' * \boldsymbol{\pi} * \mathcal{U}'^{\dagger} *)$ has to be interpreted in terms of a Taylor expansion, with non-commuting $\mathcal{U}' * \boldsymbol{x}_\mu * \mathcal{U}'^{\dagger}$ and $\mathcal{U}' * \boldsymbol{\pi}_\mu * \mathcal{U}'^{\dagger}$ properly symmetrized according to the previously discussed Wigner-Weyl ordering. We illustrate this at the example of xp which is transformed by $\mathcal{U}'$ into

$$\mathcal{U}' * xp * \mathcal{U}'^{\dagger} = \frac{1}{2}\mathcal{U}' * (x * p + p * x) * \mathcal{U}'^{\dagger} = \frac{1}{2}\left(\mathcal{U}' * x * \mathcal{U}'^{\dagger} * \mathcal{U}' * p * \mathcal{U}'^{\dagger} + \ldots|_{x\leftrightarrow p}\right) . \tag{3.149}$$

Now, introducing the Berry connection $\mathcal{A}'_{\boldsymbol{\pi}}(\boldsymbol{x},\boldsymbol{\pi}) \equiv i\mathcal{U}' * \partial_{\boldsymbol{\pi}}\mathcal{U}'^{\dagger}$, and likewise for $\mathcal{A}'_{\boldsymbol{x}}(\boldsymbol{x},\boldsymbol{\pi})$, we can cast the new kinetic variables into the form

$$\begin{aligned}\boldsymbol{X}' &= \boldsymbol{x} - \hbar\mathcal{A}'_{\boldsymbol{\pi}} - \hbar\mathcal{A}_{\boldsymbol{\pi}}(\boldsymbol{x} - \hbar\mathcal{A}'_{\boldsymbol{\pi}}, \boldsymbol{p} + \hbar\mathcal{A}'_{\boldsymbol{x}}) \\ \boldsymbol{\Pi}' &= \boldsymbol{p} + \hbar\mathcal{A}'_{\boldsymbol{x}} + \hbar\mathcal{A}_{\boldsymbol{x}}(\boldsymbol{x} - \hbar\mathcal{A}'_{\boldsymbol{\pi}}, \boldsymbol{p} + \hbar\mathcal{A}'_{\boldsymbol{x}}) .\end{aligned} \tag{3.150}$$

Up to now, everything is still exact to arbitrary order in $\hbar$, but the mathematical structure of this result is rather complicated. However, we see that to linear order in $\hbar$, the Berry connections simply add, and to find a suitable expression to second order in $\hbar$, we rewrite the Berry connections in terms of kinetic variables,

$$\mathcal{A}'_{\boldsymbol{x}/\boldsymbol{\pi}}(\boldsymbol{x},\boldsymbol{\pi}) = \mathcal{A}'_{\boldsymbol{X}/\boldsymbol{\Pi}} - \hbar\mathcal{A}'_{\boldsymbol{X}_k}\partial_{\boldsymbol{x}/\boldsymbol{\pi}}\mathcal{A}_{\boldsymbol{\pi}_k} + \hbar\mathcal{A}'_{\boldsymbol{\Pi}_k}\partial_{\boldsymbol{x}/\boldsymbol{\pi}}\mathcal{A}_{\boldsymbol{x}_k} + O(\hbar^2) , \tag{3.151}$$

with the definition $\mathcal{A}'_{\boldsymbol{X}/\boldsymbol{\Pi}}(\boldsymbol{X},\boldsymbol{\Pi}) = i\mathcal{U}'\partial_{\boldsymbol{X}/\boldsymbol{\Pi}}\mathcal{U}'^{\dagger}$. Expanding $\mathcal{A}_{\boldsymbol{\pi}}(\boldsymbol{x} - \hbar\mathcal{A}'_{\boldsymbol{\pi}}, \boldsymbol{p} + \hbar\mathcal{A}'_{\boldsymbol{x}}) = \mathcal{A}_{\boldsymbol{\pi}}(\boldsymbol{x},\boldsymbol{p}) - \hbar\mathcal{A}'_{\boldsymbol{\Pi}_k}\partial_{\boldsymbol{x}_k}\mathcal{A}_{\boldsymbol{\pi}} + \hbar\mathcal{A}'_{\boldsymbol{X}_k}\partial_{\boldsymbol{\pi}_k}\mathcal{A}_{\boldsymbol{\pi}} + O(\hbar)$ and using the definitions (3.50)-(3.52), we arrive at an expression valid up to second order in $\hbar$,

$$\boldsymbol{X}' = \boldsymbol{x} - \hbar\left(\mathcal{A}_{\boldsymbol{\pi}} + \mathcal{A}'_{\boldsymbol{\Pi}}\right) + \hbar\underline{\underline{\Theta}}^{\boldsymbol{\pi}\boldsymbol{\pi}}\mathcal{A}'_{\boldsymbol{X}} + \hbar\mathcal{A}'_{\boldsymbol{\Pi}}\underline{\underline{\Theta}}^{\boldsymbol{x}\boldsymbol{\pi}} , \tag{3.152}$$

$$\boldsymbol{\Pi}' = \boldsymbol{\pi} + \hbar\left(\mathcal{A}_{\boldsymbol{x}} + \mathcal{A}'_{\boldsymbol{X}}\right) + \hbar\underline{\underline{\Theta}}^{\boldsymbol{x}\boldsymbol{x}}\mathcal{A}'_{\boldsymbol{\Pi}} - \hbar\underline{\underline{\Theta}}^{\boldsymbol{x}\boldsymbol{\pi}}\mathcal{A}'_{\boldsymbol{X}} , \tag{3.153}$$

where, in higher order $\hbar$, effects due to the Berry connections that emerged as a result of the first diagonalization step essentially appear in shape of its Berry curvatures $\underline{\underline{\Theta}}$.

However, instead of further studying the most general situation, we step back to consider a simpler, albeit physically much more useful scenario which takes into account the electromagnetic field. Furthermore, we want to study the combined effect of the electromagnetic field and the Berry connections emerging from the diagonalization of a band Hamiltonian. Since our treatment is only linear in $\hbar$, we treat the electromagnetic Berry connection $q\boldsymbol{A}$ (q is the charge of the particle, so we usually have $q = -e$) on a different level than $\hbar\mathcal{A}$, thus formally treating $\hbar$ and q as independent expansion parameters.

3.2.2. Inclusion of the Electromagnetic Field

In this case, we are already starting from a theory which is gauge invariant in real space, thus formulated in terms of the minimally coupled momentum $\boldsymbol{p} - q\boldsymbol{A}(x)$, and we can think of this as already being an effective theory derived from a more complete theory. In this sense, we have to deal with the properties of a hierarchy of effective theories. Of course, qualitatively, one expects no new concepts to emerge in these effective theories at a lower

level in the hierarchy, as one could also go directly from the topmost theory to the lowest in a single step.

To begin with, we have the usual canonical pair $\boldsymbol{x}$ and $\boldsymbol{\pi}$ and the kinetic pair $\boldsymbol{x}$ and $\boldsymbol{\pi}+q\boldsymbol{A}(\boldsymbol{x})$, where $\boldsymbol{A}=(-\phi,\boldsymbol{A}_{\boldsymbol{r}})$ is the usual 4-component vector potential of the electromagnetic field. In the following, we denote $\boldsymbol{B}(\boldsymbol{r},t)=\boldsymbol{\nabla}_{\boldsymbol{r}}\times\boldsymbol{A}_{\boldsymbol{r}}$ and $\boldsymbol{E}(\boldsymbol{r},t)=-\partial_t\boldsymbol{A}_{\boldsymbol{r}}+\boldsymbol{\nabla}_{\boldsymbol{r}}\boldsymbol{A}_0$ as the external electric and magnetic fields.

The Hamiltonian is specified as $\mathcal{H}(\boldsymbol{x},\boldsymbol{\pi}+q\boldsymbol{A}(\boldsymbol{x}))$ and is diagonalized by an appropriate unitary matrix $\mathcal{U}(\boldsymbol{x},\boldsymbol{\pi}+q\boldsymbol{A}(\boldsymbol{x}))$, so that in the diagonalized frame we arrive at the kinetic pair of variables

$$\begin{aligned}\boldsymbol{X}&=\boldsymbol{x}-\hbar\mathcal{A}_{\boldsymbol{\pi}}(\boldsymbol{x},\boldsymbol{p}+q\boldsymbol{A})\\ \boldsymbol{\Pi}&=\boldsymbol{\pi}+q\boldsymbol{A}(\boldsymbol{X})+\hbar\mathcal{A}_{\boldsymbol{x}}(\boldsymbol{x},\boldsymbol{p}+q\boldsymbol{A})\ .\end{aligned}\tag{3.154}$$

Again, for simplicity, all Berry phases involved are assumed to be Abelian.

The fictitious fields in the presence of an electromagnetic field can be derived in a similar way as before by using commutator relations (3.55) and (3.65). To illustrate the procedure, we explicitly obtain the fictitious electric field by expanding the Moyal bracket to leading order in $\hbar$

$$\boldsymbol{\mathcal{E}}'^{(\boldsymbol{r})}=(\epsilon+qA_0+\hbar\mathcal{A}_t)\left(\overleftarrow{\partial_\epsilon}\overrightarrow{\partial_t}+\overleftarrow{\partial_r}\overrightarrow{\partial_p}-\overleftarrow{\partial_p}\overrightarrow{\partial_r}\right)(\boldsymbol{p}-q\boldsymbol{A}_{\boldsymbol{r}}-\hbar\mathcal{A}_{\boldsymbol{r}})\ ,\tag{3.155}$$

where here, and in the following, primed quantities describe the Berry curvatures of the complete system, i.e. they contain the combined contribution from Berry connections arising from going into the diagonalized frame and from the electromagnetic potential. One should pay attention to include also terms of the form $\partial_{P_k}A_\gamma$, when expanding the Moyal bracket in the commutators, since the usual vector potential now implicitly depends on momentum through $\boldsymbol{A}(\boldsymbol{r}+\hbar\mathcal{A}_{\boldsymbol{P}},t)$ (see also rule (3.158) below).

As it is the usual procedure in this chapter, we now transform to kinetic variables in order to get a physically more meaningful representation of the fictitious fields. In the process of doing so, one has to pay attention to the various contributions from derivatives acting on the Berry phase terms $\boldsymbol{A}$ and $\mathcal{A}$, and keeping all terms up to order $O(\hbar)$ and quadratic in the fields $O(q^2)$. Analogous to relation (3.151) and following, the rules we need to apply in our calculation can be summarized as

$$\partial_{x_j}=\partial_{X_j}-q(\partial_{R_j}A_l)\partial_{P_l}\ ,\qquad \partial_{\pi_j}=\partial_{\Pi_j}\tag{3.156}$$

$$\mathcal{A}_{x_k}=\mathcal{A}_{X_k}-q(\partial_{R_k}A_l)\mathcal{A}_{P_l}\ ,\qquad \mathcal{A}_{\pi_k}=\mathcal{A}_{\Pi_k}\tag{3.157}$$

$$\partial_{x_k}A_\gamma=\partial_{X_k}A_\gamma+\hbar(\partial_{R_l}A_\gamma)\partial_{X_k}\mathcal{A}_{P_l}\ ,\qquad \partial_{p_k}A_\gamma=\hbar(\partial_{R_l}A_\gamma)\partial_{P_k}\mathcal{A}_{P_l}\ ,\tag{3.158}$$

where γ runs from 0 to 3, and 0 is the time component of the 4-component vector $\boldsymbol{A}_\gamma$, i.e. A_0 is the scalar electric potential. The contributions to $\mathcal{A}_{\boldsymbol{x}}$ now have been split in the contribution from the system $\mathcal{A}_{\boldsymbol{X}}$ in absence of the magnetic field, and the contribution arising from an additional electromagnetic field. Note that $\mathcal{A}_{\boldsymbol{X}}$, as well as $\mathcal{A}_{\boldsymbol{P}}$ still carry the full gauge invariant momentum $\boldsymbol{P}$, and the external electromagnetic fields have been expressed in terms of the kinetic variable $\boldsymbol{X}$, so that for example $\boldsymbol{E}(\boldsymbol{X})=\boldsymbol{E}(\boldsymbol{x})+(\mathcal{A}_{\boldsymbol{P}}\partial_{\boldsymbol{r}})\boldsymbol{E}(\boldsymbol{x})$. Now, plugging these transformations back into (3.155) and after some straightforward algebra, we obtain

$$\boldsymbol{\mathcal{E}}'^{(\boldsymbol{r})}=q\boldsymbol{E}(\boldsymbol{X})+\boldsymbol{\mathcal{E}}^{(\boldsymbol{r})}+q\underline{\underline{\Theta}}^{\boldsymbol{rp}}\boldsymbol{E}+q\boldsymbol{B}\times\boldsymbol{\mathcal{E}}^{(\boldsymbol{p})}+q^2\boldsymbol{B}\times(\boldsymbol{E}\times\boldsymbol{\mathcal{B}}^{(\boldsymbol{p})})\ .\tag{3.159}$$

Here in these expressions, unprimed quantities $\boldsymbol{\mathcal{B}}$, $\boldsymbol{\mathcal{E}}$, $\underline{\underline{\Theta}}$ correspond to the Berry curvatures of the system in the diagonalized frame in absence of the external electromagnetic field $q\boldsymbol{A}$. However, they still carry the full gauge invariant momentum $\boldsymbol{P}$ and thus, implicitly depend on $q\boldsymbol{A}$, if one takes the canonical pair of variables as independent parameters.

The calculation of the remaining effective fields proceeds completely along the same lines, and the results can be summarized as

$$\boldsymbol{\mathcal{B}}'^{(r)} = q\boldsymbol{B}(\boldsymbol{R}) + \boldsymbol{\mathcal{B}}^{(r)} + q\left[\mathrm{Tr}(\underline{\underline{\Theta}}^{rp})\boldsymbol{B} - \boldsymbol{B}\underline{\underline{\Theta}}^{rp}\right] + q^2\left(\boldsymbol{\mathcal{B}}^{(p)}\cdot\boldsymbol{B}\right)\boldsymbol{B} \tag{3.160}$$

$$\boldsymbol{\mathcal{B}}'^{(p)} = \boldsymbol{\mathcal{B}}^{(p)} \tag{3.161}$$

$$\boldsymbol{\mathcal{E}}'^{(r)} = q\boldsymbol{E}(\boldsymbol{X}) + \boldsymbol{\mathcal{E}}^{(r)} + q\underline{\underline{\Theta}}^{rp}\boldsymbol{E} + q\boldsymbol{B}\times\boldsymbol{\mathcal{E}}^{(p)} + q^2\boldsymbol{B}\times(\boldsymbol{E}\times\boldsymbol{\mathcal{B}}^{(p)}) \tag{3.162}$$

$$\boldsymbol{\mathcal{E}}'^{(p)} = \boldsymbol{\mathcal{E}}^{(p)} + q\boldsymbol{E}\times\boldsymbol{\mathcal{B}}^{(p)} \tag{3.163}$$

$$\underline{\underline{\Theta}}'^{rp}_{ij} = \underline{\underline{\Theta}}^{rp}_{ij} + q\left[\left(\boldsymbol{\mathcal{B}}^{(p)}\cdot\boldsymbol{B}\right)\delta_{ij} - \mathcal{B}^{(p)}_i B_j\right] \ , \tag{3.164}$$

which all appear in a manifest gauge invariant manner. It is important to note that these results have to be substituted into the equations of motion (3.103), (3.104) and *not* (3.105), (3.106) since the latter has been obtained by dropping terms beyond leading order corrections in Berry curvatures, whereas our results for the fictitious fields are in fact higher order in Berry connections.[9] We will come back to this point later when discussing an alternative approach.

The term $\boldsymbol{E}\times\boldsymbol{\mathcal{B}}^{(p)}$ of $\boldsymbol{\mathcal{E}}'^{(p)}$ is the anomalous velocity term that is for example responsible for the quantum Hall effect, since the Berry curvature $\boldsymbol{\mathcal{B}}^{(p)}$ becomes non-trivial, when the system is in the Quantum Hall state. Similarly, in systems with spin-orbit interactions, this term constitutes the intrinsic contribution to the anomalous Hall effect. The reciprocal effect thereof is described by the term $q\boldsymbol{B}\times\boldsymbol{\mathcal{E}}^{(p)}$, where a external magnetic field transforms a momentum space electric field into a real-space one.

$\underline{\underline{\Theta}}'^{rp}$ gets modified by a magnetic field term that resembles a dipole-dipole interaction between a real-space and the momentum space magnetic field. In fact, as we saw in result (3.100), and as we will see explicitly at the end of this section, $\underline{\underline{\Theta}}'^{rp}$ is directly related to the magnetic dipole energy in the case of a two-level model, and thus, it is the magnetic field in $\underline{\underline{\Theta}}'^{rp}$ which will give rise to the magnetic energy in the Hamiltonian. Furthermore, the term quadratic in the fields can be absorbed by $\underline{\underline{\Theta}}'^{rp}$, i.e. fictitious electric field can be recast into

$$\boldsymbol{\mathcal{E}}'^{(r)} = q\boldsymbol{E} + \boldsymbol{\mathcal{E}}^{(r)} + q\underline{\underline{\Theta}}'^{rp}\boldsymbol{E} + q\boldsymbol{B}\times\boldsymbol{\mathcal{E}}^{(p)} \ . \tag{3.165}$$

From this expression, we see that the external electric field enters effectively as $q(\mathbb{1} + \underline{\underline{\Theta}}'^{rp})\boldsymbol{E}$, and the electric field acting on the system is thus renormalized. We will later study the case of an inhomogeneous magnetization texture yielding a non-vanishing $\underline{\underline{\Theta}}^{rp}$, then this term essentially gives rise to a change in resistance within regions of a finite magnetization gradient. An analogous renormalization of the external magnetic field appears also in the result for $\boldsymbol{\mathcal{B}}'^{(r)}$.

There is an alternative, albeit less straightforward, approach to obtain the results (3.160)-(3.164) by using a similar method as for the transformation from canonical to kinetic variables in (3.45)-(3.48). However, one should pay attention to the iterative nature of the parameter transformation (3.154), for example $\boldsymbol{A}(\boldsymbol{X}) = \boldsymbol{A}(\boldsymbol{x} - \hbar\mathcal{A}_{\boldsymbol{\pi}}(\boldsymbol{x}, \boldsymbol{p} + q\boldsymbol{A}(\boldsymbol{x})))$, so the vector potential $\boldsymbol{A}$ depends itself again on $\boldsymbol{A}$, and furthermore, the derivatives within the Moyal

[9] $q^2\hbar$ actually already corresponds to terms of third order in the expansion.

product act on all these nested terms. It is exactly this recursion that gives rise to the terms quadratic and higher order in the fields (c.f. the last terms in $\boldsymbol{\mathcal{B}}'^{(r)}$ and $\boldsymbol{\mathcal{E}}'^{(r)}$).

To leading order in $\hbar$, with everything expressed in terms of kinetic variables $\mathbf{\Pi}$ and $\boldsymbol{X}$, one obtains an alternative formulation of the equations of motion in the presence of electromagnetic field and Berry curvature effects,

$$\frac{\mathrm{d}\boldsymbol{R}}{\mathrm{d}t} = \frac{\partial\bar{\mathcal{H}}}{\partial\boldsymbol{P}} + \frac{\mathrm{d}\boldsymbol{R}}{\mathrm{d}t}\underline{\underline{\mathcal{J}}} - \boldsymbol{\mathcal{E}}^{(p)} - \frac{\mathrm{d}\boldsymbol{P}}{\mathrm{d}t}\times\boldsymbol{\mathcal{B}}^{(p)} \ , \tag{3.166}$$

$$\frac{\mathrm{d}\boldsymbol{P}}{\mathrm{d}t} = -\frac{\partial\bar{\mathcal{H}}}{\partial\boldsymbol{R}} + \underline{\underline{\mathcal{J}}}\frac{\mathrm{d}\boldsymbol{P}}{\mathrm{d}t} + \boldsymbol{\mathcal{E}}^{(r)} + \frac{\mathrm{d}\boldsymbol{R}}{\mathrm{d}t}\times\boldsymbol{\mathcal{B}}^{(r)} + q\boldsymbol{E}(\boldsymbol{R}) + q\frac{\mathrm{d}\boldsymbol{R}}{\mathrm{d}t}\times\boldsymbol{B}(\boldsymbol{R}) \ , \tag{3.167}$$

in a form equivalent to (3.105) and (3.106). Now solving these equations iteratively up to order $q^2\hbar$, thus casting it into the form (3.105) and (3.106), one can identify the combined effective fields and obtains exactly those expressions found earlier in (3.160)-(3.164). In fact, the nested structure of the parameter transformation has been mapped onto the iterative solution of the kinetic equation. It is possible in this form due to the rather simple structure of the vector potential for the electromagnetic field, while retaining only effects up to first order in Berry curvatures emerging from an explicit diagonalization in band space. For the general situation as depicted in (3.150), we did not find an analogous expression.

Before continuing, let us give the short remark that the electric field can be also treated on the level of the Hamiltonian in the form of a scalar electric potential, which means $\boldsymbol{E} \equiv 0$ in all the primed Berry curvatures above. However, in the equations of motion (3.103) and (3.104), we have instead $-\frac{\partial\bar{\mathcal{H}}}{\partial\boldsymbol{R}} = q\boldsymbol{E}$ which exactly reproduces all the electric field dependent terms found in this section.

Finally, let us discuss how the Hamiltonian and operators in the diagonalized frame are modified in the presence of the electromagnetic field.
When we use result (3.25) to transform an operator $\mathcal{O}$ into the rotated frame, we encounter the term $-\frac{i\hbar}{4}\left(\left\{\mathcal{A}_{\boldsymbol{p}}, \left[\mathcal{A}_{\boldsymbol{r}}, \bar{\mathcal{O}}_0\right]\right\} - \left\{\mathcal{A}_{\boldsymbol{r}}, \left[\mathcal{A}_{\boldsymbol{p}}, \bar{\mathcal{O}}_0\right]\right\}\right)$ which can be rewritten by splitting off the magnetic field contribution

$$\begin{aligned} -\frac{i\hbar}{4}\left(\left\{\mathcal{A}_{\boldsymbol{P}}, \left[\mathcal{A}_{\boldsymbol{R}}, \bar{\mathcal{O}}_0\right]\right\} - \left\{\mathcal{A}_{\boldsymbol{R}}, \left[\mathcal{A}_{\boldsymbol{P}}, \bar{\mathcal{O}}_0\right]\right\}\right) \\ + \frac{iq\hbar}{4}(\partial_{R_k}A_l)\left(\left\{\mathcal{A}_{P_k}, \left[\mathcal{A}_{P_l}, \bar{\mathcal{O}}_0\right]\right\} - \left\{\mathcal{A}_{P_l}, \left[\mathcal{A}_{P_k}, \bar{\mathcal{O}}_0\right]\right\}\right) \ , \end{aligned} \tag{3.168}$$

where we used rule (3.157). The last term of order $q\hbar$ can be also recast into

$$-\frac{i\hbar}{4}\left(\left\{\mathcal{A}_{\boldsymbol{P}}, \left[\mathcal{A}_{\boldsymbol{R}}, \bar{\mathcal{O}}_0\right]\right\} - \left\{\mathcal{A}_{\boldsymbol{R}}, \left[\mathcal{A}_{\boldsymbol{P}}, \bar{\mathcal{O}}_0\right]\right\}\right) + \frac{iq\hbar}{4}\epsilon_{ijk}B_k\left\{\mathcal{A}_{P_i}, \left[\mathcal{A}_{P_j}, \bar{\mathcal{O}}_0\right]\right\} \ . \tag{3.169}$$

When the observable $\bar{\mathcal{O}}_0$ possesses non-trivial matrix structure, the commutator $\left[\mathcal{Y}_1, \bar{\mathcal{O}}_0\right]$ will induce more explicit magnetic field dependent terms through $\mathcal{Y}_1$ (see also equation (3.28)). In particular, the Hamiltonian in the rotated frame reads

$$\begin{aligned} \bar{\mathcal{H}} = \bar{\mathcal{H}}_0(\boldsymbol{X}, \mathbf{\Pi}) - \frac{i\hbar}{4}\mathcal{P}_d\left(\left\{\mathcal{A}_{\boldsymbol{P}}, \left[\mathcal{A}_{\boldsymbol{R}}, \bar{\mathcal{H}}_0\right]\right\} - \left\{\mathcal{A}_{\boldsymbol{R}}, \left[\mathcal{A}_{\boldsymbol{P}}, \bar{\mathcal{H}}_0\right]\right\}\right)\mathcal{P}_d \\ + \frac{iq\hbar}{4}\epsilon_{ijk}B_k\mathcal{P}_d\left\{\mathcal{A}_{P_i}, \left[\mathcal{A}_{P_j}, \bar{\mathcal{H}}_0\right]\right\}\mathcal{P}_d + O(\hbar^2) \end{aligned} \tag{3.170}$$

and, using results (3.100) and (3.164), we find for a system with a two level band structure

$$\bar{\mathcal{H}}_{\mathcal{M}} = \mathrm{Tr}_2\left\{\bar{\mathcal{H}}_0 \mathrm{Tr}\underline{\underline{\Theta}}'^{\boldsymbol{rp}}\right\}\ \mathbb{1}_2 = \mathrm{Tr}_2\left\{\bar{\mathcal{H}}_0\left(\mathrm{Tr}\underline{\underline{\Theta}}^{\boldsymbol{rp}} + 2q\boldsymbol{B}\cdot\boldsymbol{\mathcal{B}}^{(\boldsymbol{p})}\right)\right\}\ \mathbb{1}_2\ . \tag{3.171}$$

In two dimensions, $\underline{\underline{\Theta}}'^{\boldsymbol{rp}}_{33}$ is zero,[10] and thus $\mathrm{Tr}\underline{\underline{\Theta}}'^{\boldsymbol{rp}} = \mathrm{Tr}\underline{\underline{\Theta}}^{\boldsymbol{rp}} + q\boldsymbol{B}\cdot\boldsymbol{\mathcal{B}}^{(\boldsymbol{p})}$, i.e. a factor 2 less than in the 3D case, and likewise, in 1D $\mathrm{Tr}\underline{\underline{\Theta}}'^{\boldsymbol{rp}} = \mathrm{Tr}\underline{\underline{\Theta}}^{\boldsymbol{rp}}$. Nevertheless, we see that the magnetic field couples in the shape of a dipole-dipole term $\boldsymbol{B}\cdot\boldsymbol{\mathcal{B}}^{(\boldsymbol{p})}$ to the momentum space magnetic field $\boldsymbol{\mathcal{B}}^{(\boldsymbol{p})}$. Since the magnetic dipole energy is already of order $\hbar$, we can equally write $\boldsymbol{B}(\boldsymbol{X})$ and $\boldsymbol{B}(\boldsymbol{x})$, since substituting canonical and kinetic variables affects only higher orders in $\hbar$.

3.3. The Dirac Equation

In order to illustrate our formalism, we will first study the Dirac equation and thereafter, we study the interesting scenario of a topological insulator coupled to a ferromagnet with arbitrary magnetization texture. The Dirac equation and its descendants like the Pauli Hamiltonian are the most fundamental equations in condensed matter physics, nevertheless, we present some new and interesting insight into the rich physics revealed by this rather simple equation.

We consider the Dirac Hamiltonian in the presence of a scalar potential and minimally coupled to the magnetic field [124],

$$H = c\boldsymbol{\alpha}(\boldsymbol{p} - q\boldsymbol{A}) + mc^2\beta + V(\boldsymbol{x})\mathbb{1}_4\ , \tag{3.172}$$

where m is the rest mass and $\boldsymbol{p}$ the momentum of the electron. As

$$\boldsymbol{\alpha} = \begin{pmatrix} 0 & \boldsymbol{\sigma} \\ \boldsymbol{\sigma} & 0 \end{pmatrix}\ , \qquad \beta = \begin{pmatrix} \mathbb{1}_2 & 0 \\ 0 & -\mathbb{1}_2 \end{pmatrix}\ , \tag{3.173}$$

H acts on the 4-dimensional Dirac Spinor and thus can be considered as a 4-band model.

The Foldy-Wouthuysen transformation [107] which brings the Dirac equation into diagonal form is described by the unitary matrix

$$\mathcal{U}_0 = \frac{(E_P + mc^2)\mathbb{1}_4 + c\beta\boldsymbol{\alpha}\boldsymbol{P}}{\sqrt{E_P(E_P + mc^2)}}\ , \tag{3.174}$$

where $E_P = c\sqrt{P^2 + m^2c^2}$ is the relativistic energy of the electron with gauge invariant momentum P. Performing, as outlined before, the diagonalizion with respect to $\mathcal{U}_0$, we arrive at

$$\bar{\mathcal{H}} = \mathcal{U} * H * \mathcal{U}^\dagger = E_P\sigma_0 \otimes \tau_z + \left(V(\boldsymbol{r})\sigma_0 + \hbar(\partial_{\boldsymbol{r}}V)\mathcal{A}^{(d)}_{\boldsymbol{P}} + qE_P\boldsymbol{B}\cdot\boldsymbol{\mathcal{B}}^{(\boldsymbol{p})}\right) \otimes \tau_0\ . \tag{3.175}$$

The 2×2-matrices τ_i denote the Pauli matrices in electron-positron space, while σ_i describes the usual spin degree of freedom. As discussed in the section dealing with the external magnetic field, the magnetic dipole term is given in terms of an interaction term between

[10] However, even in lower dimensional system we are still using all three dimensions in our vector calculus and according to (3.164), $\underline{\underline{\Theta}}'^{\boldsymbol{rp}}_{33} \neq 0$, so we have to pay attention to these subtleties for dimensions ≤ 2.

magnetic field $\boldsymbol{B} = \boldsymbol{\nabla} \times \boldsymbol{A}$ and the fictitious momentum space magnetic field $\boldsymbol{\mathcal{B}}^{(\boldsymbol{p})}$, to be specified below. We note that in this case, all the correction terms are equal for both electron and positron bands, albeit the term positron becomes only meaningful when all negative energy states are completely occupied.

The full matrix structure of the Berry phase, split into diagonal and off-diagonal parts, i.e. $\mathcal{A}_{\boldsymbol{P}} = \mathcal{A}^{(d)}_{\boldsymbol{P}} \otimes \tau_0 + \mathcal{A}^{(o)}_{\boldsymbol{P}} \otimes \tau_y$, reads

$$\mathcal{A}^{(d)}_{\boldsymbol{P}} = \frac{c^2 \boldsymbol{P} \times \boldsymbol{\sigma}}{2E_P(E_P + mc^2)} \approx \frac{\lambda_c}{4\hbar} \frac{\boldsymbol{P} \times \boldsymbol{\sigma}}{mc} \ , \tag{3.176}$$

$$\mathcal{A}^{(o)}_{\boldsymbol{P}} = \frac{c\boldsymbol{\sigma}}{2E_P} - \frac{\boldsymbol{P}(\boldsymbol{P}\boldsymbol{\sigma})\ c^3}{2E_P^2(E_P + mc^2)} \approx \frac{\lambda_c}{2\hbar}\boldsymbol{\sigma} \ , \tag{3.177}$$

where in the last step, we are dropping terms of order $O(p/mc)^2$. For completeness, let us also specify the first order correction to $\mathcal{U}$ which in this case absorbs the off-diagonal elements of the Berry phase matrix $\mathcal{A}_{\boldsymbol{P}}$ and the magnetization term $\propto \boldsymbol{B}$,

$$\begin{aligned} \left[\mathcal{Y}_1, \bar{\mathcal{H}}_0\right] &= \hbar(\partial_{\boldsymbol{r}} V)\mathcal{A}^{(o)}_{\boldsymbol{p}} \otimes \tau_y + \frac{\hbar q\ \boldsymbol{B}\cdot\boldsymbol{P}}{2E_P(E_P + mc^2)} \otimes \tau_x \\ \Rightarrow \mathcal{Y}_1 &= -\frac{i\hbar}{2E_P}(\partial_{\boldsymbol{r}} V)\mathcal{A}^{(o)}_{\boldsymbol{P}} \otimes \tau_x + \frac{i\hbar q\ \boldsymbol{B}\cdot\boldsymbol{P}}{4E_P^2(E_P + mc^2)} \otimes \tau_y \ , \end{aligned}$$

which is indeed anti-Hermitian.

The kinetic variables for both positive and negative energy states read explicitly

$$\begin{aligned} \boldsymbol{P} &= \boldsymbol{p} - q\boldsymbol{A}(\boldsymbol{r}) - q\hbar \boldsymbol{B} \times \mathcal{A}^{(d)}_{\boldsymbol{P}} \ , \\ \boldsymbol{R} &= \boldsymbol{r} + \hbar \mathcal{A}^{(d)}_{\boldsymbol{P}} \ , \end{aligned}$$

so that the Berry curvature is also equal for both bands, and yields

$$\boldsymbol{\mathcal{B}}^{(\boldsymbol{p})} = -\frac{\hbar mc^4}{2E_P^3}\boldsymbol{\sigma} - \frac{\boldsymbol{P}(\boldsymbol{P}\cdot\boldsymbol{\sigma})\ \hbar c^4}{2E_P^3(E_P + mc^2)} \approx -\frac{\lambda_c^2}{2\hbar}\boldsymbol{\sigma} \ , \tag{3.178}$$

where again, in the last step we took the non-relativistic limit. Of course, the general expressions are still valid for arbitrary velocities, for example, in the opposite, the ultra-relativistic limit, we find

$$\boldsymbol{\mathcal{B}}^{(\boldsymbol{p})} \overset{p \gg mc}{\to} -\frac{\boldsymbol{P}(\boldsymbol{P}\cdot\boldsymbol{\sigma})\hbar}{2P^4} \ .$$

Using the results (3.160) - (3.164), we immediately find $\boldsymbol{\mathcal{E}}^{(\boldsymbol{r})} = 0 = \boldsymbol{\mathcal{E}}^{(\boldsymbol{p})}$ and

$$\begin{aligned} \boldsymbol{\mathcal{B}}^{(\boldsymbol{r})} &= q\boldsymbol{B}(\boldsymbol{R}) + q^2 \left(\boldsymbol{\mathcal{B}}^{(\boldsymbol{p})}\cdot\boldsymbol{B}\right)\boldsymbol{B} \\ \underline{\underline{\Theta}}^{\boldsymbol{rp}}_{ij} &= q\left[\left(\boldsymbol{\mathcal{B}}^{(\boldsymbol{p})}\cdot\boldsymbol{B}\right)\delta_{ij} - \mathcal{B}^{(\boldsymbol{p})}_i B_j\right] \ , \end{aligned} \tag{3.179}$$

where here, we used $\boldsymbol{E}(\boldsymbol{R}) = 0$, since we are already using the scalar potential $V(\boldsymbol{R})$ here, and as discussed before, one would get an equivalent result by instead using the full results (3.160) - (3.164).

In terms of kinetic variables, the Hamiltonian $\bar{\mathcal{H}}$ can now be rewritten (let us restrict ourselves to the positive energy branch, whose excitations correspond to electrons, so that $q = -e$), neglecting terms of order $\hbar^2$,

$$\bar{\mathcal{H}} = E_P + V(\boldsymbol{R}) + qE_P \boldsymbol{B}(\boldsymbol{R}) \cdot \boldsymbol{\mathcal{B}}^{(p)} \ , \tag{3.180}$$

so that in view of this, the spin-orbit interaction that appears in the rotated frame can be reinterpreted as being a result of the shift the kinetic position operator attains. However, we should keep in mind that this shift is gauge dependent and becomes physically meaningful only when integrated over the whole momentum space (which then is equivalent to the polarization) or in the form of the Berry curvature, viz the momentum space magnetic field appearing in the kinetic equations. In the non-relativistic limit, the magnetic dipole energy is just the usual Zeeman term

$$\bar{\mathcal{H}}_{\mathcal{M}} = -\boldsymbol{\mu}_s \cdot \boldsymbol{B} \ , \tag{3.181}$$

where we introduced the magnetic moment of the electron spin, $\boldsymbol{\mu}_s = -g_s \mu_{\mathrm{B}} \boldsymbol{\sigma}/2 = -\mu_{\mathrm{B}} \boldsymbol{\sigma}$, and we assume a g-factor of 2 within the validity of the Dirac theory without quantum corrections from the radiative field, and $\mu_{\mathrm{B}} = \frac{e\hbar}{2m}$ is the Bohr magneton.

Using results (3.103) and (3.104) together with (3.179) and (3.180), we obtain the equations of motion of a relativistic electron wave-packet which moves in an electromagnetic field that is smooth on the scale of the Compton wavelength λ_c. We do not explicitly write the expression here, however, our result is consistent with the work of Bliokh [125].

For the sake of our discussion, we will nevertheless specify the equations of motion in absence of a magnetic field,

$$\frac{\mathrm{d}\boldsymbol{R}}{\mathrm{d}t} = \frac{\partial \bar{\mathcal{H}}}{\partial \boldsymbol{P}} - \frac{\mathrm{d}\boldsymbol{P}}{\mathrm{d}t} \times \boldsymbol{\mathcal{B}}^{(p)} = \frac{\partial \bar{\mathcal{H}}}{\partial \boldsymbol{P}} + \frac{\lambda_c^2}{2\hbar} \frac{\mathrm{d}\boldsymbol{P}}{\mathrm{d}t} \times \boldsymbol{\sigma} \ , \tag{3.182}$$

$$\frac{\mathrm{d}\boldsymbol{P}}{\mathrm{d}t} = -\frac{\partial \bar{\mathcal{H}}}{\partial \boldsymbol{R}} = -e\boldsymbol{E}(\boldsymbol{R}) \ , \tag{3.183}$$

whose anomalous velocity term is a factor 2 larger than what one would obtain from the Hamiltonian (3.175), naively taking the canonical variable $\boldsymbol{r}$ to be the physical position operator.

The particle density is, according to results (3.118) and (3.179), given by

$$n(\boldsymbol{R}, t) = \int \frac{\mathrm{d}^3 P}{(2\pi\hbar)^3} \ \mathrm{Tr}_4 \bar{\rho} \left(1 - 2q\boldsymbol{B} \cdot \boldsymbol{\mathcal{B}}^{(p)}\right) \ , \tag{3.184}$$

and let us take the vacuum state with all negative energies filled, so that $\bar{\rho} = \Theta(-\tau_z E_P)$ and the first term gives simply the vacuum charge. However, from the correction factor proportional to the magnetic field one might conclude that a sufficiently strong magnetic field leads to a charge accumulation with respect to the vacuum state, but these kinds of questions are beyond the present work. Also, the momentum integration diverges logarithmically and so it would require techniques of renormalization. On the other hand, this kind of charge accumulation is also present in topological insulators, as we will find out in the next section.

It is also insightful to study the current density in the presence of the electromagnetic field, because it gives a direct meaning to the divergence-free current terms in (3.119). For the

simplicity of our discussion, we restrict ourselves to the non-relativistic limit, where $\boldsymbol{\mathcal{B}}^{(\boldsymbol{p})} = -\frac{\lambda_c^2}{2\hbar}\boldsymbol{\sigma} = \frac{\boldsymbol{\mu}_s}{emc^2}$ and $E_P = mc^2 + \boldsymbol{P}^2/2m$, and furthermore, we treat external fields $\boldsymbol{E}$ and $\boldsymbol{B}$ only to linear order. Since we want to study excitations of positive energy, we ignore the completely filled lower band, therefore we safely can drop all corrections due to $\underline{\underline{\Theta}}^{\boldsymbol{rp}}$, since in the non-relativistic situation, factors like $D = 1 - \mathrm{Tr}\underline{\underline{\Theta}}^{\boldsymbol{rp}} = 1 - \frac{2\bar{\mathcal{H}}_{\mathcal{M}}}{mc^2}$ are relevant only for enormous magnetic fields of $\approx 10^{10}T$.

Then our charge density is

$$n(\boldsymbol{R},t) = -e\int \frac{\mathrm{d}^3P}{(2\pi\hbar)^3}\ \bar{\rho}\ ,$$

so that the charge current density becomes with the help of (3.103) and the definition of the spin magnetic moment (c.f. Eq. (3.181))

$$\boldsymbol{j}(\boldsymbol{R},t) = -e\int \frac{\mathrm{d}^3P}{(2\pi\hbar)^3}\ \frac{\boldsymbol{P}}{m}\bar{\rho} - \frac{e}{mc^2}n(\boldsymbol{R},t)\ \boldsymbol{E}\times\boldsymbol{\mu}_s - \boldsymbol{\mu}_s\times\boldsymbol{\nabla}_{\boldsymbol{R}}\, n(\boldsymbol{R},t)\ , \tag{3.185}$$

where the surface term vanishes since we assume our electron momentum to be peaked around some mean value $\boldsymbol{P}_c$. The density $\bar{\rho}$ can be explicitly determined from equation (3.125), here however, we only integrate this equation over all momenta and arrive at the continuity equation

$$\partial_t n(\boldsymbol{R},t) + \boldsymbol{\nabla}_{\boldsymbol{R}}\cdot\boldsymbol{j}(\boldsymbol{R},t) = 0\ . \tag{3.186}$$

The first term in (3.185) is the usual definition of a non-relativistic current, and the second term is the anomalous velocity contribution due to the electric field. Like for the electron wave-packet considered in equation (3.182), using the non-relativistic Pauli Hamiltonian without the distinction between canonical and kinetic variables would yield an anomalous velocity term that is just half of the correct value. However, the last term seems unusual at first as it constitutes a persistent current which itself gives rise to a magnetic moment,

$$\frac{1}{2}\int \mathrm{d}^3R\ \boldsymbol{R}\times\boldsymbol{j}_{\mathrm{per}} = -\frac{1}{2}\int \mathrm{d}^3R\ \boldsymbol{R}\times(\boldsymbol{\mu}_s\times\boldsymbol{\nabla}_{\boldsymbol{R}}\, n) = \boldsymbol{\mu}_s\int \mathrm{d}^3R\ n(\boldsymbol{R},t) = \mathcal{N}\boldsymbol{\mu}_s\ , \tag{3.187}$$

where $\mathcal{N} = 1$ is the number of electrons. This result suggests that the notion of electron spin and this internal persistent current are just different interpretations of the same effect. For example, a magnetic field couples to this circular current via the magnetic moment it generates, and gives rise to the Zeeman energy (3.181). This comes close to the original suggestion of an internal rotation of the electron by Uhlenbeck and Goudsmit [126], yet unlike their idea, it is not the motion of a solid object, instead it is a genuine quantum phenomena, and thus does not suffer the same deficiencies concerning rotation velocities of the electron that would have to be faster than the speed of light.

As discussed before, the spin-orbit term in the Pauli Hamiltonian is *not* gauge invariant, it gives the correct energy spectrum, but not the correct equations of motion. That is why it has not been realized for a long time, as the Pauli Hamiltonian has been mainly put to test with electronic spectra in atoms or solid matter. To explicitly show this point, we go into a different rotated frame so that the Berry connection is changed to $\mathcal{A}_{\boldsymbol{p}} \to \mathcal{A}_{\boldsymbol{p}} + \hbar\boldsymbol{\nabla}_{\boldsymbol{p}}\chi(\boldsymbol{p})$, and we get an additional term in the Pauli Hamiltonian $\hbar(\boldsymbol{\nabla}_{\boldsymbol{p}}\chi)(\partial_{\boldsymbol{r}}V)$. Let us assume for the moment that we are working in momentum space and in the operator representation of

quantum mechanics, where the Hamiltonian formally looks the same. Now, performing a local gauge transformation in momentum space by adding the phase factor $e^{i\chi(\boldsymbol{p})}$ to the wave function, we obtain $e^{-i\chi(\boldsymbol{p})}V(\boldsymbol{r})e^{i\chi(\boldsymbol{p})} = V(\boldsymbol{r} - \hbar\boldsymbol{\nabla}_{\boldsymbol{p}}\chi) = V(\boldsymbol{r}) - \hbar(\boldsymbol{\nabla}_{\boldsymbol{p}}\chi)(\partial_{\boldsymbol{r}}V) + O(\hbar^2)$ which exactly cancels the additional term, and we are left with the original Hamiltonian. Usually, one enforces gauge-invariance in real space to obtain the electromagnetic field. This is a an example of gauge invariance in reciprocal space which leads to the phenomena of spin-orbit interaction, or the anomalous velocity.

In the above analysis, we needed to drop terms of order $\hbar^2$, though here, $\hbar$ is just a formal expansion parameter, the real relevant scale being the Compton wavelength $\lambda_c \equiv \frac{\hbar}{mc}$, when we are assuming that we restrict ourselves to diagonalization matrices $\mathcal{U}_0$ that yield Berry connections $\mathcal{A}_{\boldsymbol{p}}$ with this property. Thus, here we assumed that $\boldsymbol{\nabla}_{\boldsymbol{p}}\chi$ shows the same characteristics in the sense of a low-energy expansion as does $\mathcal{A}_{\boldsymbol{p}}$, i.e. $\boldsymbol{\nabla}_{\boldsymbol{p}}\chi = O(\lambda_c)$. This implies that, having a certain physical regime in mind, some diagonalization matrices $\mathcal{U}_0$ work better than others in the sense that our real expansion parameter is not $\hbar$, but one that is even better suited for the specific physical regime. For example, here, we find that the order of $\hbar\mathcal{A}^{(d)}$ is $\frac{\hbar p}{4m^2c^2} = \lambda_c\frac{v}{c}$ which is to be compared with our position coordinate, where one realizes that corrections are indeed small unless the potential $V(\boldsymbol{r})$ varies strongly on the scale of the Compton wavelength λ_c. The latter is indeed the case for the Coulomb delta-like potential of the nucleus of an atom, and this leads to corrections like the Darwin term which is essential to understand atomic spectra [124]. In conclusion, our real expansion parameter is actually λ_c/ξ, where ξ denotes typical length scales of our system. Here however, just for reasons of simplicity, we have chosen to perform an additional non-relativistic expansion, by keeping only leading order terms in v/c, though we could have kept them and obtain a result valid for relativistic electrons but with Potentials that are smooth on the scale of the Compton wave-length.

Sometimes, one interprets the terms appearing in the Pauli Hamiltonian as being a result from what one called *Zitterbewegung*, and which one envisages as helical motion of the electron. Then the spin-orbit interaction and its physical consequences can be understood as a result of this motion. However, this idea is misleading since, in the effective theory, such motion does not exist when the energy of the excitation is low enough and thus is confined to a single band. When the energy is large enough, there could be interactions with the lower bands by creating virtual electron-positron pairs and then it is not really a good idea to speak of a single electron. In conclusion, one should think of *Zitterbewegung* only in the historical context, where one was still pondering about how to make sense out of the Dirac equation in terms of a single-particle theory which, as we know today is an incomplete description for relativistic electrons.

However, in the case of massless Dirac-Fermions and if one considers excitations in the vicinity of the Dirac point, both positive and negative energy states have to be taken into account simultaneously so that excitations are not confined to positive or negative energies alone. In this scenario as for example in Graphene, one obtains those features termed *Zitterbewegung* [127].

On the other side, in the description restricted to positive energies it makes no sense to talk of point particles, since we cannot resolve beyond the scale of the Compton wave-length. As such, the electron is naturally delocalized in space and we found the appearance of an internal motion in the form of circular persistent currents giving rise to a magnetic dipole moment,

and which exactly corresponds to the spin magnetic moment of the electron.

3.4. Topological Insulators Exchange Coupled to a Ferromagnet with General Magnetization Texture

In order to make use of the full range of our results derived previously, we study the surface Dirac model with arbitrary spatial and time-dependent exchange induced magnetization texture in this section. First, we consider a very general two-band model and find the formulation thereof in the diagonalized frame. Then we will study its topological properties after which we investigate the transport properties when the Fermi-level is shifted into the bands and in the presence of impurities. Finally, we study also the implications of the Dirac Fermions on the magnetization dynamics.

3.4.1. General Two Band Model

Our system has the Hamiltonian

$$\mathcal{H} = -v\boldsymbol{\sigma}(\hat{\boldsymbol{e}}_{\boldsymbol{z}}\times\boldsymbol{p}) - \boldsymbol{M}(\boldsymbol{r},t)\boldsymbol{\sigma} = -\boldsymbol{\zeta}(\boldsymbol{r},\boldsymbol{p},t)\cdot\boldsymbol{\sigma}\ , \tag{3.188}$$

where we defined the vector $\boldsymbol{\zeta}(\boldsymbol{r},\boldsymbol{p},t) \equiv \boldsymbol{M}(\boldsymbol{r},t) + v(\hat{\boldsymbol{e}}_{\boldsymbol{z}}\times\boldsymbol{p})$ which in this form can be rather general with respect to the p-dependence defining the band structure. It can be considered as an effective magnetic field that encodes the complicated dependence on time, space and momentum, and is coupled to the electron spin in the Zeeman-like term. Later, for the explicit calculation of results, we will however return to the leading order term linear in momentum. As in the previous example of the Dirac equation, this system then essentially behaves relativistically. This Hamiltonian is formally equivalent in both operator representation of quantum theory and the Wigner representation, so we can start right away with diagonalization which in this particular case amounts to rotating the spin locally in phase-space and time to point along the direction of $\boldsymbol{\zeta}(\boldsymbol{r},\boldsymbol{p},t)$. There are many possibilities to construct such unitary spin-rotation matrices that perform this task, but in the end, as discussed at length above, this is nothing but the gauge degree of freedom, and our final results representing physical quantities do not depend on the particular choice. We choose

$$\mathcal{U}_0 = \frac{\zeta\mathbb{1}_2 + \sigma_z\mathcal{H}}{\sqrt{2\zeta(\zeta - M_z)}}\ , \tag{3.189}$$

which readily yields

$$\mathcal{U}_0\mathcal{H}\mathcal{U}_0^\dagger = \zeta\sigma_z\ , \tag{3.190}$$

and we defined $\zeta \equiv |\boldsymbol{\zeta}|$ and $M_z = \zeta_3$ is the z-component of $\boldsymbol{\zeta}$. This results shows, to zeroth order in $\hbar$, the dispersion

$$\zeta = \sqrt{M_z^2 + (vp_x + M_y)^2 + (vp_y - M_x)^2} \tag{3.191}$$

of the two positive and negative energy branches. If the Fermi level is at zero energy, i.e. within the gap of energy $2M_z$, the spectrum is particle hole symmetric. M_x and M_y merely shifts the spectrum in the p_x-p_y plane.

In order to reduce redundancy during the calculation, we first treat $\boldsymbol{\zeta} = (\zeta_1, \zeta_2, \zeta_3)$ as independent parameters, and find the Berry connection $\mathcal{A}_{\boldsymbol{\zeta}} = \mathcal{A}^{(d)}_{\boldsymbol{\zeta}} + \mathcal{A}^{(o)}_{\boldsymbol{\zeta}}$

$$\mathcal{A}^{(d)}_{\boldsymbol{\zeta}} = \frac{\boldsymbol{\zeta}\times\hat{\boldsymbol{e}}_{\boldsymbol{z}}}{2\zeta(\zeta - M_z)}\sigma_z \ , \tag{3.192}$$

$$\mathcal{A}^{(o)}_{\boldsymbol{\zeta}} = -\frac{\boldsymbol{\sigma}\times\hat{\boldsymbol{e}}_{\boldsymbol{z}}}{2\zeta} + \frac{(\boldsymbol{\zeta}\times\hat{\boldsymbol{e}}_{\boldsymbol{z}})\cdot\boldsymbol{\sigma}}{2\zeta^2(\zeta - M_z)}(\zeta\hat{\boldsymbol{e}}_{\boldsymbol{z}} - \boldsymbol{\zeta}) \ , \tag{3.193}$$

with the corresponding Berry curvature

$$\boldsymbol{\mathcal{B}}^{(d)}_{\boldsymbol{\zeta}} = \hbar\epsilon_{ijk}\hat{\boldsymbol{e}}_i\partial_{\zeta_j}\mathcal{A}_{\zeta_k} = \sigma_z\frac{\hbar}{2}\frac{\boldsymbol{\zeta}}{\zeta^3} \ . \tag{3.194}$$

Then, $\mathcal{A}_{\boldsymbol{p}} = (\partial_{\boldsymbol{p}}\zeta_k)\mathcal{A}_{\boldsymbol{\zeta}_k} = v\mathcal{A}_{\boldsymbol{\zeta}}\times\hat{\boldsymbol{e}}_{\boldsymbol{z}} + (\partial_{\boldsymbol{p}}M_z)\mathcal{A}_{\zeta_3}$ and $\mathcal{A}_{\boldsymbol{x}} = (\partial_{\boldsymbol{x}}M_k)\mathcal{A}_{\boldsymbol{\zeta}_k}$, while all the desired Berry curvatures can be derived using (i,j are placeholders for any combination of $\boldsymbol{x}$ and $\boldsymbol{\pi}$)

$$\begin{aligned}\hbar(\partial_i\mathcal{A}^{(d)}_j - \partial_j\mathcal{A}^{(d)}_i) = \boldsymbol{\mathcal{B}}^{(d)}_{\boldsymbol{\zeta}}\cdot(\partial_i\boldsymbol{\zeta}\times\partial_j\boldsymbol{\zeta}) &= \sigma_z\frac{\hbar}{2}\frac{\boldsymbol{\zeta}\cdot(\partial_i\boldsymbol{\zeta}\times\partial_j\boldsymbol{\zeta})}{\zeta^3} \\ &= \sigma_z\frac{\hbar}{2}\hat{\boldsymbol{\zeta}}\cdot(\partial_i\hat{\boldsymbol{\zeta}}\times\partial_j\hat{\boldsymbol{\zeta}}) \ .\end{aligned} \tag{3.195}$$

Since $\mathrm{Tr}_2\sigma_z = 0$, we can directly see that the sum rule (3.66) is fulfilled for all Berry curvatures. All the dipole terms are then given by $\underline{\underline{\Omega}} = \zeta\underline{\underline{\Theta}}\sigma_z$ as a result of relation (3.99).

Let us first look at a general momentum dependent mass term $M_z(p)$ and its p-dependence is assumed to be isotropic in momentum space, so that the momentum space magnetic field takes the form

$$\boldsymbol{\mathcal{B}}^{(\boldsymbol{p})} = \sigma_z\frac{\hbar}{2}\frac{v^2}{\zeta^3}\left(M_z(p) - p\frac{\partial M_z}{\partial p} + (\hat{\boldsymbol{e}}_{\boldsymbol{z}}\times\boldsymbol{M})\frac{\boldsymbol{p}}{vp}\frac{\partial M_z}{\partial p}\right)\hat{\boldsymbol{e}}_{\boldsymbol{z}} \ . \tag{3.196}$$

The first Chern number [128] is then simply the Skyrmion number of the vector field

$$\begin{aligned}C_1 &= \frac{1}{2\pi\hbar}\int \mathrm{d}^2p\ \boldsymbol{\mathcal{B}}^{(\boldsymbol{p})}\cdot\hat{\boldsymbol{e}}_{\boldsymbol{z}} = \frac{1}{4\pi}\int \mathrm{d}^2p\ \hat{\boldsymbol{\zeta}}\cdot(\partial_{p_x}\hat{\boldsymbol{\zeta}}\times\partial_{p_y}\hat{\boldsymbol{\zeta}}) \\ &= \sigma_z\frac{v^2}{4\pi}\int \mathrm{d}^2p\ \frac{M_z(p) - p\partial_pM_z}{(M_z(p)^2 + v^2p_x^2 + v^2p_y^2)^{3/2}} = \frac{\sigma_z}{2}\int_0^\infty \mathrm{d}p\ \partial_p\frac{-M_z(p)}{(M_z(p)^2 + v^2p^2)^{1/2}} \\ &= \frac{\sigma_z}{2}\left(\mathrm{sgn}(M_z(0)) - \mathrm{sgn}(M_z(\infty))\right) \ ,\end{aligned} \tag{3.197}$$

and is the topological quantum number characterizing the state of matter described by our Hamiltonian $\mathcal{H}$. We see that, when $M_z(0)$ and $M_z(\infty)$ have the same sign, we are in the topologically trivial regime and if they have opposite sign, the Hamiltonian (3.188) describes a topological quantum state. In the derivation, we assumed that $M_z(p)$ asymptotically behaves at least as $O(p^2)$ when $p \to \infty$. If $M_z(p)$ goes slower to infinity than p^2, or even does not vary significantly with p, we simply get

$$C_1 = \frac{\sigma_z}{2}\,\mathrm{sgn}(M_z(0))$$

for the Cern number which then characterizes a half-integer quantum Hall state. Here, and in the subsequent investigation, we can interpret σ_z as the band index, where $\sigma_z = -1$ for the lower (valence) band and $\sigma_z = +1$ for the upper (conduction) band.

In the following, we will only consider the latter scenario of constant M_z. Then the real space magnetic field is

$$\boldsymbol{\mathcal{B}}^{(r)} = \sigma_z \frac{\hbar}{2} \hat{\boldsymbol{e}}_{\boldsymbol{z}} \frac{1}{\zeta^3} (\partial_x \boldsymbol{M} \times \partial_y \boldsymbol{M}) \cdot \boldsymbol{\zeta} \ , \tag{3.198}$$

and the corresponding effective electric fields read

$$\boldsymbol{\mathcal{E}}^{(p)} = \sigma_z \frac{\hbar}{2} \hat{\boldsymbol{\zeta}} \cdot \left(\partial_{\boldsymbol{p}} \hat{\boldsymbol{\zeta}} \times \partial_t \hat{\boldsymbol{\zeta}} \right) = \sigma_z \frac{\hbar}{2} \frac{v}{\zeta^3} \left(\boldsymbol{\zeta} \partial_t M_z - M_z \partial_t \boldsymbol{M} \right) \tag{3.199}$$

$$\boldsymbol{\mathcal{E}}^{(r)} = \sigma_z \frac{\hbar}{2} \hat{\boldsymbol{\zeta}} \cdot \left(\partial_{\boldsymbol{r}} \hat{\boldsymbol{\zeta}} \times \partial_t \hat{\boldsymbol{\zeta}} \right) = \sigma_z \frac{\hbar}{2} \frac{1}{\zeta^3} \boldsymbol{\zeta} \cdot (\partial_{\boldsymbol{r}} \boldsymbol{M} \times \partial_t \boldsymbol{M}) \ , \tag{3.200}$$

and finally the tensor

$$\underline{\underline{\Theta}}^{\boldsymbol{rp}}_{ij} = \sigma_z \frac{\hbar}{2} \frac{v}{\zeta} (-\hat{\boldsymbol{\zeta}}) \cdot ((\hat{\boldsymbol{e}}_{\boldsymbol{z}} \times \hat{e}_j \partial_{r_i}) \times \hat{\boldsymbol{\zeta}}) \ . \tag{3.201}$$

In the presence of an external electromagnetic field, the effective fields are simply modified according to (3.160)-(3.164) which of course satisfies $\boldsymbol{\nabla}_{\boldsymbol{R}} \times \boldsymbol{\mathcal{E}}^{(r)} + \partial_t \boldsymbol{\mathcal{B}}^{(r)} = 0$.

The Hamiltonian in the rotated frame takes the form

$$\begin{aligned} \bar{\mathcal{H}} &= \zeta \sigma_z + \mathrm{Tr} \underline{\underline{\Omega}}^{\boldsymbol{rp}} = \zeta \sigma_z + \zeta \mathrm{Tr}_2 \left\{ \frac{\sigma_z}{2} \mathrm{Tr} \underline{\underline{\Theta}}'^{\boldsymbol{rp}} \right\} \sigma_0 \\ &= \zeta \sigma_z + \frac{\hbar}{2} \frac{v}{\zeta^2} \left(q v M_z (\boldsymbol{B} \hat{\boldsymbol{e}}_{\boldsymbol{z}}) - \boldsymbol{\zeta} \cdot ((\hat{\boldsymbol{e}}_{\boldsymbol{z}} \times \boldsymbol{\nabla}) \times \boldsymbol{M}) \right) \sigma_0 \ , \end{aligned} \tag{3.202}$$

where we used expression (3.100) which in the case of a two level system relates $\underline{\underline{\Theta}}^{\boldsymbol{rp}}$ to $\underline{\underline{\Omega}}^{\boldsymbol{rp}}$ and thus the magnetic dipole energy $\bar{\mathcal{H}}_{\mathcal{M}}$, and from (3.164) we know $\mathrm{Tr} \underline{\underline{\Theta}}'^{\boldsymbol{rp}} = \mathrm{Tr} \underline{\underline{\Theta}}^{\boldsymbol{rp}} + q \boldsymbol{B} \boldsymbol{\mathcal{B}}^{(p)}$.

We can further rewrite the magnetic dipole energy as

$$\bar{\mathcal{H}}_{\mathcal{M}} = -\boldsymbol{\mu} \cdot \left(\boldsymbol{B}(\boldsymbol{R}, t) - \frac{1}{qv} (\hat{\boldsymbol{e}}_{\boldsymbol{z}} \times \boldsymbol{\nabla}) \times \boldsymbol{M} \right) \equiv -\boldsymbol{\mu} \cdot \boldsymbol{\mathcal{B}}^{\mathrm{eff}} \tag{3.203}$$

where we defined the magnetic moment

$$\boldsymbol{\mu} = -\frac{\hbar}{2} \frac{q v^2}{\zeta} \hat{\boldsymbol{\zeta}} \tag{3.204}$$

with an effective mass $m_{\mathrm{eff}} = \zeta / v^2$ as compared to the Bohr magneton $\mu_{\mathrm{B}} = \frac{e\hbar}{2m}$ for the spin of a free relativistic electron.

3.4.2. Topological Properties

Let us first discuss these results for completely filled bands, for which one essentially has to perform the integral over the complete momentum space [11]

$$\sigma_z \frac{M_z \hbar}{2} \int \frac{\mathrm{d}^2 P}{(2\pi\hbar)^2} \frac{1}{\zeta^3} = \frac{M_z}{4\pi\hbar} \int \frac{P \mathrm{d} P}{(v^2 P^2 + M_z^2)^{3/2}} = \frac{\sigma_z}{2hv^2} \mathrm{sgn}(M_z) = \frac{C_1}{hv^2} \ , \tag{3.205}$$

[11] We can simply put $\rho \equiv 1$, since the integral is well converging, no special care is required for large momentum.

where the components M_x and M_y disappear, because they merely shift the momentum. When the Fermi-level is inside the gap, i.e. only the lower band is occupied, then $C_1 = -\frac{1}{2}\,\mathrm{sgn}(M_z)$. Next, we find that

$$\int \frac{\mathrm{d}^2P}{(2\pi\hbar)^2}\underline{\underline{\Theta}}^{\boldsymbol{rp}} = \frac{C_1}{hv}\partial_{r_i}M_j \ , \tag{3.206}$$

which, according to (3.75), (3.82) or (3.118) is related to local charge density excitations in the system,

$$n(\boldsymbol{R},t) = -\int \frac{\mathrm{d}^2P}{(2\pi\hbar)^2}\mathrm{Tr}\underline{\underline{\Theta}}^{\boldsymbol{rp}} = -\frac{C_1}{hv}\left(\boldsymbol{\nabla}\cdot\boldsymbol{M} + vq\boldsymbol{B}(\boldsymbol{R})\hat{\boldsymbol{e}}_{\boldsymbol{z}}\right) = -\frac{C_1}{hv}\boldsymbol{\mathcal{B}}^{\mathrm{eff}}\cdot\hat{\boldsymbol{e}}_{\boldsymbol{z}} \ , \tag{3.207}$$

where $n(\boldsymbol{R},t)$ describes the additional charge with respect to the homogeneous ground state, and in the last step, we introduced the effective magnetic field as in (3.203) which describes the total action of the external magnetic field and the effect of the ferromagnetic exchange field. This induced charge due to a magnetization texture on top of a topological insulator has been found in [129] and is given by the divergence of the magnetization structure $\boldsymbol{\nabla}\cdot\boldsymbol{M}$. The magnetic field term of this result is well known in the context of the integer quantum Hall effect.

For the moment, we only need to consider the fictitious electric field $\boldsymbol{\mathcal{E}}^{(\boldsymbol{p})}$ from the expression of the current density (3.119), since, as we will find out shortly, the other terms only yield a finite contribution, when the Fermi level is not inside the gap. Performing the momentum integration, one readily finds

$$\boldsymbol{j}(\boldsymbol{R},t) = -\int \frac{\mathrm{d}^2P}{(2\pi\hbar)^2}\ \left(\boldsymbol{\mathcal{E}}^{(\boldsymbol{p})} + q\boldsymbol{E}\times\boldsymbol{\mathcal{B}}^{(\boldsymbol{p})}\right) = \frac{C_1}{hv}\partial_t\boldsymbol{M}_\perp + \frac{qC_1}{h}\hat{\boldsymbol{e}}_{\boldsymbol{z}}\times\boldsymbol{E} \ , \tag{3.208}$$

where $\boldsymbol{M}_\perp$ is the magnetization in the x-y plane. The first term of this result emerges from the effective field $\boldsymbol{\mathcal{E}}^{(\boldsymbol{p})}$ and describes an adiabatic pumping process, which has also been derived in the work of Nomura *et al.* [129]. The second term is due to $q\boldsymbol{E}\times\boldsymbol{\mathcal{B}}^{(\boldsymbol{p})}$, and constitutes the counterpart to the magnetic field term in the induced density $n(\boldsymbol{R},t)$, and consequently describes the transverse Hall current in the Quantum Hall state. We readily find that the continuity equation is satisfied,

$$\partial_t n(\boldsymbol{R}) + \boldsymbol{\nabla}\cdot\boldsymbol{j}(\boldsymbol{R}) = 0 \ , \tag{3.209}$$

by making use of the Maxwell equations for the external electromagnetic field, $\boldsymbol{\nabla}\times\boldsymbol{E}+\partial_t\boldsymbol{B} = 0$.

According to the definition of the polarization (3.141), the ferromagnetic exchange field $\boldsymbol{M}(\boldsymbol{R},t)$ gives rise to the topological contribution to the electric polarization,

$$\boldsymbol{\mathfrak{P}}(\boldsymbol{R},t) = \frac{C_1}{hv}\boldsymbol{M}_\perp(\boldsymbol{R},t) \ , \tag{3.210}$$

and is a direct result of the coupling between spin and orbit degrees of freedom. In the derivation thereof, we assume that time-dependency of $\boldsymbol{M}(\boldsymbol{R},t)$ is sufficiently slow to be adiabatic, moreover, in the case of stationary $\boldsymbol{M}$, we argue that we adiabatically turn on the exchange field from $\boldsymbol{M}(\boldsymbol{R},\tau=0) = 0$ to $\boldsymbol{M}(\boldsymbol{R},\tau=T) = \boldsymbol{M}(\boldsymbol{R},t)$.

The terms are proportional to the Chern number C_1 and constitute the topological response of the system, since they are invariant with respect to smooth deformations of the system, as long as the Fermi level resides inside the gap which here is given by the mass M_z. The topological response can be conveniently encoded in the Chern-Simons action [128],

$$\delta S_{\mathrm{CS}} = -\frac{qC_1}{2h} \int \mathrm{d}^2 R \int \mathrm{d}t \; \epsilon^{\mu\nu\tau} \mathcal{A}^{\mathrm{eff}}_{\mu} \partial_{\nu} \mathcal{A}^{\mathrm{eff}}_{\tau} \; , \tag{3.211}$$

so that the particle current is $j_\mu(\boldsymbol{R}) = \delta S_{\mathrm{CS}}/\delta A^{\mathrm{eff}}_{\mu} = (n, \boldsymbol{j})_\mu$. Greek indices run over $0, 1, 2$ and denote temporal (t) and spatial (X, Y) variables, while the effective vector potential that is linked to $\boldsymbol{\mathcal{B}}^{\mathrm{eff}}(\boldsymbol{R}, t)$ is defined as

$$\boldsymbol{\mathcal{A}}^{\mathrm{eff}}(\boldsymbol{R}, t) = (A_0, \boldsymbol{A} + \frac{1}{qv} \; \hat{\boldsymbol{e}}_{\boldsymbol{z}} \times \boldsymbol{M}) \; , \tag{3.212}$$

in accordance with [129].

We remark that, within this 2-dimensional description of the surface electrons, only the M_x and M_y components contribute to $\boldsymbol{\mathcal{B}}^{\mathrm{eff}}$, while M_z appears as a mass term that yields different effects. The reason is that M_z cannot be combined with the momentum as it is the case for the other two components. Therefore, it only makes sense to consider the z-component of $\boldsymbol{\mathcal{B}}^{\mathrm{eff}}$,

$$\boldsymbol{\mathcal{B}}^{\mathrm{eff}} \cdot \hat{\boldsymbol{e}}_{\boldsymbol{z}} \equiv \hat{\boldsymbol{e}}_{\boldsymbol{z}} \cdot \boldsymbol{B}(\boldsymbol{R}) + \frac{1}{qv} \boldsymbol{\nabla} \cdot \boldsymbol{M} \tag{3.213}$$

and moreover, the transverse components of $\boldsymbol{B}(\boldsymbol{R})$ are not coherently treated in this reduced 2 dimensional description, for we cannot minimally couple to p_z as it does not exist. For this reason, it is meaningful only to consider the z-component of the external magnetic field and we should resort to the full 3D dimensional bulk description of the strong topological insulator [130], in order to properly treat all components of the full external magnetic field. The full 4-band low-energy effective description which is for example applicable for Bi_2Te_3 or Bi_2Se_3, can then be also used to study thin films.

3.4.3. Towards, and In The Metallic Regime

If we drive our system into the metallic regime by shifting the Fermi level into the bands, we will get additional non-topological contributions which can be calculated straightforwardly using the formalism described in section 3.1.5. In a quasi-stationary situation, the density matrix is essentially the equilibrium one,

$$\bar{\rho}_{\mathrm{eq}} = f_{\mathrm{D}}(E - E_{\mathrm{F}}) \; \delta(E - (\sigma_z \zeta + \bar{\mathcal{H}}_{\mathcal{M}})) \; , \tag{3.214}$$

and we can integrate over the gauge invariant energy, since it plays no role in the present investigation (we essentially evaluate all transport quantities at the Fermi level E_{F}, like the relaxation times), so that

$$\begin{aligned} \bar{\rho}_{\mathrm{eq}}(t, \boldsymbol{R}, \boldsymbol{P}) &= f_{\mathrm{D}}(\sigma_z \zeta(t, \boldsymbol{R}, \boldsymbol{P}) + \bar{\mathcal{H}}_{\mathcal{M}} - E_{\mathrm{F}}) \\ &= \bar{\rho}_0 + \bar{\rho}_1 = f_{\mathrm{D}}(\sigma_z \zeta - E_{\mathrm{F}}) + \sigma_z \bar{\mathcal{H}}_{\mathcal{M}} \partial_\zeta \bar{\rho}_0 \; , \end{aligned} \tag{3.215}$$

which in the zero temperature approximation simply becomes a delta function, $f'_{\rm D}(\zeta\sigma_z - E_{\rm F}) = -\delta(\zeta\sigma_z - E_{\rm F})$, and which naturally is zero when $|E_{\rm F}| \leq |M_z|$, i.e. when the Fermi level is inside the gap.

The presence of impurities leads to momentum relaxation which in the simplest model can be incorporated phenomenologically by introducing the relaxation time τ, or as in section 2.2.1, by calculating the self-energy for the impurity potentials which leads to the appearance of the collision integral in the transport equation. Then, assuming low-energy transport and isotropic scattering, one can reduce the effect of the collision integral to a single parameter, the scattering time evaluated at the Fermi-level $\tau = \tau(E_{\rm F})$. Either way, and neglecting gradient corrections to the collision integral, one arrives at the Boltzmann equation in relaxation time approximation which in the rotated frame takes the form (see eqn. (3.125))

$$\left(\partial_t + \frac{{\rm d}\boldsymbol{R}}{{\rm d}t}\boldsymbol{\nabla}_R + \frac{{\rm d}\boldsymbol{P}}{{\rm d}t}\boldsymbol{\nabla}_P\right)\bar{\rho} = -\frac{\bar{\rho} - \bar{\rho}_{\rm eq}}{\tau} \ . \tag{3.216}$$

With the help of expressions (3.103) and (3.104), one can solve this equation for the non-equilibrium part of the density matrix, $\bar{\rho} = \bar{\rho}_{\rm neq} + \bar{\rho}_{\rm eq}$ which in linear response reads

$$\bar{\rho}_{\rm neq} = -\tau\left(\partial_t\bar{\rho}_0 - e\frac{\partial\bar{\rho}_0}{\partial\boldsymbol{P}}(\mathbb{1} + \underline{\underline{\Theta}}^{\boldsymbol{rp}})\boldsymbol{E} + e(\boldsymbol{E}\times\boldsymbol{\mathcal{B}}^{(\boldsymbol{p})})\cdot\frac{\partial\bar{\rho}_0}{\partial\boldsymbol{R}}\right) \ . \tag{3.217}$$

We should emphasize that the persistent current contributions in (3.119) are crucial for the correct density, since they cancel terms that would be divergent upon momentum integration. In particular, when the Fermi level is inside the gap, these dipolar terms give finite contributions which exactly compensate the terms due to $\underline{\underline{\Theta}}^{\boldsymbol{rp}}$ and $\boldsymbol{\mathcal{B}}^{(\boldsymbol{p})}$ in equation (3.119) together with (3.103). This is also the reason why we needed to consider only the effective electric field $\boldsymbol{\mathcal{E}}^{(\boldsymbol{p})}$ for the topological contribution of the current (3.207). Let us therefore bring the expression for the current density into a more convenient form.
According to result (3.99), we have the simple relation $\underline{\underline{\Omega}} = \sigma_z\zeta\underline{\underline{\Theta}}$ in the case of a two band model, and splitting off the magnetic dipole energy from the density matrix $\bar{\rho}_{\rm eq} = \bar{\rho}_0 + \bar{\rho}_1 = \bar{\rho}_0 + \sigma_z\bar{\mathcal{H}}_{\mathcal{M}}\partial_\zeta\bar{\rho}_0$, we find that many terms cancel in the expression for the equilibrium current density (3.119), so that using identity (3.116), and after some algebra, one eventually arrives at

$$\begin{aligned}\boldsymbol{j}_{\rm eq}(\boldsymbol{R},t) = \int\frac{{\rm d}^2P}{(2\pi\hbar)^2}\ {\rm Tr}_2\bar{\rho}_0\left(\frac{\partial\zeta}{\partial\boldsymbol{P}}\sigma_z - \boldsymbol{\mathcal{E}}^{(\boldsymbol{p})} - q\boldsymbol{E}\times\boldsymbol{\mathcal{B}}^{(\boldsymbol{p})}\right)\\ + \int\frac{{\rm d}^2P}{(2\pi\hbar)^2}\ {\rm Tr}_2\left(\frac{\partial\bar{\rho}_0}{\partial\boldsymbol{P}}{\rm Tr}\underline{\underline{\Omega}}^{\boldsymbol{rp}} - \frac{\partial\bar{\rho}_0}{\partial\boldsymbol{R}}\times\boldsymbol{\Omega}^{\boldsymbol{pp}} - \underline{\underline{\Omega}}^{\boldsymbol{rp}}\frac{\partial\bar{\rho}_0}{\partial\boldsymbol{P}}\right) \ .\end{aligned} \tag{3.218}$$

In this expression, we can simply substitute the primed quantities from (3.160)-(3.164) in order to obtain the influence of an external magnetic field. The second integral in this result now gives only contributions that are on-shell, due to the appearance of derivatives of the density matrix, which become sharply peaked around the Fermi level $E_{\rm F}$ for sufficiently low temperatures.

Let us first consider the equilibrium current, i.e. in absence of time-dependence and the electric field, then $\bar{\rho}_0 = f_{\rm D}(\sigma_z\zeta - E_{\rm F})$ and due to $\frac{\partial\bar{\rho}_0}{\partial\boldsymbol{R}} = \sigma_z f'_{\rm D}(\sigma_z\zeta - E_{\rm F})\frac{\partial\zeta}{\partial\boldsymbol{R}}$, contributions

from the two bands have opposite signs. Since $\bar{\rho}_0$ is isotropic in momentum space, only the last integral in (3.218) contributes to the equilibrium current, and we obtain

$$\begin{aligned}\boldsymbol{j}_{\mathrm{eq}}(\boldsymbol{R}) &= \sum_{\sigma_z} \frac{\hbar v^2}{2} \sigma_z (\hat{\boldsymbol{e}}_{\boldsymbol{z}} \times \boldsymbol{\nabla}) M_z \int \frac{\mathrm{d}^2 P}{(2\pi\hbar)^2} \frac{1}{\zeta} f'_{\mathrm{D}}(\sigma_z \zeta - E_{\mathrm{F}}) \\ &= -\frac{1}{2h} \Theta(|E_{\mathrm{F}}| - |M_z|) \operatorname{sgn}(E_{\mathrm{F}}) \ (\hat{\boldsymbol{e}}_{\boldsymbol{z}} \times \boldsymbol{\nabla}) M_z \ , \end{aligned} \tag{3.219}$$

where we used the zero-temperature approximation $f'_{\mathrm{D}}(\epsilon) = -\delta(\epsilon)$ and the sum over σ_z is equal to taking the trace over the bands. Since $\boldsymbol{\nabla} \cdot (\hat{\boldsymbol{e}}_{\boldsymbol{z}} \times \boldsymbol{\nabla}) = 0$, this equilibrium current (3.219) is divergence-free and appears at gradients of the mass term M_z, and in particular, we find the current flow along domain boundaries that lead to circular currents. This equilibrium current is independent of E_{F}, however, of opposite sign for the two bands and vanishes when E_{F} is inside the gap. We will consistently recover this behavior later in section 4.5, when studying domain walls on strong topological insulators, or in section 4.3, where the zero energy bound states at a domain-wall are found to be chiral. Furthermore, we will find later that this current is responsible for an anisotropic exchange interaction contribution for the magnetization $\boldsymbol{M}$.

We can now also study what happens to the topological contributions to the densities (3.207) and (3.208), when the Fermi level moves into the band,

$$n(\boldsymbol{R}) = -\sum_{\sigma_z} \int \frac{\mathrm{d}^2 P}{(2\pi\hbar)^2} \ f_{\mathrm{D}}(\sigma_z \zeta - E_{\mathrm{F}}) \mathrm{Tr} \underline{\underline{\Theta}}^{\boldsymbol{rp}} = \frac{M_z}{2hv|E_{\mathrm{F}}|} \left(\boldsymbol{\nabla} \cdot \boldsymbol{M} + vq \boldsymbol{B}(\boldsymbol{R}) \hat{\boldsymbol{e}}_{\boldsymbol{z}} \right) \ , \tag{3.220}$$

$$\boldsymbol{j}(\boldsymbol{R}) = -\sum_{\sigma_z} \int \frac{\mathrm{d}^2 P}{(2\pi\hbar)^2} \ f_{\mathrm{D}}(\sigma_z \zeta - E_{\mathrm{F}}) \left(\boldsymbol{\mathcal{E}}^{(\boldsymbol{p})} + q \boldsymbol{E} \times \boldsymbol{\mathcal{B}}^{(\boldsymbol{p})} \right) = -\frac{M_z}{2hv|E_{\mathrm{F}}|} \left(\partial_t \boldsymbol{M}_\perp + vq \ \hat{\boldsymbol{e}}_{\boldsymbol{z}} \times \boldsymbol{E} \right) \ . \tag{3.221}$$

If the Fermi-level is inside the gap, we need to substitute $|E_{\mathrm{F}}| = |M_z|$ and recover results (3.207) and (3.208) and when it moves into either of the two bands, it monotonously decreases as the Fermi level moves further away from the gap.

We have seen that the response due to the external electromagnetic field and the ferromagnetic exchange field $\boldsymbol{M}$ always appeared in the combined form $\boldsymbol{\mathcal{B}}^{\mathrm{eff}}$, so one might conclude that both can be simply mapped onto each other, and it is sufficient to consider only either of them, however, this conclusion is too premature. Of course, such a mapping would only make sense for the M_x and M_y components since there is no momentum in z-direction which could absorb M_z, so we forget about the M_z-component for the moment. At best, it would be possible to treat this question within the full bulk description of the STI mentioned earlier. Indeed, on the one side, the topologically induced charge and currents due to a magnetization structure appears on equal footing as the external electromagnetic field and likewise for the Hamiltonian (see result (3.203)), so the energy spectrum can be simply mapped onto each other by virtue of (3.213). Yet, on the other side, the kinetic variables differ, which results in different equations of motion that cannot be mapped onto each other easily, and which is best seen at equation of motion for the kinetic momentum (3.167), where the external magnetic field enters as expected, whereas the action of $\boldsymbol{M}$ does *not* enter as $\boldsymbol{\nabla} \cdot \boldsymbol{M}$, as $\boldsymbol{\mathcal{B}}^{\mathrm{eff}}$ would suggest.

Instead, it enters as $\boldsymbol{\mathcal{B}}^{(r)}$ according to result (3.198), which is rather different. Furthermore, we will find an explicit dependency on the combination $\boldsymbol{\nabla}\times\boldsymbol{M}$ later in result (3.233). In conclusion, it means that despite the identical band structure, we have a different motion of the electrons. The situation of spin-momentum locking due to the Rashba spin-orbit term in (3.188) is actually quite different from the study of ferromagnetic conductors with momentum isotropic dispersion $\propto p^2\mathbb{1}$, where the diagonalization transformation depends only on position [73], so that the momentum operator turns into its gauge invariant counterpart, analogously to an external magnetic field. Thus, both magnetic and exchange fields can be mapped onto each other, at least as long as transitions between spin-up and -down bands can be neglected.

This system describing a topological state of matter has the property that zero bound states may emerge under certain conditions, which will be investigated in section (4.3). However, since these states lie within the gap, they are not straightforwardly accessible within this formulation, as they involve coherent excitations shared between two bands.

3.4.4. Magnetization Dynamics and Transport Properties

Finally, we are interested in the representation of the Pauli spin-operator $\boldsymbol{\sigma}$ in the diagonalized frame, which can be rather straightforwardly obtained by virtue of results (3.83) and (3.84). In order to do so, we first need to rotate $\boldsymbol{\sigma}$ by $\mathcal{U}_0$, so that for the diagonal part, we simply have

$$\bar{\boldsymbol{\Sigma}}_0^{(d)} = \mathcal{P}_d\mathcal{U}_0\,\boldsymbol{\sigma}\,\mathcal{U}_0^\dagger\mathcal{P}_d = -\hat{\boldsymbol{\zeta}}\sigma_z\ , \tag{3.222}$$

and our notation is such that $\bar{\boldsymbol{\Sigma}}$ denotes the spin operator in the diagonalized frame, in contrast to the usual Pauli matrices $\boldsymbol{\sigma}$. Then from (3.83) and (3.84) one finds $\bar{\boldsymbol{\Sigma}}_1^{(d)} = \sigma_z\mathrm{Tr}\underline{\underline{\Theta}}^{\boldsymbol{p}}\hat{\boldsymbol{\zeta}}$. The off-diagonal part $\bar{\boldsymbol{\Sigma}}_0^{(o)}$ is not gauge-invariant, and becomes meaningful only after plugging it into the expression for the corresponding density (3.120), so we explicitly give only the result $\frac{\hbar}{2}\{\mathcal{A}_\alpha,\bar{\boldsymbol{\Sigma}}_0^{(o)}\} = \frac{\hbar}{2}\hat{\boldsymbol{\zeta}}\times\partial_\alpha\hat{\boldsymbol{\zeta}}$.

Furthermore, we need to determine $\mathcal{Y}_1$ which, in the present gauge, is given by the condition $[\mathcal{Y}_1,\bar{\mathcal{H}}_0] = \hbar\mathcal{A}_t$, and it is easily found using for example (3.29). Then,

$$\mathcal{P}_d\left[\mathcal{Y}_1,\bar{\boldsymbol{\Sigma}}_0^{(o)}\right]\mathcal{P}_d = -\sigma_z\frac{\hbar}{2\zeta^3}\,(\boldsymbol{\zeta}\times\partial_t\boldsymbol{\zeta}) \tag{3.223}$$

is gauge-invariant and incorporates the dynamics of diagonalization transformation due to $\mathcal{U}$ specified in Eq. (3.189). As we will see later, this term will be responsible for the appearance of the contributions analogous to the fictitious electric field term $\boldsymbol{\mathcal{E}}^{(\boldsymbol{p})}$ and thus, shows the importance discussed at the beginning of this chapter.

Plugging our results for $\bar{\boldsymbol{\Sigma}}$ into (3.120), one obtains an expression for direct calculation of spin-expectation values. Here, we give the spin quasi-probability distribution

$$\begin{aligned}\mathfrak{s}(\boldsymbol{R},t,\boldsymbol{P}) \equiv\ \mathrm{Tr}_2\bar{\rho}\bar{\boldsymbol{\Sigma}}_0^{(d)} + \frac{\hbar}{2\zeta^2}\mathrm{Tr}_2\left[\left(\boldsymbol{\zeta}\times\frac{\partial\boldsymbol{\zeta}}{\partial R_k}\right)\frac{\partial\bar{\rho}}{\partial P_k} - \left(\boldsymbol{\zeta}\times\frac{\partial\boldsymbol{\zeta}}{\partial P_k}\right)\frac{\partial\bar{\rho}}{\partial R_k}\right]\\ - \frac{\hbar}{2\zeta^3}\left[(\boldsymbol{\zeta}\times\partial_t\boldsymbol{\zeta}) - vqM_z\boldsymbol{E}_\perp\right]\ \mathrm{Tr}_2\bar{\rho}\sigma_z\ ,\end{aligned} \tag{3.224}$$

which, after integration over all momenta $\boldsymbol{P}$, gives the physically meaningful spin-density and then corresponds to the spin-density operator $\boldsymbol{S}(\boldsymbol{r}) = \delta(\hat{\boldsymbol{r}} - \boldsymbol{r})\boldsymbol{\sigma}$ in the original frame.

After all, this result should be related to the current, since in the original frame we have the simple expression (4.4) which in the rotated frame translates into the current

$$\boldsymbol{j} = v\hat{\boldsymbol{e}}_{\boldsymbol{z}} \times \mathfrak{s} \ , \tag{3.225}$$

and thus is directly related to the expectation value of the magnetization. In fact, it can be shown that $v\hat{\boldsymbol{e}}_{\boldsymbol{z}} \times \mathfrak{s}$ is equivalent to (3.114) for the present Hamiltonian, or more directly, it is the same as result (3.218) which is derived above for the case of a two-band model. For example, the last term in (3.224) is easily seen to be equivalent to $-\boldsymbol{\mathcal{E}}^{(\boldsymbol{p})}$. So, in the current study, the x and y-components of the spin-density can be directly obtained from the current-density (e.g. from result (3.221)), while the z-component should be calculated using (3.224).

The results obtained in the following can be used to study the magnetization dynamics of ultra-thin magnetic films deposited on top of the topological insulator. There are few works that address these questions [131, 132], and we will recover some of their results and discuss the differences and new findings. Now it is just a matter of substituting the densities into expression (3.224) and integrate over all momenta, which poses no major difficulties, so we present the results right away.

First, the external electric field induces the non-equilibrium spin-density

$$\boldsymbol{s}_E(\boldsymbol{R}, t) = \frac{\sigma_\parallel}{ve}(\hat{\boldsymbol{e}}_{\boldsymbol{z}} \times \boldsymbol{E}) \ , \tag{3.226}$$

which according to (3.225) gives rise to the expected charge current density, $\boldsymbol{j}_E = \sigma_\parallel \boldsymbol{E}$, with the expression for the longitudinal conductivity,

$$\sigma_\parallel \equiv \Theta(|E_\mathrm{F}| - |M_z|)\frac{e^2\tau(E_\mathrm{F}^2 - M_z^2)}{4\pi\hbar^2|E_\mathrm{F}|} \ . \tag{3.227}$$

Of course, $\sigma_\parallel$ is zero when E_F lies inside the gap and which is the purpose of the Heaviside theta function here. The contribution $\boldsymbol{s}_E$ has been obtained in the work of Yokoyama *et al.* [131], and constitutes an additional anisotropy field for the magnetization dynamics.

Furthermore, the intrinsic contribution to the spin density, which is a direct consequence of the Berry curvature $\boldsymbol{\mathcal{E}}^{(\boldsymbol{p})}$, is readily found to be

$$\boldsymbol{s}_\mathrm{in}(\boldsymbol{R}, t) = \frac{\sigma_\mathrm{H}}{ev}\left[\boldsymbol{E}_\perp + \frac{1}{ve}\hat{\boldsymbol{e}}_{\boldsymbol{z}} \times \partial_t \boldsymbol{M}\right], \tag{3.228}$$

which can be directly obtained by virtue of the current density (3.221) and (3.225), and the Hall conductivity is given by

$$\sigma_\mathrm{H} \equiv \frac{e^2 M_z}{4\pi\hbar|E_\mathrm{F}|} \ . \tag{3.229}$$

Alternatively, one can substitute $\bar{\rho}_\mathrm{eq}$ into the last term of (3.224) and arrive at the same result. The density $\boldsymbol{s}_\mathrm{in}$ relates to the Hall current $\boldsymbol{j}_\mathrm{H} = \sigma_\mathrm{H}\hat{\boldsymbol{e}}_{\boldsymbol{z}} \times \boldsymbol{E}$, which is readily seen using

(3.225). This term has been obtained for the case of the Fermi-level inside the gap [132], so that only the topological contribution remains, which corresponds to the given result for $\boldsymbol{s}_{\text{in}}$ with $E_{\text{F}} = M_z$.

The plain magnetization of the bands is

$$\boldsymbol{s}_0(\boldsymbol{R},t) = \frac{(|E_{\text{cutoff}}| - |E_{\text{F}}|)M_z}{2\pi\hbar^2 v^2}\hat{\boldsymbol{e}}_{\boldsymbol{z}} = s_{0,\text{gap}}(\boldsymbol{R},t)\hat{\boldsymbol{e}}_{\boldsymbol{z}} - \frac{|E_{\text{F}}|M_z}{2\pi\hbar^2 v^2}\hat{\boldsymbol{e}}_{\boldsymbol{z}} \tag{3.230}$$

where the cutoff energy $|E_{\text{cutoff}}| > |E_{\text{F}}|$ has been introduced to cope with the diverging momentum integral, and is defined such that when the Fermi level is inside the gap it yields the equilibrium magnetization of the completely filled lower band. We see that for a homogeneous magnetization, we can induce only a z-components with the same orientation as M_z, since the transverse components M_x and M_y merely shift the momentum and thus play no role after isotropic momentum integration. As the Fermi-level moves away from the gap, it symmetrically reduces this value. As we will see now, the situation changes when the magnetization is inhomogeneous so that there are non-vanishing gradients.

All the remaining contributions to $\boldsymbol{s}$ are only non-vanishing when the Fermi level is inside the bands. Then, evaluating for $\bar{\rho}_{\text{eq}}$ from (3.215), we find the induced anisotropic exchange interaction mediated by the Dirac Fermions,

$$\boldsymbol{s}_{\text{xc}}(\boldsymbol{R},t) = \Theta(|E_{\text{F}}| - |M_z|)\frac{\text{sgn}(E_{\text{F}})}{4\pi\hbar v}\ \left[\hat{\boldsymbol{e}}_{\boldsymbol{z}}(\boldsymbol{\nabla}\cdot\boldsymbol{M}) - \boldsymbol{\nabla}M_z\right]\ , \tag{3.231}$$

with the respective current (3.219). We see that this term has opposite signs for conduction and valence bands, which stems from the fact that both bands have opposite chirality.

Using the non-equilibrium density calculated in (3.217), we obtain the contribution from the Dirac Fermions to the Gilbert damping

$$\boldsymbol{s}_{\text{damp}}(\boldsymbol{R},t) = -\alpha_{xy}\partial_t M_\perp - \alpha_z\partial_t\boldsymbol{M}_z\ . \tag{3.232}$$

The in-plane component of the Gilbert damping tensor is $\alpha_{xy} \equiv \frac{\sigma_\parallel}{e^2v^2}$ and the out-of-plane component $\alpha_z \equiv \frac{2\tau M_z\sigma_{\text{H}}}{\hbar e^2v^2}\Theta(|E_{\text{F}}| - |M_z|)$. Note that we always have $\alpha_{xy}, \alpha_z > 0$, so that the prefactor of these terms is always negative, no matter in which band the Fermi level sits and independent of the sign of M_z. After all, it represents damping of the magnetization, so this property is vital and leads to a positive Gilbert damping parameter $\underline{\underline{\alpha}}$. The Gilbert damping is anisotropic with respect to the z-axis, which is to be expected due to the inherent asymmetry of the topological insulator. The work of Yokoyama and coworkers considered only small deviations with respect to the fixed z-axis, so they obtained only the damping for magnetization dynamics in the x-y axis [131]. If one considers arbitrary magnetization textures $\boldsymbol{M}$ like in a domain wall or a vortex, one should expect that also M_x and M_y components acquire significant values, but then those are subject to the out-of-plane component of the Gilbert damping tensor, α_z.

Near the band edge, α_{xy} is rather small compared to α_z, so Gilbert damping for the z-component of a spin is suppressed as opposed to the strongly damped in-plane components.

In the presence of an external electric field along with an inhomogeneous magnetization we obtain additional contributions due to the gradient corrections of $\boldsymbol{M}(\boldsymbol{R},t)$,

$$\boldsymbol{s}_{\text{grad}}(\boldsymbol{R},t) = \frac{M_z}{E_{\text{F}}}\frac{\hbar\sigma_\parallel}{2eE_{\text{F}}^2}\left[\boldsymbol{E}\cdot(\boldsymbol{\nabla}\times\boldsymbol{M})\ \hat{\boldsymbol{e}}_{\boldsymbol{z}} - (\hat{\boldsymbol{e}}_{\boldsymbol{z}}\times\boldsymbol{E})(\boldsymbol{\nabla}\cdot\boldsymbol{M})\right]\ , \tag{3.233}$$

which, unlike $\boldsymbol{s}_E$, has opposite sign when the Fermi level is in the conduction or the valence band, as it is the case for the exchange contribution. Furthermore, the gradient corrections to the torque $\boldsymbol{s}_{\text{grad}}$ become relevant in the presence of inhomogeneous magnetization textures and this contribution is smaller than $\boldsymbol{s}_E$ by a factor of $(M/E_{\text{F}})(v\tau/l_{\text{DW}}) = (M/E_{\text{F}})(l_{\text{mfp}}/l_{\text{DW}})$, where l_{mfp} is the mean-free path and l_{DW} is the characteristic length scale of the magnetization structure. When E_{F} and M are of similar order of magnitude and the domain walls are rather short or in clean samples, this term becomes important. Note that this does not correspond to the gradient term calculated in [131], there this term is independent of τ and therefore constitutes the gradient corrections to the intrinsic electric field term s_{in} as opposed to here, which are gradient corrections to the dissipative electric field term $\boldsymbol{s}_E$. The term calculated here has an additional factor $\frac{\hbar\tau M_z}{E_{\text{F}}^2}$ which is larger in clean samples.

The first term $\boldsymbol{E}\cdot(\boldsymbol{\nabla}\times\boldsymbol{M}) = \hat{\boldsymbol{e}}_{\boldsymbol{z}}\cdot(\boldsymbol{E}_\perp\times\boldsymbol{\nabla})M_z$ gives rise to a spin-accumulation along the z-direction in presence of an applied electric field, while the second terms yields an in-plane spin-accumulation which translates into the additional charge current $\boldsymbol{j}_{\text{grad}} = \delta\sigma_\parallel\boldsymbol{E}$ and thus corresponds to a change in the local conductivity

$$\frac{\delta\sigma_\parallel}{\sigma_\parallel} = -\frac{M_z}{E_{\text{F}}}\frac{\hbar v}{2E_{\text{F}}}\boldsymbol{\nabla}\cdot\frac{\boldsymbol{M}_\perp}{E_{\text{F}}}\ , \tag{3.234}$$

which ultimately gives rise to the domain-wall resistance on top of the topological insulator in the diffusive regime. We can see that the sign of the conductivity change does not depend on the sign of $\boldsymbol{M}$, but it depends on the relative sign between M_z and $M_\perp$. Also, the domain-wall resistance is expected to have opposite signs in the two bands of positive and negative energies.

Last but not least, this spin density gives rise to a torque which is exerted on the magnetization $\boldsymbol{M}$ and the resulting dynamics is described by the Landau-Lifshitz-Gilbert equation, as for example discussed in section 2.5.2, and here takes the form

$$M_d(\partial_t\boldsymbol{m} + \alpha_d\boldsymbol{m}\times\partial_t\boldsymbol{m}) = -g\mu_{\text{B}}M_d\boldsymbol{m}\times\boldsymbol{H}_{\text{eff}} + \boldsymbol{\mathcal{T}}_{\text{el}} = -g\mu_{\text{B}}M_d\boldsymbol{m}\times\boldsymbol{H}_{\text{eff}} + \boldsymbol{M}\times\boldsymbol{s}\ . \tag{3.235}$$

Here, we see that the torque essentially appears as an additional contribution to the effective magnetic field. Obviously, $\boldsymbol{s}_0$ provides an intrinsic anisotropy axis along the z-direction which can be tilted by application of an electric field in-plane of the surface. For a given $\boldsymbol{E}$-field, the in-plane tilt angle is result of an interplay between $\boldsymbol{s}_{\text{in}}$ and $\boldsymbol{s}_E$, and thus depends on the ratio $\sigma_{\text{H}}/\sigma_\parallel$ which can be controlled by shift of the Fermi-level E_{F} and the magnetization M_z. Essentially, in this topological system the electric field takes the same role that the external magnetic field has in conventional ferromagnets.

It is also interesting to note that in the Stoner limit of itinerant ferromagnetism, we find a simple relation for the Gilbert damping constant of in-plane non-equilibrium magnetizations. This can be found using $\boldsymbol{\mathcal{T}}_{\text{el}} = 0$ and considering small in-plane excitations, i.e. $\boldsymbol{M} = M_z\hat{\boldsymbol{e}}_{\boldsymbol{z}}+\boldsymbol{u}$ (similar to [131]), so that

$$\boldsymbol{\mathcal{T}}_{\text{el}} = \boldsymbol{M}\times(\boldsymbol{s}_{\text{in}} + \boldsymbol{s}_{\text{damp}} + \boldsymbol{s}_0) = 0 \tag{3.236}$$

and substituting the above results readily yields $\alpha_{xy}^{(\text{St})} = \frac{\sigma_\parallel}{\sigma_{\text{H}}}$.

We remark that we ignored the effect of screening in this investigation. When the Fermi-level is inside or near the gap however, screening is suppressed. Deeper in the metallic regime, it

should be taken into account, which can be implemented straightforwardly by introducing the screening potential φ_{ee} due to electron-electron interaction. The Thomas-Fermi screening length has been calculated in the work of [133].

3.5. Conclusions and Outlook

In this chapter, we first studied a very general Hamiltonian that contains an additional matrix structure describing different bands, and the goal was to bring this Hamiltonian into band-diagonal form which has been achieved by performing a rotation in band-space. The diagonal representation is very practical when one wants to study the low-energy response of the system because then, only one or few degenerate bands are relevant. Since in the very general case this diagonalization involves the pair of non-commutating position $\boldsymbol{r}$ and momentum $\boldsymbol{p}$ operators, we performed the diagonalization perturbatively in $\hbar$ by using the Wigner representation. We investigated the Hamiltonian and physical observables in the rotated frame and how Berry phases emerge naturally during this diagonalization procedure. Essentially, Berry phases describe corrections to the canonical variables like position and momentum due to inter-band scattering.

Moreover, we discussed the general gauge-transformation in $2\times(3+1)$-dimensional parameter space consisting of $\boldsymbol{r}$, $\boldsymbol{p}$, time t and energy ϵ and required our effective theory to be invariant with respect to this transformation, since this additional degree of freedom should not change the physics of the low energy effective theory. This freedom corresponds to the different choices of unitary transformations we can find to arrive at the same diagonal representation of the Hamiltonian. This lead us to the introduction of gauge-invariant kinetic quantities, and we expressed the Hamiltonian and observables in terms of these kinetic variables, which naturally leads to the appearance of Berry curvatures which are gauge invariant and describe all kinds of intrinsic effects. In addition to Berry curvatures, we identified further gauge invariant objects which are related to circular, or persistent currents, which itself interact with magnetic fields or with each other and give for example rise to energy terms, like the Zeeman interaction.

In order to obtain a comprehensive effective description, we discussed that the Hamiltonian alone is not sufficient. To this end, we formulated the Hamiltonian, density operators, and quasi-probability densities in the rotated frame in terms of gauge invariant kinetic variables $\boldsymbol{R}$ and $\boldsymbol{P}$. These kinetic variables in the rotated frame are strongly linked to the kinetic variables of the original theory, as opposed to the canonical variables. In fact, as we have seen, the kinetic variables essentially turn into the kinetic ones of the original theory. The canonical ones are, on the other side, responsible for the proper quantum structure due to their canonical commutation relations which defines the quantization. Therefore, both the canonical and kinetic variables are an important part of our effective description, and only then will it be consistent. Using these kinetic variables, we formulated a Boltzmann transport equation that incorporates intrinsic effects expressed in terms of Berry curvature effects. To this end, we consistently defined various quasi-probability densities which are connected by a conservation law: Liouville's theorem in extended phase space. These can be used to obtain physically meaningful densities and currents within the effective description. Furthermore, it is rather straightforward to include impurity scattering in the same manner as in section

2.4.5, albeit with additional corrections that appear in terms of Berry curvatures and which requires further investigation.

Then one could study a variety of systems that involve both spin-orbit interaction (SOI) and an inhomogeneous and time-dependent magnetization. This is interesting for spin-orbit coupled semiconductors where one has different types like Rashba SOI, Dresselhaus SOI or in the case of strong SIO in III-V ferromagnetic semiconductors one can utilize the Luttinger Hamiltonian for hole transport. In these systems the electron or hole spin is intricately coupled to both momentum and orbital degrees of freedom. In addition, one has magnetic and non-magnetic impurity scattering that adds additional complexity to the system and is naturally studied in terms of a collision integral within the Boltzmann approach. For these reasons, the formalism developed in this chapter seems practical to study various transport and dynamical properties of these systems.

Despite performing a formal expansion in $\hbar$, similar to treating the semiclassical limit, we never abandon the quantum description. One major advantage compared to other semiclassical approaches is that there is no need for a re-quantization. In fact, our real expansion parameter might be a different one, like the Compton wave-length as we have seen in the case of the relativistic Dirac equation. Also, our approach is systematic in the sense that we can go to arbitrary order in $\hbar$ or inter-band coupling. In this respect, it is also very interesting to look at terms second order in $\hbar$ which yield important contributions, for example the Darwin term in the case of the low-energy limit of the relativistic Dirac equation. Furthermore, new physical phenomena emerge at $O(\hbar^2)$, like the magneto-electric coupling in insulators which received new attention recently, also due to the discovery of topological insulators [134, 135].

As we have seen throughout this chapter, is it important to keep information about the Berry phases in effective theories, since they are essential when studying the dynamics of the system. The Hamiltonian is enough to study properties like the energy spectrum of the system. However, for example dynamical observables like current attain important Berry phase contributions that lead to a correction of a factor 2 in the case of the Dirac equation or in their non-relativistic counterparts in spin-orbit coupled semiconductor systems. Essentially, the same conclusion has been reached in [109] for the case of the relativistic Dirac equation. Only when we make the distinction between kinetic and canonical variables will the resulting current be gauge invariant. We also established a link between gauge invariance in momentum space and the spin-orbit interaction.

Finally, we studied transport and magnetization dynamics in the system of surface Dirac Fermions with proximity induced ferromagnetism in the diffusive regime. We calculated densities and currents and obtain for example the spin-accumulation and domain-wall resistance due to inhomogeneous magnetization textures in addition to the anisotropic Gilbert-damping constant. Furthermore, we found the anisotropic exchange interaction mediated by the Dirac quasiparticles. Other terms like electric field terms already published in other works were reproduced. In the Stoner limit of itinerant ferromagnetism, the simple relation $\alpha_{xy}^{(\mathrm{St})} = \frac{\sigma_{\parallel}}{\sigma_{\mathrm{H}}}$ for the in-plane component of the Gilbert damping constant holds.

In summary, we found a consistent and gauge invariant effective description that can be used to study the low-energy response of the system, where the non-equilibrium excitations are confined within a single band, or several degenerate bands. Our treatment shows how low energy effective theories arise from more comprehensive theories which usually are itself

already effective theories and what role gauge transformations, kinetic variables and canonical variables play in this course of this reduction scheme. Since the external electromagnetic field is already described in terms of a gauge invariant kinetic momentum, we discuss hierarchies of effective theories, which allow us to include the electromagnetic field conveniently into our description.

4. Transport and Bound States on Topological Insulators with Induced Ferromagnetism

4.1. Introduction to Topological Insulators

Topological insulators are a new class of materials that do not fit into the traditional characterization scheme of Landau which describes phases of matter in terms of spontaneously broken symmetries. These topological materials are subject of two recent reviews [136, 137]. The beginning of the field of topological states of matter dates back to 1980, when the Quantum Hall state was discovered by placing a 2-dimensional electron gas into a strong perpendicular magnetic field. This state does not break any symmetries but is characterized by a topological invariant, the quantized Hall conductivity $\sigma_{xy} = ne^2/h$ which is invariant with respect to smooth deformations of the system and cannot change unless the system undergoes a quantum phase transition [138, 139].

A new generation of topological insulators without time-reversal breaking mechanism was first proposed theoretically by Bernevig *et al.* in HgTe quantum wells [140], and has been observed experimentally shortly after [141]. This was the demonstration the two-dimensional quantum spin-Hall insulator (QSH), a time-reversal invariant topological state as opposed to the quantum Hall state, and carries a pair of time-reversal invariant edge state which can be detected in transport experiments [142, 143]. This state is characterized by a $\mathbb{Z}_2$ topological invariant which can take the two values 0 for the topologically trivial state and 1 for the topologically non-trivial state [144, 145].

Furthermore, Fu and Kane predicted $Bi_{1-x}Sb_x$ to be a three dimensional strong topological insulator (STI) with topologically non-trivial surface states [145], which was later seen experimentally by angle-resolved photoemission spectroscopy (ARPES) [146]. However, this material has a small bulk energy gap and a rather complicated structure of the surface states so that soon, it was predicated that the materials Bi_2Se_3, Bi_2Te_3 and Sb_2Te_3 should exhibit a much larger bulk gap of ≈ 0.3 eV [130]. Experimentally, these materials have been confirmed to show a single Dirac cone with linear dispersion on its surface [130, 147]. These materials are known for their excellent thermoelectric properties and it turns out that the major ingredient that drives a material into a topological state is the spin-orbit interaction which is also rather large in the mentioned materials. The topological nature of the surface states has been also shown experimentally by a direct measurement of the spin-texture which also demonstrates the spin-momentum locking that ultimately leads to a the topological quantum Berry phase of π. The large energy gap and the special electronic structure of the surface states makes materials like Bi_2Se_3 very interesting for high-temperature spintronics applications.

The key essence of topological states of matter is the spatial separation of bound states which manifests itself in the exponentially localized surface states. These states are robust against

perturbations since they are protected by the bulk band gap. In a semiclassical picture, the robustness of the surface states can be understood in terms of a destructive interference of time-reversed paths [137], which is a consequence of the mysterious fact that the wave function flips sign when the spin is rotated by 2π.

Topological states of matter could be also realized using rather conventional ingredients, like semiconductor heterostructures coupled ferromagnets and s-wave superconductors [148, 149].

A general theoretical description using topological field theory can be found in [128] and a definition of topological order parameters in interacting systems is discussed in Reference [150]. Many interesting phenomena are proposed to emerge from this new class of materials, like a condensed matter realization of axion physics [151], proximity induced superconductivity gives rise to unconventional superconductivity [152, 153] and is a promising candidate to realize Majorana Fermions [154, 155, 156] which are of interest for topologically protected quantum computing. Furthermore, fractional charge of quasi-particles and a quantized current have been predicted for the quantum spin Hall state [157]. And finally, the vacuum of the Standard Model is also of topological nature [158]. Therefore, it is also of very fundamental interest to study the properties of these special states of matter.

4.1.1. 3D Strong Topological Insulators (STI)

In this chapter, our interest lies in the family of so-called strong topological insulators (STI) like Bi_2Se_3. The notion of strong arises from the fact that in three dimensions there are different ways to realize topological states, and one finds four topological invariants to characterize these states, $(\nu_0; \nu_1, \nu_2, \nu_3)$ [145]. The most straightforward way to create a 3-dimensional topological insulator is by simply stacking weakly interacting layers of 2D QSH insulators, so that the edge states become anisotropic surface states. This kind is referred to as weak topological insulator with $\nu_0 = 0$ and ν_1, ν_2, ν_3 representing the Miller indices of the orientation of the layers. However, these surface states are not robust against disorder and will be subject to Anderson localization. On the other side, the STI is a genuine 3-dimensional variant characterized by $\nu_0 = 1$ and has a surface electronic structure which in the simplest case is a single Dirac cone described by the surface Hamiltonian

$$\mathcal{H}_{\text{surface}} = \hbar v_F \boldsymbol{\sigma} \cdot \boldsymbol{k} \ , \tag{4.1}$$

where $\boldsymbol{\sigma}$ is the vector of spin-Pauli matrices and $\boldsymbol{k}$ is the momentum in the surface plane. This dispersion clearly shows the spin-momentum locking which is characteristic for the surface states of time-reversal invariant STI. Therefore, for each momentum $\boldsymbol{k}$ one has only one spin-state which is of opposite direction for $\boldsymbol{k}$ and $-\boldsymbol{k}$, therefore prohibiting back-scattering and thus also Anderson localization due to disorder.

For a surface with a mirror plane, the symmetry requires

$$\mathcal{H}_{\text{surface}} = \hbar v_F \boldsymbol{\sigma} \cdot (\hat{\boldsymbol{e}}_{\boldsymbol{z}} \times \boldsymbol{k}) = \hbar v_F (k_y \sigma_x - k_x \sigma_y) \ , \tag{4.2}$$

which is the dispersion realized in Bi_2Se_3 to a very good approximation and for low enough energies. In fact, this material has to date the simplest surface structure and it comes very close to the ideal linearly dispersing Dirac cone [159]. It essentially corresponds to $\frac{1}{4}$ of Graphene, and the appearance of a single Dirac cone at the surface is only possible due to a

spatial separation of the pair of Dirac cones required by the Fermion doubling-theorem [160]. Essentially, the two cones sit on opposite surfaces and do not interact due to large spatial separation along with exponential localization at the surface. In fact, when the distance becomes smaller like in thin films, the surface states hybridize and a gap opens in the surface spectrum [161].

It seems that Bi_2Se_3 becomes the reference material for strong topological insulators due to its large band gap allowing stable surface states even at room-temperature, while the surface states itself are very close to the idealized Dirac cone. Furthermore, the stoichiometric pure compound allows one to create samples of higher purities as for example compared to the alloy $Bi_{1-x}Sb_x$. On the other side, in the related material Bi_2Te_3 the surface Dirac cone clearly shows hexagonal warping due to the underlying hexagonal symmetry [162].

On the theoretical side, a 4-band model Hamiltonian for a full description of the 3D STI has been derived from $\boldsymbol{k}\cdot\boldsymbol{p}$ perturbation theory and symmetry considerations [163]. There are few works dealing with transport theories for the topological surface states. A diffusion equation that describes spin and charge coupled transport has been derived in [164], and a more comprehensive theory of surface charge transport in topological insulators can be found in Ref. [133]. It should be noted that in contrast to the 2D QSH state, the quasiparticle motion on the surface of the strong topological insulator is diffusive and not ballistic. This is due to the surface roughness and the presence of impurities or dopants near the surface.

Finally, experimentally it is still challenging to perform real transport experiments on the topological surface states, since bulk contributions are dominating, so the current approach is to separate bulk from surface contributions. But the field of topological insulators is just at its beginning, so there is much to be expected in the future.

4.1.2. Strong Topological Insulator with Induced Ferromagnetism

We have learned that topologically protected surface states are robust against disorder however, this is only true for non-magnetic impurities. Magnetic impurities on the surface like iron open a mass gap in the Dirac dispersion [165]. On the other side, non-magnetic impurities can be used to tune the Fermi level, which can be done individually for bulk and surface states by controlled addition of impurities to the surface of the topological insulator [147, 159]. A systematic experimental study on the influence of different kind of impurities on the topological spin-structure of Bi_2Se_3 can be found in Ref. [166].

The general form of the Hamiltonian which we will mainly study for the rest of this chapter reads

$$H = \hbar v \hat{\boldsymbol{e}}_{\boldsymbol{z}}(\boldsymbol{\sigma}\times\boldsymbol{k}) - \boldsymbol{M}(\boldsymbol{r},t)\boldsymbol{\sigma} - \mu(\boldsymbol{r},t)\sigma_0 \ , \tag{4.3}$$

where the first term is simply the surface low energy description for Bi_2Se_3 introduced in Eq. (4.2) and the second term describes the proximity induced ferromagnetism with the effective ferromagnetic order parameter $\boldsymbol{M}(\boldsymbol{r})$, exchange coupled to the spin $\boldsymbol{\sigma}$ of the Dirac Fermions. Finally, chemical doping shifts the Fermi-level $\mu(\boldsymbol{r})$ which can also depend on position $\boldsymbol{r}$ by performing spatially dependent doping. This projected Hamiltonian description is sufficient as long as the Fermi-level and energies of external perturbation are low enough, so that there is no interference with the bulk band states. In this case, a more complete

description like the aforementioned full 3-dimensional 4-band theory is required. However, for the rest of this work it is assumed that the projected description is sufficient, in particular we are only interested in the low-energy transport regime.

Furthermore, the quantum anomalous Hall effect (QAH) has been predicted in the Bi_2X_3 system of topological insulators when doped with Fe or Cr [167]. Essentially, the magnetic doping leads to a finite mass $M_z \neq 0$ which opens a gap in the surface spectrum and drives the system into the quantum anomalous Hall state which in analogy to the quantum Hall state is characterized by a quantized Hall conductance, but it has the big advantage that no external magnetic field is needed.

Using the same Hamiltonian (4.3), Yokoyama *et al.* considered a ferromagnet/ferromagnet junction on the surface of a topological insulator and calculated the tunneling conductance through the interface barrier [168]. Furthermore, the effects of the Dirac Fermions on the magnetization dynamics are subject of Ref. [131]. Finally, Garate and Franz treated the inverse spin-galvanic effect in such systems [132].

The system described by (4.3) featuring an interaction of the Dirac Fermions with ferromagnetism exhibits interesting physical phenomena, such as bound states that can exist at a domain wall or at magnetization structures in general. This will be investigated in this chapter, but we will also go beyond equilibrium phenomena and explore the non-equilibrium aspects of Dirac fermions moving through inhomogeneous magnetization structures.

4.2. General Properties of Dirac Fermions with Induced Ferromagnetism

In this section, we will first investigate some basic properties of the Hamiltonian (4.3), which will help us to better understand the discussion in the subsequent sections.

4.2.1. Densities and Quantum Equations of Motion

By writing down the Heisenberg equation of motion for the position operator, we obtain for the velocity operator

$$\boldsymbol{v} \equiv \frac{\mathrm{d}\boldsymbol{r}}{\mathrm{d}t} = \frac{1}{i\hbar}\left[\boldsymbol{r}, H\right] = v\hat{\boldsymbol{e}}_{\boldsymbol{z}}\times\boldsymbol{\sigma} \ , \tag{4.4}$$

which also relates to the current operator. This can be easily shown by calculating $\partial_t\rho$, where $\rho = \Psi^\dagger\Psi$ is the density operator and Ψ is the many particle field operator in the Heisenberg picture, and which yields the continuity equation

$$\partial_t\Psi^\dagger\Psi + \boldsymbol{\nabla}\Psi^\dagger\boldsymbol{v}\Psi = \partial_t\rho + \boldsymbol{\nabla}\boldsymbol{j} = 0 \ . \tag{4.5}$$

We note that the current density $\boldsymbol{j} = v\Psi^\dagger(\hat{\boldsymbol{e}}_{\boldsymbol{z}}\times\boldsymbol{\sigma})\Psi$ is completely defined by the spin direction, a direct consequence of the spin-momentum locking on the surface of the topological insulator. Thus, creating an excitation with a certain, but fixed spin direction, the group velocity is already determined. Later, we will see that this leads to the chiral character of the bound

states that can exist at the interface between two ferromagnets of different magnetization directions on top of the topological insulator.

We are also interested in the equation of motion for the spin,

$$\frac{\mathrm{d}\boldsymbol{\sigma}}{\mathrm{d}t} = 2\hbar v\boldsymbol{\sigma}\times(\hat{\boldsymbol{e}}_{\boldsymbol{z}}\times\boldsymbol{k}) + 2\boldsymbol{\sigma}\times\boldsymbol{M} = 2\hbar v\left((\boldsymbol{k}\boldsymbol{\sigma})\hat{\boldsymbol{e}}_{\boldsymbol{z}} - \boldsymbol{k}\sigma_z\right) + 2\boldsymbol{\sigma}\times\boldsymbol{M}\ , \tag{4.6}$$

which describes precession around the effective field $2v(\hat{\boldsymbol{e}}_{\boldsymbol{z}}\times\boldsymbol{k}) + 2\boldsymbol{M}$ which is momentum-dependent.

For the sake of completeness, let us also remark that in order to have a closed set of operator equations that describe the surface physics of the topological insulator, in addition to $\frac{\mathrm{d}\boldsymbol{x}}{\mathrm{d}t}$ and $\frac{\mathrm{d}\boldsymbol{\sigma}}{\mathrm{d}t}$, we need the equation of motion for $\boldsymbol{k}$,

$$\frac{\mathrm{d}\boldsymbol{k}}{\mathrm{d}t} = \boldsymbol{\nabla}(\boldsymbol{M}\boldsymbol{\sigma}) + (\boldsymbol{\nabla}\mu)\sigma_0\ , \tag{4.7}$$

where on the right-hand side, $\boldsymbol{\nabla}$ only acts on $B(\boldsymbol{x})$ and μ and thus, it is not to be treated as a differential operator.

In the case of an arbitrary inhomogeneous magnetization, we can find an interesting relation for the spin-density $\boldsymbol{s} \equiv \Psi^\dagger\boldsymbol{\sigma}\Psi$ of an eigenstate of the general Hamiltonian (4.3). In order to find it, we take the curl of the current density,

$$\boldsymbol{\nabla}\times\boldsymbol{j} = v\hat{\boldsymbol{e}}_{\boldsymbol{z}}\left(\boldsymbol{\nabla}\cdot\boldsymbol{s}\right) = v\hat{\boldsymbol{e}}_{\boldsymbol{z}}\left(\boldsymbol{\nabla}\cdot\Psi^\dagger\boldsymbol{\sigma}\Psi\right) \tag{4.8}$$

which relates the current to the divergence of the spin density, i.e. the sources for the transverse spin density are given by the curl of the current. Multiplying the eigenvalue equation $H\Psi = E\Psi$ with σ_z from the right, we obtain

$$v\hbar\boldsymbol{\sigma}\cdot\boldsymbol{\nabla}\Psi = \sigma_z\left(E + \mu(\boldsymbol{r}) + \boldsymbol{M}(\boldsymbol{r})\boldsymbol{\sigma}\right)\Psi\ , \tag{4.9}$$

so that we can use this equation and its adjugate to plug it into (4.8), which yields

$$\begin{aligned}\hat{\boldsymbol{e}}_{\boldsymbol{z}}\cdot(\boldsymbol{\nabla}\times\boldsymbol{j}) = v\left(\boldsymbol{\nabla}\cdot\boldsymbol{s}\right) &= \frac{1}{\hbar}\Psi^\dagger\left\{E + \mu(\boldsymbol{r}) + \boldsymbol{M}(\boldsymbol{r})\boldsymbol{\sigma}, \sigma_z\right\}\Psi \\ &= \frac{2}{\hbar}\left((E+\mu)s_z + M_z\rho\right)\ .\end{aligned} \tag{4.10}$$

The source for circulating (or persistent) currents is given by M_z times the quasiparticle density $\rho = \Psi^\dagger\Psi$ of the Dirac fermion plus the contribution from the z component of the spin density with the prefactor being essentially the eigenenergy of the state. This relation will manifest itself in the bound states we will calculate later analytically (see Figure 4.10).

Homogeneous case and density of states

Let us begin very simply by considering a constant exchange field $\boldsymbol{M}$ and ignoring the chemical potential μ. Then, the diagonalization is very straightforward since the Hamiltonian

$$H_{\boldsymbol{k}} = \hbar v\hat{\boldsymbol{e}}_{\boldsymbol{z}}(\boldsymbol{\sigma}\times\boldsymbol{k}) - \boldsymbol{M}\cdot\boldsymbol{\sigma}$$

is diagonal in $\boldsymbol{k}$-space so that only 2×2 spin-space remains to be brought into diagonal form. This can be achieved by the unitary transformation

$$U_{\boldsymbol{k}} = \frac{1}{\sqrt{2\epsilon_{\boldsymbol{k}}}} \begin{pmatrix} \sqrt{\epsilon_{\boldsymbol{k}} - M_z} & \sqrt{\epsilon_{\boldsymbol{k}} + M_z} \\ -\hbar v \frac{ik_x - k_y}{\sqrt{\epsilon_{\boldsymbol{k}} - M_z}} & \hbar v \frac{ik_x - k_y}{\sqrt{\epsilon_{\boldsymbol{k}} + M_z}} \end{pmatrix} \tag{4.11}$$

that diagonalizes $H_{\boldsymbol{k}}$,

$$U_{\boldsymbol{k}}^\dagger H_{\boldsymbol{k}} U_{\boldsymbol{k}} = \begin{pmatrix} \epsilon_{\boldsymbol{k}} & 0 \\ 0 & -\epsilon_{\boldsymbol{k}} \end{pmatrix} , \tag{4.12}$$

and the energy dispersion is $\epsilon_{\boldsymbol{k}} = \sqrt{\hbar^2 v^2 k^2 + M_z^2}$ which is shown in Fig. 4.1(a).

We now calculate the spin-resolved density of states which is defined by

$$\nu(\epsilon) = \int \frac{\mathrm{d}^2 k}{(2\pi)^2}\ \delta(\epsilon - H_{\boldsymbol{k}}) , \tag{4.13}$$

where we note that we can ignore the component $\boldsymbol{M}_\perp = (M_x, M_y)$ in the plane of the topological insulator, since it merely renormalizes the momenta k_x, k_y and thus can be transformed away in the above integral, leaving us solely with the mass term or energy gap M_z:

$$\nu(\epsilon) = \int \frac{\mathrm{d}^2 k}{(2\pi)^2}\ \delta\left(\epsilon - \hbar v \hat{\boldsymbol{e}}_{\boldsymbol{z}} (\boldsymbol{\sigma} \times \boldsymbol{k}) + M_z \sigma_z\right). \tag{4.14}$$

Applying the transformation (4.11), we obtain

$$\begin{aligned} \nu(\epsilon) &= \int \frac{\mathrm{d}^2 k}{(2\pi)^2}\ U_{\boldsymbol{k}}\ \delta\left(\epsilon - U_{\boldsymbol{k}}^\dagger H_{\boldsymbol{k}} U_{\boldsymbol{k}}\right)\ U_{\boldsymbol{k}}^\dagger \\ &= \int \frac{\mathrm{d}^2 k}{(2\pi)^2} \left[\delta(\epsilon - \epsilon_{\boldsymbol{k}}) \frac{1}{2}\left(\sigma_0 + \frac{H_{\boldsymbol{k}}}{\epsilon_{\boldsymbol{k}}}\right) + \delta(\epsilon + \epsilon_{\boldsymbol{k}}) \frac{1}{2}\left(\sigma_0 - \frac{H_{\boldsymbol{k}}}{\epsilon_{\boldsymbol{k}}}\right)\right] . \end{aligned} \tag{4.15}$$

The first term due to $H_{\boldsymbol{k}}$ is linear in $\boldsymbol{k}$ and thus vanishes upon integration, so that we finally have

$$\nu(\epsilon) = \frac{|\epsilon|}{4\pi v} \left[\sigma_0 - \frac{M_z}{\epsilon}\sigma_z\right] \Theta(|\epsilon| - |M_z|) . \tag{4.16}$$

For $M_z \to 0$, we obtain a simple linear spectral density $\nu(\epsilon) = \frac{|\epsilon|}{4\pi v}\sigma_0 = \frac{|k|}{4\pi}\sigma_0$. For $M_z \neq 0$ it becomes gapped ($|\epsilon| \geq |M_z|$) an attains a spin-z component which has the same sign for all states in one band, and is shown in Figure 4.1(b).

Considering the eigenstates of the homogeneous Hamiltonian, $|\psi_{\boldsymbol{k}}^\pm\rangle = e^{i\boldsymbol{k}\boldsymbol{r}}|\chi_{\boldsymbol{k}}^\pm\rangle$, $H_{\boldsymbol{k}}|\psi_{\boldsymbol{k}}^\pm\rangle = \pm\epsilon_k|\psi_{\boldsymbol{k}}\rangle$ we obtain the energy $\epsilon_k = \pm|v\hat{\boldsymbol{e}}_{\boldsymbol{z}} \times \boldsymbol{k} + \boldsymbol{M}|$ and

$$\langle \chi_{\boldsymbol{k}}^\pm | \boldsymbol{\sigma} | \chi_{\boldsymbol{k}}^\pm \rangle = \mp \frac{1}{\epsilon_k} \left(v\hat{\boldsymbol{e}}_{\boldsymbol{z}} \times \boldsymbol{k} + \boldsymbol{M}\right) , \tag{4.17}$$

so that the expectation value of the velocity is $\langle \psi_{\boldsymbol{k}}^\pm | \boldsymbol{v} | \psi_{\boldsymbol{k}}^\pm \rangle = \pm\frac{1}{\epsilon_k}(v\boldsymbol{k} - \hat{\boldsymbol{e}}_{\boldsymbol{z}} \times \boldsymbol{M}) = \pm\frac{\partial \epsilon_k}{\partial \boldsymbol{k}}$, as expected.

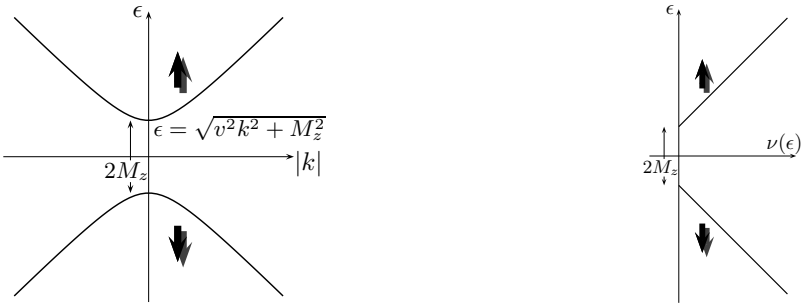

(a) Energy dispersion (b) Density of states

Figure 4.1.: Dispersion relation (a) and density of states (b) on the surface of a topological insulator in presence of a magnetic field which opens a gap of $2M_z$. Note that in-plane components of the magnetic field merely renormalize the momentum vector $\boldsymbol{k}$ and thus do not change the spectrum. The net spin polarization of the states is along the z-direction and indicated by the arrows.

4.2.2. Gauge Transformation

We start with the Hamiltonian for the surface of the STI and the general magnetization field $\boldsymbol{M}(\boldsymbol{r})$

$$\mathcal{H} = i\hbar v\boldsymbol{\sigma}(\hat{\boldsymbol{e}}_{\boldsymbol{z}}\times\boldsymbol{\nabla}) - \boldsymbol{M}(\boldsymbol{r})\boldsymbol{\sigma} - \mu(\boldsymbol{r}) \ , \tag{4.18}$$

where $\boldsymbol{r}$ describes the position on the surface which is chosen to be the x-y plane and likewise, $\boldsymbol{\nabla} = (\partial_x, \partial_y, 0)$. First, we divide the magnetization components perpendicular to $\hat{\boldsymbol{e}}_{\boldsymbol{z}}$ into two components, $\boldsymbol{M}_\perp = \boldsymbol{M}_\mathrm{l} + \boldsymbol{M}_\mathrm{t}$, where the divergence-free part has the property

$$\boldsymbol{\nabla}\boldsymbol{M}_\mathrm{t} = \partial_x M_x^\mathrm{t} + \partial_y M_y^\mathrm{t} = 0 \tag{4.19}$$

and the curl-free part satisfies

$$\hat{\boldsymbol{e}}_{\boldsymbol{z}}\cdot(\boldsymbol{\nabla}\times\boldsymbol{M}_\mathrm{l}) = -\boldsymbol{\nabla}\cdot(\hat{\boldsymbol{e}}_{\boldsymbol{z}}\times\boldsymbol{M}_\mathrm{l}) = \partial_x M_y^\mathrm{l} - \partial_y M_x^\mathrm{l} = 0 \ . \tag{4.20}$$

Now, by performing the local gauge transformation

$$|\psi\rangle \to \exp\left\{\frac{i}{v\hbar}\int^{\boldsymbol{r}} \mathrm{d}^2\boldsymbol{r}'\cdot(\hat{\boldsymbol{e}}_{\boldsymbol{z}}\times\boldsymbol{M}_\mathrm{t}(\boldsymbol{r}'))\right\}|\psi\rangle \ , \tag{4.21}$$

we can eliminate the divergence-free part $\boldsymbol{M}_\mathrm{t}$. The line integral is well defined since it does not depend on the path of integration due to the integrands vanishing curl, $\boldsymbol{\nabla}\times(\hat{\boldsymbol{e}}_{\boldsymbol{z}}\times\boldsymbol{M}_\mathrm{t}(\boldsymbol{r})) = \hat{\boldsymbol{e}}_{\boldsymbol{z}}(\boldsymbol{\nabla}\cdot\boldsymbol{M}_\mathrm{t}) = 0$. However, this additional prefactor of $|\psi\rangle$ is a pure phase and is not of any physical significance. Therefore, we can restrict ourselves to problems of the form

$$\mathcal{H} = i\hbar v\boldsymbol{\sigma}(\hat{\boldsymbol{e}}_{\boldsymbol{z}}\times\boldsymbol{\nabla}) - \boldsymbol{M}_\mathrm{l}(\boldsymbol{r})\boldsymbol{\sigma} - M_z(\boldsymbol{r})\sigma_z - \mu(\boldsymbol{r}) \ , \tag{4.22}$$

or since we can introduce a scalar potential such that $\boldsymbol{M}_\mathrm{l} = \boldsymbol{\nabla}\varphi_\mathrm{m}$, where $\varphi_\mathrm{m}(\boldsymbol{r})$ can be considered as the magnetic potential, we can also write,

$$\mathcal{H} = i\hbar v\boldsymbol{\sigma}(\hat{\boldsymbol{e}}_{\boldsymbol{z}}\times\boldsymbol{\nabla}) - \boldsymbol{\sigma}\cdot\boldsymbol{\nabla}\varphi_\mathrm{m} - M_z\sigma_z - \mu \ , \tag{4.23}$$

where we did not explicitly write the $\boldsymbol{r}$ dependence for clarity. φ_{m} will be useful later for the general solution of the zero energy bound state. It is also possible to define a magnetic charge $\rho_{\mathrm{m}}(\boldsymbol{r})$ by virtue of a Poison equation,

$$\Delta\varphi_{\mathrm{m}} = \boldsymbol{\nabla}\cdot\boldsymbol{M}_{\mathrm{l}} = \rho_{\mathrm{m}} \ . \tag{4.24}$$

Thus, the energy spectrum of the system STI with a ferromagnetic layer on top and arbitrary magnetization texture depends only the M_z component and the magnetic charge of the vector field, $\rho_{\mathrm{m}}(\boldsymbol{r})$. Note that time-dependent $\boldsymbol{M}_{\mathrm{t}}$ would also renormalize the chemical potential $\mu(\boldsymbol{r})$ with a term that is given by the time derivative of the exponent in Eq. (4.21).

Time-dependent case

In the general time-dependent case on the other hand, we can transform away the chemical potential μ in Hamiltonian (4.3) by means of a local gauge transformation which would give rise to an additional contribution to $\boldsymbol{M}_{\mathrm{t}}(\boldsymbol{r},t)$,

$$\boldsymbol{M}_{\mathrm{t}} \to \boldsymbol{M}_{\mathrm{t}} + \int^{t} \mathrm{d}t' v(\hat{\boldsymbol{e}}_{\boldsymbol{z}}\times\boldsymbol{\nabla})\mu(\boldsymbol{r},t') \ . \tag{4.25}$$

Therefore, in the general time-dependent case, the effects due to a scalar potential $\mu(\boldsymbol{r},t)$ and due to $\boldsymbol{M}_{\mathrm{t}}(\boldsymbol{r},t)$ can be mapped onto each other, so only one of them has to be considered when solving the time-dependent Dirac equation.

4.2.3. Wave Equation in the Schrödinger Form

We start from the time-dependent Dirac equation for the surface states

$$i\hbar v\boldsymbol{\sigma}(\hat{\boldsymbol{e}}_{\boldsymbol{z}}\times\boldsymbol{\nabla})\Psi = (i\hbar\partial_t + \boldsymbol{\sigma}\boldsymbol{M}_{\perp} + M_z\sigma_z)\Psi \ , \tag{4.26}$$

with the most general fields $\boldsymbol{M}(\boldsymbol{r},t)$ and chemical potential $\mu(\boldsymbol{r},t)$, and where the scalar potential term μ has already been absorbed into $\boldsymbol{M}_{\perp} = \boldsymbol{M}_{\mathrm{l}} + \boldsymbol{M}_{\mathrm{t}}$ by the gauge transformation discussed above. We transform this equation into a wave equation for the two component spinor Ψ by multiplying the whole equation with $iv\boldsymbol{\sigma}(\hat{\boldsymbol{e}}_{\boldsymbol{z}}\times\boldsymbol{\nabla})$ from the left, and obtain after some straightforward algebra[1]

$$\begin{aligned}\hbar^2(\partial_t^2 - v^2\boldsymbol{\nabla}^2)\Psi = &-(M^2 + M_z^2)\Psi \\ &+ \hbar\left[iv\hat{\boldsymbol{e}}_{\boldsymbol{z}}(\boldsymbol{\nabla}\times\boldsymbol{M}_{\perp}) + v\sigma_z(\boldsymbol{\nabla}\boldsymbol{M}_{\perp}) - 2iv(\hat{\boldsymbol{e}}_{\boldsymbol{z}}\times\boldsymbol{M}_{\perp})\boldsymbol{\nabla} - v\boldsymbol{\sigma}(\nabla\boldsymbol{M}_z) + i\boldsymbol{\sigma}(\partial_t\boldsymbol{M})\right]\Psi \ .\end{aligned} \tag{4.27}$$

We can also rewrite this equation using the Peierls substituted momentum $\boldsymbol{\nabla} \to \boldsymbol{\nabla} - \frac{i}{\hbar}\boldsymbol{A}_{\mathrm{eff}}$,

$$\hbar^2\partial_t^2\Psi - \hbar^2v^2\left(\boldsymbol{\nabla} - \frac{i}{\hbar v}(\hat{\boldsymbol{e}}_{\boldsymbol{z}}\times\boldsymbol{M}_{\perp})\right)^2\Psi = -M_z^2\Psi + \hbar\left[v\sigma_z(\boldsymbol{\nabla}\boldsymbol{M}_{\perp}) - v\boldsymbol{\sigma}(\nabla\boldsymbol{M}_z) + i\boldsymbol{\sigma}(\partial_t\boldsymbol{M})\right]\Psi \tag{4.28}$$

[1] We use $(\boldsymbol{\sigma}(\hat{\boldsymbol{e}}_{\boldsymbol{z}}\times\boldsymbol{\nabla}))^2 = \boldsymbol{\nabla}^2$ and $\boldsymbol{\sigma}(\hat{\boldsymbol{e}}_{\boldsymbol{z}}\times\boldsymbol{\nabla})(\boldsymbol{\sigma}\boldsymbol{M}_{\perp}) = \hat{\boldsymbol{e}}_{\boldsymbol{z}}(\boldsymbol{\nabla}\times\boldsymbol{M}_{\perp}) - i\sigma_z(\boldsymbol{\nabla}\boldsymbol{M}_{\perp}) - (\boldsymbol{\sigma}\boldsymbol{M}_{\perp})\boldsymbol{\sigma}(\hat{\boldsymbol{e}}_{\boldsymbol{z}}\times\boldsymbol{\nabla}) - 2(\hat{\boldsymbol{e}}_{\boldsymbol{z}}\times\boldsymbol{M}_{\perp})\boldsymbol{\nabla}$.

If we identify the vector potential as $\boldsymbol{M}_\perp = -v\hat{\boldsymbol{e}}_{\boldsymbol{z}} \times \boldsymbol{A}_{\text{eff}}$ in this equation, we obtain the (effective) magnetic field that we already encountered in (3.213)

$$\boldsymbol{B}_{\text{eff}} = \boldsymbol{\nabla} \times \boldsymbol{A}_{\text{eff}} = \hat{\boldsymbol{e}}_{\boldsymbol{z}} \frac{1}{v} (\boldsymbol{\nabla} \cdot \boldsymbol{M}_\perp) \ , \tag{4.29}$$

which appears not only in the usual orbital term but also as a Zeeman term on the right-hand side of Eqn. (4.28). We see that coupling between the two spin-components is now only due to gradients $\boldsymbol{\nabla} M_z$ and $\partial_t \boldsymbol{M}$. If the latter two vanish, we essentially have to solve two independent Schrödinger equations for the spin-up and -down components, with the difference that the time derivative appears in second order. For stationary states, $-\partial_t^2 \to E^2$, so that energy eigenvalues are simply the square roots of the Schrödinger eigenenergies. This manifests itself in analytical expressions for the eigenvalues, for example, as we will find below in (4.33) or (4.106).

For a general time and spatially-varying magnetization, $\boldsymbol{S}_{\text{eff}} \equiv i\hbar(\partial_t \boldsymbol{M}) - v\hbar(\nabla \boldsymbol{M}_z)$ appears as a spin-motive force that linearly couples to the spin like in a Zeeman term, and we can write compactly,

$$-\hbar^2 \partial_t^2 \Psi = v^2 \left(\boldsymbol{p} + \boldsymbol{A}_{\text{eff}}\right)^2 \Psi + M_z^2 \Psi - \left(\boldsymbol{B}_{\text{eff}} + \boldsymbol{S}_{\text{eff}}\right) \boldsymbol{\sigma} \Psi \ , \tag{4.30}$$

Here, M_z^2 appears as a scalar potential and for constant M_z, it simply opens a gap in the energy spectrum. The influence of the magnetization has been reduced to the effective electromagnetic potential $\boldsymbol{A}_{\text{eff}}$ and to $\boldsymbol{S}_{\text{eff}}$. The external magnetic field and some implications will be treated in the next section.

4.2.4. External Magnetic Field

An external magnetic field can be simply incorporated by the usual minimal coupling to the momentum, $\boldsymbol{\nabla} \to \boldsymbol{\nabla} - i\frac{q}{\hbar}\boldsymbol{A}$. Like in the previous section, we obtain the stationary wave equation for the Dirac spinor Ψ

$$v^2 \left(\boldsymbol{p} + q\boldsymbol{A}\right)^2 \Psi = (E^2 - M_z^2)\Psi + \hbar q v^2 (\boldsymbol{\nabla} \times \boldsymbol{A}) \sigma_z \Psi \ , \tag{4.31}$$

where we also kept a constant mass term M_z. The major difference to (4.30) is that here, the appearance of the vector potential is a result of enforcing gauge invariance, so that we have to distinguish between kinetic can canonic momentum. This is different in (4.30), where the effective vector potential is a result of the induced exchange field, and kinetic and canonic momentum are the same. This has been discussed very generally in chapter 3.

Note that the external magnetic field can have only a z-component (i.e. $\boldsymbol{B} = \boldsymbol{\nabla} \times \boldsymbol{A} = \hat{\boldsymbol{e}}_{\boldsymbol{z}} B(x, y)$), since x and y-components cannot be described by means of a Peierls substitution as we have only ∂_x and ∂_y derivatives available. For a complete inclusion of the magnetic field, one has to resort to a 3D-bulk model, for example the effective 4-band model derived in Ref. [163]. However, as Yang and Han conclude in Ref. [169], the surface projection along with the Peierls substitution are in good accord with the full four-band model, only when the surface states begin to merge with the bulk states differences arise, unsurprisingly.

It is now obvious that the above equation describes a free (non-relativistic) 2D electron gas subject to a perpendicular magnetic field. If we take B as constant, we can use the well

known solution [170],

$$v^2 \left(\boldsymbol{p} - q\boldsymbol{A}\right)^2 |\Psi_{m,n}\rangle = 2q\hbar v^2 B(n + \frac{1}{2})|\Psi_{m,n}\rangle = \hbar^2\omega_c^2(n + \frac{1}{2})|\Psi_{m,n}\rangle \ , \tag{4.32}$$

where m is the eigenvalue of the angular momentum operator L_z and the quantum number n denotes the Landau level. Note that it is the Zeeman-like coupling term $\sigma_z B_z$ that exactly cancels the zero-point energy and gives us the well known result for Landau levels of Dirac fermions [171],

$$E_n = \pm\sqrt{M_z^2 + 2q\hbar v^2 Bn} \ . \tag{4.33}$$

We remark that within a semiclassical description, it is the Berry phase that cancels the zero point energy since it accumulates a phase of π around a closed orbit [109]. Finally, the Landau level have been experimentally observed in Bi_2Se_3 using scanning tunneling microscope (STM) imaging [172, 173], although transport experiments are yet to be seen due to the general challenges that have to be overcome, as discussed in the introduction. Landau levels on a sphere have been derived in [174] using a description of the Dirac equation in curved two-dimensional space.

4.2.5. Semiclassical Orbits

In the previous chapter, we presented a semiclassical formulation of transport in systems with non-trivial band structure. Also, we already studied a range of phenomena exposed by the Hamiltonian (4.3) in section 3.4. Here, we merely want to illustrate some basic features of bound states that can be found in these kinds of systems and which we will recover later in this chapter in an exact quantum mechanical treatment. To this end, we adopt the most crude semiclassical description by simply considering the Hamiltonian equations of motion derived from the classical energy

$$H_\mathrm{c} = \sqrt{(vp_x + M_y(\boldsymbol{r}))^2 + (vp_y - M_x(\boldsymbol{r}))^2 + M_z(\boldsymbol{r})^2} \ , \tag{4.34}$$

which corresponds to the Hamilton function so that the equations of motion are given by

$$\begin{aligned} \frac{\mathrm{d}\boldsymbol{r}}{\mathrm{d}t} &= \frac{\partial H_\mathrm{c}}{\partial \boldsymbol{p}} \\ \frac{\mathrm{d}\boldsymbol{p}}{\mathrm{d}t} &= -\frac{\partial H_\mathrm{c}}{\partial \boldsymbol{r}} \ . \end{aligned}$$

Eliminating the momentum $\boldsymbol{p}$, we arrive at

$$\frac{H_c}{v^2}\frac{\mathrm{d}^2\boldsymbol{r}}{\mathrm{d}t^2} = \frac{\mathrm{d}\boldsymbol{r}}{\mathrm{d}t} \times \boldsymbol{B}_\mathrm{eff} - \frac{1}{2H_\mathrm{c}}\boldsymbol{\nabla} M_z^2 \ , \tag{4.35}$$

which essentially describes the motion of a particle in the effective magnetic field $\boldsymbol{B}_\mathrm{eff}$ defined in (4.29), and the effective electric field $-\frac{1}{2H_\mathrm{c}}\boldsymbol{\nabla} M_z^2$. Note that $\frac{\mathrm{d}H_\mathrm{c}}{\mathrm{d}t} = 0$ due to energy conservation, so that H_c is the energy of the particle in its orbit, and the mass of the quasi-particle is essentially given by its energy $\frac{H_c}{v^2}$, as expected from a relativistic theory.

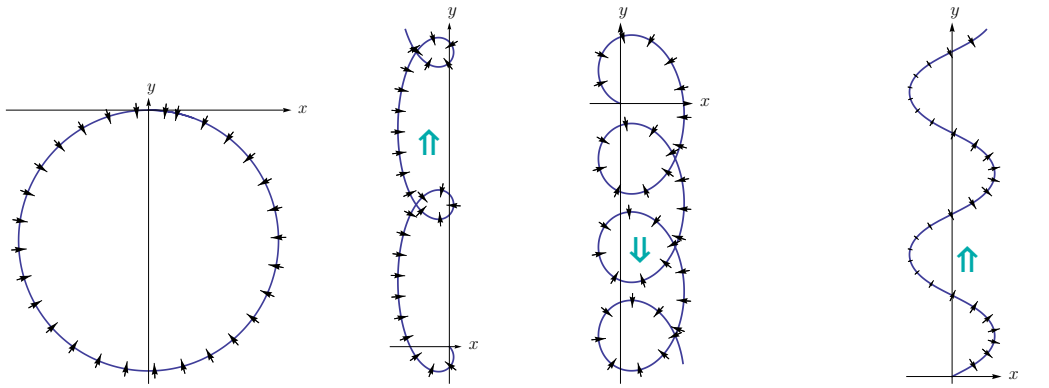

(a) $\boldsymbol{M} = \hat{\boldsymbol{e}}_{\boldsymbol{x}} \tanh(x)$ (b) $\boldsymbol{M} = \hat{\boldsymbol{e}}_{\boldsymbol{z}} \tanh(x)$

Figure 4.2.: Semiclassical orbits for Dirac fermions at domain walls with two different configurations of the magnetization. The three pictures in (a) show respectively, a localized (or closed) orbit and upward/downward moving (indicated by the blue double-arrow) helical orbits. The local spin direction is indicated by the small black arrows whose size represents the magnitude of the in-plane component. We see that the electron quasiparticle probability becomes more asymmetric with respect to the two sides of the domain wall, as the momentum p_y along the domain wall (and consequently the group velocity along y-direction) becomes larger. The picture in (b) shows the situation for a magnetization perpendicular to the 2D Dirac fermion gas. The orbits essentially undergo sinusoidal propagation. Contrary to the configuration in (a), the quasiparticle probability distribution is symmetric on both sides of the wall however, the spin-direction is asymmetric. We will recover these features when studying the exact bound states within full quantum theory.

We can also investigate the spin-direction (on the Bloch sphere) of the quasiparticle as it travels around its orbit (indicated by the black arrows in Figure 4.2). It is simply given by

$$\boldsymbol{s} = -\frac{1}{H_{\mathrm{c}}} \begin{pmatrix} M_x - v p_y \\ M_y + v p_x \\ M_z \end{pmatrix} \tag{4.36}$$

which can be obtained from result (3.222).

We see that we have two ways of creating localized states, the first one through $\boldsymbol{B}_{\mathrm{eff}}$ which is realized by a domain wall of the form $\boldsymbol{M} = \hat{\boldsymbol{e}}_{\boldsymbol{x}} \tanh(x)$ and is illustrated in Figure 4.2(a). Likewise, a domain wall of the form $\boldsymbol{M} = \hat{\boldsymbol{e}}_{\boldsymbol{z}} \tanh(x)$ leads to confinement through a scalar potential and is illustrated in 4.2(b). These are exactly the two types of domain walls we will investigate in detail later using the full quantum description.

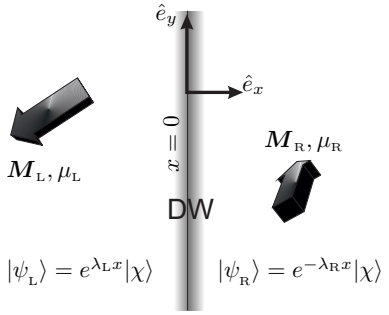

Figure 4.3.: A sketch of the interface geometry where a domain wall (DW) divides two regions of different magnetization vector $\boldsymbol{M}$ and chemical potential μ. The domain wall is assumed to be much smaller than any other relevant length scale, consequently treated as sharp interface. Due to the boundary condition at $x = 0$, the Dirac spinor $|\chi\rangle$ is the same on both sides of the interface.

4.3. Interface States and Zero Energy Bound States

Using a simple semiclassical picture in the previous section, we have seen the possibility of bound states in the system of Dirac fermions coupled to an inhomogeneous ferromagnetic exchange field. In this section, we want to explore this more accurately using a complete quantum description of the system. However, we restrict ourselves to rather simple situations and states for which analytical solutions can be found rather straightforwardly.

4.3.1. F-F Interface on Top of a Topological Insulator

Without loss of generality, we assume that the interface lies along the $\hat{\boldsymbol{e}}_{\boldsymbol{y}}$ direction so that we can expect a bound state in the $\hat{\boldsymbol{e}}_{\boldsymbol{x}}$ direction, while the transverse wave-vector q along the $\hat{\boldsymbol{e}}_{\boldsymbol{y}}$ direction is a good quantum number. For this geometry, we have $\boldsymbol{k} = -i\partial_x \hat{\boldsymbol{e}}_{\boldsymbol{x}} + q\hat{\boldsymbol{e}}_{\boldsymbol{y}}$, so that the Hamiltonian has the form (here, we set $\hbar = 1$)

$$H = iv\sigma_y \partial_x + qv\sigma_x - \boldsymbol{M}_{\mathrm{L}}\boldsymbol{\sigma} - \Delta\boldsymbol{M}\theta(x)\boldsymbol{\sigma} - \mu_{\mathrm{L}} - \Delta\mu\ \theta(x)\ , \tag{4.37}$$

where $\Delta\boldsymbol{M} = \boldsymbol{M}_{\mathrm{R}} - \boldsymbol{M}_{\mathrm{L}}$ is the difference between the magnetization on the left and right side, and likewise for the chemical potential $\Delta\mu = \mu_{\mathrm{R}} - \mu_{\mathrm{L}}$. The situation is illustrated in Figure 4.3.

On either side of the interface, we anticipate a solution of the form

$$|\psi_{\mathrm{L}}\rangle = e^{iqy + \lambda_{\mathrm{L}} x}|\chi\rangle\ , \qquad |\psi_{\mathrm{R}}\rangle = e^{iqy - \lambda_{\mathrm{R}} x}|\chi\rangle \tag{4.38}$$

with the two inverse localization lengths λ_{L} and λ_{R}, while the spinor $|\chi\rangle$ has to be equal on both sides due to the boundary condition for the wave function at the interface $x = 0$, which requires the wave function to be continuous. The two solutions obey the eigenvalue equation for $x < 0$ and $x > 0$, respectively

$$\left(iv\lambda_{\mathrm{L}}\sigma_y + qv\sigma_x - \boldsymbol{M}_{\mathrm{L}}\boldsymbol{\sigma} - \mu_{\mathrm{L}}\sigma_0\right)|\chi\rangle = E|\chi\rangle\ , \tag{4.39}$$

$$\left(-iv\lambda_{\mathrm{R}}\sigma_y + qv\sigma_x - \boldsymbol{M}_{\mathrm{R}}\boldsymbol{\sigma} - \mu_{\mathrm{R}}\sigma_0\right)|\chi\rangle = E|\chi\rangle\ , \tag{4.40}$$

with energy eigenvalue E. When multiplied by $\mp i\sigma_y$ from the left, these equations yield by virtue of $(\boldsymbol{a}\cdot\boldsymbol{\sigma})(\boldsymbol{b}\cdot\boldsymbol{\sigma}) = (\boldsymbol{a}\cdot\boldsymbol{b})\sigma_0 + i\boldsymbol{\sigma}\cdot(\boldsymbol{a}\times\boldsymbol{b})$ the following expression

$$(v\lambda_{\mathrm{L/R}} \pm i(\hat{\boldsymbol{e}}_{\boldsymbol{y}}\cdot\boldsymbol{M}_{\mathrm{L/R}}))\,|\chi\rangle = (\pm vq\sigma_z \pm \boldsymbol{\sigma}\cdot(\hat{\boldsymbol{e}}_{\boldsymbol{y}}\times\boldsymbol{M}_{\mathrm{L/R}}) \mp i(\mu_{\mathrm{L/R}} - E)\sigma_y)\,|\chi\rangle \ . \tag{4.41}$$

Adding both yields the simple eigenvalue equation

$$(v(\lambda_{\mathrm{L}} + \lambda_{\mathrm{R}}) - i(\hat{\boldsymbol{e}}_{\boldsymbol{y}}\cdot\Delta\boldsymbol{M}))\,|\chi\rangle = -\left((\hat{\boldsymbol{e}}_{\boldsymbol{y}}\times\Delta\boldsymbol{M})\cdot\boldsymbol{\sigma} - i\Delta\mu\sigma_y\right)|\chi\rangle \ , \tag{4.42}$$

from which we immediately identify the bound state to be an eigenstate of the 2×2 matrix on the right-hand side. For $\Delta\mu \neq 0$, these two states are not orthogonal since this operator is not Hermitian in that case, but we will see that only one of those two states is a bound one. At any rate, the normalized states $\langle\chi_\pm|\chi_\pm\rangle = 1$ are characterized by the following expectation value:

$$\langle\chi_\pm|\boldsymbol{\sigma}|\chi_\pm\rangle = \sin(\varphi/2)\frac{\Delta\boldsymbol{M}_\perp}{|\Delta\boldsymbol{M}_\perp|} \pm \cos(\varphi/2)\frac{\hat{\boldsymbol{e}}_{\boldsymbol{y}}\times\Delta\boldsymbol{M}_\perp}{|\Delta\boldsymbol{M}_\perp|} \quad . \tag{4.43}$$

Here, we introduced the angle $\sin(\varphi/2) \equiv -\frac{\Delta\mu}{|\Delta\boldsymbol{M}_\perp|} \neq 0$ that parametrizes the potential barrier $\Delta\mu$, and $\Delta\boldsymbol{M}_\perp$ is simply component of $\Delta\boldsymbol{M}$ within the x-z plane.

The inverse localization lengths of the bound state on either side of the contact are explicitly given by

$$\begin{aligned} v\lambda_{\mathrm{L}} = &- i\hat{\boldsymbol{e}}_{\boldsymbol{y}}\cdot\boldsymbol{M}_{\mathrm{L}} + qv\,(\sin(\varphi/2)\hat{\boldsymbol{e}}_{\boldsymbol{z}} \mp \cos(\varphi/2)\hat{\boldsymbol{e}}_{\boldsymbol{x}})\cdot\frac{\Delta\boldsymbol{M}_\perp}{|\Delta\boldsymbol{M}_\perp|} + \\ &\frac{1}{|\Delta\boldsymbol{M}_\perp|}\left(\pm\cos(\varphi/2)\ \Delta\boldsymbol{M}_\perp\cdot\boldsymbol{M}_{\mathrm{L}} + \sin(\varphi/2)\hat{\boldsymbol{e}}_{\boldsymbol{y}}\cdot(\boldsymbol{M}_{\mathrm{L}}\times\boldsymbol{M}_{\mathrm{R}})\right) \end{aligned} \tag{4.44}$$

$$\lambda_{\mathrm{R}} = \lambda_{\mathrm{L}}^*|_{\boldsymbol{M}_{\mathrm{L}}\leftrightarrow\boldsymbol{M}_{\mathrm{R}}} \ , \tag{4.45}$$

where the upper/lower sign corresponds to $|\chi_\pm\rangle$, and which has to be chosen such that $\mathrm{Re}\,\lambda_{\mathrm{L}}, \mathrm{Re}\,\lambda_{\mathrm{R}} > 0$. Comparing the terms in the above expressions, we find almost all terms to be of opposite sign in λ_{L} versus λ_{R}, which implies that the increase of these terms makes the bonding weaker on one side and stronger on the other. The only term that contributes to a binding on both sides is $\cos(\varphi/2)\ \Delta\boldsymbol{M}_\perp\cdot\boldsymbol{M}_{\mathrm{L}}$.

For the moment, we neglect the influence of finite q with the additional assumption that $\varphi = 0$. Then this gives rise to the constraint $\mathrm{sgn}(\boldsymbol{M}_{\mathrm{L}}^2 - \boldsymbol{M}_{\mathrm{L}}\cdot\boldsymbol{M}_{\mathrm{R}}) = \mathrm{sgn}(\boldsymbol{M}_{\mathrm{R}}^2 - \boldsymbol{M}_{\mathrm{L}}\cdot\boldsymbol{M}_{\mathrm{R}})$, or

$$\left(\frac{|\boldsymbol{M}_{\mathrm{L}}|}{|\boldsymbol{M}_{\mathrm{R}}|} - \cos\theta\right)\left(\frac{|\boldsymbol{M}_{\mathrm{R}}|}{|\boldsymbol{M}_{\mathrm{L}}|} - \cos\theta\right) > 0 \ , \tag{4.46}$$

where θ is the angle between $\boldsymbol{M}_{\mathrm{L}}$ and $\boldsymbol{M}_{\mathrm{R}}$. Thus, the existence of a bound state depends on the relative angle θ and the relative magnitude of the magnetization vectors, $\frac{|\boldsymbol{M}_{\mathrm{R}}|}{|\boldsymbol{M}_{\mathrm{L}}|}$. A phase diagram for the existence of a bound states is shown in figure 4.4(a).

In the end, we find that the bound state is always given by $|\chi\rangle \equiv |\chi_-\rangle$. This does not change, even when $\varphi \neq 0$ or $q \neq 0$ due to the above observation that all other relevant terms in λ_{L} and λ_{R} are equal, but of opposite sign. Also, note that the M_y-component plays no major role for the bound state other than giving rise to an oscillatory modulation of the bound state wave function, but it does not alter energies or any other expectation values of physical relevance.

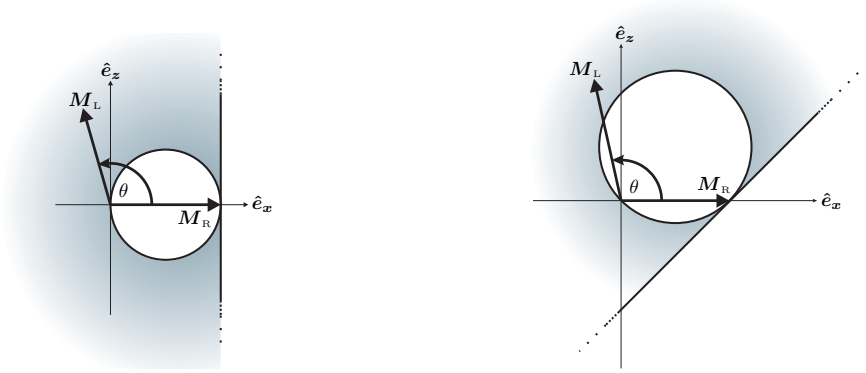

(a) $\Delta\mu = 0$ (b) $\sin(\varphi/2) \equiv -\frac{\Delta\mu}{|\Delta \boldsymbol{M}_\perp|} = 1$

Figure 4.4.: Phase diagrams showing the existence of a bound state (indicated by the shading) at the interface between two ferromagnets with magnetizations $\boldsymbol{M}_\mathrm{R}$ and $\boldsymbol{M}_\mathrm{L}$. Only the relative orientation of $\boldsymbol{M}_\mathrm{R}$ and $\boldsymbol{M}_\mathrm{L}$ is relevant for the existence of a bound state, and *not* its absolute orientation in the x-z plane. Therefore, without loss of generality we can align $\boldsymbol{M}_\mathrm{R}$ along the x-direction. The boundaries are defined by a circle with center $\boldsymbol{M}_\mathrm{R}/2$ and radius $\boldsymbol{M}_\mathrm{R}/2$ and the vertical line tangent to the circle at $\boldsymbol{M}_\mathrm{R}$. Plot (b) depicts the case of non-vanishing chemical potential difference $\Delta\mu$, parametrized by the angle φ which here is chosen to be $\varphi = \pi/2$. Note that changing the sign of φ simply yields a diagram that is the mirror image with respect to the direction $\boldsymbol{M}_\mathrm{R}$.

This is not surprising, since according to section 4.2.2, this component can be eliminated by virtue of a gauge transformation.

In the case of a finite potential difference $\Delta\mu = -|\Delta \boldsymbol{M}_\perp| \sin(\varphi/2)$, we first note that for $|\Delta\mu| > |\Delta M_\perp|$, the important contribution to λ becomes imaginary and thus, a bound state is not possible. For $|\varphi| \leq \pi$, we have the following constraints for the exsistance of a bound state,

$$\cos(\varphi/2)\left(\frac{|\boldsymbol{M}_\mathrm{L}|}{|\boldsymbol{M}_\mathrm{R}|} - \cos\theta\right) - \sin(\varphi/2)\sin\theta > 0$$

and

$$\cos(\varphi/2)\left(\frac{|\boldsymbol{M}_\mathrm{R}|}{|\boldsymbol{M}_\mathrm{L}|} - \cos\theta\right) + \sin(\varphi/2)\sin\theta > 0 \ .$$

In Figure 4.4(b), we show how finite φ modifies the bound state phase diagram.

The energy of the bound states is then readily obtained by taking the expectation value of $|\psi\rangle$ with respect to the Hamiltonian,

$$E(q) = \langle\psi|H|\psi\rangle = E_0 + v_\mathrm{DW} q \tag{4.47}$$

where the constant part of the energy reads

$$E_0 = -\sin(\varphi/2)\frac{(\boldsymbol{M}_\mathrm{R})_\perp^2 - (\boldsymbol{M}_\mathrm{L})_\perp^2}{2|\Delta \boldsymbol{M}_\perp|} - \cos(\varphi/2)\ \frac{\hat{\boldsymbol{e}}_{\boldsymbol{y}}\cdot(\boldsymbol{M}_\mathrm{L}\times\boldsymbol{M}_\mathrm{R})}{|\Delta \boldsymbol{M}_\perp|}\ , \tag{4.48}$$

$$\tag{4.49}$$

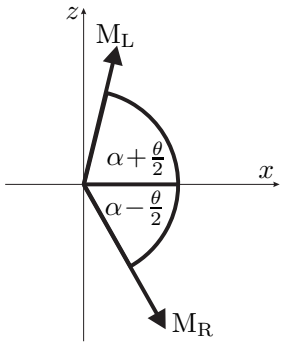

Figure 4.5.: Definitions of the angles θ and α in the x-z plane. The interface defined by the domain wall is perpendicular to this plane, i.e. along the y direction.

and we assume without loss of generality that $\mu_{\rm L} = -\mu_{\rm R}$. The group velocity for propagation along the domain wall is

$$v_{\rm DW} = v\langle\psi|\boldsymbol{\sigma}\hat{\boldsymbol{e}}_{\boldsymbol{x}}|\psi\rangle = v\,[\sin(\varphi/2)\hat{\boldsymbol{e}}_{\boldsymbol{x}} - \cos(\varphi/2)\hat{\boldsymbol{e}}_{\boldsymbol{z}}]\cdot\frac{\Delta\boldsymbol{M}_\perp}{|\Delta\boldsymbol{M}_\perp|}\ . \tag{4.50}$$

Note that the energy shift E_0 of the bound state changes sign when we exchange the two magnetizations $\boldsymbol{M}_{\rm R} \leftrightarrow \boldsymbol{M}_{\rm L}$, and it is zero only when $\boldsymbol{M}_{\rm L}$ and $\boldsymbol{M}_{\rm R}$ are anti-parallel. Essentially, the dispersion with the transverse momentum q is linear, so that the group velocity is constant with its sign determining the chirality of the bound state. Of course, what one sees here is the chirality of the underlying metallic states on the surface of the topological insulator, which manifests itself in the chirality of the bound states at a domain wall.

Finally, in the case $|\boldsymbol{M}_{\rm L}| = |\boldsymbol{M}_{\rm R}| = M$, we give a simple expression for the energy dispersion of the bound state

$$E(q) = -M\cos(\varphi/2)\cos(\theta/2)\,\mathrm{sgn}(\theta) - vq\cos(\varphi/2+\alpha)\ , \tag{4.51}$$

where θ is the angle between $\boldsymbol{M}_{\rm L}$ and $\boldsymbol{M}_{\rm R}$ in the x-z plane.[2] α describes the absolute orientation of $\Delta\boldsymbol{M}_\perp$ in the x-z plane (see Fig. 4.5). We can see that the group velocity does not depend on the relative angle θ, only on the sum $\varphi/2+\alpha$ which combines the strength of the potential barrier φ and the absolute position α of the two vectors in the x-z plane. On the other side, the energy shift E_0 is essentially controlled by the relative angle θ.

4.3.2. Zero Energy Bound States

We now want to study the zero energy bound states of a system with a general stationary magnetic texture $\boldsymbol{M}(\boldsymbol{r})$ and $M_z(\boldsymbol{r})$. Its interest lies in the fact that the zero energy bound state is essentially responsible for the half-integer quantum Hall effect, as it for example the case in graphene which exhibits a zero energy Landau level due to its relativistic dispersion [2]. The zero energy state contributes only half-a-degree of freedom as compared to finite energy excitations.

[2] Note that we define θ to be in the interval $-\pi..\pi$, so that we have $\mathrm{sgn}(\sin\theta/2) = \mathrm{sgn}(\theta)$.

The Hamiltonian to be utilized here reads

$$\mathcal{H} = i\hbar v \boldsymbol{\sigma}(\hat{\boldsymbol{e}}_{\boldsymbol{z}} \times \boldsymbol{\nabla}) - \boldsymbol{\sigma}(\boldsymbol{M}_{\mathrm{l}} + \boldsymbol{M}_{\mathrm{t}}) - M_z \sigma_z \ , \tag{4.52}$$

where $\boldsymbol{\nabla} \cdot \boldsymbol{M}_{\mathrm{t}} = 0$ and $\hat{\boldsymbol{e}}_{\boldsymbol{z}}(\boldsymbol{\nabla} \times \boldsymbol{M}_{\mathrm{l}}) = 0$, so that we can introduce the potentials φ_{t} and φ_{l} such that

$$\boldsymbol{M}_{\mathrm{l}} = \boldsymbol{\nabla}\varphi_{\mathrm{l}} \ , \qquad \varphi_{\mathrm{l}}(\boldsymbol{r}) = \int^{\boldsymbol{r}} \mathrm{d}\boldsymbol{r}' \cdot \boldsymbol{M}_{\mathrm{l}}(\boldsymbol{r}') \tag{4.53}$$

$$\boldsymbol{M}_{\mathrm{t}} = (\hat{\boldsymbol{e}}_{\boldsymbol{z}} \times \boldsymbol{\nabla})\varphi_{\mathrm{t}} \ , \qquad \varphi_{\mathrm{t}}(\boldsymbol{r}) = -\int^{\boldsymbol{r}} \mathrm{d}\boldsymbol{r}' \cdot (\hat{\boldsymbol{e}}_{\boldsymbol{z}} \times \boldsymbol{M}_{\mathrm{t}}(\boldsymbol{r}')) \ . \tag{4.54}$$

We make an ansatz for the wave function (the work of Aharonov and Casher [175] use the same basic idea)

$$\Psi(\boldsymbol{r}) = e^{-\frac{i}{\hbar v}\varphi_{\mathrm{t}} - \frac{1}{\hbar v}\sigma_z \varphi_{\mathrm{l}}} \chi(\boldsymbol{r}) \ , \tag{4.55}$$

which solves the eigenvalue equation for $|E| = |M_z|$ in the case of constant mass term M_z. Generally, there is a whole set of zero energy bound states which can be easily specified by noting that

$$i\boldsymbol{\sigma}(\hat{\boldsymbol{e}}_{\boldsymbol{z}} \times \boldsymbol{\nabla}) e^{i\boldsymbol{q}\boldsymbol{r} + \sigma_z (\boldsymbol{r} \times \boldsymbol{q})\hat{\boldsymbol{e}}_{\boldsymbol{z}}} = 0 \ , \tag{4.56}$$

so that in carthesian coordinates the general solution for the zero energy bound states reads

$$|\psi_{\boldsymbol{q}}\rangle = e^{-\frac{i}{\hbar v}\varphi_{\mathrm{t}} - \frac{1}{\hbar v}\sigma_z \varphi_{\mathrm{l}}} e^{i\boldsymbol{q}\boldsymbol{r} + \sigma_z (\boldsymbol{r} \times \boldsymbol{q})\hat{\boldsymbol{e}}_{\boldsymbol{z}}} |s\rangle \ . \tag{4.57}$$

The condition for the existence of a localized state is $\sigma_z \varphi_{\mathrm{l}}(|\boldsymbol{r}| \to \infty) \to +\infty$, where we have to choose spin-up or spin-down eigenstate such that σ_z provides the proper positive sign, which leads to a convergent solution (4.57) in all directions of space. The constraint on the size of $\boldsymbol{q}$ is such that the term $\boldsymbol{r} \times \boldsymbol{q}$ does not destroy the binding character of φ_{l}. The quantum number $\boldsymbol{q}$ is convenient for one-dimensional problems however, in two dimensions it is not easy to create a set of orthogonal states starting from the $\boldsymbol{q}$ quantum number.

For two-dimensional central symmetric problems, the best choice to tackle problems is to use the polar coordinate representation (r, ϕ), in which we simply have

$$i\boldsymbol{\sigma}(\hat{\boldsymbol{e}}_{\boldsymbol{z}} \times \boldsymbol{\nabla}) = \begin{pmatrix} 0 & \partial_- \\ -\partial_+ & 0 \end{pmatrix} \ , \tag{4.58}$$

where we introduced

$$\partial_\pm = \partial_x \pm i\partial_y = (\hat{\boldsymbol{e}}_{\boldsymbol{x}} \pm i\hat{\boldsymbol{e}}_{\boldsymbol{y}}) \cdot \boldsymbol{\nabla} = (\hat{\boldsymbol{e}}_{\boldsymbol{x}} \pm i\hat{\boldsymbol{e}}_{\boldsymbol{y}}) \cdot (\hat{\boldsymbol{e}}_r \partial_r + \frac{1}{r}\hat{\boldsymbol{e}}_\phi \partial_\phi) = e^{\pm i\phi}\left(\partial_r \pm \frac{i}{r}\partial_\phi\right) \ , \tag{4.59}$$

since $\hat{\boldsymbol{e}}_r = (\cos\phi, \sin\phi)$ and $\hat{\boldsymbol{e}}_\phi = (-\sin\phi, \cos\phi)$. Now, the general homogeneous solution of $i\boldsymbol{\sigma}(\hat{\boldsymbol{e}}_{\boldsymbol{z}} \times \boldsymbol{\nabla})|\chi\rangle = 0$ is straightforwardly found to be

$$|\chi_m\rangle = e^{im\phi\sigma_z} r^m |s\rangle \ , \tag{4.60}$$

where $m \in \mathbb{Z}$ is the rotational quantum number. Instead of (4.57), the general solution in polar coordinates takes the form

$$|\psi_m\rangle = e^{-\frac{i}{\hbar v}\varphi_{\mathrm{t}}(r) - \frac{1}{\hbar v}\sigma_z \varphi_{\mathrm{l}}(r)} \ e^{im\phi\sigma_z} r^m |s\rangle \ , \tag{4.61}$$

and the regularity of the wave function at $r = 0$ requires $m \geq 0$.

4.3.3. Zero Energy Bound States in a Perpendicular Magnetic Field – Zeroth Landau Level

The zero energy Landau level gives rise to interesting physical effects and essentially is responsible for the half integer quantum hall effect, which was measured in graphene [2] and topological insulators [172, 173].

We start from the topological surface states and apply a constant magnetic field along the z-direction, $\boldsymbol{B} = B\hat{\boldsymbol{e}}_{\boldsymbol{z}}$ that corresponds to the vector potential

$$\boldsymbol{A} = \frac{1}{2}B(\hat{\boldsymbol{e}}_{\boldsymbol{z}} \times \boldsymbol{r}) \tag{4.62}$$

in a symmetric gauge, and which is minimally coupled to the momentum $\boldsymbol{p} - q\boldsymbol{A}$, so that the contribution to the magnetization

$$\boldsymbol{M}_{\mathrm{l}} = \frac{vq}{2}B\boldsymbol{r} \tag{4.63}$$

is of the longitudinal type because $\boldsymbol{\nabla}\times\boldsymbol{M}_{\mathrm{l}} = 0$. The corresponding scalar potential is according to (4.53)

$$\varphi_{\mathrm{l}}(\boldsymbol{r}) = \frac{vq}{2}B\frac{r^2}{2} \tag{4.64}$$

and depends only on the modulus of $\boldsymbol{r}$, therefore making the problem radially symmetric. The general solution for the zero energy Landau levels ($n = 0$) then is readily obtained from (4.61)

$$|n = 0, m\rangle = \exp\left\{-\sigma_z \frac{qB}{4}r^2\right\}\ e^{im\phi\sigma_z} r^m |s\rangle\ , \tag{4.65}$$

where $|s\rangle$ is one of the two eigenstates of σ_z and is determined by the sign of the magnetic field B.

We have seen that the proximity induced ferromagnetism essentially leads to an effective magnetic field (4.29), and the effects one obtains are therefore reminiscent to those of an externally applied magnetic field. One may wonder whether those two different scenarios can be completely mapped to each other. Lets put aside the question whether it is possible at all to find an appropriate magnetization structure that reproduces the vector potential A, like in the present situation where $\boldsymbol{M}_{\mathrm{eff}} = \frac{vq}{2}B\boldsymbol{r}$ and the corresponding magnetization would have to be a vortex structure which is pointing radially outward (like in Fig. 4.6(a)) and with linearly increasing magnitude of the magnetization. This would at best be realized in some finite region of space where the resulting effective magnetic field can be taken approximately as a constant and pointing along the z-direction.
As long as only momentum independent observables are studied, both cases should indeed yield identical results, for example true for the energy spectrum or the charge current (4.4). These are actually the relevant observables in this section, so we can conclude that treating the inhomogeneous magnetization structures is not different to an external magnetic field. Essentially, the key difference is that the external magnetic field is a consequence of enforcing gauge-invariance, whereas it is not the case for $\boldsymbol{M}(\boldsymbol{r})$. On the other side, if one has to

deal with observables that involve the momentum $\boldsymbol{k}$, one has to distinguish between gauge invariant kinetic momentum and canonical momentum. The implications of the appearance of gauge invariant kinetical variables in effective theories have been studied at length in chapter 3.

4.3.4. Zero Energy Bound State in 2-Dimensional Structures

In magnetic nanostructures, one often encounters vortices in equilibrium magnetization configurations with the potential application in magnetic data storage [176] due to the rather small size of the vortex core of ≈ 10nm.

The mathematical description of the magnetic configuration of general vortices is given by

$$\boldsymbol{M}(\boldsymbol{r}) = M\sqrt{1-m_z^2(r)}\begin{pmatrix}\cos(p\phi+\phi_0)\\ \sin(p\phi+\phi_0)\\ 0\end{pmatrix} + Mm_z(r)\,\hat{\boldsymbol{e}}_{\boldsymbol{z}} \tag{4.66}$$

where $p \in \mathbb{Z}$ is an integer number denoting the order of the vortex. $m_z(r)$ is a radial function peaked at $r = 0$ and falling off to zero for large distances from the center and describes to pointing up or down of the magnetization at the vortex core. The sign of m_z specifies the polarity of the vortex, i.e. whether the magnetization in the core is pointing upward or downward. The first term in (4.66) describes the in-plane component of the magnetization with the two parameters p and ϕ_0. For the case $p = 1$ and $\phi_0 = \pm\frac{\pi}{2}$, the magnetization curls around the center with the sign of ϕ_0 denoting the chirality of the vortex.

We solve the simpler problem of the r-independent configuration by first taking $m_z = 0$

$$\boldsymbol{M}(\boldsymbol{r}) = M\begin{pmatrix}\cos(p\phi+\phi_0)\\ \sin(p\phi+\phi_0)\\ 0\end{pmatrix} \tag{4.67}$$

and we can treat the r-dependence along with the $m_z(r)$ component perturbatively later.

After some calculus, we find that

$$\varphi_{\mathrm{l}} = \frac{Mr}{2-p}\cos\left((p-1)\phi+\phi_0\right)\ , \tag{4.68}$$

$$\varphi_{\mathrm{t}} = \frac{Mr}{2-p}\sin\left((p-1)\phi+\phi_0\right)\ , \tag{4.69}$$

and for the special case $p = 2$,

$$\varphi_{\mathrm{l}} = Mr\sin\left(\phi+\phi_0\right)\ , \tag{4.70}$$

$$\varphi_{\mathrm{t}} = -Mr\cos\left(\phi+\phi_0\right)\ , \tag{4.71}$$

so that ($\boldsymbol{\nabla} = \hat{\boldsymbol{e}}_r\partial_r + \hat{\boldsymbol{e}}_\phi\frac{1}{r}\partial_\phi$)

$$\boldsymbol{M}_{\mathrm{l}} = \boldsymbol{\nabla}\varphi_{\mathrm{l}} \tag{4.72}$$

$$\boldsymbol{M}_{\mathrm{t}} = (\hat{\boldsymbol{e}}_{\boldsymbol{z}}\times\boldsymbol{\nabla})\varphi_{\mathrm{t}} \tag{4.73}$$

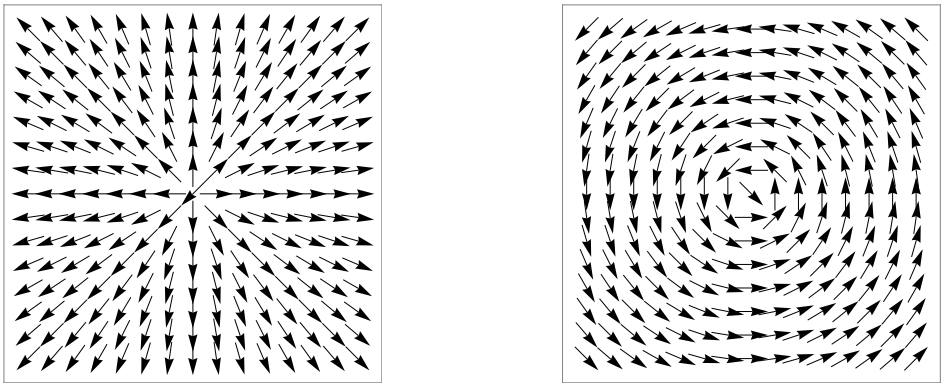

(a) Radial Vortex (b) Chiral Vortex

Figure 4.6.: Plots of the vortex structure defined by (4.67) for $p = 1$ and $\phi_0 = 0$ in (a) while in (b), the chiral vortex with $\phi_0 = \frac{\pi}{2}$ is sketched.

and $\boldsymbol{M} = \boldsymbol{M}_\mathrm{l} + \boldsymbol{M}_\mathrm{t}$.

According to result (4.61), we can readily write the general solution for the zero energy bound state,

$$e^{-\frac{i}{v}\varphi_\mathrm{t}(r)-\frac{1}{v}\sigma_z\varphi_\mathrm{l}(r)}\; e^{im\phi\sigma_z} r^m |s\rangle \ . \tag{4.74}$$

Only the curl-free part $\boldsymbol{M}_\mathrm{l}$ of the vector field is responsible for the emergence of a bound state and thus, there are severe restrictions on the term $\sigma_z\varphi_\mathrm{l}(r) = \sigma_z \frac{Mr}{2-p}\cos\left((p-1)\phi + \phi_0\right)$, since it has to be positive for all values of ϕ, i.e. the bound state should be stable in all directions in space. This essentially is only the case for $p = 1$, but we need one additional condition namely, we have to require that $\cos(\phi_0) \neq 0$ in order to obtain a finite longitudinal component. Unfortunately, $p = 1$ and $\phi = \frac{\pi}{2}$ is exactly the interesting vortex to be found as domain walls in nano structures and is shown in Figure 4.6(b). In Figure. 4.6(a), we show the magnetization structure for $\phi = 0$ which exhibits zero energy bound states labeled by the quantum number m.

On the other side, having the alternative dispersion $\boldsymbol{\sigma}\cdot\boldsymbol{\nabla}$ (see Eqn. 4.1) as in graphene, and which might be realized in a topological insulator yet to be discovered, the roles of $\boldsymbol{M}_\mathrm{l}$ and $\boldsymbol{M}_\mathrm{t}$ would simply exchange, rendering the chiral vortex the one which exhibits bound states. In this case, the vortex usually encountered in nano-structures would yield the desired bound states which could be studied for example by measuring the Hall conductivity at the Dirac point. In fact, this situation is then similar to the zero energy Landau levels that lead to the half-integer quantum Hall conductance.

In order to determine the spatial extension of the m-th bound state, we simply calculate the expectation value of the radial position operator r with respect to the wave function $\psi_m(r) = e^{-Mr}e^{im\phi}r^m$, and we obtain

$$\frac{\langle\psi_m|r|\psi_m\rangle}{\langle\psi_m|\psi_m\rangle} = \frac{\int \mathrm{d}^2 r\, e^{-2Mr} r^{2m+1}}{\int \mathrm{d}^2 r\, e^{-2Mr} r^{2m}} = \frac{1+m}{M} \ . \tag{4.75}$$

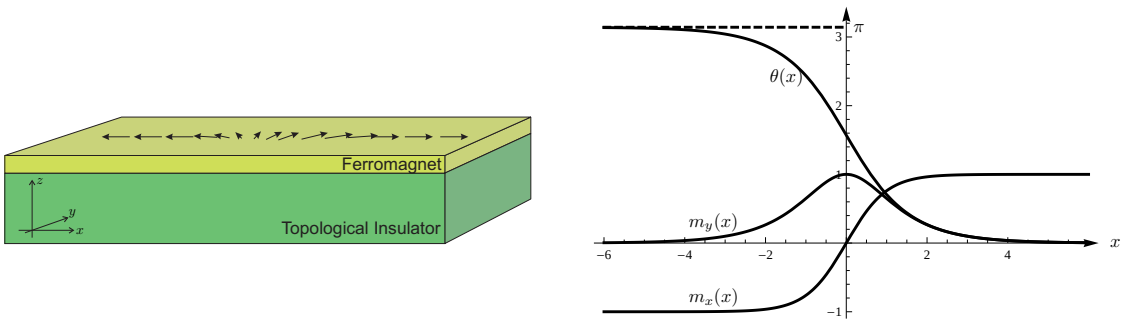

(a) STI with thin ferromagnet

(b) Magnetization

Figure 4.7.: (a) The system of topological insulator with an insulating ferromagnetic layer on top which contains a tail-to-tail domain wall and the magnetization stays always within the plane of the STI. The functional dependence of the magnetization is plotted in (b).

Consequently, the number of bound states scales with the linear dimension of the system.

There is another problem related to these zero energy bound states namely, a non-zero mass component M_z shifts the energies away from zero, which is evident from the Hamiltonian (4.52) and noting that the zero energy state is an eigenstate of σ_z. For constant M_z, the energy is simply shifted by $|M_z|$ and, as it is the case for the vortices around its core, an inhomogeneous M_z can be treated using perturbation theory to obtain an estimate for the energy shift,

$$\Delta E = -\frac{\langle\psi_m|M_z\sigma_z|\psi_m\rangle}{\langle\psi_m|\psi_m\rangle} \ , \tag{4.76}$$

which generally yields a finite contribution.

4.4. Finite Width Domain Wall - The x-y Configuration

In the previous sections, we thoroughly studied the appearance of bound states at sharply defined interfaces between regions of different physical properties. We also studied the zero bound states that might exist at magnetization structures localized in a finite region of space, like domain walls or vortices. However, now we are also interested in whether more bound states might exist at energies different from zero and also, how transport channels are affected by the presence of domain walls. In order to do so, we diagonalize the Dirac equation in the presence of a quasi one-dimensional domain wall of arbitrary width, and study its properties using the exact eigensystem.

The Hamiltonian which we employ subsequently is

$$\mathcal{H} = i\hbar v\boldsymbol{\sigma}\cdot(\hat{\boldsymbol{e}}_{\boldsymbol{z}}\times\boldsymbol{\nabla}) - M\boldsymbol{m}(\boldsymbol{r})\cdot\boldsymbol{\sigma} \tag{4.77}$$

and describes the dispersion of the surface Dirac states, exchange coupled to the magnetization profile $\boldsymbol{m}(x)$ with constant magnitude M. The domain wall profile is encoded in the spatially

dependent magnetization direction $\boldsymbol{m}$ and in the following, we will study different quasi-one-dimensional domain wall configurations.

As we will find out later, it is of advantage to first solve the configuration of the Néel wall illustrated in Figure 4.7(a), where the magnetization vector far away from the domain-wall is perpendicular to the wall and the magnetization rotates in the plane of the topological insulator. The magnetization vector has the explicit form

$$\boldsymbol{m}(\boldsymbol{r}) = \begin{pmatrix} \cos\theta(x) \\ \sin\theta(x) \\ 0 \end{pmatrix} , \tag{4.78}$$

where the angle $\theta(x)$ has the analytical form

$$\cos\theta(x) = \tanh\left(\frac{x}{w}\right) \tag{4.79}$$

when one considers the simplest mean-field model of a ferromagnet with exchange constant A and anisotropy constant K, so that the length of the domain wall becomes $w = \sqrt{A/K}$. The functional dependence of the magnetization is plotted in Figure 4.7(b).

We now want to solve the full eigenvalue problem

$$\mathcal{H}|\Psi\rangle = \left[i\hbar v\sigma_y\partial_x - i\hbar v\sigma_x\partial_y - Mm_x(x)\sigma_x - Mm_y(x)\sigma_y\right]|\Psi\rangle = E|\Psi\rangle \tag{4.80}$$

in order to find the bound states that exist at a domain wall of arbitrary width w and with the specific shape given in (4.78).

As explained in detail in a previous section, we can eliminate the m_y-component by virtue of a gauge transformation,

$$|\Psi\rangle \to \exp\left\{-i\frac{M}{\hbar v}\int^x \mathrm{d}x'\ m_y(x')\right\}|\psi\rangle = \exp\left\{-i\frac{M}{\hbar v}\int^x \mathrm{d}x'\ \sin\theta(x')\right\}|\psi\rangle = e^{i\frac{M}{\hbar v}\theta(x)}|\psi\rangle\ , \tag{4.81}$$

since $\sin\theta(x) = -\partial_x\theta(x)$.

Furthermore, our problem is effectively one-dimensional so that the solution depends only on x, while k_y is a good quantum number. Thus, we make the ansatz for the wave-function

$$|\Psi(x,y)\rangle = e^{i\frac{M}{\hbar v}\theta(x)}e^{iyk_y}|\psi(x)\rangle\ , \tag{4.82}$$

so that the reduced Hamiltonian has the following form,

$$H = i\hbar v\sigma_y\partial_x + (\hbar v k_y - M\tanh(x/w))\sigma_x\ . \tag{4.83}$$

For the sake of convenience, we rescale $x \to xw$, i.e. we measure x in units of the domain wall width w, and we eliminate $\hbar v$ by redefinition of $\Delta = \frac{Mw}{\hbar v}$, $q = k_y w$ and $\epsilon = \frac{Ew}{\hbar v}$, so that now, we have to solve the dimensionless eigenvalue equation

$$H\psi = \left[i\sigma_y\partial_x + (q - \Delta\tanh(x))\sigma_x\right]\psi = \epsilon\psi\ . \tag{4.84}$$

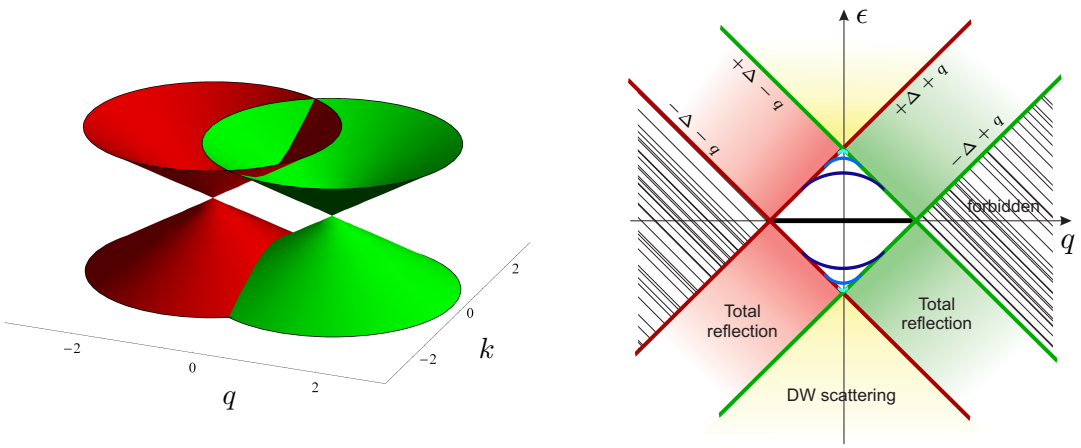

(a) Dirac cones in the bulk

(b) Projected energy diagram

Figure 4.8.: Plot (a) shows the two Dirac cones existing left (red) and right (green) of the domain wall sufficiently far away. For a given energy ϵ and transverse momentum q, a propagating solution can only exist for k-values where the two cones overlap. For other parameter ranges where an appropriate k-value can be found only for one cone, we have a totally reflecting solution. If we cannot find a k value at all, a solution does not exist or we have a bound state. The situation is illustrated in (b), where we show a projection of the left and right cones and the allowed values for the parameters ϵ and q which support states of the total system. The shaded areas contain a continuum of states, where the totally reflecting states (red and green shaded areas) can exist only on either side of the domain wall, and excitations inside the yellow shaded area exist on both sides and describe the scattering states for the domain wall. The inner diamond of this structure contains bound states which are symmetric with respect to positive and negative states, and there is a flat (dispersionless) band at $\epsilon = 0$ for $|q| \leq \Delta$.

4.4.1. Bulk Properties

We first take a closer look at Hamiltonian (4.84) by studying its bulk properties far away from the domain-wall. We investigate the asymptotics of this equation in order to find the parameter range for the existence of various types of solutions. For $x \to \mp\infty$, we have $\cos\theta \to \mp 1$, so that the bulk Hamiltonian on the left (L) and the right (R) side of the domain wall becomes

$$H_{\mathrm{L/R}} = i\sigma_y\partial_x + (q \pm \Delta)\sigma_x = -\sigma_y k_{\mathrm{L/R}} + (q \pm \Delta)\sigma_x \ , \tag{4.85}$$

and the asymptotic behavior of the exact solutions should correspond to the plane wave solutions

$$\psi_{\mathrm{L/R}} = a_{\mathrm{L/R}} e^{ixk_{\mathrm{L/R}}} |\chi_{\mathrm{L/R}}\rangle + b_{\mathrm{L/R}} e^{-ixk_{\mathrm{L/R}}} |\chi^*_{\mathrm{L/R}}\rangle \ . \tag{4.86}$$

The wave vectors for the left and the right side obey

$$k^2_{\mathrm{L/R}} = \epsilon^2 - (q \pm \Delta)^2 \ , \tag{4.87}$$

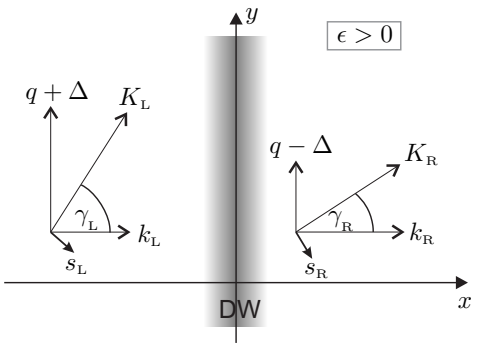

Figure 4.9.: Illustration of the various quantities that are relevant for transport across a domain wall. All parameters are defined in the bulk far away from the domain wall. The index (L/R) denotes the left and right side of the interface, k are wave vectors in the transport direction (x-direction) and q is the momentum of the Dirac Fermions parallel to the interface, which is shifted by the magnetization $\Delta > 0$ pointing along the x-direction (see Hamiltonian (4.84)). $K_{\mathrm{L/R}} = k_{\mathrm{L/R}} + i(q \pm \Delta)$ denotes the complex representation of the total vector and γ is the angle with respect to the x-direction, while s is the direction of the electron spin which is simply rotated by $-\frac{\pi}{2}$ with respect to the effective momentum K, a direct consequence of the dispersion $-\hbar v \boldsymbol{\sigma} \cdot (\hat{\boldsymbol{e}}_{\boldsymbol{z}} \times \boldsymbol{k})$. Energy conservation dictates $|K_{\mathrm{L}}| = |K_{\mathrm{R}}| = \epsilon$. This is the situation for the positive energy branch $\epsilon > 0$, while for negatives energies, s simply points into the opposite direction. Note that the z-direction is not relevant for this problem.

when we consider an eigenstate with the energy ϵ. This solution describes a Dirac cone with the center shifted to negative values at $q_0 = -\Delta$ on the left side and vice versa on the right side (see Figure 4.8). The coefficients $a_{\mathrm{L/R}}$ and $b_{\mathrm{L/R}}$ describe the amplitudes for the scattering states, and they will be given later analytically by first solving the full eigenvalue problem (4.84), and then finding the asymptotics of the solution.

The spin eigenstates of the bulk system on the left and right sides are

$$|\chi_{\mathrm{L/R}}\rangle = \frac{1}{\sqrt{2}} \begin{pmatrix} e^{-\frac{i}{2}(\gamma_{\mathrm{L/R}} - \frac{\pi}{2})} \\ e^{+\frac{i}{2}(\gamma_{\mathrm{L/R}} - \frac{\pi}{2})} \end{pmatrix} \tag{4.88}$$

with

$$e^{i\gamma_{\mathrm{L/R}}} = \frac{k_{\mathrm{L/R}} + i(q \pm \Delta)}{\epsilon} = \frac{K_{\mathrm{L/R}}}{\epsilon} \ ,$$

so that $H_{\mathrm{L/R}}|\chi_{\mathrm{L/R}}\rangle = \epsilon|\chi_{\mathrm{L/R}}\rangle$. In the end, the direction of $K_{\mathrm{L/R}}$ and thus, the corresponding angle $\gamma_{\mathrm{L/R}}$ points along the physical current flow, since $\boldsymbol{j} = v\hat{\boldsymbol{e}}_{\boldsymbol{z}} \times \boldsymbol{\sigma}$. The various quantities introduced here are illustrated in Figure 4.9. The spin expectation values in the spinor states $|\chi_{\mathrm{L/R}}\rangle$ are simply

$$\langle \chi_{\mathrm{L/R}} | \sigma_x + i\sigma_y | \chi_{\mathrm{L/R}} \rangle = e^{i(\gamma_{\mathrm{L/R}} - \frac{\pi}{2})} \ , \tag{4.89}$$

$$\langle \chi^*_{\mathrm{L/R}} | (\sigma_x + i\sigma_y) | \chi_{\mathrm{L/R}} \rangle = 1 \ , \tag{4.90}$$

and $\langle \chi_{\mathrm{L/R}} | \sigma_z | \chi_{\mathrm{L/R}} \rangle = 0$.

According to (4.4), the current is essentially given by the expectation value of the electron spin, and we can simply express it in terms of the in-plane component of the electron spin by considering the complex current

$$j \equiv j_x + ij_y = iv(\sigma_x + i\sigma_y) \ . \tag{4.91}$$

Using (4.89), we directly obtain

$$\langle \chi_{\mathrm{L/R}} | j | \chi_{\mathrm{L/R}} \rangle = v e^{i\gamma_{\mathrm{L/R}}} = v \frac{K_{\mathrm{L/R}}}{\epsilon} \ , \tag{4.92}$$

which means that the current direction is given by $\gamma_{\mathrm{L/R}}$, while its amplitude is constant and equal to $|j| = v$. The current in the transport direction is then the real part of (4.92), $v\frac{k_{\mathrm{L/R}}}{\epsilon}$ and constitutes the group velocity in transport *viz.* x-direction. The current contribution for an electron in the state $\psi_{\mathrm{L/R}}$ from Eq. (4.86) is then given by

$$\langle \psi_{\mathrm{L/R}} | j | \psi_{\mathrm{L/R}} \rangle = v|a_{\mathrm{L/R}}|^2 e^{i\gamma_{\mathrm{L/R}}} - v|b_{\mathrm{L/R}}|^2 e^{-i\gamma_{\mathrm{L/R}}} \ , \tag{4.93}$$

where the interference term drops after averaging over a finite range, a so-called coarse graining procedure. We see that the second term describes a current flow in the opposite direction.

4.4.2. Symmetries

This system exhibits a number of symmetries which can be used to easily derive other solutions from a given eigensolution. This is in particular useful, since the scattering states are doubly degenerate for each energy and we can relate them via symmetry operations, and the situation is similar between positive and negative energy solutions.
We introduce the usual space inversion symmetry operator $\mathcal{T}_x$ with the actions $\mathcal{T}_x x = -x$ and $\mathcal{T}_x \partial_x = -\partial_x$. Furthermore, we introduce $\mathcal{T}_q$ which simply flips the sign of q, i.e. $\mathcal{T}_q q = -q$. Both combined yield the space inversion operator in two dimensions, $\mathcal{T}_{\boldsymbol{r}} = \mathcal{T}_x \mathcal{T}_q$. Furthermore, we denote $\mathcal{K}$ as complex conjugation and $\mathcal{T}_M$ flips the sign of M. Some further useful properties are $\mathcal{T}_x k_{\mathrm{L/R}} = k_{\mathrm{L/R}}$ and $\mathcal{T}_M k_{\mathrm{L/R}} = k_{\mathrm{R/L}}$, while $\mathcal{K}k = -k$. Using this notation, the usual time reversal operator can be written as $\mathcal{T}_T = i\sigma_y \mathcal{T}_M \mathcal{T}_q \mathcal{K}$ with $\mathcal{T}_T^2 = -1$, so that we can summarize all symmetries

$$\begin{aligned} [\mathcal{T}_T, H] = 0 \ , \quad [\mathcal{T}_M \mathcal{T}_x \sigma_x, H] = 0 \ , \\ [\mathcal{K}, H] = 0 \ , \quad [\mathcal{T}_q \mathcal{T}_x \sigma_z, H] = 0 \ , \end{aligned} \tag{4.94}$$

where actually only three of them are independent. The space inversion symmetry operator $\mathcal{T}_q \mathcal{T}_x \sigma_z$ is used to relate totally reflecting states that only exist on either side of the boundary, and the two degenerate scattering solutions that exist for each pair of (k, q). The commutation with $\mathcal{K}$ shows that the solutions can be chosen real, which is useful for the bound states, where it is related to a vanishing current along the transport direction, since for a real spinor ψ, $j_x = -v\psi^\dagger \sigma_y \psi = 0$. Furthermore, $\mathcal{T}_M \mathcal{T}_q \sigma_y$ can be used to relate the two components of the Spinor and we will use it to derive $\varphi_\downarrow$ from $\varphi_\uparrow$.

Finally, we note that σ_z anticommutes with H, i.e. $\{H, \sigma_z\} = 0$, from which we immediately obtain $\sigma_z H|\psi_E\rangle = E\sigma_z|\psi_E\rangle = -H\sigma_z|\psi_E\rangle$. Thus, when we take an eigenstate $H|\psi_E\rangle = E|\psi_E\rangle$, we obtain the corresponding eigenstate for negative energy by virtue of

$$|\psi_{-E}\rangle = \sigma_z |\psi_E\rangle \ , \tag{4.95}$$

and furthermore, the spectrum is particle-hole symmetric.

4.4.3. The Exact Solution of the Problem

In order to solve the full eigenproblem (4.84)

$$H\begin{pmatrix}\varphi_\uparrow\\ \varphi_\downarrow\end{pmatrix} = \epsilon\begin{pmatrix}\varphi_\uparrow\\ \varphi_\downarrow\end{pmatrix} \ , \tag{4.96}$$

let us now proceed by performing the variable transformation

$$z \equiv \frac{1}{2}\left(1-\tanh x\right) \quad \Rightarrow \partial_x = -2z(1-z)\partial_z \ , \tag{4.97}$$

which leaves us with two coupled differential equations, however eliminating for example $\varphi_\downarrow$ gives us a second order differential equation. In order to bring this wave equation into hypergeometric form, we make the ansatz $\varphi_\uparrow(z) = (1-z)^{\lambda_1} z^{\lambda_2}\,\phi(z)$ and find that $\lambda_1 = -\frac{i}{2}k_{\mathrm{L}}$, $\lambda_2 = -\frac{i}{2}k_{\mathrm{R}}$ yields the differential equation

$$\left\{z(1-z)\partial_z^2 + (\gamma - (\alpha+\beta+1)z)\partial_z - \alpha\beta\right\}\phi = 0 \tag{4.98}$$

with the coefficients

$$\alpha = 1+\Delta-ik_0 \ , \quad \beta = -\Delta - ik_0 \ , \quad \gamma = 1-ik_{\mathrm{R}} \ . \tag{4.99}$$

This differential equation is well known [177] and we can directly write the final solution as (see appendix E for a short summary of useful properties of the hypergeometric and gamma functions)

$$\varphi_\uparrow(z) = \frac{e^{-\frac{i}{2}(\gamma_{\mathrm{R}}-\frac{\pi}{2})}}{\sqrt{k_{\mathrm{R}}}}(1-z)^{-\frac{i}{2}k_{\mathrm{L}}} z^{-\frac{i}{2}k_{\mathrm{R}}}\,{}_2F_1(1+\Delta-ik_0, -\Delta-ik_0, 1-ik_{\mathrm{R}}, z) \ , \tag{4.100}$$

with $k_0 = \frac{1}{2}(k_{\mathrm{L}}+k_{\mathrm{R}})$ and $\varphi_\downarrow$ is directly obtained using the symmetry $[\mathcal{T}_M\mathcal{T}_q\sigma_y, H] = 0$, so that $\varphi_\downarrow(z) = -i\mathcal{T}_M\mathcal{T}_q\varphi_\uparrow(z)$ and thus,

$$\varphi_\downarrow(z) = \frac{e^{+\frac{i}{2}(\gamma_{\mathrm{R}}-\frac{\pi}{2})}}{\sqrt{k_{\mathrm{R}}}}(1-z)^{-\frac{i}{2}k_{\mathrm{L}}} z^{-\frac{i}{2}k_{\mathrm{R}}}\,{}_2F_1(1-\Delta-ik_0, \Delta-ik_0, 1-ik_{\mathrm{R}}, z) \ . \tag{4.101}$$

The prefactor of this solution is chosen such that it directly reflects the symmetry properties of the system, i.e. $\mathcal{T}_M\mathcal{T}_q\sigma_y\psi = \psi$, and it will in particular be useful later when we need the asymptotic expansion of the scattering states in order to study transport across the domain wall.

It is also possible that both wave-vectors $k_{\mathrm{L/R}}$ become imaginary when q and ϵ lie within the inner diamond in Figure 4.8(b), and thus describe the bound states shown in this diagram. If only one of k_{L} or k_{R} is imaginary (green or red shaded area in Figure 4.8(b)), it describes evanescent modes, i.e. the incoming wave from the right or left, respectively, is totally reflected at the domain wall. The scattering states appear when the Dirac fermion can exist on both sides of the domain wall, i.e. $k_{\mathrm{L/R}}$ is a purely real wave-vector and describes plane waves with dispersion $\epsilon = \sqrt{(q\pm\Delta)^2 + k_{\mathrm{L/R}}^2}$. In this regime, there exist two degenerate solutions and we can most conveniently obtain the other independent solution by using our symmetry relations, namely $[\mathcal{H}, \mathcal{T}_q\mathcal{T}_x\sigma_z] = 0$ so that

$$\psi_2 = e^{-i\frac{\pi}{2}}\mathcal{T}_q\mathcal{T}_x\sigma_z\psi_1 \ .$$

ψ_1 describes an incoming wave from the left that is partially reflected and transmitted to the right side, and likewise, ψ_2 describes an incoming wave from the right side. These two solutions are orthogonal, $\langle\psi_1|\psi_2\rangle = 0$.

Asymptotic solutions

In order to study the properties of this solution, it is interesting to know the asymptotic expansion for values of x far away from the domain wall. With begin with the definition of the coefficient

$$A(k_{\mathrm{L}}, k_{\mathrm{R}}) = \frac{\sqrt{\frac{1}{4}\left(k_{\mathrm{L}}+k_{\mathrm{R}}\right)^2+\Delta^2}}{\sqrt{|k_{\mathrm{L}}k_{\mathrm{R}}|}} \frac{\Gamma(1-ik_{\mathrm{L}})\Gamma(1-ik_{\mathrm{R}})}{\Gamma(1-\Delta-\frac{i}{2}(k_{\mathrm{L}}+k_{\mathrm{R}}))\Gamma(1+\Delta-\frac{i}{2}(k_{\mathrm{L}}+k_{\mathrm{R}}))} \tag{4.102}$$

with the properties $A(k_{\mathrm{L}}, k_{\mathrm{R}})^* = A(-k_{\mathrm{L}}, -k_{\mathrm{R}})$, $\mathcal{T}_q A(k_{\mathrm{L}}, k_{\mathrm{R}}) = A(k_{\mathrm{R}}, k_{\mathrm{L}}) = A(k_{\mathrm{L}}, k_{\mathrm{R}})$ and $\mathcal{T}_M A(k_{\mathrm{L}}, k_{\mathrm{R}}) = A(k_{\mathrm{L}}, k_{\mathrm{R}})$. $\Gamma(x)$ is the gamma function (see appendix E or [177] for a reference), and corresponds to a generalization of the faculty, since for $n \in \mathbb{N}$, $\Gamma(1+n) = n!$.

By making a series expansion of the hypergeometric function around $z = 1$ ($x \to -\infty$) and $z = 0$ ($x \to +\infty$) (see series expansions (E.1) and (E.4)), the asymptotics of (4.100) and (4.101) can be compactly written as

$$\psi_1 = \begin{cases} A(k_{\mathrm{L}}, k_{\mathrm{R}}) \dfrac{e^{ik_{\mathrm{L}}x}}{\sqrt{v_{\mathrm{L}}}}|\chi_{\mathrm{L}}\rangle - A(-k_{\mathrm{L}}, k_{\mathrm{R}}) \dfrac{e^{-ik_{\mathrm{L}}x}}{\sqrt{v_{\mathrm{L}}}}|\chi_{\mathrm{L}}^*\rangle & x \to -\infty \\ \dfrac{e^{ik_{\mathrm{R}}x}}{\sqrt{v_{\mathrm{R}}}}|\chi_{\mathrm{R}}\rangle & x \to +\infty\ . \end{cases} \tag{4.103}$$

For a certain value of the transverse momentum $q > 0$ and energy $\epsilon > \Delta$, the states are doubly degenerate and we have to find the second independent solution, which can be most easily done with the help of the symmetry $[\mathcal{H}, \mathcal{T}_q\mathcal{T}_x\sigma_z] = 0$, so that $\psi_2 = e^{-i\frac{\pi}{2}}\mathcal{T}_q\mathcal{T}_x\sigma_z\psi_1$, and using $\mathcal{T}_q k_{\mathrm{L/R}} = k_{\mathrm{R/L}}$, $\mathcal{T}_q e^{i\gamma_{\mathrm{L/R}}} = e^{-i\gamma_{\mathrm{R/L}}}$ and $\mathcal{T}_q e^{-i\frac{\pi}{2}}\sigma_z|\chi_{\mathrm{L/R}}\rangle = |\chi_{\mathrm{R/L}}^*\rangle$, we readily find

$$\psi_2 = \begin{cases} \dfrac{e^{-ik_{\mathrm{L}}x}}{\sqrt{v_{\mathrm{L}}}}|\chi_{\mathrm{L}}^*\rangle & x \to -\infty \\ A(k_{\mathrm{L}}, k_{\mathrm{R}}) \dfrac{e^{-ik_{\mathrm{R}}x}}{\sqrt{v_{\mathrm{R}}}}|\chi_{\mathrm{R}}^*\rangle + A(k_{\mathrm{L}}, -k_{\mathrm{R}}) \dfrac{e^{ik_{\mathrm{R}}x}}{\sqrt{v_{\mathrm{R}}}}|\chi_{\mathrm{R}}\rangle & x \to +\infty\ . \end{cases} \tag{4.104}$$

These asymptotic expansions can then be used to study ballistic transport, for example. First however, we will investigate the bound states that appear at the domain wall.

4.4.4. Bound States at the Domain Wall

We are now looking for bound states, i.e. solutions with imaginary wave-vector $-ik_{\mathrm{R/L}} > 0$, so that the wave function becomes exponentially localized at the domain wall. We can easily investigate this with the help of the asymptotic expansion (4.103), and since $\frac{1}{\Gamma(-n)} = 0$ for $n \geq 0$, we find from definition (4.102) that $A(k_{\mathrm{L}}, k_{\mathrm{R}}) = 0$, provided that

$$-\frac{i}{2}(k_{\mathrm{L}}+k_{\mathrm{R}}) = \Delta - n\ , \quad n = 0, 1, 2 \ldots \lfloor\Delta\rfloor\ . \tag{4.105}$$

Using relation (4.87), we find for the energies of the bound states

$$\epsilon_{n,q} = \epsilon_{n,0}\sqrt{1 - \frac{q^2}{(\Delta - n)^2}} \ , \tag{4.106}$$

with the energy for zero transverse momentum $q = 0$,

$$\epsilon_{n,0} = \sqrt{(2\Delta - n)n} \ . \tag{4.107}$$

Therefore, we expect a total number of $\lfloor \Delta \rfloor + 1$ bound states for energies $\epsilon \geq 0$. Due to $\{\mathcal{H}, \sigma_z\} = 0$, the spectrum is symmetric with respect to positive and negative energies, so in total, we have $2\lfloor \Delta \rfloor + 1$ bound states at the domain wall, counting the zero energy state $n = 0$ only once. In fact, we see that the hypergeometric function in (4.100) and (4.101) terminates when the above condition is fulfilled and thus, we can directly obtain the wave function of the bound states in analytical form as a power series in $z = \frac{1}{2}(1 - \tanh x)$.

Once $\epsilon_{n,q} = \Delta - |q|$, the bound states merge with the continuum (see Figure 4.8(b)) and become evanescent modes, i.e. a incoming wave that is totally reflected at the domain wall and decays exponentially on the other side of the wall. If the energy of an state is $\epsilon \geq \Delta + |q|$, it becomes a scattering state which is doubly degenerate and exists as a plane wave on both sides of the wall. From the condition $\epsilon_{n,q} = \Delta - |q|$, one obtains the minimal and maximal values for the transverse momentum,

$$q_{\max}^{(n)} = \frac{(\Delta - n)^2}{\Delta} \ , \tag{4.108}$$

so that the bound state exists only for $|q| \leq q_{\max}^{(n)}$. For $n = 0$, we have a dispersionless (flat) band for values of the transverse momentum $|q| \leq \Delta$.

Restoring original units, we get for the dispersion relation

$$E_n(k_y) = \sqrt{(2M - nE_w)\, nE_w}\ \sqrt{1 - \frac{\hbar^2 v^2 k_y^2}{(M - nE_w)^2}} \ , \tag{4.109}$$

and for the maximal transverse momentum

$$(k_y)_{\max}^{(n)} = \frac{(M - nE_w)^2}{\hbar v M} \ , \tag{4.110}$$

where we introduced the energy $E_w \equiv \frac{\hbar v}{w}$ which corresponds to the localization energy of a particle confined within the extensions of the domain wall of width w, as it would be obtained in a semiclassical Bohr-Sommerfeld quantization scheme. The square root dependence of the energy is typical for Dirac fermions, and we have already seen an example thereof in the case of Landau levels for Dirac fermions in equation (4.33).

Actually, in the limit of wide walls and sufficiently low orbit n, the energy $E_n(0) \to \sqrt{2MnE_w}$, which is identical to the Landau-level spectrum of result (4.33), when we use the fact that in the center of the wall the effective field defined by (4.29) is constant for wide walls, $B_{\text{eff}} \to \frac{M}{vw}$. Of course, when the quantum number n becomes comparable to Δ, we obtain corrections from the Landau level result as expressed by (4.109), since the orbits become large and extend into the outer regions of the domain wall where the assumption of constant B_{eff} no longer is valid.

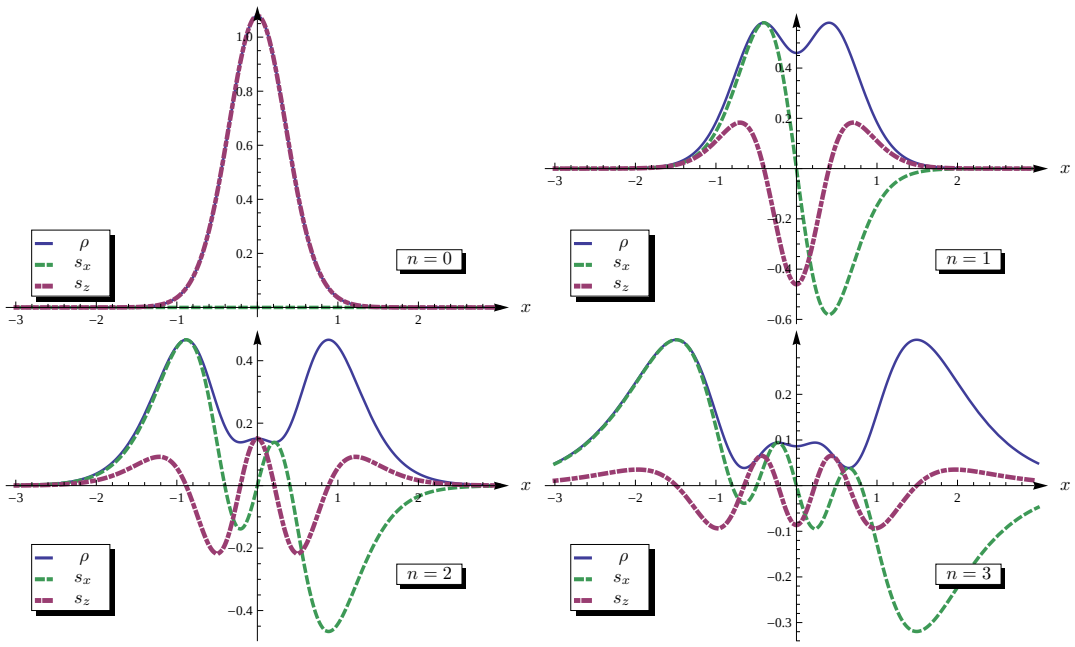

Figure 4.10.: The 4 bound states at the domain wall for the parameters $\Delta = \frac{Mw}{\hbar v} = 3.9$ and $q = 0$. In this case, all the spin expectation values are zero, except for $n = 0$, i.e. $\langle \psi_{n,0} | \boldsymbol{\sigma} | \psi_{n,0} \rangle = \delta_{n,0}\, \hat{\boldsymbol{e}}_{\boldsymbol{z}}$. The s_x component essentially corresponds to the current along the domain wall, since $j_y(x) = v s_x(x)$ can be interpreted as a current density (see continuity equation (4.5)). We see that on the left side of the domain wall ($x < 0$) the current flows in positive direction, and in the opposite direction on the other side ($x > 0$), thus constituting a persistent current circulating around the whole domain wall. We also note that whenever s_x attains a maximum, s_z goes through zero (except for $n = 0$). This is nothing but a manifestation of relation (4.10), which for the present case reads $\frac{\partial s_x}{\partial x} = 2\epsilon_{n,q} s_z$. This implies that circulating currents will enclose regions of finite s_z, with the sign of s_z given by the chirality of current flow. The states for $n \geq 1$ correspond to the first type of semiclassical orbit shown in Figure 4.2(a). The sign of s_x is also consistent in both semiclassical and quantum picture.

Let us now discuss the wave functions of these bound states by plugging the energy dispersion (4.106) into definition (4.87), so that we obtain the inverse localization lengths for the left and right side of the domain wall,

$$-ik_{\mathrm{L/R}} = \Delta - n \pm \frac{\Delta\, q}{\Delta - n}\ . \tag{4.111}$$

Of course, for higher n (i.e. higher excited states), the Dirac fermions become less localized and spread farther out.

Furthermore, due to the symmetry $[\mathcal{K}, \mathcal{H}] = 0$, we can choose our solutions $\varphi_\uparrow$ and $\varphi_\downarrow$ to be real, which leads to a vanishing y-component of the spin-expectation value. This in turn implies that there is no current flow in transport direction, since $\boldsymbol{j} = v\hat{\boldsymbol{e}}_{\boldsymbol{z}} \times \boldsymbol{\sigma}$.

Let us first focus on the zero energy bound state $n = 0$, which we find by plugging $-ik_{\mathrm{L/R}} =$

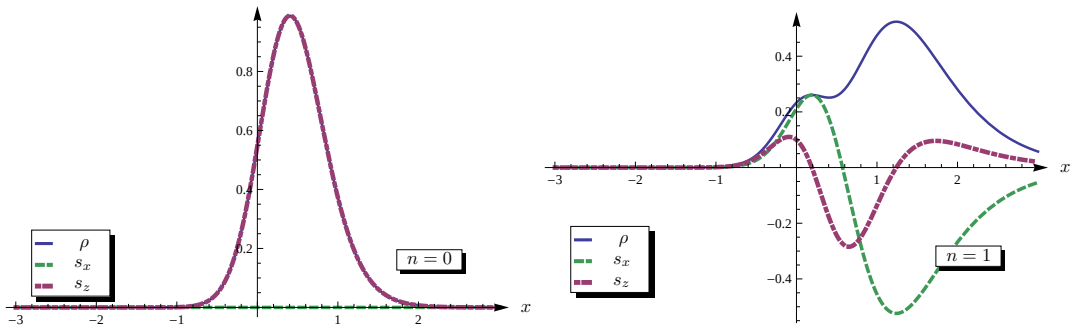

Figure 4.11.: The bound states for finite transverse momentum q are asymmetric. We chose the parameters $\Delta = 3.9$ and $q = 1.5$, so that there are in total 2 bound states at the domain wall. We see that the density distribution becomes asymmetric, which is a feature also exhibited by the semiclassical orbits. The state $n = 1$ corresponds to the third type of semiclassical orbit shown in Figure 4.2(a), with a group velocity pointing along the negative y-axis, since $\partial_q \epsilon_{n,q} < 0$. On the right side of the domain wall, $s_x < 0$. Note that the state with $n = 0$ is not captured by semiclassical descriptions since it involves a coherent excitation between the upper and lower band, i.e. it sits at the Dirac point. As in Figure 4.10, the identity $\frac{\partial s_x}{\partial x} = 2\epsilon_{n,q} s_z$ applies here too.

$\Delta(1 \pm q)$ into (4.100) and (4.101),

$$\begin{aligned} \varphi_{\uparrow}^{(0,q)}(x) &= \mathcal{N}_0 \frac{e^{qx}}{(\cosh x)^{\Delta}} \ , \\ \varphi_{\downarrow}^{(0,q)}(x) &= 0 \ , \end{aligned} \tag{4.112}$$

which has been properly normalized to $\int_{-\infty}^{+\infty} dx \ \left(|\varphi_{\uparrow}|^2 + |\varphi_{\downarrow}|^2\right) = 1$ by setting the normalization factor to $\mathcal{N}_0^2 = \frac{\Gamma(1+2\Delta)}{2^{2\Delta}\Delta\Gamma(\Delta-q)\Gamma(\Delta+q)}$. The higher excited states can be straightforwardly obtained by substituting (4.111) into (4.100) and (4.101), and this step terminates the hypergeometric series, turning the solution into a polynomial of degree n.

The spin densities are defined as

$$\boldsymbol{s}(x) = (s_x, s_y, s_z) = \psi^{\dagger}\boldsymbol{\sigma}\psi = \left(2\mathrm{Re}\,\varphi_{\uparrow}^{*}\varphi_{\downarrow}, 2\mathrm{Im}\,\varphi_{\uparrow}^{*}\varphi_{\downarrow}, \varphi_{\uparrow}^{*}\varphi_{\uparrow} - \varphi_{\downarrow}^{*}\varphi_{\downarrow}\right) \ , \tag{4.113}$$

and the probability density of an excitation in the bound state is simply $\rho(x) = \varphi_{\uparrow}^{*}\varphi_{\uparrow} + \varphi_{\downarrow}^{*}\varphi_{\downarrow}$. As noted above, s_y vanishes identically, and the other densities for the bound states are shown in figures 4.10 and 4.11. We see that $s_x(-x) = s_x$ is antisymmetric while s_z and ρ are symmetric in the case $q = 0$. For finite transverse momentum q, the bound states become asymmetric and attain a higher weight on one side of the domain wall, which is clear, since according to (4.87), one side is energetically favorable.

The spin-expectation values in these states are obtained by integrating $\boldsymbol{s}(x)$ over all $x \in \mathbb{R}$,

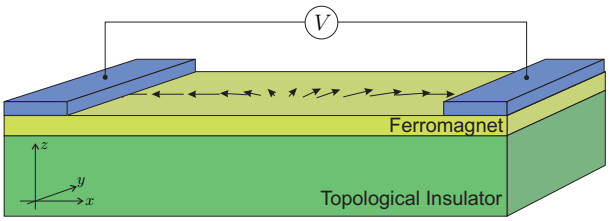

Figure 4.12.: The experimental setup for studying ballistic transport through a domain wall. Two leads with external voltage bias V are attached to the structure of topological insulator coated with a thin ferromagnetic layer.

and can be summarized as

$$\langle\psi_{n,q}|\sigma_x|\psi_{n,q}\rangle = -\frac{q\ \epsilon_{n,0}^2}{(\Delta-n)^2\epsilon_{n,q}} = \frac{\partial\epsilon_{n,q}}{\partial q}\ , \tag{4.114}$$

$$\langle\psi_{n,q}|\sigma_y|\psi_{n,q}\rangle = 0\ , \tag{4.115}$$

$$\langle\psi_{n,q}|\sigma_z|\psi_{n,q}\rangle = \delta_{n,0}\ , \tag{4.116}$$

where the expectation value of σ_z is a direct result of the symmetry $\{\mathcal{H},\sigma_z\}=0$, since $\sigma_z|\psi_{n,q}\rangle$ is the state belonging to the negative energy eigenvalue $-\epsilon_{n,q}$ and which is orthogonal to its positive energy counterpart. Of course, the zero energy bound state is its own counterpart $\sigma_z|\psi_{n,q}\rangle = |\psi_{n,q}\rangle$ so for $n=0$, Eq. (4.116) constitutes just the normalization of the state. Finally, the expectation value of σ_x exhibits the asymmetry induced by the transverse momentum q and vanishes for $q=0$. In fact, from relation (4.91) we see that the expectation value of σ_x is directly related to the current in the transverse direction, i.e. along the domain wall, and it simply yields the usual definition of the group velocity derived from the dispersion (4.109),

$$j_y = v\langle\psi_{n,q}|\sigma_x|\psi_{n,q}\rangle = v\frac{\partial\epsilon_{n,q}}{\partial q}\ . \tag{4.117}$$

4.4.5. Scattering States and Ballistic Transport

We consider the experimental setup for ballistic transport across the domain wall illustrated in Figure 4.12 and which we study using the formalism of scattering theory. The general scattering problem can be treated by finding the asymptotics of our exact wave-functions, which generally is of the form (see [122] for the general scattering formalism and Landauer formula)

$$\psi = \begin{cases} a_{\rm L}\dfrac{e^{ik_{\rm L}x}}{\sqrt{v_{\rm L}}}|\chi_{\rm L}\rangle + b_{\rm L}\dfrac{e^{-ik_{\rm L}x}}{\sqrt{v_{\rm L}}}|\chi_{\rm L}^*\rangle & x\to-\infty \\ a_{\rm R}\dfrac{e^{-ik_{\rm R}x}}{\sqrt{v_{\rm R}}}|\chi_{\rm R}^*\rangle + b_{\rm R}\dfrac{e^{ik_{\rm R}x}}{\sqrt{v_{\rm R}}}|\chi_{\rm R}\rangle & x\to+\infty\ . \end{cases} \tag{4.118}$$

The coefficients $a_{\rm L/R}$ describe the amplitudes of the incoming waves, while $b_{\rm L/R}$ are the amplitudes of the outgoing scattered wave. The scattering region in this particular case is the domain wall described by the magnetization profile (4.78). For finite transverse momentum

q, the longitudinal (along the transport direction) group velocities on the left and the right side of the domain wall differ and explicitly read (see result (4.92))

$$v_{\mathrm{L/R}} = v\frac{k_{\mathrm{L/R}}}{\epsilon} \ , \tag{4.119}$$

and have been incorporated into the definition of the scattering states, so that the coefficients a,b correspond to transmission and reflection amplitudes. The ingoing and outgoing coefficients are related through the scattering matrix

$$\begin{pmatrix} b_{\mathrm{L}} \\ b_{\mathrm{R}} \end{pmatrix} = \underline{\underline{S}} \begin{pmatrix} a_{\mathrm{L}} \\ a_{\mathrm{R}} \end{pmatrix} = \begin{pmatrix} r & t' \\ t & r' \end{pmatrix} \begin{pmatrix} a_{\mathrm{L}} \\ a_{\mathrm{R}} \end{pmatrix} = \begin{pmatrix} r & t \\ t & -r^* \frac{t}{t^*} \end{pmatrix} \begin{pmatrix} a_{\mathrm{L}} \\ a_{\mathrm{R}} \end{pmatrix} \ . \tag{4.120}$$

The reflection and transmission coefficients are readily extracted from the asymptotic expansion (4.103) and (4.104),

$$r = \frac{-A(-k_{\mathrm{L}}, k_{\mathrm{R}})}{A(k_{\mathrm{L}}, k_{\mathrm{R}})} \ , \tag{4.121}$$

$$t = \frac{1}{A(k_{\mathrm{L}}, k_{\mathrm{R}})} \ , \tag{4.122}$$

and our solutions indeed show the symmetry that is required for the scattering matrix to be unitary, $\underline{\underline{S}}^\dagger \underline{\underline{S}} = \underline{1}_2$. Current conservation is also incorporated into this condition of unitarity, which can be seen by explicitly considering ψ_1 from result (4.103) which in the present language can be written as

$$\psi_1 = \begin{cases} \dfrac{e^{ik_{\mathrm{L}}x}}{\sqrt{v_{\mathrm{L}}}}|\chi_{\mathrm{L}}\rangle + r\dfrac{e^{-ik_{\mathrm{L}}x}}{\sqrt{v_{\mathrm{L}}}}|\chi_{\mathrm{L}}^*\rangle & x \to -\infty \\ t\dfrac{e^{ik_{\mathrm{R}}x}}{\sqrt{v_{\mathrm{R}}}}|\chi_{\mathrm{R}}\rangle & x \to +\infty \ . \end{cases} \tag{4.123}$$

The state ψ_1 yields the current contribution in the transport direction

$$j_x \propto 1 - |r|^2 = |t|^2 \ , \tag{4.124}$$

as is directly obtained using result (4.93) and taking the real part thereof. Thus, $R_q(\epsilon) = |r|^2$ and $T_q(\epsilon) = |t|^2$ can indeed be given a physically meaningful definition as reflection and transmission probabilities, respectively. These probabilities explicitly depend on energy ϵ and transverse momentum q.

Using our results (4.102) and (4.122) and some properties of the Gamma function (E.8)-(E.12), we eventually arrive at the transmission probability

$$T_q(\epsilon) = \frac{\sinh(\pi k_{\mathrm{L}})\sinh(\pi k_{\mathrm{R}})}{\sin^2(\pi\Delta) + \sinh^2\left(\frac{1}{2}(k_{\mathrm{L}} + k_{\mathrm{R}})\pi\right)} \ , \tag{4.125}$$

where $k_{\mathrm{L/R}}$ is given in (4.87).

A central result in quantum transport is the Landauer formula for the linear conductance G

$$G = \frac{e^2}{2\pi\hbar}\sum_q T_q(\epsilon_{\mathrm{F}}) \ , \tag{4.126}$$

which states that the current is essentially given by the sum over all transverse channels, each with a weight given by the transmission probability. The fundamental conductance quantum $G_Q = \frac{e^2}{2\pi\hbar}$ is the numerical contribution of each channel to the conductance [122]. In linear response, the current is then simply given by $j_x W = I = GV$, where V is the externally applied voltage and W is the transverse dimension of the ballistic contact, while j_x is the current density (per unit length) along the x-direction. In the linear transport regime, all quantities are evaluated at the Fermi level ϵ_F.

The transverse momentum q runs over all values that lie inside the shaded yellow area in Figure 4.8(b), i.e. $|q| \leq \epsilon_\mathrm{F} - \Delta$, and beyond this range, we either have total reflection or no states at all, so there is no contribution. Therefore,

$$G = G_Q \, \frac{W}{2\pi} \int_{-(\epsilon_\mathrm{F}-\Delta)}^{\epsilon_\mathrm{F}-\Delta} \mathrm{d}q \; T_q(\epsilon_\mathrm{F}) \; , \tag{4.127}$$

where we rewrote the sum as an integral and $\frac{W}{2\pi}$ is the density in k_y-space. In absence of the domain wall, the conductance simply becomes

$$G_0 = G_Q \, \frac{W}{2\pi} \int_{-\epsilon_\mathrm{F}-\Delta}^{\epsilon_\mathrm{F}-\Delta} \mathrm{d}q = G_Q \, \frac{W\epsilon_\mathrm{F}}{\pi} \; . \tag{4.128}$$

We are now interested in change of the conductance due to the presence of the domain wall, so we define a domain wall resistance as

$$\delta G = -\frac{G_\mathrm{DW} - G_0}{G_0} = \delta G_\mathrm{T} + \delta G_\mathrm{DW} \; , \tag{4.129}$$

which we split into a topological contribution δG_T and the contribution δG_DW that is dependent on the specific domain wall profile. In particular, the former depends only on the magnetization M *viz.* Δ, and does not depend on the details of the domain wall, while the latter depends for example on the domain wall width. The topological contribution is due to the mere reduction of states available for transport across the domain wall, since some of them become totally reflecting. This can be seen in Figure 4.8(b) for example, since in the presence of the domain wall, the contributing transport channels get reduced to the yellow area, while without the domain wall the whole area within the red cone would be available. We remark that the appearance of the two Dirac cones on both sides that are shifted with respect to each other, is due to the opposite magnetization direction on both sides. These observations lead to

$$\delta G_\mathrm{T} = \frac{\Delta}{\epsilon_\mathrm{F}} = \frac{M}{E_\mathrm{F}} > 0 \; , \tag{4.130}$$

and is the fraction of the contribution from the red shaded area of totally reflecting states to the total contribution from the Dirac cone (yellow + red shaded areas in fig. 4.8(b)). In the end, δG_T incorporates the differences in the bulk spectrum on both sides of the wall, as far as it concerns transport at the Fermi level.

The remaining contribution from the domain wall is then related to the reflection from the wall profile and is explicitly given by

$$\delta G_\mathrm{DW} = \frac{1}{2\epsilon_\mathrm{F}} \int_{-(\epsilon_\mathrm{F}-\Delta)}^{\epsilon_\mathrm{F}-\Delta} \mathrm{d}q \; \left(1 - T_q(\epsilon_\mathrm{F})\right) = \frac{1}{2\epsilon_\mathrm{F}} \int_{-(\epsilon_\mathrm{F}-\Delta)}^{\epsilon_\mathrm{F}-\Delta} \mathrm{d}q \; R_q(\epsilon_\mathrm{F}) \; . \tag{4.131}$$

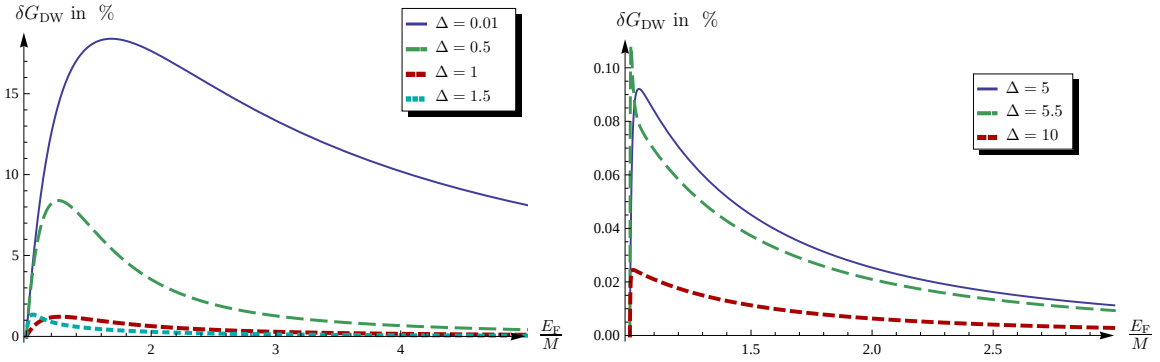

(a) short wall widths

(b) larger wall widths

Figure 4.13.: Relative decrease in the conductance due to the presence of the domain wall. We see that the values are rather large for sharp walls and decrease significantly when the wall width becomes of the order of the magnetic length $\hbar v/M$. The blue curve is already pretty close to the asymptotic curve for the limit of sharp walls, $\Delta \to 0$ (see Figure 4.15(a)).

We study δG_{DW} as a function of the two relevant parameters $\tilde{E_{\mathrm{F}}} = E_{\mathrm{F}}/M$, the Fermi level in units of the magnetic exchange field M, and $\Delta = w/l_M$, i.e. the domain wall width in units of the magnetic length $l_M = \hbar v/M$. We introduce the new integration variable $\zeta = q/\Delta$ in order to bring the above expression into the more convenient form

$$\delta G_{\mathrm{DW}} = \frac{1}{2\tilde{E_{\mathrm{F}}}} \int_{-(\tilde{E_{\mathrm{F}}}-1)}^{\tilde{E_{\mathrm{F}}}-1} \mathrm{d}\zeta \left(1 - \frac{\sinh(\pi\Delta\, k_+)\ \sinh(\pi\Delta\, k_-)}{\sin^2(\pi\Delta) + \sinh^2\left(\frac{\pi\Delta}{2}(k_+ + k_-)\right)} \right) , \tag{4.132}$$

where $k_\pm \equiv \sqrt{\tilde{E}_{\mathrm{F}}^2 - (1 \pm \zeta)^2}$. This integral is evaluated numerically and plotted in Figure 4.13 as a function of the Fermi level E_{F}/M for various values of $\Delta = w/l_M$.

When Δ is an odd multiple of $1/2$, we can see slightly enhanced peaks when E_{F} is close to M (see for example the green curve for $\Delta = 5.5$ in diagram 4.13(b)). This behavior can be traced back to the term $\sin^2(\pi\Delta)$ in the denominator of the transmission probability (4.125) which is zero for Δ being an integer number and thus enhances transmission. For Δ being an odd multiple of $1/2$, this term is maximal and reduces transmission so that reflection increases and so does δG_{DW}. When the Fermi level E_{F} approaches M and eventually reaches the crossing point of the left and right Dirac cones (crossing of red and green line in Figure 4.8(b)), the number of states available for transport drastically reduces and one reaches the point of minimal conductance which is not well described in our theory. At this point, transport is due to evanescent modes [127, 178], which is beyond the present study.

The total change in conductance $\delta G = \delta G_{\mathrm{T}} + \delta G_{\mathrm{DW}}$ is shown in Figure 4.14, and we find that the topological contribution δG_{T} strongly dominates, except for short walls for which $\Delta \lesssim 1$.

We also study the behavior of δG_{DW} with the wall width, which is shown in Figure 4.15. As before, the change in conductance is largest for sharp walls and monotonically decreases as the wall width becomes larger. As the fermi level moves deeper into the metallic regime, we also see an overall decrease of the change in conductance.

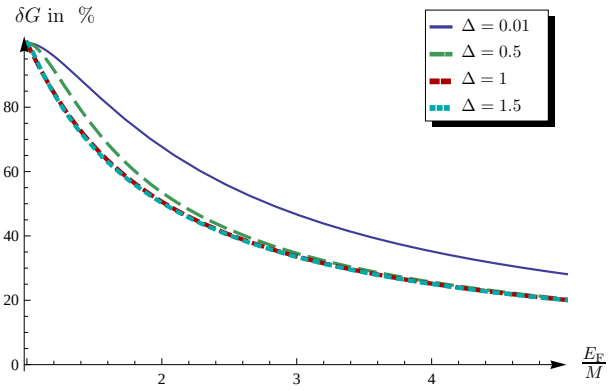

Figure 4.14.: A plot of the total reduction of the conductance due to the domain wall, $\delta G = \delta G_{\mathrm{T}} + \delta G_{\mathrm{DW}}$. The parameters are the same as in Figure 4.13(a), and for values of Δ significantly larger than 1, the contribution of δG_{T} dominates and thus, in the above plot the red and cyan lines already lie very close together. Experimentally, one could subtract the topological contribution (determined by measuring the bulk properties) in order to obtain the contribution from the domain wall profile.

Let us now consider the two limits of sharp (abrupt) walls and very wide walls for which we will derive analytical expressions.

Sharp wall

In this regime, w is very small compared to the magnetic length l_M, so that $\Delta \ll 1$ and we can expand $\sin(\pi\Delta) \approx \pi\Delta$ and $\sinh(\pi\Delta\, k) \approx \pi\Delta\, k$ in the result for the transmission probability (4.125), and find an expression that only depends on $\tilde{E_{\mathrm{F}}} \equiv \epsilon_{\mathrm{F}}/\Delta = E_{\mathrm{F}}/M$

$$\delta G_{\mathrm{DW}} \overset{\Delta \ll 1}{\to} \frac{1}{\tilde{E_{\mathrm{F}}}} \int_0^{\tilde{E_{\mathrm{F}}}-1} \mathrm{d}\zeta \, \left(1 - \frac{4k_+k_-}{4 + k_+ + k_-}\right) \, . \tag{4.133}$$

For $\tilde{E_{\mathrm{F}}} \gg 1$, we can approximately solve the integral and find the asymptotic result

$$\delta G_{\mathrm{DW}} \overset{\substack{\Delta \ll 1 \\ \tilde{E_{\mathrm{F}}} \gg 1}}{\to} \frac{1}{3\tilde{E_{\mathrm{F}}}} = \frac{M}{3E_{\mathrm{F}}} \, , \tag{4.134}$$

which equals to one third of the topological contribution δG_{T}. Therefore, the domain wall contribution δG_{DW} is at best 1/3 of the topological contribution δG_{T}, since for wider walls δG_{DW} decreases further, while δG_{T} does not depend on the wall width.

Wide wall

Here, we investigate the opposite regime of wide walls where $\Delta \gg 1$, so that we can replace the hyperbolic sines by its exponential representation,

$$\delta G_{\mathrm{DW}} = \frac{1}{\tilde{E_{\mathrm{F}}}} \int_0^{\tilde{E_{\mathrm{F}}}-1} \mathrm{d}\zeta \, \left(1 - \frac{\left(1 - e^{-2\pi\Delta\, k_+}\right)\left(1 - e^{-2\pi\Delta\, k_-}\right)}{4\sin^2(\pi\Delta)\; e^{-\pi\Delta(k_+ + k_-)} + \left(1 - e^{-\pi\Delta(k_+ + k_-)}\right)^2}\right)$$

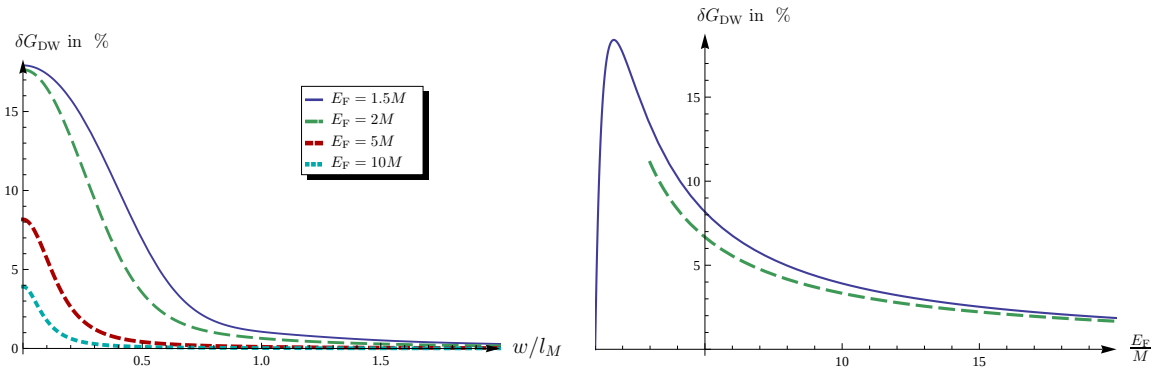

(a) Change in conductance as a function of width

(b) Limit of a short domain wall

Figure 4.15.: The plot on the left shows the dependence of the domain wall resistance on the wall width w in units of the magnetic length $l_M = \hbar v/M$, and we can see a monotonic decrease with wall width. For widths much larger than the magnetic length l_M, we find the analytic dependence $\propto 1/w^2$. The right plot shows the situation for a sharp wall $w \to 0$ together with the approximate solution (4.134) (green dashed line). The maximum is at ≈ 1.68 so that the highest possible value achievable is $\delta G_{\mathrm{DW}} \lesssim 18.4\%$.

and note that due to the largeness of Δ, only exponentials whose argument vanishes at some point during integration can contribute. This is the case for $e^{-2\pi\Delta\, k_+}$, since $k_+ \to 0$ for $\zeta \to \tilde{E_{\mathrm{F}}} - 1$, whereas $k_- \geq 2\sqrt{\tilde{E_{\mathrm{F}}} - 1}$ (we assume that $\tilde{E_{\mathrm{F}}}$ is sufficiently larger than 1) in the whole region of integration. Therefore, almost all the terms play no role during integration, and we can evaluate the much simpler integral

$$\delta G_{\mathrm{DW}} \overset{\Delta \gg 1}{\to} \int_0^1 \mathrm{d}\zeta\; e^{-2\pi\Delta \tilde{E_{\mathrm{F}}}\sqrt{1-\zeta^2}} \overset{\Delta \gg 1}{\to} \int_0^\infty \mathrm{d}z\; z\, e^{-2\pi\Delta \tilde{E_{\mathrm{F}}} z} = \frac{\hbar^2 v^2}{(2\pi E_{\mathrm{F}})^2}\; \frac{1}{w^2}\;, \tag{4.135}$$

where we rescaled the integration variable and set the lower integration bound to 0, since relevant contributions arise only for values of ζ close to 1. In a second step, we once more changed the integration variable to $z = \sqrt{1-\zeta^2}$, expand the prefactor around $z = 0$ and set the upper integration limit to ∞ since now, contributions to the integral only come from values $z \ll 1$.[3]

We find that the ballistic domain wall resistance δG_{DW} decays with the inverse square of the domain wall width, but the topological contribution $\delta G_{\mathrm{T}} = \frac{M}{E_{\mathrm{F}}}$ is also present in limit and is the dominating one. We note that the diffusive version of the conductance change found in chapter 3.4.4 is of the same type as δG_{T}, which can be seen by integrating the local contribution (3.234) over the contact of length L, and for the one-dimensional domain-wall geometry considered in this section,

$$\frac{\delta G_{\mathrm{diff}}}{G_{\mathrm{diff}}} = -\frac{M_z}{E_{\mathrm{F}}}\frac{\hbar v}{2E_{\mathrm{F}}L}\frac{M_x(+\infty) - M_x(-\infty)}{E_{\mathrm{F}}}\;. \tag{4.136}$$

We can see that this result depends only on the total change of the magnetization $M_x(+\infty) - M_x(-\infty)$, as it is the case for δG_{T}.

[3] This is essentially the method of the steepest descent or the saddle point method [179].

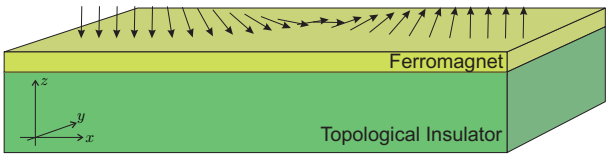

Figure 4.16.: The system of topological insulator with an insulating ferromagnetic layer on top which contains a Néel domain wall, and contrary to the previous system of Figure 4.7(a), corresponds to a mass domain wall.

4.4.6. Negative Energies

As we found earlier, the solutions for the negative energy branch can easily be obtained by operating σ_z onto our positive energy solutions. However, we use $e^{-i\frac{\pi}{2}\sigma_z}$ instead, which yields again solutions with the same symmetry properties. In fact, this operator acts on spin-space only, so its effect is directly seen by analyzing

$$e^{-i\frac{\pi}{2}\sigma_z}|\chi\rangle = e^{-i\frac{\pi}{2}\sigma_z}|\chi\rangle = \frac{1}{\sqrt{2}}\begin{pmatrix} e^{-\frac{i}{2}(\gamma+\frac{\pi}{2})} \\ e^{\frac{i}{2}(\gamma+\frac{\pi}{2})} \end{pmatrix} , \tag{4.137}$$

which is nothing but a rotation of the spin in the x-y-plane by π. This also becomes evident by looking at the spin densities (4.113) of the negative energy states, which are given by

$$\boldsymbol{s}_-(x) = \psi^\dagger e^{+i\frac{\pi}{2}\sigma_z}\boldsymbol{\sigma}e^{-i\frac{\pi}{2}\sigma_z}\psi = (-s_x, -s_y, s_z)$$

and just have a flipped spin-polarization in the plane of the topological insulator. Due to $\boldsymbol{j} = v\hat{\boldsymbol{e}}_{\boldsymbol{z}}\times\boldsymbol{\sigma}$, this reverses the current direction. However, due to the symmetry $[\mathcal{H}, \mathcal{T}_q\mathcal{T}_x\sigma_z] = 0$, the transmission probability does not change, so that the domain wall resistance is the same when the Fermi level is in the lower band, i.e. it depends only on the absolute value of the Fermi energy $|E_\mathrm{F}|$.

4.5. Finite Width Domain Wall - The z-y Configuration

Let us turn our attention to the z-y configuration which describes a Néel wall between two QAH states of opposite chirality. The solution of this problem is much less involved than before since we can make heavy use of the results from the previous section. Here, we have to solve the Hamiltonian

$$\mathcal{H}_{zy} = i\hbar v\sigma_y\partial_x + k_y\sigma_x - M\boldsymbol{m}(x)\boldsymbol{\sigma} \tag{4.138}$$

with the magnetization profile

$$\boldsymbol{m}(\boldsymbol{r}) = \begin{pmatrix} 0 \\ \sin\theta(x) \\ \cos\theta(x) \end{pmatrix} \tag{4.139}$$

and which is depicted in Figure 4.16.

4.5.1. The Exact Solution

At any rate, we can reuse the results from the previous section by noting that for the case $k_y = 0$, the two configurations can be mapped onto each other by performing a rotation around the y-axis by $\frac{\pi}{2}$. The unitary spin rotation matrix is given by

$$\mathcal{U} = e^{-i\frac{\pi}{4}\sigma_y} \ ,$$

which performs $\mathcal{U}\sigma_x\mathcal{U}^\dagger = -\sigma_z$ and $\mathcal{U}\sigma_z\mathcal{U}^\dagger = \sigma_x$. Thus, the transformed Hamiltonian which additionally has been brought into dimensionless form, reads

$$\mathcal{U}\,\mathcal{H}_{zy}\,\mathcal{U}^\dagger = i\sigma_y\partial_x - q\sigma_z - \Delta\sin\theta\,\sigma_y - \Delta\cos\theta\,\sigma_x = \mathcal{H}_{xy}(q=0) - q\sigma_z \ , \tag{4.140}$$

which is of the form of Hamiltonian (4.80), with the only difference that the transverse momentum q now couples to $-\sigma_z$ instead of σ_x in $\mathcal{H}_{xy}$. In the present case however, it is much easier to treat finite q since, once we know the eigensystem for $q = 0$, i.e. the basis in which $\mathcal{H}_{xy}$ is diagonal, we find that σ_z in this basis has also a very simple structure. We will now explicitly illustrate this by determining the bound states of this system.

We denote the eigenstates with eigenenergy $\pm\epsilon_{n,0}$ from result (4.107) as $|\pm n\rangle$, so that

$$\mathcal{H}_{xy}(q=0)|\pm n\rangle = \pm\epsilon_{n,0}|\pm n\rangle \ .$$

We then write $\mathcal{H}_{xy}(q=0) - q\sigma_z$ in the basis $(\dots, |-2\rangle, |-1\rangle, |0\rangle, |+1\rangle, |+2\rangle, \dots)$, and it has the simple matrix form

$$\begin{pmatrix}
\ddots & & & & & & \iddots \\
& \epsilon_{2,0} & & & & -q & \\
& & \epsilon_{1,0} & & q & & \\
& & & -q & & & \\
& & -q & & -\epsilon_{1,0} & & \\
& -q & & & & -\epsilon_{2,0} & \\
\iddots & & & & & & \ddots
\end{pmatrix} \ , \tag{4.141}$$

where entries not shown are zero. As inferred from the symmetry $\{\mathcal{H}_{xy}, \sigma_z\} = 0$, we see that σ_z only couples pairs of positive and negative energy, with the only exception of the zero energy bound state. For $n > 0$, the negative energy state corresponding to $|+n\rangle$ is given by $|-n\rangle = \sigma_z|+n\rangle$, so that $\langle +n|\sigma_z|-n\rangle = 1$ and $\langle \pm n|\sigma_z|\pm n\rangle = 0$. Essentially, we now have to diagonalize the 2×2 sub-blocks

$$\begin{pmatrix} \epsilon_{n,0} & -q \\ -q & -\epsilon_{n,0} \end{pmatrix} \tag{4.142}$$

in the subspace $(|n\rangle, |-n\rangle)$ with obvious eigenenergies

$$\pm\epsilon_{n,q} = \pm\sqrt{\epsilon_{n,0}^2 + q^2} \ , \tag{4.143}$$

and the corresponding eigenstates

$$|\pm n, q\rangle = \frac{\mp q\sigma_z + (\epsilon_{n,0} + \epsilon_{n,q})\sigma_0}{\sqrt{2\epsilon_{n,q}(\epsilon_{n,q} + \epsilon_{n,0})}}\ |\pm n\rangle \ . \tag{4.144}$$

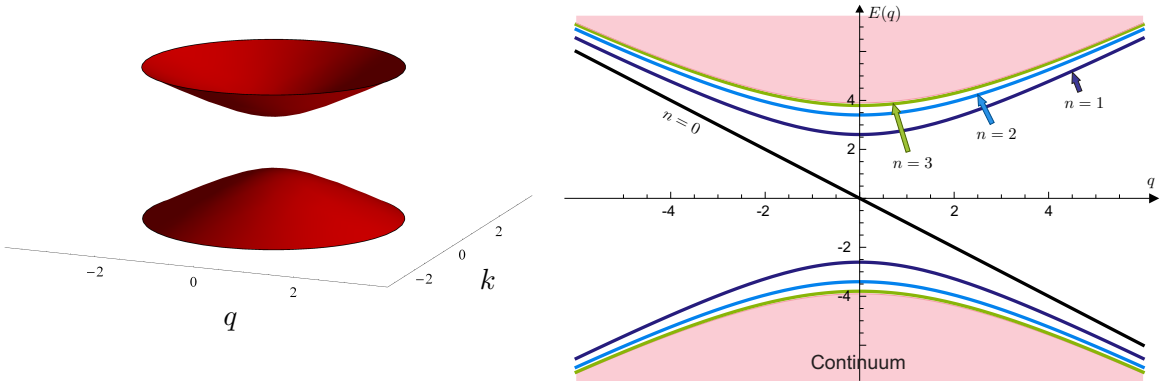

(a) Bulk spectrum

(b) Spectrum in presence of a mass domain-wall

Figure 4.17.: The bulk spectrum is, contrary to the previous study of the x-y configuration, identical on both sides of the domain wall and is shown in (a). However, here we have an additional subtlety, since the mass term due to the M_z component of the domain wall drives the system into the QAH state which is of opposite chirality on both sides of the domain wall due to opposite sign of M_z. As thoroughly discussed in chapter 3, the difference emerges for example in the Berry curvatures for quasi-particle transport in this system. The Berry curvatures do not coincide on both sides of the domain-wall, albeit the band structures are identical. Plot (b) shows the spectrum including the bound states at the domain-wall.

However, there is one exception to this namely, the zero energy state $|0\rangle$ which is invariant under the operation of σ_z and thus, we get $-q\langle 0|\sigma_z|0\rangle = -q$ which gives us directly the linearly dispersing chiral state plotted as black straight line in Figure 4.17(b). The dispersion of the other bound states is also shown along with the region of continuum states which we treat in the next section. Like for the x-y wall configuration, we have a total of $2\lfloor\Delta\rfloor + 1$ bound states which are symmetric with respect to positive and negative energies, with the major difference being the $n = 0$ state which is chiral in the present configuration. Also, as opposed to before, here is no upper bound for the value of q at which the bound states merge with the continuum. The bulk spectrum as it appears in absence of, or far away from the domain-wall is shown in Figure 4.17(a).

We obtain the spinor in the original frame by undoing the rotation, i.e. $\psi_{\pm n,q}(x) = \mathcal{U}^\dagger|\pm n, q\rangle$. As in (4.113), we are interested in the spin and quasi-particle densities which can be related to the densities for $q = 0$ by the result

$$\rho'^{(n,q)} = \psi^\dagger_{\pm n,q}\psi_{\pm n,q} = \rho^{(n,0)}(x) \mp \frac{q}{\epsilon_{n,q}} s_z^{(n,0)}(x) \ , \tag{4.145}$$

where the densities $\rho^{(n,0)}(x)$ and $\boldsymbol{s}^{(n,0)}(x)$ were calculated in the previous section, c.f. Eqn (4.113). In order to derive this relation, we simply substituted (4.144) into the definition of

the densities. Furthermore

$$s_x'^{(n,q)} = \psi^\dagger_{\pm n,q}\sigma_x\psi_{\pm n,q} = -s_z^{(n,0)}(x) \pm \frac{q}{\epsilon_{n,q}}\rho^{(n,0)}(x) \ , \tag{4.146}$$

$$s_y'^{(n,q)} = \psi^\dagger_{\pm n,q}\sigma_y\psi_{\pm n,q} = \pm\frac{\epsilon_{n,0}}{\epsilon_{n,q}}\ \boldsymbol{s}_y^{(n,0)} \ , \tag{4.147}$$

$$s_z'^{(n,q)} = \psi^\dagger_{\pm n,q}\sigma_z\psi_{\pm n,q} = \pm\frac{\epsilon_{n,0}}{\epsilon_{n,q}}\ \boldsymbol{s}_x^{(n,0)} \ , \tag{4.148}$$

where in the last two relations we made use of (4.138) and the fact that the perpendicular spin matrices $\boldsymbol{\sigma}_\perp = (\sigma_x, \sigma_y)$ anti-commute with σ_z, i.e. $\{\boldsymbol{\sigma}_\perp, \sigma_z\} = 0$. The densities for $q = 0$ are identical to those shown in Figure 4.10, with the difference that $s_x' \hat{=} -s_z$ and $s_z' \hat{=} s_x$. In the semiclassical orbit shown in Figure 4.2(b), we can also see the asymmetry in s_x' reduced by a finite value of q.

Using the results from (4.114)-(4.116), we can now readily give the expectation values of the spin-densities

$$\langle\psi_{\pm n,q}|\boldsymbol{\sigma}|\psi_{\pm n,q}\rangle = \begin{cases} -\hat{\boldsymbol{e}}_{\boldsymbol{x}} & n = 0 \\ \pm\dfrac{q}{\epsilon_{n,q}}\hat{\boldsymbol{e}}_{\boldsymbol{x}} & n > 0 \ , \end{cases} \tag{4.149}$$

so that the current flow along the domain wall becomes as expected, $j_y = vs_x' = \pm v\frac{\partial\epsilon_{n,q}}{\partial q}$.

It is also interesting to note that the spin-density of the zeroth bound state is compatible to the semiclassical expression (3.231), $\boldsymbol{s}_{\rm xc}(\boldsymbol{R}, t) \propto [\hat{\boldsymbol{e}}_{\boldsymbol{z}}(\boldsymbol{\nabla}\cdot\boldsymbol{M}) - \boldsymbol{\nabla}M_z]$. For the x-y domain wall configuration of the previous section, we have a non-vanishing $\boldsymbol{\nabla}\cdot\boldsymbol{M}$ which yields a finite s_z component. In the present z-y configuration on the other side, $-\boldsymbol{\nabla}M_z = -\hat{\boldsymbol{e}}_{\boldsymbol{x}}\partial_x M_z$ correctly predicts finite s_x with the same magnitude as before however, of opposite sign.

4.5.2. Scattering States and Ballistic Transport

For the scattering states, it is of course also possible to take advantage of the results obtained in the previous section. First, we note that $k_{\rm L} = k_{\rm R} = k$, since the bulk band structure is identical on both sides of the domain wall. We determine the scattering states for finite q exactly as we did in the case of the bound states. It boils down to transforming the two orthogonal solutions from (4.103) and (4.104) independently with a relation like (4.144). Since this transformation only affects spin-space, it acts only on the spinors $|\chi_{\rm L/R}\rangle$ defined in (4.88), so we essentially need to consider

$$|\chi_{k,q}\rangle = \frac{\mp q\sigma_z + (\epsilon_{k,0} + \epsilon_{k,q})\sigma_0}{\sqrt{2\epsilon_{k,q}(\epsilon_{k,q} + \epsilon_{k,0})}}\ |\chi_{k,0}\rangle \ , \tag{4.150}$$

where the full energy dispersion becomes

$$\pm\epsilon_{k,q} = \pm\sqrt{\epsilon_{k,0}^2 + q^2} = \pm\sqrt{\Delta^2 + k^2 + q^2} \ , \tag{4.151}$$

just as in (4.143).

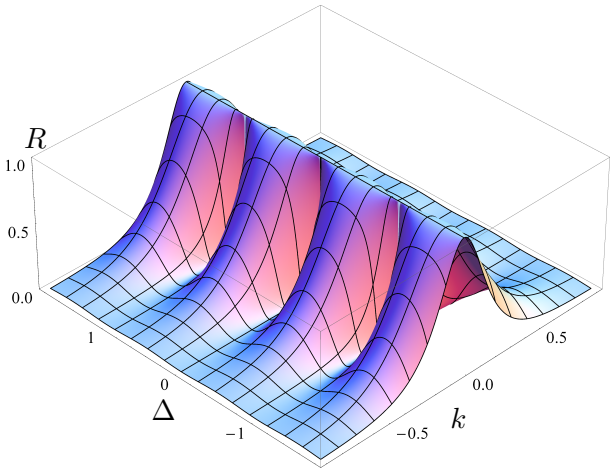

Figure 4.18.: A plot of the reflection probability (4.152) as a function of $\Delta = w/l_{\mathrm{M}}$ and the momentum k in units of the inverse wall width. We see that the reflection probability is strongly suppressed whenever the wall width is an integer multiple of the magnetic length l_{M}.

In the end, the spinors $|\chi_{k,q}\rangle$ directly relate to the group velocity by virtue of

$$\langle\chi_{k,q}|j_x|\chi_{k,q}\rangle = -v\langle\chi_{k,q}|\sigma_y|\chi_{k,q}\rangle = \mp v\frac{\epsilon_{k,0}}{\epsilon_{k,q}}\langle\chi_{k,0}|\sigma_y|\chi_{k,0}\rangle = \pm v\frac{k}{\epsilon_{k,q}} \ ,$$

where we first used (4.147) and then (4.89). Using (4.146), we can readily see that

$$\langle\chi_{k,q}|j_y|\chi_{k,q}\rangle = \pm v\frac{q}{\epsilon_{k,q}} \ ,$$

and thus is consistent with the definition of the group velocity, or current as $\boldsymbol{j} = \boldsymbol{\nabla}_{k,q}\epsilon_{k,q}$.

We see that finite q only modifies the spinor structure to yield the expected group velocity and therefore, the transmission coefficients remain independent of q. Thus, the transmission probability can be directly obtained from (4.125) and noting that $k_{\mathrm{L}} = k_{\mathrm{R}} = k$,

$$R(\Delta,k) = \frac{\sin^2(\pi\Delta)}{\sin^2(\pi\Delta)+\sinh^2(\pi k)} \ , \tag{4.152}$$

$$T(\Delta,k) = \frac{\sinh^2(\pi k)}{\sin^2(\pi\Delta)+\sinh^2(\pi k)} \ , \tag{4.153}$$

which obviously satisfies the conservation law $R+T=1$. The reflection probability is plotted in Figure 4.18.

We now calculate the ballistic conductivity using the Landauer formula (for definitions see (4.126))

$$G = G_Q\,\frac{W}{2\pi}\int_{-k_{\mathrm{F}}}^{k_{\mathrm{F}}}\mathrm{d}q\;T\left(\Delta,\sqrt{k_{\mathrm{F}}^2-q^2}\right) \ , \tag{4.154}$$

where we introduced the magnitude of the wave vector at the Fermi energy $k_{\mathrm{F}} = \sqrt{\epsilon_{\mathrm{F}}^2-\Delta^2}$. Since we evaluate the transmission probability on-shell (i.e. on states with energy equal to the

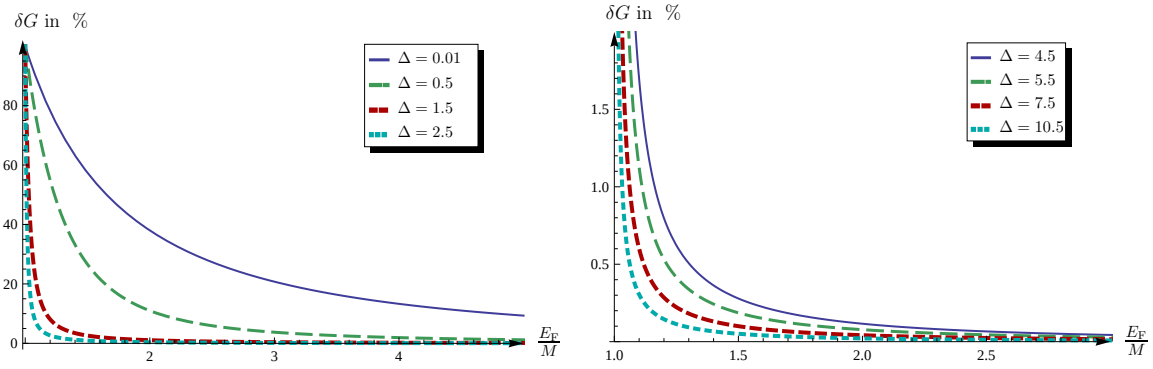

(a) short wall widths (b) larger wall widths

Figure 4.19.: Relative decrease in the conductance due to the presence of the domain wall. We see that the values are rather large for sharp walls and decrease significantly when the wall width becomes of the order of the magnetic length $\hbar v/M$. The blue curve in (a) for $\Delta = 0.01$ is already very close to the asymptotic curve for the limit $\Delta \to 0$, and coincides with the analytical result for an abrupt wall given in (4.156). Note that we considered only values of Δ which are an odd multiple of $1/2$, since the wall becomes transparent when Δ is an integer number.

Fermi level), the additional constraint $\epsilon_{\mathrm{F}} = \sqrt{\Delta^2 + k^2 + q^2}$ leads to an implicit dependency on q through the momentum k in the above integration.

In absence of the domain wall, the conductance simply becomes $G_0 = G_Q \, \frac{W}{2\pi} \, 2k_{\mathrm{F}}$, so with the same definition as in (4.129), we need to solve the following integral in order to obtain the change in conductance,

$$\begin{aligned} \delta G = -\frac{G_{\mathrm{DW}} - G_0}{G_0} &= \frac{1}{2k_{\mathrm{F}}} \int_{-k_{\mathrm{F}}}^{k_{\mathrm{F}}} \mathrm{d}q \; \frac{\sin^2(\pi\Delta)}{\sin^2(\pi\Delta) + \sinh^2\left(\pi\sqrt{k_{\mathrm{F}}^2 - q^2}\right)} \\ &= \int_0^1 \mathrm{d}\zeta \; \frac{\sin^2(\pi\Delta)}{\sin^2(\pi\Delta) + \sinh^2\left(\pi k_{\mathrm{F}}\sqrt{1-\zeta^2}\right)} \, , \end{aligned} \tag{4.155}$$

Note that contrary to the previous domain wall configuration, there is no topological contribution δG_{T}, since the bulk spectrum is identical on both sides of the wall. The value of δG is shown in Figure 4.19 as a function of the Fermi level E_{F} for various values of the parameter Δ, and in Figure 4.20 as a function of the wall width w.

The change in conductance, and thus the reflection at the domain wall is strongly suppressed when the wall width w equals the magnetic length l_{M}, or equivalently, when the localization energy E_w matches the magnetic energy M. This is a direct consequence of the transmission probability (4.153), since the wall becomes transparent whenever Δ is an integer number, i.e. then $T = 1$ for all momenta k and q. This is contrary to the x-y wall configuration, where this transparency occurs only at the singular point $q = 0$ *viz.* $k_{\mathrm{L}} = k_{\mathrm{R}}$, so that the signatures are far less pronounced than in the present situation. In particular, only the first minimum is really noticeable in the plots (for example, note the difference between the two curves for $\Delta = 1$ and $\Delta = 1.5$ in Figure 4.13(a)).

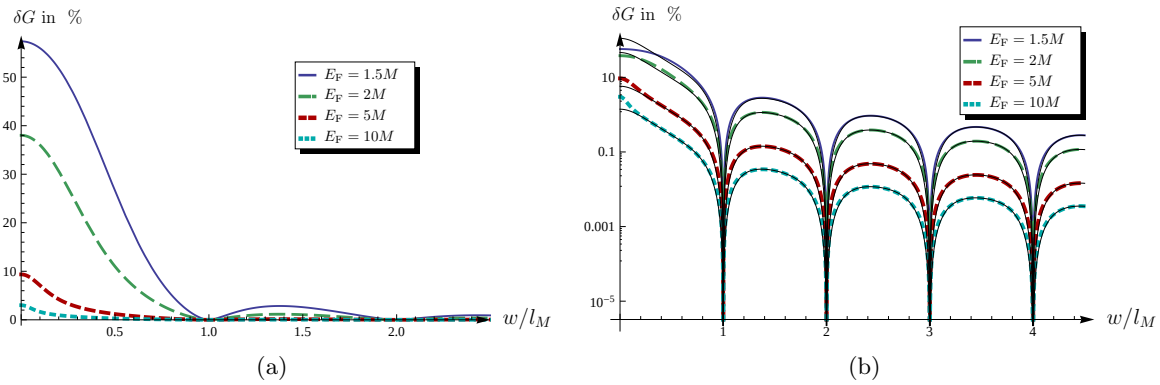

Figure 4.20.: The plot in (a) shows the dependence of the domain wall resistance on the wall width w in units of the magnetic length $l_M = \hbar v/M$, and we can see a monotonous decrease with wall width along with a periodic modulation due to the factor from eq. (4.158). Whenever the domain wall width is an integer multiple of the magnetic length, the domain becomes transparent for the Dirac Fermions and δG drops to zero. Figure (b) shows the same diagram as in (a) on a logarithmic scale, together with the approximate formula (4.157) (black thin lines). We can see a very good agreement, except for very sharp domain walls.

To further discuss these results, we analytically investigate the two opposite limits of short and wide walls.

Abrupt wall

When the wall is much shorter than any other relevant transport length scales of the system, i.e. $\Delta, k_\mathrm{F} \ll 1$, we can expand the sines and perform the integration analytically,

$$\delta G \overset{w \ll l_\mathrm{M}}{\to} \int_0^1 \mathrm{d}\zeta \, \frac{\Delta^2}{\Delta^2 + k_\mathrm{F}^2(1-\zeta^2)} = \frac{\Delta^2}{2\epsilon_\mathrm{F} k_\mathrm{F}} \log\left(\frac{\epsilon_\mathrm{F} + k_\mathrm{F}}{\epsilon_\mathrm{F} - k_\mathrm{F}}\right) . \tag{4.156}$$

For $E_\mathrm{F} \gg M$, we find the asymptotic behavior $\delta G \to \frac{M^2 \log(2E_\mathrm{F}/M)}{E_\mathrm{F}^2}$, while in the opposite limiting case when the Fermi level comes close to the band edge $E_\mathrm{F} \approx M$, we have $\delta G \to 1$, i.e. the abrupt domain wall blocks all transport channels. However, in the latter case, we should be careful, since transport at the Dirac point or at band edges is not well described in the present theory (see remark following equation (4.132)).

Wide wall

In order to obtain an analytical result for the limit of wide walls $\Delta, k_\mathrm{F} \gg 1$, we use very similar tricks as before in the derivation of (4.135). We find

$$\delta G \overset{\Delta \gg 1}{\to} \int_0^\infty \mathrm{d}z \; z \, \frac{\sin^2(\pi\Delta)}{\sin^2(\pi\Delta) + \sinh^2(\pi k_\mathrm{F} z)} \approx \frac{\log 2}{\pi^2} \frac{\hbar^2 v^2}{E_\mathrm{F}^2 - M^2} \, \frac{1}{w^2} f(\Delta) , \tag{4.157}$$

with the modulation function

$$f(\Delta) = \frac{2\sin^2(\pi\Delta)}{1+\sin^2(\pi\Delta)} \ . \tag{4.158}$$

We see that the envelope decreases with $1/w^2$ as it was the case for the in-plane x-y configuration of the domain wall (see result (4.135)). There however, the reduction of the reflection probability for w an integer multiple of l_{M} plays no role in the wide wall limit, which is contrary to the present configuration, where the modulation function (4.158) still goes to zero for Δ an integer number. We find that the approximate formula fits well already for $\Delta \gtrsim 0.5$, and in Figure 4.20(b), we show a comparison between numerical integration and the approximate solution (4.157).

4.6. Conclusion and Outlook

In this chapter, we have performed a detailed study of the consequence of proximity induced ferromagnetism on the system of topologically protected surface Dirac Fermions. The ferromagnetic order parameter is inhomogeneous and describes domain-walls or vortices. We also established a connection to similar effects caused by an externally applied magnetic field, and found that formally, it can be treated analogous to an inhomogeneous magnetization. We have seen that Dirac Fermions with an induced inhomogeneous exchange field exhibit a range of interesting physics, and the fully quantum theoretical study in this chapter complements the semiclassical analysis in 3.4.

We studied bound states in various magnetization configurations, in particular domain-walls but also two-dimensional structures like vortices. In particular, we focused on the zero energy bound states, which are, analogous the zero energy Landau levels in an external magnetic field, responsible for the half-integer Quantum Hall conductivity at Dirac point.

Subsequently, we exactly solved the Dirac equation for an analytical model describing a domain-wall of finite width and used the solution to study bound states and ballistic transport properties. We found that in addition to the zero energy bound state, additional bound states appear depending on the ratio of wall width and magnetic length l_M. Domain walls of larger width support more bound states.

Then, we studied the change in the ballistic conductance due to the presence of a domain wall. We first investigated a tail-to-tail domain wall where the magnetization always remains in the plane of the topological insulator surface. We found that there is a constant change in conductance independent of the domain-wall profile or width and which is due to the reduction of states available for transport, ultimately arising from the shift of the Dirac cone in momentum space due to the different magnetization directions left and right of the wall. In additional to this constant change, there is another contribution which depends on the wall width however, it is found to be generally smaller than the former contribution.

Furthermore, we saw that magnetizations with an in-plane component shift the Dirac cone in momentum space and thus, this can be utilized to block transport across barriers defined by domain walls or more general magnetization structures. This gives interesting perspectives to control transport in these topological materials. One could for example think of a double

domain wall, where the middle region serves as a tunnel barrier with the tunneling rate influenced by the distance of the two walls. In that respect, it is very important to study the influence of disorder, since momentum non-conservative scattering opens new channels that were blocked in the ballistic regime. Due to surface imperfections or doping, the topological surface metal tends to be in the diffusive rather than in the ballistic regime, so that disorder is an important aspect in topological insulators.

Finally, we studied a second type of domain-wall which connects two QAH states of different chirality *viz.* a mass domain wall. Contrary to the previous wall configuration, there is no constant contribution to the domain-wall conductance and we find that the change vanishes as $1/w^2$ in the limit of wide walls. In addition however, we found a modulation with a factors which vanishes exactly as the wall width is an integer multiple of the magnetic length l_M. Essentially, whenever this condition is met, the wall becomes transparent for all incoming Dirac Fermions. This suppression of back-reflection at the domain wall seems to be a destructive interference effect related to the topological nature of the surface states. The influence of disorder on this interference effect should also be investigated. However, the domain-wall conductance modulations with the factor $\sin^2(\pi w/l_M)$ are not expected to be affected, as long as the wall width w and the magnetic length $l_M = \frac{\hbar v}{M}$ are much smaller than the mean-free path.

5. Conclusions and Outlook

We have seen that a magnetization varying in space and time gives rise to a various effects even in a rather simple electronic system like a metal with a quadratic dispersion. In semiconductors, spin-orbit interaction adds an additional ingredient giving rise to even richer physics. The broad range of interest and possible applicability shows itself in the research activity in associated fields like spintronics, magnetotransport, magnetization dynamics and domain-wall motion. Recently, a new candidate entered the arena: the class of topological materials which have very interesting properties both for fundamental research and technological applications. Of course, these materials show their true power only in combination with other systems like ferromagnets which itself can possess a non-trivial magnetization texture. As we have seen, the interplay of inhomogeneous magnetization and the topological surface states encoded in the Dirac dispersion gives rise to a range interesting effects, despite the simplicity of the effective two-band model.

The big advantage of our kinetic equation approach presented and discussed in the first part of this work is that it features a comprehensive description of all relevant phenomena exhibited by ferromagnetic conductors in presence of spatially and time-varying magnetization. We can thus obtain a wide range of effects in terms of microscopic parameters and within the same model, mathematical framework and identical assumptions, which gives us a set of results consistent with each other. Moreover, in the Stoner limit we can derive the Landau-Lifshitz-Gilbert equation directly from our kinetic equation without any additional ingredients and it also includes the exchange interaction along with most other terms commonly used. Our approach also allows us to include spin-orbit interaction which gives rise to an big variety of additional phenomena which are studied in the field of spintronics, which however would be subject of future research.

In a somewhat related matter, effective theories are widely used to investigate the physical mechanisms with the help of simple models. This starts with the widely employed non-relativistic Pauli Hamiltonian and is standard procedure in the field of spintronics where one studies spin-orbit coupled semiconductors. Usually, when deriving these low-energy effective theories, focus is put only on the Hamiltonian, and afterwards, the complete description of the system is based solely on this Hamiltonian. However, as we have seen in the case of the Pauli Hamiltonian which we obtained in a rigorous manner within our formalism, one has to distinguish between canonical and kinetic variables, otherwise one obtains for example in incorrect expression for the current, with the additional complication that both Hamiltonian and the current would *not* be gauge invariant. This problem can only be resolved by discriminating between kinetic and canonical variables. Since the Pauli Hamiltonian shares many similarities with the low-energy effective models employed in spin-orbit coupled semiconductors, the same should apply for them. Therefore, the relevance for the field of spintronics should be investigated further.

At any rate, the framework developed in chapter 3 is well suited to investigate systems that exhibit intrinsic effects like anomalous Hall effect or the topological Hall effect due to a magnetization structure. The complete set of intrinsic responses of the system is encoded in the various Berry curvatures, and thus can be studied rather generally without the necessity to consider a particular system. For example, a non-vanishing divergence of the magnetization texture gives rise to a charge accumulation in the surface electron system that we found to be related to a Berry curvature.

Additionally, the presence of impurities leads to extrinsic effects like side-jump and skew-scattering ultimately giving rise to the anomalous Hall effect and underlining the importance of scattering mechanisms. Scattering is affected additionally by the presence of magnetization structures and it would be interesting to study these and related phenomena in the framework developed in chapter 3 which might give further insight from a different point of view. Due to the Boltzmann transport formulation, scattering can be naturally incorporated into the formalism, which has been already utilized in the present work to straightforwardly obtain the diffusive domain-wall resistance for the topological surface states. Therefore, it would be interesting to study spin-orbit coupled semiconductors with various types of impurities and possibly also the presence of an inhomogeneous and time-varying magnetization within the framework developed. To this end, an extension of the formalism to second order in $\hbar$ is desirable, which then would describe additional effects like the Darwin term in the Pauli Hamiltonian. Also it would be also interesting to investigate to which extent many-body effects can be incorporated into the semiclassical description.

Despite the power of a semiclassical description and the insight gained along with it, various other effects require a full quantum theoretical treatment. This is true for the investigation of surface Dirac Fermions that can be confined at inhomogeneous magnetization structures and which we studied in the last part of this work. We found that in addition to the zero energy bound state, which is strongly linked to the half-integer quantum Hall effect, there can be more bound states which we investigated in some detail. In regard to ballistic transport through a domain wall located on top of the topological insulator and thus interacting with the surface Dirac Fermions, the situation seems even more interesting. In the case of a mass-domain wall in particular, the wall becomes transparent for all incoming Dirac quasi-particles for certain wall widths, which leads to characteristic oscillations in the domain-wall resistance as one varies the domain wall width. This effect seems to be of topological nature, which leads to a destructive interference suppressing the back-scattering from the wall. The question of the origin of this effect and further implications should be addressed in additional investigations. At any rate, it is clear that topological states of matter exhibit fascinating new and rich physics and it remains tantalizing to see what the future has in store for us.

A. The Wigner function

In this appendix, we will give a short introduction to Wigner picture along with some basic properties used in this work. For compact notation, we use 4-component notation $\boldsymbol{x} = (t, \boldsymbol{r})$ and $\boldsymbol{\pi} = (\epsilon, -\boldsymbol{p})$, so that the Wigner transformation is defined as

$$\int \mathrm{d}^4 z \; e^{i\boldsymbol{z}\boldsymbol{\pi}/\hbar} A\left(\boldsymbol{x} + \frac{\boldsymbol{z}}{2}, \boldsymbol{x} - \frac{\boldsymbol{z}}{2}\right) = A(\boldsymbol{x}, \boldsymbol{\pi}) \; . \tag{A.1}$$

In the Wigner picture, operator multiplication has to be carried out by applying the Moyal product

$$* \equiv \exp \frac{i\hbar}{2} \Lambda \; , \tag{A.2}$$

and the differential operator Λ defined as

$$\Lambda = - \overleftarrow{\partial}_{\boldsymbol{x}} \overrightarrow{\partial}_{\boldsymbol{\pi}} + \overleftarrow{\partial}_{\boldsymbol{\pi}} \overrightarrow{\partial}_{\boldsymbol{x}} \; , \tag{A.3}$$

where $\overleftarrow{\partial}$ and $\overrightarrow{\partial}$ denote derivatives acting only to the left and right, respectively. The Moyal product obeys the axiom of associativity,

$$A * B * C = A * (B * C) = (A * B) * C \; , \tag{A.4}$$

and also

$$(A * B)^\dagger = B^\dagger * A^\dagger \; , \tag{A.5}$$

however, the Moyal product is non-commutative, i.e. $A * B \neq B * A$. In fact, one defines the Moyal bracket

$$\frac{1}{i\hbar} \left[A \overset{*}{,} B\right] = \frac{1}{i\hbar} \left(A * B - B * A\right) \; , \tag{A.6}$$

which is identical to the usual commutator in quantum theory.

The back transformation is readily given by

$$G(\boldsymbol{x} + \frac{\boldsymbol{z}}{2}, \boldsymbol{x} - \frac{\boldsymbol{z}}{2}) = \int \frac{\mathrm{d}^4 \pi}{(2\pi\hbar)^4} \; e^{-i\boldsymbol{z}\boldsymbol{\pi}/\hbar} G(\boldsymbol{x}, \boldsymbol{\pi}) \tag{A.7}$$

or equivalently,

$$G(\boldsymbol{x}, \boldsymbol{x}') = \int \frac{\mathrm{d}^4 \pi}{(2\pi\hbar)^4} \; e^{-i(\boldsymbol{x}-\boldsymbol{x}')\boldsymbol{\pi}/\hbar} G\left(\frac{\boldsymbol{x} + \boldsymbol{x}'}{2}, \boldsymbol{\pi}\right) \tag{A.8}$$

For example, consider a function in Wigner representation that is localized in phase space

$$G(\boldsymbol{x}, \boldsymbol{\pi}) = \delta(\boldsymbol{x} - \boldsymbol{x}_0)\delta(\boldsymbol{\pi} - \boldsymbol{\pi}_0) \tag{A.9}$$

it is in usual quantum-mechanical representation

$$G(\boldsymbol{x} + \frac{\boldsymbol{z}}{2}, \boldsymbol{x} - \frac{\boldsymbol{z}}{2}) = \delta(\boldsymbol{x} - \boldsymbol{x}_0)e^{-i\boldsymbol{z}\boldsymbol{\pi}_0/\hbar} \tag{A.10}$$

which is completely non-local along the off-diagonal where $x = x_0$ expressing Heisenberg uncertainty of position and momentum.

Using (A.8), the quantum average of a operator $G(\boldsymbol{x}, \boldsymbol{x}')$ is simply given by

$$\int \mathrm{d}^3x G(\boldsymbol{x}, \boldsymbol{x}) = \int \mathrm{d}^3x \int \frac{\mathrm{d}^4\pi}{(2\pi\hbar)^4}\ G\left(\boldsymbol{x}, \boldsymbol{\pi}\right) \tag{A.11}$$

Wigner function or Wigner quasi-probability distribution

The Wigner transformation of the usual quantum mechanical density matrix is called the Wigner function

$$P(\boldsymbol{r}, \boldsymbol{p}, t) = \frac{1}{(2\pi\hbar)^3} \int \mathrm{d}^3z\ e^{-i\boldsymbol{p}\boldsymbol{z}/\hbar} \langle \boldsymbol{r} - \tfrac{\boldsymbol{z}}{2} | \hat{\rho}(t) | \boldsymbol{r} + \tfrac{\boldsymbol{z}}{2} \rangle\ , \tag{A.12}$$

which is a so-called quasi-probability distribution. Since it have negative values, it cannot be interpreted as a probability density in the usual sense. However, the integral

$$n(\boldsymbol{r}, t) = \int \mathrm{d}^3p\ P(\boldsymbol{r}, \boldsymbol{p}, t) \tag{A.13}$$

yields the usual particle density distribution in real space, which is a physically measurable quantity.

Weyl-Wigner ordering

The back transformation of an arbitrary function or r and p yields in the operator representation a fully symmetrized expression, for example, transforming back the term $x^m p^n$ (we consider a one-dimensional scenario for simplicity and the generalization to higher dimensions is straightforward), we obtain

$$\begin{aligned}
&\int \frac{\mathrm{d}p}{2\pi\hbar}\ e^{i(x-x')p/\hbar}\ \frac{(x+x')^m}{2^m} p^n = \frac{(x+x')^m}{2^m}(-i\hbar\partial_x)^n \int \frac{\mathrm{d}p}{2\pi\hbar}\ e^{i(x-x')p/\hbar} \\
&= \frac{(x+x')^m}{2^m}(-i\hbar\partial_x)^n \delta(x-x') = \frac{1}{2^m}\sum_{k=0}^{m} \binom{m}{k} (x^k(-i\hbar\partial_x)^n x^{m-k}\delta(x-x')
\end{aligned}$$

which directly translates into

$$\frac{1}{2^m}\sum_{k=0}^{m} \binom{m}{k} \hat{x}^k \hat{p}^n \hat{x}^{m-k}.$$

For example, xp becomes symmetrized as $\frac{1}{2}(\hat{x}\hat{p} + \hat{p}\hat{x})$.

B. Beyond linear response

This chapter is an extension to the treatment in section 2.2.4 which focused on the linear response regime. Here, we will attempt an exact derivation, albeit it will be a series expansion in external perturbations given by ∂_{neq} form Eq. (2.41).

To take into account the energy ω-dependency in the quantities $\delta\hat{G}$ and $\hat{A}$ exactly, we have to consider all moments, that is, we need to calculate the quantities

$$\hat{g}^{(n)}(\boldsymbol{k},\boldsymbol{r},t) = \int \frac{\mathrm{d}\omega}{2\pi i}\, \xi^n\, \delta\hat{G}(\boldsymbol{k},\omega,\boldsymbol{r},t)\ , \tag{B.1}$$

where $\xi \equiv \omega - E_{\mathrm{F}}$ and which are related by a hierarchy of equations. Actually, it is the collision integral $\hat{\mathcal{I}}[\delta\hat{G}]$ that keeps us from finding an exact equation for $\hat{g}^{(0)}$ alone. In order to find the aforementioned hierarchy, we multiply the kinetic equation by ξ^n and integrate over energy. The ansatz (2.42) gives rise to two terms on either side of equation (2.37) and thus, we have to treat four distinct contributions.

The first one,

$$\begin{aligned} -i\int \frac{\mathrm{d}\omega}{2\pi i}\left[(\epsilon\hat{1}-\hat{H}\,\tilde{*}\,\delta\hat{G}\right]\xi^n &= \int \frac{\mathrm{d}\omega}{2\pi i}\,\xi^n\partial_{\mathrm{neq}}\delta\hat{G} \\ &\quad + i\int \frac{\mathrm{d}\omega}{2\pi i}\left(\hat{H}\tilde{*}(\xi+\tfrac{i}{2}\overleftarrow{\partial}_{\mathrm{neq}})^n\delta\hat{G} - \delta\hat{G}(\xi-\tfrac{i}{2}\overrightarrow{\partial}_{\mathrm{neq}})^n\tilde{*}\hat{H}\right) \end{aligned} \tag{B.2}$$

Now, the idea is that $\hat{H}$ does not depend on ω, so we can replace $\tilde{*}$ simply by $\circ$, since ∂_ω acting towards $\delta\hat{G}$ can be disposed of by noting that we now have to integrate a total derivative $\partial_\omega(\cdots)$ of an expression which vanishes at infinity, a property here inherited from $\delta\hat{G}$. Therefore,

$$\begin{aligned} -i\int \frac{\mathrm{d}\omega}{2\pi i}\Big[(\epsilon\hat{1}-\hat{H}\,\tilde{*}\,\delta\hat{G}\Big]\xi^n & \\ &= \partial_{\mathrm{neq}}\hat{g}^{(n)} + i\int \frac{\mathrm{d}\omega}{2\pi i}\left(\hat{H}\circ(\xi+\tfrac{i}{2}\overleftarrow{\partial}_{\mathrm{neq}})^n\delta\hat{G} - \delta\hat{G}(\xi-\tfrac{i}{2}\overrightarrow{\partial}_{\mathrm{neq}})^n\circ\hat{H}\right) \\ &= \partial_{\mathrm{neq}}\hat{g}^{(n)} + \sum_{m=0}^{n}\binom{n}{m}\left(\frac{i}{2}\right)^m i\left[\partial_{\mathrm{neq}}^m\hat{H}\,\hat{\circ}\,\hat{g}^{(n-m)}\right]_{(-1)^m} \end{aligned} \tag{B.3}$$

after making use of definition (B.1).

We want to apply the same trick for the collision integral

$$\begin{aligned} \int \frac{\mathrm{d}\omega}{2\pi i}\,\xi^n\mathcal{I}[\delta\hat{G}] = \int \frac{\mathrm{d}^3k'}{(2\pi)^3}\int \frac{\mathrm{d}\omega}{2\pi i}\,\xi^n & \\ \frac{1}{2}\left[\left\{\underline{\hat{\chi}}\delta\hat{G}(\boldsymbol{k}',\omega,\boldsymbol{r},t)\,\tilde{*}\,\hat{A}(\boldsymbol{k},\omega,\boldsymbol{r},t)\right\} - \left\{\underline{\hat{\chi}}\hat{A}(\boldsymbol{k}',\omega,\boldsymbol{r},t)\,\tilde{*}\,\delta\hat{G}(\boldsymbol{k},\omega)\right\}\right]\ , & \end{aligned}$$

so we have to convey the ω-dependency of the $\hat{A}$ factors to the other side of the $\tilde{*}$-operators, which is performed by first moving the ω-dependecy into a translation operator and then shifting this factor accross $\tilde{*}$,

$$\hat{B}(\omega)\tilde{*}\hat{A}(\omega) = \hat{B}(\omega)\tilde{*}e^{\xi\partial_{E_\mathrm{F}}}\hat{A}(E_\mathrm{F}) = e^{(\xi-\frac{i}{2}\partial_\mathrm{neq})\partial_{E_\mathrm{F}}}\hat{B}(\omega)\tilde{*}\hat{A}(E_\mathrm{F}) \ ,$$

where ∂_neq now acts on $\hat{A}$ *and* $\hat{B}$. Since there is now only ω-dependency on either of the two sides of $\tilde{*}$, the aforementioned argument applies and the collision integral becomes

$$\begin{aligned}
\int \frac{\mathrm{d}\omega}{2\pi i}\, \xi^n \mathcal{I}[\delta\hat{G}] &= \frac{1}{2}\int \frac{\mathrm{d}^3k'}{(2\pi)^3}\int \frac{\mathrm{d}\omega}{2\pi i} \\
e^{(\xi-\frac{i}{2}\partial_\mathrm{neq})\partial_{E_\mathrm{F}}} &\left[\underline{\hat{\chi}}\delta\hat{G}(\boldsymbol{k}',\omega)(\xi-\tfrac{i}{2}\partial_\mathrm{neq})^n\circ\hat{A}(\boldsymbol{k},E_\mathrm{F}) - \delta\hat{G}(\boldsymbol{k},\omega)(\xi-\tfrac{i}{2}\partial_\mathrm{neq})^n\circ\underline{\hat{\chi}}\hat{A}(\boldsymbol{k}',E_\mathrm{F})\right] + \text{h.c.} \\
&= \frac{1}{2}\int \frac{\mathrm{d}^3k'}{(2\pi)^3}\sum_{m=0}^{\infty}\frac{1}{m!}\sum_{k=0}^{m}\binom{m}{k}\sum_{l=0}^{n}\binom{n}{l}\left(\frac{i}{2}\right)^{k+l} \\
&\partial_\mathrm{neq}^k\partial_{E_\mathrm{F}}^m\left(\left\{\partial_\mathrm{neq}^l\hat{A}(\boldsymbol{k},E_\mathrm{F})\stackrel{\circ}{,}\underline{\hat{\chi}}\hat{g}^{(m+n-k-l)}(\boldsymbol{k}')\right\}_{(-1)^{k+l}} - \right. \\
&\left.\left\{\partial_\mathrm{neq}^l\underline{\hat{\chi}}\hat{A}(\boldsymbol{k}',E_\mathrm{F})\stackrel{\circ}{,}\hat{g}^{(m+n-k-l)}(\boldsymbol{k})\right\}_{(-1)^{k+l}}\right) \ , \qquad \text{(B.4)}
\end{aligned}$$

where h.c. denotes that the hermitian conjugate should be added and we omitted the $\boldsymbol{r},t$ arguments for brevity. Note that it is this additional energy dependency in the scattering rates implicitly appearing in the collision integral that couples the different equations in the hierarchy for the $\hat{g}^{(n)}$. If it were not for this collision integral, there would be no such coupling and we would obtain a resulting equation for $\hat{g}^{(0)}$ alone which is much easier to solve.

Concerning the source terms, it is practical to write the source $\hat{\mathcal{J}}_\mathrm{t}$ stemming from the transport part

$$\begin{aligned}
\hat{\mathcal{J}}_\mathrm{t}^{(n)} &= \int \frac{\mathrm{d}\omega}{2\pi i}\xi^n i\left[(\omega\hat{1}-\hat{H})\stackrel{\tilde{*}}{,} i\hat{A}(\boldsymbol{k},\omega)f_\mathrm{D}(\omega)\right] \\
&= \int \frac{\mathrm{d}\omega}{2\pi i}\xi^n\left\{-\left[(\omega\hat{1}-\hat{H})\stackrel{\tilde{*}}{,}\hat{A}(\boldsymbol{k},\omega)f_\mathrm{D}(\omega)\right] + \left[(\omega\hat{1}-\hat{H})\stackrel{\tilde{*}}{,}\hat{A}(\boldsymbol{k},\omega)\right]f_\mathrm{D}(\omega)\right\} \\
&= \int \frac{\mathrm{d}\omega}{2\pi i}\xi^n\left\{\left[\hat{H}\stackrel{\tilde{*}}{,}\hat{A}(\boldsymbol{k},\omega)f_\mathrm{D}(\omega)\right] - \left[\hat{H}\stackrel{\tilde{*}}{,}\hat{A}(\boldsymbol{k},\omega)\right]f_\mathrm{D}(\omega)\right\} \ ,
\end{aligned}$$

where we could add the second term which vanishes by virtue of equation (2.39) and whereafter the two ω-terms cancel each other. Yet again, moving all the omega dependency on one side of the $\tilde{*}$-operator and performing the above trick yields

$$\begin{aligned}
\hat{\mathcal{J}}_\mathrm{t}^{(n)} &= \int \frac{\mathrm{d}\omega}{2\pi i}\hat{A}(\boldsymbol{k},\omega)\left(f_\mathrm{D}(\omega-\tfrac{i}{2}\partial_\mathrm{neq}) - f_\mathrm{D}(\omega)\right)(\xi-\tfrac{i}{2}\partial_\mathrm{neq})^n\circ\hat{H} + \text{h.c.} \\
&= -\frac{1}{4\pi}\int \mathrm{d}\omega\sum_{k=0}^{\infty}\frac{1}{(k+1)!}\left(-\frac{i}{2}\right)^k\partial_\omega^{k+1}f_\mathrm{D}(\omega)\ \hat{A}(\boldsymbol{k},\omega)(\xi-\tfrac{i}{2}\partial_\mathrm{neq})^n\circ\partial_\mathrm{neq}^{k+1}\hat{H} + \text{h.c.} \ ,
\end{aligned}$$

and after partial integration

$$\begin{aligned}
\hat{\mathcal{J}}_{\mathrm{t}}^{(n)} &= \frac{1}{4\pi}\int \mathrm{d}\omega \left(-\frac{\partial f_{\mathrm{D}}}{\partial \omega}\right) \sum_{k=0}^{\infty} \frac{1}{(k+1)!} \left(\frac{i}{2}\right)^k \partial_\omega^k \hat{A}(\boldsymbol{k},\omega)(\xi - \tfrac{i}{2}\partial)^n \circ \partial^{k+1}\hat{H} + \mathrm{h.c.} \\
&= \frac{1}{4\pi}\int \mathrm{d}\omega \left(-\frac{\partial f_{\mathrm{D}}}{\partial \omega}\right) \sum_{k=0}^{\infty} \frac{1}{(k+1)!} \left(\frac{i}{2}\right)^k \sum_{l=0}^{k} \binom{k}{l} \\
&\qquad \partial_\omega^{k-l}\hat{A}(\boldsymbol{k},\omega)\ \ \partial_\omega^{l}(\xi - \tfrac{i}{2}\partial_{\mathrm{neq}})^n \circ \partial_{\mathrm{neq}}^{k+1}\hat{H} + \mathrm{h.c.} \\
&= \frac{1}{4\pi}\int \mathrm{d}\omega \left(-\frac{\partial f_{\mathrm{D}}}{\partial \omega}\right) \sum_{k=0}^{\infty} \frac{1}{(k+1)!} \left(\frac{i}{2}\right)^k \sum_{l=0}^{\min\{k,n\}} \binom{k}{l} \frac{n!}{(n-l)!} \\
&\qquad \partial_\omega^{k-l}\hat{A}(\boldsymbol{k},\omega)\ \ (\xi - \tfrac{i}{2}\partial_{\mathrm{neq}})^{n-l} \circ \partial_{\mathrm{neq}}^{k+1}\hat{H} + \mathrm{h.c.}
\end{aligned}$$

and rearranging the summation $l = s$, $k = m + s$, where now $m = 0...\infty$, $s = 0...n$, so that

$$\begin{aligned}
\hat{\mathcal{J}}_{\mathrm{t}}^{(n)} &= \frac{1}{4\pi}\int \mathrm{d}\omega \left(-\frac{\partial f_{\mathrm{D}}}{\partial \omega}\right) \sum_{m=0}^{\infty} \frac{1}{m!} \sum_{s=0}^{n} \frac{1}{m+s+1} \left(\frac{i}{2}\right)^{m+s} \binom{n}{s} \\
&\qquad \partial_\omega^{m}\hat{A}(\boldsymbol{k},\omega)\ \ (\xi - \tfrac{i}{2}\partial_{\mathrm{neq}})^{n-s} \circ \partial_{\mathrm{neq}}^{m+s+1}\hat{H} + \mathrm{h.c.}\ .
\end{aligned}$$

To further simplify the equation, let us make use of the zero-temperature approximation, i.e. that $-\frac{\partial f_{\mathrm{D}}}{\partial \omega} = \delta(\omega - E_{\mathrm{F}})$ which forces $\xi = 0$ and apply the identity

$$\sum_{s=0}^{n} \binom{n}{s} \frac{1}{m+s+1}(-1)^{n-s} = (-1)^n \frac{n!m!}{(n+m+1)!}$$

so that we finally obtain

$$\hat{\mathcal{J}}_{\mathrm{t}}^{(n)} = \quad (-1)^n \frac{n!}{4\pi} \sum_{m=0}^{\infty} \frac{1}{(n+m+1)!} \left(\frac{i}{2}\right)^{n+m} \left\{ \partial_{E_{\mathrm{F}}}^{m}\hat{A}(\boldsymbol{k}, E_{\mathrm{F}}) \circ \partial_{\mathrm{neq}}^{n+m+1}\hat{H} \right\}_{(-1)^{m+n}} . \quad \text{(B.5)}$$

The derivation of the collision source terms walks along the same lines, that is

$$\begin{aligned}
\hat{\mathcal{J}}_{\mathrm{c}}^{(n)} &= \int \frac{\mathrm{d}\omega}{2\pi i}\ \xi^n \mathcal{I}[i\hat{A} f_{\mathrm{D}}(\omega)] = \\
&= \frac{1}{4\pi}\int \frac{\mathrm{d}^3k'}{(2\pi)^3} \int \mathrm{d}\omega \xi^n\ \left(f_{\mathrm{D}}(\omega)\underline{\hat{\chi}}\hat{A}(\boldsymbol{k}',\omega)\tilde{*}\hat{A}(\boldsymbol{k},\omega) - \underline{\hat{\chi}}\hat{A}(\boldsymbol{k}',\omega)\tilde{*}\hat{A}(\boldsymbol{k},\omega) f_{\mathrm{D}}(\omega) \right) + \mathrm{h.c.} \\
&= \frac{1}{4\pi}\int \frac{\mathrm{d}^3k'}{(2\pi)^3} \int \mathrm{d}\omega\ \left(f_{\mathrm{D}}(\omega)\underline{\hat{\chi}}\hat{A}(\boldsymbol{k}',\omega) \left(\xi - \tfrac{i}{2}\partial_{\mathrm{neq}}\right)^n \tilde{*}\hat{A}(\boldsymbol{k},\omega) \right. \\
&\qquad \left. - \underline{\hat{\chi}}\hat{A}(\boldsymbol{k}',\omega) \left(\xi - \tfrac{i}{2}\partial_{\mathrm{neq}}\right)^n \tilde{*}\hat{A}(\boldsymbol{k},\omega) f_{\mathrm{D}}(\omega) \right) + \mathrm{h.c.}
\end{aligned}$$

and using that

$$\int \mathrm{d}\omega \left(f_{\mathrm{D}}(\omega)\hat{B}(\omega)\tilde{*}\hat{A}(\omega) - \hat{B}(\omega)\tilde{*}\hat{A}(\omega)f_{\mathrm{D}}(\omega)\right) =$$

$$\sum_{m=0}^{\infty} \frac{1}{(m+1)!} \left(\tfrac{i}{2}\right)^{m+1} \partial_{\mathrm{neq}}^{m+1} \int \mathrm{d}\omega f_{\mathrm{D}}(\omega) \underbrace{\left[(-1)^{m+1}\hat{B}\circ\partial_{\omega}^{m+1}\hat{A} - \partial_{\omega}^{m+1}\hat{B}\circ\hat{A}\right]}_{-\partial_{\omega}\sum_{k=0}^{m}(-1)^{m-k}\left(\partial_{\omega}^{k}\hat{B}\right)\circ\left(\partial_{\omega}^{m-k}\hat{A}\right)} =$$

$$- \sum_{m=0}^{\infty} \frac{1}{(m+1)!} \left(\tfrac{i}{2}\right)^{m+1} \partial_{\mathrm{neq}}^{m+1} \sum_{k=0}^{m}(-1)^{m-k} \int \mathrm{d}\omega \left(-\frac{\partial f_{\mathrm{D}}}{\partial\omega}\right) \left(\partial_{\omega}^{k}\hat{B}\right)\circ\left(\partial_{\omega}^{m-k}\hat{A}\right) \ ,$$

where along the derivation we made use of the fact that $m = 0$ has no contribution and we integrated by parts with respect to ω. We thus obtain

$$\begin{aligned}
\hat{\mathcal{J}}_{\mathrm{c}}^{(n)} &= \frac{-1}{4\pi}\int\frac{\mathrm{d}^3k'}{(2\pi)^3}\sum_{m=0}^{\infty}\frac{\left(\frac{i}{2}\right)^{m+1}}{(m+1)!}\partial_{\mathrm{neq}}^{m+1}\sum_{k=0}^{m}(-1)^{m-k}\int\mathrm{d}\omega\left(-\tfrac{\partial f_{\mathrm{D}}}{\partial\omega}\right) \\
&\qquad \left(\partial_{\omega}^{k}\hat{\underline{\chi}}\hat{A}(\boldsymbol{k}',\omega)\left(\xi-\tfrac{i}{2}\partial_{\mathrm{neq}}\right)^{n}\right)\circ\left(\partial_{\omega}^{m-k}\hat{A}(\boldsymbol{k},\omega)\right) + \mathrm{h.c.} \\
&= \frac{-1}{4\pi}\int\frac{\mathrm{d}^3k'}{(2\pi)^3}\sum_{m=0}^{\infty}\frac{\left(\frac{i}{2}\right)^{m+1}}{(m+1)!}\partial_{\mathrm{neq}}^{m+1}\sum_{k=0}^{m}(-1)^{m-k}\int\mathrm{d}\omega\left(-\tfrac{\partial f_{\mathrm{D}}}{\partial\omega}\right)\sum_{l=0}^{\min\{n,k\}}\binom{k}{l}\frac{n!}{(n-l)!} \\
&\qquad \left(\partial_{\omega}^{k-l}\hat{\underline{\chi}}\hat{A}(\boldsymbol{k}',\omega)\right)\circ\left(\left(\xi-\tfrac{i}{2}\partial_{\mathrm{neq}}\right)^{n-l}\partial_{\omega}^{m-k}\hat{A}(\boldsymbol{k},\omega)\right) + \mathrm{h.c.}\ .
\end{aligned}$$

Again making use of zero temperature approximation and rearranging summation by transformation $m = u + s$, $l = s$, $k = t + s$ with boundaries $u = 0...\infty$, $t = 0...u$ and $s = 0...n$, which yields the final result

$$\begin{aligned}
\hat{\mathcal{J}}_{\mathrm{c}}^{(n)} &= \frac{1}{4\pi}\int\frac{\mathrm{d}^3k'}{(2\pi)^3}\sum_{u=0}^{\infty}\sum_{t=0}^{u}\sum_{s=0}^{n}\frac{\left(\frac{i}{2}\right)^{u+n+1}}{(u+s+1)!}\partial_{\mathrm{neq}}^{u+s+1}(-1)^{1+n+u-t-s}\frac{(t+s)!}{t!}\binom{n}{s} \\
&\qquad \left(\partial_{E_{\mathrm{F}}}^{t}\hat{\underline{\chi}}\hat{A}(\boldsymbol{k}',E_{\mathrm{F}})\right)\circ\left(\partial_{\mathrm{neq}}^{n-s}\partial_{E_{\mathrm{F}}}^{u-t}\hat{A}(\boldsymbol{k},E_{\mathrm{F}})\right) + \mathrm{h.c.} \\
&= \frac{1}{4\pi}\int\frac{\mathrm{d}^3k'}{(2\pi)^3}\sum_{u=0}^{\infty}\sum_{t=0}^{u}\sum_{s=0}^{n}\binom{n}{s}\frac{(t+s)!\ (-1)^{t+s}}{(u+s+1)!\ t!}\left(\tfrac{i}{2}\right)^{u+n+1} \\
&\qquad \partial_{\mathrm{neq}}^{1+u+s}\left\{\partial_{\mathrm{neq}}^{n-s}\partial_{E_{\mathrm{F}}}^{u-t}\hat{A}(\boldsymbol{k},E_{\mathrm{F}})\stackrel{\circ}{,}\partial_{E_{\mathrm{F}}}^{t}\hat{\underline{\chi}}\hat{A}(\boldsymbol{k}',E_{\mathrm{F}})\right\}_{(-1)^{1+n+u}} \ . \qquad \text{(B.6)}
\end{aligned}$$

For the most simple case, where we treat external perturbations, be it in time or externally applied electric field, to linear order only, equations (B.3),(B.4),(B.5),(B.6) drastically simplify to yield the kinetic equation valid for describing the low-energy behavior. Furthermore, it turns out that, generally, $\hat{g}^{(n)}$ is of order $(\boldsymbol{E},\partial_t)^{n+1}$, i.e. the index n specifies the order in external perturbations that lead to non-equilibrium excitations. It is for this reason that we do not need to go beyond $\hat{g}^{(0)} \equiv \hat{g}$, so that we can restrict ourselves to the lowest equation in the hierarchy:

$$\hat{\mathcal{J}}_{\mathrm{t}} = \frac{1}{4\pi}\left\{\hat{A}(\boldsymbol{k},E_{\mathrm{F}},\boldsymbol{r},t)\stackrel{\circ}{,}\partial_{\mathrm{neq}}\hat{H}\right\} \qquad \text{(B.7)}$$

$$\hat{\mathcal{J}}_{\mathrm{c}} = \frac{1}{4\pi}\partial_{\mathrm{neq}}\int\frac{\mathrm{d}^3k'}{(2\pi)^3}\ \frac{1}{2i}\left[\hat{\underline{\chi}}\hat{A}(\boldsymbol{k}',E_{\mathrm{F}},\boldsymbol{r},t)\stackrel{\circ}{,}\hat{A}(\boldsymbol{k},E_{\mathrm{F}},\boldsymbol{r},t)\right] \ . \qquad \text{(B.8)}$$

$$i\left[\hat{H}\circ\hat{g}(\boldsymbol{k},\boldsymbol{r},t)\right]=\hat{\mathcal{J}}_{\mathrm{t}}+\hat{\mathcal{J}}_{\mathrm{c}}$$
$$+\frac{1}{2}\int\frac{\mathrm{d}^3k'}{(2\pi)^3}\left(\left\{\hat{A}(\boldsymbol{k},E_{\mathrm{F}},\boldsymbol{r},t)\circ\underline{\hat{\chi}}\hat{g}(\boldsymbol{k}',\boldsymbol{r},t)\right\}-\left\{\underline{\hat{\chi}}\hat{A}(\boldsymbol{k}',E_{\mathrm{F}},\boldsymbol{r},t)\circ\hat{g}(\boldsymbol{k},\boldsymbol{r},t)\right\}\right)\ ,$$

where we note that the term $\partial_{\mathrm{neq}}\hat{g}(\boldsymbol{k},\boldsymbol{r},t)$ can be neglected since it is of higher order in $\boldsymbol{E},\partial_t$. Also, in the above formulas, the spectral densities $\hat{A}$ need to be only of zeroth order in $\boldsymbol{E},\partial_t$. Note that there are never any corrections of order $\frac{1}{\tau E_{\mathrm{F}}}$ in the kinetic equation for $\hat{g}$ or $\hat{G}^<$; the only corrections we have (within our approach) are the aforementioned non-linear corrections in ∂_t and $\boldsymbol{E}$, so as long as we stay in the linear response regime, the above equations are exact, except for the restriction concerning precession and which is discussed below. However, in determining the spectral densities, there will be a broadening of the delta-peaked spectrum we are employing here (Eq. (D.3)) due to the influence of scattering. Those corrections are of order $\frac{1}{\tau E_{\mathrm{F}}}$, but we do not need to take them into account due to the condition $\tau E_{\mathrm{F}}\gg 1$ and besides, these corrections are of no interest to the problem under investation. However, when $\tau\Delta\approx 1$ and Δ is not small compared to E_{F}, there will be some smearing of the quantities, since the delta-spectrum has to be replaced by Lorentzians of width $1/\tau$. Concerning time-dependency and precession, there is another important point which has been also discussed in section 2.2.4. Let us look at two limiting cases. First, for $\Delta\approx E_{\mathrm{F}}$, the terms $\partial_t\hat{g}$ become very important, since $\hat{g}$ includes rapidly oscillating terms and we then cannot linearize with respect to ∂_t. Then we have to consider (2.44) as an effective equation in which ∂_t does not act on Δ-oscillations. Second, for $\Delta\ll E_{\mathrm{F}}$, we can directly apply our equations and ∂_t does describe the precession which now is a slow time-scale. However, in the regime $\Delta\ll E_{\mathrm{F}}$, corrections to the spectrum become irrelevant, however, in our model then exhibits$\tau_\uparrow=\tau_\downarrow$ which is undesired in the case of the domain-wall resistance.

C. Details on deriving the hierarchy of equations

We start out with the kinetic equation (2.64) and (2.45) by taking $(-e)\,\langle v_x^n\ (2.64)\rangle$ and by introducing

$$\hat{g}^{(n)} = (-e)\,\langle v_x^n\ \hat{g}\rangle = (-e)\int \frac{\mathrm{d}^3k}{(2\pi)^3} v_x^n\ \hat{g}\ ,$$
$$\hat{a}^{(n)} = \left\langle v_x^n\ \hat{A}\right\rangle = \int \frac{\mathrm{d}^3k}{(2\pi)^3} v_x^n\ \hat{A}\ .$$

Afterwards, employing an expansion of $\circ = e^{\frac{i}{2}(\overleftarrow{\partial_x}\overrightarrow{\partial_{kx}} - \overleftarrow{\partial_{kx}}\overrightarrow{\partial_x})} \approx 1 + \frac{i}{2}(\cdots) - \frac{1}{8}(\cdots)^2$ and making use of relation (2.68), we obtain

$$\left\langle v_x^n\ \frac{i}{2}\left[\hat{f}(x) \circ \hat{g}(x,k)\right]\right\rangle = \frac{i}{2}\left[\hat{f},\hat{g}^{(n)}\right] + \frac{n}{2m_\mathrm{e}}\frac{1}{2}\left\{\partial\hat{f},\hat{g}^{(n-1)}\right\} - \frac{n(n-1)}{8m_\mathrm{e}^2}\frac{i}{2}\left[\partial^2\hat{f},\hat{g}^{(n-2)}\right]\ ,$$
$$\left\langle v_x^n\ \frac{1}{2}\left\{\hat{f}(x) \circ \hat{g}(x,k)\right\}\right\rangle = \frac{1}{2}\left\{\hat{f},\hat{g}^{(n)}\right\} - \frac{n}{2m_\mathrm{e}}\frac{i}{2}\left[\partial\hat{f},\hat{g}^{(n-1)}\right] - \frac{n(n-1)}{8m_\mathrm{e}^2}\frac{1}{2}\left\{\partial^2\hat{f},\hat{g}^{(n-2)}\right\}\ ,$$

where we are able to truncate the series since our treatment includes only terms up to order q^2 and subsequent terms would contribute only to higher orders.

This yields the following equation

$$\begin{aligned}\partial\hat{g}^{(n+1)} - \Delta\frac{i}{2}\left[\vec{m}\hat{\vec{\sigma}},\hat{g}^{(n)}\right] - \frac{n}{m_\mathrm{e}}\frac{1}{2}\left\{\frac{\Delta}{2}\partial\vec{m}\hat{\vec{\sigma}} + (\partial\delta\mu),\hat{g}^{(n-1)}\right\} + \frac{\Delta n(n-1)}{8m_\mathrm{e}^2}\frac{i}{2}\left[\partial^2\vec{m}\hat{\vec{\sigma}},\hat{g}^{(n-2)}\right]\\ = \frac{1}{2}\left\{\hat{a}^{(n)},\underline{\hat{\chi}}\hat{g}^{(0)}\right\} - \frac{1}{2}\left\{\underline{\hat{\chi}}\hat{a}^{(0)},\hat{g}^{(n)}\right\} + \frac{n}{2m_\mathrm{e}}\frac{i}{2}\left(\left[\hat{a}^{(n-1)},\partial\underline{\hat{\chi}}\hat{g}^{(0)}\right] + \left[\partial\underline{\hat{\chi}}\hat{a}^{(0)},\hat{g}^{(n-1)}\right]\right)\\ - \frac{n(n-1)}{8m_\mathrm{e}^2}\frac{1}{2}\left(\left\{\hat{a}^{(n-2)},\partial^2\underline{\hat{\chi}}\hat{g}^{(0)}\right\} - \left\{\partial^2\underline{\hat{\chi}}\hat{a}^{(0)},\hat{g}^{(n-2)}\right\}\right)\ , \quad \text{(C.1)}\end{aligned}$$

where the action of $\underline{\hat{\chi}}$ is defined in (2.28).

We also need to know the spectral density $\hat{a}^{(n)}$ up to order q^2. We find for even and odd moments, respectively

$$\begin{aligned}\hat{a}^{(2n)} &= 2\pi\left(\nu_0^{(n)}\hat{1} + \nu_\mathrm{s}^{(n)}\vec{m}\hat{\vec{\sigma}}\right) + 2\pi\left(\beta_0^{(n)}\hat{1} + \beta_\mathrm{s}^{(n)}\vec{m}\hat{\vec{\sigma}}\right)(\partial\vec{m})^2 + 2\pi\beta_\perp^{(n)}(\partial^2\vec{m})_\perp\hat{\vec{\sigma}}\ ,\\ \hat{a}^{(2n+1)} &= 2\pi\alpha_\perp^{(n)}\vec{m}\times\partial\vec{m}\hat{\vec{\sigma}}\ , \quad \text{(C.2)}\end{aligned}$$

where $(\partial^2 \boldsymbol{m})_\perp$ denotes that we only take the component perpendicular to $\vec{m}$. The coefficients for a $d = 3$ dimensional electron gas are given by

$$\begin{aligned}
\alpha_\perp^{(n)} &= \frac{1}{2}\left[\frac{2}{\Delta}\nu_{\mathrm{s}}^{(n+1)} - \nu_0'^{(n+1)}\right] \\
\beta_\perp^{(n)} &= -\frac{1}{\Delta}\alpha_\perp^{(n)} - \frac{2n(2n-1)}{8m_{\mathrm{e}}^2}\nu_{\mathrm{s}}^{(n-1)} \\
\beta_0^{(n)} &= -\frac{2n-1}{4m_{\mathrm{e}}}\alpha_\perp^{(n-1)} + \frac{2n-1}{m_{\mathrm{e}}}\nu_0^{(n-1)}\frac{\delta\mu}{q^2} \\
\beta_{\mathrm{s}}^{(n)} &= -\frac{1}{2\Delta}\alpha_\perp^{(n)} - \frac{2n-1}{8m_{\mathrm{e}}}\nu_{\mathrm{s}}^{(n-1)}\left[1 - \frac{8m_{\mathrm{e}}}{q^2}\delta\mu\right] ,
\end{aligned}$$

using the definitions

$$\begin{aligned}
\nu_0^{(n)}(\omega) &= \frac{1}{2}\left[\nu_\uparrow^{(n)}(\omega) + \nu_\downarrow^{(n)}(\omega)\right] \\
\nu_{\mathrm{s}}^{(n)}(\omega) &= \frac{1}{2}\left[\nu_\uparrow^{(n)}(\omega) - \nu_\downarrow^{(n)}(\omega)\right] \\
\nu_{\uparrow,\downarrow}^{(n)}(\omega) &= \frac{\nu_{\uparrow,\downarrow}(\omega)}{1+2n}\left[\frac{2}{m_{\mathrm{e}}}\left(\omega \pm \frac{\Delta}{2}\right)\right]^n .
\end{aligned}$$

$\nu_{\uparrow,\downarrow}$ specified without any argument implies that we take its value at the Fermi-level, i.e. more specifically $\nu_{\uparrow,\downarrow}^{(n)} \equiv \nu_{\uparrow,\downarrow}^{(n)}(E_{\mathrm{F}})$.

The chemical potential $\delta\mu$ is obtained from the condition that

$$\begin{aligned}
&\int_{-\infty}^{+\infty}\frac{\mathrm{d}\omega}{2\pi}\, f_{\mathrm{D}}(\omega)\ \mathrm{Tr}\left\{\hat{a}^{(0)}(\omega) - \hat{a}^{(0)}(\omega)|_{q=0}\right\} = \int_{-\infty}^{+\infty}\mathrm{d}\omega f_{\mathrm{D}}(\omega)\ 2\beta_0^{(0)}q^2 = \\
&\quad\int_{-\infty}^{+\infty}\mathrm{d}\omega f_{\mathrm{D}}(\omega)\ \frac{2}{m_{\mathrm{e}}}\left(\frac{1}{4}\alpha_\perp^{(-1)}q^2 - \nu_0^{(-1)}\delta\mu\right) = \frac{1}{2}\alpha_\perp^{(0)}q^2 + 2\nu_0^{(0)}\delta\mu \stackrel{!}{=} 0 ,
\end{aligned} \tag{C.3}$$

since in the zero-temperature approximation

$$\int_{-\infty}^{+\infty}\mathrm{d}\omega\ f_{\mathrm{D}}(\omega)\nu_{\uparrow,\downarrow}^{(n)}(\omega) = \int^{E_{\mathrm{F}}}\mathrm{d}\omega\ \nu_{\uparrow,\downarrow}^{(n)}(\omega) = \frac{m_{\mathrm{e}}}{2n+1}\nu_{\uparrow,\downarrow}^{(n+1)} .$$

Therefore, we immediately arrive at the shift in the chemical potential

$$\delta\mu = -\frac{1}{4\nu_0^{(0)}}q^2\alpha_\perp^{(0)} = \frac{q^2}{2m_{\mathrm{e}}}\frac{1}{4}\left(1 - \frac{2}{\Delta}\frac{m_{\mathrm{e}}\nu_{\mathrm{s}}^{(1)}}{\nu_0^{(0)}}\right) , \tag{C.4}$$

which yields result (2.57), once we plug in all definitions and by noting that $\nu_0^{(0)} = \nu_0$, $\nu_{\mathrm{s}}^{(0)} = P\nu_0$ and $\nu_{\mathrm{s}}^{(1)} = \frac{\nu_0}{3m_{\mathrm{e}}}(2PE_{\mathrm{F}} + \Delta)$. Substituting $\delta\mu$ back into the expressions for β, we can now write

$$\begin{aligned}
\beta_0^{(n)} &= -\frac{2n-1}{4m_{\mathrm{e}}}\alpha_\perp^{(n-1)} - \frac{\nu_0'^{(n)}}{4\nu_0^{(0)}}\alpha_\perp^{(0)} \\
\beta_{\mathrm{s}}^{(n)} &= -\frac{1}{2\Delta}\alpha_\perp^{(n)} - \frac{1}{4\Delta}\frac{\nu_{\mathrm{s}}^{(1)}}{\nu_0^{(0)}}\nu_{\mathrm{s}}'^{(n)} .
\end{aligned}$$

Later, we will also need

$$\underline{\hat{\chi}}\hat{a}^{(0)} = \underline{\hat{\chi}}\hat{a}_0^{(0)} + \underline{\hat{\chi}}\hat{a}_q^{(0)} \to \frac{1}{\tau}(\hat{1} + P\gamma\vec{m}\hat{\vec{\sigma}}) + \frac{1}{\tau\nu_0}\left(\beta_0^{(0)}\hat{1} + \beta_{\rm s}^{(0)}\gamma\vec{m}\hat{\vec{\sigma}}\right)q^2 + \frac{1}{\tau\nu_0}\beta_\perp^{(0)}(1 - \frac{\tau}{T_2})(\partial^2\vec{m})_\perp\hat{\vec{\sigma}} \ ,$$

where we write $\hat{a}_0^{(0)}$ to indicate that we take the zeroth order in q only and accordingly, $\hat{a}_q^{(0)}$ contains all corrections to the density of states due to a magnetization gradient.

Next, we will change the 2×2 spin-matrix representation to the 4×4 matrix representation in the basis introduced above, $(+,-,\uparrow,\downarrow)$. This change of basis implies a local rotation of the basis in spin space to align the magnetization direction $\vec{m}$ along the new z-axis, which corresponds to the gauge transformation introduced above. The various vectors we will encounter in the following derivation transform in the following manner:

$$\begin{aligned} \vec{m}\hat{\vec{\sigma}} &\to \hat{\sigma}_z \\ \partial\vec{m}\hat{\vec{\sigma}} &\to q\hat{\sigma}_y \\ \vec{m}\times\partial\vec{m} &\to -q\sigma_x \\ \partial^2\vec{m}\hat{\vec{\sigma}} = (\partial^2\vec{m})_\perp\hat{\vec{\sigma}} + (\vec{m}\partial^2\vec{m})\vec{m}\hat{\vec{\sigma}} &\to (\partial q)\hat{\sigma}_y - q^2\hat{\sigma}_z \ , \end{aligned}$$

and we note that $-\vec{m}\partial^2\vec{m} = (\partial\vec{m})^2 = q^2$. In the following, we specify substitution rules that perform this transformation:

$$\begin{array}{ll} \frac{i}{2}[\hat{\sigma}_i, \hat{n}] & \to \underline{\underline{M}}_i\vec{n} \\ \frac{1}{2}\{\hat{\sigma}_i, \hat{n}\} & \to \underline{\underline{K}}_i\vec{n} \end{array} \ , \tag{C.5}$$

where

$$\underline{\underline{M}}_x = \frac{i}{2}\begin{pmatrix} 0 & 0 & 1 & -1 \\ 0 & 0 & -1 & 1 \\ 1 & -1 & 0 & 0 \\ -1 & 1 & 0 & 0 \end{pmatrix} \quad \underline{\underline{M}}_y = \frac{1}{2}\begin{pmatrix} 0 & 0 & -1 & 1 \\ 0 & 0 & -1 & 1 \\ 1 & 1 & 0 & 0 \\ -1 & -1 & 0 & 0 \end{pmatrix} \quad \underline{\underline{M}}_z = \begin{pmatrix} -i & 0 & 0 & 0 \\ 0 & i & 0 & 0 \\ 0 & 0 & 0 & 0 \\ 0 & 0 & 0 & 0 \end{pmatrix}$$

$$\underline{\underline{K}}_x = \frac{1}{2}\begin{pmatrix} 0 & 0 & 1 & 1 \\ 0 & 0 & 1 & 1 \\ 1 & 1 & 0 & 0 \\ 1 & 1 & 0 & 0 \end{pmatrix} \qquad \underline{\underline{K}}_y = \frac{i}{2}\begin{pmatrix} 0 & 0 & 1 & 1 \\ 0 & 0 & -1 & -1 \\ -1 & 1 & 0 & 0 \\ -1 & 1 & 0 & 0 \end{pmatrix} \quad \underline{\underline{K}}_z = \begin{pmatrix} 0 & 0 & 0 & 0 \\ 0 & 0 & 0 & 0 \\ 0 & 0 & 1 & 0 \\ 0 & 0 & 0 & -1 \end{pmatrix}$$

constitute matrices in $(+,-,\uparrow,\downarrow)$ representation. The action of $\underline{\hat{\chi}}$ turns into

$$\underline{\hat{\chi}}\hat{n} \to \frac{1}{2\pi\nu_0\tau}\underline{\chi}\vec{n}$$

with the matrix

$$\underline{\chi} = \underline{\underline{1}} + \tau\begin{pmatrix} -\frac{1}{T_2} & 0 & 0 & 0 \\ 0 & -\frac{1}{T_2} & 0 & 0 \\ 0 & 0 & -\frac{1}{2T_1} & \frac{1}{2T_1} \\ 0 & 0 & \frac{1}{2T_1} & -\frac{1}{2T_1} \end{pmatrix} .$$

As a consequence of the gauge transformation, the derivative transforms into

$$\partial \to \underline{\underline{\partial}} \equiv \underline{\underline{1}}\partial + q\underline{\underline{M}}_x \ .$$

Now with these rules at hand, the change of representation is straightforward and we obtain

$$\underline{\underline{\partial}}\vec{g}^{(n+1)} + \hat{\underline{\underline{\Pi}}}\vec{g}^{(n)} = \underline{\underline{\Xi}}_0^{(n)}\vec{g}^{(0)} + \underline{\underline{\Xi}}_q^{(n)}\vec{g}^{(0)} - \hat{\underline{\underline{\Pi}}}_q^{(n)}\vec{g}^{(n)} + \underline{\zeta}_1^{(n)}\vec{g}^{(n-1)} + \underline{\zeta}_2^{(n)}\vec{g}^{(n-2)} \tag{C.6}$$

where zeroth order relaxation and precession terms are

$$\frac{1}{2}\left\{\hat{\underline{\chi}}\hat{a}_0^{(0)}, \hat{g}^{(n)}\right\} - \Delta\frac{i}{2}\left[\vec{m}\hat{\vec{\sigma}}, \hat{g}^{(n)}\right] \to \left[\frac{1}{\tau}(\underline{\underline{1}} + P\gamma\underline{\underline{K}}_z) - \Delta\underline{\underline{M}}_z\right]\vec{g}^{(n)} \equiv \hat{\underline{\underline{\Pi}}}\vec{g}^{(n)} \tag{C.7}$$

and magnetization gradient correction to relaxation rates yield

$$\frac{1}{2}\left\{\hat{\underline{\chi}}\hat{a}_q^{(0)}, \hat{g}^{(n)}\right\} \to \frac{1}{\nu_0\tau}\left[q^2\beta_0^{(0)}\underline{\underline{1}} + q^2\beta_{\mathrm{s}}^{(0)}\gamma\underline{\underline{K}}_z + (\partial q)\beta_\perp^{(0)}(1 - \frac{\tau}{T_2})\underline{\underline{K}}_y\right]\vec{g}^{(n)} \equiv \hat{\underline{\underline{\Pi}}}_q^{(n)}\vec{g}^{(n)} \ . \tag{C.8}$$

Corrections that depend on lower moments $\vec{g}^{(n)}$ in the hierarchy read explicitly

$$\begin{aligned}\frac{\Delta n}{2m_{\mathrm{e}}}\frac{1}{2}\left\{\partial\vec{m}\hat{\vec{\sigma}}, \hat{g}^{(n-1)}\right\} + \frac{n}{m_{\mathrm{e}}}(\partial\delta\mu)\hat{g}^{(n-1)} + \frac{n}{2m_{\mathrm{e}}}\frac{i}{2}\left[\partial\hat{\underline{\chi}}\hat{a}^{(0)}, \hat{g}^{(n-1)}\right] \\ \to \left[q\frac{\Delta n}{2m_{\mathrm{e}}}\underline{\underline{K}}_y + \frac{n}{m_{\mathrm{e}}}(\partial\delta\mu)\underline{\underline{1}} + q\frac{n}{2m_{\mathrm{e}}}\frac{P\gamma}{\tau}\underline{\underline{M}}_y\right]\vec{g}^{(n-1)} \equiv \underline{\zeta}_1^{(n)}\vec{g}^{(n-1)}\end{aligned} \tag{C.9}$$

and

$$\begin{aligned}-\frac{\Delta n(n-1)}{8m_{\mathrm{e}}^2}\frac{i}{2}\left[\partial^2\vec{m}\hat{\vec{\sigma}}, \hat{g}^{(n-2)}\right] + \frac{n(n-1)}{8m_{\mathrm{e}}^2}\frac{1}{2}\left\{\partial^2\hat{\underline{\chi}}\hat{a}^{(0)}, \hat{g}^{(n-2)}\right\} \\ \to \frac{n(n-1)}{8m_{\mathrm{e}}^2}\left[\Delta\left(q^2\underline{\underline{M}}_z - (\partial q)\underline{\underline{M}}_y\right) - \frac{P\gamma}{\tau}\left(q^2\underline{\underline{K}}_z - (\partial q)\underline{\underline{K}}_y\right)\right]\vec{g}^{(n-2)} \equiv \underline{\zeta}_2^{(n)}\vec{g}^{(n-2)} \ .\end{aligned} \tag{C.10}$$

Furthermore, we have source terms appearing in the equation, whereof the zeroth order term simply is

$$\frac{1}{2}\left\{\hat{a}_0^{(2n)}, \hat{\underline{\chi}}\hat{g}^{(0)}\right\} \to \frac{1}{\nu_0\tau}\left[\nu_0^{(n)}\underline{\underline{1}} + \nu_{\mathrm{s}}^{(n)}\underline{\underline{K}}_z\right]\underline{\chi}\vec{g}^{(0)} \equiv \underline{\underline{\Xi}}_0^{(2n)}\vec{g}^{(0)} \tag{C.11}$$

for even indices and $\underline{\underline{\Xi}}_0^{(2n+1)} = 0$ for odd indices. The corresponding gradient corrections are, for even indices

$$\begin{aligned}\frac{1}{2}\left\{\hat{a}_q^{(2n)}, \hat{\underline{\chi}}\hat{g}^{(0)}\right\} + \frac{2n}{2m_{\mathrm{e}}}\frac{i}{2}\left[\hat{a}^{(2n-1)}, \partial\hat{\underline{\chi}}\hat{g}^{(0)}\right] - \frac{2n(2n-1)}{8m_{\mathrm{e}}^2}\frac{1}{2}\left\{\hat{a}^{(2n-2)}, \partial^2\hat{\underline{\chi}}\hat{g}^{(0)}\right\} \\ \to \frac{1}{\tau\nu_0}\left[q^2\beta_0^{(n)}\underline{\underline{1}} + q^2\beta_{\mathrm{s}}^{(n)}\underline{\underline{K}}_z + (\partial q)\beta_\perp^{(n)}\underline{\underline{K}}_y - q\frac{2n}{2m_{\mathrm{e}}}\alpha_\perp^{(n-1)}\underline{\underline{M}}_x\underline{\underline{\partial}}\right. \\ \left. -\frac{2n(2n-1)}{8M^2}\left(\nu_0^{(n-1)}\underline{\underline{1}} + \nu_{\mathrm{s}}^{(n-1)}\underline{\underline{K}}_z\right)\underline{\underline{\partial}}^2\right]\underline{\chi}\vec{g}^{(0)} \equiv \underline{\underline{\Xi}}_q^{(2n)}\vec{g}^{(0)} \ .\end{aligned}$$

and for odd indices

$$\begin{aligned}\frac{1}{2}\left\{\hat{a}_q^{(2n+1)}, \hat{\underline{\chi}}\hat{g}^{(0)}\right\} + \frac{2n+1}{2m_{\mathrm{e}}}\frac{i}{2}\left[\hat{a}^{(2n)}, \partial\hat{\underline{\chi}}\hat{g}^{(0)}\right] \\ \to \frac{1}{\tau\nu_0}\left[-q\alpha_\perp^{(n)}\underline{\underline{K}}_x + \frac{2n+1}{2m_{\mathrm{e}}}\nu_{\mathrm{s}}^{(n)}\underline{\underline{M}}_z\underline{\underline{\partial}}\right]\underline{\chi}\vec{g}^{(0)} \equiv \underline{\underline{\Xi}}_q^{(2n+1)}\vec{g}^{(0)} \ .\end{aligned}$$

For our purpose, we only need the first 5 equations, since, as stated previously, in our regime of investigation we need to know only up to $\hat{g}^{(4)}$. Explicitly, these equations read

$$\underline{\underline{\partial}}\vec{j} + (\underline{\underline{\Pi}} - \underline{\underline{\Xi}}_0^{(0)})\vec{n} = (\underline{\underline{\Xi}}_q^{(0)} - \underline{\underline{\Pi}}_q^{(0)})\vec{n} \tag{C.12}$$

$$\underline{\underline{\partial}}\vec{S} + \underline{\underline{\Pi}}\vec{j} = \underline{\underline{\Xi}}_q^{(1)}\vec{n} - \underline{\underline{\Pi}}_q^{(1)}\vec{j} + \underline{\zeta}_1^{(1)}\vec{n} \tag{C.13}$$

$$\underline{\underline{\partial}}\vec{T} + \underline{\underline{\Pi}}\vec{S} - \underline{\underline{\Xi}}_0^{(2)}\vec{n} = \underline{\underline{\Xi}}_q^{(2)}\vec{n} - \underline{\underline{\Pi}}_q^{(2)}\vec{S} + \underline{\zeta}_1^{(2)}\vec{j} + \underline{\zeta}_2^{(2)}\vec{n} \tag{C.14}$$

$$\underline{\underline{\partial}}\vec{U} + \underline{\underline{\Pi}}\vec{T} = \underline{\underline{\Xi}}_q^{(3)}\vec{n} + \underline{\zeta}_1^{(3)}\vec{S} + O(q^3) \tag{C.15}$$

$$\underline{\underline{\Pi}}\vec{U} - \underline{\underline{\Xi}}_0^{(4)}\vec{n} = O(q)\ , \tag{C.16}$$

where we defined $\vec{n} = \vec{g}^{(0)}$, $\vec{j} = \vec{g}^{(1)}$, $\vec{S} = \vec{g}^{(2)}$, $\vec{T} = \vec{g}^{(3)}$ and $\vec{U} = \vec{g}^{(4)}$. Here, we already dropped terms that would only contribute to higher orders than q^2. Note that $\Gamma = \underline{\underline{\Pi}} - \underline{\underline{\Xi}}_0^{(0)}$.

Our aim is to obtain a differential equation of the form (2.76),

$$\left(\hat{\underline{\underline{\Gamma}}} - \underline{\underline{D}}\partial^2\right)\vec{n} = \underline{\underline{W}}(q)\vec{n}\ , \tag{C.17}$$

where

$$\underline{\underline{W}}(q) = \underline{\underline{Y}}_{q\partial}q\partial + \underline{\underline{Y}}_{\partial q}\partial q + \underline{\underline{Y}}_{\partial qq\partial}\partial q^2\partial + \underline{\underline{Y}}_{q\partial q\partial}q\partial q\partial + \underline{\underline{Y}}_{\partial q\partial q}\partial q\partial q. \tag{C.18}$$

To achieve this, we unite the set of equations (C.12)-(C.16) iteratively by eliminating every moment except $\vec{n}$. We do this order by order in q, ∂ and in the following, we give only terms that are relevant to our result. The zeroth order is simply $\vec{S}_0' = \underline{\underline{\Pi}}^{-1}\underline{\underline{\Xi}}_0^{(2)}\vec{n}$ and $\vec{U}_0 = \underline{\underline{\Pi}}^{-1}\underline{\underline{\Xi}}_0^{(4)}\vec{n}$ while the odd moments $\vec{j}, \vec{T}$ vanish as $q, \partial \to 0$. $\vec{S}_0$, when plugged into equation (C.13) will yield a term that resembles a diffusion term, but will not yet be of the desired form as given by (2.75). In order to transform the diffusion term into the form which permits convenient solution of the differential equation, we will multiply equation (C.17) to the left with $\underline{\underline{\Pi\mathcal{A}}}$ and then subtract it from the equation (C.14) which provides $\vec{S}$. We thus obtain a new $\vec{S}_0 = \left(\underline{\underline{\Pi}}^{-1}\underline{\underline{\Xi}}_0^{(2)} + \underline{\underline{\mathcal{A}\hat{\Gamma}}}\right)\vec{n}$ with the choice of $\underline{\underline{\mathcal{A}}}$ determined by the condition that $\vec{S}_0 \stackrel{!}{=} \underline{\underline{\Pi D}}\vec{n}$ which in turn translates into

$$\underline{\underline{\mathcal{A}}} = \left(\underline{\underline{\Pi D}} - \underline{\underline{\Pi}}^{-1}\underline{\underline{\Xi}}_0^{(2)}\right)\underline{\underline{\Gamma}}^{-1} \tag{C.19}$$

and, since $\underline{\underline{\Gamma}}$ is singular in longitudinal subspace as it possesses one vanishing eigenvalue, $\underline{\underline{\Gamma}}^{-1}$ has to be considered as the pseudo inverse.

In order to obtain the form reminiscent of the spin-charge diffusion equation (2.70), we rewrite equation (C.13)

$$\underline{\underline{\Pi}}\left(\vec{j} + \underline{\underline{D}}\partial\vec{n}\right) = \underline{\underline{\Pi D}}\partial\vec{n} - \underline{\underline{\partial}}\vec{S} + \underline{\underline{\Xi}}_q^{(1)}\vec{n} - \underline{\underline{\Pi}}_q^{(1)}\vec{j} + \underline{\zeta}_1^{(1)}\vec{n}\ , \tag{C.20}$$

where now the right-hand side of this equation is of order q, in particular the difference $\underline{\underline{\Pi D}}\ \vec{n} - \vec{S}$ no longer contributes to the zeroth order solution, as opposed to $\vec{S}$ itself.

Before proceeding with higher orders, we define for convenience

$$\begin{aligned}
\underline{\underline{\Pi}}_q^{(n)} &= \underline{\underline{\Pi}}_{qq}^{(n)} q^2 + \underline{\underline{\Pi}}_{\partial q}^{(n)} (\partial q - \partial q) \\
\underline{\zeta}_1^{(n)} &= \underline{\zeta}_{1,q}^{(n)} q + \underline{\zeta}_{1,\partial qq}^{(n)} (\partial q^2 - q^2 \partial) \\
\underline{\zeta}_2^{(n)} &= \underline{\zeta}_{2,qq}^{(n)} q^2 + \underline{\zeta}_{2,\partial q}^{(n)} (\partial q - \partial q) \\
\underline{\underline{\Xi}}_q^{(2n)} &= \underline{\underline{\Xi}}_{qq}^{(2n)} q^2 + \underline{\underline{\Xi}}_{\partial q}^{(2n)} \partial q + \underline{\underline{\Xi}}_{q\partial}^{(2n)} q\partial \\
\underline{\underline{\Xi}}_q^{(2n+1)} &= \underline{\underline{\Xi}}_q^{(2n+1)} q + \underline{\underline{\Xi}}_{\partial}^{(2n+1)} \partial \ ,
\end{aligned}$$

where we remind that ∂ acts on everything to its right so that $\underline{\underline{\Xi}}_q$ actually are differential operators.

The first order is given by ($\vec{j} = (\underline{\underline{\mathcal{J}}}_q q + \underline{\underline{\mathcal{J}}}_\partial \partial)\, \vec{n}$, etc.)

$$\begin{aligned}
\underline{\underline{\mathcal{J}}}_q &= -\underline{\underline{\Pi}}^{-1} \left(\underline{\underline{M}}_x \underline{\underline{\Pi}} \underline{\underline{D}} - \underline{\underline{\Xi}}_q^{(1)} - \underline{\zeta}_{1q}^{(1)} \right) \\
\underline{\underline{\mathcal{J}}}_\partial &= -\underline{\underline{D}} + \underline{\underline{\Pi}}^{-1} \underline{\underline{\Xi}}_\partial^{(1)} \\
\underline{\underline{\mathcal{T}}}_q &= -\underline{\underline{\Pi}}^{-1} \left(\underline{\underline{M}}_x \underline{\underline{\Pi}}^{-1} \underline{\underline{\Xi}}_0^{(4)} - \underline{\underline{\Xi}}_q^{(3)} - \underline{\zeta}_{1q}^{(3)} \underline{\underline{\Pi}} \underline{\underline{D}} \right) \\
\underline{\underline{\mathcal{T}}}_\partial &= -\underline{\underline{\Pi}}^{-1} \left(\underline{\underline{\Pi}}^{-1} \underline{\underline{\Xi}}_0^{(4)} - \underline{\underline{\Xi}}_\partial^{(3)} \right) \ ,
\end{aligned}$$

the second order terms are

$$\begin{aligned}
\underline{\underline{Y}}_{\partial q} &= \underline{\underline{\Pi}}^{-1} \underline{\underline{M}}_x \underline{\underline{\Pi}} \underline{\underline{D}} + \underline{\underline{\Xi}}_{\partial q}^{(0)} - \underline{\underline{\Pi}}_{\partial q}^{(0)} - \underline{\underline{\Pi}}^{-1} \left(\underline{\underline{\Xi}}_q^{(1)} + \underline{\zeta}_{1q}^{(1)} \right) \\
\underline{\underline{Y}}_{q\partial} &= \underline{\underline{M}}_x \underline{\underline{D}} + \underline{\underline{\Xi}}_{q\partial}^{(0)} + \underline{\underline{\Pi}}_{\partial q}^{(0)} - \underline{\underline{M}}_x \underline{\underline{\Pi}}^{-1} \underline{\underline{\Xi}}_\partial^{(1)} \\
\underline{\underline{\mathcal{S}}}_{\partial q} &= \underline{\underline{\Pi}}^{-1} \left(-\underline{\underline{\mathcal{T}}}_q - \underline{\underline{\Pi}}_{\partial q}^{(2)} \underline{\underline{\Pi}} \underline{\underline{D}} + \left(\underline{\underline{\Xi}}_{\partial q}^{(2)} + \underline{\zeta}_{2\partial q}^{(2)} \right) \right) - \underline{\underline{\mathcal{A}}} Y_{\partial q} \\
\underline{\underline{\mathcal{S}}}_{q\partial} &= \underline{\underline{\Pi}}^{-1} \left(-\underline{\underline{M}}_x \underline{\underline{\mathcal{T}}}_\partial + \underline{\underline{\Pi}}_{\partial q}^{(2)} \underline{\underline{\Pi}} \underline{\underline{D}} + \underline{\zeta}_{1q}^{(2)} \underline{\underline{\mathcal{J}}}_\partial + \left(\underline{\underline{\Xi}}_{q\partial}^{(2)} - \underline{\zeta}_{2\partial q}^{(2)} \right) \right) - \underline{\underline{\mathcal{A}}} Y_{q\partial}
\end{aligned}$$

and finally, the 3 remaining coefficients in equation (C.18),

$$\begin{aligned}
\underline{\underline{Y}}_{\partial qq\partial} &= \underline{\underline{\Pi}}^{-1} \left(\underline{\underline{M}}_x \underline{\underline{\mathcal{S}}}_{q\partial} + \underline{\underline{\Pi}}_{qq}^{(1)} \underline{\underline{\mathcal{J}}}_\partial + \underline{\zeta}_{1\partial qq}^{(1)} \right) \\
\underline{\underline{Y}}_{q\partial q\partial} &= \underline{\underline{M}}_x \underline{\underline{\Pi}}^{-1} \left(\underline{\underline{\mathcal{S}}}_{q\partial} + \underline{\underline{\Pi}}_{\partial q}^{(1)} \underline{\underline{\mathcal{J}}}_\partial \right) \\
\underline{\underline{Y}}_{\partial q\partial q} &= \underline{\underline{\Pi}}^{-1} \left(\underline{\underline{M}}_x \underline{\underline{\mathcal{S}}}_{\partial q} - \underline{\underline{\Pi}}_{\partial q}^{(1)} \underline{\underline{\mathcal{J}}}_q \right) \ .
\end{aligned}$$

To solve equation (C.17), we use the method elaborated upon previously in section 2.3.4, so that by use of equations (2.93) and (2.97) we end up with

$$\delta\rho_{\mathrm{DW}} = \left[\frac{K}{\lambda} \left[2(\underline{\underline{Y}}_{\partial q})_{\mathrm{lt}} \underline{\underline{\mathcal{F}}} (\underline{\underline{Y}}_{q\partial})_{\mathrm{tl}} + (\underline{\underline{Y}}_{\partial q})_{\mathrm{lt}} \underline{\underline{\mathcal{F}}} (\underline{\underline{Y}}_{\partial q})_{\mathrm{tl}} + (2\underline{\underline{Y}}_{\partial qq\partial} + \underline{\underline{Y}}_{q\partial q\partial} + \underline{\underline{Y}}_{\partial q\partial q})_{\mathrm{ll}} \right] \vec{n}_0 \right]_{\mathrm{c}} \quad \text{(C.21)}$$

where the outer bracket denotes that we take the charge component.

D. Details on solving the kinetic equation in the general time-dependent case

In this appendix, we describe the hierarchy of equations obtained from Eqns. (2.44), (2.45) and which are utilized to obtain all the results discussed in section 2.4 and 2.5.

To begin with, let us define the moments of the Greens function $\hat{g}$,

$$\begin{aligned}
\hat{n}(\boldsymbol{r},t) &= \int \frac{\mathrm{d}^3k}{(2\pi)^3}\hat{g}(\boldsymbol{k},\boldsymbol{r},t) \equiv \langle \hat{g} \rangle \\
\hat{\boldsymbol{j}}(\boldsymbol{r},t) &= \langle \boldsymbol{v}_{\boldsymbol{k}}\hat{g} \rangle \\
\hat{\underline{\underline{T}}}(\boldsymbol{r},t) &= \left\langle \left(\boldsymbol{v}_{\boldsymbol{k}} \circ \boldsymbol{v}_{\boldsymbol{k}} - \underline{\underline{1}}\frac{1}{3}v_{\boldsymbol{k}}^2 \right)\hat{g} \right\rangle \ ,
\end{aligned} \tag{D.1}$$

where the second moment $\hat{\underline{\underline{T}}}$ is defined such that the isotropic part is projected out. Note that the definitions represent quasi-particle densities, so in order to obtain the respective charge-densities we simply have to multiply with the factor $(-e)$. We do not need more than the first three moments for the present study up to second order spatial magnetization gradients.

We also need the respective moments of the spectral density which read

$$\begin{aligned}
\hat{a}^{(0)}(\boldsymbol{r},t) &= \left\langle \hat{A} \right\rangle \\
\hat{\boldsymbol{a}}^{(1)}(\boldsymbol{r},t) &= \left\langle \boldsymbol{v}_{\boldsymbol{k}}\hat{A} \right\rangle = O(\boldsymbol{\partial}_r\vec{m}) \\
\hat{\underline{\underline{a}}}^{(2)}(\boldsymbol{r},t) &= \left\langle \left(\boldsymbol{v}_{\boldsymbol{k}} \circ \boldsymbol{v}_{\boldsymbol{k}} - \underline{\underline{1}}\frac{1}{3}v_{\boldsymbol{k}}^2 \right)\hat{A} \right\rangle = \left\langle \boldsymbol{v}_{\boldsymbol{k}} \circ \boldsymbol{v}_{\boldsymbol{k}}\hat{A} \right\rangle - \underline{\underline{1}}\frac{2}{dm_{\mathrm{e}}}\frac{1}{2}\{\hat{E}_{\mathrm{F}},\hat{a}^{(0)}\} = O(\boldsymbol{\partial}_r\vec{m})^2 \ ,
\end{aligned} \tag{D.2}$$

where we can see that the definition of the moments is such that the n-th moment is of the order $O(\boldsymbol{\partial}_r\vec{m})^n$, a condition we can use to also define higher order moments. For example, the fourth moment $b^{(3)}$ would have $\boldsymbol{\partial}_r^3$ terms but no $\boldsymbol{\partial}_r$ terms.

The moments $\hat{a}^{(0)}$, $\hat{\boldsymbol{a}}^{(1)}$, $\hat{\underline{\underline{a}}}^{(2)}$ can be obtained by $\boldsymbol{k}$-integrating the spectral density $\hat{A} = \hat{A}_0 + \hat{A}_1 + \ldots$, which has for example the first order correction

$$\hat{A}_1 = \ -\frac{\pi}{2}\hat{\vec{\sigma}}\left(\vec{m}\times(\partial_t + \boldsymbol{v}_k\boldsymbol{\partial}_r)\vec{m}\right)\left[\partial_\epsilon\left[\delta(\epsilon-\epsilon_{\boldsymbol{k}}^{\uparrow}) + \delta(\epsilon-\epsilon_{\boldsymbol{k}}^{\downarrow})\right] - \frac{2}{\Delta}\left[\delta(\epsilon-\epsilon_{\boldsymbol{k}}^{\uparrow}) - \delta(\epsilon-\epsilon_{\boldsymbol{k}}^{\downarrow})\right]\right] \ . \tag{D.3}$$

The explicit expression for $\hat{a}^{(0)}$ can be found in (2.128).

After a longer derivation, we come up with the following set of equations we can employ to obtain our results in the regime of interest, i.e. $\tau\Delta \gg 1$ and gradients up to order $(\boldsymbol{\partial}_r\vec{m})^2$. In

particular, we want corrections to the spin-charge current which are up to $\partial_t \boldsymbol{\partial}_r$ and $E(\boldsymbol{\partial}_r \vec{m})^2$, so that we only need the first three equations in the hierarchy,

$$\underline{\underline{\hat{\Gamma}}}\hat{n} + \boldsymbol{\partial}_r \hat{\boldsymbol{j}} = \hat{\mathcal{J}}^{(0)} \tag{D.4}$$

$$\underline{\underline{\hat{\Pi}}}\hat{\boldsymbol{j}} + \boldsymbol{\partial}_r \underline{\underline{\hat{T}}} + \hat{\boldsymbol{\mathcal{T}}}^{(1)}_{\hat{n}} = \frac{1}{2}\left\{\hat{\boldsymbol{a}}^{(1)}, \underline{\hat{\chi}}\hat{n}\right\} + \hat{\boldsymbol{\mathcal{C}}}^{(1)}_{\hat{n}} + \hat{\boldsymbol{\mathcal{J}}}^{(1)} \tag{D.5}$$

$$\underline{\underline{\hat{\Pi}}}\,\underline{\underline{\hat{T}}} + \underline{\underline{\hat{\mathcal{T}}}}^{(2)}_{\hat{j}} - \underline{\underline{1}}\frac{1}{d}\mathrm{Tr}\underline{\underline{\hat{\mathcal{T}}}}^{(2)}_{\hat{j}} + \underline{\underline{\hat{\mathcal{T}}}}'^{(2)}_{\hat{n}} = \underline{\underline{\hat{\mathcal{C}}}}^{(2)}_{\hat{j}} - \underline{\underline{1}}\frac{1}{d}\mathrm{Tr}\underline{\underline{\hat{\mathcal{C}}}}^{(2)}_{\hat{j}} + \underline{\underline{\hat{\mathcal{C}}}}'^{(2)}_{\hat{n}} + \underline{\underline{\hat{\mathcal{J}}}}^{(2)} \ , \tag{D.6}$$

where

$$\hat{\boldsymbol{\mathcal{T}}}^{(1)}_{\hat{n}} = \frac{1}{2m_{\mathrm{e}}}\left(\frac{2}{d}\boldsymbol{\partial}_r\{\hat{E}_{\mathrm{F}}, \hat{n}\} - \{\boldsymbol{\partial}_r \hat{E}_{\mathrm{F}}, \hat{n}\}\right) \tag{D.7}$$

$$\hat{\boldsymbol{\mathcal{C}}}^{(1)}_{\hat{n}} = \frac{1}{4im_{\mathrm{e}}}\left(\frac{2}{d}\boldsymbol{\partial}_r\left([\underline{\hat{\chi}}\hat{a}^{(0)}, \hat{n}] - [\underline{\hat{\chi}}\hat{n}, \hat{a}^{(0)}]\right) - \left([\boldsymbol{\partial}_r\underline{\hat{\chi}}\hat{a}^{(0)}, \hat{n}] - [\boldsymbol{\partial}_r\underline{\hat{\chi}}\hat{n}, \hat{a}^{(0)}]\right)\right) \ , \tag{D.8}$$

and the spin-resolved Fermi-energy is defined as $\hat{E_{\mathrm{F}}} \equiv E_{\mathrm{F}}\hat{1} + \frac{\Delta}{2}\vec{m}\hat{\vec{\sigma}}$. $d = 3$ is the dimensionality and the two tensors $\underline{\underline{\hat{\mathcal{T}}}}^{(2)}_{\hat{j}}$ arising from the commutator on the left-hand side of the kinetic equation (2.44) and $\underline{\underline{\hat{\mathcal{C}}}}^{(2)}_{\hat{j}}$ originating from the collision integral (2.45) are defined as

$$\begin{aligned}
\underline{\underline{\hat{\mathcal{T}}}}^{(2)}_{\hat{j}} &= \frac{1}{2m_{\mathrm{e}}}\left(\frac{2}{d+2}\boldsymbol{\partial}_r^\dagger\{\hat{E}_{\mathrm{F}}, {}^\dagger\hat{\boldsymbol{j}}\} - \{\boldsymbol{\partial}_r^\dagger \hat{E}_{\mathrm{F}}, {}^\dagger\hat{\boldsymbol{j}}\}\right) \ , \\
\underline{\underline{\hat{\mathcal{C}}}}^{(2)}_{\hat{j}} &= \frac{1}{4im_{\mathrm{e}}}\left(\frac{2}{d+2}\boldsymbol{\partial}_r^\dagger[\underline{\hat{\chi}}\hat{a}^{(0)}, {}^\dagger\hat{\boldsymbol{j}}] - [\boldsymbol{\partial}_r^\dagger\underline{\hat{\chi}}\hat{a}^{(0)}, {}^\dagger\hat{\boldsymbol{j}}]\right) \ .
\end{aligned} \tag{D.9}$$

In these expressions, the tensorial structure is due to the special symmetrizing contraction denoted by † and is defined by $\boldsymbol{a}(\boldsymbol{\partial}_r^\dagger \ldots {}^\dagger\hat{\boldsymbol{j}})\boldsymbol{b} \equiv (\boldsymbol{a}\boldsymbol{\partial}_r)\ldots(\hat{\boldsymbol{j}}\boldsymbol{b}) + (\boldsymbol{b}\boldsymbol{\partial}_r)\ldots(\hat{\boldsymbol{j}}\boldsymbol{a})$. Note that we have defined spin-relaxation $\underline{\underline{\hat{\Gamma}}}$ and momentum relaxation $\underline{\underline{\hat{\Pi}}}$

$$\begin{aligned}
\underline{\underline{\hat{\Gamma}}}\hat{\mathcal{X}} &\equiv \frac{\Delta - \delta\Delta}{2i}\left[\vec{m}\hat{\vec{\sigma}}, \hat{\mathcal{X}}\right] + \frac{1}{2}\left\{\underline{\hat{\chi}}\hat{a}^{(0)}, \hat{\mathcal{X}}\right\} - \frac{1}{2}\left\{\underline{\hat{\chi}}\hat{\mathcal{X}}, \hat{a}^{(0)}\right\} \\
\underline{\underline{\hat{\Pi}}}\hat{\mathcal{X}} &\equiv \frac{\Delta - \delta\Delta}{2i}\left[\vec{m}\hat{\vec{\sigma}}, \hat{\mathcal{X}}\right] + \frac{1}{2}\left\{\underline{\hat{\chi}}\hat{a}^{(0)}, \hat{\mathcal{X}}\right\} \ ,
\end{aligned} \tag{D.10}$$

where both incorporate also precession and gradient corrections to the scattering rates enter through $\hat{a}^{(0)}$ and $\delta\Delta$.

We can drop the contributions $\underline{\underline{\hat{\mathcal{T}}}}'^{(2)}_{\hat{n}}$ and $\underline{\underline{\hat{\mathcal{C}}}}'^{(2)}_{\hat{n}}$ in the third equation and which is used to obtain the second moment of our distribution, $\underline{\underline{\hat{T}}}$. Since it only contain terms like $\boldsymbol{\partial}_r[\boldsymbol{\partial}_r\vec{m}\hat{\vec{\sigma}}, \hat{n}]$ and because $\hat{n} = O(E\boldsymbol{\partial}_r) + O(\partial_t)$, these terms would go beyond our regime. Let us specify these terms nevertheless in order to obtain a closed set of three equations valid under the assumption that only the first three moments of the Greens functions, $\hat{n}$, $\hat{\boldsymbol{j}}$ and $\underline{\underline{\hat{T}}}$ are relevant.

$$\begin{aligned}
\underline{\underline{\hat{\mathcal{T}}}}'^{(2)}_{\hat{n}} &= \frac{\Delta}{8im_{\mathrm{e}}^2}\left\{\frac{2}{d+2}\left(\underline{\underline{1}}\boldsymbol{\partial}_r[\boldsymbol{\partial}_r\vec{m}\hat{\vec{\sigma}}, \hat{n}] + \boldsymbol{\partial}_r^\dagger[{}^\dagger\boldsymbol{\partial}_r\vec{m}\hat{\vec{\sigma}}, \hat{n}]\right) - \frac{1}{2}[\boldsymbol{\partial}_r^\dagger\,{}^\dagger\boldsymbol{\partial}_r\vec{m}\hat{\vec{\sigma}}, \hat{n}]\right\} \\
\underline{\underline{\hat{\mathcal{C}}}}'^{(2)}_{\hat{n}} &= \frac{1}{8m_{\mathrm{e}}^2}\Bigg\{\frac{2}{d+2}\Big[\underline{\underline{1}}\boldsymbol{\partial}_r\left(\{\hat{a}^{(0)}, \boldsymbol{\partial}_r\underline{\hat{\chi}}\hat{n}\} - \{\boldsymbol{\partial}_r\underline{\hat{\chi}}\hat{a}^{(0)}, \hat{n}\}\right) \\
&\qquad + \boldsymbol{\partial}_r^\dagger\left(\{\hat{a}^{(0)}, {}^\dagger\boldsymbol{\partial}_r\underline{\hat{\chi}}\hat{n}\} - \{{}^\dagger\boldsymbol{\partial}_r\underline{\hat{\chi}}\hat{a}^{(0)}, \hat{n}\}\right)\Big] \\
&\qquad - \frac{1}{2}\{\hat{a}^{(0)}, \boldsymbol{\partial}_r^\dagger\,{}^\dagger\boldsymbol{\partial}_r\underline{\hat{\chi}}\hat{n}\} + \frac{1}{2}\{\boldsymbol{\partial}_r^\dagger\,{}^\dagger\boldsymbol{\partial}_r\underline{\hat{\chi}}\hat{a}^{(0)}, \hat{n}\}\Bigg\} \ .
\end{aligned} \tag{D.11}$$

The source terms that appear in these equations can be summarized as follows,

$$
\begin{aligned}
\hat{\mathcal{J}}_t^{(0)} &= -\frac{1}{2\pi} e\boldsymbol{E}\hat{\boldsymbol{a}}^{(1)} + \frac{1}{2\pi}\frac{1}{2}\{\partial_t \hat{H}, \hat{a}^{(0)}\} \\
\hat{\mathcal{J}}_c^{(0)} &= \frac{1}{4\pi}\partial_t \frac{1}{2i}[\hat{\underline{\underline{\chi}}}\hat{a}^{(0)}, \hat{a}^{(0)}] \\
\hat{\boldsymbol{\mathcal{J}}}_t^{(1)} &= -\frac{1}{2\pi} e\boldsymbol{E}\hat{\underline{\underline{a}}}^{(2)} + \frac{1}{2\pi}\frac{1}{2}\{\partial_t \hat{H}, \hat{\boldsymbol{a}}^{(1)}\} - \frac{1}{2\pi}\frac{1}{4im_{\mathrm{e}}}\left(\frac{2}{d}\boldsymbol{\partial}_r[\partial_t \hat{H}, \hat{a}^{(0)}] - [\boldsymbol{\partial}_r \partial_t \hat{H}, \hat{a}^{(0)}]\right) \\
\hat{\boldsymbol{\mathcal{J}}}_c^{(1)} &= \frac{e\boldsymbol{E}}{4\pi m_{\mathrm{e}}}\frac{1}{2i}[\hat{\underline{\underline{\chi}}}\hat{a}^{(0)}, \hat{a}^{(0)}] \\
&\qquad + \frac{1}{4\pi}\partial_t\left(\frac{1}{2i}[\hat{\underline{\underline{\chi}}}\hat{a}^{(0)}, \hat{\boldsymbol{a}}^{(1)}] + \frac{1}{4m_{\mathrm{e}}}\left(\frac{2}{d}\boldsymbol{\partial}_r\{\hat{\underline{\underline{\chi}}}\hat{a}^{(0)}, \hat{a}^{(0)}\} - \{\boldsymbol{\partial}_r \hat{\underline{\underline{\chi}}}\hat{a}^{(0)}, \hat{a}^{(0)}\}\right)\right) \\
\hat{\underline{\underline{\mathcal{J}}}}_t^{(2)} &= \frac{e}{4\pi m_{\mathrm{e}}}\frac{2}{d+2}\left(-\boldsymbol{E}^{\dagger}\{\hat{E_{\mathrm{F}}}^{\dagger}\hat{\boldsymbol{a}}^{(1)}\} + \underline{\underline{1}}\frac{2}{d}\{\hat{E_{\mathrm{F}}}, \boldsymbol{E}\hat{\boldsymbol{a}}^{(1)}\}\right. \\
&\qquad \left. + \frac{\Delta}{4im_{\mathrm{e}}}\left(\underline{\underline{1}}[\boldsymbol{E}\boldsymbol{\partial}_r \vec{m}\hat{\vec{\sigma}}, \hat{a}^{(0)}] + \boldsymbol{E}^{\dagger}[^{\dagger}\boldsymbol{\partial}_r \vec{m}\hat{\vec{\sigma}}, \hat{a}^{(0)}]\right)\right) + O(\partial_t \boldsymbol{\partial}_r^2) \\
\hat{\underline{\underline{\mathcal{J}}}}_c^{(2)} &= \frac{e}{8\pi m_{\mathrm{e}}}\frac{2}{d+2}\left(-i\boldsymbol{E}^{\dagger}[\hat{\underline{\underline{\chi}}}\hat{a}^{(0)}, ^{\dagger}\,\hat{\boldsymbol{a}}^{(1)}] + i\underline{\underline{1}}\frac{2}{d}[\hat{\underline{\underline{\chi}}}\hat{a}^{(0)}, \boldsymbol{E}\hat{\boldsymbol{a}}^{(1)}]\right. \\
&\qquad + \frac{1}{2m_{\mathrm{e}}}\left(\underline{\underline{1}}\boldsymbol{E}\{\boldsymbol{\partial}_r \hat{a}^{(0)}, \hat{\underline{\underline{\chi}}}\hat{a}^{(0)}\} + \boldsymbol{E}^{\dagger}\{^{\dagger}\boldsymbol{\partial}_r \hat{a}^{(0)}, \hat{\underline{\underline{\chi}}}\hat{a}^{(0)}\}\right)\Big) \\
&\qquad - \frac{2e}{32\pi m_{\mathrm{e}}^2}\boldsymbol{E}^{\dagger}\ \{\hat{a}^{(0)}, ^{\dagger}\,\boldsymbol{\partial}_r \hat{\underline{\underline{\chi}}}\hat{a}^{(0)}\} + O(\partial_t \boldsymbol{\partial}_r^2)\ . \qquad \text{(D.12)}
\end{aligned}
$$

$\delta\mu$ enters the above set of equations only through $\hat{H}$ in $\hat{\mathcal{J}}_{\mathrm{t}}$ and indirectly through the density of states $\hat{a}$.

E. The Hypergeometric function ${}_2F_1$ and the Gamma function Γ

The hypergeometric function ${}_2F_1(a,b;c;z)$ is defined as [177]

$$ {}_2F_1(a,b;c;z) = \sum_{n=0}^{\infty} \frac{(a)_n (b)_n}{(c)_n} \frac{z^n}{n!} \ , \tag{E.1} $$

and satisfies the differential equation

$$ \left\{ z(1-z)\partial_z^2 + [c-(a+b+1)z]\,\partial_z - ab \right\} \ {}_2F_1(a,b;c;z) = 0 \ . \tag{E.2} $$

$(a)_n$ is the Pochhammer symbol and defined as

$$ (a)_n = \frac{\Gamma(a+n)}{\Gamma(a)} \ . \tag{E.3} $$

The Hypergeometric function has a branch cut on the real axis for $\mathrm{Re}\, z >= 1$, and the series expansion for $z \to 1$ and $c-a-b \notin Z$, $\mathrm{Re}\,(c-a-b) \geq 0$ reads ($\xi > 0$)

$$ {}_2F_1(a,b;c;1-\xi) = \frac{\Gamma(c)\Gamma(c-a-b)}{\Gamma(c-a)\Gamma(c-b)} \left(1+O(\xi)\right) + \frac{\Gamma(c)\Gamma(a+b-c)}{\Gamma(a)\Gamma(b)} \xi^{c-a-b} \left(1+O(\xi)\right) \ , \tag{E.4} $$

which can be found using Kummer's solution

$$ \begin{aligned} {}_2F_1(a,b;c;z) = {} & \frac{\Gamma(c-a-b)\Gamma(c)}{\Gamma(c-a)\Gamma(c-b)} \, {}_2F_1(a,b;1+a+b-c;1-z) \\ & + \frac{\Gamma(a+b-c)\Gamma(c)}{\Gamma(a)\Gamma(b)} (1-z)^{c-a-b} \, {}_2F_1(c-a,c-b;1+c-a-b;1-z) \ , \end{aligned} \tag{E.5} $$

together with the series representation used to define the hypergeometric function. For $z=1$, ${}_2F_1(a,b;c;z)$ has the following explicit values

$$ {}_2F_1(a,b;c;1) = \frac{\Gamma(c)\Gamma(c-a-b)}{\Gamma(c-a)\Gamma(c-b)} \qquad \text{if } \mathrm{Re}\,(c-a-b) > 0 \tag{E.6} $$

$$ {}_2F_1(-n,b;c;1) = \frac{(c-b)_n}{(c)_n} \qquad \text{if } n \in \mathbb{N}_0 \ . \tag{E.7} $$

Finally, we summarize some interesting relations between Gamma functions,

$$\Gamma(z+1) = z\Gamma(z) \tag{E.8}$$

$$\Gamma(z)\Gamma(-z) = -\frac{\pi}{z\sin(\pi z)} \tag{E.9}$$

$$\Gamma(1+z)\Gamma(1-z) = \frac{\pi z}{\sin(\pi z)} \tag{E.10}$$

$$\Gamma(\frac{1}{2}+z)\Gamma(\frac{1}{2}-z) = \frac{\pi}{\cos(\pi z)} \tag{E.11}$$

$$\Gamma(2z) = \frac{2^{2z-1}}{\sqrt{\pi}}\Gamma(z)\Gamma(z+\frac{1}{2}) \tag{E.12}$$

Bibliography

[1] S. S. P. Parkin, M. Hayashi & L. Thomas, Science **320**, 190 (2008).

[2] Y. Zhang, Y.-W. Tan, H. L. Stormer & P. Kim, Nature **438**, 201 (2005).

[3] S. Datta & B. Das, Applied Physics Letters **56**, 665 (1990).

[4] E. B. Myers, D. C. Ralph, J. A. Katine, R. N. Louie & R. A. Buhrman, Science **285**, 867 (1999).

[5] S. Urazhdin, N. O. Birge, W. P. Pratt & J. Bass, Phys. Rev. Lett. **91**, 146803 (2003).

[6] B. Özyilmaz, A. D. Kent, D. Monsma, J. Z. Sun, M. J. Rooks & R. H. Koch, Phys. Rev. Lett. **91**, 067203 (2003).

[7] J. Grollier, V. Cros, A. Hamzic, J. M. George, H. Jaffrès, A. Fert, G. Faini, J. B. Youssef & H. Legall, Appl. Phys. Lett. **78**, 3663 (2001).

[8] J. A. Katine, F. J. Albert, R. A. Buhrman, E. B. Myers & D. C. Ralph, Phys. Rev. Lett. **84**, 3149 (2000).

[9] T. Ono, H. Miyajima, K. Shigeto, K. Mibu, N. Hosoito & T. Shinjo, Science **284**, 468 (1999), http://www.sciencemag.org/content/284/5413/468.full.pdf.

[10] L. Thomas, M. Hayashi, X. Jiang, R. Moriya, C. Rettner & S. S. P. Parkin, Nature **443**, 197 (2006).

[11] M. Hayashi, L. Thomas, Y. Bazaliy, C. Rettner, R. Moriya, X. Jiang & S. Parkin, Phys. Rev. Lett. **96**, 197207 (2006).

[12] M. Hayashi, L. Thomas, C. Rettner, R. Moriya, Y. B. Bazaliy & S. S. P. Parkin, Phys. Rev. Lett. **98**, 037204 (2007).

[13] L. Thomas, R. Moriya, C. Rettner & S. S. Parkin, Science **330**, 1810 (2010), http://www.sciencemag.org/content/330/6012/1810.full.pdf.

[14] M. Hayashi, L. Thomas, R. Moriya, C. Rettner & S. S. P. Parkin, Science **320**, 209 (2008), http://www.sciencemag.org/content/320/5873/209.full.pdf.

[15] J. C. Slonczewski, Journal of Magnetism and Magnetic Materials **159**, L1 (1996).

[16] L. Berger, Phys. Rev. B **54**, 9353 (1996).

[17] M. Tsoi, A. G. M. Jansen, J. Bass, W.-C. Chiang, M. Seck, V. Tsoi & P. Wyder, Phys. Rev. Lett. **80**, 4281 (1998).

[18] Y. Tserkovnyak, A. Brataas, G. E. W. Bauer & B. I. Halperin, Rev. Mod. Phys. **77**, 1375 (2005).

[19] S. Zhang & Z. Li, Phys. Rev. Lett. **93**, 127204 (2004).

[20] G. Tatara & H. Kohno, Phys. Rev. Lett. **92**, 086601 (2004).

[21] J. Xiao, A. Zangwill & M. D. Stiles, Phys. Rev. B **73**, 054428 (2006).

[22] H. Kohno, G. Tatara & J. Shibata, J. Phy. Soc. Jap **75**, 113706 (2006).

[23] Y. Tserkovnyak, H. J. Skadsem, A. Brataas & G. E. W. Bauer, Phys. Rev. B **74**, 144405 (2006).

[24] R. A. Duine, A. S. N. nez, J. Sinova & A. H. MacDonald, Phys. Rev. B **75**, 214420 (2007).

[25] H. Kohno & J. Shibata, J. Phy. Soc. Jap **76**, 063710 (2007).

[26] G. Tatara, H. Kohno, J. Shibata, Y. Lemaho & K.-J. Lee, Journal of the Physical Society of Japan **76**, 054707 (2007).

[27] G. Tatara & P. Entel, Phys. Rev. B **78**, 064429 (2008).

[28] F. Piéchon & A. Thiaville, Phys. Rev. B **75**, 174414 (2007).

[29] G. Tatara, H. Kohno & J. Shibata, Journal of the Physical Society of Japan **77**, 031003 (2008).

[30] S. A. Yang, G. S. D. Beach, C. Knutson, D. Xiao, Q. Niu, M. Tsoi & J. L. Erskine, Phys. Rev. Let. **102**, 067201 (2009).

[31] S. E. Barnes, J. Ieda & S. Maekawa, Appl. Phys. Lett. **89**, 122507 (2006).

[32] P. Levy & S. Zhang, Phys. Rev. Lett. **79**, 5110 (1997).

[33] G. Tatara & H. Fukuyama, Phys. Rev. Lett. **78**, 3773 (1997).

[34] A. Brataas, G. Tatara & G. Bauer, Phys. Rev. B **60**, 3406 (1999).

[35] R. P. van Gorkom, A. Brataas & G. E. W. Bauer, Phys. Rev. Lett. **83**, 4401 (1999).

[36] G. Tatara, Int. J. of Mod. Phys. B **15**, 321 (2001).

[37] V. Dugaev, J. Barnas, A. Lusakowski & L. Turski, Phys. Rev. B **65**, 224419 (2002).

[38] F. Bergeret, A. Volkov & K. Efetov, Phys. Rev. B **66**, 184403 (2002).

[39] E. Simanek, Phys. Rev. B **63**, 224412 (2001).

[40] E. Simanek & A. Rebei, Phys. Rev. B **71**, 172405 (2005).

[41] U. Ruediger, J. Yu, S. Zhang, A. Kent & S. Parkin, Phys. Rev. Lett. **80**, 5639 (1998).

[42] U. Ebels, A. Radulescu, Y. Henry, L. Piraux & K. Ounadjela, Phys. Rev. Lett. **84**, 983 (2000).

[43] A. Aziz, S. J. Bending, H. G. Roberts, S. Crampin, P. J. Heard & C. H. Marrows, Phys. Rev. Lett. **97**, 206602 (2006).

[44] C. Hassel, M. Brands, F. Y. Lo, A. D. Wieck & G. Dumpich, Phys. Rev. Lett. **97**, 226805 (2006).

[45] C. Marrows, Adv. in Phys. **54**, 585 (2005).

[46] A. Kent, J. Yu, U. Rudiger & S. Parkin, J Phys.-Cond. Mat **13**, R461 (2001).

[47] J. D. Burton, R. F. Sabirianov, S. S. Jaswal, E. Y. Tsymbal & O. N. Mryasov, Phys. Rev. Lett. **97**, 077204 (2006).

[48] A. A. Kovalev, K. Výborný & J. Sinova, Phys. Rev. B **78**, 041305 (2008).

[49] A. A. Kovalev, Y. Tserkovnyak, K. Výborný & J. Sinova, Phys. Rev. B **79**, 195129 (2009).

[50] J. Rammer & H. Smith, Rev. Mod. Phys. **58**, 323 (1986).

[51] G. Mahan, *Many-Particle Physics* (Plenum New York, 2000).

[52] M. H. Levitt, *Spin Dynamics: Basics of Nuclear Magnetic Resonance, 2nd edition* (John Wiley & Sons, New York, 2008).

[53] K. Capelle, G. Vignale & B. Gyorffy, Phys. Rev. Lett. **8720**, 206403 (2001).

[54] J. Kudrnovský, V. Drchal, C. Blaas, P. Weinberger, I. Turek & P. Bruno, Phys. Rev. B **62**, 15084 (2000).

[55] V. Drchal, J. Kudrnovský, P. Bruno, P. H. Dederichs, I. Turek & P. Weinberger, Phys. Rev. B **65**, 214414 (2002).

[56] J. van Hoof, K. Schep, P. Kelly & G. Bauer, Journal of Magnetism and Magnetic Materials **177**, 188 (1998), International Conference on Magnetism.

[57] J. Velev & W. H. Butler, Phys. Rev. B **69**, 094425 (2004).

[58] J. Kudrnovsky, V. Drchal, I. Turek, P. Streda & P. Bruno, Surface Science **482**, 1107 (2001).

[59] S. V. Faleev, F. Léonard, D. A. Stewart & M. van Schilfgaarde, Phys. Rev. B **71**, 195422 (2005).

[60] M. A. M. Gijs & G. E. W. Bauer, Adv. Phys. **46**, 285 (1997).

[61] D. Huertas-Hernando, Y. V. Nazarov & W. Belzig, Phys. Rev. Lett. **88**, 047003 (2002).

[62] A. Cottet & W. Belzig, Phys. Rev. B **72**, 180503 (2005).

[63] D. Huertas Hernando, Y. V. Nazarov, A. Brataas & G. E. W. Bauer, Phys. Rev. B **62**, 5700 (2000).

[64] T. Valet & A. Fert, Phys. Rev. B **48**, 7099 (1993).

[65] G. Tatara & H. Kohno, Phys. Rev. B **67**, 113316 (2003).

[66] G. Tatara, H. Kohno & J. Shibata, Physics Reports **468**, 213 (2008).

[67] D. Loss, P. Goldbart & A. V. Balatsky, Phys. Rev. Lett. **65**, 1655 (1990).

[68] A. Takeuchi & G. Tatara, Journal of the Physical Society of Japan **77**, 074701 (2008).

[69] S. Zhang, P. M. Levy & A. Fert, Phys. Rev. Lett. **88**, 236601 (2002).

[70] S. E. Barnes & S. Maekawa, Phys. Rev. Lett. **98**, 246601 (2007).

[71] R. A. Duine, Phys. Rev. B **77**, 014409 (2008).

[72] R. A. Duine, Phys. Rev. B **79**, 014407 (2009).

[73] Y. Tserkovnyak & C. H. Wong, Phys. Rev. B **79**, 014402 (2009).

[74] C. H. Wong & Y. Tserkovnyak, Phys. Rev. B **80**, 184411 (2009).

[75] Y. Taguchi, Y. Oohara, H. Yoshizawa, N. Nagaosa & Y. Tokura, Science **291**, 2573 (2001).

[76] P. Bruno, V. K. Dugaev & M. Taillefumier, Phys. Rev. Lett. **93**, 096806 (2004).

[77] A. Neubauer, C. Pfleiderer, B. Binz, A. Rosch, R. Ritz, P. G. Niklowitz & P. Böni, Phys. Rev. Lett. **102**, 186602 (2009).

[78] M. Onoda, G. Tatara & N. Nagaosa, Journal of the Physical Society of Japan **73**, 2624 (2004).

[79] A. Takeuchi, K. Hosono & G. Tatara, Phys. Rev. B **81**, 144405 (2010).

[80] Y. Tserkovnyak, E. M. Hankiewicz & G. Vignale, Phys. Rev. B **79**, 094415 (2009).

[81] Y. L. Maho, J.-V. Kim & G. Tatara, Phys. Rev. B **79**, 174404 (2009).

[82] H. J. Skadsem, Y. Tserkovnyak, A. Brataas & G. E. W. Bauer, Phys. Rev. B **75**, 094416 (2007).

[83] E. M. Hankiewicz, G. Vignale & Y. Tserkovnyak, Phys. Rev. B **78**, 020404 (2008).

[84] I. Garate & A. MacDonald, Phys. Rev. B **79**, 064403 (2009).

[85] I. Garate & A. MacDonald, Phys. Rev. B **79**, 064404 (2009).

[86] Z. Li & S. Zhang, Phys. Rev. Lett. **92**, 207203 (2004).

[87] Z. Li & S. Zhang, Phys. Rev. B **70**, 024417 (2004).

[88] A. Thiaville, Y. Nakatani, J. Miltat & Y. Suzuki, Europhys. Lett. **69**, 990 (2005).

[89] V. K. Dugaev, V. R. Vieira, P. D. Sacramento, J. Barnaś, M. A. N. Araújo & J. Berakdar, Phys. Rev. B **74**, 054403 (2006).

[90] M. D. Stiles, W. M. Saslow, M. J. Donahue & A. Zangwill, Phys. Rev. B **75**, 214423 (2007).

[91] M. Thorwart & R. Egger, Phys. Rev. B **76**, 214418 (2007).

[92] S. E. Barnes & S. Maekawa, Phys. Rev. Lett. **95**, 107204 (2005).

[93] G. Tatara, T. Takayama, H. Kohno, J. Shibata, Y. Nakatani & H. Fukuyama, Journal of the Physical Society of Japan **75**, 064708 (2006).

[94] J. Shibata, Y. Nakatani, G. Tatara, H. Kohno & Y. Otani, Phys. Rev. B **73**, 020403 (2006).

[95] F. Colaiori, G. Durin & S. Zapperi, Phys. Rev. B **76**, 224416 (2007).

[96] J.-i. Ohe & B. Kramer, Phys. Rev. Lett. **96**, 027204 (2006).

[97] A. V. Khvalkovskiy, K. A. Zvezdin, Y. V. Gorbunov, V. Cros, J. Grollier, A. Fert & A. K. Zvezdin, Phys. Rev. Lett. **102**, 067206 (2009).

[98] M. E. Lucassen & R. A. Duine, Phys. Rev. B **80**, 144421 (2009).

[99] M. E. Lucassen, H. J. van Driel, C. M. Smith & R. A. Duine, Phys. Rev. B **79**, 224411 (2009).

[100] A. Goussev, M. Robbins, J. & V. Slastikov, Phys. Rev. Lett. **104**, 147202 (2010).

[101] D. Culcer, M. E. Lucassen, R. A. Duine & R. Winkler, Phys. Rev. B **79**, 155208 (2009).

[102] A. K. Nguyen, H. J. Skadsem & A. Brataas, Phys. Rev. Lett. **98**, 146602 (2007).

[103] M. Eltschka *et al.*, Phys. Rev. Lett. **105**, 056601 (2010).

[104] G. Malinowski *et al.*, Journal of Physics D: Applied Physics **43**, 045003 (2010).

[105] R. Moriya, L. Thomas, M. Hayashi, Y. B. Bazaliy, C. Rettner & S. S. P. Parkin, Nat Phys **4**, 368 (2008).

[106] C. Burrowes *et al.*, Nat Phys **6**, 17 (2010).

[107] L. L. Foldy & S. A. Wouthuysen, Phys. Rev. **78**, 29 (1950).

[108] E. Wigner, Phys. Rev. **40**, 749 (1932).

[109] D. Xiao, M.-C. Chang & Q. Niu, Rev. Mod. Phys. **82**, 1959 (2010).

[110] J. N. Fuchs, F. Piéchon, M. O. Goerbig & G. Montambaux, The European Physical Journal B - Condensed Matter and Complex Systems **77**, 351 (2010), 10.1140/epjb/e2010-00259-2.

[111] K. M. D. Hals, A. K. Nguyen, X. Waintal & A. Brataas, Phys. Rev. Lett. **105**, 207204 (2010).

[112] R. D. King-Smith & D. Vanderbilt, Phys. Rev. B **47**, 1651 (1993).

[113] N. Nagaosa, J. Sinova, S. Onoda, A. H. MacDonald & N. P. Ong, Rev. Mod. Phys. **82**, 1539 (2010).

[114] M. N. Leuenberger & D. Loss, Phys. Rev. B **63**, 054414 (2001).

[115] G. Sundaram & Q. Niu, Phys. Rev. B **59**, 14915 (1999).

[116] P. Gosselin, J. Hanssen & H. Mohrbach, Phys. Rev. D **77**, 085008 (2008).

[117] R. Winkler, *Spin-orbit Coupling Effects in Two-dimensional Electron and Hole Systems* (Springer-Verlag Berlin Heidelberg, 2003).

[118] J. E. Moyal, Mathematical Proceedings of the Cambridge Philosophical Society **45**, 99 (1949).

[119] H. P. Breuer & F. Petruccione, *The Theory of Open Quantum Systems* (Oxford U. Press, 2002).

[120] D. Xiao, J. Shi & Q. Niu, Phys. Rev. Lett. **95**, 137204 (2005).

[121] A. Shelankov, Journal of Low Temperature Physics **60**, 29 (1985), 10.1007/BF00681651.

[122] Y. V. Nazarov & Y. M. Blanter, *Quantum Transport: Introduction to Nanoscience* (Cambridge University Press, 2009).

[123] D. J. Thouless, Phys. Rev. B **27**, 6083 (1983).

[124] F. Schwabl, *Advanced Quantum Mechanics* (Springer-Verlag Berlin Heidelberg, 2008).

[125] K. Y. Bliokh, EPL (Europhysics Letters) **72**, 7 (2005).

[126] G. E. Uhlenbeck & S. Goudsmit, Nature **117**, 264 (1926).

[127] M. Katsnelson, Eur. Phys. J. B **51**, 157 (2006).

[128] X.-L. Qi, T. L. Hughes & S.-C. Zhang, Phys. Rev. B **78**, 195424 (2008).

[129] K. Nomura & N. Nagaosa, Phys. Rev. B **82**, 161401 (2010).

[130] H. Zhang, C.-X. Liu, X.-L. Qi, X. Dai, Z. Fang & S.-C. Zhang, Nat Phys **5**, 438 (2009).

[131] T. Yokoyama, J. Zang & N. Nagaosa, Phys. Rev. B **81**, 241410 (2010).

[132] I. Garate & M. Franz, Phys. Rev. Lett. **104**, 146802 (2010).

[133] D. Culcer, E. H. Hwang, T. D. Stanescu & S. Das Sarma, Phys. Rev. B **82**, 155457 (2010).

[134] A. M. Essin, A. M. Turner, J. E. Moore & D. Vanderbilt, Phys. Rev. B **81**, 205104 (2010).

[135] S. Coh, D. Vanderbilt, A. Malashevich & I. Souza, Phys. Rev. B **83**, 085108 (2011).

[136] J. C. Y. Teo & C. L. Kane, Phys. Rev. Lett. **104**, 046401 (2010).

[137] X.-L. Qi & S.-C. Zhang, Physics Today **63**, 33 (2010).

[138] D. J. Thouless, M. Kohmoto, M. P. Nightingale & M. den Nijs, Phys. Rev. Lett. **49**, 405 (1982).

[139] X.-G. Wen, Advances in Physics **44**, 405 (1995).

[140] B. A. Bernevig, T. L. Hughes & S.-C. Zhang, Science **314**, 1757 (2006).

[141] M. König, H. Buhmann, L. W. Molenkamp, T. Hughes, C.-X. Liu, X.-L. Qi & S.-C. Zhang, Journal of the Physical Society of Japan **77**, 031007 (2008).

[142] M. König, S. Wiedmann, C. Brüne, A. Roth, H. Buhmann, L. W. Molenkamp, X.-L. Qi & S.-C. Zhang, Science **318**, 766 (2007).

[143] A. Roth, C. Brüne, H. Buhmann, L. W. Molenkamp, J. Maciejko, X.-L. Qi & S.-C. Zhang, Science **325**, 294 (2009).

[144] C. L. Kane & E. J. Mele, Phys. Rev. Lett. **95**, 146802 (2005).

[145] L. Fu & C. L. Kane, Phys. Rev. B **76**, 045302 (2007).

[146] D. Hsieh, D. Qian, L. Wray, Y. Xia, Y. S. Hor, R. J. Cava & M. Z. Hasan, Nature **452**, 970 (2008).

[147] Y. L. Chen *et al.*, Science **325**, 178 (2009).

[148] J. D. Sau, R. M. Lutchyn, S. Tewari & S. Das Sarma, Phys. Rev. Lett. **104**, 040502 (2010).

[149] J. Alicea, Phys. Rev. B **81**, 125318 (2010).

[150] Z. Wang, X.-L. Qi & S.-C. Zhang, Phys. Rev. Lett. **105**, 256803 (2010).

[151] R. Li, J. Wang, X.-L. Qi & S.-C. Zhang, Nat Phys **6**, 284 (2010).

[152] J. Linder, Y. Tanaka, T. Yokoyama, A. Sudbø & N. Nagaosa, Phys. Rev. Lett. **104**, 067001 (2010).

[153] J. Linder, Y. Tanaka, T. Yokoyama, A. Sudbø & N. Nagaosa, Phys. Rev. B **81**, 184525 (2010).

[154] L. Fu & C. L. Kane, Phys. Rev. Lett. **100**, 096407 (2008).

[155] L. Fu & C. L. Kane, Phys. Rev. Lett. **102**, 216403 (2009).

[156] A. R. Akhmerov, J. Nilsson & C. W. J. Beenakker, Phys. Rev. Lett. **102**, 216404 (2009).

[157] X.-L. Qi, T. L. Hughes & S.-C. Zhang, Nat Phys **4**, 273 (2008).

[158] G. Volovik, JETP Letters **91**, 55 (2010), 10.1134/S0021364010020013.

[159] D. Hsieh *et al.*, Nature **460**, 1101 (2009).

[160] H. B. Nielsen & M. Ninomiya, Physics Letters B **130**, 389 (1983).

[161] Y. Zhang *et al.*, Nat Phys **6**, 584 (2010).

[162] Z. Alpichshev, J. G. Analytis, J.-H. Chu, I. R. Fisher, Y. L. Chen, Z. X. Shen, A. Fang & A. Kapitulnik, Phys. Rev. Lett. **104**, 016401 (2010).

[163] C.-X. Liu, X.-L. Qi, H. Zhang, X. Dai, Z. Fang & S.-C. Zhang, Phys. Rev. B **82**, 045122 (2010).

[164] A. A. Burkov & D. G. Hawthorn, Phys. Rev. Lett. **105**, 066802 (2010).

[165] Y. L. Chen *et al.*, Science **329**, 659 (2010).

[166] L. A. Wray *et al.*, Nat Phys **7**, 32 (2011).

[167] R. Yu, W. Zhang, H.-J. Zhang, S.-C. Zhang, X. Dai & Z. Fang, Science **329**, 61 (2010).

[168] T. Yokoyama, Y. Tanaka & N. Nagaosa, Phys. Rev. B **81**, 121401 (2010).

[169] Z. Yang & J. H. Han, Phys. Rev. B **83**, 045415 (2011).

[170] P. Phillips, *Advanced Solid State Physics* (Westview Press, 2003).

[171] J. W. McClure, Phys. Rev. **104**, 666 (1956).

[172] T. Hanaguri, K. Igarashi, M. Kawamura, H. Takagi & T. Sasagawa, Phys. Rev. B **82**, 081305 (2010).

[173] P. Cheng *et al.*, Phys. Rev. Lett. **105**, 076801 (2010).

[174] D.-H. Lee, Phys. Rev. Lett. **103**, 196804 (2009).

[175] Y. Aharonov & A. Casher, Phys. Rev. A **19**, 2461 (1979).

[176] K. Yamada, S. Kasai, Y. Nakatani, K. Kobayashi, H. Kohno, A. Thiaville & T. Ono, Nat Mater **6**, 270 (2007).

[177] I. Gradshteyn & I. Ryzhik, *Table of Integrals, Series, and Products (Seventh Edition)* (Academic Press, 2007).

[178] R. Danneau, F. Wu, M. Craciun, S. Russo, M. Tomi, J. Salmilehto, A. Morpurgo & P. Hakonen, Journal of Low Temperature Physics **153**, 374 (2008), 10.1007/s10909-008-9837-z.

[179] M. Hazewinkel, *Encyclopaedia of Mathematics* (Springer, 1994).